Green Chemistry and Sustainable Technology

Bhalchandra M. Bhanage
Masahiko Arai *Editors*

Transformation and Utilization of Carbon Dioxide

Springer

Green Chemistry and Sustainable Technology

Series Editors

For further volumes:
http://www.springer.com/series/11661

Green Chemistry and Sustainable Technology

Aims and Scope

The series *Green Chemistry and Sustainable Technology* aims to present cutting-edge research and important advances in green chemistry, green chemical engineering and sustainable industrial technology. The scope of coverage includes (but is not limited to):

- Environmentally benign chemical synthesis and processes (green catalysis, green solvents and reagents, atom-economy synthetic methods etc.)
- Green chemicals and energy produced from renewable resources (biomass, carbon dioxide etc.)
- Novel materials and technologies for energy production and storage (biofuels and bioenergies, hydrogen, fuel cells, solar cells, lithium-ion batteries etc.)
- Green chemical engineering processes (process integration, materials diversity, energy saving, waste minimization, efficient separation processes etc.)
- Green technologies for environmental sustainability (carbon dioxide capture, waste and harmful chemicals treatment, pollution prevention, environmental redemption etc.)

The series *Green Chemistry and Sustainable Technology* is intended to provide an accessible reference resource for postgraduate students, academic researchers and industrial professionals who are interested in green chemistry and technologies for sustainable development.

Bhalchandra M. Bhanage • Masahiko Arai
Editors

Transformation and Utilization of Carbon Dioxide

Springer

Editors
Bhalchandra M. Bhanage
Department of Chemistry
Institute of Chemical Technology
Mumbai, India

Masahiko Arai
Division of Chemical Process Engineering
Faculty of Engineering, Hokkaido University
Sapporo, Japan

ISSN 2196-6982 ISSN 2196-6990 (electronic)
ISBN 978-3-642-44987-1 ISBN 978-3-642-44988-8 (eBook)
DOI 10.1007/978-3-642-44988-8
Springer Heidelberg New York Dordrecht London

Library of Congress Control Number: 2014931416

Printed on acid-free paper

Springer is part of Springer Science+Business Media (www.springer.com)

Preface

Carbon dioxide is one of the green house gases and the emission and accumulation of a huge amount of CO_2 causes significant and negative effects on the global environment. It is crucial, therefore, to take effective measures to reduce CO_2 emission and treat the CO_2 emitted. Carbon dioxide is a safe and abundant resource of C and O and the production of useful chemicals from CO_2 conforms to the Green Chemistry principles. Carbon dioxide may replace harmful reactants like CO and phosgene currently used in chemical reaction processes. Carbon dioxide is a stable and less reactive molecule and, hence, the CO_2 activation has been investigated so far by using various catalysts and processes. The practical use of CO_2 as a reactant could also have a contribution to the reduction of the undesired CO_2 in the environment.

This book is dedicated to a wide-angle review of chemical transformation and utilization of CO_2 in 14 chapters. It is composed of four parts, which are chemical (organic and inorganic), electro- and photo-chemical, and biochemical transformation of CO_2 to a number of organic and inorganic, small- and large-scale products. The last two chapters deal with the application of CO_2 as a promoter as well as a reactant in organic synthetic reactions.

Part I, consisting of seven chapters, deals with the use of CO_2 in chemical reactions. In Chap. 1, Prof. Kühn and coworkers describe valorization of CO_2 to organic products using organocatalysts. Chapters 2 and 3 give several examples of direct and indirect utilization of CO_2 to valuable products using heterogeneous catalysts. In Chap. 4, Prof. Beller and coworker review hydrogenation and related reduction of CO_2 using molecular catalysts. Professor Arena and coworkers describe hydrogenation of CO_2 to bulk chemicals like methanol and dimethyl ether in Chap. 5. Professor Ross describes fundamentals and perspectives of syngas production using CO_2 reforming in Chap. 6. In Chap. 7, Prof. Rieger and coworkers explain utilization of CO_2 as a C-1 block for the synthesis of polycarbonates. These chapters demonstrate the usefulness and potential of CO_2 as a reactant.

Part II consists of four chapters dedicated to photocatalytic, electrochemical, and inorganic reactions of CO_2. Professor Krebs and coworker explore the possibilities of using flexible substrates as basis for CO_2 fixation and photocatalytic reduction in

Chap. 8. Chapter 9, contributed by Prof. Yamashita and co-workers, describes reductive conversion of CO_2 by using various photocatalyst materials. In Chap. 10, Prof. Senboku explains electrochemical fixation of CO_2. Chapter 11 of Prof. Baciocchi and co-workers describes accelerated carbonation processes for CO_2 capture, storage, and utilization.

Part III is directed to biological reactions of CO_2, consisting of Chap. 12 of Prof. Das and coworker. This chapter summarizes the role of various biological processes available for CO_2 mitigation and discusses the use of terrestrial plants, algae, cyanobacteria, carbonic anhydrase enzyme, and various other bacteria in CO_2 sequestration.

Part IV deals with the reactions in/under dense phase CO_2 in two chapters. In Chap. 13, Prof. He and co-workers describe homogeneous catalysis promoted by CO_2. Chapter 14 explains the potential of multiphase catalytic reactions in/under dense phase CO_2, in which CO_2 is utilized as a reaction promoter.

We believe/hope that this book will be useful to readers in various fields who take practical and scientific interests in the current and future *Transformation and Utilization of Carbon Dioxide*. All these chapters have been written by overseas experts in the related fields. We would like to express our sincere thanks to the authors for their excellent contributions to this book and their names are listed on separate pages. We are also thankful to Springer for their support in publishing this book.

Sapporo, Japan — Masahiko Arai
Mumbai, India — Bhalchandra M. Bhanage

Contents

Contributors

Peter T. Altenbuchner Technische Universität München, WACKER-Lehrstuhl für Makromolekulare Chemie, Garching, Germany

Michael H. Anthofer Catalysis Research Center, Technische Universität München, München, Germany

Masahiko Arai Division of Chemical Process Engineering, Faculty of Engineering, Hokkaido University, Sapporo, Japan

Francesco Arena Department of Electronic Engineering, Industrial Chemistry and Engineering, University of Messina, Messina, Italy

Renato Baciocchi Laboratory of Environmental Engineering, Department of Civil Engineering and Computer Science Engineering, University of Rome "Tor Vergata", Rome, Italy

Matthias Beller Leibniz-Institut für Katalyse Eingetragener Verein an der Universität Rostock, Rostock, Germany

Bhalchandra M. Bhanage Department of Chemistry, Institute of Chemical Technology, Mumbai, India

Mirza Cokoja Catalysis Research Center, Technische Universität München, München, Germany

Giulia Costa Laboratory of Environmental Engineering, Department of Civil Engineering and Computer Science Engineering, University of Rome "Tor Vergata", Rome, Italy

Debabrata Das Department of Biotechnology, Indian Institute of Technology, Kharagpur, India

Zhen-Feng Diao State Key Laboratory of Elemento-Organic Chemistry, Nankai University, Tianjin, People's Republic of China

Shin-ichiro Fujita Division of Chemical Process Engineering, Faculty of Engineering, Hokkaido University, Sapporo, Japan

Kojirou Fuku Division of Materials and Manufacturing Science, Graduate School of Engineering, Osaka University, Suita, Osaka, Japan

Elements Strategy Initiative for Catalysts Batteries ESICB, Kyoto University, Katsura, Kyoto, Japan

Liang-Nian He State Key Laboratory of Elemento-Organic Chemistry, Nankai University, Tianjin, People's Republic of China

Jacob Jensen Department of Energy Conversion and Storage, Technical University of Denmark, Roskilde, Denmark

Stefan Kissling Technische Universität München, WACKER-Lehrstuhl für Makromolekulare Chemie, Garching, Germany

Frederik C. Krebs Department of Energy Conversion and Storage, Technical University of Denmark, Roskilde, Denmark

Fritz E. Kühn Catalysis Research Center, Technische Universität München, München, Germany

Kanhaiya Kumar Department of Biotechnology, Indian Institute of Technology, Kharagpur, India

Ran Ma State Key Laboratory of Elemento-Organic Chemistry, Nankai University, Tianjin, People's Republic of China

Giovanni Mezzatesta Department of Electronic Engineering, Industrial Chemistry and Engineering, University of Messina, Messina, Italy

Kohsuke Mori Division of Materials and Manufacturing Science, Graduate School of Engineering, Osaka University, Suita, Osaka, Japan

Elements Strategy Initiative for Catalysts Batteries ESICB, Kyoto University, Katsura, Kyoto, Japan

Bernhard Rieger Technische Universität München, WACKER-Lehrstuhl für Makromolekulare Chemie, Garching, Germany

Julian R.H. Ross University of Limerick, Limerick, Ireland

Hisanori Senboku Division of Chemical Process Engineering, Faculty of Engineering, Hokkaido University, Sapporo, Hokkaido, Japan

Lorenzo Spadaro Department of Electronic Engineering, Industrial Chemistry and Engineering, University of Messina, Messina, Italy

Giuseppe Trunfio Department of Electronic Engineering, Industrial Chemistry and Engineering, University of Messina, Messina, Italy

Rahul A. Watile Department of Chemistry, Institute of Chemical Technology, Mumbai, India

Michael E. Wilhelm Catalysis Research Center, Technische Universität München, München, Germany

Hiromi Yamashita Division of Materials and Manufacturing Science, Graduate School of Engineering, Osaka University, Suita, Osaka, Japan

Elements Strategy Initiative for Catalysts Batteries ESICB, Kyoto University, Katsura, Kyoto, Japan

Zhen-Zhen Yang State Key Laboratory of Elemento-Organic Chemistry, Nankai University, Tianjin, People's Republic of China

Hiroshi Yoshida Division of Chemical Process Engineering, Faculty of Engineering, Hokkaido University, Sapporo, Japan

Carolin Ziebart Leibniz-Institut für Katalyse Eingetragener Verein an der Universität Rostock, Rostock, Germany

Daniela Zingaretti Laboratory of Environmental Engineering, Department of Civil Engineering and Computer Science Engineering, University of Rome "Tor Vergata", Rome, Italy

Part I
Chemical Reactions

Chapter 1
Valorization of Carbon Dioxide to Organic Products with Organocatalysts

Michael H. Anthofer, Michael E. Wilhelm, Mirza Cokoja, and Fritz E. Kühn

1.1 Introduction

Humankind is facing an increasing problem with energy supply. Society must meet the needs of the steadily increasing world population [1], and additionally, industrially emerging countries exhibit a rising energy demand in order to improve their living standard. Today, the main energy sources are fossil carriers such as petroleum and, to a minor extent, coal [2]. Other sources are either ecologically or politically problematic, such as nuclear power, or they are not yet efficient enough, depend on climatic fluctuations, or are difficult to store (solar and wind power). Hence, if the world continues to rely on carbon compounds as energy carriers, with the energy stored in chemical bonds, other renewable resources have to be considered. So far, however, the main alternative carbon feedstock – natural gas, carbon dioxide, and biomass (starch, cellulose, lignin) – have primarily been used for direct combustion, and their transformation into value-added chemicals is considered as notoriously difficult due to their chemical inertness [3–6]. For this reason, catalysis research is increasingly devoted to finding ways to develop high-performance catalysts for the valorization of renewable carbon feedstocks [7–9]. Numerous approaches have already been presented in the literature. However, they are often associated with a significant carbon footprint, which is thus rendering these approaches useless, at least on a larger scale [10–14].

Carbon dioxide is in a special spotlight as a renewable C_1-feedstock, since it is ubiquitous and readily available, either from decomposition of organic matter or artificially. Whereas CO_2 can be transformed to carbohydrates in nature – which is the basis of life on Earth – from a chemical (industrial) point of view, CO_2 appeared

Michael H. Anthofer and Michael. E. Wilhelm equally contributed to this article.

M.H. Anthofer • M.E. Wilhelm • M. Cokoja (✉) • F.E. Kühn (✉)
Catalysis Research Center, Technische Universität München, Ernst-Otto-Fischer-Straße 1, D-85747 Garching bei München, Germany
e-mail: mirza.cokoja@ch.tum.de; fritz.kuehn@ch.tum.de

B.M. Bhanage and M. Arai (eds.), *Transformation and Utilization of Carbon Dioxide*, Green Chemistry and Sustainable Technology, DOI 10.1007/978-3-642-44988-8_1,

to be a dead end for all organic compounds. The idea behind the use of CO_2 as feedstock for chemicals and fuels is nevertheless attractive: the direct energy supply via combustion of carbonaceous energy carriers produces CO_2, which could be converted back into the energy carrier, thereby leading to an artificial carbon cycle, leading to a recycling of CO_2 and balancing the anthropogenic emission into the atmosphere [15]. Evidently, the activation of CO_2 can only be realized using catalysts (and – in many cases additional – cheap energy sources). In this case, the classic heterogeneous catalysts fail to convert CO_2 at mild temperatures, which would warrant a multiton plant scale. On the other hand, homogeneous catalysts usually operate at significantly milder conditions [16–18]. From all possible transformations of CO_2 to C_1 or higher chemicals with molecular catalysts in solution, the most promising reactions in terms of energy balance, catalyst performance, reusability, and scale-up perspective would be:

- Reduction to CO
- Hydrogenation with H_2 to formate, methanol, or methane
- Formation of (poly)carbonate

The reduction reactions appear particularly attractive, since the products are all significantly more reactive than CO_2 or can themselves be used as energy carriers. However, these processes are to date either not efficient enough, or they involve hydrogen, which is currently expensive (steam reforming process) and therefore an undesired reactant. As long as there are no promising approaches to access H_2 from water cheaply, e.g., photochemically, these reactions are prohibitive for industry. Contrasting this, the synthesis of carbonates and polycarbonates from CO_2 and epoxides is a well-known and established procedure using various high-performance metal catalysts [19–25]. Yet, for all reactions, there is plenty of room for improvement of the catalyst design, efficiency, and reaction conditions in order to establish a process for the valorization of CO_2 (in the multimillion ton scale).

In comparison to molecular metal catalysts, metal-free catalysts are not so widespread. However, the application of organocatalysts would – in most cases – easily outcompete metal catalysts in many regards, not only in price or stability but also in terms of "green chemistry," avoiding heavy metal waste or intricate catalyst recovery. This chapter presents a comprehensive overview of catalytic transformations of CO_2 to organic products – most notably carbonates – employing molecular metal-free catalysts reported in the literature to date.

1.2 Ionic Compounds as Catalysts for the Green Synthesis of Cyclic Carbonates from Epoxides and Carbon Dioxide

The reaction with epoxides to cyclic carbonates (Scheme 1.1) is one of the best-studied methods for the chemical fixation of CO_2 in homogeneous phase. The most important cyclic carbonates are ethylene carbonate (EC), propylene carbonate (PC),

Scheme 1.1 Conversion of carbon dioxide and epoxides into cyclic carbonates

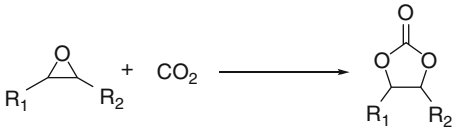

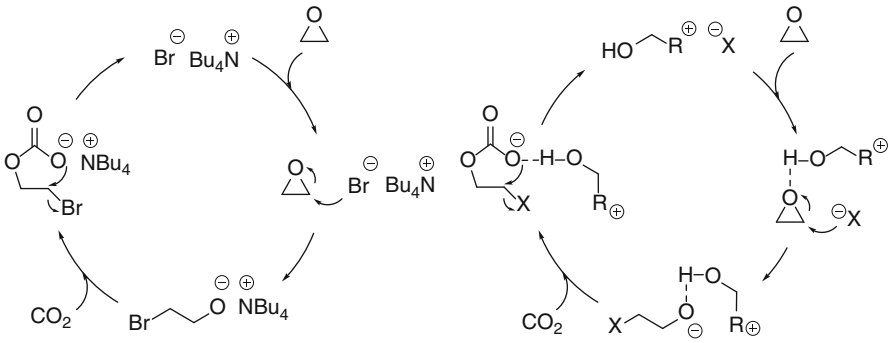

Scheme 1.2 Proposed mechanisms for the chemical fixation of CO_2 with EO using TBAB as catalyst and a proposed cooperative mechanism for hydroxyl-functionalized ionic liquids (HFILs)

and styrene carbonate (SC). Five-membered cyclic carbonates can be used as polar aprotic solvents, electrolytes in secondary batteries, valuable precursors for polycarbonate and polyurethane materials, and intermediates in organic synthesis [26]. The first successful approach was carried out by Calo et al. by dissolving propylene oxide (PO) in tetrabutylammonium bromide (TBAB) or tetrabutylammonium iodide (TBAI) at atmospheric CO_2 pressure to yield PC [27]. The observed activity of the catalytic system decreases in order of TBAI > TBAB due to the higher nucleophilicity of iodide in comparison to bromide. In addition, an increase of chain length from tetraethylammonium bromide (TEAB) to TBAB results in a higher yield of PC. After the reaction is completed, the pure cyclic carbonate can be easily separated by vacuum distillation or extraction with ethyl acetate, which allows the recycling of the ammonium salt. For getting a better understanding of the reaction mechanism, investigations toward the cycloaddition of epoxides with CO_2 using TBAB as catalyst were studied in various reports. Proposed mechanisms are illustrated in Scheme 1.2 [27, 28].

The bromide anion performs a nucleophilic attack to form an oxyanion species. This species reacts with CO_2 to result in cyclic carbonate formation after intramolecular cyclic elimination. Further experimental and theoretical studies of the catalytic behavior, in dependency of the used anion with a consistent cation, show a higher activity in the order Cl > Br > I, which was not in accord with the calculated relative energy of the rate-determining step [28]. Nevertheless, lowering of the activation energies and thus higher activity could be confirmed experimentally and theoretically.

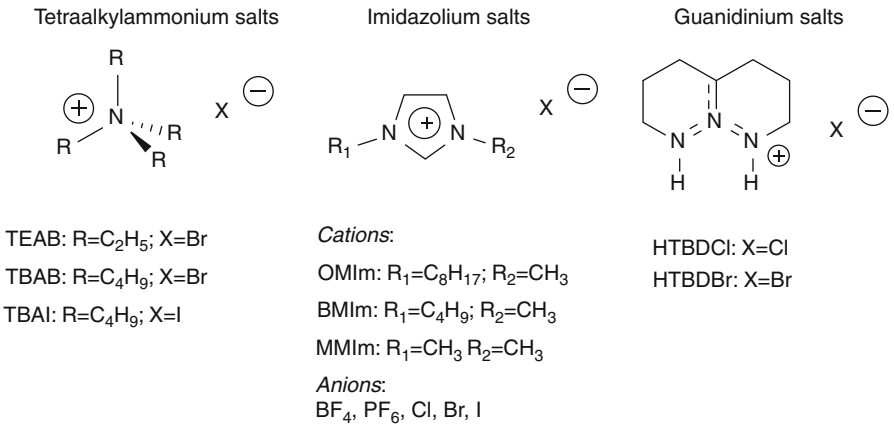

Fig. 1.1 Representative tetraalkylammonium-, imidazolium-, and guanidinium-based ionic liquids

The first quantitative conversion of propylene oxide (PO) to propylene carbonate (PC) was observed in 2001 by Peng and Deng, using 2.5 mol-% of 1-butyl-3-methylimidazolium tetrafluoroborate ($BMImBF_4$) under 25 bar CO_2 pressure at 110 °C after 6 h (TOF = 6.6 h^{-1}) [29]. The group investigated the influence of cation and anion of the ionic liquid (IL) and asserted an increase in the catalytic activity in order imidazolium > pyridyl for the cation and PF_6 > Cl > BF_4 for the anion. In later works, the catalytic activity of several ammonium halides and imidazolium-based ILs could be further improved by microwave irradiation instead of heating [30]. A representative overview of different ILs active as organocatalysts for the fixation of CO_2 is given in Fig. 1.1.

In the next step, imidazolium-based ILs were used as catalyst with supercritical CO_2 ($scCO_2$) as solvent and reactant. Therefore, 1-octyl-3-methylimidazolium tetrafluoroborate ($OMImBF_4$) was found to be an excellent catalyst under supercritical conditions. Nearly 100 % yield and selectivity of PC was determined at 140 bar CO_2 pressure and 100 °C after 5 min (TOF = 517 h^{-1}) [31]. The TOF value is nearly 80 times faster than previously reported [29]. Ikushima et al. detected an increase of the yield of PC by increasing the chain length of the alkyl side chain of the imidazolium cation from C_2 to C_8, due to higher solubility of CO_2 and PO in the IL phase [31]. Furthermore, theoretical studies indicate cooperative interactions between cation and anion, which stabilize intermediates and transition states through hydrogen bonding. Therefore, the ring-opening of PO as the rate-determining step is facilitated, leading to enhanced catalytic activity [32]. By comparison of 1-butyl-3-methylimidazolium chloride (BMImCl) and 1-butyl-3-methylimidazolium bromide (BMImBr) for the synthesis of PC, TOFs of 5 h^{-1} (BMImCl) and 37 h^{-1} (BMImBr) were found at 100 °C, 35 bar CO_2 pressure after 1 h [33]. Hence, the activity of the catalyst decreases in order of Br > Cl.

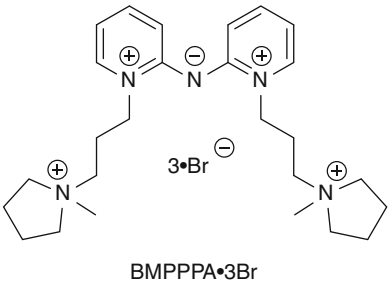

Fig. 1.2 BMPPPA·3Br as reaction medium and efficient organocatalyst for CO_2 fixation into cyclic carbonates

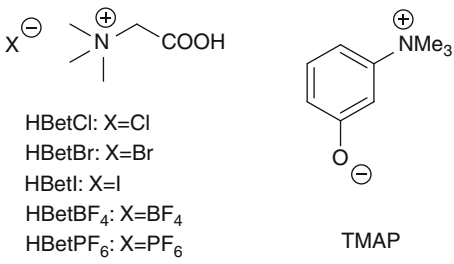

Fig. 1.3 Betaine-based salts and TMAP as bifunctional organocatalysts bearing a betaine framework

Wong et al. prepared the new IL BMPPPA · 3Br (Fig. 1.2) with a Lewis acidic cation, which is a promising catalyst for the activation of epoxides in the cycloaddition with CO_2. This IL catalyzes the formation of PC with a yield and selectivity of ≥99 % at 80 °C, 40 bar CO_2 pressure after 3 h and could be recycled for more than ten times without any loss of activity. Small amounts of water (2 % w/w) are needed to liquefy the IL at 80 °C in order to function also as reaction medium [34].

Task-specific ILs (TSILs) bearing a functional group, allowing the activation of PO or CO_2 or both, are the next generation of ILs for the formation of cyclic carbonates. First, a series of hydroxyl-functionalized ionic liquids (HFILs) was developed, characterized, and found to be efficient and reusable catalysts for the synthesis of cyclic carbonates with high selectivity in the absence of any cocatalyst and any cosolvents [35]. Hydroxyl groups in the catalyst were proposed to polarize the C–O bond via hydrogen bonding and therefore facilitate the nucleophilic attack of the halide anion, as illustrated in Scheme 1.2. 1-(2-hydroxyethyl)-3-methylimidazolium bromide (HEMImBr) was most efficient for the synthesis of PC with 99 % conversion of PO and a selectivity of 99.8 % under the optimized reaction conditions (catalyst loading: 1.6 mol-%, 125 °C, 20 bar CO_2, 1 h).

Similar to hydroxyl groups, carboxylic acid groups as hydrogen bond donors can also accelerate the ring-opening reaction of the epoxide. Through direct protonation of anhydrous betaine, a series of bifunctional catalysts was synthesized, allowing the polarization of the epoxide through hydrogen bonding and at the same time the ring-opening of the epoxide with the respective anion (Fig. 1.3) [36].

The catalytic activity for the formation of PC increases in order HBetI > HBetCl > HBetBr > $HBetBF_4$ > $HBetPF_6$. Under catalytic conditions, 2.5 mol-% HBetI

(80 bar CO_2 pressure, 140 °C, 8 h) result in a yield of 98 % PC and the catalyst was recycled for at least three times. Based on these results, organocatalysts bearing an ammonium betaine moiety have been developed as a new catalytic motif for the activation of carbon dioxide and epoxides to produce cyclic carbonates under milder reaction conditions [37]. After screening several catalysts, 3-trimethylammoniumphenolate (TMAP) was shown to be the most active for the conversion of PO to PC with a yield of 99 % under relatively mild reaction conditions (catalyst loading: 3 mol-%, 10 bar CO_2 pressure, 120 °C, 24 h). Additionally, TMAP is capable to form a CO_2 adduct at 15 °C which is also promising for carbon capture and storage (CCS). Another attempt for a bifunctional catalyst system was using α-amino acids in $scCO_2$ due to the same background as mentioned before for betaine. After a screening, L-histidine turned out to be the most active catalyst leading to the corresponding cyclic carbonates in good to excellent yields with a catalyst loading of 0.8 mol-% at 130 °C under 80 bar CO_2 [38]. Natural alpha-amino acids-derived ionic liquids, comprising BMIm cation and amino acid anion, were found to be efficient catalysts for the coupling of various epoxides and CO_2. Cyclic carbonates could be produced in good yields and selectivity without any additional organic solvent or halogen [39]. Using a modified amino acid IL with triethylamine (NEt_3) as cocatalyst, the catalytic activity of the L-proline-based ionic liquid was greatly enhanced. Up to 97 % isolated yield of cyclic carbonate was achieved at 90 °C under atmospheric CO_2 pressure without organic solvent and metal component [40].

Another way for the fixation of CO_2 in cyclic carbonates are CO_2 adducts of N-heterocyclic carbenes (NHCs). Therefore, the thermal stable 1,3-bis (2,6-diisopropylphenyl)imidazolium-2-carboxylate (IPr-CO_2) was found to catalyze the reaction of PO with CO_2 to PC. Under the optimized reaction conditions (catalyst loading: 0.5 mol-%, 2 mL CH_2Cl_2, 20 bar CO_2, 120 °C, 24 h), a quantitative conversion of PO with a selectivity ≥99 % for PC was observed [41]. Ikariya et al. also developed a series of different NHC-CO_2 adducts which were active toward the cycloaddition of CO_2 with epoxides. With a catalyst loading of 5.0 mol-%, styrene oxide was converted with a selectivity ≥99 % to the corresponding cyclic carbonate in a yield of 98 % under optimized reaction conditions (45 bar CO_2 pressure, 100 °C, 24 h) [42].

Cheng et al. found a single Lewis base catalyst for the formation of cyclic carbonates from CO_2 and terminal epoxides in water without suffering selectivity [43]. It is proposed that water and the anion of the Lewis base play a synergistic effect in accelerating the ring-opening reaction. Among the investigated catalysts, triphenylbutylphosphonium iodide (PPh_3BuI) was the most active with a yield of 95 % and a selectivity of 98 % for the conversion of ethylene oxide (EO) to ethylene carbonate (EC) under optimized reaction conditions (0.5 mol-% PPh_3BuI, 33.5 mol-% water, 110 °C, 25 bar CO_2 pressure, 0.5 h). The catalyst could be recycled for at least ten times without significant loss of activity.

A series of easily prepared Lewis basic ILs were developed for cyclic carbonate synthesis from epoxide and CO_2 without utilization of any organic solvents or additives (Fig. 1.4) [44]. The presence of a tertiary nitrogen atom in the cation has

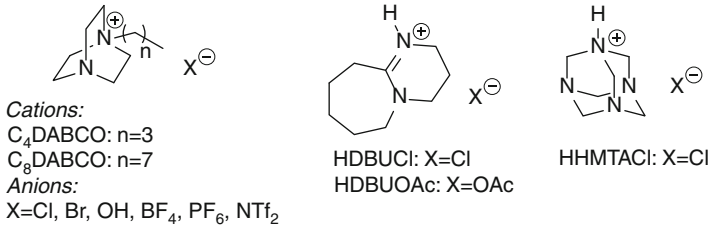

Fig. 1.4 Lewis basic ionic liquids

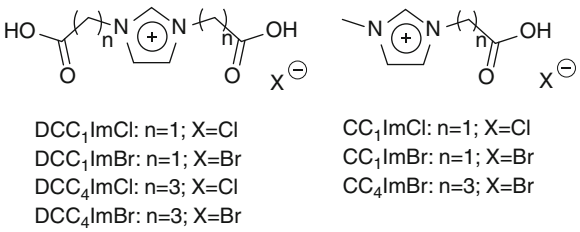

Fig. 1.5 Imidazolium-based acid–base bifunctional catalysts (ABBCs)

the potential to form a carbamate species as an activated form of CO_2. Additionally, the epoxide could be activated through hydrogen bonding of the proton attached to the ammonium nitrogen atom of the IL. In dependence of the cation, the catalytic activity decreases in order of $HDBU^+ > HTBD^+ \sim OMIm^+ > C_4DABCO^+ \sim C_8DABCO^+ > BMIm^+ > HHMTA^+$. After 2 h, 97 % yield and a selectivity $\geq$99 % toward the formation of PC were attained, when 1.0 mol-% 1,8-diazabicyclo [5.4.0]undec-7-enium chloride ([HDBU]Cl) was used as a catalyst at 140 °C under 10 bar CO_2 pressure. Furthermore, the catalyst could be recycled over five times without appreciable loss of catalytic activity. Also, hydroiodides of amidines catalyze the reaction of CO_2 and epoxides. Under ambient pressure and temperature, the corresponding cyclic carbonates were obtained in moderate to high yields [45]. Furthermore, hydroiodides of secondary and primary amines were found to be efficient catalysts for PC synthesis [46]. Detailed investigation showed that the catalytic activity is strongly dependent on the counter anions of the ammonium salts. Iodide catalyzes the reaction efficiently, whereas bromide and chloride show almost no activity. In addition, the activity of the catalyst increases with increasing bulkiness of the substituents on the ammonium nitrogen atoms, since PC synthesis becomes more efficient as the parent amines become more basic. After performing a catalyst screening, dicyclohexylammonium iodide (DCAI) was determined to be the most active catalyst. SC was successfully synthesized out of SO by using 5 mol-% DCAI dissolved in 1-methyl-2-pyrrolidone (NMP) at 45 °C under atmospheric CO_2 pressure after 24 h in a yield of 85 % and a selectivity $\geq$99 %.

New acid–base bifunctional catalysts (ABBCs), containing one or two Brønsted acidic sites in the imidazolium-based cationic part and a Lewis basic site in the anionic part, were determined as efficient catalysts for the synthesis of cyclic carbonates without the use of additional cocatalyst or cosolvent (Fig. 1.5) [47]. Imidazolium was

Scheme 1.3 Preparation of amidinium halides

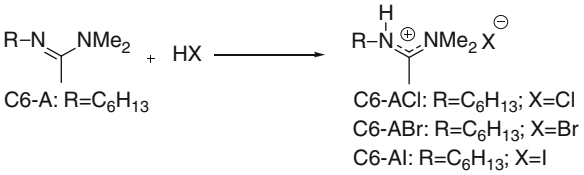

used as cationic structural motif due to a decrease of catalytic activity in order of imidazolium- > bipyridinium- > isonicotinic-based ABBCs. The catalytic cycle is proposed to be the same as it is for HFILs and illustrated in Scheme 1.2.

Among all catalysts, 1,3-(bis-3-carboxypropyl)imidazolium bromide DCC_4ImBr was the most active and could be recycled for five times without loss of activity. Almost quantitative yield of PC can be achieved in 1 h at 100 °C under 20 bar CO_2. Park et al. synthesized ILs with carboxylic acid moieties in their backbones and observed a higher activity for the cycloaddition reaction of CO_2 with various epoxides for ABBCs, compared to HFILs and ILs without any functional groups [48].

Tassaing and coworkers investigated the catalytic cycloaddition of PO to CO_2 at 80 °C and 80 bar CO_2 pressure via in situ FTIR and Raman spectroscopy using the primarily tetraalkylammonium, imidazolium, and guanidinium salts mentioned in Fig. 1.1 [49]. Among all investigated ILs, 1,5,7-triazabicyclo[4.4.0]dec-5-enium bromide (HTBDBr) and 1-methyl-3-methylimidazolium iodide (MMImI) showed the highest activity. The spectroscopic results show the possibility of activating the epoxide through hydrogen bonding and stabilization of the oxyanion intermediate. This is comparable to other works and fits to the illustrated mechanism in Scheme 1.2 [35, 44, 48, 50–52]. Therefore, SO was converted to SC with a yield of 87 % using 1 mol-% HTBDBr at 80 °C under 10 bar CO_2 pressure after 20 h. If the reaction is carried out at 80 bar CO_2, the yield of SC is only about 88 %. By pressurizing the reaction with less than 10 bar CO_2, the yield decreases to 65 %. Nevertheless, no recycling experiments were carried out to show the efficiency of the catalytic system.

The IL-catalyzed reaction of PO and CO_2 to PC was also studied in a microreactor using 2-hydroxyethyltributylammonium bromide (HETBABr) as catalyst. After a parameter variation, the results show that the residence time can be dramatically reduced from several hours in a conventional stirred reactor to about 10 s in a microreactor. Almost quantitative yield of PC can be reached at 35 bar at a residence time of 14 s. The TOF value varies in the range of 3,000–14,000 h^{-1} compared to 60 h^{-1} in the conventional stirred reactor. This work opens the possibility for the commercialization of the metal-free conversion of CO_2 to cyclic carbonates [53].

Amidinium halide catalysts were synthesized (see Scheme 1.3) and employed in the synthesis of cyclic carbonates using an in situ-prepared, reversible, room-temperature ionic liquid (RTIL), amidinium carbamates, as solvent [54].

Amidinium carbamates (C6-A-CO_2) were prepared by exposing equimolar mixtures of C6-A and a primary amine to CO_2 gas. 2 mol-% C6-AI in C6-A-CO_2

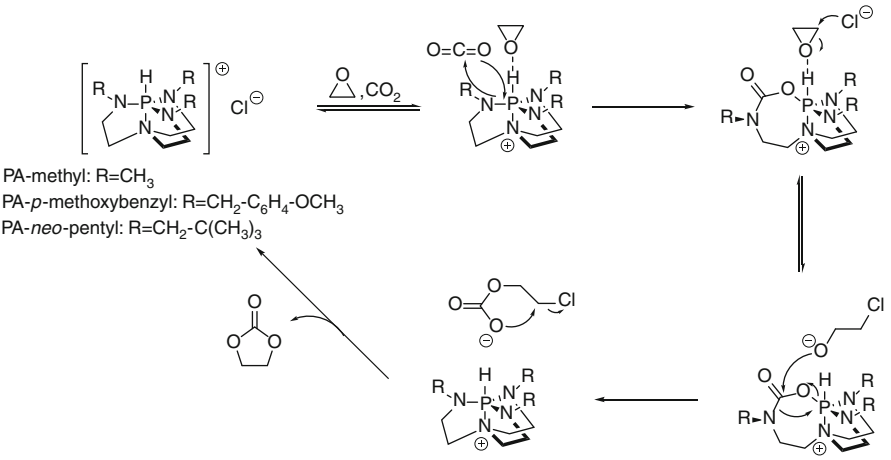

Scheme 1.4 Proposed mechanism for the azaphosphatrane derivatives catalyzed cycloaddition of EO and CO_2

at 50 °C under 25 bar CO_2 pressure lead to a yield of 99 % of SC after 8 h. Product and any unreacted epoxide were extracted easily upon addition of an immiscible, lower density liquid to the RTIL reaction mixture. This process was repeated three times with the same RTIL without any obvious decrease in catalytic activity. This system is an attractive alternative for preparing cyclic carbonates and CO_2 storage due to the reusability and the rather low temperatures and CO_2 pressures.

Latest research efforts lead to azaphosphatrane (AP) derivatives as a new class of catalysts [55]. AP can be a tunable alternative to known ammonium halides, but their catalytic behavior strongly depends on their substitution pattern cause of the proposed mechanism. The authors propose an activation of the epoxide through hydrogen bonding of the phosphonium cation and an insertion of CO_2 into the P–N bond. The formed tricyclic phosphoryl-carbamate species is very sensitive. Bulkier substituents prevent degradation of the catalyst and lead to a higher activity (Scheme 1.4). AP-*neo*-pentyl with the most bulky substituents is the most stable and active catalyst in this work. A kinetic experiment with 1.0 mol-% AP-*neo*-pentyl leads to 50 % yield of SC in toluene as solvent at 100 °C under atmospheric CO_2 pressure after 7 h.

1.3 Formation of Cyclic Carbonates Catalyzed by Immobilized Ionic Liquids

The separation of homogeneous catalysts from the reaction mixture is often associated with complicated procedures, which possibly prevent the industrial application. In order to facilitate the recycling of ionic liquids as metal-free catalysts for

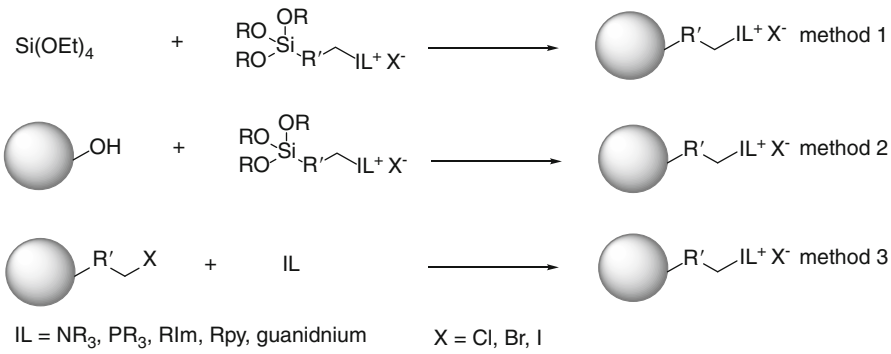

Scheme 1.5 Methods for the covalent immobilization of ILs on supporting material

the cycloaddition of CO_2, the immobilization on solid carriers leading to supported ionic liquid phase (SILP) materials is a promising concept. The obtained heterogeneous catalysts do not only offer advantages with regard to catalyst separation and reusability but also the selectivity and reaction rate can be increased through the proper use of the supporting material.

Impregnation of ILs via physical adsorption on carrier materials illustrates one route for the preparation of SILPs. The synthesis of this type of catalysts is carried out by dispersing the support materials in the respective solvent, adding the desired amount of IL followed by evaporation of the solvent. By using this method, Wang et al. prepared silica gel-supported tetraalkylammonium and imidazolium salts, which gave full conversion of PO with a selectivity up to 98 % for PC under supercritical conditions (150–160 °C, 80 bar CO_2) [56, 57]. Zhu et al. immobilized choline chloride/urea on molecular sieves and achieved quantitative conversion of PO after 5 h at 110 °C [58]. In all of these cases, the catalytic activity of the respective ILs is nearly unaffected by their immobilization. However, the resulting catalysts can be separated from the reaction mixture by simple filtration and are recyclable for several times.

The covalent immobilization of ILs on amorphous or mesoporous silica and zeolites represents another possibility for the synthesis of SILP catalysts. This can be accomplished by the cocondensation of trialkoxysilylalkyl-functionalized ILs and triethoxysilane (Method 1, Scheme 1.5) [59, 60] or the reaction of these ILs with hydroxyl groups on the surface of the supporting material (Method 2, Scheme 1.5) [61, 62]. In addition to that, the quaternization of terminally monohalogenated alkyl-functionalized carrier materials can also be used to produce SILP materials (Method 3, Scheme 1.5) [63, 64]. The reaction conditions for the formation of cyclic carbonates with the corresponding catalysts and supporting materials together with the synthetic methods are given in Table 1.1.

These covalently immobilized IL catalysts are not only easily recyclable from the reaction mixture, but also show a higher catalytic activity than the homogeneous analogs, which is not convenient to other catalytic reactions. This derives from a synergistic effect from the silanol groups on the surface of the silica material, which

Table 1.1 Formation of cyclic carbonates with silica-based SILP catalysts

IL	Support material	Method	Substrate	Cat. loading	T [°C]	p (CO_2) [bar]	t [h]	Conversion [%]	Selectivity [%]	Ref.
MImCl	Silica gel	1	PO	17.6 wt.-%	120	[a]	8.0	86	Not given	[60]
BImBr	Silica gel	1	AGE	11.0 wt.-%	110	35.5	6.0	99	93	[65]
BImI	Silica gel	2	AGE	11.0 wt.-%	110	7.6	3.0	78	100	[68]
MImOH	Silica gel	2	PO	1.8 mol-%	120	20.0	4.0	95	100	[61]
EtImBr	MCM-41	3	AGE	11.0 wt.-%	110	21.0	6.0	99	95	[66]
CC_3ImBr	Silica gel	2	PO	21.5 wt.-%	110	16.0	3.0	100	99	[69]
Br-EImBr	MCM-41	3	SO	8.3 wt.-%	140	40.0	4.0	100	99	[70]
EImBr	SBA-15	1	PGE	8.9 wt.-%	140[b]	9.7	0.25	91	100	[67]
PBGCl	Silica gel	1	PO	23.1 wt.-%	120	45.0	4.0	100	>99	[59]
4-pyr-pyI	Silica gel	3	SO	0.8 mol-%	100	10.0	20.5	91	98	[71]
PBu_3I	Silica gel	3	PO	1.0 mol-%	100	100.0	1	100	100	[63]
PPh3Br	Silica gel	2	PO	1.0 mol-%	90	10.0	6	100	99	[62]
NEt_3Cl	MCM-41	3	AGE	22.4 wt.-%	110	17.6	6	73	99	[72]
HETABr	SBA-15	2	PO	1.0 mol-%	110	20.0	2	99	99	[73]

Br-E 3-(2-Bromoethyl), *PBG* pentabutyl-guaniddinium, *4-pyr-py* 4-pyrrolidinopyridinium, *HOEtTA* 4-(2-Hydroxy-ethyl)-1,2,4-triazolium, *AGE* allyl glycidyl ether

[a] $PO/CO_2 = 2/1$

[b] 100 W

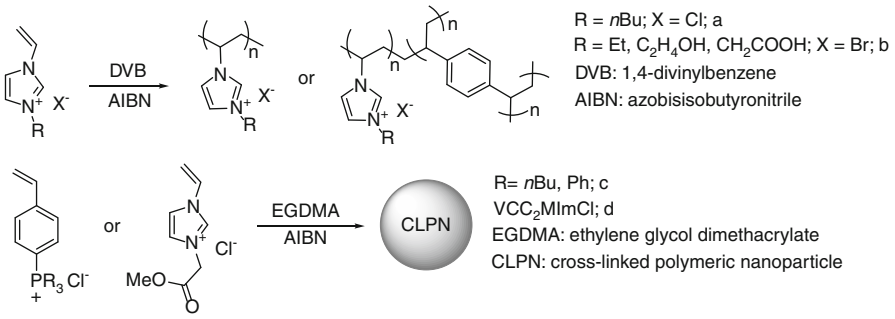

Scheme 1.6 Preparation of SILP catalysts by radical polymerization

activate the epoxide, thus facilitating the nucleophilic attack [63]. The influence of the catalyst loading on the reactivity of the system was examined and it was pointed out that higher amount of immobilized IL and more bulky catalysts lead to a decrease in the reactivity. This is caused by the reduced space within the pores of the MCM-41 material and the lower amount of surface hydroxyl groups [65, 66]. Dharman et al. further investigated the influence of the structure of the silica support on the microwave-assisted synthesis of allyl glycidyl carbonate. It was found that silica supports with relatively large pores (>4 nm) showed higher catalytic activities and that microwave induction leads to a dramatically decrease of the reaction time [67]. Sakai et al. could show that the acidity of the surface hydroxy groups also affects the catalytic activity of the SILP catalysts.

Thereby, immobilization of phosphonium halides on Toyonite and especially basic alumina led to a lower catalytic activity of the SILP material, than the use of silica as the support material [62].

As mentioned before, the use of hydroxyl-functionalized ILs as catalysts results in a higher reactivity. This also applies to SILP catalysts with OH-containing ILs, which was shown by the comparison of immobilized HOETABr and unfunctionalized ETABr as catalyst [73].

Another possibility for the synthesis of organocatalytic active SILPs is the polymerization or copolymerization of vinyl-functionalized ILs (Scheme 1.6). The first example for this kind of SILP catalyst was given by Han and coworkers who polymerized 3-butyl-1-vinylimidazolium chloride (VBImCl) or copolymerized the IL and divinylbenzene (DVB) with AIBN as the initiator (Scheme 1.6, *a*). The resulting insoluble highly cross-linked polymer-supported IL was able to catalyze the formation of PC with a yield of 97 % at 110 °C (60 bar CO_2, 7 h, 0.2 mmol active sites). In comparison to BMImCl, it also showed slightly higher reactivity and was easily recyclable for at least four times by simple filtration [74]. Recently, Wang and Cheng prepared a series of hydroxyl- and carboxyl-functionalized polymers and copolymers of VImBr with DVB (Scheme 1.6, *b*). The quantitative conversion of PO to PC was achieved after 4 h at 130 °C and 25 bar CO_2 pressure with 1.0 mol-% of the immobilized CC_2ImBr catalyst. The superior reactivity of the functionalized catalyst derives again from the activation of the epoxide through

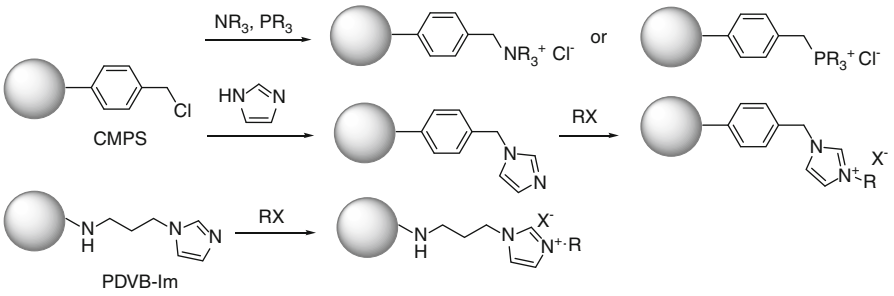

Scheme 1.7 SILP synthesis with functionalized PS resin as the solid phase

hydrogen bonds inducing a positive effect on the ring-opening [75]. Xiong et al. synthesized cross-linked polymeric nanoparticles (CLPN) as SILP catalysts for the synthesis of various carbonates including PC. The copolymerization of 4-vinylbenzyl-triphenylphosphorous chloride or the respective butyl analog and ethylene glycol dimethacrylate (EGDMA) in a ratio of 2:1 initiated by AIBN gave the most active catalysts (Scheme 1.6, *c*). The SILP materials could catalyze the formation of PC with excellent yields of >99 % and a selectivity of up to 100 % (30 bar CO_2, 3 h, CLPN-PBu_3Cl: 140 °C, PPh_3Cl: 160 °C) and were reusable for at least 4 times [76, 77]. The same group applied this method to develop a 3-(2-methoxy-2-oxyl ethyl)-imidazolium chloride (VCC_2MImCl)-based CLPN catalyst (EGDMA/IL/AIBN: 2/1/~0.07) (Scheme 1.6, *d*). The cycloaddition of CO_2 to PO was conducted with nearly quantitative yield and 100 % selectivity at relatively harsh conditions (160 °C, 50 bar CO_2, 12 h), when compared to the phosphorous-based CLNPs [78]. In all of these cases, the copolymers showed higher reactivity than the polymerized vinyl-substituted ILs. This derives most probably due to the very high density of active sites in the homopolymers, leading to the insufficient use of catalytic active centers [75].

Furthermore, the grafting of ILs on functionalized polymers displays an alternative method for the preparation of SILP catalysts. Through the coupling of tertiary amines or phosphines with chloromethylated polystyrene resin (CMPS, cross-linked by copolymerization with varying degrees of DVB; DC, degree of cross-linking), it is possible to synthesize polymer-supported quaternary onium salts. For the immobilization of imidazolium salts on CMPS, imidazole firstly is reacted with the resin and is functionalized in the second step. As an alternative, commercially available cross-linked divinylbenzene polymer, grafted with 1-(3-aminopropyl) imidazole (PDVB-Im), is converted to the corresponding halide to obtain the desired product (Scheme 1.7). The PS-based SILP catalysts with the corresponding supporting materials and reaction conditions for the cycloaddition reaction of CO_2 are given in Table 1.2.

Immobilized quaternary onium salts and their application as SILP catalysts for the cycloaddition of CO_2 to PMO were first introduced in the year 1993. It was pointed out that the length of the alkyl chain attached to the supported IL strongly affects the reactivity, which reached a maximum for $R = n - Bu$ [79].

Table 1.2 Catalytic formation of CCs through SILP catalysts obtained by grafting of ILs on functionalized PS resins

Supported IL	DC [%]	Substrate	T [°C]	t [h]	pCO_2 [bar]	Cat. loading [mol-%]	Conversion [%]	Selectivity [%]	Ref.
P(*n*Bu)$_3$Cl	2	PMO	100	24	atm[a]	1.0	93	100	[79]
N(*n*Bu)$_3$Cl	2	GMA	110	6	atm[b]	1.0	*	*	[80]
N(Me)$_3$Cl[c]	1	PO	100	24	80.0	5.0	99	100	[81]
N(Me)$_3$Cl	2	PO	150	5	20.0	1.1	96	99	[82]
NEt(C_2H_4OH)$_2$Br[d]	2	PO	110	4	20.0	2.0	99	99	[83]
P(*n*Bu)$_3$Cl	2	PO	150	6	50.0	3.2[e]	93	100	[84]
HEImI	6	PO	120	4	25.0	1.6	99	99	[85]
HeMImCl	1	AGE	120	4	15.5	11.0[e]	83	99	[86]
DHPImBr	2	PO	125	3	20.0	1.2	99	97	[87]
HEImBr[f]	1	PO	140	4	20.0	0.44	98	100	[88]
CC_3ImBr[f]	1	PO	140	4	20.0	0.44	96	100	[89]

*k-values are given

PMO 2-phenoxymethyloxirane, *GMA* glycidyl methacrylate, *HE* 1-(2-hydroxyethyl), *HeM* 1-*n*-hexyl-3-methyl, *DHP* 1-(2,3-di-hydroxyl-propyl)

[a]CO_2 flow, 40 mL/min

[b]10 mL/min

[c]Ion exchange resin

[d]Prepared by quaternization of PS-N(C_2H_4OH)$_2$ with EtBr

[e]wt.-%

[f]Resin, PDVB-Im

This indicates that more sterically hindered alkyl structures inhibit the approach of the epoxide to the reactive sites, while shorter chain lengths of the ILs result in a less lipophilic catalyst [80]. A series of imidazolium-based SILP catalysts were prepared later. The ILs containing hydroxyl groups showed higher catalytic activity than the unfunctionalized ILs due to the epoxide activation through hydrogen bonds [85]. This was also shown by other groups through comparison of the catalytic activity of PS-HEImBr, PS-CC_3ImBr, and unfunctionalized ILs under the investigated reaction conditions [88, 89]. In addition to that, ILs containing two or more hydroxyl groups were immobilized to further increase the activity of the resulting SILP materials [83, 87]. The reactivity of the PS-HEImX also strongly depends on the anion and decreased in the order of I ~ Br > Cl in accordance to the nucleophilicity [85].

The quaternization of cross-linked (2 %) poly-(4-vinylpyridine) with halides is another example for the preparation of polymer-bound IL catalysts. The resulting pyridinium-based IL (best catalyst: RX = 1-*n*-butylbromide) is able to catalyze the fixation of CO_2 to glycidyl phenyl ether in a yield of >99 % (100 °C, 1 bar CO_2, 12 h, 5.0 wt.-% cat. loading) [90]. The protonation of polyanilines with HX also creates highly active SILP catalysts. When HI was used as the doping agent (protonation degree: 3.0 mmol g^{-1}), the resulting SILP-like material could catalyze the formation of PC at 115 °C in a yield of 99 % (50 bar CO_2, 6 h, 20 wt.-%) [91]. Han and coworkers prepared porous polymer bead SILP catalysts by suspension copolymerization of 1-vinylimidazole and DVB with AIBN as initiator and subsequent quaternization of the supported imidazole. The 3-*n*-butyl-iodide-functionalized IL, supported on a polymer with a high-surface area, and amount of immobilized IL, gave more active catalysts for the conversion of AGE, whereas nonporous polymer beads as carrier material resulted in a decrease in reactivity [92]. Tubular microporous organic networks, with imidazolium iodide as the active species for the coupling of CO_2 with epoxides, are also accessible via Sonogashira coupling of a tetrahedral building block and the corresponding diiodoimidazolium salt. The generated SILP catalyst gave a yield of 87 % PC using a relatively low catalyst loading of 0.065 mol-% (150 °C, 10 bar CO_2, 10 h) [93]. Alternatively, tubular heterogeneous SILP catalysts can be obtained by esterification of carboxy group containing carbon nanotubes with hydroxyl-functionalized imidazolium salts. The grafting of MImI resulted in a SILP which catalyzed the formation of SC in a yield of 97 % at 115 °C (6 h, 18.2 bar CO_2, 2.1 wt.-%) [40]. Recently, He and coworkers developed a SILP, which performs as a homogeneous catalyst under supercritical conditions but is easily separable after the completion of the reaction. This was achieved by the formation of a fluoroacrylate/chloromethylstyrene copolymer (10/1) and subsequent reaction with P(*n*Bu)$_3$ [94]. The preparation of multilayered SILP catalyst illustrates a combined method for the immobilization of imidazolium-based IL on silica or SBA materials and organic polymers. For that purpose, a bis-vinylimidazolium salt is linked to a mercapto-modified polystyrene or silica (amorphous or SBA-15) by the thiol-ene reaction. High excess of the IL results in a high loading of imidazolium units within the SILP material (up to 3.40 mmol g^{-1}). SBA-15-supported imidazolium bromides showed the highest

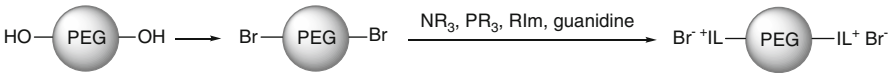

Scheme 1.8 Preparation of PEG-supported ILs

catalytic activity in the high-throughput conversion of PO (84 %, 95 % selectivity) under $scCO_2$ (150 °C, 100 bar CO_2, 1 mol-%, 3 h) because of the higher surface area of the silica material [95]. All of the above listed insoluble SILP catalysts based on PS or other polymers are recyclable through simple filtration from the reaction mixture and therefore provide the capability of an effective chemical fixation of CO_2 to cyclic carbonates.

As an inexpensive, thermally stable, and nontoxic supporting material, polyethylene glycols (PEGs) represent a green alternative to the already mentioned supporting materials. The easiest and most applied method for the synthesis of PEG-supported ILs displays the bromination of the polymer chain ends and the subsequent reaction with the desired IL (Scheme 1.8).

The first example of the application of this class of SILP catalysts for the synthesis of cyclic carbonates was shown by He et al. in 2006. The coupling of NBu_3 with PEG_{6000} resulted in an increase of catalytic activity due to the changes of physical properties of the reaction mixture. Under $scCO_2$ (120 °C, 80 bar CO_2), an excellent PC yield (98 %) and selectivity (99 %) could be achieved after 6 h reaction time with a relatively low catalyst loading (0.5 mol-%). Moreover, the catalyst could be recycled by simple filtration from the cooled reaction mixture [96]. The reaction of a pentaalkylguanidine with PEG_{6000} was realized by the same group. The prepared catalysts gave an even better PC yield (99 %) at milder reaction conditions (110 °C, 40 bar CO_2, 4 h, 0.5 mol-%). However, the catalyst recycling had to be carried out by extraction with diethyl ether [97]. In addition to that, He and coworkers also synthesized a series of PEG_{150}-grafted imidazolium salts (MMImX, MImBr, X = Cl, Br, I) and guanidinium bases (DBN, DBU, TBD). The resulting TBD-based catalyst was able to catalyze the formation of PC in nearly quantitative yield (>99 %) at relatively mild reaction conditions (120 °C, 10 bar CO_2, 8 h, 1 mol-%). Most probably, the formation of an activated carbamate species, through the reaction of CO_2 with the secondary amino group of TBD, which was detected by in situ FTIR, enhances the reactivity [98]. Furthermore, these catalysts can also be used for the catalytic conversion of CO_2 with aziridines to form oxazolidinones. Hereby, the DBN-based catalysts showed not only high reactivity but also good regioselectivities [99]. An example for a phosphonium bromide-based SILP catalyst was given by Bhanage et al. through the reaction of PPh_3 with PEG_{600}. The conversion of SO or epichlorohydrin to the respective carbonates could be catalyzed in excellent yields and selectivities (>98 %), whereas the formation of PC was rather poor (60 % yield) under the investigated reaction conditions (100 °C, 27 bar CO_2, 3 h, 5 wt.-%) [100]. Very recently, Park and coworkers published their work on the conversion of AGE with CO_2, catalyzed by imidazolium salts supported on PEG_{4000}. For the grafting of the IL,

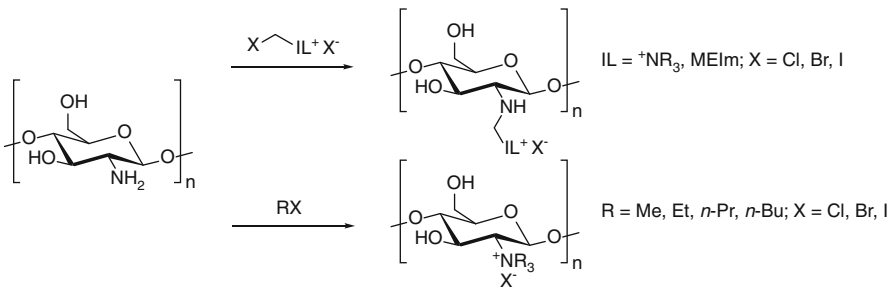

Scheme 1.9 Synthesis of chitosan-based SILP catalysts

one chain-end hydroxyl group of the polymer is firstly transformed with succinic anhydride to the corresponding succinic acid and then esterified with HAImX (A = Me, Et, *n*-Bu; X = Cl, Br, I). The catalyst with immobilized MImCl showed the highest reactivity reaching a conversion and selectivity of 98 % at 140 °C (18.9 bar CO_2, 4 h, 2.3 mol-%) [101].

Considering the biocompatibility, biodegradability, and high availability of the biopolymer chitosan (CS), it represents a suitable supporting material for ILs in terms of green chemistry. The hitherto known methods for the grafting of ILs on chitosan are shown in Scheme 1.9.

The immobilization of 3-chloro-2-hydroxypropyl trialkylammonium halides on chitosan was the first CS-SILP catalyst investigated for the cycloaddition of CO_2 with epoxides. He and coworkers have shown that CS as a supporting material could enhance the catalytic activity of the immobilized IL through a synergistic effect, which derives from the coexistence of hydrogen bond donors (-OH of CS) and the halide anions of the ammonium moiety ($N^+R_3X^-$) [102, 103]. With CS-$N^+Me_3Cl^-$ as the model catalyst (1.7 mmol-%), an excellent PC yield (98 %) and selectivity (>99 %) were reached, however under relatively harsh reaction conditions (160 °C, 40 bar CO_2, 6 h) [102]. Park et al. synthesized a series of CS-SILP catalysts through the quaternization of the CS-amino group with alkyl halides [103, 104]. The efficiency of the catalyst preparation could be increased drastically through microwave irradiation, yielding CS-$N^+Me_3I^-$ as the most reactive species. The resulting system was able to catalyze the formation of PC with good yields (89 %) and excellent selectivities (>99 %) at comparably mild reaction conditions (120 °C, 11.7 bar CO_2, 6 h, 1.6 mmol-%) [104]. Moreover, SILP catalysts are accessible through the grafting of Br-EMImBr on CS. In comparison to the PS-bound catalysts, the CS-EMImBr showed higher activity due to the already mentioned synergistic effect of the carrier material. As a result, excellent yields and selectivities (96 % and >99 % for PC) could be achieved (120 °C, 20 bar CO_2, 4 h, 1 mmol-%) [105]. Another example for a biopolymer as carrier material was given by Park et al. who used carboxymethyl cellulose for the non-covalently immobilization of imidazolium salts. DFT calculations have shown that the nucleophilic attack at the epoxide is facilitated via hydrogen bonds from the carboxyl and hydroxyl functional groups of the biopolymer. This synergistic effect results in a

high activity of the iodide-containing SILP catalyst for the formation of PC (yield and selectivity >98 %) under relatively mild conditions (110 °C, 18 bar CO_2, 2 h, 1.2 mmol-%) [106].

1.4 Formation of Cyclic Carbonates Catalyzed by Nitrogen Donor Bases

Organic nitrogen bases represent another class of metal-free catalysts for the transformation of carbon dioxide. The most commonly used bases for this purpose are illustrated in Fig. 1.6.

To the best of the authors' knowledge, the first example for the nitrogen base-mediated cycloaddition of CO_2 to epoxides was reported by Sartori et al. in 2003. The guanidine MTBD (7-methyl-1,5,7-triazabicyclo[4.4.0]dec-5-ene) and the supported analog (MCM-41 as carrier material) were used as catalysts for the formation of a variety of carbonates including SC. However, harsh reaction conditions (140 °C, 50 bar CO_2, 4 mol-%) and long reaction times (20–40 h) were necessary to obtain full conversion of SO (95 % yield) [107]. Furthermore, TBD was used as catalytic active species supported on silica or as molecular organocatalyst in several other works [108–110]. The reactivity of the catalysts in the cycloaddition reaction is strongly influenced by their basicity. Therefore, the use of TBD, which represents a stronger base than, for example, DBU, resulted in more active organocatalysts [109]. In addition, Sun and coworkers have shown that the surface hydroxyl groups of the silica supporting material dramatically enhance the catalytic activity of TBD. For this purpose, the reactivity of the TBD/SiO_2 catalyst was compared with a methyl-modified silica species. It was pointed out that the surface hydroxyl groups play an important role in the reaction, since the conversion of PO dropped from >99 to <1 % (150 °C, 20 bar CO_2, 20 h, 6.4 wt.-%) when the modified material was used as catalyst [108]. A possible application of the well-known transesterification catalyst DMAP for the chemical fixation of CO_2 with epoxides was first discovered by Manikandan et al. in 2004. It was found that DMAP, which should be used as the cocatalyst, was able to catalyze the conversion of epichlorohydrin to the

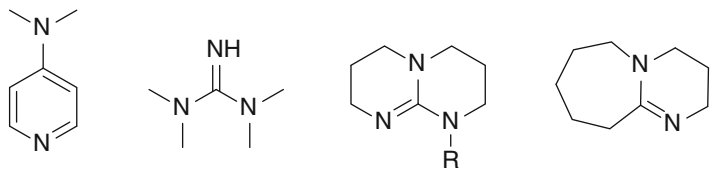

Fig. 1.6 Structures of most frequently used bases for CO_2 activation

respective carbonate by itself [111]. This was also shown by Jones and Shiels who used homogeneous and SBA-15-supported DMAP for the formation of PC. The molecular DMAP showed slightly higher reactivity (85 % yield, 100 % selectivity) under the investigated reaction conditions (120 °C, 17.2 bar CO_2, 4 h, 0.4 mol-%) [112]. Another class of N-donor base catalysts for the cycloaddition of CO_2 were prepared by Ratnasamy and coworkers via the covalent immobilization of adenine, guanine, imidazole, and primary alkyl amines on SBA-15 [113, 114]. The resulting adenine catalyst, which showed the highest reactivity, could catalyze the conversion of SO in good yields (86 %) and excellent selectivities for SC (97 %) under comparably mild reaction conditions (120 °C, 6.9 bar CO_2, 8 h) [114]. The non-covalently immobilization of polyvinyl pyridine on silica also leads to organocatalytic active solid basic materials. The optimized catalyst (10 wt.-% PVP on SiO_2) gave 93 % yield of PC at 150 °C and 55 bar CO_2 after 6 h [115]. The recently reported preparation of TMG-SiO_2 nanoparticles is another possibility for the synthesis of solid base catalysts. The grafting of TMG on 3-chloropropyl-modified silica from rice husk ash gave amorphous spherical particles with a mean size of 19.6 nm. The cycloaddition of CO_2 to PO was carried out with 92 % conversion and 98 % selectivity for PC at 130 °C and 50 bar CO_2 for 8 h [116].

Park and coworkers synthesized and applied melamine-bridged periodic mesoporous organosilica (PMO) as organocatalyst for the cycloaddition of CO_2 to epoxides. In PMO, the organic moieties are integrated in the silica framework forming an ordered mesoporous type of organic–inorganic material. Through the incorporation of large-sized melamine-based triorganosilsesquioxane as organic linker, a well-ordered hexagonal mesostructural organocatalyst could be synthesized. After 10 h at 100 °C and 5.5 bar CO_2, around 40 % conversion of PO to PC with a high selectivity could be achieved [117]. The use of as-synthesized covalent triazine frameworks (CTF) for the metal-free catalytic valorization of CO_2 to carbonates was reported by Roeser and coworkers. Under investigated reaction conditions, the crystalline CTF was significantly less active than the amorphous high-surface area (HSA) analog. Furthermore, the pyridinic CTF (CTF-P) showed higher reactivity than the benzylic CTF, because of the higher basicity leading to an increased extent of CO_2 absorption. The CTF-P-HSA was able to catalyze the full conversion of epichlorohydrin to the respective cyclic carbonate with a selectivity of 96 % within 4 h under relatively mild reaction conditions (130 °C, 6.9 bar CO_2) [118]. A possible mechanism for the formation of cyclic carbonates via nitrogen base-catalyzed cycloaddition reaction of CO_2 with epoxides is shown in Scheme 1.10 with SiO_2-TMG as the model catalyst [110, 116].

In the first step, CO_2 is absorbed through reaction with the Lewis basic sites to form a carbamate species [107, 110, 114, 116, 117]. The resonance stabilization of the resulting cation enhances the stability of the cationic intermediate. The nucleophilic attack of the carbamate anion at the less sterically hindered carbon atom of the epoxide leads to the ring-opening of the epoxide. The formed anion intramolecularly attacks the carbonyl carbon atom forming a five-membered cyclic species. Finally, PC is eliminated from the surface regenerating the catalyst [110, 116].

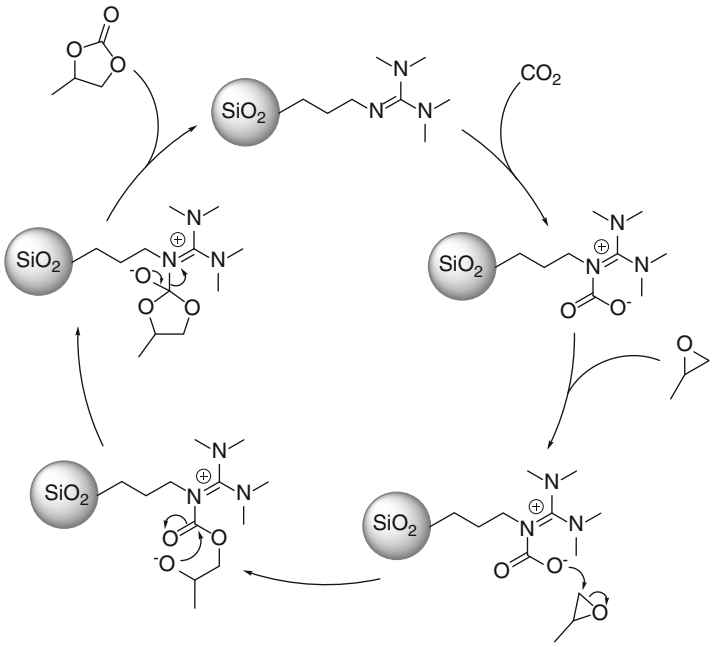

Scheme 1.10 TMG-SiO_2-catalyzed cycloaddition reaction of CO_2 to PO [116]

1.4.1 Binary Catalyst Systems for the Cycloaddition of Epoxides and CO_2

In the following chapter, binary catalyst systems for the chemical fixation of CO_2 and epoxides (Scheme 1.1) are introduced. All of them show a cooperative effect between a hydrogen bond donor and a nucleophile and the mechanism is proposed to be identical according to HFILs (Scheme 1.2). The first approaches of binary catalyst systems were carried out using phenol as hydrogen bond donor [119–121]. Nevertheless, using phenol as catalyst results in a low selectivity because also the side reaction to 1-phenoxypropan-2-ol takes place. Therefore, different groups did a broad catalyst screening with different aliphatic and aromatic alcohols and found 1,2-benzenediol (BDO) and 1,2,3-benzenetriol (BTO) in combination with TBAB or TBAI as cocatalyst to be the most active [51, 121]. Furthermore, there are other catalytic systems based on cellulose [122], β-cyclodextrin [123], lecithin [124], pentaerythritol [125], and lignin [52] in combination with potassium iodide (KI) as cocatalyst. An overview of these binary catalyst systems is listed in Table 1.3 with their optimum reaction conditions.

Other reports describe the influence of the hydrogen bond donor character using theoretical calculation methods. It was found that the catalytic activity strongly depends on the distance between the two hydroxyl groups [121, 126]. Additional calculations concerning the BTO/TBAI system suggest a stabilization of the

Table 1.3 Overview of selected effective binary catalyst systems

Catalyst	Co-catalyst	Molar ratio[a]	Substrate	T [°C]	p(CO_2) [bar]	t [h]	Conv. [%]	Sel. [%]	Recycling runs	Reference
Cellulose	KI	66[b]/1.5	PO	110	20	2	99	99	5	[122]
β-cyclo-dextrin	KI	8.7[b]/2.5	PO	120	60	4	98	99	5	[123]
Lecithin	KI	1.25/1.25	PO	100	20	4	98	98	–	[124]
Lignin	KI	0.67[c]/2	PO	140	20	12	91	99	5	[52]
BDO	TBAB	5/1	PO	100	30	0.5	92	99	–	[121]
BTO	TBAI	5/5	PO	45	10	16	100	99	2[d]	[51]

[a]In relation to the substrate (mol-% cat./mol-% co-cat.)
[b]Amount in wt.-%
[c]Mol-% of active OH-groups
[d]Loss of activity with each run

Scheme 1.11 Stabilization of the oxyanion intermediate by BTO

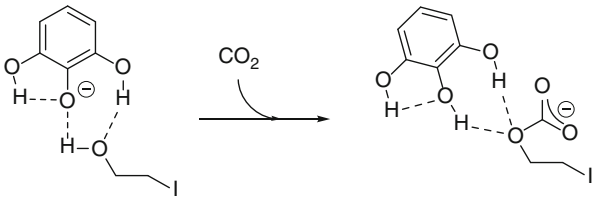

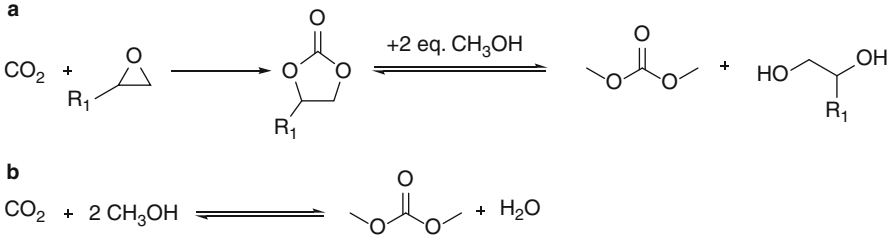

Scheme 1.12 Synthesis of DMC by (**a**) transesterification of cyclic carbonates with MeOH or (**b**) by direct synthesis of CO_2 and MeOH

oxyanion before and after the insertion of CO_2 by the adjacent hydroxyl groups of BTO (see Scheme 1.11). After activating the epoxide via hydrogen bonding, the following oxyanion intermediate is stabilized by hydrogen bonding of the neighboring hydroxyl groups. For the same reason, glycerol is also an efficient catalyst for the chemical fixation of CO_2 with epoxides [82]. However, glycerol is not a suitable catalyst since during the reaction glycerol carbonate (GC) is also formed. This prevents the systems to be recycled for several times since glycerol is also consumed as substrate. Nevertheless, GC offers a lot of other opportunities and is an attractive target molecule for the chemical fixation of CO_2 [127].

1.5 Synthesis of Dimethyl Carbonate (DMC)

Utilizing CO_2 as a feedstock for the green synthesis of DMC, there are two possible routes for reaching this goal in an environmentally friendly and cheap way. DMC can be synthesized either by the transesterification of a cyclic carbonate with methanol (MeOH) (Scheme 1.12a) or by the direct synthesis from CO_2 and MeOH (Scheme 1.12b). The first route represents an indirect way for DMC synthesis out of CO_2 because cyclic carbonates can be produced from CO_2 and epoxide, as described in Sects. 1.2, 1.3, and 1.4. High CO_2 pressure in the transesterification reaction of a cyclic carbonate with MeOH is required to prevent decarboxylation of the cyclic carbonate and is not directly involved in the reaction procedure. For this reason, only the one-pot synthesis out of an epoxide, CO_2, and MeOH is mentioned in the following sections of this chapter.

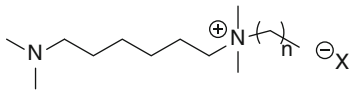

n=1, X=Br: $Me_2NC_6NMe_3Br$
n=5, X=Br: $Me_2NC_6NMe_2HexBr$
n=3, X=I: $Me_2NC_6NMe_2BuI$
n=3, X=NTf_2: $Me_2NC_6NMe_2BuNTf_2$
n=3, X=Br: $Me_2NC_6NMe_2BuBr$
n=3, X=Cl: $Me_2NC_6NMe_2BuCl$
n=3, X=BF_4: $Me_2NC_6NMe_2BuBF_4$

Scheme 1.13 Overview of ILs bearing a tertiary amino moiety and a quaternary ammonium group

1.5.1 One-Pot Synthesis of DMC from Methanol, CO_2 and Epoxides

Wang et al. showed a good activity toward the one-pot synthesis out of methanol, CO_2, and EO for using the mixture KI:K_2CO_3 (weight ratio 1:1) under supercritical conditions (150 °C, 150 bar CO_2 pressure, 2 h, 2 wt.-% catalyst) [128]. A detailed investigation showed an increasing yield of the desired products at higher temperature, whereas the CO_2 pressure has more or less no effect on the yield. Increasing the EO content results in a better selectivity. Kinetic studies confirmed a relatively high reaction rate for EC formation [129]. Due to a low reaction rate for the transesterification with MeOH to form DMC, this step is proposed to be the rate-determining step in the one-pot synthesis. Also, amines were found to be active and therefore DBU served as a suitable catalyst for the reaction of glycidyl phenyl ether, MeOH, and CO_2 (150 bar) at 150 °C to reach high yields of DMC and the corresponding 1,2-diol (>95 %) [130]. Extension of this one-pot coproduction of DMC and 1,2-diols to the synthesis of other symmetric dialkyl carbonates leads to yields of 63 % diethyl carbonate (DEC) and 44 % dibutyl carbonate (DBC) under similar reaction conditions. Changwen et al. adopted a mixture of $BMImBF_4$ and sodium methanolate (NaOMe) as catalyst for the one-pot synthesis [131]. Under optimized reaction conditions (40 bar, 5 h, 150 °C), the conversion of PO was >95 %, reaching a yield of 67 % DMC paired with a selectivity <10 % for the by-products. A binary catalyst system consisting of TBAB as the cycloaddition catalyst to form cyclic carbonates and tri(*n*-butyl)amine (NBu_3) as a possible transesterification catalyst was introduced [132]. Under optimized reaction conditions (2.5 mol-% catalyst loading, 150 °C, 150 bar, 8 h), PO, SO, and 2-(phenoxymethyl)oxirane (PMO) exhibit 59 %, 80 %, and 84 % of DMC yield, respectively.

An inorganic base (K_2CO_3) and a phosphonium halide-functionalized PEG ($BrBu_3PPEG_{6000}PBu_3Br$) binary system was developed as heterogeneous catalyst and shown to be active for the one-pot synthesis of DMC even under low CO_2 pressure (2 bar) [133]. The cycloaddition to form the cyclic carbonate was carried out at 120 °C under 10 bar CO_2 for 6 h. Afterward, MeOH was added and the mixture was further heated for 1.5 h at 100 °C while removing DMC via distillation. It was possible to reach yields up to 97 % DMC even in the fourth run of the catalytic cycle. Moreover, leaching of the catalyst could be also excluded via ^{31}P-NMR after recovering the catalyst by filtration. Novel ILs bearing both a tertiary amino moiety and a quaternary ammonium group were synthesized and tested toward the one-step synthesis of DMC (Scheme 1.13) [134]. Under 20 bar CO_2 pressure at 150 °C and a

catalyst loading of 1.3 mol-%, quantitative conversion of EO was observed after 8 h with a selectivity of 74 % toward DMC using $Me_2NC_6NMe_2BuI$ as catalyst. Additionally, the catalyst could be reused for several times.

Zheng and coworkers systematically screened binary catalysts for the one-pot synthesis of DMC and found that in presence of H_2O, commercial quaternary ammonium salts/K_2CO_3, pyridinium salts/K_2CO_3, and KI/K_2CO_3 were remarkably effective for DMC synthesis with no need for separation of EC [135]. Nearly quantitative conversion of EO and 82 % yield of DMC were obtained under relatively mild reaction conditions. The cycloaddition was carried out at 120 °C under 25 bar CO_2 pressure for 1 h with 0.018 mol-% H_2O, 0.45 mol-% K_2CO_3, and 1.88 mol-% KI. After adding MeOH, the temperature was decreased to 60 °C and further reacted for 0.5 h. This system could be easily recovered and reused for 12 times without obvious loss of its catalytic activity. However, this study shows an incompatibility of imidazolium salts with inorganic alkaline toward the one-pot synthesis of DMC possibly because of the reactive C2 proton of the imidazolium ring.

Newer research effort showed that also a CTF is an active catalyst for synthesizing DMC out of PO, CO_2, and MeOH in one-pot [118]. At 20 bar CO_2 and 160 °C, a conversion of 95 % PO was observed with a selectivity of 17 % toward DMC. This is the first example using a porous organic coordination polymer for DMC synthesis.

1.5.2 Direct Synthesis of DMC from CO_2 and Methanol

A first example for the direct synthesis of DMC was carried out using different bases and methyl iodide (MeI) as a promoter for the reaction [136], where dimethyl ether (DME) is formed as a by-product. Further investigations for this reaction showed the highest activity for K_2CO_3 as a catalyst using MeI as the promoter for the reaction [137]. Arai et al. observed two maxima in DMC formation at 45 and 80 bar CO_2 pressure while DME formation decreases with higher pressure. Additional mechanistic studies suggest a parallel pathway for DMC and DME formation, whereas MeI is involved in both. Using other alcohols than MeOH leads to a lower reactivity. In both cases, the optimized reaction conditions lead to a yield of less or about 4 % DMC with a rather bad selectivity. Catalytic experiments with potassium methanolate (KOMe) as catalyst and MeI as promoter raised the yield of DMC to 16 % with a selectivity of $\geq$99 % at 80 °C and 20 bar CO_2 pressure, whereas there is a second maximum of yield at 72 bar [138]. Thus, higher pressures are not required for an effective synthesis of DMC. Wang et al. used KOH as a catalyst for the direct synthesis of DMC with MeI and studied the effects of adding the IL EMImBr to the reaction mixture [139]. Therefore, an increase of the yield from 8 % DMC without EMImBr to 11 % in the presence of the IL was observed at a CO_2 pressure of 20 bar. The reason for higher DMC yield in presence of EMImBr may be ascribed to the strong polarity and electrostatic field of the IL, which may stabilize the charged intermediate. Interestingly, also in this case, two maxima for the yield of DMC were found at 20 and 73 bar CO_2 pressure, which

is similar to previous described works. Later work deals with the thermodynamics of DMC synthesis and it could be shown that the reaction does not spontaneously occur in view of thermodynamics using K_2CO_3, KOMe, or KOH as catalyst [140]. This may offer new possibilities for the design of effective organocatalytic systems for the synthesis of DMC.

1.6 Further Organocatalytic Transformations of CO_2

1.6.1 Organocatalytic Reduction of CO_2 into Value-Added Chemicals

Employing CO_2 as a true C_1 building block and therefore preparing a wide spectrum of chemicals, catalytic reactions that are able to promote the complete deoxygenation of CO_2 are required. For example, NHCs reversibly form zwitterionic CO_2 adducts, which are considered to be key intermediates in the reductive deoxygenation of CO_2. The role of NHC during catalysis was investigated theoretically and experimentally [141, 142], and for using diphenylsilane as a sacrificial reducing agent, CH_3OH could be detected upon workup.

Cantat and coworkers developed the organocatalytic formylation reaction of N–H bonds by using CO_2 and hydrosilanes to yield formamides. To achieve complete deoxygenation, they proposed that the amide function could react in a cascade reaction with a nucleophile (Scheme 1.14), such as an amine, which results in a substitution of the C═O bond in the formamide derivative [143–145].

The formylation was successfully catalyzed by nitrogen bases, such as TBD with using silanes instead of H_2 as reducing agent, allowing the utilization of an organocatalyst which avoids any toxic and/or expensive metal. The reaction takes place at 100 °C under CO_2 pressure <3 bar without an additional solvent and promotes the formylation of a wide spectrum of amines due to the mild reaction conditions, while using H_2 as reducing agent, the reaction is limited to only a few amines [143]. Nevertheless, this system is limited to basic amines and only

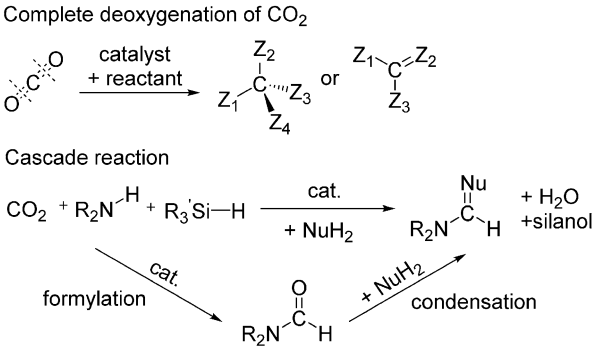

Scheme 1.14 Principles of complete deoxygenation of CO_2 and the cascade reaction for substitution of C═O bond in the formamide derivative

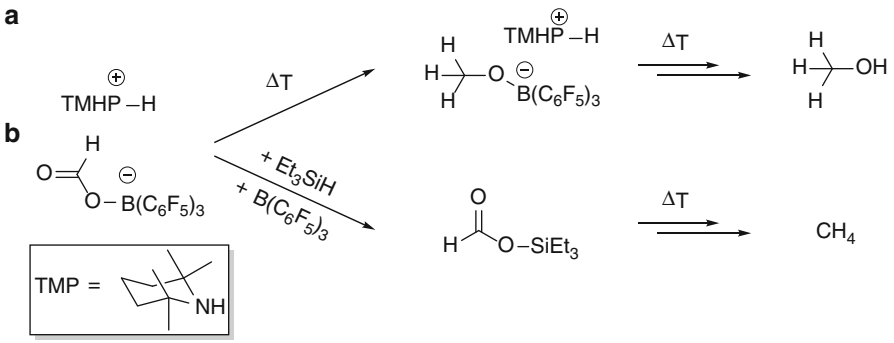

Scheme 1.15 Formation of (**a**) methanol and (**b**) methane out of the boratocarbamate-TMPH ion pair

proceeds at 100 °C, whereas low temperatures and broad application spectra are required for CO_2 recycling in an environmentally friendly way. Further investigations demonstrated that the formylation step is also effectively catalyzed by NHCs. NHCs are efficient catalysts for the conversion of amines, anilines, imines, and N-heterocycles at room temperature, and, therefore, NHCs are more attractive for a sustainable recycling of CO_2 [144]. Also, the cascade reductive functionalization of CO_2 into benzimidazoles, quinazolinones, formamidines, and their derivatives is catalyzed by NHCs and TBD at 70 °C [145]. The results show a difference in selectivity between the two classes of organocatalyst and suggest a different activation pathway in the reductive functionalization of CO_2, which has to be confirmed by further investigations.

Another way for the nonmetal-mediated reduction of CO_2 is the use of frustrated Lewis pairs (FLPs) [146]. Therefore, the stoichiometric reduction of CO_2 to CH_3OH was investigated in detail and it was found that a system consisting of 2,2,6,6-tetramethylpiperidine (TMP) and tris(pentafluorophenyl)borane [$B(C_6F_5)_3$] activates CO_2 to form a boratocarbamate-TMPH ion pair (Scheme 1.15) [147]. Heating this ion pair at 160 °C under a H_2 atmosphere leads quantitatively to $CH_3OB(C_6F_5)_2$ after 6 d, and after vacuum distillation of the solvent, 17–25 % CH_3OH could be isolated. Another study dealing with an analogous FLP showed a conversion of this species in the presence of triethylsilane (TES) to a silylcarbamate and the known ion pair $[TMPH]^+[HB(C_6F_5)_3]^-$, which was recently shown to react with CO_2 via transfer of the hydride from the hydridoborate to form the formatoborate $[TMPH]^+[HC(O)OB(C_6F_5)_3]^-$ [148]. In the presence of extra B $(C_6F_5)_3$ (0.1–1.0 equiv.) and excess TES, the formatoborate is rapidly hydrosilated to form a formatosilane and regenerate $[TMPH]^+[HB(C_6F_5)_3]^-$. The formatosilane in turn is rapidly hydrosilated by the $B(C_6F_5)_3/Et_3SiH$ system to CH_4, with $(Et_3Si)_2O$ as the by-product. At low concentration of Et_3SiH, it is possible to isolate intermediate CO_2 reduction products, whereas addition of more CO_2/Et_3SiH results in resumed hydrosilylation. All the results indicate a robust, living tandem catalytic system for the deoxygenative reduction of CO_2 to CH_4.

1.7 Conclusions

It is shown that many promising concepts for the development of highly efficient organocatalysts for the transformation of carbon dioxide to (bulk) chemicals are at hand. Particularly in the field of the synthesis of cyclic carbonates, the variation of organic substituents allows for tailoring the desired parameters in order to enhance the catalyst activity in a similar fashion as it is possible with metal catalysts. A drawback of most organocatalysts is still that usually rather high temperatures and CO_2 pressures are required. However, in the last years, significant improvements could be achieved. Therefore, different catalysts were developed which allow the activation of the epoxide and/or CO_2 leading to lower reaction temperature and CO_2 pressure. Furthermore, the simple separation and reuse of a catalyst for several times is very important for industrial application, which was proven and realized for IL catalysts in the formation of cyclic carbonates. Alternative ways for sustainable CO_2 fixation represent the synthesis of DMC and the reduction to methanol or methane. Nevertheless, the known organocatalytic systems still need optimization regarding catalyst design to reach satisfying conversion under mild reaction conditions. Considering all these facts, organocatalytic systems open the possibility for a green and sustainable valorization of CO_2 with regard to a CO_2-emission point of view as well as for industrial applications.

References

1. Brundtland GH (1987) United Nations report: our common future, Oxford University Press.
2. BP Statistical Review of World Energy (2012) Statistical review of world energy. BP p. l. c.
3. Aresta M, Dibenedetto A (2004) The contribution of the utilization option to reducing the CO_2 atmospheric loading: research needed to overcome existing barriers for a full exploitation of the potential of the CO_2 use. Catal Today 98(4):455–462, http://dx.doi.org/10.1016/j.cattod.2004.09.001
4. Bozell JJ, Petersen GR (2010) Technology development for the production of biobased products from biorefinery carbohydrates-the US Department of Energy's "Top 10" revisited. Green Chem 12(4):539–554. doi:10.1039/B922014C
5. Marshall A-L, Alaimo PJ (2010) Useful products from complex starting materials: common chemicals from biomass feedstocks. Chem Eur J 16(17):4970–4980. doi:10.1002/chem.200903028
6. Ruppert AM, Weinberg K, Palkovits R (2012) Hydrogenolyse goes Bio: Von Kohlenhydraten und Zuckeralkoholen zu Plattformchemikalien. Angew Chem 124(11):2614–2654. doi:10.1002/ange.201105125
7. Arakawa H, Aresta M, Armor J, Barteau M, Beckman EJ, Bell AT, Bercaw JE, Creutz C, Dinjus E, Dixon DA, Domen K, Dubois DL, Eckert J, Fujita E, Gibson DH, Goddard WA, Goodman WD, Keller J, Kubas GJ, Kung HH, Lyons JE, Manzer L, Marks TJ, Morokuma K, Nicholas KM, Periana R, Que L, Rostrup-Nielson J, Sachtler WMH, Schmidt LD, Sen A, Somorjai GA, Stair PC, Stults BR, Tumas W (2001) Catalysis research of relevance to carbon management: progress, challenges, and opportunities. Chem Rev 101(4):953–996. doi:10.1021/cr000018s
8. Omae I (2006) Aspects of carbon dioxide utilization. Catal Today 115(1–4):33–52, http://dx.doi.org/10.1016/j.cattod.2006.02.024

9. Omae I (2012) Recent developments in carbon dioxide utilization for the production of organic chemicals. Coordination Chem Rev 256(13–14):1384–1405, http://dx.doi.org/10.1016/j.ccr.2012.03.017
10. Song C (2006) Global challenges and strategies for control, conversion and utilization of CO_2 for sustainable development involving energy, catalysis, adsorption and chemical processing. Catal Today 115(1–4):2–32, http://dx.doi.org/10.1016/j.cattod.2006.02.029
11. Centi G, Iaquaniello G, Perathoner S (2011) Can we afford to waste carbon dioxide? Carbon dioxide as a valuable source of carbon for the production of light olefins. ChemSusChem 4(9):1265–1273. doi:10.1002/cssc.201100313
12. Peters M, Köhler B, Kuckshinrichs W, Leitner W, Markewitz P, Müller TE (2011) Chemical technologies for exploiting and recycling carbon dioxide into the value chain. ChemSusChem 4(9):1216–1240. doi:10.1002/cssc.201000447
13. Quadrelli EA, Centi G, Duplan J-L, Perathoner S (2011) Carbon dioxide recycling: emerging large-scale technologies with industrial potential. ChemSusChem 4(9):1194–1215. doi:10.1002/cssc.201100473
14. Gallezot P (2012) Conversion of biomass to selected chemical products. Chem Soc Rev 41(4):1538–1558. doi:10.1039/C1CS15147A
15. Olah GA, Prakash GKS, Goeppert A (2011) Anthropogenic chemical carbon cycle for a sustainable future. J Am Chem Soc 133(33):12881–12898. doi:10.1021/ja202642y
16. Aresta M, Dibenedetto A (2007) Utilisation of CO_2 as a chemical feedstock: opportunities and challenges. Dalton Trans 28:2975–2992. doi:10.1039/B700658F
17. Cokoja M, Bruckmeier C, Rieger B, Herrmann WA, Kühn FE (2011) Transformation of carbon dioxide with homogeneous transition-metal catalysts: a molecular solution to a global challenge? Angew Chem Int Ed 50(37):8510–8537. doi:10.1002/anie.201102010
18. Drees M, Cokoja M, Kühn FE (2012) Recycling CO_2? Computational considerations of the activation of CO_2 with homogeneous transition metal catalysts. ChemCatChem 4(11):1703–1712. doi:10.1002/cctc.201200145
19. Coates GW, Moore DR (2004) Discrete metal-based catalysts for the copolymerization of CO_2 and epoxides: discovery, reactivity, optimization, and mechanism. Angew Chem Int Ed 43(48):6618–6639. doi:10.1002/anie.200460442
20. Sakakura T, Kohno K (2009) The synthesis of organic carbonates from carbon dioxide. Chem Commun 11:1312–1330. doi:10.1039/B819997C
21. Darensbourg DJ (2010) Chemistry of carbon dioxide relevant to its utilization: a personal perspective. Inorg Chem 49(23):10765–10780. doi:10.1021/ic101800d
22. Decortes A, Castilla AM, Kleij AW (2010) Salen-complex-mediated formation of cyclic carbonates by cycloaddition of CO_2 to epoxides. Angew Chem Int Ed 49(51):9822–9837. doi:10.1002/ange.201002087
23. Kember MR, Buchard A, Williams CK (2011) Catalysts for CO_2/epoxide copolymerisation. Chem Commun 47(1):141–163. doi:10.1039/C0CC02207A
24. Klaus S, Lehenmeier MW, Anderson CE, Rieger B (2011) Recent advances in CO_2/epoxide copolymerization—new strategies and cooperative mechanisms. Coordination Chem Rev 255(13–14):1460–1479, http://dx.doi.org/10.1016/j.ccr.2010.12.002
25. Lu X-B, Darensbourg DJ (2012) Cobalt catalysts for the coupling of CO_2 and epoxides to provide polycarbonates and cyclic carbonates. Chem Soc Rev 41(4):1462–1484. doi:10.1039/C1CS15142H
26. Shaikh A-AG, Sivaram S (1996) Organic carbonates. Chem Rev 96(3):951–976. doi:10.1021/cr950067i
27. Calo V, Nacci A, Monopoli A, Fanizzi A (2002) Cyclic carbonate formation from carbon dioxide and oxiranes in tetrabutylammonium halides as solvents and catalysts. Org Lett 4(15):2561–2563. doi:10.1021/ol026189w
28. Wang J-Q, Dong K, Cheng W-G, Sun J, Zhang S-J (2012) Insights into quaternary ammonium salts-catalyzed fixation carbon dioxide with epoxides. Catal Sci Technol 2(7):1480–1484. doi:10.1039/c2cy20103h

29. Peng J, Deng Y (2001) Cycloaddition of carbon dioxide to propylene oxide catalyzed by ionic liquids. New J Chem 25(4):639–641. doi:10.1039/B008923K
30. Dharman MM, Choi H-J, Park S-W, Park D-W (2010) Microwave assisted synthesis of cyclic carbonate using homogeneous and heterogeneous ionic liquid catalysts. Top Catal 53(7–10):462–469. doi:10.1007/s11244-010-9473-0
31. Kawanami H, Sasaki A, Matsui K, Ikushima Y (2003) A rapid and effective synthesis of propylene carbonate using a supercritical CO_2-ionic liquid system. Chem Commun 7:896–897. doi:10.1039/B212823C
32. Sun H, Zhang D (2007) Density functional theory study on the cycloaddition of carbon dioxide with propylene oxide catalyzed by alkylmethylimidazolium chlorine ionic liquids. J Phys Chem A 111(32):8036–8043. doi:10.1021/jp073873p
33. Kim HS, Kim JJ, Kim H, Jang HG (2003) Imidazolium zinc tetrahalide-catalyzed coupling reaction of CO_2 and ethylene oxide or propylene oxide. J Catal 220(1):44–46, http://dx.doi.org/10.1016/S0021-9517(03)00238-0
34. Wong W-L, Chan P-H, Zhou Z-Y, Lee K-H, Cheung K-C, Wong K-Y (2008) A robust ionic liquid as reaction medium and efficient organocatalyst for carbon dioxide fixation. ChemSusChem 1(1–2):67–70. doi:10.1002/cssc.200700097
35. Sun J, Zhang S, Cheng W, Ren J (2008) Hydroxyl-functionalized ionic liquid: a novel efficient catalyst for chemical fixation of CO_2 to cyclic carbonate. Tetrahedron Lett 49(22):3588–3591. doi:10.1016/j.tetlet.2008.04.022
36. Zhou Y, Hu S, Ma X, Liang S, Jiang T, Han B (2008) Synthesis of cyclic carbonates from carbon dioxide and epoxides over betaine-based catalysts. J Mol Catal A-Chem 284(1–2):52–57. doi:10.1016/j.molcata.2008.01.010
37. Tsutsumi Y, Yamakawa K, Yoshida M, Ema T, Sakai T (2010) Bifunctional organocatalyst for activation of carbon dioxide and epoxide to produce cyclic carbonate: betaine as a new catalytic motif. Org Lett 12(24):5728–5731. doi:10.1021/ol102539x
38. Qi C, Jiang H (2010) Histidine-catalyzed synthesis of cyclic carbonates in supercritical carbon dioxide. Sci China-Chem 53(7):1566–1570. doi:10.1007/s11426-010-4019-7
39. Wu F, Dou X-Y, He L-N, Miao C-X (2010) Natural amino acid-based ionic liquids as efficient catalysts for the synthesis of cyclic carbonates from CO_2 and epoxides under solvent-free conditions. Lett Org Chem 7(1):73–78
40. Gong Q, Luo H, Cao J, Shang Y, Zhang H, Wang W, Zhou X (2012) Synthesis of cyclic carbonate from carbon dioxide and epoxide using amino acid ionic liquid under 1 atm pressure. Aust J Chem 65(4):381–386. doi:10.1071/ch11462
41. Zhou H, Zhang W-Z, Liu C-H, Qu J-P, Lu X-B (2008) CO_2 adducts of N-heterocyclic carbenes: thermal stability and catalytic activity toward the coupling of CO_2 with epoxides. J Org Chem 73(20):8039–8044. doi:10.1021/jo801457r
42. Kayaki Y, Yamamoto M, Ikariya T (2009) N-heterocyclic carbenes as efficient organocatalysts for CO2 fixation reactions. Angew Chem-Int Ed 48(23):4194–4197. doi:10.1002/anie.200901399
43. Sun J, Ren J, Zhang S, Cheng W (2009) Water as an efficient medium for the synthesis of cyclic carbonate. Tetrahedron Lett 50(4):423–426. doi:10.1016/j.tetlet.2008.11.034
44. Yang Z-Z, He L-N, Miao C-X, Chanfreau S (2010) Lewis basic ionic liquids-catalyzed conversion of carbon dioxide to cyclic carbonates. Adv Synth Catal 352(13):2233–2240. doi:10.1002/adsc.201000239
45. Aoyagi N, Furusho Y, Endo T (2012) Remarkably efficient catalysts of amidine hydroiodides for the synthesis of cyclic carbonates from carbon dioxide and epoxides under mild conditions. Chem Lett 41(3):240–241. doi:10.1246/cl.2012.240
46. Aoyagi N, Furusho Y, Endo T (2013) Convenient synthesis of cyclic carbonates from CO_2 and epoxides by simple secondary and primary ammonium iodides as metal-free catalysts under mild conditions and its application to synthesis of polymer bearing cyclic carbonate moiety. J Polymer Sci Part A-Polymer Chem 51(5):1230–1242. doi:10.1002/pola.26492
47. Sun J, Han L, Cheng W, Wang J, Zhang X, Zhang S (2011) Efficient acid-base bifunctional catalysts for the fixation of CO_2 with epoxides under metal- and solvent-free conditions. Chemsuschem 4(4):502–507. doi:10.1002/cssc.201000305

48. Han L, Choi S-J, Park M-S, Lee S-M, Kim Y-J, Kim M-I, Liu B, Park D-W (2012) Carboxylic acid functionalized imidazolium-based ionic liquids: efficient catalysts for cycloaddition of CO_2 and epoxides. React Kinet Mech Catal 106(1):25–35. doi:10.1007/s11144-011-0399-8
49. Foltran S, Alsarraf J, Robert F, Landais Y, Cloutet E, Cramail H, Tassaing T (2013) On the chemical fixation of supercritical carbon dioxide with epoxides catalyzed by ionic salts: an in situ FTIR and Raman study. Catal Sci Technol 3(4):1046–1055. doi:10.1039/c2cy20784b
50. Xiao L, Lv D, Wu W (2011) Brønsted acidic ionic liquids mediated metallic salts catalytic system for the chemical fixation of carbon dioxide to form cyclic carbonates. Catal Lett 141 (12):1838–1844. doi:10.1007/s10562-011-0682-3
51. Whiteoak CJ, Nova A, Maseras F, Kleij AW (2012) Merging sustainability with organocatalysis in the formation of organic carbonates by using CO_2 as a feedstock. ChemSusChem 5(10):2032–2038. doi:10.1002/cssc.201200255
52. Wu Z, Xie H, Yu X, Liu E (2013) Lignin-based green catalyst for the chemical fixation of carbon dioxide with epoxides to form cyclic carbonates under solvent-free conditions. ChemCatChem. doi:10.1002/cctc.201200894
53. Zhao Y, Yao C, Chen G, Yuan Q (2013) Highly efficient synthesis of cyclic carbonate with CO_2 catalyzed by ionic liquid in a microreactor. Green Chem 15(2):446–452. doi:10.1039/c2gc36612f
54. Yu T, Weiss RG (2012) Syntheses of cyclic carbonates with amidinium halide catalysts in reusable, reversible, room-temperature ionic liquids or acetonitrile. Green Chem 14 (1):209–216. doi:10.1039/c1gc16027c
55. Chatelet B, Joucla L, Dutasta J-P, Martinez A, Szeto KC, Dufaud V (2013) Azaphosphatranes as structurally tunable organocatalysts for carbonate synthesis from CO_2 and epoxides. J Am Chem Soc 135(14):5348–5351. doi:10.1021/ja402053d
56. Wang J-Q, Kong D-L, Chen J-Y, Cai F, He L-N (2006) Synthesis of cyclic carbonates from epoxides and carbon dioxide over silica-supported quaternary ammonium salts under supercritical conditions. J Mol Catal A Chem 249(1–2):143–148, http://dx.doi.org/10.1016/j.molcata.2006.01.008
57. Wang J-Q, Yue X-D, Cai F, He L-N (2007) Solventless synthesis of cyclic carbonates from carbon dioxide and epoxides catalyzed by silica-supported ionic liquids under supercritical conditions. Catal Commun 8(2):167–172, http://dx.doi.org/10.1016/j.catcom.2006.05.049
58. Zhu A, Jiang T, Han B, Zhang J, Xie Y, Ma X (2007) Supported choline chloride/urea as a heterogeneous catalyst for chemical fixation of carbon dioxide to cyclic carbonates. Green Chem 9(2):169–172. doi:10.1039/B612164K
59. Xie H, Duan H, Li S, Zhang S (2005) The effective synthesis of propylene carbonate catalyzed by silica-supported hexaalkylguanidinium chloride. New J Chem 29(9):1199–1203. doi:10.1039/B504822B
60. Lai G, Peng J, Li J, Qiu H, Jiang J, Jiang K, Shen Y (2006) Ionic liquid functionalized silica gel: novel catalyst and fixed solvent. Tetrahedron Lett 47(39):6951–6953, http://dx.doi.org/10.1016/j.tetlet.2006.07.122
61. Zhang X, Wang D, Zhao N, Al-Arifi ASN, Aouak T, Al-Othman ZA, Wei W, Sun Y (2009) Grafted ionic liquid: catalyst for solventless cycloaddition of carbon dioxide and propylene oxide. Catal Commun 11(1):43–46, http://dx.doi.org/10.1016/j.catcom.2009.08.007
62. Sakai T, Tsutsumi Y, Ema T (2008) Highly active and robust organic-inorganic hybrid catalyst for the synthesis of cyclic carbonates from carbon dioxide and epoxides. Green Chem 10(3):337–341. doi:10.1039/B718321F
63. Takahashi T, Watahiki T, Kitazume S, Yasuda H, Sakakura T (2006) Synergistic hybrid catalyst for cyclic carbonate synthesis: remarkable acceleration caused by immobilization of homogeneous catalyst on silica. Chem Commun 15:1664–1666. doi:10.1039/B517140G
64. Udayakumar S, Park S-W, Park D-W, Choi B-S (2008) Immobilization of ionic liquid on hybrid MCM-41 system for the chemical fixation of carbon dioxide on cyclic carbonate. Catal Commun 9(7):1563–1570, http://dx.doi.org/10.1016/j.catcom.2008.01.001
65. Udayakumar S, Raman V, Shim H-L, Park D-W (2009) Cycloaddition of carbon dioxide for commercially-imperative cyclic carbonates using ionic liquid-functionalized porous amorphous silica. Appl Catal A Gen 368(1–2):97–104, http://dx.doi.org/10.1016/j.apcata.2009.08.015

66. Udayakumar S, Lee M-K, Shim H-L, Park S-W, Park D-W (2009) Imidazolium derivatives functionalized MCM-41 for catalytic conversion of carbon dioxide to cyclic carbonate. Catal Commun 10(5):659–664, http://dx.doi.org/10.1016/j.catcom.2008.11.017
67. Dharman MM, Choi H-J, Kim D-W, Park D-W (2011) Synthesis of cyclic carbonate through microwave irradiation using silica-supported ionic liquids: effect of variation in the silica support. Catal Today 164(1):544–547, http://dx.doi.org/10.1016/j.cattod.2010.11.009
68. Han L, Park S-W, Park D-W (2009) Silica grafted imidazolium-based ionic liquids: efficient heterogeneous catalysts for chemical fixation of CO_2 to a cyclic carbonate. Energy Environ Sci 2(12):1286–1292. doi:10.1039/B910763K
69. Han L, Choi H-J, Choi S-J, Liu B, Park D-W (2011) Ionic liquids containing carboxyl acid moieties grafted onto silica: synthesis and application as heterogeneous catalysts for cycloaddition reactions of epoxide and carbon dioxide. Green Chem 13(4):1023–1028. doi:10.1039/C0GC00612B
70. Appaturi JN, Adam F (2013) A facile and efficient synthesis of styrene carbonate via cycloaddition of CO2 to styrene oxide over ordered mesoporous MCM-41-Imi/Br catalyst. Appl Catal B Environ 136–137:150–159, http://dx.doi.org/10.1016/j.apcatb.2013.01.049
71. Motokura K, Itagaki S, Iwasawa Y, Miyaji A, Baba T (2009) Silica-supported aminopyridinium halides for catalytic transformations of epoxides to cyclic carbonates under atmospheric pressure of carbon dioxide. Green Chem 11(11):1876–1880. doi:10.1039/B916764C
72. Udayakumar S, Son Y-S, Lee M-K, Park S-W, Park D-W (2008) The synthesis of chloropropylated MCM-41 through co-condensation technique: the path finding process. Appl Catal A Gen 347(2):192–199, http://dx.doi.org/10.1016/j.apcata.2008.06.009
73. Cheng W, Chen X, Sun J, Wang J, Zhang S (2013) SBA-15 supported triazolium-based ionic liquids as highly efficient and recyclable catalysts for fixation of CO_2 with epoxides. Catal Today 200:117–124, http://dx.doi.org/10.1016/j.cattod.2012.10.001
74. Xie Y, Zhang Z, Jiang T, He J, Han B, Wu T, Ding K (2007) CO_2 cycloaddition reactions catalyzed by an ionic liquid grafted onto a highly cross-linked polymer matrix. Angew Chem Int Ed 46(38):7255–7258. doi:10.1002/anie.200701467
75. Shi T-Y, Wang J-Q, Sun J, Wang M-H, Cheng W-G, Zhang S-J (2013) Efficient fixation of CO_2 into cyclic carbonates catalyzed by hydroxyl-functionalized poly(ionic liquids). RSC Adv 3(11):3726–3732. doi:10.1039/C3RA21872D
76. Xiong Y, Wang H, Wang R, Yan Y, Zheng B, Wang Y (2010) A facile one-step synthesis to cross-linked polymeric nanoparticles as highly active and selective catalysts for cycloaddition of CO_2 to epoxides. Chem Commun 46(19):3399–3401. doi:10.1039/B926901K
77. Xiong Y, Wang Y, Wang H, Wang R (2011) A facile one-step synthesis to ionic liquid-based cross-linked polymeric nanoparticles and their application for CO_2 fixation. Polym Chem 2(10):2306–2315. doi:10.1039/C1PY00201E
78. Xiong Y, Wang Y, Wang H, Wang R, Cui Z (2012) Novel one-step synthesis to cross-linked polymeric nanoparticles as highly active and selective catalysts for cycloaddition of CO_2 to epoxides. J Appl Polym Sci 123(3):1486–1493. doi:10.1002/app.34622
79. Nishikubo T, Kameyama A, Yamashita J, Tomoi M, Fukuda W (1993) Insoluble polystyrene-bound quaternary onium salt catalysts for the synthesis of cyclic carbonates by the reaction of oxiranes with carbon dioxide. J Polym Sci A Polym Chem 31(4):939–947. doi:10.1002/pola.1993.080310412
80. Park D-W, Yu B-S, Jeong E-S, Kim I, Kim M-I, Oh K-J, Park S-W (2004) Comparative studies on the performance of immobilized quaternary ammonium salt catalysts for the addition of carbon dioxide to glycidyl methacrylate. Catal Today 98(4):499–504, http://dx.doi.org/10.1016/j.cattod.2004.09.003
81. Du Y, Cai F, Kong D-L, He L-N (2005) Organic solvent-free process for the synthesis of propylene carbonate from supercritical carbon dioxide and propylene oxide catalyzed by insoluble ion exchange resins. Green Chem 7(7):518–523. doi:10.1039/B500074B
82. Ma J, Song J, Liu H, Liu J, Zhang Z, Jiang T, Fan H, Han B (2012) One-pot conversion of CO_2 and glycerol to value-added products using propylene oxide as the coupling agent. Green Chem 14(6):1743–1748. doi:10.1039/C2GC35150A

83. Chen X, Sun J, Wang J, Cheng W (2012) Polystyrene-bound diethanolamine based ionic liquids for chemical fixation of CO_2. Tetrahedron Lett 53(22):2684–2688, http://dx.doi.org/10.1016/j.tetlet.2012.03.058
84. Xiong Y, Bai F, Cui Z, Guo N, Wang R (2013) Cycloaddition reaction of carbon dioxide to epoxides catalyzed by polymer-supported quaternary phosphonium salts. J Chem 2013:9. doi:10.1155/2013/261378
85. Sun J, Cheng W, Fan W, Wang Y, Meng Z, Zhang S (2009) Reusable and efficient polymer-supported task-specific ionic liquid catalyst for cycloaddition of epoxide with CO_2. Catal Today 148(3–4):361–367, http://dx.doi.org/10.1016/j.cattod.2009.07.070
86. Yu J-I, Choi H-J, Selvaraj M, Park D-W (2011) Catalytic performance of polymer-supported ionic liquids in the cycloaddition of carbon dioxide to allyl glycidyl ether. React Kinet Mech Catal 102(2):353–365. doi:10.1007/s11144-010-0280-1
87. Watile RA, Deshmukh KM, Dhake KP, Bhanage BM (2012) Efficient synthesis of cyclic carbonate from carbon dioxide using polymer anchored diol functionalized ionic liquids as a highly active heterogeneous catalyst. Catal Sci Technol 2(5):1051–1055. doi:10.1039/C2CY00458E
88. Dai W-L, Chen L, Yin S-F, Li W-H, Zhang Y-Y, Luo S-L, Au C-T (2010) High-efficiency synthesis of cyclic carbonates from epoxides and CO_2 over hydroxyl ionic liquid catalyst grafted onto cross-linked polymer. Catal Lett 137(1–2):74–80. doi:10.1007/s10562-010-0346-8
89. Zhang Y, Yin S, Luo S, Au CT (2012) Cycloaddition of CO_2 to epoxides catalyzed by carboxyl-functionalized imidazolium-based ionic liquid grafted onto cross-linked polymer. Indus Eng Chem Res 51(10):3951–3957. doi:10.1021/ie203001u
90. Ochiai B, Endo T (2007) Polymer-supported pyridinium catalysts for synthesis of cyclic carbonate by reaction of carbon dioxide and oxirane. J Polym Sci A Polym Chem 45 (23):5673–5678. doi:10.1002/pola.22316
91. He J, Wu T, Zhang Z, Ding K, Han B, Xie Y, Jiang T, Liu Z (2007) Cycloaddition of CO_2 to epoxides catalyzed by polyaniline salts. Chem Eur J 13(24):6992–6997. doi:10.1002/chem.200700210
92. Han L, Choi H-J, Kim D-K, Park S-W, Liu B, Park D-W (2011) Porous polymer bead-supported ionic liquids for the synthesis of cyclic carbonate from CO_2 and epoxide. J Mol Catal A Chem 338(1–2):58–64, http://dx.doi.org/10.1016/j.molcata.2011.02.001
93. Cho HC, Lee HS, Chun J, Lee SM, Kim HJ, Son SU (2011) Tubular microporous organic networks bearing imidazolium salts and their catalytic CO_2 conversion to cyclic carbonates. Chem Commun 47(3):917–919. doi:10.1039/C0CC03914D
94. Song Q-W, He L-N, Wang J-Q, Yasuda H, Sakakura T (2013) Catalytic fixation of CO_2 to cyclic carbonates by phosphonium chlorides immobilized on fluorous polymer. Green Chem 15(1):110–115. doi:10.1039/C2GC36210D
95. Aprile C, Giacalone F, Agrigento P, Liotta LF, Martens JA, Pescarmona PP, Gruttadauria M (2011) Multilayered supported ionic liquids as catalysts for chemical fixation of carbon dioxide: a high-throughput study in supercritical conditions. ChemSusChem 4(12):1830–1837. doi:10.1002/cssc.201100446
96. Du Y, Wang J-Q, Chen J-Y, Cai F, Tian J-S, Kong D-L, He L-N (2006) A poly(ethylene glycol)-supported quaternary ammonium salt for highly efficient and environmentally friendly chemical fixation of CO_2 with epoxides under supercritical conditions. Tetrahedron Lett 47(8):1271–1275, http://dx.doi.org/10.1016/j.tetlet.2005.12.077
97. Dou X-Y, Wang J-Q, Du Y, Wang E, He L-N (2007) Guanidinium salt functionalized PEG: an effective and recyclable homo-geneous catalyst for the synthesis of cyclic carbonates from CO_2 and epoxides under solvent-free conditions. Synlett 2007:3058–3062. doi:10.1055/s-2007-992362
98. Yang Z-Z, Zhao Y-N, He L-N, Gao J, Yin Z-S (2012) Highly efficient conversion of carbon dioxide catalyzed by polyethylene glycol-functionalized basic ionic liquids. Green Chem 14(2):519–527. doi:10.1039/C2GC16039K
99. Zhao Y-N, Yang Z-Z, Luo S-H, He L-N (2013) Design of task-specific ionic liquids for catalytic conversion of CO_2 with aziridines under mild conditions. Catal Today 200:2–8, http://dx.doi.org/10.1016/j.cattod.2012.04.006

100. Patil YP, Tambade PJ, Jagtap SR, Bhanage BM (2008) Synthesis of 2-oxazolidinones/2-imidazolidinones from CO_2, different epoxides and amino alcohols/alkylene diamines using $Br^{-}Ph_3{}^{+}P$-PEG600-$P^{+}Ph_3Br^{-}$ as homogenous recyclable catalyst. J Mol Catal A Chem 289(1–2):14–21, http://dx.doi.org/10.1016/j.molcata.2008.03.019
101. Choi H-J, Selvaraj M, Park D-W (2013) Catalytic performance of immobilized ionic liquid onto PEG for the cycloaddition of carbon dioxide to allyl glycidyl ether. Chem Eng Sci 100:242–248. doi:http://dx.doi.org/10.1016/j.ces.2012.11.014
102. Zhao Y, Tian J-S, Qi X-H, Han Z-N, Zhuang Y-Y, He L-N (2007) Quaternary ammonium salt-functionalized chitosan: an easily recyclable catalyst for efficient synthesis of cyclic carbonates from epoxides and carbon dioxide. J Mol Catal A Chem 271(1–2):284–289, http://dx.doi.org/10.1016/j.molcata.2007.03.047
103. Tharun J, Hwang Y, Roshan R, Ahn S, Kathalikkattil AC, Park D-W (2012) A novel approach of utilizing quaternized chitosan as a catalyst for the eco-friendly cycloaddition of epoxides with CO_2. Catal Sci Technol 2(8):1674–1680. doi:10.1039/C2CY20137B
104. Tharun J, Kim DW, Roshan R, Hwang Y, Park D-W (2013) Microwave assisted preparation of quaternized chitosan catalyst for the cycloaddition of CO_2 and epoxides. Catal Commun 31:62–65, http://dx.doi.org/10.1016/j.catcom.2012.11.018
105. Sun J, Wang J, Cheng W, Zhang J, Li X, Zhang S, She Y (2012) Chitosan functionalized ionic liquid as a recyclable biopolymer-supported catalyst for cycloaddition of CO_2. Green Chem 14(3):654–660. doi:10.1039/C2GC16335G
106. Roshan KR, Mathai G, Kim J, Tharun J, Park G-A, Park D-W (2012) A biopolymer mediated efficient synthesis of cyclic carbonates from epoxides and carbon dioxide. Green Chem 14(10):2933–2940. doi:10.1039/C2GC35942A
107. Barbarini A, Maggi R, Mazzacani A, Mori G, Sartori G, Sartorio R (2003) Cycloaddition of CO_2 to epoxides over both homogeneous and silica-supported guanidine catalysts. Tetrahedron Lett 44(14):2931–2934, http://dx.doi.org/10.1016/S0040-4039(03)00424-6
108. Zhang X, Zhao N, Wei W, Sun Y (2006) Chemical fixation of carbon dioxide to propylene carbonate over amine-functionalized silica catalysts. Catal Today 115(1–4):102–106, http://dx.doi.org/10.1016/j.cattod.2006.02.028
109. Zhang X, Zhang Y, Yang Y, Wei Q, Zhang X (2008) Chemical fixation of carbon dioxide to propylene carbonate over TBD/SiO_2 and DBU/SiO_2 catalysts. React Kinet Catal Lett 94(2):385–390. doi:10.1007/s11144-008-5275-9
110. Yu KMK, Curcic I, Gabriel J, Morganstewart H, Tsang SC (2009) Catalytic coupling of CO2 with epoxide over supported and unsupported amines. J Phys Chem A 114(11):3863–3872. doi:10.1021/jp906365g
111. Sankar M, Tarte NH, Manikandan P (2004) Effective catalytic system of zinc-substituted polyoxometalate for cycloaddition of CO_2 to epoxides. Appl Cataly A Gen 276(1–2):217–222, http://dx.doi.org/10.1016/j.apcata.2004.08.008
112. Shiels RA, Jones CW (2007) Homogeneous and heterogeneous 4-(N, N-dialkylamino)pyridines as effective single component catalysts in the synthesis of propylene carbonate. J Mol Catal A Chem 261(2):160–166, http://dx.doi.org/10.1016/j.molcata.2006.08.002
113. Srivastava R, Srinivas D, Ratnasamy P (2005) CO_2 activation and synthesis of cyclic carbonates and alkyl/aryl carbamates over adenine-modified Ti-SBA-15 solid catalysts. J Catal 233(1):1–15, http://dx.doi.org/10.1016/j.jcat.2005.03.023
114. Srivastava R, Srinivas D, Ratnasamy P (2006) Sites for CO_2 activation over amine-functionalized mesoporous Ti(Al)-SBA-15 catalysts. Micropor Mesopor Mater 90(1–3):314–326, http://dx.doi.org/10.1016/j.micromeso.2005.10.043
115. Jagtap SR, Raje VP, Samant SD, Bhanage BM (2007) Silica supported polyvinyl pyridine as a highly active heterogeneous base catalyst for the synthesis of cyclic carbonates from carbon dioxide and epoxides. J Mol Catal A Chem 266(1–2):69–74, http://dx.doi.org/10.1016/j.molcata.2006.10.033
116. Adam F, Batagarawa MS (2013) Tetramethylguanidine–silica nanoparticles as an efficient and reusable catalyst for the synthesis of cyclic propylene carbonate from carbon dioxide and propylene oxide. Appl Catal A Gen 454:164–171, http://dx.doi.org/10.1016/j.apcata.2012.12.009

117. Prasetyanto EA, Ansari MB, Min B-H, Park S-E (2010) Melamine tri-silsesquioxane bridged periodic mesoporous organosilica as an efficient metal-free catalyst for CO_2 activation. Catal Today 158(3–4):252–257, http://dx.doi.org/10.1016/j.cattod.2010.03.081
118. Roeser J, Kailasam K, Thomas A (2012) Covalent triazine frameworks as heterogeneous catalysts for the synthesis of cyclic and linear carbonates from carbon dioxide and epoxides. ChemSusChem 5(9):1793–1799. doi:10.1002/cssc.201200091
119. Huang J-W, Shi M (2003) Chemical fixation of carbon dioxide by NaI/PPh_3/PhOH. J Org Chem 68(17):6705–6709. doi:10.1021/jo0348221
120. Shen Y-M, Duan W-L, Shi M (2003) Phenol and organic bases co-catalyzed chemical fixation of carbon dioxide with terminal epoxides to form cyclic carbonates. Adv Synth Catal 345(3):337–340. doi:10.1002/adsc.200390035
121. Wang J-Q, Sun J, Cheng W-G, Dong K, Zhang X-P, Zhang S-J (2012) Experimental and theoretical studies on hydrogen bond-promoted fixation of carbon dioxide and epoxides in cyclic carbonates. Phys Chem Chem Phys 14(31):11021–11026. doi:10.1039/c2cp41698k
122. Liang S, Liu H, Jiang T, Song J, Yang G, Han B (2011) Highly efficient synthesis of cyclic carbonates from CO_2 and epoxides over cellulose/KI. Chem Commun 47(7):2131–2133. doi:10.1039/c0cc04829a
123. Song J, Zhang Z, Han B, Hu S, Li W, Xie Y (2008) Synthesis of cyclic carbonates from epoxides and CO_2 catalyzed by potassium halide in the presence of [small beta]-cyclodextrin. Green Chem 10(12):1337–1341. doi:10.1039/B815105A
124. Song J, Zhang B, Zhang P, Ma J, Liu J, Fan H, Jiang T, Han B (2012) Highly efficient synthesis of cyclic carbonates from CO_2 and epoxides catalyzed by KI/lecithin. Catal Today 183(1):130–135. doi:10.1016/j.cattod.2011.08.042
125. Zhou L, Liu Y, He Z, Luo Y, Zhou F, Yu E, Hou Z, Eli W (2013) Pentaerythritol and KI: an efficient catalytic system for the conversion from CO_2 and epoxides to cyclic carbonates. J Chem Res 2:102–104. doi:10.3184/174751913x13571500195988
126. Ma J, Liu J, Zhang Z, Han B (2012) The catalytic mechanism of KI and the co-catalytic mechanism of hydroxyl substances for cycloaddition of CO_2 with propylene oxide. Green Chem 14(9):2410–2420. doi:10.1039/c2gc35711a
127. Sonnati MO, Amigoni S, de Givenchy EPT, Darmanin T, Choulet O, Guittard F (2013) Glycerol carbonate as a versatile building block for tomorrow: synthesis, reactivity, properties and applications. Green Chem 15(2):283–306. doi:10.1039/c2gc36525a
128. Cui H, Wang T, Wang F, Gu C, Wang P, Dai Y (2003) One-pot synthesis of dimethyl carbonate using ethylene oxide, methanol, and carbon dioxide under supercritical conditions. Indus Eng Chem Res 42(17):3865–3870. doi:10.1021/ie021014b
129. Cui H, Wang T, Wang F, Gu C, Wang P, Dai Y (2004) Kinetic study on the one-pot synthesis of dimethyl carbonate in supercritical CO_2 conditions. Indus Eng Chem Res 43(24):7732–7739. doi:10.1021/ie049715r
130. Kishimoto Y, Ogawa I (2004) Amine-catalyzed, one-pot coproduction of dialkyl carbonates and 1,2-diols from epoxides, alcohols, and carbon dioxide. Indus Eng Chem Res 43(26):8155–8162. doi:10.1021/ie040006n
131. Chen X, Hu C, Su J, Yu T, Gao Z (2006) One-pot synthesis of dimethyl carbonate catalyzed by [bmim]BF_4/CH_3ONa. Chin J Catal 27(6):485–488, http://dx.doi.org/10.1016/S1872-2067(06)60029-6
132. Tian J-S, Wang J-Q, Chen J-Y, Fan J-G, Cai F, He L-N (2006) One-pot synthesis of dimethyl carbonate catalyzed by n-Bu_4NBr/n-Bu_3N from methanol, epoxides, and supercritical CO_2. Appl Catal A Gen 301(2):215–221, http://dx.doi.org/10.1016/j.apcata.2005.12.002
133. Tian J-S, Miao C-X, Wang J-Q, Cai F, Du Y, Zhao Y, He L-N (2007) Efficient synthesis of dimethyl carbonate from methanol, propylene oxide and CO_2 catalyzed by recyclable inorganic base/phosphonium halide-functionalized polyethylene glycol. Green Chem 9(6):566–571. doi:10.1039/B614259A
134. Li J, Wang L, Shi F, Liu S, He Y, Lu L, Ma X, Deng Y (2011) Quaternary ammonium ionic liquids as bi-functional catalysts for one-step synthesis of dimethyl carbonate from ethylene oxide, carbon dioxide and methanol. Catal Lett 141(2):339–346. doi:10.1007/s10562-010-0498-6

135. Wang J-Q, Sun J, Shi C-Y, Cheng W-G, Zhang X-P, Zhang S-J (2011) Synthesis of dimethyl carbonate from CO_2 and ethylene oxide catalyzed by K_2CO_3-based binary salts in the presence of H_2O. Green Chem 13(11):3213–3217. doi:10.1039/C1GC15812K
136. Fang S, Fujimoto K (1996) Direct synthesis of dimethyl carbonate from carbon dioxide and methanol catalyzed by base. Appl Catal Gen 142(1):1–3. doi:10.1016/0926-860X(96)00081-6
137. S-i F, Bhanage BM, Ikushima Y, Arai M (2001) Synthesis of dimethyl carbonate from carbon dioxide and methanol in the presence of methyl iodide and base catalysts under mild conditions: effect of reaction conditions and reaction mechanism. Green Chem 3(2):87–91. doi:10.1039/B100363L
138. Cai Q, Jin C, Lu B, Tangbo H, Shan Y (2005) Synthesis of dimethyl carbonate from methanol and carbon dioxide using potassium methoxide as catalyst under mild conditions. Catal Lett 103(3–4):225–228. doi:10.1007/s10562-005-7158-2
139. Wang H, Lu B, Cai QH, Wu F, Shan YK (2005) Synthesis of dimethyl carbonate from methanol and carbon dioxide catalyzed by potassium hydroxide under mild conditions. Chin Chem Lett 16(9):1267
140. Cai Q, Lu B, Guo L, Shan Y (2009) Studies on synthesis of dimethyl carbonate from methanol and carbon dioxide. Catal Commun 10(5):605–609, http://dx.doi.org/10.1016/j.catcom.2008.11.002
141. Riduan SN, Zhang Y, Ying JY (2009) Conversion of carbon dioxide into methanol with silanes over N-heterocyclic carbene catalysts. Angew Chem Int Ed 48(18):3322–3325. doi:10.1002/anie.200806058
142. Huang F, Lu G, Zhao L, Li H, Wang Z-X (2010) The catalytic role of N-heterocyclic carbene in a metal-free conversion of carbon dioxide into methanol: a computational mechanism study. J Am Chem Soc 132(35):12388–12396. doi:10.1021/ja103531z
143. Das Neves Gomes C, Jacquet O, Villiers C, Thuéry P, Ephritikhine M, Cantat T (2012) A diagonal approach to chemical recycling of carbon dioxide: organocatalytic transformation for the reductive functionalization of CO_2. Angew Chem 124(1):191–194. doi:10.1002/ange.201105516
144. Jacquet O, Das Neves Gomes C, Ephritikhine M, Cantat T (2012) Recycling of carbon and silicon wastes: room temperature formylation of N–H bonds using carbon dioxide and polymethylhydrosiloxane. J Am Chem Soc 134(6):2934–2937. doi:10.1021/ja211527q
145. Jacquet O, Das Neves Gomes C, Ephritikhine M, Cantat T (2013) Complete catalytic deoxygenation of CO_2 into formamidine derivatives. ChemCatChem 5(1):117–120. doi:10.1002/cctc.201200732
146. Stephan DW, Erker G (2010) Frustrated Lewis pairs: metal-free hydrogen activation and more. Angew Chem Int Ed 49(1):46–76. doi:10.1002/anie.200903708
147. Ashley AE, Thompson AL, O'Hare D (2009) Non-metal-mediated homogeneous hydrogenation of CO_2 to CH_3OH. Angew Chem Int Ed 48(52):9839–9843. doi:10.1002/anie.200905466
148. Berkefeld A, Piers WE, Parvez M (2010) Tandem frustrated Lewis pair/tris(pentafluorophenyl) borane-catalyzed deoxygenative hydrosilylation of carbon dioxide. J Am Chem Soc 132(31):10660–10661. doi:10.1021/ja105320c

Chapter 2
Direct Transformation of Carbon Dioxide to Value-Added Products over Heterogeneous Catalysts

Shin-ichiro Fujita, Masahiko Arai, and Bhalchandra M. Bhanage

2.1 Introduction

Carbon dioxide (CO_2) is one of the greenhouse gases arising from human activities, and hence its accumulation in the atmosphere should be controlled by removing it from industrial emissions to avoid global warming. Thus, large amounts of CO_2 would be available [1–4]. On the other hand, CO_2 is recognized to be an abundant, cheap, recyclable, and nontoxic carbon source that can sometimes replace toxic chemicals such as phosgene, isocyanates, or carbon monoxide [2, 5–9]. It has been considered that utilization of CO_2 is more attractive rather than storage, if economical processes are available. Under these circumstances, chemical fixation of CO_2 into valuable chemicals is still gaining considerable interest.

Heterogeneous catalysts are widely used in industries because of their advantages in the separation and recycling and their applicability for flow reaction systems. Unfortunately, conventional heterogeneous catalysts are sometimes less active and/or selective in comparison to such homogeneous ones as metal complexes and organic bases including ionic liquids. A class of heterogeneous catalysts can be built of those homogeneous ones immobilized on solids of metal oxides or polymers. These immobilized catalysts can have not only high activity and/or selectivity but also the advantages in the catalyst separation, enabling more efficient and economical reaction processes.

During the last two decades, a variety of catalysts have been employed for the chemical fixation of CO_2. In this chapter, the utilization of heterogeneous catalysts for

S.-i. Fujita (✉) • M. Arai
Division of Chemical Process Engineering, Faculty of Engineering,
Hokkaido University, Sapporo 060-8628, Japan
e-mail: sfuji@eng.hokudai.ac.jp; marai@eng.hokudai.ac

B.M. Bhanage
Department of Chemistry, Institute of Chemical Technology,
Mumbai 400019, India
e-mail: bhanage@ictmumbai.edu.in

B.M. Bhanage and M. Arai (eds.), *Transformation and Utilization of Carbon Dioxide*,
Green Chemistry and Sustainable Technology, DOI 10.1007/978-3-642-44988-8_2,

the synthesis of cyclic carbonate from CO_2 and epoxides and of dimethyl carbonate (DMC) from CO_2 and methanol has been reviewed. The catalysts described will include immobilized organic base catalysts as well as conventional inorganic solid catalysts of metal oxides, clays, and zeolites. A few related reactions will also be described.

2.2 Synthesis of Cyclic Carbonate via Cycloaddition of CO_2 to Epoxide

2.2.1 Use of Inorganic Catalysts for CO_2 Cycloaddition

The five-member cyclic carbonates have several applications [6–8]; e.g., ethylene carbonate is an excellent solvent for many polymers and resins. Another important application includes the use as an intermediate for the manufacture of several important chemicals like dialkyl carbonates, glycols, carbamates, pyrimidines, purines, etc. These five-member cyclic carbonates were conventionally produced via a corrosive, poisonous, and hazardous route involving glycol and phosgene. Then manufacturers shifted to the production based on the cycloaddition of CO_2 to epoxide (Scheme 2.1) in the presence of base catalysts.

Yano et al. first reported the use of a metal oxide catalyst for the reaction of CO_2 and epoxide. They showed that a commercial MgO could catalyze the reactions of CO_2 with propylene oxide (PO) and styrene oxide (SO) to give cyclic carbonates [10]. It gave 60 % and 41 % yields of styrene carbonate (SC) and propylene carbonate (PC), respectively, at 135 °C and 2 MPa of CO_2 for 12 h in a solvent of dimethylformamide (DMF). CO_2 pressure showed no effect on the carbonate yield in a region between 0.2 and 2.8 MPa. When a chiral epoxide was used as the substrate, interestingly, the chirality was retained in the cyclic carbonate product.

Yamaguchi et al. used Mg–Al mixed oxides prepared from hydrotalcite for the reactions of CO_2 with several epoxides [11]. Corresponding cyclic carbonates were obtained with excellent yields at 100–120 °C and 0.5 MPa of CO_2 for 15–24 h in DMF. The Mg/Al ratio of the mixed oxide was significant for its catalytic activity, and the best value was 5. Based on the catalyst characterization results, the authors proposed that the O and Al atoms involved in Mg–O–Al bonds act as basic and acidic sites, respectively, and they cooperatively activate an epoxide molecule.

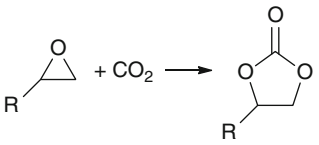

R = H (EO: ethylene oxide, EC: ethylene carbonate)
CH_3 (PO: propylene oxide, PC: propylene carbonate)
C_6H_5 (SO: styrene oxide, SC: styrene carbonate)

Scheme 2.1 Synthesis of cyclic carbonate via cycloaddition of CO_2 to epoxide. Abbreviations for a few representative substrates and products are also given

No use of organic solvent makes the reaction system more preferable. A few groups have reported the CO_2 cycloaddition reactions under such conditions. Bhanage et al. employed several metal oxide catalysts of MgO, CaO, ZnO, Zr_2O, La_2O_3, CeO_2, and Al_2O_3 for the reaction of CO_2 and propylene oxide (PO) to propylene carbonate (PC) [12]. MgO was found to be the best among the metal oxides examined. It gave a PC yield of 32 % with a PC selectivity of 92 % at 150 °C and 8 MPa of CO_2 for 15 h. Although a higher PC yield of 54 % was obtained with La_2O_3, the PC selectivity was lower (75 %). Basic properties of these catalysts were investigated by temperature programmed desorption (TPD) of adsorbed CO_2. It was suggested that both moderately and strongly basic sites are active sites for the reaction, and MgO has a large amount of moderately basic sites, resulting in its high activity and selectivity. The reaction of CO_2 and styrene oxide (SO) to styrene carbonate (SC) was also examined with MgO. For this reaction, MgO gave a poor product yield (16 %) because of low selectivity.

Tu and Davis prepared cesium-loaded zeolite X (Cs/KX) catalysts and used them for the synthesis of ethylene carbonate (EC) from CO_2 and ethylene oxide (EO) [13]. The activity of the zeolite catalyst was slightly lower than MgO, but the former catalyst was much more tolerant of water moisture than the latter one. Wet Cs/KX selectively produced EC, while wet MgO mostly produced mono-, di-, and triethylene glycol, which were formed by hydrolysis of EO and following dehydration reactions. Interestingly, the wet Cs/KX afforded a much higher EC yield than dry Cs/KX, although the reason was unknown.

Smectite is one of the layered clay minerals, and its acidic and basic properties are tunable [14]. Fujita et al. developed new types of catalysts based on Mg- and/or Ni-containing smectite catalysts, in which various amounts of alkali metals such as Na, K, and Li are incorporated [15, 16]. These catalysts were highly active and selective for PC synthesis from CO_2 and PO without organic solvent. The catalytic activity strongly depends on the amount of alkali atoms incorporated. The most active smectite catalyst gave a PC yield of 81 % with a PC selectivity of 94 % at 150 °C and 8 MPa of CO_2 for 15 h. The turnover number obtained with the most active smectite catalyst was about five times of that obtained with MgO, which was considered to be the best catalyst among the conventional metal oxide catalysts tested, as stated above. TPD of adsorbed CO_2 suggested that the smectite catalysts had large amounts of strongly basic sites, resulting in their high activities. They also studied in detail the optimization of the reaction conditions for this reaction [16]. The CO_2 pressure does not significantly affect the conversion and the selectivity in the region between 3 and 10 MPa; however, both the conversion and the selectivity decrease sharply at 15 MPa. It is highly probable that the reaction system consists of three phases: CO_2–liquid–solid at the lower pressures, while it should be in a homogeneous phase at 15 MPa. Such a phase change would cause an increase in the volume at the location where the reaction proceeds. Hence, the concentration of the catalyst and/or PO would be low at 15 MPa, resulting in low PO conversion at this elevated pressure. The effect of reaction temperature on the reaction of PO and CO_2 was investigated. The PO conversion was found to increase with the temperature, as expected; however, the selectivity decreased at 170 °C and thus the optimum reaction temperature was 150 °C.

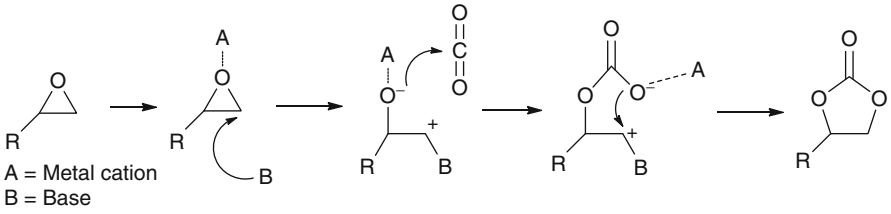

Scheme 2.2 A generally accepted reaction mechanism for CO_2 cycloaddition to epoxide catalyzed by acid-base bi-functional systems

As mentioned above, MgO gave a reasonable SC yield from CO_2 and SO at 135 °C in the presence of DMF; however, it gave a poor SC yield even at 150 °C in the absence of DMF, suggesting positive effects of DMF on the reaction. Yasuda et al. carried out the PC synthesis with MgO, Mg–Al mixed oxide, or SmOCl in the presence and absence of DMF and showed that the presence of DMF enhanced the PC yield twice or more irrespective of the catalyst used [17]. Similar results were also reported for the cyclic carbonate synthesis using Nb_2O_3 and DMF and using titanosilicate and 4-(dimethylamino)pyridine (DMAP) [18, 19]. Furthermore, Mori et al. reported that, when even a catalytic amount of DMAP was combined with zinc-based hydroxyapatite (ZnHAP), a good SC yield of 79 % was obtained at 100 °C and 0.5 MPa of CO_2 for 20 h, although ZnHAP had no activity and the activity of DMAP was very low [20]. Thus, it is highly probable that the occurrence of the synergetic effect is common in the bifunctional catalyst systems consisting of inorganic metal compounds and organic bases. A general reaction mechanism for those bifunctional catalyst systems can be drawn as Scheme 2.2. The Lewis acidic center of metal cation would interact with the oxygen atom of the epoxide, and the base would attack the less hindered carbon atom of the epoxide ring. Such cooperative activation of the epoxide should make the ring opening easier, being the reason for the promotional effects of the base. It is also possible that base activates a CO_2 molecule. In the absence of organic bases, the oxygen atoms on the metal oxide surface would act as Lewis base, but it would be less effective than the organic base.

2.2.2 *Use of Immobilized Organic Base Catalysts for CO_2 Cycloaddition*

It is well known that organic bases of amines, ammonium salts, phosphonium salts, imidazolium salts, etc., can be homogeneous catalysts for the cyclic carbonate synthesis via CO_2 cycloaddition to epoxides [7, 8, 21, 22]. Several groups examined the immobilization of those catalysts onto a solid support to facilitate the catalyst separation from the products. In this subsection, some representative examples of the CO_2 cycloaddition reactions using such immobilized catalysts are described.

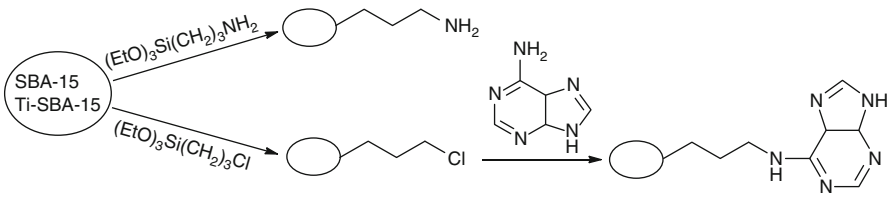

Scheme 2.3 Immobilization of propylamine and adenine on SBA-15 or Ti-SBA-15

To synthesize zeolites, tetraalkyl ammonium salts are used as the template. Srivastava et al. reported that as-synthesized zeolite-beta, which contained the template of tetramethylammonium bromide, could produce a few types of cyclic carbonates via CO_2 cycloaddition with very high yields at 120 °C and 0.7 MPa of CO_2 for 3–8 h without any solvent [23]. The catalyst could be recycled eight times with little loss in activity. The turnover frequency (TOF) value based on the amount of the ammonium template contained was almost the same with that of homogeneously used ammonium bromide. However, the authors pointed out that over the as-synthesized zeolite-beta, the reaction takes place only at the surface, and therefore, the ammonium molecules in the inside part of the zeolite are not accessible for the reaction. Thus, it is highly probable that the actual TOF of the solid catalyst is much higher than the observed one. This may be explained by the presence of surface silanol group as described below.

The same group also reported the covalent immobilization of organic amines (propylamine, adenine) on mesoporous materials of SBA-15 and Ti-SBA-15 by using silane coupling reagents (Scheme 2.3) [24]. The catalytic activity of the immobilized catalyst for CO_2 cycloaddition increased with the Ti content. FTIR spectra of the catalysts measured under several conditions suggested the activation of CO_2 on the base sites, because the cyclic carbonate yield was well correlated with the peak intensity of surface carbamate species. The authors proposed that the coexistence of epoxide activated on Ti sites and CO_2 activated on base sites is significant for the reaction. Recycling of adenine-modified Ti-SBA-15 was tested. In the absence of any organic solvent, the activity gradually decreased with recycling, while such deactivation was much less in the presence of acetonitrile solvent. When the deactivated catalyst was washed with organic solvents, the initial activity was almost restored. It was also confirmed that some heavy carbonaceous products accumulated on the catalyst surface, resulting in the deactivation. So, at least for this catalyst, the use of organic solvent is required.

The advantage of immobilizing homogeneous catalysts on solid materials is not only the easier separation of the catalyst but also the usability of it for the continuous operation using a fixed-bed flow reactor. Takahashi et al. first reported the use of silica-immobilized tetraalkyl phosphonium bromide for a flow reactor [25]. The phosphonium bromide was immobilized on silica in a similar way to Scheme 2.3. They carried out the PC synthesis using 10 MPa of CO_2 for more than 1,000 h. Unfortunately, the reaction temperature was required to be increased from the initial one of 90–160 °C for keeping the yield above 80 %, suggesting that some

Scheme 2.4 Cooperative activation of an epoxide molecule on silica-immobilized phosphonium halides

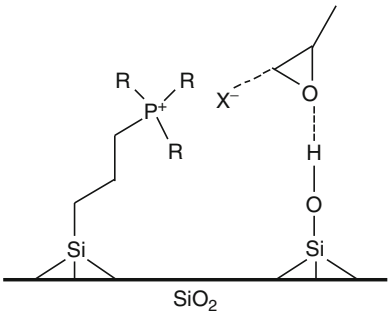

leaching of the phosphonium bromide from the support might occur; however, the selectivity to PC was kept over 99.9 % during the whole of the reaction run. In the same paper [25], they reported interesting synergistic effects of the immobilization of phosphonium halides on silica. They also carried out the reaction runs in a batch reactor and showed that the TOF of the immobilized phosphonium halides was more than 300 times larger compared to that of corresponding phosphonium halides that were used homogeneously. However, such enhancement in the activity was not observed by the immobilization on polystyrene. The surprising enhancement of the activity by supporting on silica was ascribed to the cooperational activation of the epoxide by the acidic surface silanol groups and the halide anion of the immobilized phosphonium salts (Scheme 2.4). The most active immobilized catalyst could almost quantitatively convert PO to PC at 100 °C and 10 MPa of CO_2 for a short reaction time of 1 h.

The acidity of the OH group on the solid surface was also suggested to affect the activity of immobilized onium halide catalysts. Sakai et al. prepared immobilized phosphonium halide catalysts using silica, aluminosilicate, and basic alumina as the support materials [26]. The activity for the CO_2 cycloaddition to epoxyhexane was in the order of silica $>$ aluminosilicate $>$ basic alumina, which is the same order as that of the acidity of the OH group on the support surface, and hence they ascribed the differences in the activity among the catalysts to those in the acidity of the OH group of the supports. This also supports the cooperative activation mechanism shown in Scheme 2.4. The enhancement of the activity by the immobilization was also observed with imidazolium and aminopyridinium halides [27, 28]. Thus, the synergistic effects of the immobilization on inorganic materials having surface hydroxyl groups are common. Over the immobilized catalysts, the mean pore size, the total pore volume, and the amount of surface hydroxyl groups were also found to be important factors determining the catalyst performance for CO_2 cycloaddition [26, 29].

Zinc tetrahalide onium salts prepared from zinc halide and onium halide were found to be excellent catalysts for the CO_2 cycloaddition [30–32]. They could give high cyclic carbonate yields under very mild conditions. This is ascribed to the cooperational activation of epoxide ring by Lewis acidic Zn center and basic halide anion, which is similar to Scheme 2.2. Qiao et al. applied this strategy for

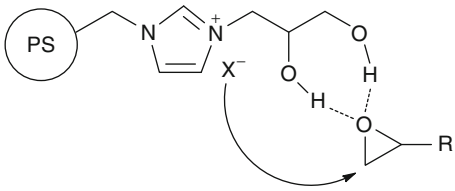

Scheme 2.5 Activation of an epoxide molecule by polystyrene-supported diol-functionalized imidazolium halide

polymer-immobilized imidazolium catalysts [33]. They immobilized imidazolium on polystyrene by copolymerization of 1-vinyl-3-butylimidazolium salts and styrene and further treated the copolymers with zinc halides. The resulting immobilized catalysts could show high TOF values up to about 3,800 h^{-1} at 120 °C. This TOF value was comparable to those obtained with very active homogeneous catalyst systems reported so far.

Very recently, Watile et al. developed diol-functionalized imidazolium halide immobilized on polystyrene (PS) as the catalyst for the CO_2 cycloaddition and showed that the diol-functionalization is more effective for the reaction than the mono hydroxyl-functionalization [34]. The PC yield obtained with 1-(2,3-di-hydroxyl-propyl)-imidazolium bromide was higher than that with a corresponding mono hydroxyl-functionalized imidazolium halide of 1-(2-hydroxyl-ethyl)-imidazolium bromide. It was proposed that the epoxide is activated by chelate-type hydrogen bonding of its O atom with the vicinal two hydroxyl groups of the functionalized imidazolium halide (Scheme 2.5).

Recent advance in the preparation of microporous materials is the development of zeolitic imidazole frameworks (ZIFs), in which metal atoms such as Zn are linked through N atoms by ditropic imidazolate to form neutral frameworks [35, 36]. ZIFs have uniform micropores, high surface areas, and open porous framework structures, making them interesting materials for adsorption and catalytic applications. The co-presence of the Lewis acidic Zn center and the N basic moieties in ZIF would make ZIF a candidate of the catalyst for the CO_2 cycloaddition reaction. Recently, Miralda et al. prepared non-functionalized and ethylene diamine-functionalized ZIF-8 (one kind of ZIF) catalysts and used them for the CO_2 cycloaddition to epichlorohydrin [37]. The nonfunctionalized ZIF-8 produced chloropropylene carbonate with a 44 % yield at 80 °C and 0.7 MPa of CO_2 for 4 h; however, the selectivity to cyclic carbonate was 52 %. By-products were a diol (24 % selectivity) and a dimer of the substrate (24 % selectivity). At a higher temperature of 100 °C, the conversion was increased, but the carbonate yield was decreased because of the increase in the dimer formation. The functionalization of ZIF-8 with amine improved both the yield of and the selectivity to the carbonate (73 % and 73 %), and the formation of the dimer was ceased. Unfortunately, the catalytic properties of both nonfunctionalized and functionalized ZIF-8 catalysts were unstable. They lost about half of their initial activities after the first recycling. This was ascribed to the accumulation of carbonaceous materials on the catalysts. Furthermore, after the second recycling, the zeolitic structures of both two catalysts were destroyed. The authors examined ZIF-8 for only the

substrate of epichlorohydrin. It is not clear at present whether the deactivation occurs with other epoxides. The loss of their structural features was proposed to result from the co-presence of CO_2 at high pressure and the carbonaceous materials. ZIFs are a new class of porous materials on which the number of studies is limited. Further studies on them may improve their catalytic performance and stability.

2.3 Synthesis of Dimethyl Carbonate from CO_2 and Methanol

Dimethyl carbonate (DMC) finds such applications as a solvent, an octane enhancer, and a reagent for carbonylation and methylation, replacing poisonous phosgene and dimethyl sulfate [5, 9, 38]. In addition, DMC is a precursor for polycarbonate resins, which have been commercially produced by polycondensation between bisphenol-A and phosgene. Thus, DMC can be regarded as a safe replacement for phosgene. Currently, DMC is synthesized by phosgenation of methanol, by oxidative carbonylation of methanol (non-phosgene route), or by a reaction of carbon monoxide with methyl nitrite. Methyl nitrite is produced from methanol, oxygen, and nitric oxide. These routes use poisonous and/or corrosive gases such as phosgene, hydrogen chloride, nitric oxide, and carbon monoxide and also bear potential explosion hazards in the case of methanol carbonylation. Hence, the direct synthesis of DMC from CO_2 and methanol (Scheme 2.6) is an attractive alternative and, hence, one of the promising reactions for the chemical fixation of CO_2.

Fang and Fujimoto [39] reported that various inorganic bases catalyze the direct DMC synthesis in the presence of methyl iodide as a promoter. Among the base catalysts examined, potassium carbonate was the most effective. Although the yield of DMC obtained with this catalyst was higher than those with organometallic complexes, the range of reaction conditions used was quite limited. Fujita et al. studied the influence of reaction conditions and the reaction mechanism in detail [40]. It was found that two maxima in the DMC formation appear at CO_2 pressures of 4.5 and 8 MPa, while the formation of a by-product, dimethyl ether (DME), decreased monotonically with increasing CO_2 pressure. DMC formation increased almost linearly with the amount of either methyl iodide or potassium carbonate when their concentrations were low. Mechanistic studies suggested that DMC and DME are produced in parallel pathways and methyl iodide is involved in both the formation of DMC and DME, as illustrated in Scheme 2.7. The catalyst was deactivated in the course of the reaction and methyl iodide was essentially a reactant rather than a promoter for the reaction. This is likely because the

Scheme 2.6 Synthesis of DMC from CO_2 and methanol

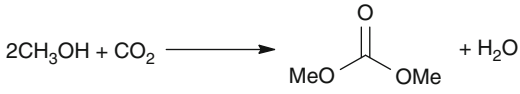

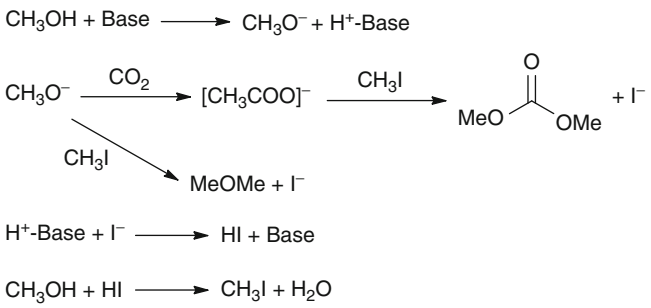

Scheme 2.7 Reaction mechanism of DMC synthesis in the presence of base and CH_3I

regeneration of methyl iodide from methanol and HI produced is difficult under the present reaction conditions. The residual HI instead reacted with potassium carbonate as confirmed by IR spectroscopy.

The direct DMC synthesis using solid catalysts in the absence of methyl iodide was also reported. Tomishige et al. found that ZrO_2 and CeO_2–ZrO_2 mixed oxide catalysts were selective for the direct DMC synthesis reaction under such conditions [41–43]. CeO_2–ZrO_2 mixed oxides were more active than pure ZrO_2. Based on temperature programmed desorption of NH_3 and CO_2, they proposed that acid–base pairs are active sites for the reaction. Jung and Bell also drew the same conclusion from IR measurements of the surface species formed on ZrO_2 [44, 45]. It was also reported that the enhancement in the acidity of ZrO_2 by supporting phosphoric or tungstophosphoric acid significantly improved the catalytic activity [46, 47]. Thus, several ZrO_2-based catalysts were disclosed; however, the DMC yields obtained were far from satisfactory because of the reaction equilibrium limitation. Lately, Tomishige and Kunimori [48] showed that the DMC yield can be improved by using dimethyl acetal (DMP) as a dehydration reagent. Hence, removal of H_2O from the reaction system is significant to get DMC in high yields; however, the amount of DMP added should be controlled. With too much DMP, the DMC formation decreased and the formation of undesirable by-product dimethyl ether increased. It was also shown that diethyl carbonate could be synthesized from ethanol and CO_2, although its yield was lower than that of DMC.

An analogous reaction to the DMC synthesis from CO_2 and methanol is diphenyl carbonate (DPC) synthesis from CO_2 and phenol. DPC is an important precursor of aromatic polycarbonate. It is conventionally synthesized from phosgene and phenol. Also for the synthesis of DPC, the replacement of phosgene with CO_2 is significant. Although it has been known that Lewis acid compounds of zinc halides can catalyze this reaction with or without base in a solvent of CCl_4, the use of CCl_4 is essential for the reaction, because CCl_4 is considered to be transformed to phosgene in the reaction system [49–51]. One can say that those systems are the reaction using in situ generated phosgene. Furthermore, the use of toxic CCl_4 should be avoided. Li and Su tried the reaction using ZrO_2 without any solvent at an elevated temperature and CO_2 pressure [52]. Unfortunately, the catalyst could

produce no DPC. Products observed were hydroxybenzyl phenol, diphenyl ether, and other compounds. For the DPC synthesis, further development of the catalyst is required. It may be a key issue how effectively to create a new bond between the carbon atom of CO_2 and the O atom of phenol.

2.4 Other Reactions for Transformation of CO_2

In the foregoing sections, the utilization of heterogeneous catalysts for the cyclic carbonate synthesis from CO_2 and epoxide and for the DMC synthesis from CO_2 and methanol was reviewed. In this section, a few related reactions in the presence of heterogeneous catalysts have been described.

Tomishige et al. examined the reaction of CO_2 and glycol to produce cyclic carbonate with CeO_2–ZrO_2 mixed oxide catalysts (Scheme 2.8) [53]. This is another route to synthesize cyclic carbonate from CO_2. Using the substrates of glycols cheaper than epoxides is of benefit. They optimized the catalyst composition (Ce/Zr ratio) and the calcination condition. Even after the optimization, however, the carbonate yields obtained were very low because of the reaction equilibrium limitation. Removal of H_2O from the reaction system would be essential to obtain high yields of the carbonate, similar to the cases of direct DMC synthesis from CO_2 and methanol.

Carbamates are another important class of organic compounds that meet a variety of applications for the production of polyurethanes, pesticides, fungicides, and medicinal drugs. They are commercially produced with the use of toxic phosgene. Another route producing carbamate is the reaction of primary amine, CO_2, and alkyl halide (Scheme 2.9). It is a benign way to synthesize carbamate avoiding the use of toxic phosgene, isocyanate, and CO. Srivastava et al. who used as-synthesized zeolite and amine-modified SBA-15 and Ti-SBA-15 for the CO_2 cycloaddition as described in Sect. 2.2.2, also examined the same catalysts for the carbamate synthesis [23, 24]. From various aliphatic and aromatic amines, their carbamates were produced with high selectivity under mild conditions (at 80 °C and 0.34 MPa of CO_2) in the absence of solvent. FTIR spectra of the catalysts measured again revealed that the product yield was well correlated with the peak intensity of

Scheme 2.8 Synthesis of cyclic carbonate from CO_2 and glycol

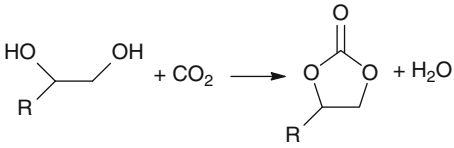

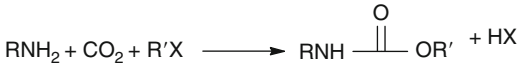

Scheme 2.9 Synthesis of carbamate from primary amine, CO_2, and alkyl halide

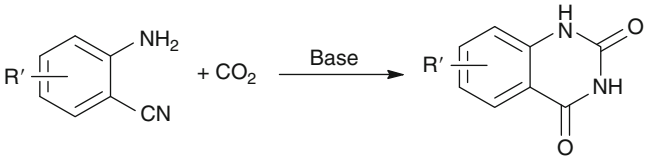

Scheme 2.10 Synthesis of quinazoline-2,4(1*H*,3*H*)-diones from CO_2 and 2-aminobenzonitriles

Scheme 2.11 Oxidation of benzene to phenol with CO_2

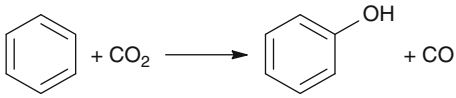

surface carbamate species. The coexistence of Ti sites and base sites was again suggested to be significant for the reaction. Adenine-modified Ti-SBA-15, which was deactivated by recycling in the absence of solvent, could be recycled for the carbamate synthesis without loss of activity even in the absence of solvent. These catalysts would be of promise for realizing carbamate synthesis processes from CO_2 using solid catalysts.

The reactions of CO_2 and aminobenzonitriles produce rather complex compounds of quinazoline-2,4(1H,3H)-diones (Scheme 2.10), which are important because of their biological activity and widely used as key structures in medical drugs. Patil et al. employed a series of MgO/ZrO_2 catalysts for this reaction [54]. When 2-aminobenzonitrile was used as the substrate, pure MgO and ZrO_2 gave the product yields of 44 % and 18 %, respectively, at 130 °C and 3.5 MPa of CO_2 (at room temperature) for 12 h in DMF solvent. MgO/ZrO_2 catalysts (MgO loading 5–15 %) gave higher product yields and an almost quantitative yield was obtained with 10 % MgO/ZrO_2. MgO/SiO_2 showed lower activity. FTIR of the catalysts and CO_2 TPD measurements suggested some interaction between MgO and ZrO_2. The most active catalyst gave good to excellent product yields from a broad range of aminobenzonitriles. The selection of the solvent was significant. The product yield obtained with DMSO was almost the same with DMF, while other polar and nonpolar solvents were ineffective (0–10 % yields). The catalyst was recyclable without loss of activity. The same group also reported the use of inorganic base of Cs_2CO_3 and of organic one of 1-butyl-3-methyl imidazolium hydroxide [55, 56]. The catalytic performance of the best MgO/ZrO_2 catalyst was comparable with those bases.

In all the above-mentioned reactions, CO_2 was used as the source of carbonyl group. CO_2 can be an oxidant for the direct synthesis of phenol from benzene (Scheme 2.11). Goettmann et al. first reported that graphitic carbon nitride C_3N_4 can catalyze this reaction in the co-presence of organic bases [57]. Lately, Ansari et al. studied the influence of starting compounds to prepare C_3N_4 on the activity [58]. In these studies, a high reaction temperature (150 °C) and long reaction time (10–20 h) were required to get reasonable product yields. So, further improvement of the catalyst activity is still required to synthesize phenol in large scales.

The by-product of CO can be used for other synthetic reactions, being an advantage of this reaction. Furthermore, the current industrial phenol manufacturing processes (the cumene process) suffer from the formation of large amounts of acetone as a by-product. Considering these, the oxidation of benzene with CO_2 would be a new and highly desirable route for utilization of CO_2.

2.5 Concluding Remarks

This chapter has reviewed the utilization of heterogeneous catalysts for the transformation of CO_2 to valuable chemicals. The reactions described are the CO_2 cycloaddition to epoxide producing cyclic carbonate (Scheme 2.1), the synthesis of DMC from CO_2 and methanol (Scheme 2.6), and other several related reactions (Schemes 2.8, 2.9, 2.10, and 2.11). These reactions are benign synthesis ways to avoid the use of toxic chemicals of phosgene, CO, isocyanate, etc.

Inorganic heterogeneous catalysts of a few metal oxides, an alkali-loaded zeolite, and smectites are effective for the CO_2 cycloaddition in the absence of any organic solvent. Furthermore, their activities are enhanced by the co-presence of basic organic solvents. This enhancement is ascribed to the cooperative activation of the epoxide ring by the metal center and the base (Scheme 2.2). Synergistic effect is observed on immobilization of organic bases including imidazolium halides on inorganic solids having surface hydroxyl groups. This is also explained by a similar cooperative activation mechanism (Scheme 2.4). Highly active heterogeneous bifunctional catalyst systems can also be realized by modification (treatment with zinc halide or substituting with alkyl diol) of imidazolium halides immobilized on polymers (Scheme 2.5). One of ZIFs, which are a new class of porous materials, can be used for the CO_2 cycloaddition.

DMC can be produced from CO_2 and methanol in the presence of potassium carbonate as a catalyst and methyl iodide as a promoter; however, the catalyst is deactivated by transformation to potassium iodide, and methyl iodide acts as a reactant rather than a promoter (Scheme 2.6). Even in the absence of methyl iodide, ZrO_2-based catalysts can selectively catalyze the DMC synthesis, and the removal of H_2O from the reaction system is essential to get high DMC yields because of the reaction equilibrium limitation.

For the cyclic carbonate synthesis from CO_2 and glycol, CeO_2–ZrO_2 is selective, but it can give only low product yields because of the reaction equilibrium limitation. Organic bases (tetraalkyl ammonium halides, adenine) immobilized on zeolite or Ti-SBA-15 can give excellent product yields for the synthesis of carbamates from CO_2, primary amines, and alkyl halides. Also for this reaction, the coexistence of acid Ti sites and base sites is suggested to be an important factor. MgO/ZrO_2 is effective for the synthesis of quinazoline-2,4(1H,3H)-diones from CO_2 and aminobenzonitriles. Graphitic carbon nitride can catalyze the oxidation of benzene to phenol with CO_2 that would be a new and highly desirable route for the utilization of CO_2.

References

1. Edwards JH (1995) Potential sources of CO_2 and options for its large–scale utilization now and in future. Catal Today 23:59–66
2. Aresta M, Tomasi I (1997) Carbon dioxide utilization in the chemical industry. Energy Convers Manage 38(Suppl):S373–S378
3. Arakawa H, Aresta M, Armor JM et al (2001) Catalysis research of relevance to carbon management: progress, challenges and opportunities. Chem Rev 101:953–996
4. Zevenhoven R, Eloneva S, Teir S (2006) Chemical Fixation of CO_2 in carbonates: routes to valuable products and long–term storage. Catal Today 115:73–79
5. Ono Y (1997) Catalysis in the production and reactions of dimethyl carbonate, an environmentally benign building block. Appl Catal A Gen 155:133–166
6. Bigi F, Maggi R, Sartori G (2000) Selected synthesis of ureas through phosgene substitutes. Green Chem 2:140–148
7. Sakakura T, Choi JC, Yasuda H (2007) Transformation of carbon dioxide. Chem Rev 107:2365–2387
8. Sakakura T, Kohno K (2009) The synthesis of organic carbonates from carbon dioxide. Chem Commun, pp 1312–1330
9. Shaikh AA, Sivaram S (1996) Organic carbonates. Chem Rev 96:951–976
10. Yano T, Matsui H, Koike T et al (1997) Magnesium oxide-catalysed reaction of carbon dioxide with an epoxide with retention of stereo chemistry. Chem Commun, pp 1129–1130
11. Yamaguchi K, Ebitani K, Yoshida T et al (1999) Mg-Al mixed oxides as highly active acid–base catalysts for cycloaddition of carbon dioxide to epoxides. J Am Chem Soc 121:4526–4527
12. Bhanage BM, Fujita S, Ikushima Y, Arai M (2001) Synthesis of dimethyl carbonate and glycols from carbon dioxide, epoxides and methanol using heterogeneous basic metal oxide catalysts with high activity and selectivity. Appl Catal A Gen 219:259–266
13. Tu M, Davis RJ (2001) Cycloaddition of CO_2 to epoxides over solid base catalysts. J Catal 199:85–91
14. Nishiyama Y, Arai M, Guo SL et al (1993) Catalytic properties of hectorite-like smectites containing nickel. Appl Catal A Gen 95:171–181
15. Fujita S, Bhanage BM, Ikushima Y et al (2002) Chemical fixation of carbon dioxide to propylene carbonate using smectite catalysts with high activity and selectivity. Catal Lett 79:95–98
16. Bhanage BM, Fujita S, Ikushima Y et al (2003) Synthesis of dimethyl carbonate and glycols from carbon dioxide, epoxides and methanol using heterogeneous Mg containing smectite catalysts: effect of reaction variables on activity and selectivity performance. Green Chem 5:71–75
17. Yasuda H, He LN, Sakakura T (2002) Cyclic carbonate synthesis from supercritical carbon dioxide and epoxide over lanthanide oxychloride. J Catal 209:547–550
18. Arest M, Dibenedetto A, Gianfrate L et al (2003) Nb(V) compounds as epoxides carboxylation catalysts: the role of the solvent. J Mol Catal A Chem 204–205:245–252
19. Srivastava R, Srinivas D, Ratnasamy P (2003) Synthesis of polycarbonate precursors over titanosilicate molecular sieves. Catal Lett 91:133–139
20. Mori K, Mitani Y, Hara T et al (2005) A single-site hydroxyapatite-bound zinc catalyst for highly efficient chemical fixation of carbon dioxide with epoxides. Chem Commun, pp 3331–3333
21. Sun J, Fujita S, Arai M (2005) Development in the green synthesis of cyclic carbonate from carbon dioxide using ionic liquids. J Organometal Chem 690:3490–3497
22. North M, Pasquale R, Young C (2010) Synthesis of cyclic carbonates from epoxides and CO_2. Green Chem 12:1514–1539
23. Srivastava R, Srinivas D, Ratnasamy P (2005) Zeolite–based organic–inorganic hybrid catalysts for phosgene–free and solvent–free synthesis of cyclic carbonates and carbamates at mild conditions utilizing CO_2. Appl Catal A Gen 289:128–134

24. Srivastava R, Srinivas D, Ratnasamy P (2005) CO_2 activation and synthesis of cyclic carbonates and alkyl/aryl carbamates over adenine-modified Ti-SBA-15 solid catalysts. J Catal 233:1–5
25. Takahasi T, Watanuki T, Kitazume S et al (2006) Synergistic hybrid catalyst for cyclic carbonate synthesis: remarkable acceleration caused by immobilization of homogeneous catalyst on silica. Chem Commun, pp 1664–1666
26. Sakai T, Tsutsumi Y, Ema T (2008) Highly active and robust organic–inorganic hybrid catalyst for the synthesis of cyclic carbonates from carbon dioxide and epoxides. Green Chem 10:337–341
27. Dai WL, Chen L, Yin SF et al (2010) 3-(2-hydroxyethyl)-1-propylimidazolium bromide immobilized on SBA-15 as efficient catalyst for the synthesis of cyclic carbonates via the coupling of carbon dioxide and epoxides. Catal Lett 135:295–304
28. Motokura K, Itagaki S, Iwasawa Y et al (2009) Silica-supported aminopyridinium halides for catalytic transformations of epoxides to cyclic carbonates under atmospheric pressure of carbon dioxide. Green Chem 11:1876–1880
29. Udayakumar S, Lee MK, Shim HL, Park DW (2009) Functionalization of organic ions on hybrid MCM-41 for cycloaddition reaction: the effective conversion of carbon dioxide. Appl Catal A Gen 365:88–95
30. Kim HS, Kim JJ, Kim H, Jang HG (2003) Imidazolium zinc tetrahalide-catalyzed coupling reaction of CO_2 and ethylene oxide or propylene oxide. J Catal 220:44–46
31. Palgunadi J, Kwon O-S, Lee H et al (2004) Ionic liquid-derived zinc tetrahalide complexes: structure and application to the coupling reactions of alkylene oxides and CO_2. Catal Today 98:511–514
32. Fujita S, Nishiura M, Arai M (2010) Synthesis of styrene carbonate from carbon dioxide and styrene oxide with various zinc halide-based ionic liquids. Catal Lett 135:263–268
33. Qiao K, Ono F, Bao Q et al (2009) Efficient synthesis of styrene carbonate from CO_2 and styrene oxide using zinc catalysts immobilized on soluble imidazolium-styrene copolymers. J Mol Catal A Chem 303:30–34
34. Watile RA, Desmukh KM, Dhake KP, Bhanage BM (2012) Efficient synthesis of cyclic carbonate from carbon dioxide using polymer anchored diol functionalized ionic liquids as a highly active heterogeneous catalyst. Catal Sci Technol 2:1051–1055
35. Huang X-C, Lin Y-Y, Zhang J-P, Chen X-M (2006) Ligand-directed strategy for zeolite-type metal-organic frameworks: zinc(II) imidazolates with unusual zeolitic topologies. Angew Chem Int Ed 45:1557–1559
36. Banerjee R, Furukawa H, Britt D et al (2009) Control of pore size and functionality in isoreticular zeolitic imidazolate frameworks and their carbon dioxide selective capture properties. J Am Chem Soc 131:3875–3877
37. Miralda CM, Macias EE, Zhu M et al (2011) Zeolitic imidazole freamwork-8 catalysts in the conversion of CO_2 to chloropropene carbonate. ACS Catal 2:180–183
38. Ono Y (1997) Dimethyl carbonate for environmentally benign reactions. Catal Today 35:15–25
39. Fang S, Fujimoto K (1996) Direct synthesis of dimethyl carbonate from carbon dioxide and methanol catalyzed by base. Appl Catal A Gen 142:L1–L3
40. Fujita S, Bhanage BM, Ikushima Y, Arai M (2001) Synthesis of dimethyl carbonate from carbon dioxide and methanol in the presence of methyl iodide and base catalysts under mild conditions: effect of reaction conditions and reaction mechanism. Green Chem 3:87–91
41. Tomishige K, Sakaihori T, Ikeda Y, Fujimoto K (1999) A novel method of direct synthesis of dimethyl carbonate from methanol and carbon dioxide catalyzed by zirconia. Catal Lett 58:225–229
42. Ikeda Y, Sakaihori T, Tomishige K, Fujimoto K (2000) Catalytic properties and structure of zirconia catalysts for direct synthesis of dimethyl carbonate from methanol and carbon dioxide. Catal Lett 66:59–62
43. Tomoshige K, Furusawa Y, Ikeda Y et al (2002) CeO_2–ZrO_2 solid solution catalyst for selective synthesis of dimethyl carbonate from methanol and carbon dioxide. Catal Lett 76:71–74

44. Jung KT, Bell AT (2001) An in situ infrared study of dimethyl carbonate synthesis from carbon dioxide and methanol over zirconia. J Catal 204:339–347
45. Jung KT, Bell AT (2001) Effects of catalyst phase structure on the elementary processes involved in the synthesis of dimethyl carbonate from methanol and carbon dioxide over zirconia. Top Catal 20:97–105
46. Tomishige K, Ikeda Y, Sakaihori T, Fujimoto K (2000) Promoting effect of phosphoric acid on zirconia catalysts in selective synthesis of dimethyl carbonate from methanol and carbon dioxide. J Catal 195:355–362
47. Jiang C, Guo Y, Wang C et al (2003) Synthesis of dimethyl carbonate from methanol and carbon dioxide in the presence of polyoxometalates under mild conditions. Appl Catal A Gen 256:203–212
48. Tomishige K, Kunimori K (2002) Catalytic and direct synthesis of dimethyl carbonate starting from carbon dioxide using CeO_2–ZrO_2 solid solution heterogeneous catalyst: effect of H_2O removal from the reaction system. Appl Catal A Gen 237:103–109
49. Li Z, Qin Z (2007) Synthesis of diphenyl carbonate from phenol and carbon dioxide in carbon tetrachloride with zinc halides as catalyst. J Mol Catal A Chem 264:255–259
50. Fan G, Fujita S, Zou B et al (2009) Synthesis of diphenyl carbonate from phenol and carbon dioxide in the presence of carbon tetrachloride with zinc chloride. Catal Lett 133:280–287
51. Fan G, Wang Z, Zou B, Wang B (2011) Synthesis of diphenyl carbonate from compressed carbon dioxide and phenol without use of organic solvent. Fuel Process Technol 92:1052–1055
52. Li Z, Su K (2007) The direct reaction between CO_2 and phenol catalyzed by bifunctional catalyst ZrO_2. J Mol Catal A Chem 277:180–184
53. Tomishige K, Yasuda H, Yoshida Y et al (2004) Catalytic performance and properties of ceria based catalysts for cyclic carbonate synthesis from glycol and carbon dioxide. Green Chem 6:206–214
54. Patil YP, Tambade PJ, Parghi KD et al (2009) Synthesis of quinazoline-2,4(1*H*,3*H*)-diones from carbon dioxide and aminobenzonitriles using MgO/ZrO_2 as a solid base catalyst. Catal Lett 133:71–74
55. Patil YP, Tambade PJ, Jagtop SR, Bhange BM (2008) Cesium carbonate catalyzed efficient synthesis of quinazoline-2,4(1*H*,3*H*)-diones using carbon dioxide and 2-aminobenzonitriles. Green Chem Lett Rev 1:127–132
56. Patil YP, Tambade PJ, Desmukh KM et al (2009) Synthesis of quinazoline-2,4(1*H*,3*H*)-diones from carbon dioxide and aminobenzonitriles using [Bmim]OH as a homogeneous recyclable catalyst. Catal Today 148:355–360
57. Goettmann F, Thomas A, Antonietti M (2007) Metal-free activation of CO_2 by mesoporous graphitic carbon nitride. Angew Chem Int Ed 46:2717–2720
58. Ansari MB, Min B-H, Mo Y-H, Park S-E (2011) CO_2 activation and promotional effect in the oxidation of cyclic olefins over mesoporous carbon nitrides. Green Chem 13:1416–1421

Chapter 3
Indirect Utilisation of Carbon Dioxide in Organic Synthesis for Valuable Chemicals

Rahul A. Watile, Bhalchandra M. Bhanage, Shin-ichiro Fujita, and Masahiko Arai

3.1 Introduction

Carbon dioxide (CO_2) has attracted much attention from the scientific community because of its potential greenhouse effect as a result of its steadily increasing concentrations in the atmosphere [1–4]. Moreover, CO_2 is nontoxic, nonflammable, abundant and economical C1 feedstock. Currently, carbon dioxide is used industrially for the synthesis of urea, salicylic acid, inorganic carbonates, methanol, cyclic carbonates and polycarbonates [2–7]. Major emphasis is to replace phosgene-based routes by introducing CO_2 into organic substrates for synthesis of various chemicals [5].

However, in industry, around 105 million tons of CO_2 are utilised for the production of urea. On the other hand, cyclic carbonates (80,000 t), salicylic acid (90,000 t) and polypropylene carbonate (70,000 t) are produced on industrial scale [6, 8]. In addition to these commercial industrial processes using CO_2, there are a lot of interesting approaches for the application of CO_2. The simplest kind of reaction is the insertion of CO_2, e.g. to obtain carbamates [6, 9, 10], carboxylated allyl derivatives [11], acetic acid [12, 13], dialkyl carbonates [14–17], polypyrones [18], lactones [19–21] and polyurethanes [22, 23]. Although a lot of research has been done on CO_2 fixation reaction, there is still a challenge in utilising the CO_2 as such in organic transformation due to the requirement of high reaction temperatures (250–300 °C) and high pressures (50–100 atm) as well as thermodynamics limitations in such direct reaction [24–27]. The development of a practical catalytic

R.A. Watile • B.M. Bhanage (✉)
Department of Chemistry, Institute of Chemical Technology, Mumbai 400019, India
e-mail: bm.bhanage@ictmumbai.edu.in

S.-i. Fujita • M. Arai
Division of Chemical Process Engineering, Faculty of Engineering, Hokkaido University, Sapporo 060-8626, Japan
e-mail: marai@eng.hokudai.ac.jp

B.M. Bhanage and M. Arai (eds.), *Transformation and Utilization of Carbon Dioxide*, Green Chemistry and Sustainable Technology, DOI 10.1007/978-3-642-44988-8_3,

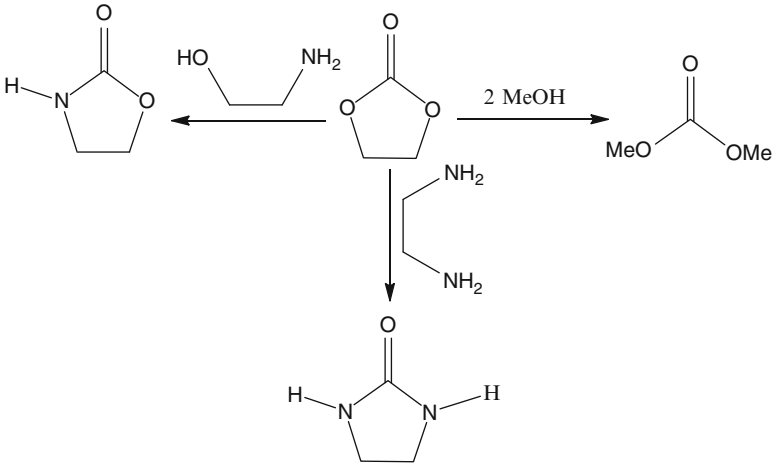

Scheme 3.1 Organic carbonate used as sources of carbon dioxide for the industrially important chemicals

system for CO_2 fixation reaction still remains a challenge, as high activation energy barriers have to be overcome for the cleavage of the C–O bonds of CO_2 [28].

Cyclic carbonates are valuable synthetic targets; since their commercialisation in the mid-1950s, the coupling of CO_2 to epoxide to cyclic carbonates is one of the most promising reactions in this area of replacing existing poisonous phosgene-based synthesis. Cyclic carbonates have interesting applications as excellent aprotic polar solvents, electrolytes in secondary batteries, engineering plastics and as raw materials in the synthesis of polycarbonates and polyurethanes [10, 29–31]. Recently, it has been shown that organic carbonates, e.g. EC, PC and DMC, can be used as a carbonylation reagent for several organic transformations such as producing various important chemicals such as dimethyl carbonate (DMC) via transesterification of EC with methanol. Furthermore, these carbonates have been successfully applied to the carbonylation of bifunctional substrates, such as diamines, and amino alcohols which have been converted into cyclic carbamates [32–34], N,N-bis(hydroxyalkyl)ureas [35, 36] and cyclic ureas [37]. Detailed developments in these areas are discussed here (Scheme 3.1). Salicylic acid is a crucial intermediate for the synthesis of Aspirin. More than 100 years ago, the Kolbe–Schmitt reaction for the synthesis of salicylic acid was developed and still it is a topic of research [6, 8].

CO_2 hydrogenation is an example that produces various chemicals depending on the catalysts used. Effective copper-based catalysts have been explored for the methanol synthesis from CO_2 [38]. Recently, the direct reduction of CO_2 to methanol at mild conditions [39] and the development of new highly active catalysts for the production of formic acid and its derivatives by CO_2 hydrogenation are still desirable [40–44]. The hydrogenation of carbon dioxide to CO, methane or methanol has been far less explored, as these reactions are unfavourable from a

thermodynamic point of view. The hydrogenation of CO_2 into CH_3OH has been extensively investigated, and Cu-/Zn-based catalyst was found to be highly selective, but under relatively harsh reaction conditions (250 °C, 50 atm) [45, 46]. Therefore, the methanol production from CO_2 by direct hydrogenation under mild reaction conditions is still a great challenge for both academia and industry [42, 47–49]. Recently Milstein and co-workers developed an indirect approach from CO_2 to methanol through homogeneous hydrogenation of carbonates or carbamates using pincer-type Ru(II) catalysts, under mild conditions [50]. Especially, the hydrogenation of DMC has established a bridge from CO_2 to methanol [24], as DMC can be produced from CO_2 and methanol [51]. In the present chapter, we focus our results on many of these reactions (Scheme 3.1). Relevant studies by other research groups are also compared.

3.2 Use of Organic Carbonates as Carbonylation Reagent

In recent years, it has been observed that organic carbonates, e.g. dimethyl carbonate (DMC) and ethylene carbonate (EC), are of significant interest, because these compounds can be produced from CO_2 and used as a carbonylation reagent for several synthetic protocols. EC is produced in large scale from CO_2 with ethylene oxide. It can react with other compounds, producing several valuable chemicals (Scheme 3.1).

Organic carbonates are used as sources of CO_2 for the synthesis of industrially important chemicals (Scheme 3.1). This chapter mainly focuses on the ideal alternative routes for the synthesis of DMC, 1,3-disubstituted urea and 2-oxazolidinones/2-imidazolidinones via transesterification of EC with methanol, transamination of EC with primary amine and transamination reaction of EC with diamines/β-amino alcohols, respectively, which will be described in the following section. Milstein et al. reported for the first time catalytic hydrogenation of organic carbonates to methanol, their mild hydrogenation which can provide alternative and mild approaches to the indirect hydrogenation of CO_2. Detailed developments of indirect CO_2 fixation reactions will be described in the following section.

3.3 Synthesis of DMC via Transesterification of EC

DMC has drawn specific attention as a nontoxic, noncorrosive and environmentally friendly building block for the production of polycarbonates and variety of chemicals. DMC finds extensive applications as a solvent and an octane booster in gasoline to meet oxygenate specifications and is used as a starting material for organic synthesis via carbonylation and methylation as well as promising substitute for poisonous phosgene and dimethyl sulphate [52, 53]. In addition, it is used as an electrolyte in lithium batteries due to its high dielectric constant [54]. Traditionally,

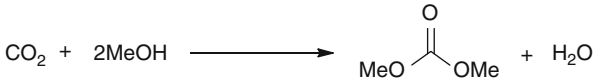

Scheme 3.2 Synthesis of DMC from CO_2

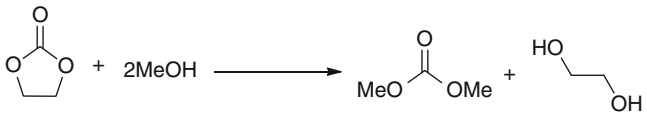

Scheme 3.3 Synthesis of DMC via transesterification of cyclic carbonate with methanol

DMC is synthesised by oxidative carbonylation of methanol (non-phosgene route) or by phosgenation of methanol. Both routes involve the use of poisonous and corrosive gases of chlorine, phosgene and carbon monoxide. Therefore, the development of green and efficient route for DMC synthesis is till desirable.

From the green chemistry point of view, direct synthesis of DMC from CO_2 is one of the promising reactions for the chemical fixation of CO_2 (Scheme 3.2) [2, 55], which is more attractive compared with other commercial processes including methanolysis of phosgene, carbon monoxide and carbonylation of methanol using toxic, corrosive, flammable and explosive gases. Various catalysts are reported for the direct synthesis of DMC from methanol and carbon dioxide, including organometallic compounds [56], CeO_2–ZrO_2 [57] and $H_3PW_{12}O_{40}$/ZrO_2 [58]. Among these catalysts, CeO_2–ZrO_2 showed a significant catalytic activity for direct synthesis of DMC from methanol and CO_2 due to its acid–base bifunctional property. Although several reports exist for the direct DMC synthesis, usually the reaction conditions employed are not mild, i.e. high reaction temperatures, long reaction times and high CO_2 pressures are needed. So the development of more efficient and practical route for DMC synthesis is still desired.

DMC can also be synthesised via one-pot reaction directly from epoxides, CO_2 and methanol [59]; however, undesired side reaction such as ring opening of epoxides by methanol led to relatively lower DMC selectivity. The more promising approach for synthesis of DMC based on transesterification of cyclic carbonates with methanol comes forward (Scheme 3.3). The process for the synthesis of DMC from the transesterification of EC with methanol was developed by Texaco Chemical [60] (Scheme 3.3). Recently, Zhang et al. reported carboxylic functionalised imidazolium ionic liquid as a catalyst for transesterification of cyclic carbonates with methanol to DMC [61]. Ju et al. reported that DMC was prepared from methanol and EC in the presence of 1-alkyl-3-methylimidazolium ionic liquids at 160 °C and 2 MPa CO_2 [62]. Yang et al. reported DMC synthesis (with 81 % yield) via transesterification of EC with methanol, and it was achieved by employing the Lewis basic ILs derived from DABCO as efficient and recyclable catalysts [63]. Most of the reported heterogeneous catalysts require harsh reaction conditions like high temperature and pressure to obtain even a moderate yield of DMC

[64–67]. Feng et al. used amino-functionalised MCM-41 as a heterogeneous catalyst to obtain 44 mol% DMC yield at 160 °C [68]. Kinfton and Duranleau reported organic phosphine/amine catalysts supported on partially cross-linked polymer for the synthesis of DMC which gave 58 % conversion of EC [69]. Tatsumi et al. reported K-TS-1 as an effective catalyst with DMC yield of 57 % [64]. Watanabe and Tatsumi demonstrated the use of Mg–Al hydrotalcite materials as an active catalyst for transesterification reaction and they observed 70 % EC conversion with 58 % DMC yield. The major drawback of all mentioned heterogeneous catalyst systems is that they gave lower yields of DMC. Although great advances have been made, most of the catalytic system suffer from low catalytic activity, high reaction temperature and the use of expensive metallic compounds that are often required. There is a need to develop a suitable catalytic system for the synthesis of DMC via transesterification of cyclic carbonate. After considering all the merits and the demerits of the reported methods, one of our contribution in the investigation of transesterification of EC with methanol for synthesis of DMC is using poly-4-vinyl pyridine (PVP) as a novel, homogeneous recyclable base catalyst [70] (Scheme 3.3). Basic properties of the catalyst was examined by temperature programmed desorption (TPD) of adsorbed CO_2 using a conventional flow reactor. Basicity of PVP is responsible for high activity and selectivity for the synthesis of DMC. Optimisation of the reaction parameters were investigated for the transesterification reaction of EC with methanol in presence of PVP which results in the formation of DMC and EG. The higher conversion of EC (96 %) and higher yield of DMC (82 %) and EG (75 %) was observed at 140 °C reaction temperature, 20 wt-% of PVP loading and for reaction time of 4 h. It has been observed that the CO_2 pressure does not have any influence on the conversion of EC and yield of DMC/EG. It was found that the catalyst could be active up to three consecutive recycles without significant loss in its catalytic activity and selectivity.

3.4 Synthesis of 2-Oxazolidinones/2-Imidiazolidinones via Transesterification of EC with β-Amino Alcohols/1,2-Diamines

Synthesis of five-member oxazolidinones and imidiazolidinones, possessing wide application as intermediates, chiral auxiliaries and building blocks for biologically active pharmaceutical agents, in organic synthesis are desirable [71, 72]. They show good antibacterial properties, hence widely used in pharmaceuticals, cosmetics, pesticides and so on. Chiral 2-oxazolidinones have been used as chiral auxiliaries in a wide range of asymmetric synthesis [73–75]. 2-Imidiazolidinones have recently attracted much attention due to their diverse applications as intermediates for biologically active pharmaceutical molecules, such as the HIV protease inhibitors, DMP 323 and DMP 450 [76]. The developments of greener and efficient route for

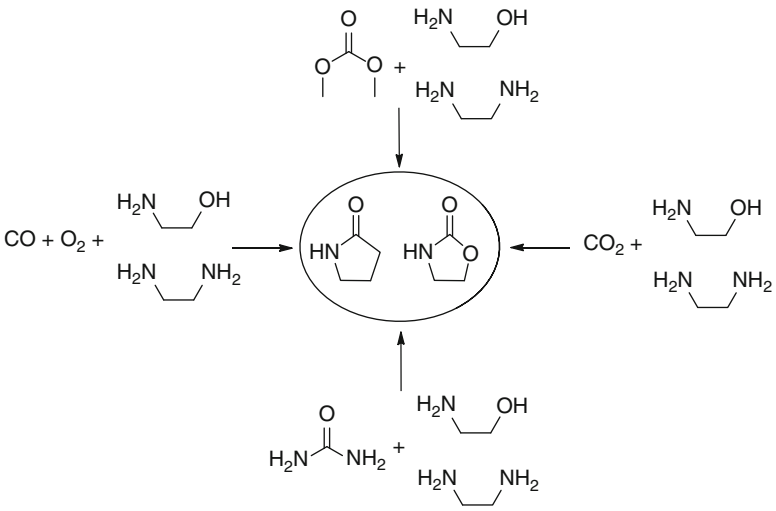

Scheme 3.4 Various routes for the synthesis of 2-imidiazolidinones and 2-oxazolidinones

synthesis of 2-oxazolidinones/2-imidiazolidinones have attracted much more attention in recent years.

Usually 2-imidiazolidinones and 2-oxazolidinones are synthesised by carbonylation of 1,2-diamines and β-amino alcohols with several reagents like phosgene [77], urea, dialkyl carbonates [78, 79] or the mixture CO/O_2 via oxidative carbonylation (Scheme 3.4). However, the mentioned synthesis routes are often associated with the use of high pressure, high temperature, formation of side product like polyurea and risk associated with explosion hazards using CO/O_2 mixtures [80, 81].

Direct addition of CO_2 with alkylene diamines and amino alcohols to produce 2-imidiazolidinones and 2-oxazolidinones is the most desired route (Scheme 3.4). However, the synthesis is often associated with the use of high pressure and high temperature and formation of side product [82]. Hence, development of an alternative for improving the yield as well as selectivity is more desirable. The 2-imidiazolidinones/2-oxazolidinones could be synthesised using transamination reaction of EC with diamines/β-amino alcohols in the presence of a base catalyst (Scheme 3.5) [83]. This reaction can be considered as indirect CO_2 fixation reaction, since EC is synthesised with a quantitative yield by the cycloaddition of CO_2 to epoxides [84, 85]. Recently, Xiao et al. reported the synthesis of 2-imidiazolidinones/2-oxazolidinones from EC with 1,2-diamines/β-amino alcohols in the presence of a homogenous catalyst [83]. However, it suffers from the major drawback of catalyst–product separation. We investigated transamination reaction of EC with diamines/β-amino alcohols using heterogeneous base catalysts such as basic metal oxides for the first time, an indirect CO_2 fixation reaction [86] (Scheme 3.5). Several commercially available metal oxides such as MgO, CaO, ZnO, ZrO_2, CeO_2 and La_2O_3 were screened for the reaction. The basic properties of

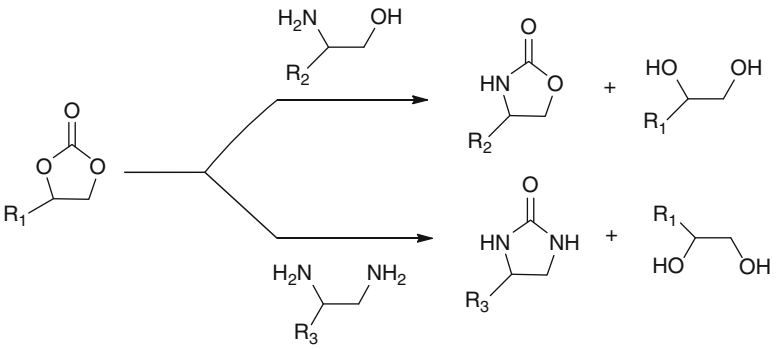

Scheme 3.5 Synthesis of 2-oxazolidinones/2-imidiazolidinones from cyclic carbonates and β-amino alcohols/1, 2-diamines

the catalysts were examined by temperature programmed desorption (TPD) of adsorbed CO_2 using a conventional flow reactor. It was observed that among the various metal oxide catalysts screened, only MgO gave excellent yield of 2-oxazolidinones (83 %) after 6 h. CaO and CeO_2 were also found to give good yield of 2-oxazolidinones 68 % and 72 %, respectively. The effects of various reaction parameters like reaction time, reaction temperature, solvent effect and catalyst loading on the reaction system were also examined. It was observed that the yields of the 2-oxazolidinones were found to increase to 83 % at a temperature of 80 °C after the reaction time of 6 h in the ethanol solvent. It was observed that the catalyst can be reused for four conjugative recycle runs without any significant loss in the catalytic activity.

3.5 Synthesis of 1,3-Disubstituted Symmetrical/ Unsymmetrical Urea

1,3-Disubstituted ureas are very important classes of nitrogen-containing compounds, having a wide range of application in dyes for cellulose fibre, as antioxidants in gasoline, as corrosion inhibitors and intermediates for carbamate synthesis [87] as well as showing pharmacological and physiological activities. Recently, special interest in these compounds has arisen, since substituted ureas having amino acid group have been used for brain cancer treatment and were proven to have a marked inhibitory effect on HIV protease enzyme [88]. Traditionally, *N*,*N*′-alkyl aryl ureas and *N*,*N*′-dialkyl ureas are prepared by the nucleophilic addition of aryl amines and alkyl amines to phosgene or isocyanates. However, phosgene or isocyanates are highly toxic and hazardous reagents. Therefore, these routes are not considered as eco-friendly routes for the urea synthesis. Oxidative carbonylation of amine with CO is one of the phosgene-free alternative routes for the urea synthesis

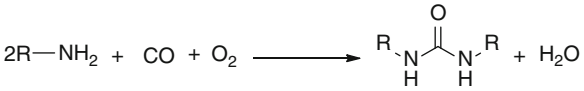

Scheme 3.6 Synthesis of substituted ureas via oxidative carbonylation of amines with CO

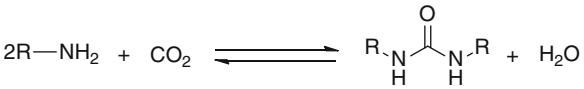

Scheme 3.7 Synthesis of substituted ureas from CO_2 and amines

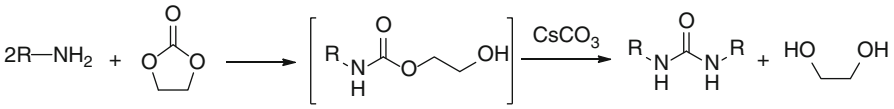

Scheme 3.8 Synthesis of symmetrical 1,3-disubstituted urea

(Scheme 3.6). Various homogeneous metal catalysts, including Au [89], Pd [90] and W [91], have been reported for the synthesis of 1, 3-disubstituted ureas via oxidative carbonylation. Deng et al. demonstrated the use of ZrO_2–SO_2 supported palladium catalyst for the synthesis of 1,3-disubstituted ureas [92]. This method suffers from the drawback associated with the tremendous toxicity of CO as well as the risk associated with the use of explosive mixture of CO and O_2. Hence, an idea of direct synthesis of 1,3-disubstituted ureas from CO_2 and amines came forward (Scheme 3.7) [93–98].

Different catalysts have been reported for the synthesis of 1, 3-disubstituted urea from CO_2, such as $RuCl_3 3H_2O/Bu_3P$ and Ph_3SbO/P_4S_{10} [99]. Water is formed during the course of reaction. The dehydrating agents such as $POCl_3$, propargyl alcohols [96], diorganophosphites [98], Me_3NSO_3 [97] and carbodiimide [95] are required to increase the yield of the target product. Vos and co-workers achieved the synthesis of symmetrical and unsymmetrical urea in good yields from CO_2 and amines using Cs^+ base catalysts and N-methylpyrrolidone as the solvent without a dehydrating agent [93]. With increasing demands for safer and cleaner processes, the hazardous phosgene process has to be essentially replaced by more environmentally friendly processes; e.g. the transesterification of EC with amine (Scheme 3.8) shows promise as a phosgene-free route.

From the literature, we observed that EC-based CO_2 fixation reactions have received much more attention to organic chemistry because these are considered to be indirect CO_2 fixation reactions. EC represents an effective carbonylating reagent [100] (Scheme 3.8). In 1998, Yasuoka et al. patented a synthesis of 1,3-disubstituted urea via transamination reaction of EC with an excess of butylamine in methanolic NaOMe solution (28 %) and in an autoclave at 100 °C. It gave the product 1,3-dibutylurea in 85 % yield [101]. There are very few reports

on transamination reaction between EC and amines. Arai and co-workers reported the synthesis of both symmetrical and unsymmetrical 1,3-disubstituted urea using alkali metal oxides as heterogeneous base catalyst for the first time [102, 103]. Recently, our group reported the synthesis of 1,3-disubstituted symmetrical/unsymmetrical urea via transamination of in situ generated 2-hydorxycarbamate (Scheme 3.8) [104] using Cs_2CO_3 as heterogeneous base catalysts. Various commercially available basic catalysts like alkali metal carbonates/hydroxides/halides were screened for the reaction. It can be seen that among the various base catalysts screened, only Cs_2CO_3 was the most successful base delivering 1,3-dibutylurea in quantitative yield. Other carbonate bases were not as effective for the transamination reaction. The high catalytic reactivity of Cs_2CO_3 is attributed to the unprecedented 'cesium effect' [104, 105] and due to the softness of Cs cation, which makes Cs_2CO_3 highly soluble in reaction mixture. Hence, we thought this methodology therefore will contribute to existing cesium base-promoted transformations, whereas alkali metal halide was found to be inactive for the synthesis of 1,3-dibutylurea. Hence, in order to optimise reaction conditions, we examined the effect of temperature and reaction time on the 1,3-disubstituted urea synthesis. It has been observed that at 90 °C, Cs_2CO_3 gives 91 % yield of the 1,3-dibutylurea. The reaction was carried out using various aliphatic primary, secondary and heterocyclic as well as aromatic amines. It was observed that aliphatic primary amines could efficiently react with EC in the presence of Cs_2CO_3, which leads to the formation of corresponding symmetrical 1,3-disubstituted ureas. Unfortunately, aromatic amines and secondary amine are unreactive under the given optimised reaction condition.

3.6 Synthesis of Unsymmetrical 1,3-Disubstituted Ureas

On the basis of the results obtained for the synthesis of symmetrical 1,3-disubstituted urea, we next directed our attention towards the synthesis of unsymmetrical 1,3-disubstituted urea (Scheme 3.9). Recently, Saliu et al. reported the solventless method for the synthesis of unsymmetrical ureas via transamination reaction between EC and amines using 1,5,7-Triazabicyclo[4.4.0]dec-5-ene (TBD) and thioureas as organocatalysts for this reaction [106]. We developed a two-step procedure for the synthesis of unsymmetrical ureas (Scheme 3.9). In the first step a primary amine reacts with EC to give the corresponding 2-hydroxyethylcarbamate at 70 °C for 1 h in the absence of a catalyst [107]. In the second step, the 2-hydroxyethylcarbamate reacts in the presence of Cs_2CO_3 base catalyst with another primary amine or with a secondary amine to give disubstituted or trisubstituted ureas, respectively. Although this method is fast and providing high yield, the formation of symmetrical ureas as side products is its major drawback, and column chromatography is needed to obtain the desired products in high purity. Hence, development of more efficient, easily prepared and one-pot protocol for the synthesis of unsymmetrical 1,3-disubstituted urea is still highly desired.

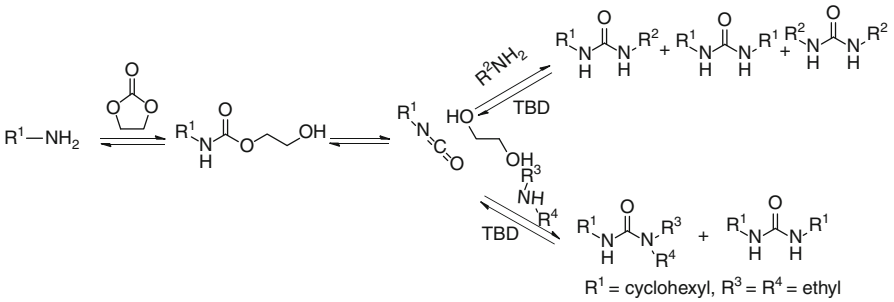

Scheme 3.9 Synthesis of unsymmetrical 1,3-disubstituted urea via transamination of EC with amines

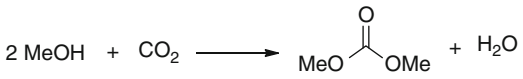

Scheme 3.10 Synthesis of DMC from carbon dioxide

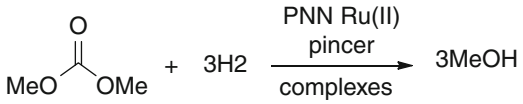

Scheme 3.11 Hydrogenation of organic carbonates (such as DMC) to methanol

3.7 Efficient Hydrogenation of Organic Carbonates: Alternative Routes to Methanol Based on CO_2

The industrial production of methanol by direct hydrogenation of CO_2 under mild conditions is an attractive goal, but a practical catalytic process has not yet been developed. Methanol is an important fuel and synthetic building block, industrially produced from syngas at high temperatures (250–300 °C) and high pressures (50–100 atm) using a copper oxide-based catalyst [25]. Hydrogenation of methyl formate to methanol is known [43, 108–111]. However, this method suffers from drawback such as the formation of CO by-product from the decomposition of methyl formate, making it less attractive for large-scale application. In contrast, the carbonylation of methanol to DMC [112] or oxidative carbonylation to DMC and the synthesis of DMC from CO_2 are known and well investigated [4] (Scheme 3.10).

To the best of our knowledge, the hydrogenation of organic carbonates (such as dimethyl carbonate) to methanol remains unknown [109, 113]. Milstein et al. reported the first examples of catalytic hydrogenation of dimethyl carbonate to methanol [114] (Scheme 3.11). They used PNN Ru(II) pincer complexes derived from pyridine- and bipyridine-based tridentate ligands. Thus, catalytic hydrogenation

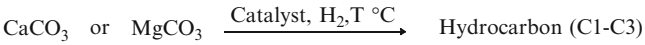

Scheme 3.12 Catalytic hydrogenation of calcium carbonate to hydrocarbons

of the organic carbonates to methanol under mild conditions could provide an indirect method to obtain methanol from CO_2. These new reactions provide interesting alternatives for the mild hydrogenation of CO_2 to methanol representing the ultimate '*green*' reactions, which is a timely topic in the context of the 'methanol economy' [24]. Further developments of catalyst and process design will still be needed for this reaction to be industrialised.

3.8 Direct Conversion of Calcium Carbonate to Hydrocarbons

One of the central challenges in the twenty-first century is the sufficient and sustainable supply of energy. At present, we derive more than 80 % of our energy from fossil fuels [115]. Inorganic carbonates constitute nontoxic, nonflammable, inexpensive natural source of carbon. Therefore, the objective of investigating the direct conversion of these carbonates into hydrocarbons is of considerable importance (Scheme 3.12).

Replacing gaseous CO_2 with solid inorganic carbonates which are abundantly present in nature, such as calcite ($CaCO_3$) and dolomite ($MgCO_3$), has many inherent advantages. In the decomposition of the carbonates, the recarbonisation process can be used to keep the resources renewable for the production of fuels and chemicals. Here, we focused on inorganic carbonates, instead of gaseous CO_2, as a source of carbon to form methane and studied the efficiency of the conversion. CNR Rao and co-workers reported for the first time the catalytic hydrogenation of inorganic carbonates to methane using Co/CoO/CaO as mixed metal oxide-based catalytic protocol (Scheme 3.12) [116]. This route can be considered as an indirect hydrogenation of CO_2 as they can be rapidly replenished by the carbonation process from CO_2. Recently, the same group reported the hydrogenation of $CaCO_3$ to form C1–C3 hydrocarbons, in the presence of iron-based catalysts [117]. Such a study would also be relevant to convert carbonaceous inorganic rocks to organics, which can be of importance in the future. The research on catalytic hydrogenations of inorganic carbonates must be developed further.

3.9 Conclusions and Future Trends

This chapter addresses recent contribution to the development of innovative and environmentally friendly chemical processes based on CO_2. The utilisation of CO_2 in organic synthesis is important with regard to securing carbon resources as well as

mitigating the greenhouse effect. It is noteworthy that cyclic carbonate synthesis has already been an industrialised process. However, the development of new catalysts for this reaction continues to be a fruitful area of research, and recent advance such as alkali metal halide-supported liquid phase catalyst (SLPC) and silica-supported catalysts have the potential to allow this industrial process to be in actual practice. The synthesis of DMC and direct hydrogenation of CO_2 to methanol are attractive goals in organic synthesis, but a practical catalytic process has not yet been developed because of the reaction equilibrium and chemical inertness of CO_2. The preferred alternatives are the transesterification of EC with methanol, transamination reaction of EC with diamines/β-amino alcohols and catalytic hydrogenation of DMC, an indirect route to methanol from CO_2. Further significant developments in catalysis and process design will occur in the next few years; thus, CO_2 can be used for synthesis of industrially important chemicals which can be used to help to limit global CO_2 emissions.

Additionally, the future of CO_2 lies in its viable conversion to CO via partial reduction using renewable source of hydrogen, and once we can get CO at ambient conditions, it opens new avenues for CO-based well-known chemistry. This reaction is overlooked so far, and research in this direction is required.

References

1. Jessop PG, Ikariya T, Noyori R (1995) Homogeneous catalysis in supercritical fluids. Science 269:1065–1069
2. Aresta M, Quaranta E (1997) Carbon dioxide: a substitute for phosgene. Chemtech 27:32–40
3. Shaikh AA, Shivaram S (1995) Organic carbonates. Chem Rev 96:951–957
4. Sakakura S, Choi JC, Yasuda H (2007) Transformation of carbon dioxide. Chem Rev 107:2365–2387
5. Pierre B, Dominque M, Dominique N (1988) Reaction of carbon dioxide with carbon -carbon bond formation catalyzed by transition-metal complexes. Chem Rev 88:747–764
6. Aresta M (2003) Carbon dioxide recovery and utilization. (A summary report of the EU Project BRITE-EURAM 1998 BBRT-CT98-5089.) Kluwer Academic Publishers, Dordrecht, 407 pp
7. Lindsey AS, Jeskey H (1957) The Kolbe-Schmitt reaction. Chem Rev 57:583–620
8. Gibson DH (1996) The organometallic chemistry of carbon dioxide. Chem Rev 96:2063–2096
9. Chaturvedi D, Ray S (2006) Versatile use of carbon dioxide in the synthesis of carbamates. Monatsh Chem 137:127–145
10. Rohr M, Geyer C, Wandeler R, Schneider MS, Murphy EF, Baiker A (2001) Solvent-free ruthenium-catalysed vinylcarbamate synthesis from phenylacetylene and diethylamine in supercritical carbon dioxide. Green Chem 3:123–125
11. Shi M, Nicholas KM (1997) Palladium-catalyzed carboxylation of allyl stannanes. J Am Chem Soc 119:5057–5058
12. Shi DX, Feng YQ, Zhong SH (2004) Photocatalytic conversion of CH_4 and CO_2 to oxygenated compounds over Cu/CdS–TiO_2/SiO_2 catalyst. Catal Today 98:505–509
13. Wilcox EM, Roberts GW, Spivey JJ (2003) Direct catalytic formation of acetic acid from CO_2 and methane. Catal Today 88:83–90

14. Sakakura T, Choi J, Saito CY, Sako T (2000) Synthesis of dimethyl carbonate from carbon dioxide: catalysis and mechanism. Polyhedron 19:573–576
15. Iwakabe K, Nakaiwa M, Sakakura T, Choi JC, Yasuda H, Takahashi T, Ooshima Y (2005) Reaction rate of the production of dimethyl carbonate directly from the supercritical CO_2 and methanol. J Chem Eng Jpn 38:1020–1024
16. Aresta M, Dibenedetto A, Fracchiolla E, Giannoccaro P, Pastore C, Papai I, Schubert G (2005) Mechanism of formation of organic carbonates from aliphatic alcohols and carbon dioxide under mild conditions promoted by carbodiimides. J Org Chem 70:6177–6186
17. Tomishige K, Sakaihori T, Ikeda Y, Fujimoto K (1999) A novel method of direct synthesis of dimethyl carbonate from methanol and carbon dioxide catalyzed by zirconia. Catal Lett 58:225–229
18. Tsuda T, Maruta K, Kitaike Y (1992) Nickel (0)-catalyzed alternating copolymerization of carbon dioxide with diynes to poly(2- pyrones). J Am Chem Soc 114:1498–1499
19. Behr A, Heite M (2000) Telomerization of carbon dioxide and 1, 3-butadiene: process development in a miniplant. Chem Eng Technol 23:952–955
20. Schulz PS, Walter O, Dinjus E (2005) Facile synthesis of a tricyclohexylphosphine-stabilized η3-allyl-carboxylato Ni(II) complex and its relevance in electrochemical butadiene carbon dioxide coupling. Appl Organomet Chem 19:1176–1179
21. Takimoto M, Mori M (2002) Novel catalytic CO_2 incorporation reaction: nickel-catalyzed regio- and stereoselective ring-closing carboxylation of bis-1,3-dienes. J Am Chem Soc 124:10008–10009
22. McGhee W, Riley D, Christ K, Pan Y, Parnas B (1995) Carbon dioxide as a phosgene replacement: synthesis and mechanistic studies of urethanes from amines, CO_2 and alkyl chlorides. J Org Chem 60:2820–2830
23. Ochiai B, Inoue S, Endo T (2005) One-pot non-isocyanate synthesis of polyurethanes from bisepoxide, carbon dioxide and diamine. J Polym Sci Part A Polym Chem 43:6613–6618
24. Olah GA, Geoppert A, Surya Prakash GK (2009) Beyond oil and gas: the methanol economy, 2nd edn. Wiley-VCH, Weinheim
25. Bart JCJ, Sneeden JJF (1987) Copper-zinc oxide-alumina methanol catalysts revisited. Catal Today 2:1–124
26. Weissermel K, Arpe HJ (2003) Industrial organic chemistry. Wiley-VCH, Weinheim, pp 30–36
27. Hansen JB, Nielsen PEH (2008) In: Ertl G, Knçzinger H, Schüth F, Weitkamp J (eds) Handbook of heterogeneous catalysis, vol 6, 3rd edn. Wiley-VCH, Weinheim, pp 2920–2949
28. Omae I (2006) Aspects of carbon dioxide utilization. Catal Today 115:33
29. Behr A (1988) Carbon dioxide as an alternative C1 synthetic unit: activation by transition-metal complexes. Angew Chem Int Ed Engl 27:661–678
30. Elvers B, Hawkins S, Schulz G (eds) (1992) Ullmann's encyclopedia of industrial chemistry A, vol 21, 5th edn. VCH, Weinheim, p 207
31. Beckman EJ (1999) Making polymers from carbon dioxide. Science 283:946–947
32. Giannoccaro P, Dibenedetto A, Gargano M, Quaranta E, Aresta M (2008) Interaction of palladium(II) complexes with amino-alcohols: synthesis of new amino-carbonyl complexes, key intermediates to cyclic carbamates. Organometallics 27:967–975
33. Gabriele B, Salerno G, Brindisi D, Costa M, Chiusoli GP (2000) Synthesis of 2-oxazolidinones by direct palladium-catalyzed oxidative carbonylation of 2-amino-1-alkanols. Org Lett 2:625–627
34. Gabriele B, Mancuso R, Salerno G, Costa DM (2003) An improved procedure for the palladium-catalyzed oxidative carbonylation of β-amino alcohols to oxazolidin-2-ones. J Org Chem 68:601–604
35. Giannoccaro P, Ferragina C, Gargano M, Quaranta E (2010) Pd-catalysed oxidative carbonylation of amino alcohols to N, N′-bis(hydroxyalkyl)ureas under mild conditions using molecular oxygen as the oxidant. Appl Catal A Gen 375:78–84
36. Diaz DJ, Hylton KG, McElwee-White L (2006) Selective catalytic oxidative carbonylation of amino alcohols to ureas. J Org Chem 71:734–738

37. Qian F, McCusker JE, Zhang Y, Main AD, Chlebowski M, Kokka M, McElwee-White L (2002) Catalytic oxidative carbonylation of primary and secondary diamines to cyclic ureas. Optimization and substituent studies. J Org Chem 67:4086–4092
38. Ushikoshi K, Mori K, Watanabe T, Saito M (1998) A 50 kg/day class test plant for methanol synthesis from CO_2 and H_2 Study. Surf Sci Catal 114:357–364
39. Das S, Mçller K, Junge K, Beller M (2011) Zinc-catalyzed chemoselective reduction of esters to alcohols. Chem Eur J 17:7414
40. Darensbourg DJ, Ovalles C, Pala M (1983) Homogeneous catalysts for carbon dioxide/hydrogen activation. Alkyl formate production using anionic ruthenium carbonyl clusters as catalysts. J Am Chem Soc 105:5937–5939
41. Tsai JC, Nicholas KM (1992) Rhodium-catalyzed hydrogenation of carbon dioxide to formic acid. J Am Chem Soc 114:5117–5124
42. Jessop PJ, Ikariya T, Noyori R (1995) Homogeneous hydrogenation of carbon dioxide. Chem Rev 95:259–272
43. Jessop PJ, Hisiao Y, Ikariya T, Noyori R (1996) Homogeneous catalysis in supercritical fluids: hydrogenation of supercritical carbon dioxide to formic acid, alkyl formates, and formamides. J Am Chem Soc 1996(118):344–355
44. Tominaga K, Sasaki Y, Kawai M, Watanabe T, Saito M (1993) Ruthenium complex catalysed hydrogenation of carbon dioxide to carbon monoxide, methanol and methane. J Chem Soc Chem Commun 7:629
45. Boddien A, Gärtner F, Federsel C, Piras I, Junge H, Jackstell R, Beller M (2012) In: Ding K, Dai L-X (eds) Organic chemistry: breakthroughs and perspectives. Wiley-VCH, Weinheim, pp 683–722
46. Wang W, Wang SP, Ma XB, Gong JL (2011) Recent advances in catalytic hydrogenation of carbon dioxide. Chem Soc Rev 40:3703
47. Marinus JM, Nico SW, Hiemstra H, Poetsch E, Casutt M (1995) Synthesis of D-(+)-biotin through selective ring closure of N-acyliminium silyl enol ethers. Angew Chem 34–21:2391–2393
48. Leitner W (1995) Carbon dioxide as a raw material: the synthesis of formic acid and its derivatives. Angew Chem Int Ed Engl 34:2207
49. Ma J, Sun N, Zhang X, Zhao N, Mao F, Wei W, Sun Y (2009) A short review of catalysis for CO_2 conversion. Catal Today 148:221
50. Balaraman E, Gunanathan C, Zhang J, Shimon LJW, Milstein D (2011) Efficient hydrogenation of organic carbonates, carbamates and formates indicates alternative routes to methanol based on CO_2 and CO. Nat Chem 3:609
51. Dixneuf PH (2011) Bifunctional catalysis: a bridge from CO_2 to methanol. Nat Chem 3:578
52. Sato Y, Yamamoto T, Souma Y (2000) Poly(pyridine-2,5-diyl)-CuCl2 catalyst for synthesis of dimethyl carbonate by oxidative carbonylation of methanol: catalytic activity and corrosion influence. Catal Lett 65:123–126
53. Pacheco MA, Marshall CL (1997) Review of dimethyl carbonate (DMC) manufacture and its characteristics as a fuel additive. Energy Fuels 11:2–29
54. Wei T, Sun Y (2003) Synthesis of dimethyl carbonate by transesterification over CaO/carbon composites. Green Chem 5:343
55. Jessop PG, Ikariya T, Noyori R (1999) Homogeneous catalysis in supercritical fluids. Chem Rev 99:475
56. Taniguchi T, Ogasawara K (1993) Lipase–triethylamine-mediated dynamic transesterification of a tricyclic acyloin having a latent meso-structure: a new route to optically pure oxodicyclopentadiene. Chem Commun 15:1399
57. Tomishige K, Furusawa Y, Ikeda Y, Asadullah M, Fujimoto K (2001) CeO_2–ZrO_2 solid solution catalyst for selective synthesis of dimethyl carbonate from methanol and carbon dioxide. Catal Lett 76:71
58. Jiang C, Guo Y, Wang C, Hu C, Wu Y, Wang E (2003) Synthesis of dimethyl carbonate from methanol and carbon dioxide in the presence of polyoxometalates under mild conditions. Appl Catal A Gen 256:203–212

59. Bhanage BM, Fujita S, Ikushima Y, Arai M (2001) Synthesis of dimethyl carbonate and glycols from carbon dioxide, epoxides, and methanol using heterogeneous basic metal oxide catalysts with high activity and selectivity. Appl Catal A Gen 219:259–266
60. Stinson S (1992) Edith M. Flanigen Wins Perkin Medal. Chem Eng News 10:25
61. Wang JQ, Sun J, Cheng WG, Shi CY, Dong K, Zhang XP, Zhang SJ (2012) Synthesis of dimethyl carbonate catalyzed by carboxylic functionalized imidazolium salt via transesterification reaction. Catal Sci Technol 2:600–605
62. Ju HY, Manju MD, Park DW (2007) Performance of ionic liquid as catalysts in the synthesis of dimethyl carbonate from ethylene carbonate and methanol. React Kinet Catal Lett 90:3
63. Yang ZZ, He LN, Dou XY, Chanfreau S (2010) Dimethyl carbonate synthesis catalyzed by DABCO-derived basic ionic liquids via transesterification of ethylene carbonate with methanol. Tetrahedron Lett 51:2931–2934
64. Tatsumi T, Watanabe Y, Koyano KA (1996) Synthesis of dimethyl carbonate from ethylene carbonate and methanol using TS-1 as solid base catalyst. Chem Commun 19:2281–2283
65. Sriniwas D, Srivasatava R, Ratnasamy P (2004) Transesterifications over titanosilicate molecular sieves. Catal Today 96:127–133
66. Fujita S, Arai M (2005) Chemical fixation of carbon dioxide: synthesis of cyclic carbonate, dimethyl carbonate, cyclic urea and cyclic urethane. J Japan Pet Inst 48:67
67. Li Y, Zhao XQ, Wang YJ (2004) Synthesis of dimethyl carbonate from propylene oxide, carbon dioxide and methanol on KOH/4A molecular sieve catalyst. Chin J Cat 25:633
68. Feng SJ, Lu ZB, He R (2004) Tertiary amino group covalently bonded to MCM-41 silica as heterogeneous catalyst for the continuous synthesis of dimethyl carbonate from methanol and ethylene carbonate. Appl Catal A Gen 272:347–352
69. Knifton JF, Duranleau RG (1991) Ethylene glycol-dimethyl carbonate cogeneration. J Mol Catal 67:389–399
70. Jagtap SR, Bhanushali MJ, Panda AG, Bhanage BM (2008) Synthesis of dimethyl carbonate via transesterification of ethylene carbonate with methanol using poly-4-vinyl pyridine as a novel base catalyst. Catal Commun 122:1928–1931
71. Dyen ME, Swern D (1967) 2-Oxazolidones. Chem Rev 67:197–246
72. Pancartov VA, Frenkel TM, Fainleib AM (1983) 2-Oxazolidinones. Russ Chem Rev 52:576–593
73. Kudo N, Taniguchi M, Furuta S, Endo T, Honma T (1998) Synthesis and herbicidal activities of 4-substituted 3-aryl-5-tert-butyl-4-oxazolin-2-ones. Agric Food Chem 46:5305–5312
74. O'Hagan D, Tavasli M (1999) 1, 2-amino alcohols and their heterocyclic derivatives as chiral auxiliaries in asymmetric synthesis. Tetrahedron Asymmetry 10:1189
75. Ager DJ, Prakash I, Schaad DR (1961) 2-Amino alcohols and their heterocyclic derivatives as chiral auxiliaries in asymmetric synthesis. Chem Rev 96:835–875
76. Hodge CN, Lam PYS, Eyermann CJ, Jadhav PK, Fernandez Ru Y, De Lucca CH, Chang CH, Kaltenbach RJC, Aldrich PE (1998) Calculated and experimental low-energy conformations of cyclic urea HIV protease inhibitors. J Am Chem Soc 120:4570–4581
77. Puschin NA, Mitic RV (1937) Compounds of phosgene with hexamethylenetetramine, m-toluidine and ethylenediamine. Justus L Ann Chem 532:300
78. Fu Y, Baba T, Ono Y (2001) Carbonylation of o-phenylenediamine and o-aminophenol with dimethyl carbonate using lead compounds as catalysts. J Catal 197:91–97
79. Baba T, Kobayashi A, Yamauchi T, Tanaka H, Aso S, Inomata M, Kawanami Y (2002) Catalytic methoxycarbonylation of aromatic diamines with dimethyl carbonate to their dicarbamates using zinc acetate. Catal Lett 82:193–197
80. Bhanage BM, Fujita SI, Ikushima Y, Arai M (2004) Non-catalytic clean synthesis route using urea to cyclic urea and cyclic urethane compounds. Green Chem 6:78–80
81. Bhanage BM, Fujita SI, Ikushima Y, Arai M (2003) Synthesis of cyclic ureas and urethanes from alkylene diamines and amino alcohols with pressurized carbon dioxide in the absence of catalysts. Green Chem 5:340–342

82. Bank MR, Cadgan JIG, Thomas DE (1991) 1,3-Oxazolidin-2-ones from 1H-aziridines by a novel stratagem which mimics the direct insertion of CO_2. J Chem Soc Perkin Trans I 1:961–962
83. Xiao LF, Xu LW, Xia CG (2007) A method for the synthesis of 2-oxazolidinones and 2-imidazolidinones from five-membered cyclic carbonates and -aminoalcohols or 1,2-diamines. Green Chem 9:369–372
84. Tu M, Davis RJ (2001) Cycloaddition of CO_2 to epoxides over solid base catalysts. J Catal 199:85–91
85. Sun J, Fujita SI, Bhanage BM, Arai M (2004) One-pot synthesis of styrene carbonate from styrene in tetrabutylammonium bromide. Catal Today 93–95:383–388
86. Jagtap SR, Patil YP, Fujita SI, Arai M, Bhanage BM (2008) Heterogeneous base catalyzed synthesis of 2-oxazolidinones/2- imidiazolidinones via transesterification of ethylene carbonate with β-aminoalcohols/1,2-diamines. Appl Catal A Gen 341:133–138
87. Bigi F, Maggi R, Sartori G (2000) Selected syntheses of ureas through phosgene substitutes. Green Chem 2:140–148
88. Getman DP, DeCrescenzo GA, Heintz RM, Reed KL, Talley JJ, Bryant ML, Clare M, Houseman KA, Marr JJ, Mueller RA, Vazquez HML, Shieh S, Stallings WC, Stageman RA (1993) Discovery of a novel class of potent HIV-1 protease inhibitors containing the (R)-(hydroxyethyl)urea isostere. J Med Chem 1993(36):288–291
89. Shi F, Deng Y (2001) First gold(I) complex-catalyzed oxidative carbonylation of amines for the syntheses of carbamates. Chem Commun 5:443–444
90. Bartolo G, Salerno G, Mancuso R, Costa M (2004) Efficient synthesis of ureas by direct palladium- catalyzed oxidative carbonylation of amines. J Org Chem 69:4741–4750
91. McCusker JE, Main AD, Johnson KS, Grasso CA, McElwee-White L (2000) W(CO)6-Catalyzed oxidative carbonylation of primary amines to N, N′-disubstituted ureas in single or biphasic solvent systems optimization and functional group compatibility studies. J Org Chem 65:5216–5222
92. Shi F, Deng YY, Sima TL, Yang HZ (2001) A novel ZrO_2–SO_2– supported palladium catalyst for syntheses of disubstituted ureas from amines by oxidative carbonylation. Tetrahedron Lett 42:2161–2163
93. Ion A, Parvulescu V, Jacobs P, De Vos D (2007) Synthesis of symmetrical or asymmetrical urea compounds from CO_2 via base catalysis. Green Chem 9:158–161
94. Jiang T, Ma X, Zhou Y, Liang S, Zhang J, Han B (2008) Solvent-free synthesis of substituted ureas from CO_2 and amines with a functional ionic liquid as the catalyst. Green Chem 10:465–469
95. Ogura H, Tekeda K, Tokue R, Kobayashi T (1978) A convenient direct synthesis of ureas from carbon dioxide and amines. Synthesis 5:394–396
96. Fournier J, Bruneau C, Dixneuf PH, Lecolier S (1991) Ruthenium-catalyzed synthesis of symmetrical N, N-dialkylureas directly from carbon dioxide and amines. J Org Chem 56:4456–4458
97. Cooper CF, Falcone SJ (1995) A simple one-pot procedure for preparing symmetrical diarylureas from carbon dioxide and aromatic amines. Synth Commun 25:2467–2475
98. Yamazaki N, Higashi F, Iguchi T (1974) Carbonylation of amines with carbon dioxide under atmospheric conditions. Tetrahedron Lett 13:1191–1194
99. Nomura R, Hasegawa Y, Ishimoto M, Toyosaki T, Matsuda H (1992) Carbonylation of amines by carbon dioxide in the presence of an organoantimony catalyst. J Org Chem 57:7339–7342
100. Aresta M, Quaranta E, Tommasi I, Giannocarro P, Ciccarese A (1995) Enzymic versus chemical carbon dioxide utilization. Part I. The role of metal centers in carboxylation reactions. Gazz Chim Ital 125:509
101. Hayashi T, Yasuoka JEP (1998) 846679 (to Sumika Fine Chemicals Co.)
102. Fujita S, Bhanage BM, Arai M (2004) Synthesis of N, N-disubstituted urea from ethylene carbonate and amine using CaO. Chem Lett 33:742–743

103. Fujita S, Bhanage BM, Kanamura H, Arai M (2005) Synthesis of 1,3-dialkylurea from ethylene carbonate and amine using calcium oxide. J Mol Catal A Chem 230:43–48
104. Galli C (1992) "Cesium ion effect" and macrocyclization. A critical review. Org Prep Proced Int 24:287–307
105. Ostrowicki A, Vogtle F (1992) In: Weber E, Vogtle F (eds) Topics in current chemistry, vol 161. Springer, Heidelberg, p 37
106. Saliu F, Rindone B (2010) Organocatalyzed synthesis of ureas from amines and ethylene carbonate. Tetrahedron Lett 51:6301–6304
107. Jagtap SR, Patil YP, Fujita SI, Arai M, Bhanage BM (2009) Synthesis of 1,3-disubstituted symmetrical/unsymmetrical ureas via Cs_2CO_3- catalyzed transamination of ethylene carbonate and primary amines. Synth Commun 39:2093–2100
108. Jessop PG, Joo F, Tai CC (2004) Recent advances in the homogeneous hydrogenation of carbon dioxide. Coord Chem Rev 248:2425
109. Federsel C, Jackstell R, Beller M (2010) State-of-the-art catalysts for hydrogenation of carbon dioxide. Angew Chem Int Ed 49:6254–6257
110. Yu KMK, Yeung CMY, Tsang SC (2007) Carbon dioxide fixation into chemicals (methyl formate) at high yields by surface coupling over a Pd/Cu/ZnO nanocatalyst. J Am Chem Soc 129:6360
111. Tanaka R, Yamashita M, Nozaki K (2009) Catalytic hydrogenation of carbon dioxide using Ir (III) − pincer complexes. J Am Chem Soc 131:14168
112. Lee JS, Kim JC, Kim YG (1990) Methyl formate as a new building block in C1 chemistry. Appl Catal 57:1–30
113. Federsel C, Jackstell R, Boddien A, Laurenczy G, Beller M (2010) Ruthenium-catalyzed hydrogenation of bicarbonate in water. ChemSusChem 3:1048
114. Balaraman E, Gunanathan C, Zhang J, Shimon LJW, Milstein D (2011) Efficient hydrogenation of organic carbonates, carbamates and formates indicates alternative routes to methanol based on CO_2 and CO. Nat Chem 13:609
115. World Energy Council (WEC) (2010) http://worldenegy.org/wec-geis/
116. Jagadeesan D, Eswaramoorthy M, Rao CNR (2009) Investigations of the conversion of inorganic carbonates to methane. ChemSusChem 2:878
117. Jagadeesan D, Sundarayya Y, Madras G, Rao CNR (2013) Direct conversion of calcium carbonate to C1–C3 hydrocarbons. RSC Adv 3:7224

Chapter 4
Hydrogenation and Related Reductions of Carbon Dioxide with Molecular Catalysts

Carolin Ziebart and Matthias Beller

Abbreviations

Bcat	catecholborane
Bpin	pinacolborane
bpy	bipyridine
cat.	catalyst
Cp*	pentamethylcyclopentadienyl
Cy	cyclohexyl group
DBU	1,8-diazabicycloundec-7-ene
DFT	density functional theory
DHBP	4,4′-dihydroxy-2,2′-bipyridine
DHPT	4,7-dihydroxy-1,10-phenanthroline
DMFC	direct methanol fuel cells
dmpe	1,3-bis(dimethylphophino)ethane
dppm	1,2-bis(diphenylphosphino)methane
dppp	1,3-bis(diphenylphosphino)propane
EMIMCl	1-ethyl-3-methylimidazolium chloride
FLP	frustrated Lewis pairs
hex	hexyl group
IL	ionic liquid
iPr	isopropyl group
IR	infrared spectroscopy
KIE	kinetic isotope effect
MD	molecular dynamics
Me	methyl group
Mes	mesityl groups

C. Ziebart • M. Beller (✉)
Leibniz-Institute für Katalyse Eingetragener Verein an der Universität Rostock, Albert-Einstein Straße 29a, Rostock 18059, Germany
e-mail: Matthias.Beller@catalysis.de

B.M. Bhanage and M. Arai (eds.), *Transformation and Utilization of Carbon Dioxide*, Green Chemistry and Sustainable Technology, DOI 10.1007/978-3-642-44988-8_4,

MTA	methanol-to-aromatics
MTD	metadynamics
MTG	methanol-to-gasoline
MTO	methanol-to-olefins
*m*tppms	sodium diphenylphosphinobenzene-3-sulfonate
NHC	N-heterocyclic carbene
NMR	nuclear magnetic resonance spectroscopy
OAc	acetoxy group
OTf	triflate group
Ph	phenyl group
PNP	pincer ligand (P donor atoms on the side arms N ~ in the middle); analogue PNN PCP
RT	room temperature
SDQ	single doubles quadruples
tBu	tert-butyl group
TOF	turnover frequency
TON	turnover number
TMP	tetramethylpiperidine
TS	transition state
Verkade's base	2,8,9-triisopropyl-2,5,8,9-tetraaza-1-phosphabicyclo-[3, 3, 3]undecane
X	halide anions such as Cl^- Br^-

4.1 Introduction

In today's chemical industry, most of the product chains are based on fossil resources like petroleum, coal, or natural gas. Although it is known that these resources are limited, the major part is "just" burned as fuels, and CO_2 is emitted into the atmosphere with incalculable risks for climate change [1].

Therefore, new concepts for the future have to be developed to meet the increasing demand of energy and materials by ensuring environmental safety. Using the abundant greenhouse gas CO_2 as C1 building block to produce chemicals and fuels would close the anthropogenic carbon cycle and save natural resources [2].

However, the thermodynamic stability and the low reactivity of CO_2 require highly active catalysts and high energy starting materials. Nature shows that such a transformation is practicable. By using photosynthesis, the biological reduction of CO_2 with sunlight and water to organic carbohydrates, $385 \cdot 10^9$ t of CO_2 is fixed annually net [3]. Therefore, enzymes and different kind of mechanism have been evolved and optimized in billions of years by nature. Biochemical studies on active sites of these enzymes can be of benefit for understanding and developing new synthetic catalysts capable of CO_2 activation [4].

In the last decades, chemists have followed this dream and pioneering work toward catalytic transformation of CO_2 has been reported [5–7]. Especially, the reduction of CO_2 to products of higher hydrogen content is of great interest. For example, direct hydrogenation of CO_2 to MeOH with green, nonfossil-based hydrogen is discussed to be a key step for building up a methanol economy as MeOH can be converted into fuels as well as valuable chemicals such as olefins and aromatics [6, 8, 9].

Despite all improvements in the last years, the catalyst costs of homogeneous catalysts for hydrogenation of CO_2 are still too high for industrial applications and only few heterogeneous processes are established [10, 11]. However, in the last 10 years significant progress was observed that makes it more likely that industrial processes based on homogeneous catalysis will be set up, too.

This chapter summarizes recent developments in this field starting at 2005 including hydrogen and other hydride reagents. Earlier findings have been well presented by Jessop, Leitner, and others [12–15].

Before 2005, active catalyst systems have been developed to give HCOOH and formamides and their mechanism have been intensively studied. However, the separation of HCOOH from base and catalyst as well as the use of CO_2 as hydrogen storage material have been neglected—but are hot topics in this decade. Following the principles of Green Chemistry, new systems have been developed in the last years using green solvents, ambient conditions, bio-inspired catalysts, as well as non-precious metals [16]. As the combustion of fossil fuels is one of the major reasons for increasing CO_2 amount in the atmosphere, the synthesis of fuels out of CO_2 using clean, nonfossil-based H_2 is highly desirable [17]. Therefore, reducing CO_2 to MeOH or CH_4 is of great interest, and promising catalytic systems have been reported recently for gaining MeOH. Homogeneous catalysts capable of hydrogenating CO_2 to CH_4 with H_2 are still unreported, but interesting activities have been achieved using a combination of boranes and silanes.

4.2 Hydrogenation of CO_2/HCO_3^- to Formic Acid Derivatives

$$\begin{aligned} &HCO_3^- + H_2 \longrightarrow HCO_2^- + H_2O \\ &CO_2 + H_2 \xrightarrow{\text{base}} HCO_2H \cdot \text{base} \xrightarrow[-H_2O]{ROH} HCOOR \\ &CO_2 + H_2 \xrightarrow[-H_2O]{HNR_2} HCONR_2 \end{aligned} \tag{4.1}$$

The direct hydrogenation of CO_2 to HCOOH is an endergonic reaction. Therefore, base is often applied to drive the thermodynamics by proton transfer. Available products are formates, formic acid–base adducts, as well as alkyl formates in the presence of alcohols and formamides by using primary or secondary amines (Eq. 4.1).

Catalytic systems reported before 2005 are usually noble-metal systems with mono- or bisphosphine ligands as well as a few examples of bipyridine-based ligand structures. The best catalyst presented until 2005 is the $(PMe_3)_4RuCl(OAc)$ catalyst from Jessop which hydrogenates CO_2 at 50 °C and 200 bar of H_2/CO_2 with high TON of 32,000 and an astonishing TOF of 95,000 h^{-1} [18].

Since then, new ligand structures have been developed and applied successfully in the hydrogenation of CO_2 to formic acid derivatives. This section gives an overview of recent results subdivided by ligand classes.

4.2.1 Using Mono- and Bidentate Phosphine Ligands

As mentioned above, the Ru trimethylphosphine catalyst system [18] was one of the most active ones until 2005. Regarding the high interest in understanding the mechanism, several computational and analytical studies have been reported identifying possible reaction species (Scheme 4.1). All of them have in common that a Ru dihydride species **1** with four phosphine ligands exists. The dissociation of one phosphine ligand leads to *cis*-$Ru(H)_2(PMe_3)_3$. Here, Sakaki started his investigations with DFT and MP4(SDQ) methods to figure out differences between this real catalyst and the model catalyst *cis*-$Ru(H)_2(PH_3)_3$ [19]. As the PMe_3 group is more donating than its analog, the trialkyl phosphine ligand showed a stronger *trans*-influence than PH_3. Both, strong donating ligands and polar solvents, made the CO_2 insertion into the metal-H bond more favorable. This step is proposed to be the rate-determining step in the hydrogenation of CO_2 with **2** in absence of water. The catalytic cycle can be described in the following steps: CO_2 insertion into Ru(II)-H, isomerization of the ruthenium(II)-η^1-formate intermediate **3**, six-centered σ-bond-metathesis of the η^1-formate with a dihydrogen molecule **4**, and dissociation of formic acid to give again the dihydride species (Scheme 4.1, phosphine dissociation mechanism (a), phosphine groups are drawn as P for clarity).

Taking into account that water was observed to accelerate the catalytic system, the group of Sakaki presented a second computational study using *cis*-$Ru(H)_2(PMe_3)_3(H_2O)_2$ as catalytic intermediate [20]. They figured out that aqua ligands can accelerate the nucleophilic attack of the hydride ligand on the CO_2 molecule by forming hydrogen bonds (**6**). The resulting ruthenium(II)-η^1-formate **3** isomerizes fast in the presence of water which suppresses the deinsertion of CO_2. The rate-determining step now is believed to be the coordination of the H_2 molecule to the ruthenium(II)-η^2-formate complex. The last step, the heterolytic H_2 cleavage, is facilitated again by water molecules (**7**). However, Jessop's NMR results have been inconsistent with such a phosphine dissociation mechanism. For this reason, he proposed a different cycle based on the unsaturated, cationic ruthenium species $[(PMe_3)_4RuH]^+$ **8** [21]. This mechanism also explains the necessity of the added base. The base on the one hand traps the formic acid and on the other hand helps to form the active catalytic species by abstracting a hydride ligand leading from **1** to **8**.

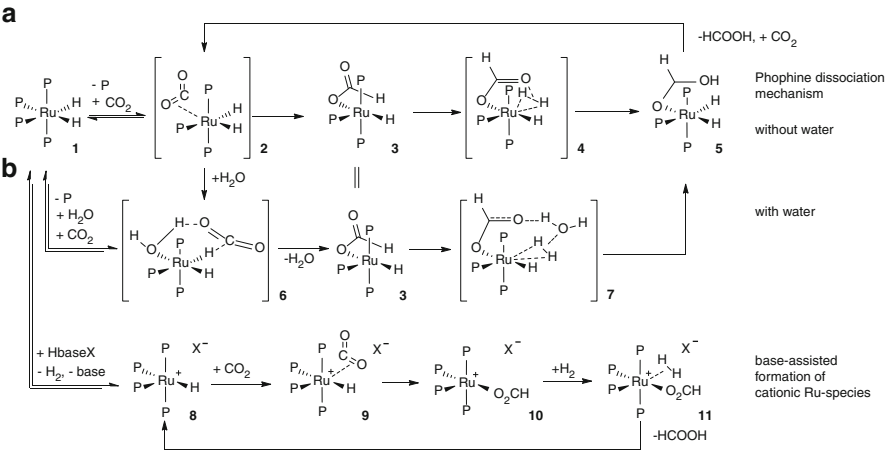

Scheme 4.1 Two different reaction pathways for the $(PMe_3)_4RuCl(OAc)$ system proposed by Sakaki and Jessop

Most recently, our group synthesized benzoyl- and naphthoyl-substituted phosphines which are stable to air and moisture [22]. The related Ru complexes showed good activity in the bicarbonate reduction with H_2 at 80 °C (TON up to 1,600). CO_2 as well as carbonyl compounds could be hydrogenated, too.

Using simple phosphite ligands at the Ru center such as [*trans*-$RuCl_2\{P(OMe)_3\}_4$], the group of Thiel achieved good TON up to 6,630 and TOF of 1,655 h^{-1} under supercritical conditions [23]. This was the first time phosphite ligands have been shown to form active complexes for the hydrogenation of CO_2. However, the application of the expensive base DBU in the presence of C_6F_5OH is a drawback and an exchange through cheaper bases is highly desirable.

Taking advantage of the water-accelerating effect, Zhao and Joó published a water-soluble [$RhCl(m$tppms$)_3$] catalyst capable of CO_2 hydrogenation to free formic acid in aqueous HCOONa solutions [24]. However, only low TON < 150 was observed after 20 h at 100 bar pressure (CO_2/H_2 – 1:1) and 50 °C. This might be due to the low basicity of the formate.

The hydrogenation of CO_2 to HCOOH is reversible. Hence, many catalyst systems have been developed which efficiently and selectively decompose HCOOH to hydrogen and CO_2 [25–27]. Hydrogen, ideally produced by renewable energy sources, for example, by electrolysis of water, is a potentially explosive, volatile gas which is usually stored in high pressure tanks [28–31]. By reacting it with CO_2 or bicarbonate, H_2 can be stored and transported easily as liquid or solid and H_2 can be released easily if needed. Therefore, researchers developed different systems capable of storing hydrogen based on CO_2/HCOOH or bicarbonate/formate. Both the groups of Papp and Joó [32] as well as our group [33] presented at the same time catalyst systems able of recharging H_2 based on a bicarbonate/formate cycle. In comparison to CO_2, bicarbonate is well soluble in water and its solutions are easy to handle and can be converted catalytically under mild conditions. As these systems work amine-free, no base evaporation is possible with the H_2 stream.

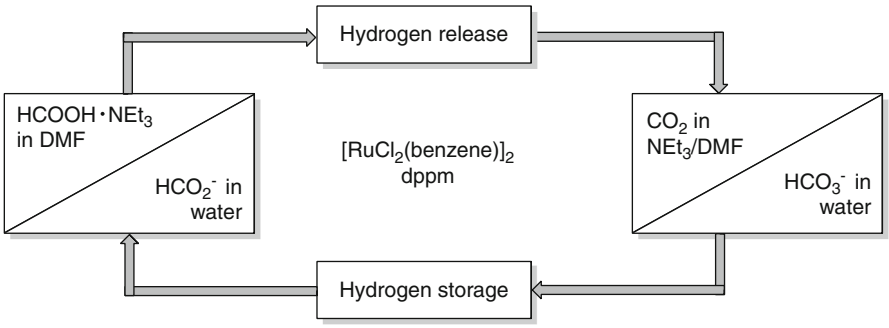

Scheme 4.2 One catalyst—two hydrogen storage systems based on CO_2 or bicarbonate by the group of Beller

Papp and Joó observed reversibility with the $[RuCl_2(m\text{tppms})_2]_2$ complex in aqueous bicarbonate solution in a sapphire NMR tube [32]. They showed three cycles of both the hydrogenation of bicarbonate to formate and the dehydrogenation of formate to bicarbonate. However, the decomposition of the formate slows down significantly at around 50 % conversion. Therefore, only half of the formate amount can be used for hydrogen storage in this system. Higher yields for the dehydrogenation of formates at even lower temperature (70 % at 40 °C) were shown by our group with a $[RuCl_2(\text{benzene})]_2$ precursor in the presence of 4 eq of dppm as ligand [33]. In comparison to earlier studies [34], the yields for the bicarbonate reduction could be improved to 96 % at 70 °C, using 80 bar of H_2 in a water-THF mixture without additional CO_2. A good TON of 1,108 was achieved after 2 h. Exchanging the sodium cation through NH_4^+ or Li^+, K^+, Mg^{2+}, and Ca^{2+}cations, the productivity decreases and often a significant amount of CO_2 is released with the H_2 during the formate decomposition. Our group also demonstrated that the catalyst is capable of hydrogen storage at RT based on CO_2/HCOOH·NEt_3 (Scheme 4.2). The catalyst system runs eight cycles without showing significant decrease in activity [35].

For the hydrogenation at RT, high formic acid amine ratios up to 2.31 were observed with TON up to 3,200. In addition, we could present an astonishing TON up to 800,000 for continuous H_2 liberation using $[RuCl_2(\text{benzene})]_2$ and dppe. However, it should be noted that the gravimetric hydrogen content of formic acid is limited to 4.4 % which is further reduced by the addition of amine or solvent.

To clarify possible reaction mechanisms for complexes with bidentate phosphine ligands, ab initio MTD and MD studies were performed by the group of Baiker for the dihydride catalyst $[Ru(dmpe)_2(H)_2]$ **13** [36]. This study was supported by further DFT calculations as well as IR and NMR experiments [37]. The authors concluded the coordination of molecular H_2 to the complex is the rate-determining step. That requires dissociation of the formate from the Ru center **14** to leave a free coordination site for the H_2. The formate anion then interacts weakly with the $Ru(H_2)^+$ complex **15** (Scheme 4.3). The activation energy for the H_2 adduct was found to be lower for the complex where the two hydrides are in *trans* position to each other (**13**). However, in solution more than 95 % of the *cis*-complex **12** was observed. The CO_2 insertion is

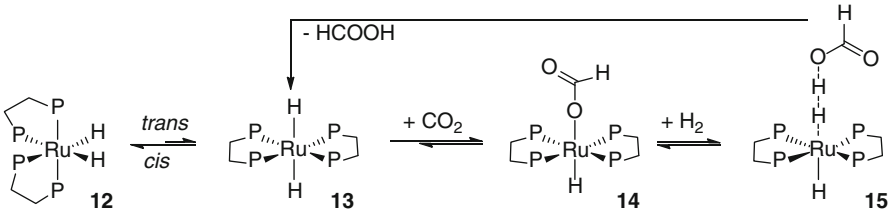

Scheme 4.3 Proposed mechanism for the $[Ru(dmpe)_2(H)_2]$ catalyzed CO_2 hydrogenation by Baiker

believed to happen via a concerted mechanism where the Ru-H bond breaks at the same time as the Ru-O-bond is formed. This can be imagined as a "formate ion" rotation.

Based on kinetic measurements by using stop-flow technique, Schindler's group calculated activation parameters for a Rh catalyst involving $[(dppp)_2RhH]$ as the active species [38]. For this complex, the following mechanism was proposed: the formation of an ionic Rh(I) formate complex through insertion of CO_2 into the Rh-H bond and subsequent dissociation of formate, followed by oxidative addition of H_2 to give an ionic Rh(III) dihydride formate complex which under reductive elimination of formic acid yields again the neutral Rh(I) complex.

In addition to catalyst variations and mechanistic studies, different kinds of concepts have been developed to solve the problem of the formic acid separation from base and catalyst. For example, the groups of Han and Leitner presented independently two systems based on ionic liquids. That the equilibrium of CO_2/H_2 to HCOOH is more favored in IL than in H_2O, due to the strong solvation of HCOOH in IL, was shown by Nakahara [39]. The idea of Han was to use an IL with an extra amine function **16** in combination with a ruthenium catalyst bound on silica [40]. By inserting a second amine function on the IL (**17**), the activity could be increased from 100 h^{-1} up to 920 h^{-1} TOF with a TON of 1,840 using 90 bar of H_2 and a total pressure of 180 bar [41]. Both systems were recycled four times using the procedure described in Fig. 4.1. Addition of water accelerates the reaction, maybe due to a decreased viscosity, interaction of water in the catalytic cycle, or bicarbonate formation as the true substrate.

Leitner and co-workers were using the IL as stationary phase containing the precursors $[Ru(cod)(methallyl)_2]$ and $PBu_4{}^+mtppms^-$ as well as additional base [42]. The formic acid extraction occurs with supercritical CO_2 in a continuous-flow single process unit where $scCO_2$ serves as mobile and extracting phase at the same time. With the base NEt_3 and EMIM Cl as IL, a TON of 516 was achieved after half an hour at 50 °C and 50 bar of both CO_2 and H_2. By exchanging the anion of the IL through HCO_2^- to give **18**, increased TON and TOF were observed.

Another interesting concept for the production and separation of pure formic acid was presented by Schaub and Paciello [43]. Key to success is the skillful choice of solvents by taking advantage of the diverse solubility and miscibility of all components (Fig. 4.2).

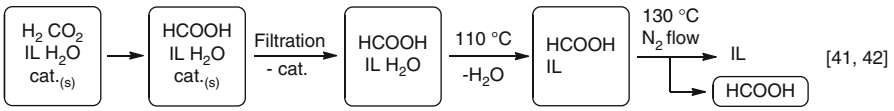

[41, 42]

or HCOOH extraction with $scCO_2$ as mobile phase and IL as stationary phase [43]

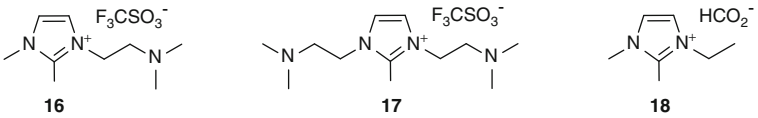

16 17 18

Fig. 4.1 Concepts for HCOOH separation using IL presented by Han and Leitner

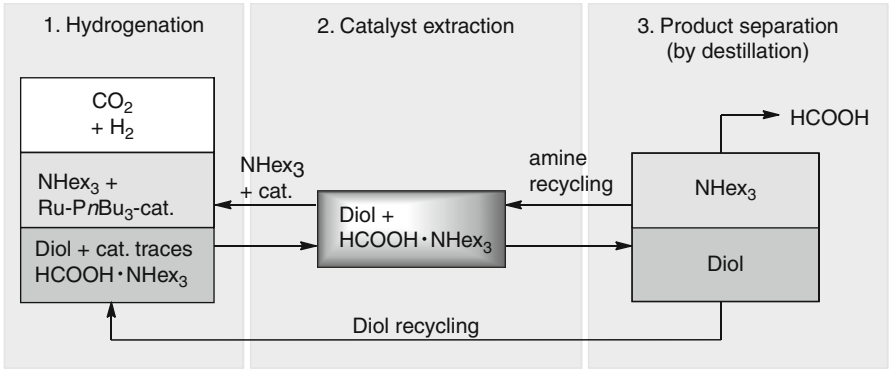

Fig. 4.2 Liquid-liquid phase process for formic acid formation and separation by Schaub and Paciello [43]

Here, in the first step, CO_2 is hydrogenated with the $[Ru(H)_2(PnBu_3)_4]$ catalyst in the presence of $NHex_3$ and a diol. The formed formic acid salts $[NHex_3 \cdot HCOOH]$ are not miscible in free amine, but good soluble in the diol phase. At the same time, most of the lipophilic catalyst stays in the unpolar amine phase. To get rid of the remaining catalyst traces, the diol phase is extracted with the resulting amine of the formic acid salt cleavage. The amine is then recycled to the hydrogenation vessel, whereas the formic acid salt enriched diol phase is treated thermally under mild conditions to give pure formic acid and free $NHex_3$ which forms again a two-phase system with the diol. Both phases are back transferred to close the process cycle.

4.2.2 Using Bipyridine-Based and Carbene-Type Ligands

A second ligand class known for CO_2 hydrogenation is based on the bipyridine structure. In this context, the groups of Ogo and Fukuzumi started kinetic

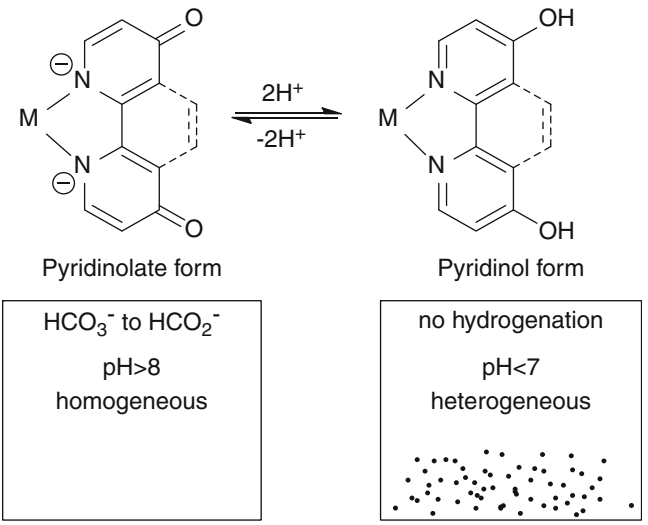

Scheme 4.4 pH switchable catalysts for CO_2 hydrogenation reported by Himeda

investigations of Ir(III) and Ru(II) bpy complexes in citric buffer solutions (pH = 3) to obtain pure formic acid [44]. By comparing TON in dependence of H_2 or CO_2 pressure, they concluded that in the case of ruthenium, the H_2 coordination to the corresponding aqua complex is rate determining. This is in contrast to the iridium complexes. Here, the authors believe that the rate-determining step is the CO_2 insertion into the active hydride complex.

By inserting hydroxy groups in *para*- or *ortho*-position at the pyridine rings, interesting behavior of the catalysts in dependence of the pH was reported. This ligand class shows an acid–base equilibrium between the pyridinol and pyridinolate form (Scheme 4.4) which influences the catalytic activity and water solubility.

In 2007, Himeda presented different catalysts for the CO_2 hydrogenation in aqueous KOH solutions to potassium formate using Ru, Ir, and Rh half-sandwich complexes bearing DHPT or DHBP ligands [45]. Under basic conditions, the deprotonated, water-soluble form exists showing strong electronic donation properties. High TON up to 220,000 was observed for an Ir DHPT complex at 120 °C and 60 bar of each CO_2 and H_2 in 48 h. Lowering the pH to acidic conditions, the pyridinol form of the catalyst predominates. The catalyst becomes insoluble in water and precipitates. Now, the catalyst can be reused easily and showed maintaining activity even after four cycles. To confirm the importance of the formation of the pyridinolate species, the hydroxy groups have been methylated resulting in significantly less active complexes. Other groups in *para*-position like carboxy or methyl groups are inferior, too [46]. For further details see review [47].

To study the effects of the ligand structure in more detail, Himeda and Fujita synthesized new iridium half-sandwich complexes differing in position and quantity of the hydroxy groups (Scheme 4.5).

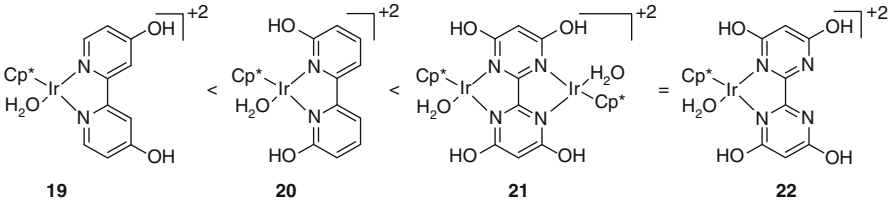

Scheme 4.5 Ligand structure study on the reactivity of Ir half-sandwich complexes by Himeda

Moving the hydroxy groups from *para* to *ortho* position (**19**–**20**) resulted in a rate enhancement by a factor of 2 comparing the initial TOF after 10 min [48]. Doubling both the quantity of the hydroxy groups as well as the amount of Ir centers **21**, another increase in the reactivity in order of 2.5 was observed for the hydrogenation of CO_2. Surprisingly, the dinuclear complex **22** showed similar activity as the mononuclear one with four hydroxy groups **21**. To explain these results, DFT studies and deuteration experiments have been performed [49]. The computational study identified the water-assisted heterolysis of H_2 to be the rate-determining step. This is in line with the NMR experiments as kinetic isotope effects of H_2O, H_2, and bicarbonate have only been observed for the ligands containing hydroxy groups in *ortho* position, not *para*. This is the first time a kinetic isotope effect was proved for the hydrogenation of CO_2, revealing that H_2O is involved in the rate-determining step. The significant increase in reactivity is believed to be caused by the high σ-donor strengths of the four O^- groups and the accelerated proton transfer by forming water bridges.

Using the binuclear Ir complex **21**, Himeda, Fujita, and Hull showed that their system is not only capable of CO_2 hydrogenation but also can decompose HCOOH to CO_2 and H_2 under acidic conditions [50]. High TON of 308,000 and very good TOF of 228,000 h^{-1} were achieved for the decomposition at 80–90 °C in the presence of HCOOH/HCOONa (1:1). Increasing the pH to basic conditions, the same catalyst hydrogenates CO_2 with TON of 153,000 and TOF of 53,800 h^{-1} in the presence of bicarbonate at 50 °C/80 °C. To rule out bicarbonate as only substrate, a test reaction without CO_2 was run yielding only a low formate production. However, long reaction times and the necessity of adding stoichiometric amounts of base or acid to switch the reaction make it so far unpractical for industrial application.

The same concept of hydrogen storage was reported by Fukuzumi using the water-soluble, proton-switchable phenylpyrazolyl organoiridium aqua complex **23** (Scheme 4.6) [51]. Both the hydrogenation of CO_2 under slightly basic conditions at RT under atmospheric pressure of H_2 and CO_2 and the formic acid decomposition under acidic conditions are possible. Due to KIE effects, the authors concluded that the rate-determining step is the formic acid decomposition via *β*-hydride elimination of the formate to release CO_2. In case of the hydrogenation of bicarbonate, both the catalyst and bicarbonate are believed to be involved in the rate-determining step as the TOF raises with increasing amount of bicarbonate. A more general view on these Ir-H complexes is presented in a review [52].

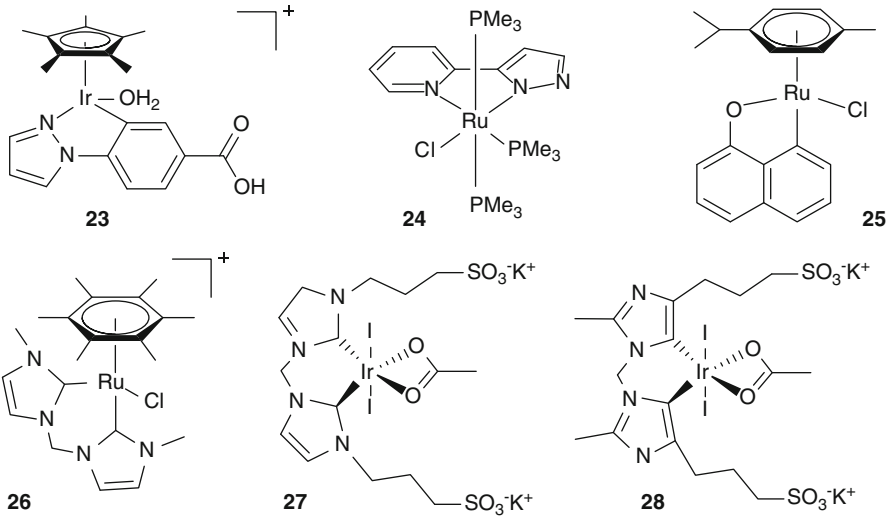

Scheme 4.6 Catalysts capable of HCOOH production by Fukuzumi, Thiel, Süss-Fink, and Peris

Further systems capable of CO_2 hydrogenation were presented by Niedner-Schatteburg, van Wüllen, and Thiel [53] using catalyst **24** and the group of Süss-Fink [54] including the arene ruthenium oxinato complex **25**. However, in all of these cases only moderate TONs were achieved.

Another interesting ligand class for the activation of CO_2 was discovered by Peris. A series of bis-*N*-heterocyclic carbene complexes with Ru **26** and Ir **27** were tested in both CO_2 hydrogenation and transfer hydrogenation [55]. As these chelating NHC ligands are known for their high thermal stability, reaction temperatures up to 200 °C are tolerated. Interestingly, if the carbene position is blocked by a methyl group, a bis-abnormal coordination of the NHC ligand to the iridium center is observed [56]. This complex **28** is even more active and the highest known TON of 1,320 was reported for transfer hydrogenation of CO_2 using *i*PrOH in aqueous KOH solutions.

4.2.3 Using Pincer Ligands

For more than 30 years, pincer-type ligands have been known [57]. The high stability of this complexes are due to the strong coordination between the tridentate ligand and the metal center. At the same time, they offer interesting redox chemistry as these noninnocent ligands are directly involved in the reaction mechanism. This enabled new and unknown reactivities. Catalytic applications of these ligand-metal cooperations are, for example, arylation and coupling reactions, alkane dehydrogenations, hydroaminations, and a bunch of hydrogenation reactions [58–61].

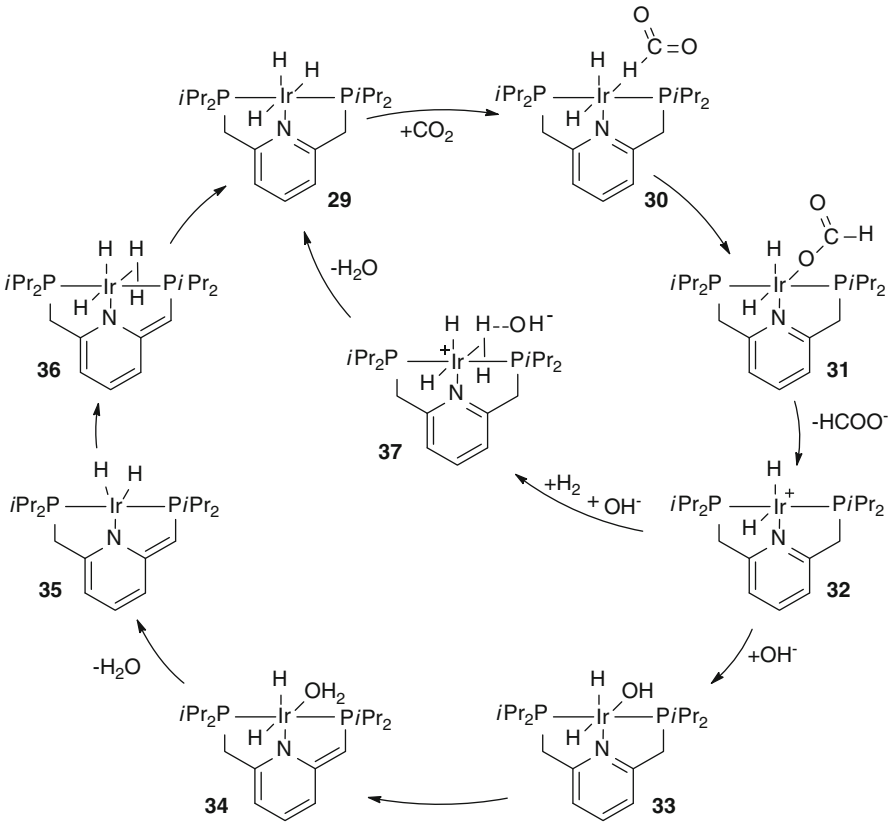

Scheme 4.7 Possible reaction mechanism for the Ir-trihydride-pincer complex of Nozaki

Recently, the first example of CO_2 hydrogenation to formate with this ligand class was presented by Nozaki. This system is highly efficient and was highlighted in 2010 [62]. In fact, Nozaki's Ir(III)$(H)_3$-pincer complex **29** achieved astonishing TON up to 3,500,000 in 48 h at 120 °C and TOF of 150,000 h^{-1} after 2 h at 200 °C using each 30 bar of CO_2 and H_2 in an aqueous KOH solution of 1 M [63]. The proposed mechanism is presented in Scheme 4.7. The first step is the CO_2 insertion into Ir-H bond of **29** forming complex **30** with the formato group in *cis* position to the N atom. After dissociation of the formate, the Ar-CH_2-P*i*Pr_2 moiety of the ligand is deprotonated followed by dearomatization of the pyridine ring. To this amido iridium dihydride complex **35**, a hydrogen molecule coordinates which is then heterolytically cleaved to give the full-aromatized Ir$(H)_3$ **29** back. Yang reported a different pathway by studying computationally PNP-pincer complexes with Ir$(H)_3$ and Fe/Co $(H)_2(CO)$ [64]. He claimed that the OH^--triggered H_2 cleavage (**37**) is more favorable than Nozaki's aromatization/dearomatization mechanism as well as Ahlquist's suggestions based on DFT studies [65]. In response Nozaki and Morokuma presented their own computational study for the CO_2 hydrogenation with complex **29** [66].

As a result, both pathways, the aromatization/dearomatization reaction as well as the hydrogenolysis suggested by Yang, are possible as their transition state energies are very similar. Deeper insight in the mechanism was provided by Hazari who examined the *trans*-influence of various ligands for insertion of CO_2 into the Ir-H bond of **29** [67]. The strongest *trans*-effect was observed by the hydride ligand which is believed to weaken the Ir-H bond by increasing the nucleophilicity of this hydride making the CO_2 insertion more favorable.

Other non-considered mechanisms were pointed out by Milstein's group. They proposed a double deprotonation by methylating a Ni(II) PNP complex where the negative charge is delocalized in the amido-type backbone [68] as well as a methylated Co(I)-pincer complex which lost a H radical by homolytic C-H bond cleavage [69]. Here, the unpaired electron is delocalized in the ligand backbone and evidence for the remaining aromaticity of the pyridine ring was detected. The abstraction of the H radical is believed to be caused by the solvent as an increase of the reaction rate was observed in aliphatic solvents.

4.2.4 Using Non-precious Metals

Despite increasing scientific interest in the hydrogenation of CO_2, the use of bio-relevant metals such as iron, manganese, or cobalt as catalysts has scarcely been investigated compared to noble-metal-based systems. Before 2005, only a few examples were reported yielding higher TON than 10 [70]. However, long reaction times and harsh conditions are needed.

In 2011, Yang predicted computationally an iron-pincer complex to be capable of CO_2 hydrogenation [64]. In the same year, Milstein presented an analog Fe complex **38** (Scheme 4.8) not only active in CO_2 hydrogenation but also in the bicarbonate reduction to formate [71]. In aqueous solutions, bicarbonate can be converted to the corresponding formate at ambient pressure and 80 °C with a moderate yield 30 % and a TON of 320. Using CO_2, even higher TON up to 600 was achieved. Based on IR and NMR experiments, a similar mechanism as for the $Ir(H)_3$-pincer complex **29** is proposed.

Whereas mono-, bi-, and tridentate phosphine ligands are well investigated for noble metals in the catalytic hydrogenation of CO_2, tetradentate ligands have not been presented at all. The application of the tetradentate phosphine ligand $P(CH_2CH_2PPh_2)_3$ in combination with $Fe(BF_4)_2{\cdot}6H_2O$ in MeOH led to the highly active complex **39** [72]. With this complex, our group showed that bicarbonate can be reduced to formate in high yields (88 %) and TON (up to 610) at 80 °C and 60 bar of H_2. Testing a variety of bidentate and tridentate ligands which failed all in generating an active catalyst in situ, it seemed to be that iron needs a very well-defined environment. Even other iron sources instead of $Fe(BF_4)_2{\cdot}6H_2O$ gave significant lower yield. Replacing bicarbonate by CO_2, methyl formate was produced in the presence of NEt_3 and the corresponding formamides were observed by using dialkyl amines as base yielding TON up to 730.

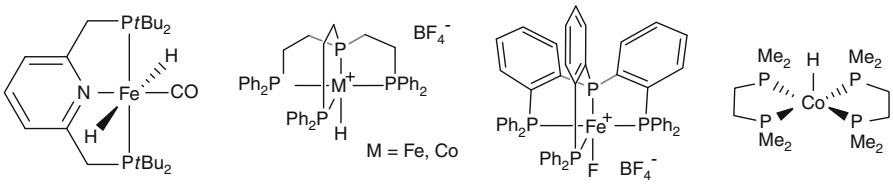

38 39 40 41

Scheme 4.8 Non-precious metals active in CO_2 hydrogenation published by Milstein, Beller, and Linehan

Changing the metal from Fe to Co, slightly higher yields were observed for the bicarbonate reduction and higher temperature was tolerated. In addition, lower H_2 pressure is applicable [73]. TON up to 3,900 for sodium formate and 1,300 for DMF could be detected. By synthesizing Co monohydride and Co dihydrogen complexes and testing them in the catalytic hydrogenation of bicarbonate, the monohydride complex was excluded as possible active species, whereas the Co dihydrogen complex was active. These results were in correlation with the performed NMR studies.

By synthesizing the phenyl-bridged analog of the tetradentate phosphine ligand mentioned above and combining it with $Fe(BF_4)_2{\cdot}6H_2O$, the most active and stable iron catalyst **40** known for the hydrogenation of bicarbonate and CO_2 was developed [74]. The crystal structure of **40** exhibited an unusual Fe-F bond, where the F^- originally came from the BF_4^- anion. Both the in situ system and the well-defined complex **40** showed the same activity, resulting in TON up to one order of magnitude higher than the previously reported Fe systems for the bicarbonate reduction (TON 7,550). With higher catalyst loading, the reaction reached its equilibrium already after 5 h with TOF up to 770 h^{-1}. Furthermore, the hydrogenation of CO_2 in the presence of base gave formic acid, methyl formate, and formamides, the latter in TON up to 5,100. NMR studies indicated that a Bianchini-type complex [75] has been formed being in equilibrium with a Fe-hydride complex where the dihydrogen ligand has been exchanged by a solvent or a CO_2 molecule. Through base-assisted heterolytic hydrogen cleavage, an active dihydride Fe complex was proposed to be formed into which CO_2 inserts to give the hydride formate complex. Dissociation of the formate followed by the coordination of a dihydrogen molecule led back to the Bianchini-type complex and HCOOH·base adduct.

Very recently, the group of Linehan published NMR experiments where Co(I) $(dmpe)_2H$ shows very high TOF up to 74,000 h^{-1} for the hydrogenation of CO_2 to formate [76]. However, by using other bases than the expensive and very unusual Verkade's base, the activity dropped down dramatically. Even with much higher catalyst loading and the use of the expensive, in CO_2 hydrogenation successfully tested base DBU, almost no activity was observed. A scale-up of this process is therefore very unlikely.

Table 4.1 Reported catalysts for the hydrosilylation of CO_2 to silyl formate

Entry	Catalyst	T [°C]	CO_2 [atm]	TON	TOF [h^{-1}]	Ref.
1	$Ru_2Cl_5(MeCN)_7$	40	14	4,619	231	[77]
2	*cis*-[$RuCl_2(MeCN)_4$]	85	10 g	–	3,700	[78]
3	Iridium complex	RT	3	112	0.8	[80]
4	Zinc complex	100	6.8	1,006	2.9	[81]
5	Cu bisphosphine complex (Ph)	60	1	8,100	1,350	[82]
6	[(NHC)Cu(O*t*Bu)]	60	1	7,489	1,248	[83]
7	Cu bisphosphine complex (*i*Pr)	60	1	70,000	2,917	[79]
8	$Rh_2(OAc)_4$	50	1	180	90	[84]
9	[Et_3SiPh][$B(C_6F_5)_4$]	30	1	–	–	[85]

4.2.5 Using Other Hydride Reagents

Parallel to the hydrogenation of CO_2, catalysts for the reduction of CO_2 to silyl formate with Hsilanes have been reported. The most recent systems are listed in Table 4.1.

In case of the $Ru_2Cl_5(MeCN)_7$, the catalyst could be recycled 10 times, resulting in an overall TON up to 4,600 [77]. The same group achieved with the similar catalyst *cis*-[$RuCl_2(MeCN)_4$] and MePhSiH high TOF of 3,400 h^{-1} yielding 96 % of silyl formate at 85 °C [78]. The highest TONs were achieved by the copper (1,2-bis(diisopropylphosphino)benzene) complex [79] with a very good TON of 70,000 after 24 h at 1 atm of CO_2 pressure.

From a mechanistic point of view, two different pathways are proposed depending on how CO_2 inserts. For the systems [79] and [80], in the first step, the silane is activated on the metal center resulting in the formation of a metal-hydride complex and the transfer of the silyl cation to an anionic ligand (Cl^- or triflate). In the second step, the silyl cation activates CO_2 and subsequent silyl formate is reductively eliminated (outer-sphere mechanism).

The other systems [79, 81–83] are believed to follow a different mechanism. Here, the active catalytic species is formed by the reaction of the precursor and silane to yield the corresponding metal-hydride complex. Into this metal-H bond inserts a CO_2 molecule to build up the metal formate complex. In the last step, this formate complex reacts with silane to regenerate the metal-H species and release silyl formate.

By adding water to silyl formate, formic acid is formed. This transformation is not really competitive with the reduction of CO_2 to formic acid using molecular hydrogen as for the latter even more active catalysts systems are known. However, using other nucleophiles, such as amines or Grignard reagents, offers new synthetic ways to a number of synthesis products (Scheme 4.9). For example, benzhydrol was formed in 77 % yield by reacting silyl formate with two equivalents of PhMgBr [84].

A stoichiometric metal-free reduction of CO_2 with trialkyl silanes and stoichiometric amounts of trityl borate was shown by the group of Müller [85]. They observed different products depending on the solvent applied. In PhCl, disilylated formic acid or disilyl methyl oxonium is formed. By quenching these intermediates

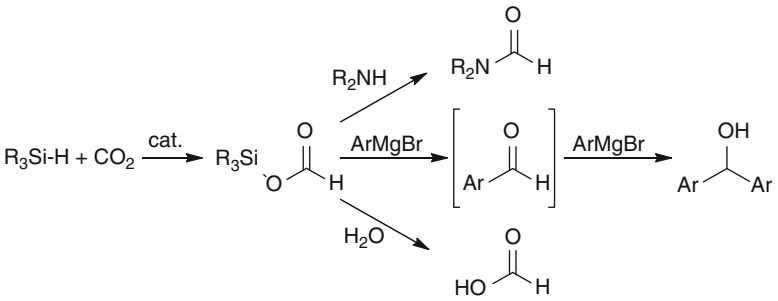

Scheme 4.9 Reduction of CO_2 to silyl formate and possible applications presented by Mizuno

with water, HCOOH and MeOH are obtained. In contrast, in PhH, the transformation of benzylic cations gives silyl ester or benzoic acid.

An example for a hydroboration of CO_2 to formate was presented by Labinger and Bercaw [86] using trialkyl boranes in the presence of Rh and Ni dmpe complexes to form formate-borane adducts. However, closing the catalytic cycle through breaking the formate-borane adducts failed.

In 2013, the group of Shintani and Nozaki presented a copper-NHC-catalyzed hydroboration of CO_2 to formic acid by quenching the reaction mixture with HCl [87]. This way, yields up to 87 % of formic acid have been observed. By adding primary or secondary amines to the reaction mixture instead of quenching with HCl, they isolated the corresponding formamides in good to very good yields (81–98 %). This *N*-formylation is also possible in one step by reacting CO_2 with pinacolborane in the presence of amine. However, the yields decreased slightly (e.g., from 84 to 71 % for *p*-anisidine).

4.3 Hydrogenation of CO_2 to MeOH

Searching for alternative sources of fuels and energy storage mediums, MeOH is considered for several good reasons. First, it can be dehydrogenated to give H_2 and, therefore, can serve as hydrogen storage carrier [88, 89]. Second, methanol has a high energy content of 22.7 MJ kg^{-1}, making it suitable for energy storage (CH_4: 24.3 MJ kg^{-1}) [6]. It can be used as liquid fuel (blended with gasoline or directly in direct methanol fuel cells, DMFC [90]) or can be converted to gasoline (MTG process). Last but not least, MeOH is a valuable feedstock as it can be transformed into ethylene or propylene in the MTO (methanol-to-olefins) process or to aromatics in the MTA (methanol-to-aromatics) process using zeolites. Therefore, MeOH covers all important basic chemicals for a wide range of product chains [6, 91]. The advantage of such a MeOH economy in comparison to the often discussed H_2-based technology is that MeOH as a liquid can be used analogous to petroleum and therefore can be transported and stored easily in the maintaining

infrastructure. In addition, MeOH is highly H_2 enriched (12.6 w%) in comparison to many other H_2 storage devices.

The most sustainable way for producing MeOH out of CO_2 and water combines the electrolysis of water to hydrogen and the subsequent hydrogenation of CO_2 to MeOH. The cost of this process will strongly depend on the electricity price for supplying the needed hydrogen amount. However, even today, this process can be competitive regarding the highly increased prices of gasoline in European countries [8]. The first commercial CO_2-to-renewable-methanol plant based on geothermal sources was established in 2012 in Iceland, producing annually 3,500 t of MeOH, and is planned to be expanded [9]. Industrial applications of homogeneous catalyst systems in this field are still far away from reality, but the first recent examples of the homogeneous catalyzed hydrogenation of carbon dioxide in the last 3 years are promising.

4.3.1 Catalytic Reduction with Hydrogen

$$CO_2 + 3\,H_2 \rightarrow CH_3OH + H_2O \tag{4.2}$$

One of the first concepts for the hydrogenation of CO_2 to MeOH (Eq. 4.2) was presented by the group of Sanford [92]. They set up a cascade by using three different catalysts: $Ru(PMe_3)_4Cl(OAc)$ for the hydrogenation of CO_2 to formic acid, $Sc(OTf)_3$ as catalyst for the esterification of the formic acid to methyl formate, and finally the Ru PNN-pincer complex **42** which converted methyl formate to methanol. Key to success was the separation of the last catalyst from the second one to avoid deactivation. Therefore, methyl formate is transferred by a temperature ramp to an outer vessel containing the pincer complex **42**. The overall TON of 21 for the transformation of $^{13}CO_2$ to MeOH is low, but showed that this reaction is achievable by homogeneous catalysis. As one reason for this low activity, Sanford recognized an inhibition of the Ru PNN-pincer complex **42** by CO_2 [93]. Two products were observed under CO_2 atmosphere (Scheme 4.10). The kinetic product **43** is observed immediately under 1 atm of CO_2 by forming a C-C bond between the CO_2 and the phosphine arm. This process is reversible. By simply keeping the complex longer under CO_2 atmosphere or heating the solution, the irreversible product **44** is formed at the amine arm of the pincer complex and single crystals could be grown from the solution.

Milstein observed a similar phenomenon with a Ru PNP ligand with two phosphine arms [94]. Here, only a reversible addition of CO_2 to the phosphine arm was found confirming Sanford's results. Calculations reveal no solvent effect on the TS energies, indicating a concerted mechanism and the absence of a charge separation like Ru^+ COO^-. Another example of CO_2-ligand interactions was shown by Oro and Langer [95] using an Ir(I) dppm catalyst. Here, CO_2 inserts

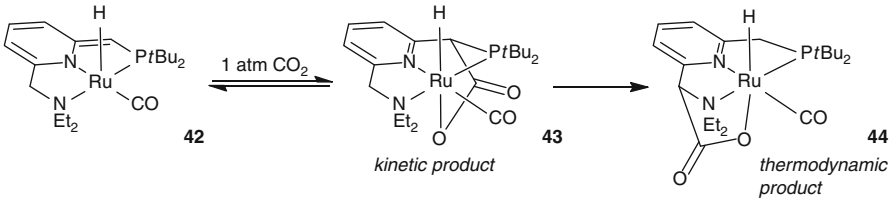

Scheme 4.10 CO_2 interactions with the Ru PNN-pincer complex observed by Sanford

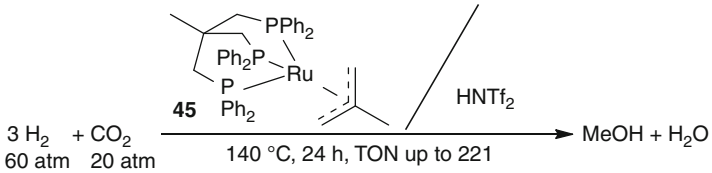

Scheme 4.11 The first homogeneous one-catalyst system for the reaction of CO_2 to MeOH reported by Leitner

into the C-H bond of the bisphosphine ligand to give the binuclear complex [IrCl(dppm)(H){$(Ph_2P)_2$C-COOH}]$_2$.

The first one-catalyst system for the production of methanol was reported by Klankermayer and Leitner [96]. Using the Ru catalyst **45** in the presence of 1 eq $HNTf_2$, MeOH is produced with a TON of 221 in a THF/EtOH mixture at 20 bar of CO_2 and 60 bar of H_2 (Scheme 4.11). They propose a cationic Ru hydrido dihydrogen complex to be the active species.

In addition to the systems mentioned above, a few concepts for the indirect conversion of CO_2 to MeOH were developed, reducing substrates which can be produced from CO_2 (Scheme 4.12). Pioneering work has been published by Milstein. Using the Ru-pincer complexes **42** or **46**, alkyl formates, organic carbonates, and carbamates [97] as well as challenging ureas [98] were converted under mild conditions in quantitative yield, often for the first time. Key to success is the unique behavior of the pincer complex being involved in the mechanism by metal-ligand cooperation. This work was also highlighted by Dixneuf [99] and Choudhury [100]. Notably, the activities need to be improved for industrial application and the economy of the process will also depend on H_2 cost.

One year later, Yang presented a DFT study on the dimethyl carbonate reduction to MeOH with the Ru NNP-pincer complex **42**. In addition, an analog Fe-pincer complex was proposed [101]. The suggested mechanism runs via three catalytic cycles, each with a direct hydride and ligand proton transfers. The cascade intermediates are methyl formate, followed by formaldehyde and subsequently MeOH as the product. The overall rate-determining step was found to be the formation of the second MeOH molecule from methyl formate in the second cycle.

However, it should be kept in mind that the reduction of dimethyl carbonate to methanol is uneconomic as the starting material with 1,000 US/t is much more

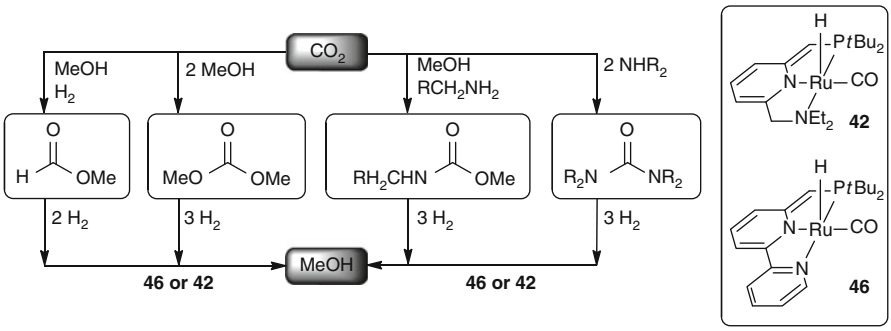

Scheme 4.12 Various ways for the indirect conversion of CO_2 to MeOH published by Milstein

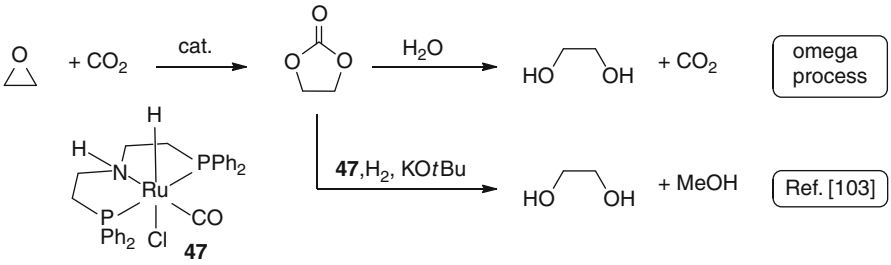

Scheme 4.13 Another concept for the indirect production of MeOH from CO_2 demonstrated by Ding

expensive than MeOH (400 US/t) [102]. Therefore, Ding et al. developed another indirect route for the MeOH production [102]. The idea is based on the omega process where ethylene carbonate, synthesized from CO_2 and ethylene oxide, is hydrolyzed to ethylene glycol and CO_2 (Scheme 4.13).

Instead of hydrolyzing the organic carbonate, this intermediate can be hydrogenated with the Ru PNP-pincer complex **47** in the presence of KO*t*Bu to give ethylene glycol and MeOH. This opens a nice way to get two bulk chemicals at the same time from reacting CO_2 with ethylene oxide. With TON up to 87,000 and TOF of 1,200 h^{-1}, high activity could be observed at almost quantitative yields. In addition, deuterated methanol could be obtained in 99 % yield by deuteration of the sterically hindered tetramethyl ethylene carbonate with D_2. Furthermore, the catalyst is able to depolymerize the widely used material poly(propylene carbonate) by hydrogenating it to MeOH and the corresponding diol. Therefore, a recycling of this material to valuable products is possible [103].

An unusual way to gain methanol is the formic acid disproportionation (Eq. 4.3). Here, formic acid is both substrate and hydrogen source. In a HCOOH/water mixture at 60 °C, the molecular iridium catalyst $[Cp^*Ir(bpy)(H_2O)](OTf)_2$ converts formic acid to methanol with a selectivity up to 12 % [104]. The selectivity increases with higher HCOOH concentration and lower temperature. Additional

H_2 suppresses the competing formate decomposition to CO_2 and H_2. As a side product methyl formate was observed through HCOOH esterification. Deuteration experiments indicate that formaldehyde is an intermediate of the catalytic cycle which is then hydrogenated to MeOH by HCOOH releasing CO_2.

$$3\,HCOOH_{(aq)} \rightarrow CH_3OH_{(aq)} + H_2O_{(l)} + 2CO_{2(g)} \quad \Delta G^{\circ}{}_{298} = -11.9\,\text{kcal}\,\text{mol}^{-1} \quad (4.3)$$

An interesting approach is the use of frustrated Lewis pairs which are capable of heterolytic H_2 activation [105]. Ashley and O'Hare applied TMP + $B(C_6F_5)_3$, forming a unique formato borate complex [TMPH]-[$HCO_2B(C_6F_5)_3$] with CO_2 under H_2 atmosphere (1–2 atm). After 6 days at 160 °C, $H_3COB(C_6F_5)_2$ was formed and 24 % yield of methanol was observed after distillation. However, the rendering of the catalytic cycle is still unachieved [106].

4.3.2 Catalytic Reduction with Other Hydride Reagents

There is a bunch of catalysts capable of reducing CO_2 using other hydride reagents such as aminoboranes, Hboranes and Hsilanes. For example, the group of Stephan presented a 1:2 mixture of $PMes_3$ and AlX_3 reacting with CO_2 to the corresponding phosphonium-carboxylate adduct. This intermediate then dehydrogenates aminoboranes at RT to give phosphonium methoxy aluminate in less than 15 min. Quenching with H_2O leads to 37–51 % yield of methanol [107].

The first catalytic metal-free hydrosilylation of CO_2 to MeOH was reported in 2009 by Zhang and Ying [108]. Using the NHC catalyst **49** under CO_2 atmosphere, first imidazolium carboxylate is formed which reacted then with diphenylsilane at RT to give CH_3OSiMe_3. Final quenching with water gives MeOH in 90 % yield based on the used Hsilane amount with TON of 1,840 and TOF of 25 h^{-1}. Therefore, it is competitive with known Ru catalysts lacking their typical drawbacks of moisture and air sensitivity. This system is even active under dried air. The first catalytic hydroboration of CO_2 to the methoxide level was reported by Guan, applying the nickel catalyst **48** [109] in the presence of HBcat. Hydrolysis gives MeOH with TON and TOF of 495 h^{-1} (based on B-H).

Comparing both systems by studying the mechanism quantum mechanically, Wang proposed that the most favorable pathway for both contains analog, experimentally detected intermediates like formoxy, acetal, and methoxide species [110, 111]. In addition, he predicted formaldehyde to be another intermediate in the catalytic cycle (Scheme 4.14). Both catalysts accelerate the hydride transfer in comparison to uncatalyzed reactions, but the mechanism of the hydride transfer is different. In the Ni/borane system, the Ni catalyst **48** acts as a shuttle, transferring the hydride from the HBcat to the C-O bonds. In the first step, CO_2 inserts into the [Ni]-H bond (**50**) forming Ni-formate. This complex reacts with catecholborane HBcat (**51**) to give formyl borate and [Ni]-H catalyst **48**. The catalyst then activates

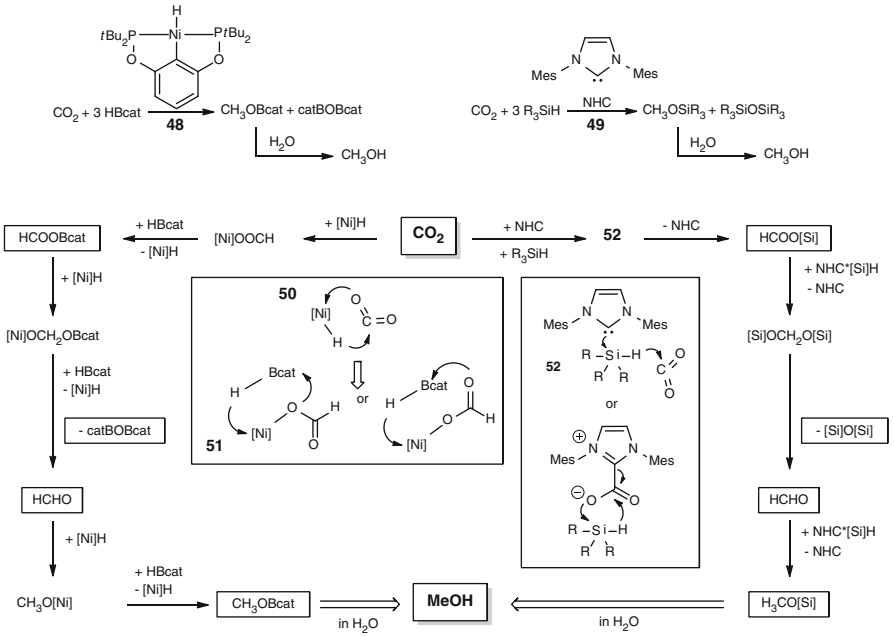

Scheme 4.14 Comparing two catalytic systems based on the DFT studies by Wang for CO_2 to MeOH using hydroboration and hydrosilylation reagents

this product by forming the acetal species. The hydride transfer to [Ni] by a second HBcat results in formaldehyde and di(boryl)ether production. Formaldehyde then inserts into the [Ni]-H, yielding the corresponding methoxide complex. A third HBcat closes the catalytic cycle by reforming the [Ni]-H catalyst and gaining the final product CH_3OBcat.

In contrast, the NHC catalyst **49** "only" activates the Si-H bond by pushing electron density to the H atoms and simplifies this way the direct hydride transfer from Hsilane to the C-O bond (**52** top). However, the NHC catalyst **49** can react with CO_2 to the corresponding imidazolium carboxylate, too. This activated CO_2 adduct can be attacked more easily by Hsilanes than unbounded CO_2 (**52** bottom).

It is noteworthy that the CO_2 reduction catalyst and the hydride source must match for achieving high activity. Exchanging the hydride source for both systems, the reduction of CO_2 to MeOH failed. The reasons are a high kinetic barrier for the reaction of the Ni-formate with silanes and the formation of a thermodynamic stable intermediate between NHC and Hboranes.

Further examples of a catalytic hydroboration with Ru catalysts were presented by Sabo-Etienne using $[RuH_2(H_2)_2(PCy_3)_2]$ in combination with pinacolborane [112, 113] and by the group of Stephan applying the precursor $[Ru(PPh_3)Cl_2]$ and the ligand $N((CH_2)_2NHP\mathit{i}Pr_2)_3$ in the presence of HBpin [114].

The first metal-free organocatalyst for hydroboration of CO_2 to MeOH was published by Maron and Fontaine [115]. The organocatalyst 1-Bcat-2-PPh_2-C_6H_4 reduces CO_2 with 3 eq of $BH_3{\cdot}SMe_2$ to give subsequent MeOH with TON >3,000 and TOF >970 h^{-1}.

4.4 Other Homogeneous Catalytic Reductions of CO_2 Using Hydride Reagents

Beside methanol, the full reduction of CO_2 to methane is an attractive and actual goal for homogeneous catalysis. However, so far homogeneous catalysts capable of hydrogenating CO_2 to methane with molecular H_2 are still unknown (Eq. 4.4). In the meantime, some efforts have been undertaken using less benign reductants such as silanes.

$$CO_2 + 4\,H_2 \;\rightarrow\; CH_4 + 2\,H_2O \tag{4.4}$$

Interestingly, Musgrave's ab initio studies claim that even in the absence of a metal, the reduction of CO_2 with ammonia boranes via simultaneous hydride and proton transfer should be possible involving the intermediates HCOOH and hydrated formaldehyde to give finally methanol [116]. Unfortunately, ammonia boranes decompose easily in the presence of acid to H_2 and NH_2BH_2. Unless this problem will be solved, the reduction will stop at the HCOOH step. The group of Wehmschulte showed that strong Lewis acids such as $[Et_2Al]^+$ can catalyze the hydrosilylation of CO_2 to methane. However, after three cycles the activity decreased, likely caused by side reactions with the solvent C_6D_6 [117].

Combining borane complexes or additional borane with hydrosilylation reagents was the key to success for improved catalytic turnover numbers. All active systems have in common that different kind of metal complexes or frustrated Lewis pairs (FLP) are needed to activate the CO_2 to form the corresponding formate complexes. The following reduction steps are believed to be catalyzed by species $[R_3Si\text{-}H\cdots BR_3]$ involving the intermediates bis(silyl)acetal, methyl silyl ether, and finally methane. Active co-catalysts are presented in Scheme 4.15.

Activities and selectivities were low for the systems using **53** [118], **54** [119], and **55** [120], whereas a good TON of 2,156 was achieved in16 h by Turculet using the Pt-pincer borane complex **56** with Et_3SiH at 65 °C and 1 atm of CO_2 [121]. A high TON of 8,300 after 72 h at RT was published by Brookhart applying the Ir^+ PCP-pincer complex **57** [122] in the presence of Me_2PhSiH.

Finally, it is worth mentioning that carbon dioxide can be used as methylation reagent for amines in the presence of silanes. Our group [123] as well as the group of Cantat [124] realized the reduction of CO_2 with a simultaneous C-N bond formation. With this method it is possible to methylate primary amines with CO_2 as C1 feedstock.

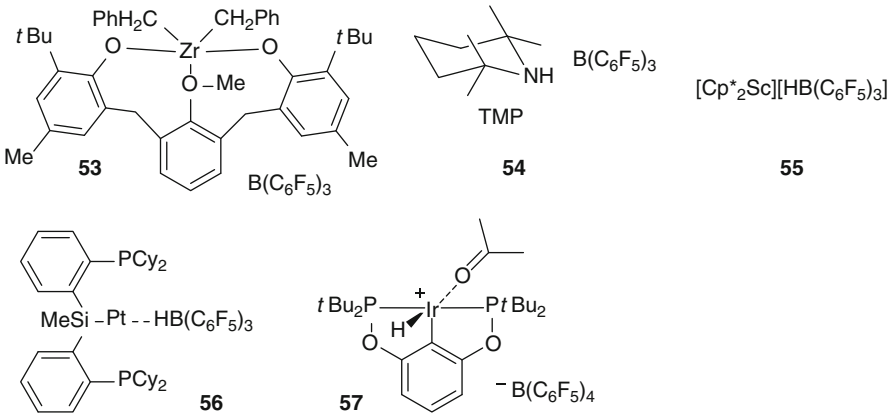

Scheme 4.15 Various co-catalysts for the $[R_3Si\text{-}H\cdots BR_3]$ catalyzed reduction of CO_2 to CH_4

4.5 Concluding Remarks

In the last decade, several improved organometallic catalysts for the hydrogenation of CO_2 to formic acid derivatives have been reported. Many of them show good activity even under ambient conditions. In addition, interesting concepts have been developed, combining both formic acid product separation and catalyst recycling. However, for industrial applications the activities and long-term stabilities of the catalysts still have to be improved. Meanwhile, also catalyst systems have been presented for hydrogen storage using carbon dioxide.

While non-precious metals such as Fe and Co were rarely known for the homogeneous CO_2 hydrogenation before 2009, much progress was achieved in this field in the last 3 years.

Very recently, also first promising systems capable of converting CO_2 to methanol became available opening new ways to a future methanol economy. On the other hand, the homogeneously catalyzed reduction of carbon dioxide to CH_4 using molecular hydrogen is still not known and more efforts are needed in this area. At this point it should be mentioned that related reductions of carbon dioxide using boranes or hydrosilylation reagents are interesting in order to understand the mechanism of such processes. Nevertheless, it should be clear that they will not be of preparative use due to price, sensitivity of the reagents, and waste generated.

What will be the future challenges in homogeneous CO_2 reductions? Obviously, for industrial implementations even better catalysts are needed. With regard to basic science, the hydrogenation of carbon dioxide with simultaneous C-C bond formation represents a grand challenge. As an example, the low temperature and selective Fischer-Tropsch reaction can be considered. Furthermore, reducing carbon dioxide directly to Co is of both industrial and academic interest. Such transformations would allow using carbon dioxide instead of toxic carbon monoxide. The key tools to achieve these goals will be catalysis and organometallic chemistry.

References

1. Cokoja M, Bruckmeier C, Rieger B, Herrmann WA, Kühn FE (2011) Umwandlung von Kohlendioxid mit Übergangsmetall-Homogenkatalysatoren: eine molekulare Lösung für ein globales Problem? Angew Chem 123(37):8662–8690. doi:10.1002/ange.201102010
2. Peters M, Köhler B, Kuckshinrichs W, Leitner W, Markewitz P, Müller TE (2011) Chemical technologies for exploiting and recycling carbon dioxide into the value chain. ChemSusChem 4(9):1216–1240. doi:10.1002/cssc.201000447
3. Geider RJ, Delucia EH, Falkowski PG, Finzi AC, Grime JP, Grace J, Kana TM, La Roche J, Long SP, Osborne BA, Platt T, Prentice IC, Raven JA, Schlesinger WH, Smetacek V, Stuart V, Sathyendranath S, Thomas RB, Vogelmann TC, Williams P, Woodward FI (2001) Primary productivity of planet earth: biological determinants and physical constraints in terrestrial and aquatic habitats. Glob Chang Biol 7(8):849–882. doi:10.1046/j.1365-2486.2001.00448.x
4. Appel AM, Bercaw JE, Bocarsly AB, Dobbek H, DuBois DL, Dupuis M, Ferry JG, Fujita E, Hille R, Kenis PJA, Kerfeld CA, Morris RH, Peden CHF, Portis AR, Ragsdale SW, Rauchfuss TB, Reek JNH, Seefeldt LC, Thauer RK, Waldrop GL (2013) Frontiers, opportunities, and challenges in biochemical and chemical catalysis of CO_2 fixation. Chem Rev. doi:10.1021/cr300463y
5. Mikkelsen M, Jorgensen M, Krebs FC (2010) The teraton challenge. A review of fixation and transformation of carbon dioxide. Energy Environ Sci 3(1):43–81
6. Bertau M, Offermanns H, Menges G, Keim W, Effenberger FX (2010) Methanol findet zu wenig Beachtung als Kraftstoff und Chemierohstoff der Zukunft [Methanol needs more attention as a fuel and raw material for the future]. Chem Ing Tech 82(12):2055–2058. doi:10.1002/cite.201000159
7. Sakakura T, Choi J-C, Yasuda H (2007) Transformation of carbon dioxide. Chem Rev 107 (6):2365–2387. doi:10.1021/cr068357u
8. Olah GA, Prakash GKS, Goeppert A (2011) Anthropogenic chemical carbon cycle for a sustainable future. J Am Chem Soc 133(33):12881–12898. doi:10.1021/ja202642y
9. Olah GA (2013) Towards oil independence through renewable methanol chemistry. Angew Chem Int Ed 52(1):104–107. doi:10.1002/anie.201204995
10. Haggin J (1994) New processes target methanol production, off-gas cleaning. Chem Eng News 72:29–31
11. Goehna H, Koenig P (1994) Producing methanol from CO_2. ChemTech 24:36–39
12. Jessop PG, Ikariya T, Noyori R (1995) Homogeneous hydrogenation of carbon dioxide. Chem Rev 95(2):259–272. doi:10.1021/cr00034a001
13. Leitner W (1995) Carbon dioxide as a raw material: the synthesis of formic acid and its derivatives from CO_2. Angew Chem Int Ed 34(20):2207–2221. doi:10.1002/anie.199522071
14. Jessop PG, Joó F, Tai C-C (2004) Recent advances in the homogeneous hydrogenation of carbon dioxide. Coord Chem Rev 248(21–24):2425–2442. doi:10.1016/j.ccr.2004.05.019
15. de Vries JG, Elsevier CJ, Jessop PG (2007) 17 homogeneous hydrogenation of carbon dioxide. Handb Homogen Hydrogen 1:489–511
16. Rothenberg G (2008) Introduction. In: Catalysis. Wiley-VCH Verlag GmbH & Co. KGaA, Weinheim, pp 1–38. doi:10.1002/9783527621866.ch1
17. Olah GA (2005) Beyond oil and gas: the methanol economy. Angew Chem Int Ed 44(18):2636–2639. doi:10.1002/anie.200462121
18. Munshi P, Main AD, Linehan JC, Tai C-C, Jessop PG (2002) Hydrogenation of carbon dioxide catalyzed by ruthenium trimethylphosphine complexes: the accelerating effect of certain alcohols and amines. J Am Chem Soc 124(27):7963–7971. doi:10.1021/ja0167856
19. Y-y O, Matsunaga T, Nakao Y, Sato H, Sakaki S (2005) Ruthenium(II)-catalyzed hydrogenation of carbon dioxide to formic acid. Theoretical study of real catalyst, ligand effects, and solvation effects. J Am Chem Soc 127(11):4021–4032. doi:10.1021/ja043697n

20. Y-y O, Nakao Y, Sato H, Sakaki S (2006) Ruthenium(II)-catalyzed hydrogenation of carbon dioxide to formic acid. Theoretical study of significant acceleration by water molecules. Organometallics 25(14):3352–3363. doi:10.1021/om060307s
21. Getty AD, Tai C-C, Linehan JC, Jessop PG, Olmstead MM, Rheingold AL (2009) Hydrogenation of carbon dioxide catalyzed by ruthenium trimethylphosphine complexes: a mechanistic investigation using high-pressure NMR spectroscopy. Organometallics 28(18):5466–5477. doi:10.1021/om900128s
22. Gowrisankar S, Federsel C, Neumann H, Ziebart C, Jackstell R, Spannenberg A, Beller M (2013) Synthesis of stable phosphomide ligands and their use in Ru-catalyzed hydrogenations of bicarbonate and related substrates. ChemSusChem 6(1):85–91. doi:10.1002/cssc.201200732
23. Muller K, Sun Y, Thiel WR (2013) Ruthenium(II)–phosphite complexes as catalysts for the hydrogenation of carbon dioxide. ChemCatChem 5(6):1340–1343. doi:10.1002/cctc.201200818
24. Zhao G, Joó F (2011) Free formic acid by hydrogenation of carbon dioxide in sodium formate solutions. Catal Commun 14(1):74–76. doi:10.1016/j.catcom.2011.07.017
25. Johnson TC, Morris DJ, Wills M (2010) Hydrogen generation from formic acid and alcohols using homogeneous catalysts. Chem Soc Rev 39(1):81–88
26. Grasemann M, Laurenczy G (2012) Formic acid as a hydrogen source – recent developments and future trends. Energy Environ Sci 5(8):8171–8181. doi:10.1039/C2EE21928J
27. Loges B, Boddien A, Gärtner F, Junge H, Beller M (2010) Catalytic generation of hydrogen from formic acid and its derivatives: useful hydrogen storage materials. Top Catal 53:902–914
28. Laurenczy G, Dalebrook AF, Gan W, Grasemann M, Moret S (2013) Hydrogen storage – beyond conventional methods. Chem Commun. doi:10.1039/C3CC43836H
29. Graetz J (2009) New approaches to hydrogen storage. Chem Soc Rev 38(1):73–82. doi:10.1039/B718842K
30. Jena P (2011) Materials for hydrogen storage: past, present, and future. J Phys Chem Lett 2 (3):206–211. doi:10.1021/jz1015372
31. Eberle U, Felderhoff M, Schüth F (2009) Chemical and physical solutions for hydrogen storage. Angew Chem Int Ed 48(36):6608–6630. doi:10.1002/anie.200806293
32. Papp G, Csorba J, Laurenczy G, Joó F (2011) A charge/discharge device for chemical hydrogen storage and generation. Angew Chem 123(44):10617–10619. doi:10.1002/ange.201104951
33. Boddien A, Gärtner F, Federsel C, Sponholz P, Mellmann D, Jackstell R, Junge H, Beller M (2011) Kohlenstoffdioxid-neutrale Wasserstoffspeicherung basierend auf Bicarbonaten und Formiaten. Angew Chem 123:6535–6538. doi:10.1002/ange.201101995
34. Federsel C, Jackstell R, Boddien A, Laurenczy G, Beller M (2010) Ruthenium-catalyzed hydrogenation of bicarbonate in water. ChemSusChem 3(9):1048–1050. doi:10.1002/cssc.201000151
35. Boddien A, Federsel C, Sponholz P, Mellmann D, Jackstell R, Junge H, Laurenczy G, Beller M (2012) Towards the development of a hydrogen battery. Energy Environ Sci 5(10):8907–8911. doi:10.1039/c2ee22043a
36. Urakawa A, Iannuzzi M, Hutter J, Baiker A (2007) Towards a rational design of ruthenium CO_2 hydrogenation catalysts by ab initio metadynamics. Chem Eur J 13(24):6828–6840. doi:10.1002/chem.200700254
37. Urakawa A, Jutz F, Laurenczy G, Baiker A (2007) Carbon dioxide hydrogenation catalyzed by a ruthenium dihydride: a DFT and high-pressure spectroscopic investigation. Chem Eur J 13(14):3886–3899. doi:10.1002/chem.200601339
38. Dietrich J, Schindler S (2008) Kinetic studies on the hydrogenation of carbon dioxide to formic acid using a rhodium complex as catalyst. Z Anorg Allg Chem 634(14):2487–2494. doi:10.1002/zaac.200800352
39. Yasaka Y, Wakai C, Matubayasi N, Nakahara M (2010) Controlling the equilibrium of formic acid with hydrogen and carbon dioxide using ionic liquid. J Phys Chem A 114 (10):3510–3515. doi:10.1021/jp908174s

40. Zhang Z, Xie Y, Li W, Hu S, Song J, Jiang T, Han B (2008) Hydrogenation of carbon dioxide is promoted by a task-specific ionic liquid. Angew Chem Int Ed 47(6):1127–1129. doi:10.1002/anie.200704487
41. Zhang Z, Hu S, Song J, Li W, Yang G, Han B (2009) Hydrogenation of CO_2 to formic acid promoted by a diamine-functionalized ionic liquid. ChemSusChem 2(3):234–238. doi:10.1002/cssc.200800252
42. Wesselbaum S, Hintermair U, Leitner W (2012) Continuous-flow hydrogenation of carbon dioxide to pure formic acid using an integrated $scCO_2$ process with immobilized catalyst and base. Angew Chem 124:8713–8716. doi:10.1002/ange.201203185
43. Schaub T, Paciello RA (2011) A process for the synthesis of formic acid by CO_2 hydrogenation: thermodynamic aspects and the role of CO. Angew Chem Int Ed 50(32):7278–7282. doi:10.1002/anie.201101292
44. Ogo S, Kabe R, Hayashi H, Harada R, Fukuzumi S (2006) Mechanistic investigation of CO_2 hydrogenation by Ru(II) and Ir(III) aqua complexes under acidic conditions: two catalytic systems differing in the nature of the rate determining step. Dalton Trans 39:4657–4663. doi:10.1039/b607993h
45. Himeda Y, Onozawa-Komatsuzaki N, Sugihara H, Kasuga K (2007) Simultaneous tuning of activity and water solubility of complex catalysts by acid–base equilibrium of ligands for conversion of carbon dioxide. Organometallics 26(3):702–712. doi:10.1021/om060899e712
46. Himeda Y, Miyazawa S, Hirose T (2011) Interconversion between formic acid and H_2/CO_2 using rhodium and ruthenium catalysts for CO_2 fixation and H_2 storage. ChemSusChem 4(4):487–493. doi:10.1002/cssc.201000327
47. Himeda Y (2007) Conversion of CO_2 into formate by homogeneously catalyzed hydrogenation in water: tuning catalytic activity and water solubility through the acid–base equilibrium of the ligand. Eur J Inorg Chem 25:3927–3941. doi:10.1002/ejic.200700494
48. Wang W-H, Hull JF, Muckerman JT, Fujita E, Himeda Y (2012) Second-coordination-sphere and electronic effects enhance iridium(III)-catalyzed homogeneous hydrogenation of carbon dioxide in water near ambient temperature and pressure. Energy Environ Sci 5:7923–7926
49. Wang W-H, Muckerman JT, Fujita E, Himeda Y (2013) Mechanistic insight through factors controlling effective hydrogenation of CO_2 catalyzed by bioinspired proton-responsive iridium(III) complexes. ACS Catal 3(5):856–860. doi:10.1021/cs400172j
50. Hull JF, Himeda Y, Wang W-H, Hashiguchi B, Periana R, Szalda DJ, Muckerman JT, Fujita E (2012) Reversible hydrogen storage using CO_2 and a proton-switchable iridium catalyst in aqueous media under mild temperatures and pressures. Nat Chem 4(5):383–388
51. Maenaka Y, Suenobu T, Fukuzumi S (2012) Catalytic interconversion between hydrogen and formic acid at ambient temperature and pressure. Energy Environ Sci 5(6):7360–7367. doi:10.1039/c2ee03315a
52. Fukuzumi S, Suenobu T (2013) Hydrogen storage and evolution catalysed by metal hydride complexes. Dalton Trans 42(1):18–28. doi:10.1039/c2dt31823g
53. Muller K, Sun Y, Heimermann A, Menges F, Niedner-Schatteburg G, van Wüllen C, Thiel WR (2013) Structure–reactivity relationships in the hydrogenation of carbon dioxide with ruthenium complexes bearing pyridinylazolato ligands. Chem Eur J 19:7825–7834. doi:10.1002/chem.201204199
54. Thai T-T, Therrien B, Suss-Fink G (2009) Arene ruthenium oxinato complexes: synthesis, molecular structure and catalytic activity for the hydrogenation of carbon dioxide in aqueous solution. J Organomet Chem 694(25):3973–3981. doi:10.1016/j.jorganchem.2009.09.008
55. Sanz S, Azua A, Peris E (2010) '([small eta]6-arene)Ru(bis-NHC)' complexes for the reduction of CO_2 to formate with hydrogen and by transfer hydrogenation with iPrOH. Dalton Trans 39(27):6339–6343. doi:10.1039/C003220D
56. Azua A, Sanz S, Peris E (2011) Water-soluble IrIII N-heterocyclic carbene based catalysts for the reduction of CO_2 to formate by transfer hydrogenation and the deuteration of aryl amines in water. Chem Eur J 17(14):3963–3967. doi:10.1002/chem.201002907
57. Albrecht M, van Koten G (2001) Platinum group organometallics based on "pincer" complexes: sensors, switches, and catalysts. Angew Chem Int Ed 40(20):3750–3781. doi:10.1002/1521-3773(20011015)40:20<3750::aid-anie3750>3.0.co;2-6

58. van der Boom ME, Milstein D (2003) Cyclometalated phosphine-based pincer complexes: mechanistic insight in catalysis, coordination, and bond activation. Chem Rev 103(5):1759–1792. doi:10.1021/cr960118r
59. Grützmacher H (2008) Cooperating ligands in catalysis. Angew Chem Int Ed 47(10):1814–1818. doi:10.1002/anie.200704654
60. van der Vlugt JI, Reek JNH (2009) Neutral tridentate PNP ligands and their hybrid analogues: versatile non-innocent scaffolds for homogeneous catalysis. Angew Chem Int Ed 48(47):8832–8846. doi:10.1002/anie.200903193
61. Musa S, Shaposhnikov I, Cohen S, Gelman D (2011) Ligand–metal cooperation in PCP pincer complexes: rational design and catalytic activity in acceptorless dehydrogenation of alcohols. Angew Chem 123(15):3595–3599. doi:10.1002/ange.201007367
62. Federsel C, Jackstell R, Beller M (2010) State-of-the-art catalysts for hydrogenation of carbon dioxide. Angew Chem Int Ed 49(36):6254–6257. doi:10.1002/anie.201000533
63. Nozaki K, Tanaka R, Yamashita M (2009) Catalytic hydrogenation of carbon dioxide using Ir (III) – pincer complexes. J Am Chem Soc 131(40):14168–14169. doi:10.1021/ja903574e
64. Yang X (2011) Hydrogenation of carbon dioxide catalyzed by PNP pincer iridium, iron, and cobalt complexes: a computational design of base metal catalysts. ACS Catal 1:849–854. doi:10.1021/cs2000329
65. Ahlquist MSG (2010) Iridium catalyzed hydrogenation of CO_2 under basic conditions-mechanistic insight from theory. J Mol Catal A Chem 324(1–2):3–8. doi:10.1016/j.molcata.2010.02.018
66. Tanaka R, Yamashita M, Chung LW, Morokuma K, Nozaki K (2011) Mechanistic studies on the reversible hydrogenation of carbon dioxide catalyzed by an Ir-PNP complex. Organometallics 30(24):6742–6750. doi:10.1021/om2010172
67. Schmeier TJ, Dobereiner GE, Crabtree RH, Hazari N (2011) Secondary coordination sphere interactions facilitate the insertion step in an iridium(III) CO_2 reduction catalyst. J Am Chem Soc 133(24):9274–9277. doi:10.1021/ja2035514
68. Vogt M, Rivada-Wheelaghan O, Iron MA, Leitus G, Diskin-Posner Y, Shimon LJW, Ben-David Y, Milstein D (2013) Anionic Nickel(II) complexes with doubly deprotonated PNP pincer-type ligands and their reactivity toward CO_2. Organometallics 32(1):300–308. doi:10.1021/om3010838
69. Khaskin E, Diskin-Posner Y, Weiner L, Leitus G, Milstein D (2013) Formal loss of an H radical by a cobalt complex via metal-ligand cooperation. Chem Commun 49(27):2771–2773. doi:10.1039/C3CC39049G
70. Tai C-C, Chang T, Roller B, Jessop PG (2003) High-pressure combinatorial screening of homogeneous catalysts: hydrogenation of carbon dioxide. Inorg Chem 42(23):7340–7341. doi:10.1021/ic034881x
71. Langer R, Diskin-Posner Y, Leitus G, Shimon LJW, Ben-David Y, Milstein D (2011) Low-pressure hydrogenation of carbon dioxide catalyzed by an iron pincer complex exhibiting noble metal activity. Angew Chem Int Ed 50(42):9948–9952. doi:10.1002/anie.201104542
72. Federsel C, Boddien A, Jackstell R, Jennerjahn R, Dyson PJ, Scopelliti R, Laurenczy G, Beller M (2010) A well-defined iron catalyst for the reduction of bicarbonates and carbon dioxide to formates, alkyl formates, and formamides. Angew Chem Int Ed 49(50):9777–9780. doi:10.1002/anie.201004263
73. Federsel C, Ziebart C, Jackstell R, Baumann W, Beller M (2012) Catalytic hydrogenation of carbon dioxide and bicarbonates with a well-defined cobalt dihydrogen complex. Chem Eur J 18(1):72–75. doi:10.1002/chem.201101343
74. Ziebart C, Federsel C, Anbarasan P, Jackstell R, Baumann W, Spannenberg A, Beller M (2012) Well-defined iron catalyst for improved hydrogenation of carbon dioxide and bicarbonate. J Am Chem Soc 134(51):20701–20704. doi:10.1021/ja307924a
75. Bianchini C, Peruzzini M, Zanobini F (1988) An exceptionally stable cis-(hydride)([eta]2-dihydrogen) complex of iron. J Organomet Chem 354(2):C19–C22. doi:10.1016/0022-328x(88)87057-8

76. Jeletic MS, Mock MT, Appel AM, Linehan JC (2013) A cobalt-based catalyst for the hydrogenation of CO_2 under ambient conditions. J Am Chem Soc. doi:10.1021/ja406601v
77. Jansen A, Pitter S (2004) Homogeneously catalysed reduction of carbon dioxide with silanes: a study on solvent and ligand effects and catalyst recycling. J Mol Catal A Chem 217 (1–2):41–45, http://dx.doi.org/10.1016/j.molcata.2004.03.041
78. Deglmann P, Ember E, Hofmann P, Pitter S, Walter O (2007) Experimental and theoretical investigations on the catalytic hydrosilylation of carbon dioxide with ruthenium nitrile complexes. Chem Eur J 13(10):2864–2879. doi:10.1002/chem.200600396
79. Motokura K, Kashiwame D, Takahashi N, Miyaji A, Baba T (2013) Highly active and selective catalysis of copper diphosphine complexes for the transformation of carbon dioxide into silyl formate. Chem Eur J 19(30):10030–10037. doi:10.1002/chem.201300935
80. Lalrempuia R, Iglesias M, Polo V, Sanz Miguel PJ, Fernández-Alvarez FJ, Pérez-Torrente JJ, Oro LA (2012) Effective fixation of CO_2 by iridium-catalyzed hydrosilylation. Angew Chem Int Ed 51(51):12824–12827. doi:10.1002/anie.201206165
81. Sattler W, Parkin G (2012) Zinc catalysts for on-demand hydrogen generation and carbon dioxide functionalization. J Am Chem Soc 134(42):17462–17465. doi:10.1021/ja308500s
82. Motokura K, Kashiwame D, Miyaji A, Baba T (2012) Copper-catalyzed formic acid synthesis from CO_2 with hydrosilanes and H_2O. Org Lett 14(10):2642–2645. doi:10.1021/ol301034j
83. Zhang L, Cheng J, Hou Z (2013) Highly efficient catalytic hydrosilylation of carbon dioxide by an N-heterocyclic carbene copper catalyst. Chem Commun 49(42):4782–4784. doi:10.1039/C3CC41838C
84. Itagaki S, Yamaguchi K, Mizuno N (2013) Catalytic synthesis of silyl formates with 1 atm of CO_2 and their utilization for synthesis of formyl compounds and formic acid. J Mol Catal A Chem 366:347–352, http://dx.doi.org/10.1016/j.molcata.2012.10.014
85. Schäfer A, Saak W, Haase D, Müller T (2012) Silyl cation mediated conversion of CO_2 into benzoic acid, formic acid, and methanol. Angew Chem Int Ed 51(12):2981–2984. doi:10.1002/anie.201107958
86. Miller AJM, Labinger JA, Bercaw JE (2011) Trialkylborane-assisted CO_2 reduction by late transition metal hydrides. Organometallics 30(16):4308–4314. doi:10.1021/om200364w
87. Shintani R, Nozaki K (2013) Copper-catalyzed hydroboration of carbon dioxide. Organometallics 32(8):2459–2462. doi:10.1021/om400175h
88. Stephan DW (2013) Catalysis: a step closer to a methanol economy. Nature 495(7439):54–55
89. Nielsen M, Alberico E, Baumann W, Drexler H-J, Junge H, Gladiali S, Beller M (2013) Low-temperature aqueous-phase methanol dehydrogenation to hydrogen and carbon dioxide. Nature 495(7439):85–89
90. (a) Surumpudi S, Narayanan SR, Vamos E, Frank HA, Halpert G, Prakash GKS, Olah GA, US Patent 6,248,460, 2001; (b) Surumpudi S, Narayanan SR, Vamos E, Frank HA, Halpert G, Olah GA, Prakash GKS, US Patent 6,444,343, 2002
91. Chang CD (1997) In: Ertl G, Knözinger H, Weitkamp J (eds) Handbook of heterogeneous catalysis. VCH, Weinheim, p 1894 and references therein
92. Huff CA, Sanford MS (2011) Cascade catalysis for the homogeneous hydrogenation of CO_2 to methanol. J Am Chem Soc 133(45):18122–18125. doi:10.1021/ja208760j
93. Huff CA, Kampf JW, Sanford MS (2012) Role of a noninnocent pincer ligand in the activation of CO_2 at (PNN)Ru(H)(CO). Organometallics 31(13):4643–4645. doi:10.1021/om300403b
94. Vogt M, Gargir M, Iron MA, Diskin-Posner Y, Ben-David Y, Milstein D (2012) A new mode of activation of CO_2 by metal–ligand cooperation with reversible C–C and M–O bond formation at ambient temperature. Chem Eur J 18(30):9194–9197. doi:10.1002/chem.201201730
95. Langer J, Fabra MJ, Garcia-Orduna P, Lahoz FJ, Oro LA (2008) A C-H activation-CO_2-carboxylation reaction sequence mediated by an 'Iridium(dppm)' species. Formation of the anionic ligand (Ph2P)2C-COOH. Chem Commun 39:4822–4824
96. Wesselbaum S, vom Stein T, Klankermayer J, Leitner W (2012) Hydrogenation of carbon dioxide to methanol by using a homogeneous ruthenium–phosphine catalyst. Angew Chem 124:7617–7620. doi:10.1002/ange.201202320

97. Balaraman E, Gunanathan C, Zhang J, Shimon LJW, Milstein D (2011) Efficient hydrogenation of organic carbonates, carbamates and formates indicates alternative routes to methanol based on CO_2 and CO. Nat Chem 3(8):609–614
98. Balaraman E, Ben-David Y, Milstein D (2011) Unprecedented catalytic hydrogenation of urea derivatives to amines and methanol. Angew Chem Int Ed 50(49):11702–11705. doi:10.1002/anie.201106612
99. Dixneuf PH (2011) Bifunctional catalysis: a bridge from CO_2 to methanol. Nat Chem 3(8):578–579
100. Choudhury J (2012) New strategies for CO2-to-methanol conversion. ChemCatChem 4:609–611. doi:10.1002/cctc.201100495
101. Yang X (2012) Metal hydride and ligand proton transfer mechanism for the hydrogenation of dimethyl carbonate to methanol catalyzed by a pincer ruthenium complex. ACS Catal 2(6):964–970. doi:10.1021/cs3000683
102. Han Z, Rong L, Wu J, Zhang L, Wang Z, Ding K (2012) Catalytic hydrogenation of cyclic carbonates: a practical approach from CO_2 and epoxides to methanol and diols. Angew Chem Int Ed 51(52):13041–13045. doi:10.1002/anie.201207781
103. Li Y, Junge K, Beller M (2013) Improving the efficiency of the hydrogenation of carbonates and carbon dioxide to methanol. ChemCatChem 5(5):1072–1074. doi:10.1002/cctc.201300013
104. Miller AJM, Heinekey DM, Mayer JM, Goldberg KI (2013) Catalytic disproportionation of formic acid to generate methanol. Angew Chem 125(14):4073–4076. doi:10.1002/ange.201208470
105. Stephan DW, Erker G (2010) Frustrated Lewis pairs: metal-free hydrogen activation and more. Angew Chem Int Ed 49(1):46–76. doi:10.1002/anie.200903708
106. Ashley AE, Thompson AL, O'Hare D (2009) Non-metal-mediated homogeneous hydrogenation of CO_2 to CH3OH. Angew Chem Int Ed 48(52):9839–9843. doi:10.1002/anie.200905466
107. Ménard G, Stephan DW (2010) Room temperature reduction of CO_2 to methanol by Al-based frustrated Lewis pairs and ammonia borane. J Am Chem Soc 132(6):1796–1797. doi:10.1021/ja9104792
108. Riduan SN, Zhang Y, Ying JY (2009) Conversion of carbon dioxide into methanol with silanes over N-heterocyclic carbene catalysts. Angew Chem Int Ed 48(18):3322–3325. doi:10.1002/anie.200806058
109. Chakraborty S, Zhang J, Krause JA, Guan H (2010) An efficient nickel catalyst for the reduction of carbon dioxide with a borane. J Am Chem Soc 132(26):8872–8873. doi:10.1021/ja103982t
110. Huang F, Lu G, Zhao L, Li H, Wang Z-X (2010) The catalytic role of N-heterocyclic carbene in a metal-free conversion of carbon dioxide into methanol: a computational mechanism study. J Am Chem Soc 132(35):12388–12396. doi:10.1021/ja103531z
111. Huang F, Zhang C, Jiang J, Wang Z-X, Guan H (2011) How does the nickel pincer complex catalyze the conversion of CO_2 to a methanol derivative? A computational mechanistic study. Inorg Chem 50(8):3816–3825. doi:10.1021/ic200221a
112. Bontemps S, Vendier L, Sabo-Etienne S (2012) Borane-mediated carbon dioxide reduction at ruthenium: formation of C1 and C2 compounds. Angew Chem Int Ed 51(7):1671–1674. doi:10.1002/anie.201107352
113. Bontemps S, Sabo-Etienne S (2013) Trapping formaldehyde in the homogeneous catalytic reduction of carbon dioxide. Angew Chem Int Ed. doi:10.1002/anie.201304025
114. Sgro MJ, Stephan DW (2012) Frustrated Lewis pair inspired carbon dioxide reduction by a ruthenium tris(aminophosphine) complex. Angew Chem 124(45):11505–11507. doi:10.1002/ange.201205741
115. Courtemanche M-A, Légaré M-A, Maron L, Fontaine F-G (2013) A highly active phosphine–borane organocatalyst for the reduction of CO_2 to methanol using hydroboranes. J Am Chem Soc 135(25):9326–9329. doi:10.1021/ja404585p

116. Zimmerman PM, Zhang Z, Musgrave CB (2010) Simultaneous two-hydrogen transfer as a mechanism for efficient CO_2 reduction. Inorg Chem 49(19):8724–8728. doi:10.1021/ic100454z
117. Khandelwal M, Wehmschulte RJ (2012) Deoxygenative reduction of carbon dioxide to methane, toluene, and diphenylmethane with [Et2Al]+ as catalyst. Angew Chem Int Ed 51(29):7323–7326. doi:10.1002/anie.201201282
118. Matsuo T, Kawaguchi H (2006) From carbon dioxide to methane: homogeneous reduction of carbon dioxide with hydrosilanes catalyzed by zirconium – borane complexes. J Am Chem Soc 128(38):12362–12363. doi:10.1021/ja0647250
119. Berkefeld A, Piers WE, Parvez M (2010) Tandem frustrated Lewis pair/Tris (pentafluorophenyl)borane-catalyzed deoxygenative hydrosilylation of carbon dioxide. J Am Chem Soc 132(31):10660–10661. doi:10.1021/ja105320c
120. Berkefeld A, Piers WE, Parvez M, Castro L, Maron L, Eisenstein O (2013) Decamethylscandocinium-hydrido-(perfluorophenyl)borate: fixation and tandem tris(perfluorophenyl) borane catalysed deoxygenative hydrosilation of carbon dioxide. Chem Sci 4(5):2152–2162. doi:10.1039/C3SC50145K
121. Mitton SJ, Turculet L (2012) Mild reduction of carbon dioxide to methane with tertiary silanes catalyzed by platinum and palladium silyl pincer complexes. Chem Eur J 18(48):15258–15262. doi:10.1002/chem.201203226
122. Park S, Bézier D, Brookhart M (2012) An efficient iridium catalyst for reduction of carbon dioxide to methane with trialkylsilanes. J Am Chem Soc 134(28):11404–11407. doi:10.1021/ja305318c
123. Li Y, Fang X, Junge K, Beller M (2013) A general catalytic methylation of amines using carbon dioxide. Angew Chem Int Ed. doi:10.1002/anie.201301349
124. Jacquet O, Frogneux X, Das Neves Gomes C, Cantat T (2013) CO_2 as a C1-building block for the catalytic methylation of amines. Chem Sci 4(5):2127–2131. doi:10.1039/C3SC22240C

Chapter 5
Latest Advances in the Catalytic Hydrogenation of Carbon Dioxide to Methanol/Dimethylether

Francesco Arena, Giovanni Mezzatesta, Lorenzo Spadaro, and Giuseppe Trunfio

5.1 Introduction

As world population growth places more demand on limited fossil fuels, the discovery of renewable energy sources becomes crucial as part of the solution to the impending energy and environmental dilemmas. Indeed, the continuously rising levels of carbon dioxide in the atmosphere, expected to double current levels (≈400 ppm) before 2050 [1], represent to date a major environmental threat, owing to the unpredictable consequences of the *greenhouse effect* responsible for the global warming and climate changes already in place [1–5]. This depends on the fact that carbon dioxide is naturally recycled through photosynthesis processes, using sun's energy, in geological times.

Therefore, systematic exploitation of renewable energy sources and recycling technologies are compulsory to attain a significant short-term cut of carbon dioxide emissions. In this context a very viable solution for the abatement of the huge releases from fossil fuel-burning power plants and other industrial flue gases, including cement factories, consists of the chemical conversion of carbon dioxide to fuels alternative to oil-derived ones, like methanol (MOH) and dimethylether (DME) [2–11].

Indeed, methanol and dimethylether are effective substitutes of LPG, gasoline and gas oil, ensuring also considerably minor VOC and PM^{10} polluting impact than crude oil-derived fuels [2, 5–7, 12]; with an average octane number of 100, the former has excellent characteristics for spark-ignited engines, while DME (currently produced by methanol dehydration) can well replace diesel in compression-ignited engines, because of its high cetane number (55–60), and LPG for household purposes [2–5, 9, 10].

F. Arena (✉) • L. Spadaro
DEEICE-UNIME + Instituto CNR-ITAE, Nicola Giordano,
Salita S. Lucia 31, 98125 Messina, Italy
e-mail: Francesco.Arena@unime.it

G. Mezzatesta • G. Trunfio
Department of Electronic Engineering, Industrial Chemistry and Engineering,
University of Messina, Messina, Italy

B.M. Bhanage and M. Arai (eds.), *Transformation and Utilization of Carbon Dioxide*,
Green Chemistry and Sustainable Technology, DOI 10.1007/978-3-642-44988-8_5,

In perspective, MOH and DME are advantageous to hydrogen as an energy carrier, as the latter is explosive and volatile and has a very low energy density, also being a prime material for synthetic hydrocarbon manufacture and chemical industry as well [2, 4–9]. A remarkable advantage of MOH and DME also over biofuels is that the former do not require shifting valuable agricultural and food resources to fuel production. Therefore, an economy based on methanol as an energy carrier could be renewable at the short timescales necessary for human needs.

Easily accessible from natural gas, MOH-based fuels would also meet the strategic goal of reducing the oil dependence of Western countries, while the exploitation of CO_2-rich natural gas fields, coupled to lower costs of syngas obtained by technologies alternative to steam reforming, like wet partial oxidation (WPOX) or auto-thermal reforming (ATR), represents further remarkable economic advantages of CO_2-hydrogenation processes over current MOH–DME synthesis technologies [5, 11–13].

Since many decades, methanol synthesis is industrially run on Cu–ZnO/Al_2O_3 catalysts, feeding syngas streams containing traces of CO_2 [2, 4, 6, 14–16], though methanol can be obtained via CO_2 hydrogenation with rates and carbon utilisation factors comparable to those of traditional route [17–19]. Despite mechanism and active sites still being a matter of debate, indeed, it is generally recognised that methanol forms from CO_2, while CO acts as *scavenger* of oxygen atoms coming from water production, hindering active metal sites [2, 4, 17, 20–22]. Then, water formation explains a lower functionality in CO_2-rich syngas streams of traditional alumina-based synthesis catalysts in comparison to zirconia ones [16, 23–28]. In fact, though the enhanced reactivity of ZrO_2-promoted Cu systems is generally ascribed to a lower water affinity than commercial alumina-based ones, valuable promoting effects of many oxide promoters and carriers on the functionality of Cu catalyst have been documented [2, 4, 28–32]. In this context, the lack of definitive evidences on the CO_2-hydrogenation mechanism of oxide-promoted Cu systems represents to date a major drawback for further catalyst advances [2, 29–32]. Despite the methanol synthesis reactions network on metal Cu has been thoroughly described by a classical Langmuir–Hinshelwood (L–H) model [17, 33, 34], a mix of *structural*, *electronic* and *chemical* effects is invoked to explain the positive influence of oxide promoters on the CO_2-hydrogenation pattern of Cu catalyst [2, 4, 28–32].

In fact, apart from the generally recognised indispensable promoting influence of ZnO on the catalytic functionality of Cu [2, 4, 30, 33, 35–39], the lack of relationships between metal exposure (MSA) and activity seems to depend on a strong "synergism" of metal and oxide phases controlling texture, exposure of active sites and interaction with reagents, products and intermediates.

5.2 Thermodynamic Aspects of Methanol Synthesis Reactions

Since almost a century, methanol synthesis is one of the most important processes of the chemical industry, methanol, with ammonia and sulphuric acid, being one of the three most produced chemicals in the world. With an overall capacity of about

Table 5.1 List of reactions of the methanol synthesis processes

Description	Reaction stoichiometry	ΔH^0 (kJ/mol)	Acronym
Methanol synthesis	$CO_2 + 3\ H_2 \leftrightarrows CH_3OH + H_2O$	−49.4	MS
Reverse water gas shift	$CO_2 + H_2 \leftrightarrows CO + H_2O$	+41.1	RWGS
CO hydrogenation	$CO + 2\ H_2 \leftrightarrows CH_3OH$	−90.5	COH
Methanol steam reforming	$CH_3OH + H_2O \leftrightarrows CO_2 + 3\ H_2$	+49.4	MSR
Water gas shift	$CO + H_2O \leftrightarrows CO_2 + H_2$	−41.1	WGS
Methanol decomposition	$CH_3OH \leftrightarrows CO + 2\ H_2$	+90.5	MD

ΔH^0 at standard conditions (25 °C and 0.1 MPa)

60 Mton *per* year [40], nowadays methanol synthesis is run on Cu–ZnO/Al_2O_3 catalysts in the range of 220–300 °C, at a pressure of 5–10 MPa, with a syngas feed generally containing 10–20 % of CO_x in H_2 [2–6, 21, 40–45].

Indeed, whatever feed composition, the chemistry of methanol synthesis processes can be described by two main reactions, both involving CO_2 as reactant: the methanol synthesis (MS) and the reverse water gas shift (RWGS). A linear combination of MS and RWGS accounts for the straight CO hydrogenation to methanol (COH), besides all those relevant processes involving CO, CO_2, H_2, CH_3OH and H_2O, like methanol steam reforming (MSR) and decomposition (MD) and water gas shift (WGS), constituting the reverse of COH, MS and RWGS, respectively (Table 5.1).

Due to the involvement of the same molecules, and perhaps of similar intermediates, the above reactions deserve analogous catalyst formulations, including copper as the active phase [1–6, 21, 33, 40–45]. In addition, they occur in a relatively narrow range of temperature (200–300 °C), the lower limit relying on kinetic factors, while, at industrial scale, yield optimisation deserves different operating pressures.

The optimum operating conditions of each process are, in fact, evident from Fig. 5.1a, showing an overview of the free energy of MS, RWGS and COH reactions in the range of 25–300 °C. Both MS and RWGS reactions are characterised by ΔG values that are always positive, rising for the former (4→56 kJ/mol) and decreasing for the latter (28→17 kJ/mol), while COH is the only favoured process ($\Delta G < 0$) below 150 °C. Furthermore, the MS and COH reactions are exothermic and accompanied by a decrease in volume, while the endothermic RWGS is favoured at higher temperatures and insensitive to pressure (Table 5.1).

Therefore, whether CO or CO_2 is the C-atom source, thermodynamic data indicate that methanol formation is favoured at lower temperatures and higher pressures as shown, in particular, by the equilibrium conversion-selectivity data of a stoichiometric (1:3) CO_2:H_2 mixture in the range of 160–260 °C (Fig. 5.1b).

At any pressure and below 160 °C, thermodynamic data show full selectivity to methanol, decreasing with temperature more steeply as pressure decreases. The CO_2 conversion lowers with temperature, though its variation is very sensitive to pressure at 160 °C (19–43 %) and almost negligible (20–25 %) at 260 °C. This is because of the prevailing contribution of MS over the RWGS reaction at lower temperature and vice versa (Fig. 5.1a).

Finally, thermodynamic data deserve a final remark concerning the methanol C-atom source. In fact, CO in the syngas feed for the methanol synthesis does not

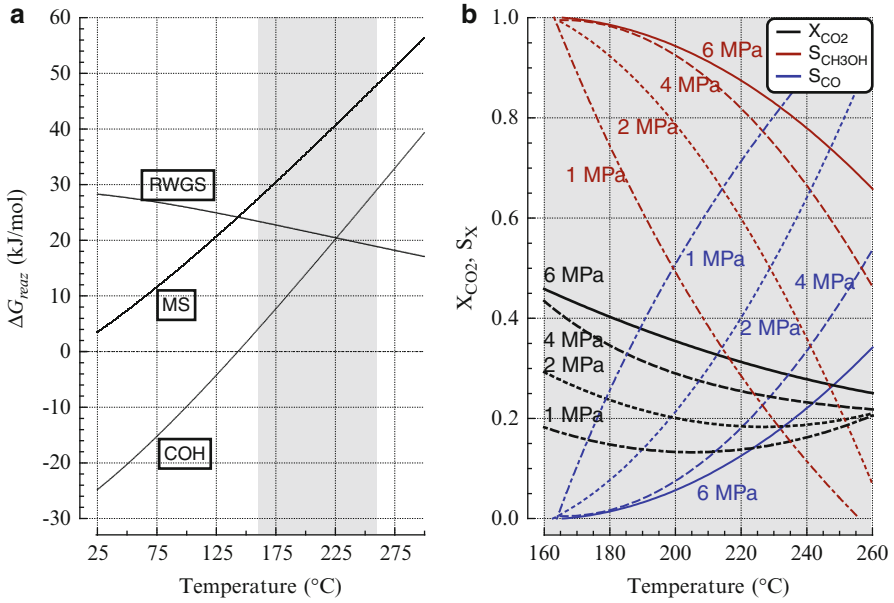

Fig. 5.1 Free energy of the MS, RWGS and COH reactions (**a**) and equilibrium conversion-selectivity values of the CO_2-hydrogenation reaction at various pressures (**b**)

take part directly in the reaction, but it rather does influence the process through two effects: (i) producing the "reactive" CO_2 intermediate via the WGS reaction and (ii) influencing morphology, state and composition of metal Cu particles. Thermodynamic data, however, suggest that it would be advantageous to the synthesis of methanol by direct hydrogenation of CO, the COH reaction being characterised by lower ΔG values in the concerned range of temperature (Fig. 5.1a). At any pressure, it would allow much higher conversion and yield per pass than current processes, proceeding through CO_2 hydrogenation, as demonstrated by the CO and CO_2-hydrogenation equilibrium values reported in Table 5.2.

Therefore, the discovery of novel catalysts producing methanol with high selectivity, directly by hydrogenation of CO (*methanation* is the competitive process), would represent a further decisive breakthrough for the MOH synthesis technology [33].

5.3 Catalysts for Methanol Synthesis

Although the thermodynamic analysis indicates low temperature and high pressure as the optimal reaction conditions for the CO_2-hydrogenation process, the activation of carbon dioxide occurs with a sufficient rate only at temperatures higher than 200 °C. At such temperatures, however, the formation of by-products like CO,

Table 5.2 Equilibrium conversion values of stoichiometric $CO–H_2$ (1:2) and $CO_2–H_2$ (1:3) mixtures at various temperatures and pressures

Temperature	Pressure					
	2 MPa	4 MPa	6 MPa	2 MPa	4 MPa	6 MPa
(°C)	X_{CO} (%)[a]			X_{CO2}–S_{CH3OH}–Y_{CH3OH} (%)[b]		
180	66	77	82	24-92-22	35-97-34	40-98-40
200	53	68	75	20-80-16	29-93-27	35-96-34
220	39	57	65	19-59-11	25-83-22	32-85-27
240	26	44	55	19-36-7	23-66-15	28-79-22
260	15	32	43	21-8-2	22-46-10	25-66-17

[a]Assuming a total selectivity to methanol (i.e. $X_{CO} = Y_{CH3OH}$)
[b]From MS and RWGS equilibrium data (Fig. 5.1b)

hydrocarbons and alcohols lowers methanol selectivity and yield; then, preferably, catalysts should be able to activate the CO_2 at temperatures as low as possible, avoiding undesired by-products formation.

Several surveys have been devoted to catalyst design, investigating the role of different active phases and their interaction with many oxide support and promoters [2, 4].

5.3.1 Active Phases

Although a variety of metal phases were investigated, a competitive catalyst formulation for the CO_2-hydrogenation process remains that of conventional synthesis catalysts, including copper and zinc oxide on an alumina carrier, in different proportions [2, 4, 6, 41]. Generally, CuO loading is comprised between 40 and 80 %, ZnO between 10 and 30 %, while Al_2O_3 represents the remaining weight fraction, being comprised between 10 and 20 % [6]. These require extremely pure syngas (i.e. S- and Cl-compound concentrations lower than 0.1 ppm) and mild operating conditions to avoid the premature ageing caused by the copper sintering [2, 41].

Then, relatively large amounts of water produced by MS and RWGS (Table 5.1) inhibit catalytically active sites, probably constituting the hardest drawback of conventional methanol synthesis catalysts, accelerating the catalyst sintering and the synthesis rate decay [4, 22–25, 45, 46]. Indeed, the presence of CO in syngas, besides serving as CO_2 source, acts as scavenger of oxygen atoms, hindering the negative effects of water formation [4, 20, 33].

Hence, catalysts for carbon dioxide hydrogenation should exhibit a higher water tolerance, suggesting that this could be at the origin of a lower functionality of the alumina-based catalysts in comparison to zirconia ones [4, 16, 24–30].

In combination with different promoters, copper is to date considered as the best active phase for the methanol synthesis reactions [2–4, 6, 31, 33, 47], as documented by a brief summary of activity data of the most used metal catalysts in Table 5.3. In particular, Cu-based catalysts exhibit the best CO_2-hydrogenation

Table 5.3 Activity data in the CO_2-hydrogenation reaction of different catalysts

Catalyst	Preparation method	P(MPa)	T (°C)	CO_2 conv. (%)	Methanol yield (%)	Ref.
Cu–ZnO/ZrO_2	Co-precipitation	8	220	21.0	14.3	[49]
Ag/ZnO/ZrO_2	Co-precipitation	8	220	2.0	1.9	[49]
Au/ZnO/ZrO_2	Co-precipitation	8	220	2.5	1.5	[49]
Pd–CeO_2	Impregnation	2	250	4.1	1.2	[50]
Pd/Zn/CNTs	Incipient wetness	3	250	6.3	6.3	[51]
G_2O_3–Pd/SiO_2	Incipient wetness	3	250	n/a	–	[52]
$LaCr_{0.5}Cu_{0.5}O_3$	Sol-gel	2	250	10.4	9.4	[53]
Pt/CeO_2	Impregnation	30	230	8.1	5.5	[54]
Ru/CeO_2	Impregnation	30	230	8.2	0	[54]
Ni/CeO_2	Impregnation	30	230	2.5	0	[54]

functionality to methanol, while, though active, Ni, Ru and Rh mainly encourage the formation of methane [47, 48]. Examples of less reactive metal components are Pd, Pt, Ag and Au, also catalysing the formation of high amounts of carbon monoxide and methane [49–54]. Moreover, Pd–ZnO catalyst supported on multiwalled carbon nanotubes (CNTs) offers very high methanol selectivity at very low conversion *per* pass, while a Pd/CeO_2 system forms preferentially formaldehyde instead of methanol (Table 5.3).

Despite the unpredictability of the catalyst performance at microscopic level, such evidences indicate that the superior methanol synthesis functionality of Cu is likely associated to its peculiar ability to hinder the breaking of the C–O bond, at variance of more active hydrogenation catalysts, like Ni, Pt, Ru and Pd, forming huge amounts of methane.

Furthermore, a very controversial issue concerns the chemical state of the active sites under stationary reaction conditions [2, 4, 11, 14–18, 33, 55]. Indeed, some claim that metal Cu atoms are uniformly active, according to a catalytic activity comparing the metal surface area [35–58], whereas others report that electron-deficient $Cu^{\delta+}$ species dissolved across the ZnO promoter are the active sites, on the basis of a superior specific activity than un-promoted systems [4, 12, 59–69]. Anyhow, strong synergistic effects on the functionality of the binary Cu–ZnO system can be grouped into the following six categories [70]:

- Formation of Cu^+ ions on the ZnO phase [59, 60, 71]
- Schottky-type junction effects at the Cu–ZnO interface [61]
- Electronic interactions between Cu and ZnO [61]
- Formation of Cu–Zn pair alloy [35, 39]
- Specific reaction at the Cu–ZnO interface [65]
- Stabilisation of Cu in a morphologically active form by ZnO [69]

Metal copper centres are by far the most accepted species responsible for the catalytic activity, though their exact nature is not fully clear, strongly depending on the gas phase composition.

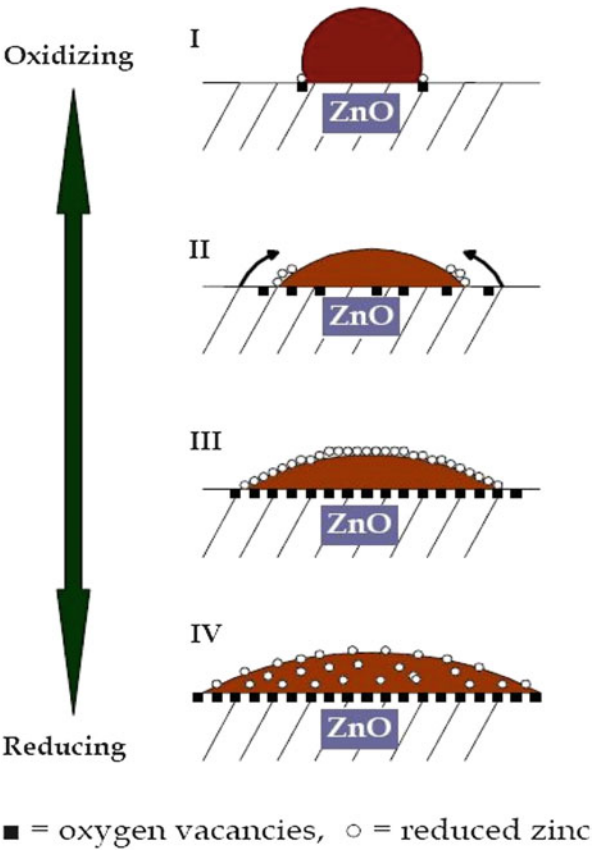

Fig. 5.2 Schematic model for the wetting/non-wetting phenomena of the Cu particles on the ZnO support [70]: (*I*) round-shaped particle under oxidising syngas conditions; (*II*) disc-like particle under more reducing conditions; (*III*) surface Zn–Cu alloying due to stronger reducing conditions; (*IV*) brass alloy formation due to severe reducing conditions

For instance, on the basis of DFT calculations, several authors conclude that open Cu surface partially covered by oxygen provides a better model for the active sites of methanol synthesis [17, 72, 73]. On the other hand, higher reducing potentials increase oxygen vacancies at the ZnO surface and spread over Cu crystallites [33, 64], ultimately resulting in the formation of Cu–Zn surface alloys [65, 66]. Reversible changes in the Cu coordination number with the particle shape on the ZnO support induced by the wetting/non-wetting phenomenon were also reported [64]. Under oxidising conditions, the ZnO surface is not wetted by copper, leading to more spherical-shaped copper particles, while a wetting transition takes place if the ZnO surface becomes oxygen deficient as the copper particles assume a "pancake" morphology, as shown in Fig. 5.2 for the wetting/non-wetting model of Cu particles on the ZnO support [64]. HRTEM investigations show that the changes for ZnO-supported samples are caused both by adsorbate-induced changes in surface energies and changes in the interfacial energy [33, 74].

Therefore, the observed dynamic restructuring in response to changes in the properties of the reaction environment demonstrates that the active sites for methanol catalysts are essentially generated during reaction [17, 33, 72–74].

5.3.2 Supports and Promoters

Although the superior reactivity of ZnO-promoted Cu catalysts is generally recognised, valuable promoting effects of many oxide promoters and carriers on the functionality of Cu catalyst have been documented.

Therefore, novel catalyst formulations and preparation methods have been proposed to improve the process performance in terms of activity, selectivity and stability [2, 4].

Among the oxide promoters of the Cu–ZnO system, ZrO_2 is of overwhelming interest because of its good mechanical and thermal stability under reducing and oxidising atmospheres, high specific surface area and a peculiar surface functionality [16, 25, 28, 70, 75]. It is not a case that pure ZrO_2 shows distinct activity and selectivity for methanol synthesis at higher reaction temperatures [70].

Then, adopting a new preparation method based on the reverse co-precipitation of precursors under ultrasound irradiation, Arena et al. synthesised Cu–ZnO/ZrO_2 catalysts with surface exposure up to 170 m^2/g and metal dispersion and surface area values up to 60 % and 60 $m_{Cu}^{2} \cdot g_{cat}^{-1}$, respectively [25]. Recently, Guo et al. obtained Cu–ZnO/ZrO_2 catalysts with favourable characteristics such as small grain size and low reduction temperature via the urea–nitrate combustion method [76]. The presence of urea distributes the combustion heat, allowing a very fast quenching effect leading to very small CuO particles that favour a stronger interaction between copper, ZnO and ZrO_2. An increase in the urea content led to the partial transformation of *t*-ZrO_2 to *m*-ZrO_2, stabilising higher concentration of the reactive intermediates that improve methanol selectivity [76].

Słoczyński et al. studied the effects of Ga, B, In, Gd, Y, Mg and Mn on Cu–ZnO/ZrO_2 catalyst, pointing out a remarkable influence on the catalyst activity [32]. The highest methanol yield was obtained by the addition of Ga, while In implies a severe activity loss. Toyir et al. reported that the addition of Ga_2O_3 to the Cu–ZnO system enhances the methanol production, due to selectivity values two times higher than that of the corresponding Cu–ZnO system [77]. Finally, studying the influence of Ce addition on $Cu/Ce_xZr_{(1-x)}O_2$ catalyst, Pokrovski and Bell observed a strong increase of the methanol selectivity [31], later confirmed by Arena et al., though a low surface exposure depresses the catalyst productivity [28–31].

5.4 Mechanistic–Kinetic Aspects of CO_2-Hydrogenation Reactions

5.4.1 Methanol Synthesis

Although bare metal Cu exhibits its own reactivity in the hydrogenation of CO_2 to methanol, well described by macro- and microkinetic models [17, 33, 72, 73], the

promoting effect of many oxide systems reflects the occurrence of structural, chemical and electronic effects, enhancing exposure and reactivity of Cu sites. In addition, it must be stressed that oxide promoters feature a peculiar surface affinity to either CO_2 or H_2 molecule that can further contribute to shape the functionality of multicomponent catalytic systems [28, 29, 36, 75–79].

Although this partially explains the high uncertainty on active sites in charge of the various surface functionalities of promoted Cu catalysts [2–4] and despite the similar physico-chemical characteristics of catalysts for methanol synthesis (MS), water gas shift (WGS), methanol steam reforming (MSR) and methanol decomposition (MD) processes [2, 4, 43, 44, 80–84] and composition and redox potential of the reacting atmosphere also influence morphology and chemical state of Cu particles indeed [85, 86].

In this respect, Klier et al. propose that oxidised Cu is active and reduced Cu is not in methanol synthesis, arguing that copper incorporated into Zn lattice, as Cu^+, is the active site for reactant adsorption [35, 83].

Quanto-chemical calculations lead several authors to conclude that MS and RWGS might not occur on clean Cu <111> surface [17, 72, 73]. However, Yang et al. suggest that methanol formation from both CO_2 and CO, along with the WGS–RWGS interconversion paths, occurs via the *carboxyl* (HOC*O) route, in agreement with the conclusions of Zhao et al., claiming yet a fundamental influence of the surface Cu oxygen coverage on the hydrocarboxyl route [72, 73]. In contrast, the microkinetic model developed by Grabow and Mavrikakis supports the formate reaction path, still driven by partially oxidised Cu facet (CO_2 → HCOO* → HCOOH* → CH_3O_2* → CH_2O* → CH_3O* → CH_3OH*) [17]. Both Cu^+ and Cu^0 seem to be active in the MD reaction, though the reducing environment suggested that the latter are the active sites [84], while Choi and Stenger came to conclusion that Cu^{2+} centres drive both MD and MSR reactions [44].

This "mimetic" nature of active sites depends on the fact that, despite all the above reactions involve the same molecular species, formation and fate of the numerous reaction intermediates strictly depend on the state of the catalyst surface under stationary conditions. For instance, while MSR and WGS reactions imply mostly oxidative conditions, MS, RWGS and MD proceed in a reducing environment. In other words, each process determines a different state of metal sites, shaping the reactivity of the active Cu phase in MS, WGS–RWGS, MD and MSR processes.

In this context, it is generally recognised as the systematic promoting influence of ZnO on the reactivity of Cu, because of a peculiar solid-state interaction pattern leading to the effects of different nature. In particular, a recognised strong Cu–ZnO synergism enhancing the catalytic functionality of the active phase has been mostly explained by four types of physical and chemical effects [2, 4, 33, 39, 71]:

(i) ZnO enhances metal dispersion, exerting a structural effect on Cu phase.
(ii) ZnO acts as a reservoir for atomic hydrogen that, spilling over the Cu surface, speeds up the hydrogenation of the formate intermediate.

(iii) ZnO confers a peculiar morphology to Cu particles, by stabilising specific active surface planes.
(iv) ZnO creates additional active sites on the Cu surface.

In addition, a peculiar solid-state interaction pattern renders the Cu–ZnO system very dynamic, accounting for marked changes in the morphology of metal particles, associated with the extent that the metal particles wet the underlying support, with composition and reduction potential of the gas mixture [64, 85, 86]. The dynamics of particle morphology can also be used to counteract the effect of sintering of copper particles [33], though morphology changes predicted by the Wülff reconstruction model were questioned [86]. Then, while a strong Cu–ZnO synergism positively influences metal dispersion, the nature of the promoting effect of ZnO is still controversial. Further possible electronic/chemical effects (ii–iv) due to the intimate contact of metal/oxide phases cannot, yet, be excluded [72, 73].

The picture is further complicated by the fact that, besides Cu and ZnO precursors, catalyst formulations generally involve an additional (*structural*) promoter, improving the dispersion and the resistance to sintering of Cu and ZnO phases [2, 4, 6]. Due to a peculiar capability to interact with both Cu and Zn precursors, stabilising highly dispersed, prevalently amorphous phases, ZrO_2 and Al_2O_3 are to date the most effective "carriers" of Cu–ZnO systems. Particularly, ZrO_2-based systems feature a superior activity than conventional Al_2O_3-based synthesis catalysts, probably because of a superior hydrophobicity favouring water desorption [2, 4, 25–28, 76, 87]. Nevertheless, as documented by Fischer and Bell, zirconia exhibits also a peculiar surface affinity to CO_2 playing an "active" role on the reactivity pattern of the Cu/ZrO_2 catalyst, favouring the formation of the reactive *formate* intermediate [75].

This seems not a peculiarity, since the formation of various reaction intermediates and precursors at the surface of Al_2O_3, SiO_2 and TiO_2 carriers was also reported [88].

Then, a network of *physical* and *chemical* effects, due to the strong synergism of the various phases, shapes the catalytic pattern of multicomponent systems, disguising the role and influence of each single promoter on the structure and reactivity of the active phase.

Taken as physical location of active sites, mostly as Cu^+ centres, the metal/oxide interface is in fact generally considered as a measure of the Cu–oxide(s) "synergism" [11, 26, 27, 35, 63]. Its crucial influence on the catalytic functionality could explain the lack of direct relationships between activity and metal surface area, recorded for both $Cu–ZnO/Al_2O_3$ [87] and $Cu–ZnO/ZrO_2$ systems [25–30].

This denotes a variable specific activity of Cu sites (e.g. TOF) with metal dispersion (Fig. 5.3), supporting the hypothesis that the reactivity of multicomponent catalysts no longer depends only on the availability of Cu sites [11, 25–30, 87, 89]. Particularly, a peculiar surface affinity to CO_2, enhancing the formation of reactive intermediates, as a key factor of the reactivity of promoted Cu catalysts could be taken into account [28, 29, 36, 87–90].

Due to the unfeasibility of getting direct information on the extent of the metal/oxide interface, our first attempts to highlight the key factor(s) controlling the reactivity of multicomponent Cu–ZnO catalysts were based on the evaluation of

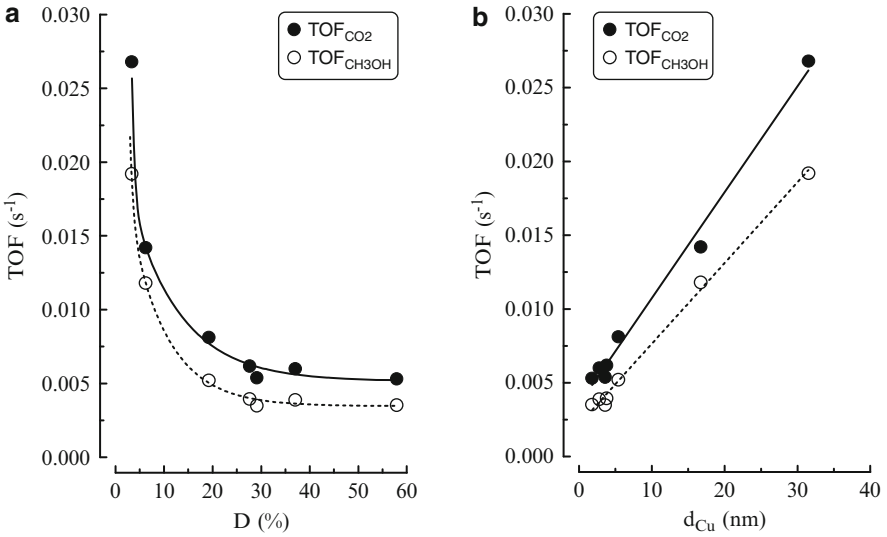

Fig. 5.3 Influence of the metal dispersion (**a**) and average metal particle diameter (**b**) on the turnover frequency of CO_2 conversion and CH_3OH formation (Reprinted from Ref. [25]. Copyright 2007, with permission from Elsevier)

the "θ" factor ($\theta = [4\cdot(MSA\cdot OSA)/(SA)^2]$, MSA, OSA and SA being metal, oxide and total surface area, respectively), taken as a measure of the degree of contact of metal and oxide phases [11].

Experimental data show typical "volcano" trends (Fig. 5.4), supporting the thought that CO_2-hydrogenation systems might bear a balanced exposure of metal (MSA) and oxide (OSA) surface [11]. This also explains the negative effect of an overwhelming MSA exposure on the reactivity of Cu–ZnO and Cu–ZnO/Al_2O_3 catalysts [87].

Chemisorption and FTIR studies on high surface area Cu–ZnO/ZrO_2 catalysts [26, 27] prove that the interaction of Cu particles with ZnO and ZrO_2 phases leads to stabilisation of $Cu^{\delta+}$ sites at the metal/oxides interface, to an extent (i.e. $Cu^{\delta+}/Cu^0$) comparable with the CO/N_2O uptake ratio [26].

Then, the normalisation of TOF to the CO/N_2O uptake (TOF_1) and oxide to metal surface area (OSA/MSA) ratios (TOF_2) results in two straight-line relationships, fairly insensitive to Cu dispersion (Fig. 5.5), supporting a direct influence of the oxide phases on the functionality of promoted Cu catalysts.

This hypothesis is supported by the conclusions of a comparative study on the effects of Ga_2O_3, Cr_2O_3, Al_2O_3 and ZrO_2 carriers on the reactivity of the Cu–ZnO system, showing different effects depending on the nature of oxide promoter [77].

In particular, these were classified into two basic categories:

- Al_2O_3 and ZrO_2 improve the metal dispersion, acting essentially as structural promoters of the active Cu phase.

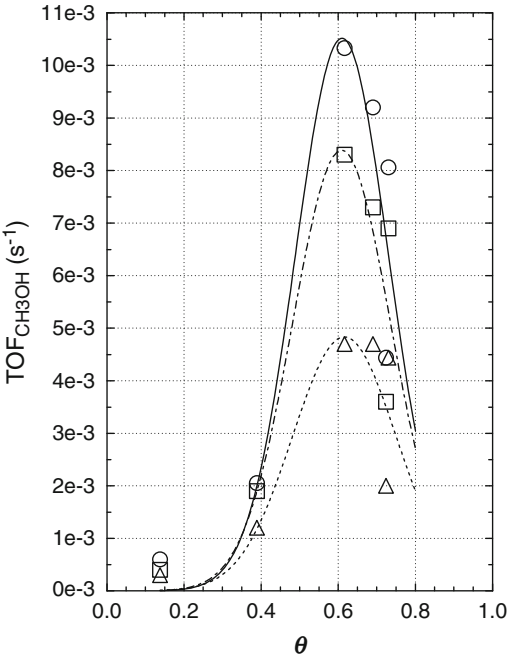

Fig. 5.4 Relationships between TOF and θ at 180 (Δ), 200 (□) and (○) 220 °C (Reprinted from Ref. [11]. Copyright 2004, with permission from Elsevier)

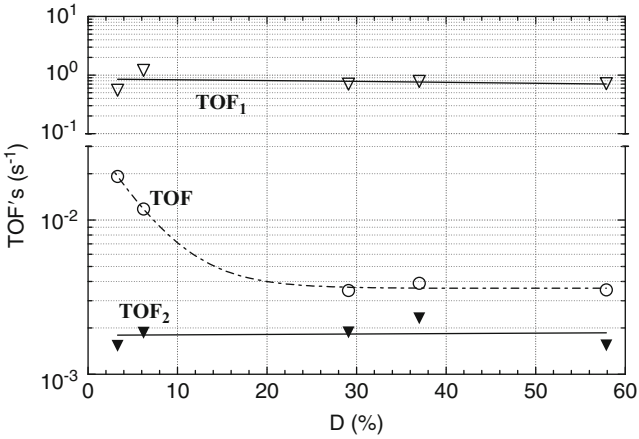

Fig. 5.5 Influence of metal dispersion on the turnover frequency (TOF) and TOF normalised to the CO/N_2O (TOF_1) and OSA/MSA (TOF_2) ratios, respectively (Reprinted from Ref. [26]. Copyright 2008, with permission from Elsevier)

- Ga_2O_3 and Cr_2O_3 enhance the specific activity of surface metal Cu atoms, acting thus as chemical/electronic promoters of the active Cu phase [77].

Likewise, the addition of ceria and ceria-yttria yields a remarkable improvement in the reactivity of the Cu/Al_2O_3 system, which was attributed to the generation of surface oxygen vacancies at ceria surface favouring CO_2 activation [89].

The peculiar promoting effect of ceria was confirmed by several studies on the influence of either ZnO or ZrO_2 substitution in $Cu–ZnO/ZrO_2$ catalysts [28–31]. Apart from a general negative influence of either ZnO or ZrO_2 replacement on total and metal surface area [28–30], activity data substantially confirm the requirement of the ZnO precursor and a progressive enhancement in the surface reactivity of the Cu–ZnO system with the extent of $CeO_2–ZrO_2$ substitution [30, 31]. Due to a much lower efficiency as structural promoter than Al_2O_3 and ZrO_2, resulting in considerably lower SA and MSA exposure, however, the $Cu–ZnO/CeO_2$ system features a lower productivity in comparison to $Cu–ZnO/Al_2O_3$ and $Cu–ZnO/ZrO_2$ catalysts [28, 29].

Nevertheless, the lack of direct relationships between activity and MSA from the specific metal surface activity data of the $Cu–ZnO/Al_2O_3$, $Cu–ZnO/ZrO_2$ and $Cu–ZnO/CeO_2$ catalysts is also evident, in this case, documenting the superior functionality of the ceria-supported catalyst at any temperature and pressure (Fig. 5.6).

Chemisorption data of the various catalysts at "steady-state" conditions, probed by temperature-programmed measurements, show a complex pattern of CO_2 and H_2 desorption (Fig. 5.7a), similar for each catalyst, along with a band of CO formation, likely due to an incipient reduction of CO_2 [28, 29]. These account for an extensive surface CO_x coverage that, referred to metal Cu surface area, gives a decreasing trend with dispersion, as shown in Fig. 5.7b. The variations are less pronounced *per* unit of total (SA) and oxide surface area (OSA). The variations are less pronounced *per* unit of total (SA) and oxide surface area (OSA).

An extent of conversion of 60–80 % to MOH and CO under H_2 stream disclosed the reactive nature of the adsorbed CO_2 species [29], while the metal-specific surface activity of the $Cu–ZnO/Al_2O_3$, $Cu–ZnO/ZrO_2$ and $Cu–ZnO/CeO_2$ catalysts depicts decreasing trends with dispersion (Fig. 5.8), similar to that found for $Cu–Zn/ZrO_2$ catalysts (Fig. 5.3) and comparable with the CO_x uptake in Fig. 5.7b.

On the other hand, unchanging values of the activity data normalised to the oxide-specific surface area (Fig. 5.8) suggest again a fundamental contribution of the oxide carrier on the CO_2-hydrogenation functionality of the Cu–ZnO system [28, 29].

Therefore, steady-state chemisorption data and structure–activity relationships suggest that oxide promoters directly affect the catalytic functionality of metal Cu, likely determining an additional availability of CO_2 adsorption–activation sites, enhancing the surface concentration of the reactive intermediate(s) [29]. On this account, the superior performance of the $Cu–ZnO/ZrO_2$ catalyst might mirror a crucial influence of the zirconia carrier on the availability and reactivity of surface sites [25–30].

Finally, experimental evidences concerning the reaction network leading to MOH and CO formation generally show a positive effect of the space velocity on methanol

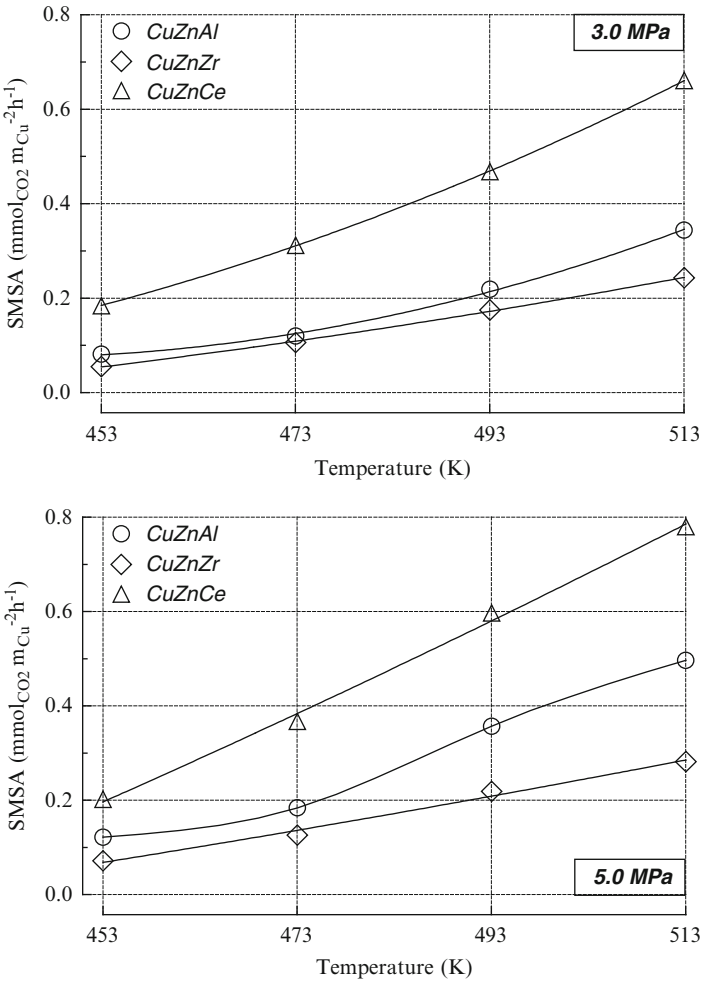

Fig. 5.6 Specific metal surface rate of CO_2 conversion in the range of 453–513 K (Adapted from Ref. [29]. Copyright 2013, with permission from Elsevier)

selectivity [28–30, 87], resulting in steadily decreasing selectivity-conversion relationships [25–27]. Altogether these evidences indicate the occurrence of a consecutive reaction network leading to the primary formation of methanol (MS) at low temperature (e.g. $T < 200$ °C) and high pressure [28, 29]. The formation of CO occurs mostly at higher temperature ($T > 200$ °C) via the consecutive and parallel MD and RWGS endothermic paths, respectively [25, 28, 29, 44, 87, 91].

Then, the mechanistic scheme proposed in Fig. 5.9 emphasises the cooperative role of the various phases on the main reaction pathway driving the primary formation of methanol at the metal/oxide interface [28].

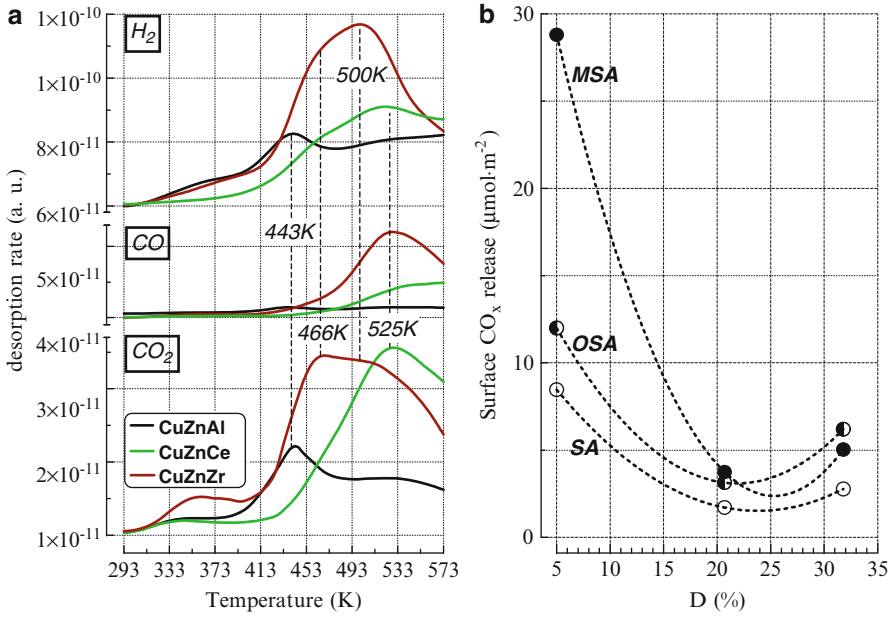

Fig. 5.7 (**a**) Temperature-programmed desorption data of CO_2, CO and H_2 of CuZnAl, CuZnZr and CuZnCe catalysts after treatment under "steady-state" reaction conditions; (**b**) relationships between the "steady-state" adsorption capacity referred to total (SA), metal (MSA) and oxide surface area (OSA) and metal dispersion (Adapted from ref. [28, 29], Copyright 2013, with permission from Elsevier)

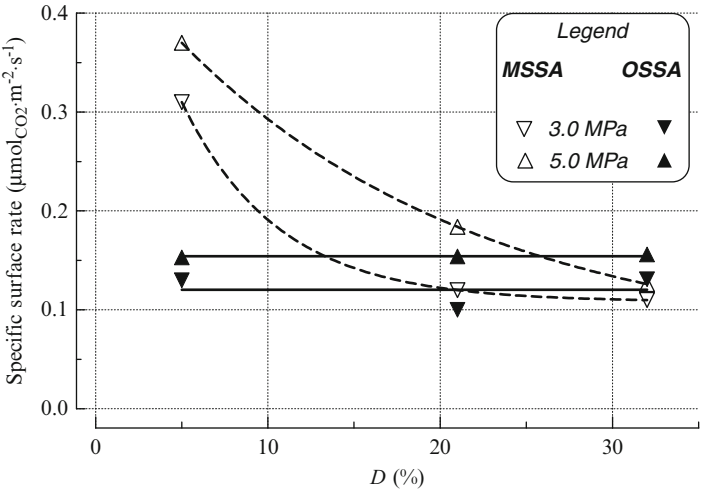

Fig. 5.8 Metal (MSSA)- and oxide (OSSA)-specific surface rates of CO_2 conversion *vs.* dispersion (Adapted from Ref. [28]. Copyright 2013, with permission from Elsevier

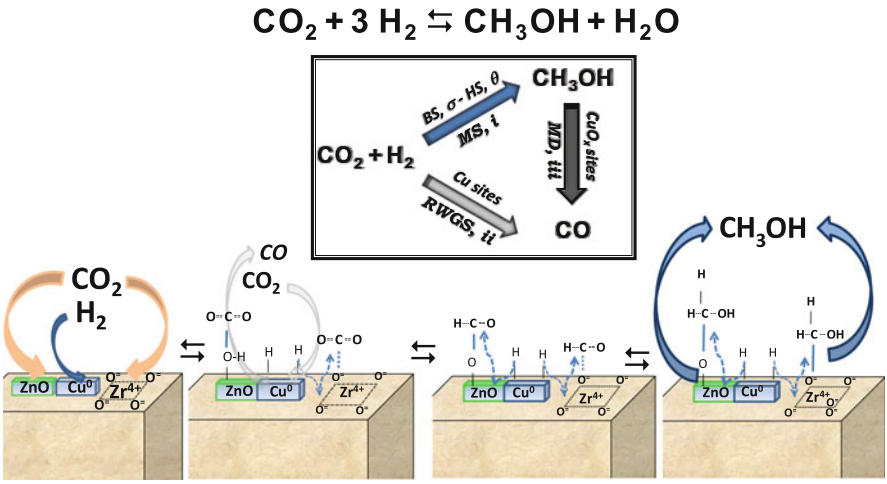

Fig. 5.9 Surface reaction mechanism of CO_2 hydrogenation to methanol on supported Cu–ZnO catalysts (Reprinted from Ref. [28]. Copyright 2013, with permission from Elsevier)

5.4.2 Direct Dimethylether Synthesis

The increasing demand of dimethylether (DME) as an alternative fuel to LPG and gas oil, coupled to the possibility of realising an effective recycle of CO_2 emissions, explains the great scientific concern on the development of the novel "one-step" DME synthesis processes via CO_2 hydrogenation.

In fact, since methanol dehydration reaction occurs in a temperature window compatible with that of the MS reaction, coupling the MS-RWGS and methanol dehydration (MDH) reactions into a "one-step" process ($2CO_2 + 6H_2 \leftrightarrows C_2H_6O + 3H_2O$) provides a strong driving force for shifting the CO_2 conversion above the equilibrium values ($2\ CH_3OH \leftrightarrows C_2H_6O + H_2O$) forced by MS-RWGS reactions (Fig. 5.1b), by in situ transformation of methanol to DME [2, 5].

Therefore, an effective synergism of MS-RWGS-MDH reactions results in remarkable economic advantages of the overall CO_2-hydrogenation process [2, 5]. However, due to quite different catalyst requirements of synthesis and dehydration processes, scouting attempts to develop bifunctional catalysts have been so far reported, using various combinations of synthesis and dehydration catalyst formulations [92–94].

In particular, adopting a co-precipitating sedimentation method, Sun et al. prepared multicomponent Cu–ZnO–ZrO_2–Al_2O_3/HZSM5 catalysts further promoted with a Pd/Al_2O_3 sample [92]. The synergistic effect of synthesis–dehydration–hydrogenation functionalities results in a strong improvement of both CO_2 conversion and MOH–DME selectivity which, at 200 °C and 3.0 MPa, reaches the remarkable level of 85–90 %, with an overwhelming formation of DME (≈75 %). However, no definitive explanation to the strong promoting influence of Pd on the functionality of the un-promoted system has been given [92].

Analogous results were obtained by Aguayo's group using Cu–ZnO/Al_2O_3 synthesis catalyst in combination with either γ-Al_2O_3 or NaHZSM5 [93, 94]. Although having considerably lower DME selectivity values (T, 275 °C; P, 4.0 MPa), a marked improvement of both conversion and selectivity led to overall MOH–DME yields much higher than the single MOH synthesis process and above the equilibrium values in the range of 240–340 °C. They also provided a kinetic model for the overall CO_2 to DME hydrogenation process, coming to the conclusion that the NaHZSM5 dehydration system could be more suitable for industrial purposes as it offers a higher resistance to deactivation by water and coke formation and a superior stability during the burn-off regeneration procedure [93].

Further attempts to synthesise DME via the CO_2-hydrogenation process have been made using "dual-bed" catalysts, obtained by physical mixing of synthesis and dehydration catalysts. A strong improvement in the process performance of the bifunctional Cu–ZnO/Al_2O_3/HZSM5 system was recently documented by Gao et al. further to the addition of La [95]. In particular, a 2 wt% of La caused a fourfold rise both in conversion and DME selectivity with respect to the un-promoted system, ascribed to both an enhanced Cu dispersion and a superior strength of acid sites. Although our preliminary attempt using Cu–ZnO/ZrO_2 and HZSM5 systems did not provide any significant improvement in CO_2 conversion or oxygenated selectivity [11], we addressed a more systematic investigation of the effects of the catalyst bed configuration on the one-step DME synthesis performances of the hybrid Cu–ZnO/ZrO_2–HZSM5 system [96]. Among the various configurations, the "mono-bed" configuration including pre-pelletised particles of both systems, with an optimum weight ratio of 1, showed the highest level of synergism, with a marked improvement of CO_2 conversion, though at the expense of MOH–DME selectivity. This could depend on the enhanced acidity or impurity present on the commercial HZSM5 system, somewhat promoting the MD reaction [96].

A preliminary study of the effects of the Ti/Zr ratio on the performances of Cu–TiO_2–ZrO_2/HZSM5 bifunctional catalysts indicated a superior performance further to the partial substitution (50/50) of zirconia with titania, though the effects of the acidic catalysts were not addressed [97].

Dual-bed Cu–ZnO–Al_2O_3–ZrO_2/HZSM5 configuration catalysts were also successfully applied in the CO_2-hydrogenation process, reaching conversion and MOH–DME yield values of 0.31 and 0.21–0.06, respectively [98]. Based on such experimental data, An et al. propose a CO_2-hydrogenation process with CO recycle to enhance both DME and MOH yields [98].

5.5 Synthesis Technologies

All commercial methanol technologies are made up of three main process sections [6, 33, 41, 99–104]:

- Synthesis gas production
- Methanol synthesis
- Methanol purification

In the design of a methanol plant, the three process sections may be considered independently, and the technology may be selected and optimised separately for each section. The criteria for the selection of technology are capital cost and plant efficiency. The syngas preparation and compression typically account for ca. 60 % of the investment, and almost all energy is consumed in this process section.

The used synthesis gas is characterised by the so-called syngas module (M), defined by the ratio $(H_2–CO_2)/(CO + CO_2)$, where $M = 2$ represents the stoichiometric synthesis gas for methanol formation [99, 100]. Hence, syngas with very high CO/CO_2 ratios reduces water formation and catalyst deactivation [6], while the presence of inerts in the syngas composition reduces the methanol formation. Typical inerts in the methanol synthesis are methane, argon and nitrogen.

Finally, the produced syngas needs a careful purification of the feedstock, since the commercial methanol catalysts may be poisoned by sulphur, chlorine compounds and metal carbonyls [6].

Currently syngas is obtained by three types of hydrocarbons reforming processes: the steam reforming (SR), the partial oxidation (POX) and the auto-thermal reforming (ATR).

The most commonly used method is the high energy-demanding SR process carried out with excess steam-to-carbon ratios, which takes place in special alloy tube reformers loaded with a nickel-based catalyst at 750–900 °C. Burners provide direct heat exchange. The exit syngas composition is a mixture of H_2, CO, CO_2 and unreacted methane accounting for an M value of ca. 3. One of the main drawbacks of this very complex technology is the long start-up time increasing the operating costs.

Unlike the SR process, the POX technology presents a simple design with small inert production without additional burners investments. It is a mature technology in which natural gas or heavy hydrocarbons are mixed in a combustion process with oxygen. The exothermic nature leads to a significant heat production requiring external utilities (water and cold air). The main drawbacks are the comparatively low hydrogen yield ($M \approx 1.8$) and the tendency to produce soot at sub-stoichiometric air/fuel ratios.

Finally, the ATR process carries out the natural gas reforming in a mixture of steam and oxygen in the presence of a catalyst reducing the investment costs by eliminating the expensive fired reformer technology. The produced heat is used to supply the heat input needed by the steam reformer.

The synthesis gas produced presents an optimal module ($\approx$2) for methanol production, implying that it is deficient in hydrogen and contains high CO_2 percentage [45]. The first ATR in operation in commercial scale at H_2O/C ratio of 0.6 was an industrial demonstration in South Africa in 1999. Very large units were started in South Africa in 2004 and Qatar in 2006 [101, 102]. A methanol plant with a single line capacity of 10,000 MTPD is in the engineering phase for start-up in Nigeria [103, 104].

5.5.1 Current Technologies

As evidenced from thermodynamic evaluations, MS and COH are exothermic reactions. Then, low reaction temperature would combine high conversion with low reaction rate. Using high amount of catalyst at lower temperature for better selectivity or high temperature for higher productivity with high recycle ratio is a possible strategy. Anyway, the optimal control of the reaction temperature is crucial for facing the important drawback of methanol selectivity.

On this account, single bed converters, using the reactor as heat exchanger, and multiple bed reactors, where the catalyst mass is separated in many sections by cooling devices (heat exchangers or direct injections of cool gas), allow an optimal temperature control.

Actually, the worldwide methanol production is essentially accomplished by the ICI (ca. 60 % of world production), Lurgi (ca. 30 %) and Haldor Topsøe (ca. 10 %) processes, including the following reactor technologies, all making use of the $Cu–ZnO/Al_2O_3$ catalysts:

- Quench reactor
- Adiabatic reactors in series
- Boiling water reactors (BWR)

The ICI process (Fig. 5.10) uses an adiabatic reactor with four catalyst beds in series (quench reactor), where the reaction is quenched by cold gas at several points. Products are cooled by exchanging with the feed and water used for the generation of high-pressure steam. Further cooling is accomplished by an air-cooled heat exchanger in which methanol and water are condensed. The subsequent gas/liquid separation takes place in a flash drum under pressure, while the unreacted gas is recycled after purging a small part, to keep the inerts level within the operating limits. Finally the methanol purification is done in two separation columns. In the first one, gases and other light impurities are removed, while in the second, methanol is separated from other heavy alcohols.

The Lurgi process employs adiabatic reactors (Fig. 5.11), normally made up of 2–4 fixed beds, placed in series with cooling systems between the reactors [105–107]. Cooling is achieved in several ways including preheating of high-pressure boiler feed water, generation of medium-pressure steam and/or by preheat of feed to the first reactor. This system features good economy of scale, and also the mechanical simplicity contributes to lower investment costs. This technology, called MegaMethanol, is developed for methanol capacities larger than one million metric tons per year as that built in 2004 in Trinidad and Tobago.

Finally, the Haldor Topsøe methanol process (Fig. 5.12) makes use of the boiling water reactors (BWR), constituted by a shell and tube heat exchanger with the catalysts installed on the tube cooled by boiling water on the shell side [108]. By controlling the pressure of the circulating boiling water, the temperature of the reaction is controlled and optimised. This type of reactor is nearly isothermal,

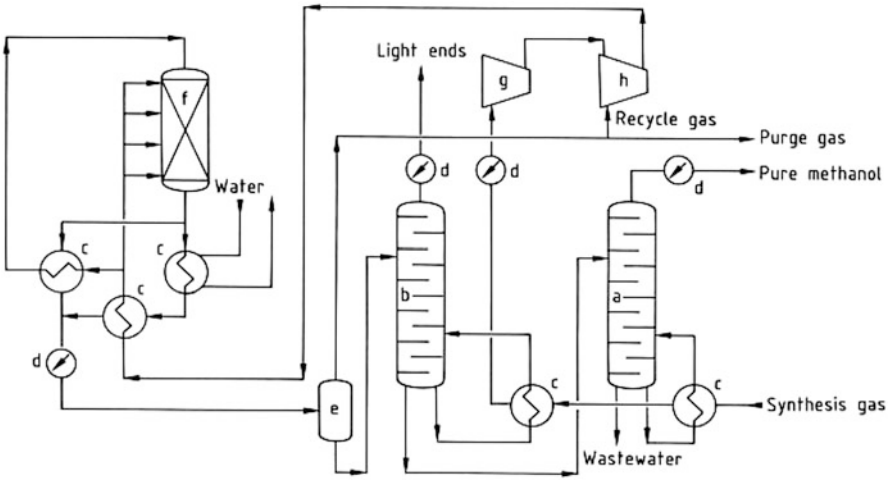

Fig. 5.10 Low-pressure methanol ICI process: (**a**) pure methanol column, (**b**) light ends column, (**c**) heat exchanger, (**d**) cooler, (**e**) separator, (**f**) reactor, (**g**) compressor, (**h**) compressor recycle stage [6]

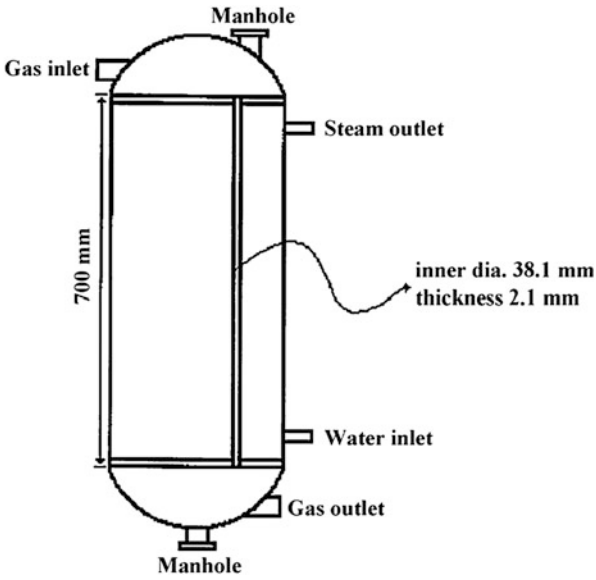

Fig. 5.11 Scheme of the Lurgi fixed-bed methanol synthesis reactor (Reprinted from Ref. [105]. Copyright 2012, with permission from Elsevier)

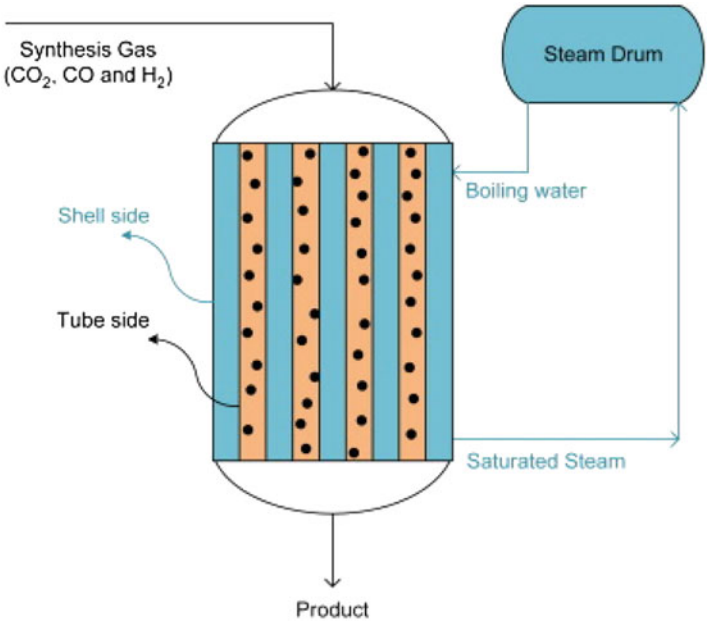

Fig. 5.12 Scheme of the Haldor Topsøe boiling water reactor (BWR) (Reprinted from Ref. [108]. Copyright 2009, with permission from IAHE)

giving a high conversion compared to the amount of catalyst installed therein. Complex mechanical design of the BWR results in relatively high investment cost and limits the maximum size of the reactor [108].

5.5.2 *Is CO_2 Hydrogenation to MOH–DME Feasible?*

Since the current lack of real application instances, the feasibility of CO_2 emissions abatement is preliminarily assessed by a recent simulation study [109].

In particular, the study addresses the design of a CO_2 to methanol process hydrogenation, which uses flue gas of a coal thermoelectric plant [109]. Through a detailed analysis of consumptions and releases, the study demonstrates that the process feasibility depends on two essential requirements:

- The availability of hydrogen, produced, for instance, from electrolysis of water by a zero-emissions electricity source (e.g. renewable and/or nuclear energy).
- The availability of waste heat in the power plant, to provide thermal energy to the process. Indeed, in the absence of these thermal sources, the CO_2 abatement is close to 0.

An overview of the process is given in Fig. 5.13. Apart from the fundamental relevance of the water electrolysis unit, the optimisation of which implies the

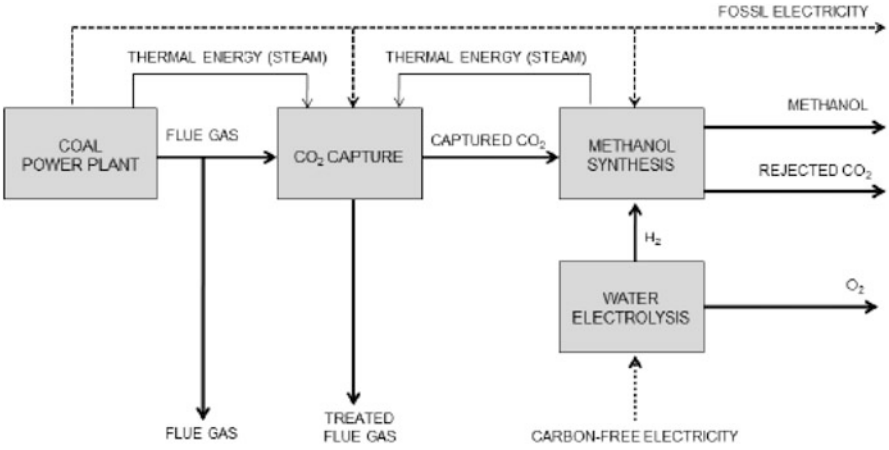

Fig. 5.13 Block diagram of the CO_2 abatement through the methanol synthesis process (Reprinted from Ref. [109]. Copyright 2012, with permission from AIDIC)

exploitation of the oxygen generated by water splitting, the process includes a chemical absorption CO_2 capture unit from the flue gas of a power plant with desulphurisation, using MEA as solvent. The synthesis reactor operates under adiabatic conditions, and it is packed with a conventional Cu–ZnO/Al_2O_3 catalyst for which, on the basis of available kinetic models, it is assumed a 33 % CO_2 conversion to methanol and a recycle ratio of 5.0. On account of this, mass, energy and CO_2 balance analysis shows that it is possible to abate a large amount of CO_2 from the production of methanol (up to 1.7 ton *per* ton of MOH) if "carbon-free" hydrogen is available.

Furthermore, An et al. proposed a CO_2 hydrogenation to DME hydrogenation process [98]. Based on a kinetic model developed for the synthesis of DME from a stoichiometric CO_2–H_2 mixture, they come to conclusion that 3 % of CO leads to a strong increase in DME and MOH yields from CO_2 hydrogenation, reaching at 270 °C levels of 37 % and 6.5 %, respectively. Since CO is continuously produced during the process, they show that its concentration can be tuned at a constant level (3 %) in the reactor effluent recycle by proper optimisation of the process conditions. A scheme of the CO_2-to-DME process is shown in Fig. 5.14.

Despite the industrial feasibility of the synthesis of methanol from CO_2 being confirmed, only small demonstration units have been developed in recent years worldwide. For instance, Carbon Recycling International (CRI) definitively proved the feasibility of the carbon dioxide recycling with its first commercial scale plant in Iceland, using available cheap geothermal energy sources to produce hydrogen by water electrolysis [5]. Another pilot plant with an annual capacity of 100 ton is under construction by the same company.

The CO_2 hydrogenation has also been demonstrated on a pilot scale in Japan, operating with a 50 kg CH_3OH/day production and selectivity to methanol of 100 % [5].

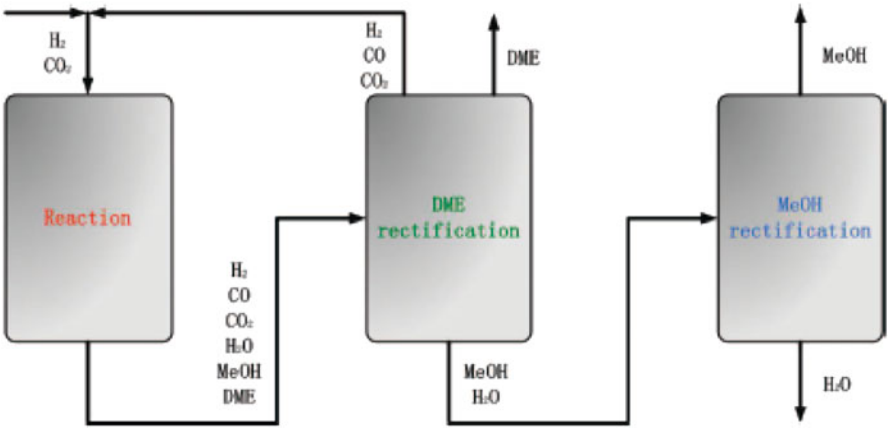

Fig. 5.14 CO_2 hydrogenation to DME process with CO recycle (Reprinted from Ref. [98]. Copyright 2008, with permission from American Chemical Society)

Further, exploring and developing new efficient catalysts formulations are generating opportunities in concepts and technologies for the chemical industry. Lurgi AG, for example, developed and thoroughly tested a high-activity catalyst for methanol synthesis from CO_2, obtaining an excellent selectivity at 260 °C, while the activity loss was comparable with that of commercial catalysts used in methanol synthesis plants [5].

5.6 Conclusions

The hydrogenation to methanol and dimethylether might become a future prospective of an efficient CO_2 recycling, since, as effective substitutes of oil-derived fuels, they would accomplish the strategic environmental goals of cutting *greenhouse gas* emissions and reducing the air pollution levels in big metropolitan areas.

Although flue gas from fuel-burning power plants, cement and other factories and syngas from ATR and POX processes are already suitable candidates for the CO_2-hydrogenation processes, however, a future scenario where the low concentration atmospheric CO_2 could be captured and recycled back to methanol/dimethylether is predictable.

In this context, despite a century since its application, the catalysis of the synthesis of methanol remains a tremendously fascinating topic, still worthy of capturing a huge scientific concern worldwide. Hence, the fundamental research in catalysis is destined to play a pivotal role in providing effective catalytic systems operating at lower temperature and pressure that, in combination with novel engineering approaches, are aimed at improving the feasibility of methanol/dimethylether synthesis technologies.

References

1. Our earth in 2050 (2013) http://greenphysicist2.blogspot.it. Accessed 28 Jun 2013
2. Wang W, Wang S, Ma X et al (2011) Recent advances in catalytic hydrogenation of carbon dioxide. Chem Soc Rev 40:3703–3727
3. Song C (2006) Global challenges and strategies for control, conversion and utilization of CO_2 for sustainable development involving energy, catalysis, adsorption and chemical processing. Catal Today 115:2–32
4. Liu X-M, Lu G-Q, Yan Z-F et al (2003) Recent advances in catalysts for methanol synthesis via hydrogenation of CO and CO_2. Ind Eng Chem Res 42:6518–6530
5. Olah GA, Goeppert A, Surya Prakash GK (2009) Chemical recycling of carbon dioxide to methanol and dimethyl ether: from greenhouse gas to renewable, environmentally carbon neutral fuels and synthetic hydrocarbons. J Org Chem 74:487–498
6. Fiedler E, Grossmann G, Kersebohm DB, Weiss G, Witte C (2000) Methanol. Ullmann's encyclopedia of industrial chemistry. Wiley, New York
7. Larminie J, Dicks A (2003) Fuel cell systems explained, 2nd edn. Wiley, New York
8. Pontzen F, Liebner W, Gronemann V et al (2011) CO_2-based methanol and DME efficient technologies for industrial scale production. Catal Today 171:242–250
9. Naik SP, Ryu T, Bui V et al (2011) Synthesis of DME from CO_2/H_2 gas mixture. Chem Eng J 167:362–368
10. Ma J, Sun NN, Zhang XL et al (2009) A short review of catalysis for CO_2 conversion. Catal Today 148:221–231
11. Arena F, Spadaro L, Di Blasi O et al (2004) Integrated synthesis of dimethylether via CO_2 hydrogenation. Stud Surf Sci Catal 147:385–390
12. Larson ED, Tingjin R (2003) Synthetic fuel production by indirect coal liquefaction. Energy Sust Dev 7:79–102
13. Jia M, Li W, Xu H et al (2002) An integrated air-POM syngas/dimethyl ether process from natural gas. Appl Catal A 233:7–12
14. Chinchen GC, Denny PJ, Jennings JR et al (1988) Synthesis of methanol: Part 1. Catalysts and kinetics. Appl Catal 36:1–65
15. Bart JCJ, Sneeden RPA (1987) Copper-zinc oxide-alumina methanol catalysts revisited. Catal Today 2:1–124
16. Yang C, Ma Z, Zhao N et al (2006) Methanol synthesis from CO_2-rich syngas over a ZrO_2 doped CuZnO catalyst. Catal Today 115:222–227
17. Grabow LC, Mavrikakis M (2011) Mechanism of methanol synthesis on Cu through CO_2 and CO hydrogenation. ACS Catal 1:365–384
18. Fujita S, Usui M, Ito H et al (1995) Mechanisms of methanol synthesis from carbon dioxide and from carbon monoxide at atmospheric pressure over Cu/ZnO. J Catal 157:403–413
19. Sun Q, Liu Z (2011) Mechanism and kinetics for methanol synthesis from CO_2/H_2 over Cu and Cu/oxide surfaces: recent investigations by first-principles-based simulation. Front Chem China 6:164–172
20. Melian-Cabrera I, Granados ML, Fierro JLG (2002) Reverse topotactic transformation of a Cu-Zn-Al catalyst during wet Pd Impregnation: relevance for the performance in methanol synthesis from CO_2/H_2 mixtures. J Catal 210:273–284
21. Waugh KC (1992) Methanol synthesis. Catal Today 15:51–75
22. Sun Q, Liu C-W, Pan W et al (1998) In situ IR studies on the mechanism of methanol synthesis over an ultrafine $Cu/ZnO/Al_2O_3$ catalyst. Appl Catal A 171:301–308
23. Inui T, Hara H, Takeguchi T et al (1997) Structure and function of Cu-based composite catalysts for highly effective synthesis of methanol by hydrogenation of CO_2 and CO. Catal Today 36:25–32
24. Saito M, Fujitani T, Takeuchi M et al (1996) Development of copper/zinc oxide-based multicomponent catalysts for methanol synthesis from carbon dioxide and hydrogen. Appl Catal A 138:311–318

25. Arena F, Barbera K, Italiano G et al (2007) Synthesis, characterization and activity pattern of Cu-ZnO/ZrO_2 catalysts in the hydrogenation of carbon dioxide to methanol. J Catal 249:185–194
26. Arena F, Italiano G, Barbera K et al (2008) Solid-state interactions, adsorption sites and functionality of Cu-ZnO/ZrO_2 catalysts in the CO_2 hydrogenation to CH_3OH. Appl Catal A 350:16–23
27. Arena F, Italiano G, Barbera K et al (2009) Basic evidences for methanol-synthesis catalyst design. Catal Today 143:80–85
28. Arena F, Mezzatesta G, Zafarana G et al (2013) Effects of oxide carriers on surface functionality and process performance of the Cu-ZnO system in the synthesis of methanol via CO_2 hydrogenation. J Catal 300:141–151
29. Arena F, Mezzatesta G, Zafarana G et al (2013) How oxide carriers control the catalytic functionality of the Cu-ZnO system in the hydrogenation of CO_2 to methanol. Catal Today 210:39–46
30. Bonura G, Arena F, Mezzatesta G et al (2011) Role of the ceria promoter and carrier on the functionality of Cu-based catalysts in the CO_2-to-methanol hydrogenation reaction. Catal Today 171:251–256
31. Pokrovski KA, Bell AT (2006) An investigation of the factors influencing the activity of $Cu/Ce_xZr_{1-x}O_2$ for methanol synthesis via CO hydrogenation. J Catal 241:276–286
32. Słoczyński J, Grabowski R, Olszewski R et al (2006) Effect of metal oxide additives on the activity and stability of Cu/ZnO/ZrO_2 catalysts in the synthesis of methanol from CO_2 and H_2. Appl Catal A 310:127–137
33. Chorkendorff I, Niemantsverdriet JW (2005) Concepts of modern catalysis and kinetics. Wiley, Weinheim
34. Askgaard TS, Norskov JK, Ovesen CV et al (1995) A kinetic model of methanol synthesis. J Catal 156:229–242
35. Nakamura J, Uchijima T, Kanai Y et al (1996) The role of ZnO in Cu/ZnO methanol synthesis catalysts. Catal Today 28:223–230
36. Ostrovskii VE (2002) Mechanisms of methanol synthesis from hydrogen and carbon oxides at Cu-Zn-containing catalysts in the context of some fundamental problems of heterogeneous catalysis. Catal Today 77:141–160
37. Granjean D, Pelipenko V, Batyrev ED et al (2011) Dynamic Cu/Zn interaction in SiO_2 supported methanol synthesis catalysts unraveled by in situ XAFS. J Phys Chem C 115:20175–20191
38. Choi Y, Futagami K, Fujitani T et al (2001) The difference in the active sites for CO_2 and CO hydrogenations on Cu/ZnO-based methanol synthesis catalysts. Catal Lett 73:27–31
39. Fujitani T, Nakamura J (2000) The chemical modification seen in the Cu/ZnO methanol synthesis catalysts. Appl Catal A 191:111–129
40. Global Methanol Market Review (2012) http://www.ptq.pemex.com. Accessed 24 Jun 2013
41. Hansen JB (1997) Methanol synthesis. In: Handbook of heterogeneous catalysis. Wiley, Weinheim
42. Kakumoto T, Watanabe T (1997) A theoretical study for methanol synthesis by CO_2 hydrogenation. Catal Today 36:39–44
43. Campbell CT, Daube KA (1987) A surface science investigation of the water-gas shift reaction on Cu(111). J Catal 104:109–119
44. Choi Y, Stenger HG (2002) Fuel cell grade hydrogen from methanol on a commercial Cu/ZnO/Al_2O_3 catalyst. Appl Catal B 38:259–269
45. Moulijn JA, Makkee M, van Diepen A (2001) Chemical process technology, 2nd edn. Wiley, New York
46. Pipitone G, Bolland O (2009) Power generation with CO_2 capture: technology for CO_2 purification. Int J Grenh Gas Con 3:528–534
47. Wambach J, Baiker A, Wokaun A (1999) CO_2 hydrogenation over metal/zirconia catalysts. Phys Chem Chem Phys 1:5071–5080

48. Razali NAM, Lee KT, Bhatia S et al (2012) Heterogeneous catalysts for production of chemicals using carbon dioxide as raw materials: a review. Renew Sust Energ Rev 16:4951–4964
49. Słoczyński J, Grabowski R, Kozłowska A et al (2004) Catalytic activity of the M/(3ZnO · ZrO_2) system (M = Cu, Ag, Au) in the hydrogenation of CO_2 to methanol. Appl Catal A 278:11–23
50. Shen W-J, Ichihashi Y, Ando H et al (2001) Effect of reduction temperature on structural properties and CO/CO_2 hydrogenation characteristics of a Pd-CeO_2 catalyst. Appl Catal A 217:231–239
51. Liang X-L, Dong X, Lin G-D et al (2009) Carbon nanotube-supported Pd-ZnO catalyst for hydrogenation of CO_2 to methanol. Appl Catal B 88:315–322
52. Collins SE, Chiavassa DL, Bonivardi AL et al (2005) Hydrogen spillover in Ga_2O_3-Pd/SiO_2 catalysts for methanol synthesis from CO_2/H_2. Catal Lett 103:83–88
53. Jia LJ, Gao J, Fang W et al (2009) Carbon dioxide hydrogenation to methanol over the pre-reduced $LaCr_{0.5}O_3$ catalyst. Catal Commun 10:2000–2003
54. Tsubaki N, Fujimoto K (2003) Promotional SMSI effect on supported palladium catalysts for methanol synthesis. Top Catal 22:325–335
55. Chinchen GC, Denny PJ, Parker DG et al (1987) Mechanism of methanol synthesis from $CO_2/CO/H_2$ mixtures over copper/zinc oxide/alumina catalysts: use of 14C-labelled reactants. Appl Catal 30:333–338
56. Deng J, Sun Q, Zhang Y et al (1996) A novel process for preparation of a Cu/ZnO/Al_2O_3 ultrafine catalyst for methanol synthesis from $CO_2 + H_2$: comparison of various preparation methods. Appl Catal A 139:75–85
57. Pan WX, Cao R, Roberts DL et al (1988) Methanol synthesis activity of CuZnO catalysts. J Catal 114:440–446
58. Ovesen CV, Stoltze P, Nørskov JK et al (1992) A kinetic model of the water gas shift reaction. J Catal 134:445–468
59. Klier K (1982) Methanol synthesis. Adv Catal 31:243–313
60. Ponec V (1992) Cu and Pd, two catalysts for CH_3OH synthesis: the similarities and the differences. Surf Sci 272:111–117
61. Frost JC (1988) Junction effect interactions in methanol synthesis catalysts. Nature 334:577–579
62. Grunwaldt J-D, Molenbroek AM, Topsøe N-Y et al (2000) In situ investigations of structural changes in Cu/ZnO catalysts. J Catal 194:452–460
63. Fujitani T, Nakamura J (1998) The effect of ZnO in methanol synthesis catalysts on Cu dispersion and the specific activity. Catal Lett 56:119–124
64. Topsøe N-Y, Topsøe H (1999) FTIR studies of dynamic surface structural changes in Cu-based methanol synthesis catalysts. J Mol Catal A 141:95–105
65. Greeley I, Gokhale AA, Kreuser J et al (2003) CO vibrational frequencies on methanol synthesis catalysts: a DFT study. J Catal 213:63–72
66. Bower M, Hadden RA, Houghton H et al (1988) The mechanism of methanol synthesis on copper/zinc oxide/alumina catalysts. J Catal 109:263–273
67. Yoshihara J, Campbell CT (1996) Methanol synthesis and reverse water-gas shift kinetics over Cu(110) model catalysts: structural sensitivity. J Catal 161:776–782
68. Günter MM, Ressler T, Bems B et al (2001) Implication of the microstructure of binary Cu/ZnO catalysts for their catalytic activity in methanol synthesis. Catal Lett 71:37–44
69. Bems B, Schur M, Dassenoy A et al (2003) Relations between synthesis and microstructural properties of copper/zinc hydroxycarbonates. Chem Eur J 9:2039–2052
70. Vukojević S (2009) Copper colloids and nanoparticular Cu/ZrO_2-based catalysts for methanol synthesis. PhD Thesis, Ruhr-Universitat, Bochum
71. Fujitani T, Nakamura I, Ueno S et al (1997) Methanol synthesis by hydrogenation of CO_2 over a Zn-deposited Cu(111): formate intermediate. Appl Surf Sci 121:583–586

72. Zhao Y-F, Yang Y, Mims C et al (2011) Insight into methanol synthesis from CO_2 hydrogenation on Cu(111): complex reaction network and the effects of H_2O. J Catal 281:199–211
73. Yang Y, Mims CA, Mei DH et al (2013) Mechanistic studies of methanol synthesis over Cu from $CO/CO_2/H_2/H_2O$ mixture: the source of C in methanol and the role of water. J Catal 298:10–17
74. Hansen PL, Wagner JB, Helveg S et al (2002) Atom-resolved imaging of dynamic shape changes in supported copper nanocrystals. Science 295:2053–2055
75. Fisher IA, Bell AT (1997) In-situ infrared study of methanol synthesis from H_2/CO_2 over $Cu/ZrO_2/SiO_2$. J Catal 172:222–237
76. Guo X, Mao D, Lu G et al (2010) Glycine-nitrate combustion synthesis of CuO-ZnO-ZrO_2 catalysts for methanol synthesis from CO_2 hydrogenation. J Catal 271:178–185
77. Toyir J, Milouna R, Elkadri NE et al (2009) Sustainable process for the production of methanol from CO_2 and H_2 using Cu/ZnO-based multicomponent catalysts. Phys Proceed 2:1075–1079
78. Fisher IA, Bell AT (1998) In situ infrared study of methanol synthesis from H_2/CO over Cu/SiO_2 and $Cu/ZrO_2/SiO_2$. J Catal 178:153–173
79. Bianchi D, Chafik T, Khalfallah M et al (1994) Intermediate species on zirconia supported methanol aerogel catalysts: III. Adsorption of carbon monoxide on copper containing solids. Appl Catal A 112:57–73
80. Jones SD, Neal LM, Hagelin-Weaver HE (2008) Steam reforming of methanol using Cu-ZnO catalysts supported on nanoparticle alumina. Appl Catal B 84:631–642
81. Mastalir H, Frank B, Szizybalski A et al (2005) Steam reforming of methanol over $Cu/ZrO_2/CeO_2$ catalysts: a kinetic study. J Catal 230:464–475
82. Mei M, Xu L, Henkelman G (2009) Potential energy surface of methanol decomposition on Cu(110). J Phys Chem C 113:4522–4537
83. Klier K, Chatikavanij V, Herman RG et al (1982) Catalytic synthesis of methanol from $CO-H_2$: IV. The effects of carbon dioxide. J Catal 74:343–360
84. Cheng W-H (1995) Reaction and XRD studies on Cu based methanol decomposition catalysts: role of constituents and development of high-activity multicomponent catalysts. Appl Catal A 130:13–30
85. Clausen BS, Schiøtz J, Gråbæk L et al (1994) Wetting/non wetting phenomena during catalysis: evidence from in situ on-line EXAFS studies of Cu-based catalysts. Top Catal 1:367–376
86. Ressler T, Kniep BL, Kasatkin I et al (2005) The microstructure of copper zinc oxide catalysts: bridging the materials gap. Angew Chem Int 44:4704–4707
87. Sun Q, Zhang Y-L, Chen H-Y et al (1997) A novel process for the preparation of Cu/ZnO and $Cu/ZnO/Al_2O_3$ ultrafine catalyst: structure, surface properties, and activity for methanol synthesis from $CO_2 + H_2$. J Catal 167:92–105
88. Bando KK, Sayama K, Kusama H et al (1997) In-situ FT_IR study on CO_2 hydrogenation catalysts supported on SiO_2, Al_2O_3, and TiO_2. Appl Catal A 165:391–409
89. Wang JB, Lee H-K, Huang T-J (2002) Synergistic catalysis of carbon dioxide hydrogenation into methanol by yttria-doped ceria/γ-alumina-supported copper oxide catalyst: effect of support and dopant. Catal Lett 83:79–86
90. Tang Q-L, Hong QJ, Liu Z-P (2009) CO_2 fixation into methanol at Cu/ZrO_2 interface from first principles kinetic Monte Carlo. J Catal 263:114122
91. Yang Y, Evans J, Rodriguez JA et al (2010) Fundamental studies of methanol synthesis from CO_2 hydrogenation on Cu(111), Cu clusters, and Cu/ZnO(0001). Phys Chem Chem Phys 12:9909–9917
92. Sun K, Lu W, Wang M et al (2004) Low-temperature synthesis of DME from CO_2/H_2 over Pd-modified CuO-ZnO-Al_2O_3-ZrO_2/HZSM-5 catalysts. Catal Commun 5:367–370
93. Aguayo AT, Ereña J, Mier D et al (2007) Kinetic modeling of dimethyl ether synthesis in a single step on a CuO-ZnO-Al2O3/γ-Al_2O_3 catalyst. Ind Eng Chem Res 46:5522–5530

94. Aguayo AT, Ereña J, Sierra I et al (2005) Deactivation and regeneration of hybrid catalysts in the single-step synthesis of dimethyl ether from syngas and CO_2. Catal Today 106:265–270
95. Gao W, Wang H, Wang Y et al (2013) Dimethyl ether synthesis from CO_2 hydrogenation on a La-modified CuO-ZnO-Al_2O_3/HZSM-5 bifunctional catalysts. J Rare Earths 31:470–476
96. Bonura G, Cordaro M, Spadaro L et al (2013) Hybrid Cu-ZnO-ZrO_2/H-ZSM5 system for the direct synthesis of DME by CO_2 hydrogenation. Appl Cat B 140–141:16–24
97. Wang S, Mao D, Guo X et al (2009) Dimethyl ether synthesis via CO_2 hydrogenation over CuO-TiO_2-ZrO_2/HZSM-5 bifunctional catalysts. Catal Commun 10:1367–1370
98. An X, Zuo Y-Z, Zhang Q et al (2008) Dimethyl ether synthesis from CO_2 hydrogenation on a CuO-ZnOAl_2O_3-ZrO_2/HZSM-5 bifunctional catalyst. Ind Eng Chem Res 47:6547–6554
99. Aasberg-Pettersen K, Nielsen CS, Dybkjær L, Perregaard J (2009) Large scale methanol synthesis from natural gas. www.topsoe.com. Accessed 24 Jun 2013
100. Lee S, Speight JG, Loyalka SK (2007) Handbook of alternative fuel technologies. Taylor & Francis, Boca Raton
101. Dybkjær I (2006) Synthesis gas technology. www.topsoe.com. Accessed 21 Jun 2013
102. Halstead K (2008) Oryx GTL from conception to reality. www.fwc.com. Accessed 21 Jun 2013
103. Petroleum Technology Quarterly (2008) www.alfalaval.com. Accessed 23 Jun 2013
104. Sørensen EL, Perregaard J (2004) Condensing methanol synthesis and ATR – the technology choice for large-scale methanol production. Stud Surf Sci Catal 147:7–12
105. Fuad MNM, Hussain MA, Zakaria A (2012) Optimization strategy for long-term catalyst deactivation in a fixed-bed reactor for methanol synthesis process. Comput Chem Eng 44:104–126
106. Tijm PJA, Waller FJ, Brown DM (2001) Methanol technology developments for the new millennium. Appl Catal A 221:275–282
107. Jahanmiri A, Eslamloueyan R (2002) Optimal temperature profile in methanol synthesis reactor. Chem Eng Commun 189(6):713–741
108. Rahimpour MR, Alizadehhesari K (2009) Enhancement of carbon dioxide removal in a hydrogen-permselective methanol synthesis reactor. Int J Hydrogen Energ 34:1349–1362
109. Van-Dal ES, Bouallou C (2012) CO_2 abatement through a methanol production process. Chem Eng Trans 29:463–468

Chapter 6
Syngas Production Using Carbon Dioxide Reforming: Fundamentals and Perspectives

Julian R.H. Ross

6.1 Introduction

Much has been written over the last few decades about the potential use of CO_2 as a feedstock in the chemical industry, and particular attention has been given to its possible use in the conversion of methane and other hydrocarbons using so-called dry reforming to give syngas, a mixture of CO and hydrogen. The CO_2 or dry reforming of methane can be represented by the equation

$$CH_4 + CO_2 \rightarrow 2CO + 2H_2 \tag{6.1}$$

In any practical application, in order to achieve acceptable conversions, this reaction would have to be carried out at very high temperature (up to as much as 1,000 °C) when the conversion would be close to chemical equilibrium. The reaction is always accompanied by the reverse water–gas shift reaction, generally fully at equilibrium:

$$CO_2 + H_2 \rightleftarrows CO + H_2O \tag{6.2}$$

A consequence of the combination of these two reactions is that the CO:H_2 ratio obtained is generally rather lower than the value of 1:1 to be expected if only the reaction of Eq. 6.1 occurred. The reaction system is further complicated by the fact that the conditions used generally favour carbon deposition. Carbon deposition can be thought of as occurring by one of three interdependent reactions:

$$2CO \rightleftarrows C + CO_2 \tag{6.3}$$

J.R.H. Ross (✉)
Charles Parsons Initiative, Department of Chemical and Environmental Sciences, University of Limerick, Limerick, Ireland
e-mail: julian.ross@ul.ie

B.M. Bhanage and M. Arai (eds.), *Transformation and Utilization of Carbon Dioxide*, Green Chemistry and Sustainable Technology, DOI 10.1007/978-3-642-44988-8_6,

$$CH_4 \rightleftarrows C + 2H_2 \tag{6.4}$$

and

$$CO + H_2 \rightleftarrows C + H_2O \tag{6.5}$$

In most practical cases, whether or not carbon deposition is likely to occur is determined by thermodynamic considerations; further, as Boudouard carbon (Eq. 6.3) is generally expected at low temperatures, carbon deposition under dry reforming conditions is most likely to occur by either methane decomposition (Eq. 6.4) or CO reduction (Eq. 6.5). The problem of carbon deposition is a key feature of the process and we will return to it many times below.

A search of Web of Science using the search terms "methane, CO_2 and reforming" shows that more than 1,900 papers with these three words in the titles and/or abstracts had been published between 1987 and mid-2013. Table 6.1 shows the approximate number of papers that include these search terms published up to 1994 and in each 5-year period since then, together with the approximate total number of citations to these papers given in each period. It is clear that there is little sign of the interest in the subject showing any decline; indeed, the yearly number of publications reached an all-time high of more than 200 in 2012, this being significantly higher than the previous maximum of 160 in 2011. As will be discussed further below, it is highly questionable if this level of activity is justified by the potential applicability of the process. The only justification for such a level of activity is probably that the work reported provides new insights into particular types of catalysts, CO_2 reforming being used as a model reaction.

Other combinations of search terms to those used in the search of the Web of Science discussed above show up significant additional material.[1] This review is based largely on the material gleaned from the search related to Table 6.1. However, some references are also included that did not show up in this search, in most cases because the keywords of the original articles were different; there is also no doubt that some important papers will have been omitted for the same reason.

Interestingly, the first paper on CO_2 reforming of methane listed in the search outlined in Table 6.1 is a relatively under-cited one by Fish and Hawn on the use of CO_2 reforming in a thermochemical cycle [1], a topic to which we will return briefly below. The second paper on the list, by Gadalla and Bowers [2], is concerned with the use of a range of commercial steam reforming catalysts, showing that the most promising results were obtained with alumina supports containing magnesium or calcium oxide. (A further paper by Gadalla and Somer [3], published in 1989, gives more details on this subject.) As will be discussed in a later section, Ni catalysts based on Mg-containing supports still appear to be among the most effective catalysts for the process.

[1] No attempt has been made to cross-check the contents of various searches that have been carried out so that the total number of papers is likely to be well in excess of 2000. More detailed Web of Science and Scopus searches have also been carried out in order to identify some of the key references on each of these subjects, and the text that follows below concentrates predominantly on these papers.

Table 6.1 The numbers of papers on the topic of dry reforming of methane published during various time periods since 1987 together with the numbers of citations listed in those time periods

Years	Up to 1995	1996–2000	2001–2005	2005–2010	2011 and later
Publications	60	280	490	670	>400
Citations	<200	2,400	7,200	1,890	1,380

Data obtained from a Web of Science (Thomson Reuters) search (May 2013) using the search terms *methane, CO_2 and reforming*

Many of the papers that have been published over the last 20 years or so justify the work carried out by claiming that a process involving the consumption of both methane and CO_2 would help to provide a solution to the emission of these two greenhouse gases. It needs to be emphasised from the outset that such claims are largely unjustified since the quantity of CO_2 that might be used in syngas production by CO_2 reforming would be negligible compared with the very large emissions of CO_2 currently causing concern, even if it was possible to collect the CO_2 in a sufficiently pure form for the CO_2 reforming reaction. Further, dry reforming produces syngas with a composition usable only in limited applications; as shown above (see Eq. 6.1), using methane as co-reactant, the syngas ratio, CO/H_2, is approximately 1.0. Much more suitable ratios can be attained by the addition of either steam or oxygen to the reactant stream, such addition also having the benefit that the potential for carbon deposition on the catalysts used in the process is significantly reduced.[2] An alternative to the dry reforming process using CO_2 in the primary feed is to operate the steam reforming reaction:

$$CH_4 + H_2O \rightarrow CO + 3H_2 \tag{6.6}$$

and then to carry out the reverse water–gas shift reaction (reverse of reaction (6.2)) in order to achieve the desired CO/H_2 ratio:

$$CO_2 + H_2 \rightarrow CO + H_2O \tag{6.7}$$

There are several advantages to be achieved using this approach, these including the following: (i) the problem of C deposition can largely be avoided since the catalysts and process conditions for the steam reforming reaction under carbon-free conditions are well established commercially; and (ii) the CO_2 required for the process can be extracted from the effluent of the reformer furnace (burning natural gas) used to heat the tubular steam reforming reactor system. Hence, the only additional processing step required is the separation unit to remove CO_2 from the combustion gases, a step also required if dry reforming is to be carried out. Further, although the cost of a steam reforming plant is very high and a major contributor to the all-over cost of any process requiring a syngas feed, it is unlikely that there will be much reduction in the total operation cost if dry reforming is used.

[2] A relatively small proportion of the papers in the recent literature have recognised these further limitations, and some of these are listed in the tables below.

Accepting, for the reasons given above, that dry reforming is unlikely to solve the greenhouse gas problem, other justifications have to be found for the very extensive work on the subject that has been carried out over recent years. As will be discussed in more detail in the following sections, much of the most recent work has been devoted to trying to find catalysts that are resistant to carbon deposition while having suitable activities and stabilities under reaction conditions.[3] Although much of the work published recently undoubtedly adds incrementally to the literature of the subject, there appear to have been no major breakthroughs: most, if not all, of the catalysts that have been examined under suitable conditions unfortunately show gradual deactivation due to carbon deposition. Further, many of the catalyst systems studied bear remarkable similarity to ones that have been studied previously for other closely related reactions, for example, the steam reforming of methane. In many cases, such similarities do not appear to have been recognised by the authors of these papers.

This review traces briefly the development of processes used for the production of syngas from methane (and higher hydrocarbons) and discusses the interest in the use of CO_2 as a co-reactant, paying particular attention to the conversion of methane. It then considers the thermodynamics of such conversion processes, highlighting the problem of carbon deposition and the need for operation at high temperature. Recognising the similarity between dry reforming and steam reforming and the fact that the latter is a well-established industrial process, mention is made of the catalysts used commercially for the steam reforming of methane and of higher hydrocarbons, with a short digression on the catalysts used for methanation. The review then considers various groups of papers that have been devoted to studies of different catalyst types, particular attention being given to the use of noble metals (particularly Pt) and other transition metals such as Ni, Co and Mo, on a variety of different supports. The review concentrates on the literature on methane reforming, but it should be recognised that many of the catalysts developed will be equally applicable to the reforming of higher hydrocarbons, the only complication being that methane is also a potential product when the methanation reaction is thermodynamically feasible (at lower temperatures, see Sect. 6.2.2).

6.2 Historical Background

6.2.1 Syngas Production from Hydrocarbons

Before embarking on a more detailed discussion of the dry reforming reaction and the catalysts that have been used for that reaction, it is sensible first to give a brief

[3] Unfortunately, a significant proportion of the papers in the recent literature report experiments carried out under unrealistic conditions, for example, at low temperatures or with non-stoichiometric reactant compositions; in any process that will be developed, the reaction will be carried out at high temperatures and pressures under conditions close to equilibrium, and any novel catalyst formulations must be tested under similar conditions.

outline of the use and importance of the steam reforming of methane as a source of syngas. The subject of the steam reforming of methane (Eq. 6.6) has been reviewed by various different authors, from the point of view of both the processes involved [4] and of the catalysts used [5]. Although, as pointed out by Rostrup-Nielsen [4], some papers and patents on the steam reforming of hydrocarbons had been published as early as 1868, the first industrial steam reformer was commissioned in Baton Rouge in 1930 by the Standard Oil of New Jersey, and this was followed by another reformer commissioned by ICI in Billingham in 1936; in both cases, the main product required was hydrogen, and so the CO formed was removed using the water–gas shift reaction. While steam reforming in the United States was usually carried out with methane as the feed hydrocarbon, the raw material of choice in Europe until the 1960s was naphtha; with the advent of European natural gas supplies in the second half of that decade, methane also became the feedstock of choice.[4] It is interesting to note that although there has been some limited commercial interest in the use of CO_2 as a feed instead of water, the only plant using a methane/CO_2 feedstock has been a pilot plant operated by Haldor Topsoe in Texas in which a sulphur-modified steam reforming catalyst is used [6]. It is also worth noting that in the so-called Midrex process for the direct reduction of iron ore, a mixed feed of methane with CO_2 and steam is used in a reformer; the CO_2 and steam for the reforming step are produced during the reduction of the iron ore, and the syngas produced in the reformer is fed directly to the reduction reactor [6, 7].

Although other active materials, notably the noble metals, have been examined for use as the active components in steam reforming catalysts, the only ones that have been used commercially are those including Ni as the active component. This is not only a matter of cost: Ni is the only non-noble transition metal that is maintained in its metallic state under steam reforming conditions since the equilibrium

$$NiO + H_2 \rightleftarrows Ni + H_2O \tag{6.8}$$

lies to the right-hand side as long as the ratio H_2/H_2O is greater than about 0.01; in other words, the nickel will be in its reduced (and active) form as long as there is approximately 1 % hydrogen in the reactant gas [5]. (With the exception of the noble metals, much higher proportions are needed for most of the other transition metals.) A variety of different Ni-containing formulations have been commercialised. However, among the most commonly used materials are the ICI (now Johnson Matthey) 46–1 catalyst (predominant components in the reduced form are Ni, alumina and K_2O with CaO, SiO_2 and MgO added as a cement binder) and the Haldor Topsoe catalyst (containing Ni, MgO and alumina). Other catalyst manufacturers supply similar materials. The potassium of the ICI formulation is added to help minimise C deposition, and the MgO of the Haldor Topsoe material

[4] Syngas could also be formed by coal gasification or by modifications of the gasification process using steam or CO_2 in the feed.

serves a similar function. As mentioned above, the catalyst used in the Haldor Topsoe pilot plant for dry reforming (see above) is partially sulphided [4, 6, 8]. This was based on work on the subject of S passivation for application in the steam reforming process [9].

6.2.2 Methanation

From a historical point of view but also in relation to work on the formulation of catalysts, it is interesting to note that there occurred in the late 1970s and early 1980s a period of very significant academic and industrial research activity on the topics of methanation and methanation catalysts. This interest arose because natural gas supplies in the United States could not keep up with demand. As a result, it was desirable to find means of converting syngas (produced from coal) into so-called synthetic natural gas (SNG):

$$CO + 3H_2 \rightarrow CH_4 + H_2O \tag{6.9}$$

This reaction is the reverse of the steam reforming reaction (Eq. 6.6) and is highly exothermic. Hence, much of the work from that period concentrated on finding catalysts with high stability at higher temperatures that also resisted carbon deposition. Many of the catalysts examined and reported in many papers of that period had great similarity to those that have been examined more recently for dry reforming. This author reviewed the literature on methanation and steam reforming in 1985 [10].

6.2.3 Methane Coupling

Following on from the great interest from the catalysis community in the topic of methanation, the subject of the oxidative coupling of methane to give C_2H_6 and C_2H_4 became predominant during the second half of the 1980s as a result of a paper by Keller and Bhasin published in 1982 [11]. These authors showed that it was possible, using a cyclic process in which methane and oxygen were fed in turn to a catalyst bed, to obtain reasonable yields of C_2 hydrocarbons, the catalysts being operated at temperatures around 800 °C. Keller and Bhasin used a range of α-alumina-supported materials (including the oxides of Cd, Sn, Sb, Tl, Bi and Pb) as catalyst and postulated that an oxidation–reduction mechanism was involved. Hinsen and Baerns were the first to carry out the reaction with methane and oxygen fed simultaneously, and they obtained good yields using a lead/γ-alumina catalyst [12]. A paper by Ito, Wang, Lin and Lunsford published in 1985 introduced the use of Li/MgO materials [13]. Many more similar catalysts were introduced over the next decade, and a number of very extensive reviews have been written on the subject [14–17].

It was soon recognised that the reaction occurs by a combination of heterogeneous reactions and gas-phase radical reactions and that the products included not only ethane and ethylene but also a mixture of higher hydrocarbons, water, CO, CO_2 and hydrogen. The participation of gas-phase reactions as well as limitations introduced by the explosive limits of methane/oxygen mixtures leads to a limit in the potential yields of C_2 hydrocarbons produced in the reaction, the best values being just above 20 %, too low to enable the reaction to have commercial application with current natural gas prices. Although papers on the subject were published in a variety of different journals, a very good overview of the work that was carried out is to be found by examining the proceedings of the earlier "Natural Gas Conversion" meetings [18–21], from the first of the series held in 1987 in Auckland, NZ, to the fourth meeting held in 1998 in Messina, Italy; by 2001, when the 6th meeting of the series was held in Alaska, the topic of methane coupling had disappeared. What had been gained from all this work was a much greater understanding in the academic community of the operation of catalytic reactors at elevated temperatures and the problems of catalyst stability. (It is of interest to note that renewed interest in methane coupling has recently been evident, this being spurred by the current low prices of natural gas.)

6.2.4 Dry Reforming and Partial Oxidation of Methane

When at the beginning of the 1990s an interest developed in the production of syngas from natural gas using either partial oxidation or "dry reforming", it was not surprising that the research community that had been involved in the work on methane coupling transferred its interest to studying one or other of these two reactions. This transfer is clearly seen in the proceedings of the "Natural Gas Conversion" meetings referred to above. The majority of the papers under the title "Methane Conversion" in the second meeting held in Oslo in 1990 [18] were related to oxidative coupling, there being none on partial oxidation or CO_2 reforming. This bias was continued at the third meeting held in Sydney in 1993 [19] with more than 20 papers on methane coupling and only four on dry reforming; two of the latter were reviews of the subject by J. R Rostrup-Nielsen and by J. H. Edwards and A. M. Maitra (discussed further in the following section). However, by the time of the fourth meeting held in the Kruger National Park in South Africa in 1995 [20], there were 16 papers on oxidative coupling, 13 papers on partial oxidation and 8 papers on CO_2 reforming. By the fifth meeting held in Taormina, Italy, in 1998 [21], the latter two topics had become the predominant subjects of interest related to methane conversion. The relevant papers from these meetings will be outlined in Sect. 6.4.1.

As discussed above (see Table 6.1), there has since 1996 been an explosive development of interest in CO_2 reforming and partial oxidation, so much so that it is virtually impossible to write a comprehensive review covering every aspect of the work that has been carried out on either topic. The following sections will therefore

concentrate on some of the more important types of catalyst that have been investigated, particular attention being paid to papers describing those types of catalyst that have reasonable stabilities under "dry reforming" conditions and to papers giving new insights into the mechanism of the reaction or advancing other approaches to the conversion process. No great detail on any of the papers is given; instead, summaries are given in tabular form of their main conclusions. Further, no attempt is made to discuss any of the parallel literature on partial oxidation, exceptions being when it has been shown that the addition of oxygen to the "dry reforming" mixture has beneficial effects or when the results on the partial oxidation reaction on a particular catalyst have some relevance to the dry reforming reaction on identical or similar catalysts. In selecting the literature for inclusion, use has been made of citation indexing, the searches being based on the use of Web of Science and/or Scopus. As a starting point, some of the papers appearing in the proceedings of the earlier Natural Gas Conversion meetings referred to above have been used to identify some of the major themes of research. Scopus and Web of Science searches have then been used to identify some of the (in most cases) more recent key papers related to each of these themes, and some of the main conclusions of these are tabulated. Finally, the main objectives and conclusions of some very recently published papers on the subject that have not yet achieved a significant citation record are summarised.

Before embarking on our summary of the literature, a brief outline of the thermodynamic limitations associated with the dry reforming reaction and associated side reactions is given since these limitations have some importance in discussing the papers from the literature.

6.3 Thermodynamics of the $CH_4 + CO_2$ Reaction

The dry reforming of methane (Eq. 6.1) is an endothermic process, and so the maximum conversion calculated thermodynamically increases with increasing temperature. This is illustrated schematically in Fig. 6.1 that shows the thermodynamic conversions for various feed compositions as a function of temperature of reaction [22]. It can be seen that a temperature in excess of about 850 °C is necessary to obtain adequate conversions using a stoichiometric CH_4/CO_2 feed (1:1).

It is to be expected that the water–gas shift reaction (Eq. 6.2) will be in equilibrium under CO_2 reforming conditions and so the CO/H_2 ratio of the product gas can be calculated easily from a knowledge of the feed compositions and the measured methane conversions. It should be noted that the so-called selectivity of the reaction is very frequently given in publications reporting the behaviour of novel catalysts; unless it is shown very clearly that the water–gas reaction is *not* in equilibrium for that catalyst system, such values have no real significance as they are thermodynamically rather than kinetically controlled.

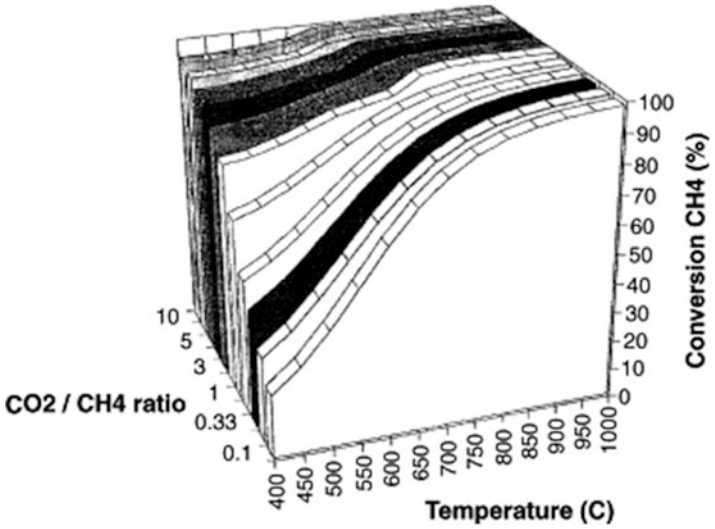

Fig. 6.1 Thermodynamically calculated conversions of methane as a function of temperature for a series of different feed ratios. Calculations carried out using HSC chemistry (version 1.10, Outokumpu Research, Finland) (Reprinted from Ref. [22]. Copyright 2005, with permission from Elsevier)

Figure 6.2 shows the yield of carbon to be expected if carbon deposition is possible for two possible cases: whether or not the water–gas shift reaction is considered to be in equilibrium [22]. This diagram was constructed assuming that there is a closed system and that the amount of carbon formed relates to the amount fed as methane and CO_2; the results should therefore be seen only as a guide as to when carbon would form in a continuous flow reactor. It is clear that carbon formation is possible over the whole range of temperatures in both cases considered (with or without the water–gas shift reaction being equilibrated), and that the amount of carbon formed will be lower at high temperatures. When the water–gas shift reaction does not take place, the amount formed at the highest temperatures is much lower; however, in most cases reported in the literature, the water–gas shift reaction is at equilibrium at the higher temperatures and so this situation does not apply. Rostrup-Nielsen uses a different approach, favouring the use of so-called carbon limit diagram, developed first for the steam reforming reaction [6, 23]. He shows that in the absence of the addition of steam, the CO_2 reforming reaction operates under conditions when carbon can form regardless of the CH_4/CO_2 ratio. He concludes that the noble metals, most of which do not form carbides (necessary intermediates in carbon formation) have a greater potential for use as CO_2 reforming than do catalyst formulations using nickel. The topic of carbon deposition will be handled further after a discussion of the types of catalyst studied.

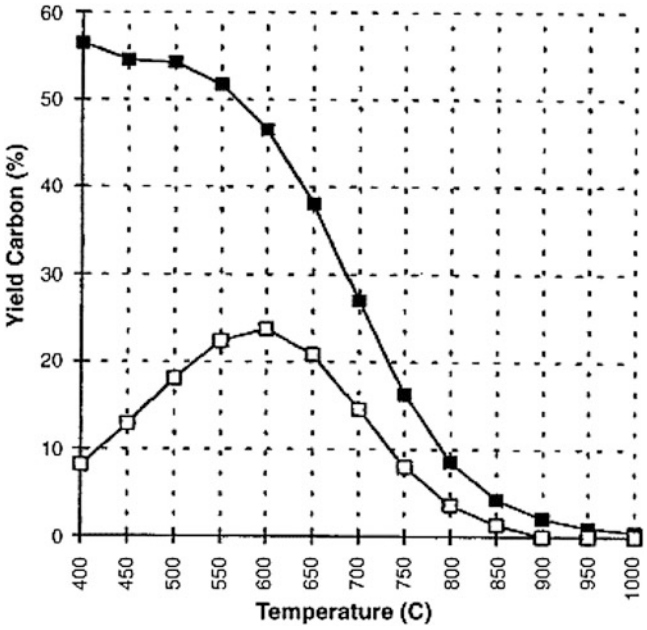

Fig. 6.2 Thermodynamically calculated proportions of carbon formed under CO_2 reforming conditions with $CH_4/H_2O = 1.0$; (■), with the reverse water–gas shift reaction in equilibrium; (□), without the reverse water–gas shift reaction (Reprinted from Ref. [22]. Copyright 2005, with permission from Elsevier)

6.4 Catalysts for the Dry Reforming of Methane

6.4.1 Papers on CO_2 Reforming Published in the Proceedings of the Natural Gas Conversion Symposia up to 1998

Tables 6.2, 6.3, and 6.4 list the relevant papers presented at the Natural Gas Conversion Symposia between 1993 and 1998: the third (held in 1993, published in 1994 [19]), the fourth (held in 1995, published in 1997 [20]) and the fifth (held and published in 1998 [21]). The following paragraphs first summarise two review articles from the third meeting and then outline some of the important aspects of the other papers, this being in preparation for a more general discussion of the literature on the subject since about 1997.

In his review delivered at the third symposium [6], Rostrup-Nielsen of Haldor Topsoe A/S (Lyngby, Denmark) gave a very clear exposition of the then-available information on the CO_2 reforming of methane, paying particular attention to earlier work on the subject. He noted that the reaction was examined by Fischer and

Table 6.2 Papers from NGC 3

Reference/year	Metal	Support	Temperature range/°C	Comments
Rostrup-Nielsen [6]	Noble metals S-passivated nickel	Alumina MgO	No specific range given	Review article, discussing process options and carbon deposition; also summarises some work from Haldor Topsoe on noble metals as CO_2 reforming catalysts
Edwards [24]	Range	Range	No specific range given	Review article, summarising types of catalysts studied up to about 1993; some discussion of possible processes
Seshan [25]	Pt, Ni	ZrO_2, Al_2O_3	390–560	Pt/ZrO_2 much more stable that Pt/Al_2O_3; 5%Ni/ZrO_2 more stable than 10%Ni/ZrO_2
Uchijima [26]	Rh	Al_2O_3, SiO_2, TiO_2	377–727	PO gives first combustion and then steam and CO_2 reforming. Rh/Al_2O_3 is 35× more active than Rh/SiO_2 for CO_2 reforming. Addition of Al_2O_3 or TiO_2 to Rh/SiO_2 gives significant promotion

Tropsch as early as 1928 [49]; these scientists studied a series of base metal catalysts and found that nickel and cobalt gave the best results, the product gas compositions being close to thermodynamic equilibrium.

Rostrup-Nielsen also summarises the work of Bodrov and Apel'baum who showed in 1967 [50] that the kinetic expression for the CO_2 reforming reaction over a nickel film was similar to what they had found previously for the steam reforming reaction [51], this indicating that the mechanism was very similar for both reactions.

Rostrup-Nielsen discussed industrial processes that involve CO_2 reforming, these including the SPARG process making use of a sulphur-passivated Ni catalyst. The original research relating to that process is detailed in a research paper by Dibbern et al. referred to above [8]. The technology used, adding traces of H_2S to the reactor feed, is similar to that previously introduced by Haldor Topsoe to enable steam reforming to be carried out at low steam/methane ratios [9]. Rostrup-Nielsen also presented in his review some data on the CO_2 reforming of methane using the noble metals and Ni supported on MgO. He concluded that the noble metals are much less susceptible to carbon poisoning due to the fact that they do not dissolve C in their bulk. He then described briefly some work in which Rh and Ru catalysts, the

Table 6.3 Papers from NGC4

Reference/ year	Metal	Support	Temperature range/°C	Comments
Cant [27]	Ni, Rh	Al_2O_3	700	Deuterium kinetic isotope effect shows differences between metals. C easily removed from Rh
Slagtern [28]	Ni	Al_2O_3	700, 800	Rare earth mixture used as promoter; similar results to using La_2O_3
Yu [29]	Ni	Al_2O_3	700, 750	CH_4 decomposition, followed by removal of C by CO_2
Zhang [30]	Ni	La_2O_3	550–750	L_2O_3 activates CO_2 and encourages removal of C from Ni
Erdöhelyi [31]	Ir	Al_2O_3, TiO_2, SiO_2, MgO	427–500, 850	C deposition limited on all samples. TiO_2 most effective support
Van Keulen [32]	Pt	ZrO_2	550–800	Optimisation of Pt/ZrO_2 with life tests
Kikuchi [33]	Ni, noble metals	Al_2O_3	500	Tested in membrane reactor system. Noble metals much less susceptible to coke formation
Ponelis [34]	Ru, Rh	SiO_2	400–900	Membrane gives significantly improved conversions at higher contact times

most promising of the metals studied, were used for carbon-free operation in a pilot plant under conditions in which carbon is favoured thermodynamically. He concluded, however, that because of their scarcity neither of these metals is likely to be used in other than niche applications. In conclusion, Rostrup-Nielsen discussed the limitations of possible processes for the use of CO-rich gases from CO_2 reforming. He pointed out that the amounts of CO_2 used in such processes will be virtually insignificant in comparison with the total worldwide emissions of CO_2. For example, the CO_2 that would be required for the production of 5 million tons of acetic acid per year (the current global rate of production) by the reaction:

$$CH_4 + CO_2 \rightarrow CH_3COOH \tag{6.10}$$

would correspond to the emission from only one 500 MW coal-based electricity power station. Yearly worldwide production of methanol is four times higher, and so supplying syngas via CO_2 reforming of methane would require the output from four such power plants. More importantly, the current technology for CO_2 extraction makes the use of CO_2 from flue gases uneconomical and so other sources of CO_2 would have to be considered. The article by Rostrup-Nielsen contains many other details (and warnings) related to the potential of a process for CO_2 reforming. Anyone working in the area should therefore read it with care.

A second review article was delivered at the same symposium; this was reported by Edwards and Maitra of CSIRO (North Ryde, Australia) [24]. Having also

Table 6.4 Papers from NGC V, SSSC 119 (1998) (Italy)

First author/ reference	Metal	Support	Temperature range/°C	Comments
Hallische [35]	Ni with Co, Ce, Cu or Fe as promoter	α-Al_2O_3	550, 730	Co, Ce, Cu promote activities $H_2/CO>1$
Buarab [36]	Ni	Various supports	600	α-Al_2O_3 most effective support; K poisons reaction
Nichio [37]	Ni	α-Al_2O_3	650–800	Best results for preparation with Ni acetylacetonate
Gronchi [38]	Ni	SiO_2, La_2O_3	600	Pulse reactor study CO_2 reacts with La_2O_3
Provendier [39]	Ni	LaNiFe perovskite	400–800	Perovskite forms Ni–Fe alloy in use. Low coke formation
Kroll [40]	Ni	SiO_2	700	Detailed kinetic study
Kim [41]	Ni	Al_2O_3	600–800	Aerogel catalyst gives low carbon deactivation K addition helpful
York [42]	Ni + W or Mo oxides	Al_2O_3	700	W improves Ni catalyst
	Mo_2C, WC	No support	850	Carbides vs. stable
Suzuki [43]	Ni	$Ca_{0.8}Sr_{0.2}TiO_3$ $BaTiO_3$	850	In situ preparation. Stable against C formation
Stagg [44]	Pt	ZrO_2 with CeO_2, La_2O_3	800	Promoters increase stability and activity
O'Connor [45]	Pt	ZrO_2	600	DRIFTS study; oxidation –reduction mechanism probable
Quincoces [46]	Ni	CaO/SiO_2	650	CaO increases activity
Nam [47]	Ni	Ni–La perovskites with Sr promotion	600–900	Addition of Ca reduces coke formation
Tomishige [48]	Ni	MgO from solid solution	500–850	Addition of small quantities of H_2 stops any deactivation

discussed the various reactions involved and their thermodynamics, these authors gave a very comprehensive review of work on CO_2 reforming published up until 1993. They showed that most of the noble metals and also nickel had been studied and that oxides such as alumina and magnesia had been used as supports for the active metals. They also pointed out that carbon deposition rates seem to depend on the support used and possibly on catalyst morphology, two factors that emerge repeatedly in more recent publications. They mentioned specifically the paper by Gadalla and Somer referred to above [3] in which the use of a Ni/MgO catalyst for up to 125 h was reported; at the end of the experiment, these authors observed only a minute trace of carbon deposition.

Edwards and Maitra also discussed the results of two papers where the activities of a series of metals are reported. In the first, by Takayasu et al. [52], Ni, Ru, Rh, Pt and Pd catalysts supported on "ultrafine single crystal MgO" were compared, the activities being in that order. In the second, by Ashcroft et al. [53], catalysts comprising of Ni, Ir, Rh, Pd and Ru supported on alumina were examined, the order of activity being in the order given. While Takayasu et al. had found that Ru was one of the most active metals, Ashcroft et al. reported that it is one of the least active. (Rostrup-Nielsen has also reported it as being very active [6].) However, both groups found that Ni and Rh are among the most active metals. Listing other papers on the topic, Edwards and Maitra also pointed out that Solymosi et al. [54] and Masai et al. [55] had previously reported that Rh supported on alumina is one of the most active catalysts for the reaction.

Edwards and Maitra closed their review [24] with a discussion of the potential application of thermochemical heat pipe applications for the recovery, storage and transmission of solar energy, showing that the CO_2 reforming reaction can be coupled with the methanation reaction to provide a method of energy transmission (a topic also mentioned briefly by Rostrup-Nielsen in his more extensive review [6]). We return briefly to this topic later (see Table 6.13).

The research papers on CO_2 reforming of methane from the meetings of the Natural Gas Conversion series listed in Tables 6.2, 6.3, and 6.4 cover the use of most of the metal/support combinations that have since been examined in more detail. The vast majority of these papers reported work involving nickel, this being supported on a variety of different oxides, in particular, alumina [6, 25, 27–29, 33, 35, 37, 41, 42], silica [31, 38, 40, 46], magnesia [6], lanthana [30, 38] and zirconia [25]. Some attention was also given to the use of catalysts derived from nickel-containing compounds or from solid solutions of NiO in MgO [48]. Most of the noble metals are also featured, particular attention being focused on Pt [2, 25, 32], Rh [26, 27, 34], Ru [34] and Ir [31], again on a variety of supports. It is interesting to note that there was a wide range in the temperatures of operation, from 400 to 900 °C. As was pointed out above, operation at high temperature is necessary to give acceptably high conversions and so the results at lower temperatures, although giving information on relative activities, have less practical relevance. It should also be noted that the paper by York et al. [42] reports the use of carbides, while the papers by Kikuchi and Chen [33] and Ponelis and Van Zyl [34] both describe the use of membrane systems.

6.4.2 Highly Cited Publications from the General Literature

In the following sections, we give a listing of the more significant papers from the recent literature under headings suggested by the brief outline given in the last paragraph. Owing to the very large literature on the subject of CO_2 reforming of methane, the papers selected for mention under each heading are chosen in relation to their citation records, recognising that those papers most frequently referred by

Table 6.5 Some of the most cited reviews on CO_2 reforming listed in the Web of Science

First author/ reference	Comments	Citations (WoS May 2013)
Wang [58]	Identifies areas for future research: effect of metal-support interaction on activity; effects of promoters; reaction kinetics and mechanism; pilot reactor performance and scaleup. Ni on some supports gives carbon-free operation	226
Hu [59]	Reviews catalysts studied, with emphasis on inhibition of C deposition (also reviews partial oxidation)	212
Ross [60]	Review of the development of Pt/ZrO_2 catalysts	134
Ross [61]	General review of CO_2 reforming	59
Bradford [62]	Reviews the use of Ni and Rh catalysts, also single crystals; also partial oxidation	552
Verykios [63]	Review concentrating on the development of Ni/La_2O_3 catalysts. $La_2O_2CO_3$ species are critical to good operation	
Armor [64]	Review largely on steam reforming but also including CO_2 reforming, particularly limitations due to C deposition and also costs of supplying pure CO_2	445
Ma [65]	Review of CO_2 conversion including $CH_4 + CO_2$ over Ni supported on a wide variety of supports	45
Kodama [66]	Review on production of fuels using sunlight including CO_2 reforming of methane	118

others are likely to be the most important in that field. In the tables, the number of citations to each of the publications given by the Web of Science in May 2013 is shown for comparison purposes; clearly this is only a snapshot of the situation, and it should also be recognised that younger publications will have correspondingly lower numbers of citations than older ones.[5] A reader with a particular interest in one or another type of catalyst would gain an up-to-date picture of the literature on that topic by doing his/her own citation study based on the appropriate key papers listed in the tables.

Table 6.5 lists some of the most cited reviews on the subject of CO_2 reforming. Some of these are very general, covering a whole range of topics from basic aspects to pilot plant results [58], while others are much more focused on one type of catalyst [60, 63]. The review by Armor [64] is of particular interest as it not only covers both steam reforming and CO_2 reforming but also deals with matters such as problems associated with purification of CO_2. Kodama [66] reviews the subject of fuel production using sunlight.

Nickel, although very active for the conversion of methane by either steam reforming or CO_2 reforming, suffers from the problem that it rapidly becomes deactivated by the formation of carbon, this carbon generally being in the form of nanotubes with a nickel crystallite at the tip. Much of the effort has therefore been in trying to find suitable additives for the catalysts that help to minimise this form of carbon deposition, often by modifying the Ni particle size or the support surface in the region of the nickel

[5] We have paid some attention to this time dependence in our choice of which papers to include.

crystallites. It is now reasonably well established that small nickel crystallites are much less susceptible to C growth, but anchoring the active metal to the support is also known to hinder filament growth. Table 6.6 lists some of the papers reporting the use of catalysts consisting of Ni supported on alumina or modified aluminas. A number of additives are seen to improve the behaviour of the catalysts in relation to the problem of carbon deposition, particularly the alkali [67, 75] and alkaline earth metals [67, 74], lanthana [71] and ceria [68, 73]; ceria is particularly effective.

The effect of reducing the particle size is seen particularly with catalysts based on Ni on MgO; see Table 6.7. This is because the precursor to the active catalyst often involves the formation of a solid solution of NiO in MgO; see, for example, references [77, 80, 83]. Catalysts based on supports such as $MgAl_2O_4$ are also very effective [81–83].

Another support that has received some attention is zirconia, sometimes alone but also often promoted by other species such as ceria [84, 85] or magnesia [83]; see Table 6.8. The effect of Ni particle size on stability has been shown for a zirconia support by Lercher et al. [86]. Other supports studied have included titania [88], lanthana [89], silica [90] and a La–Sr–Ni–Co perovskite [91]; see Table 6.9.

Noble metals have the advantage over Ni in that they do not dissolve carbon, and so the problem of the growth of carbon filaments does not occur with them. As a result, there has been a significant amount of work using catalysts containing noble metals on a variety of supports. Table 6.10 lists some highly cited papers describing the use of supported Pt catalysts on various different supports. Work from this laboratory [60, 95] and also from Bitter et al. [96] has been concerned with the use of Pt on zirconia, this usually being promoted by a small quantity of alumina. Other promoters such as La_2O_3 or CeO_2 are also possible [93].

The other noble metals have also received significant attention, particularly Rh [97–102], Ir [99, 101] and Pd [101, 103]; see Table 6.11. As discussed by Rostrup-Nielsen, a series of successful pilot plant tests have been carried out using a catalyst based on Rh. However, the cost of Rh is prohibitively high so that this work is unlikely to be applied.

Because of the high cost of the noble metals and the resultant problems of operating large scale using them, a significant amount of attention has been paid to the possibility of using MoC_2 or WC as the active component of a catalyst, it being well established that these carbides exhibit properties similar to those of the noble metals. Claridge et al. ([105], see Table 6.12) showed that both of the carbides were active for the reaction, but they reported that there was some evidence of deactivation caused by oxidation of the carbides. Work from this laboratory [106] showed that this was probably due to the fact that the entrance to the CO_2 reforming bed operates under slightly oxidising conditions, this causing the carbide to oxidise, and that the exit part of the bed was stable. The activity of a Mo_2C material supported on ZrO_2 could be improved significantly by promotion with Bi species.

Finally, Table 6.13 lists some references describing work in various laboratories on energy transport systems involving the CO_2 reforming reaction as the endothermic part of the system. It is interesting to note that despite the comments above, the metal of choice for this work appears to be Rh, probably because of the reliable performance far outweighs the disadvantage of cost.

Table 6.6 Some of the most cited papers dealing with Ni supported on Al_2O_3 or modified Al_2O_3

First author/ reference	Metal	Support	Temperature range/°C	Comments	Citations (WoS May 2013)
Horiuchi [67]	Ni	Al_2O_3		Studied effect of adding Na, K, Mg and Ca. All decrease the tendency to deposit carbon	185
Wang [68]	Ni	CeO_2–Al_2O_3		CeO_2 addition (1–5 wt% optimum) gives better activity, stability and C suppression	182
Wang [69]	Ni	Al_2O_3, SiO_2, MgO		Strong metal-support interaction improves stability and coking resistance	129
Kim [70]	Ni	Al_2O_3 aerogel	700	Aerogel supported metal more active and stable than conventional Ni/Al_2O_3 catalyst. C deposition depends on Ni particle size, being significant above 7 nm	154
Martinez [71]	Ni	Al_2O_3		Studies influence of La_2O_3 addition. La decreases rate of coking	79
Juan-Juan [72]	Ni, Ni/K	Al_2O_3	TP reaction to 900, isothermal at 700	Coking rate with K much reduced	59
Laosiripojana [73]	Ni	Al_2O_3–CeO_2	800–900	8 % CeO_2 gives greatly improved behaviour, with greatly decreased C deposition	54
Goula [74]	Ni	CaO–Al_2O_3	750	Ca content influences amounts of C on catalyst after use and also Ni morphology. Origin of C probed by tracer study	90
Osaki [75]	Ni	K–Al_2O_3		K controls Ni ensemble size and thus affects C deposition rates	93

Table 6.7 Some papers dealing with Ni supported on MgO

First author/ reference	Metal	Support	Temperature range/°C	Comments	Citations (WoS May 2013)
Rostrup-Nielsen [76]	Ni	MgO		Discussion of all aspects of the reaction over Ni catalysts	674
Tomishige [77]	Ni	MgO, Al_2O_3		Ni0.03MgO0.970 solid solution much more resistant to C deposition than Ni/MgO or Ni/Al_2O_3	239
Wei [78]	Ni	MgO		Careful kinetic analysis (with isotopic measurements) shows C–H bond activation to be sole relevant step	225
Ruckenstein [79]	Ni	MgO and other alkaline earth oxides		Ni/MgO more stable than Ni on the other supports; MgO inhibits Boudouard reaction	194
Ruckenstein [80]	Ni	MgO SiO_2 Al_2O_3	790	Combines CH_4/O_2 with CH_4/CO_2 to decrease chance of explosion. Ni/MgO solid solution catalyst most effective	59
Djaidja [81]	Ni	MgO/Al_2O_3 MgO	800	Ni/MgO sample prepared by co-precipitation less stable than one prepared by impregnation	58
Guczi [82]	Ni	$MgAl_2O_4$		Study of C species formed. Addition of Au shown to improve activity and stop formation of C nanotubes	18
Wang [83]	Ni, Co, Ni–Co	MgAlOx	750	Ni–Co catalyst is very stable; no deactivation after 2,000 h operation. XANES and EXAFS study of catalyst structure	

Table 6.8 Some papers dealing with Ni supported on zirconia

First author/ reference	Metal	Support	Temperature range/°C	Comments	Citations (WoS May 2013)
Roh [84]	Ni	Ce/ZrO_2	750	Work on steam reforming of methane using catalysts previously studied for CO_2 reforming	152
Montoya [85]	Ni	ZrO_2–CeO_2	500–800	CeO_2 stabilises tetragonal ZrO_2. Graphitic C does not cause deactivation. CeO_2 enhances reverse water–gas shift reaction	133
Lercher [86]	Ni, Pt	ZrO_2 and other supports	600, 720–780	Ni/ZrO_2 very stable if low Ni loadings used. (Ni particle size ~2 nm)	94
Nagaraja [87]	Ni	K/MgO–ZrO_2	550–750	Addition of 0.5wt%K increases activity and stability of the $Ni/MgO/ZrO_2$ catalyst	3

Table 6.9 Some papers dealing with nickel on other supports

First author/ reference	Metal	Support	Temperature range/°C	Comments	Citations (WoS May 2013)
Bradford [88]	Ni	TiO_2 (also SiO_2, MgO)	400–550	Ni/TiO_2 more active than Ni/C, Ni/SiO_2 or Ni/MgO. Ni/TiO_2 suppresses C deposition. Reverse water–gas shift reaction in equilibrium	231, 152
Zhang [89]	Ni	La_2O_3, Al_2O_3, CaO/ Al_2O_3, CaO	750	Sites at Ni–La_2O_3 interface give active and stable performance compared with other supports all of which gave continuous deactivation with time	157
Swaan [90]	Ni	SiO_2	700	Operating catalyst is Ni carbide. Deactivation by catalyst sintering and C deposition	181
Valderrama [91]	Ni–Co	La–Sr–O	600–800	La–Sr–Ni–Co–O perovskite solid solutions give rise to nano-sized crystallites stable under reforming conditions	23

Table 6.10 Some papers dealing with Pt catalysts on various supports

First author/ reference	Metal	Support	Temperature range/°C	Comments	Citations (WoS May 2013)
Ashcroft [92]	Pt and other Pt- group metals	Al_2O_3	400–800	Shows that partial oxidation and CO_2 reforming can be carried out simultaneously	437
Stagg-Williams [93]	Pt	ZrO_2, ZrO_2/La_2O_3, ZrO_2/CeO_2	800	La stabilises support. Ce improves oxygen uptake of support	124
Damyanova [94]	Pt	CeO_2–Al_2O_3	450–600	CeO_2 gives improved Pt dispersion and increased activity. Optimum 1 % CeO_2	118
Ross [60]	Pt	ZrO_2, TiO_2, Al_2O_3	550–800	Pt on ZrO_2 much more stable with respect to C deposition than other samples	130
O'Connor [95]	Pt	ZrO_2, Al_2O_3	550–800	O_2 addition to CO_2 reduces the temperature for a given conversion and also reduces carbon deposition	99
Bitter [96]	Pt	ZrO_2, SiO_2	600–800	ZrO_2 as support activates CO_2, while Pt black or SiO_2 as a support does not	113

Table 6.11 Some papers dealing with catalysts containing Rh, Ru, Ir or Pd

First author/ reference	Metal	Support	Temperature range/ °C	Comments	Citations (WoS May 2013)
Nakamura [97]	Rh	Al_2O_3, TiO_2, SiO_2	277–727	Rh/SiO_2 greatly improved by mixing with Al_2O_3, TiO_2 or MgO	109
Richardson [98]	Rh, Pt/Re	γ-Al_2O_3 washcoated on α-Al_2O_3	Pt–Re deactivates below 700 °C	Foams exhibit high effectiveness factor. Rh best overall catalyst	54
Mark [99]	Rh, Ir	Range of oxides	550–850	Specific rates constant regardless of support. H_2/CO ratio varied by addition of H_2O or O_2	129
Erdohelyi [100]	Rh	Al_2O_3, TiO_2, SiO_2, MgO	150 upwards	Methane adsorbs above 150 °C. Reaction with CO_2 occurs above 400 °C. No carbon deposition observed	29
Erdohelyi [103]	Pd	Al_2O_3, TiO_2, SiO_2, MgO	400–500	Little carbon deposited with stoichiometric gas mixture	127
Qin [101]	Ru, Rh > Ir > Pt, Pd	MgO	600–900	Compares steam and CO_2 reforming. Activity in order shown. Ru, Rh and Ir give little deactivation. Mixed reforming slower	121
Maestri [102]	Rh	Al_2O_3	300–900	Microkinetic analysis of data of Donazzi et al. [104]	44

Table 6.12 Some papers dealing with carbides as catalysts

First author/ reference	Carbide	Support	Temperature range/°C	Comments	Citations (WoS May 2013)
Claridge [105]	Mo_2C, unsupported WC	Al_2O_3, ZrO_2, SiO_2, TiO_2	850–950	Interaction with support during preparation affects activity. Oxidation of carbide causes deactivation	157
Treacy [106]	Mo_2C	Al_2O_3, ZrO_2, SiO_2	950	ZrO_2 material most stable. Addition of Bi gives higher conversions. Catalyst oxidises at entry to bed	2

Table 6.13 Some papers discussing the use of dry reforming as part of an energy transportation system

First author/ reference	Metal	Support	Temperature range/°C	Comments	Citations (WoS May 2013)
Fish [1]	–	–	–	Describes balancing of the reactions for a system including dry reforming (Sandia Natl. Labs.)	27
Levy [56]	Rh	Al_2O_3	750–900	Over 60 cycles of reforming reaction and the reverse (methanation) carried out (Weizmann Institute)	59
Worner [57]	Rh	Foam structures: α-Al_2O_3, SiC	700–860	Both inserts gave some C deposition (Deutch Zentrum Luft und Raumfahrt)	64

6.4.3 *Some Recent Publications on CO_2 Reforming of Methane*

In conclusion, we list in Table 6.14 a number of recent publications on the subject of CO_2 reforming chosen rather at random from the large number that have been published recently. Many of the themes that we have highlighted above return frequently. While some of the papers report significant improvements in previously described catalyst systems (e.g. [110, 111, 123]), others use the reaction purely as a test reaction (generally at rather lower temperatures) to provide a method of

Table 6.14 Some recent papers (2013) on methane dry reforming

First author/ reference	Metal	Support	Temperature range/°C	Comments
Asencios [107]	Ni	$MgO–ZrO_2$	750	Coupling of partial oxidation and dry reforming leads to stable operation. Optimum behaviour with 20w% Ni
Zanganeh [108]	Ni	MgO	550–750	Best results with catalyst derived from NiO/MgO solid solution with relatively low Ni content: $Ni_{0.03}$ $Mg_{0.97}O$
Zanganeh [109]	Ni	MgO	700	$Ni_{0.1}$ $Mg_{0.9}O$ samples prepared by surfactant-assisted co-precipitation gave good activities and stabilities (122 h on stream)
Chen [110]	Ni	$CeAlO_3–Al_2O_3$	800	Presence of $CeAlO_3$ phase reduces graphitic carbon deposition; this phase decomposes CO_2 giving active surface oxygen
Xiao [111]	Ni	MgO (ex solid solution)	760	Preparation based on nano-platelets giving homogeneous distribution of the Ni
Bhavani [111]	Ni–Co Ni–Mn	NiCoMnCeZrO and other combinations	800	Mixed $CH_4/O_2/CO_2$ feed. NiCoMnCeZrO gives high activity with little activity loss
Benrabaa [112]	Ni	$NiFe_2O_4$	800	Non-stoichiometric mixed spinel formed under reaction conditions
		$Ni_xFe_{2-x}O_4$		Activity improved by reduction
Gardner [113]	Ni	$Ba_{0.75}Ni_yAl_{12-y}O_{19-\delta}$	900	Activity increases with amount of Ni but C deposition also increases
Baeza [114]	Ni	$CaO–La_2O_3–ZrO_2$	400–500	CaO (2 wt%) acts as a source of CO and active O species that remove C deposited on surface
Odedairo [115]	Ni	CeO_2	700	Plasma treatment of catalyst gives clean metal–support interface and higher activity and stability than untreated sample

(continued)

Table 6.14 (continued)

First author/ reference	Metal	Support	Temperature range/°C	Comments
Ozkara-Aydinoglu [116]	Ni/Pt	Al_2O_3	580–620	Amount of Pt added has major effect on the reaction kinetics, also on level of inhibition by CO
Tao [117]	Ni	Al_2O_3	700	Sample prepared by single-step surfactant-templating method more active and stable than conventional sample
Ma [118]	Ni	Carbon nanotubes	750	Samples with Ni inside nanotubes more active and stable than those with Ni outside the tubes
Sun [119]	Ni	Mg (and or Ca) O/Al_2O_3	750	NiO/MgO solid solution formed giving active and stable catalyst; CaO addition causes decreased activity and stability
Zhu [120]	Ni	CeO_2/SiO_2	800	Investigation of the effect of calcination atmosphere. Calcination in Ar gives better performance
Albarazi [121]	Ni	CeO_2/ZrO_2/SBA-15	600–800	Promotion of Ni within pores by Ce–Zr–O improves behaviour but gives a decrease in accessibility of the active sites
San Jose-Alonso [122]	Ni or Co	Al_2O_3	700–800	Low metal contents gave low rates of C deposition. Tests for 24 h
Nagaraja [123]	Ni	K–MgO/ZrO_2	550–800	Presence of K^+ incorporated during the co-precipitation of the MgO–ZrO_2 support greatly increases the stability. No C deposition detected with most active and stable samples

characterising a catalyst system (e.g. [116, 121]). One example of an improvement is to be found in work from this laboratory ([123]; see also [87]) that shows that a very stable catalyst with good activity can be achieved with the Ni–Zr–Mg–O system as long as K^+ ions are included in the structure.

6.5 Conclusions

The dry reforming of methane has provided a fertile area of research for more than two decades, and some significant advances have been made in the design of catalysts suitable for the reaction. However, it is at present unlikely that the reaction will be used in practice unless it is combined with either partial oxidation or steam reforming in order to avoid the problems associated with carbon formation. This review has concentrated almost exclusively on the CO_2 reforming of methane, paying little attention to the reactions of other hydrocarbons. However, many of the constraints encountered equally to the reforming of other molecules such as naphtha with the added complication that methane may be formed as a product.

Dedication. The author wishes to dedicate this review to the memory of the late Laszlo Guczi with whom he collaborated in a joint project under the auspices of an ERA-Chemistry project (coordinated by Alain Keinemann) until shortly before his death in December 2012.

Acknowledgement The author wishes to thank Bhari Mallanna Nagaraja for having contributed some of the references included in this review and for having read and commented on the concept manuscript.

References

1. Fish JD, Hawn DC (1987) Closed-loop thermochemical energy-transport based on CO_2 reforming of methane – balancing the reaction systems. J Solar Energy Eng Trans ASME 109:215–220
2. Gadalla AM, Bower B (1988) The role of catalyst support on the activity of nickel for the reforming of methane with CO_2. Chem Eng Sci 43:3049–3062
3. Gadalla AM, Somer ME (1989) Synthesis and characterization of catalysts in the system Al_2O_3-MgO-NiO-Ni for methane reforming with CO_2. J Am Ceram Soc 72:683–687
4. Rostrup Nielsen JR (1984) Catalytic steam reforming. In: Anderson JR, Boudart M (eds) Catalysis – science and technology, vol 5. Springer, Berlin/Heidelberg/New York/Tokyo, pp 1–117
5. Ross JRH (1975) The steam reforming of hydrocarbons. In: Thomas JM, Roberts MW (eds) Surface and defect properties of solids, vol 4. The Chemical Society, London, pp 34–67
6. Rostrup-Nielsen JR (1994) Aspects of CO_2 reforming of methane. In: Curry-Hyde HE, Howe RF (eds) Natural gas conversion, II, vol 81, Studies in surface science and catalysis. Elsevier, Amsterdam, pp 25–41
7. The Midrex Process (2013) http://www.midrex.com
8. Dibbern HC, Olesen P, Rostrup Nielsen JR, Udengaard NR (1986) Make low H_2/CO syngas using sulfur passivated reforming. Hydrocarb Process 65:71–74
9. Rostrup Nielsen JR (1984) Sulfur-passivated nickel catalysts for carbon-free steam reforming of methane. J Catal 85:31–43
10. Ross JRH (1985) Metal catalysed methanation and steam reforming. In: Bond GC, Webb G (eds) Catalysis, vol 7, Specialist periodical report. Royal Society of Chemistry, London, pp 1–45

11. Keller GE, Bhasin MM (1982) Synthesis of ethylene via oxidative coupling of methane. 1 Determination of active catalysts. J Catal 73:9–19
12. Hinsen W, Baerns M (1983) Oxidative coupling of methane to C_2 hydrocarbons in the presence of different catalysts. Chemiker Zeitung 107:223–226
13. Ito T, Wang J-X, Lin C-H, Lunsford JH (1985) Oxidative dimerization of methane over a lithium-promoted magnesium-oxide catalyst. J Am Chem Soc 107:5062–5068
14. Lunsford JH (1991) The catalytic conversion of methane to higher hydrocarbons. "Natural gas conversion". Stud Surf Sci Catal 61:3–13
15. Hutchings GJ, Scurrell MS, Woodhouse JR (1989) Oxidative coupling of methane using oxide catalysts. Chem Soc Rev 18:251
16. Baerns M, Ross JRH (1992) Catalytic chemistry of methane conversion. Thomas JM, Zamaraev KI (eds) Perspectives in catalysis. Blackwell Scientific Publishers, Oxford, IUPAC monograph, pp 10–30
17. See also a collection of review papers in Wolf EE (eds) (1992) Methane conversion by oxidative processes – fundamental and engineering aspects. Van Nostrand Reinhold catalysis series, Van Nostrand Reinhold, New York
18. Holmen A, Jens K-J, Kolboe S (eds) (1990) Natural gas conversion, vol 61, Stud Surf Sci Catal. Elsevier, Amsterdam
19. Howe R, Curry-Hyde E (eds) (1994) Natural gas conversion III, vol 81, Stud Surf Sci Catal. Elsevier, Amsterdam
20. de Pontes M, Espinoza RL, Nicolaides C, Scholz JH, Scurrell MS (eds) (1997) Natural gas conversion IV, vol 107, Stud Surf Sci Catal. Elsevier, Amsterdam
21. Parmaliana A, Sanfilippo D, Frusteri F, Vaccari A, Arena F (eds) (1998) Natural gas conversion V, vol 119, Stud Surf Sci Catal. Elsevier, Amsterdam
22. Ross JRH (2005) Natural gas reforming and CO_2 mitigation. Catal Today 100:151–158. O'Connor AM (1994) BSc thesis, University of Limerick
23. Rostrup Nielsen JR (1993) Production of synthesis gas. Catal Today 18:305–324
24. Edwards JH, Maitra AM (1994) The reforming of methane with carbon dioxide – current status and future applications. Stud Surf Sci Catal 81:291–296
25. Seshan K, Ten Barge HW, Hally W, Van Keulen ANJ, Ross JRH (1994) Carbon dioxide reforming of methane in the presence of nickel and platinum catalysts supported on ZrO_2. Stud Surf Sci Catal 81:285–290
26. Uchijima T, Nakamura J, Sato K, Aikawa K, Kubushiro K, Kummori K (1994) Production of synthesis gas by partial oxidation of methane and reforming of methane by carbon dioxide. Stud Surf Sci Catal 81:325–327
27. Cant NW, Dümpelmann R, Maitra AM (1997) A comparison of nickel and rhodium catalysts for the reforming of methane by carbon dioxide. Stud Surf Sci Catal 107:491–496
28. Slagtern A, Olsbye U, Blom R, Dahl IM (1997) The influence of rare earth oxides on Ni/Al_2O_3 catalysts during CO_2 reforming of CH_4. Stud Surf Sci Catal 107:497–502
29. Yu C-C, Lu Y, Ding X-J, Shen S-K (1997) Studies on Ni/Al_2O_3 Catalyst for CO_2 reforming of CH_4 to synthesis gas. Stud Surf Sci Catal 107:503–510
30. Zhang Z-L, Verykios X (1997) Performance of Ni/La_2O_3 catalyst in carbon dioxide reforming of methane to synthesis gas. Stud Surf Sci Catal 107:511–516
31. Erdöhelyi A, Fodor K, Solymosi F (1997) Reaction of CH_4 with CO_2 and H_2O over supported Ir catalyst. Stud Surf Sci Catal 107:525–530
32. Van Keulen ANJ, Hegarty MES, Ross JRH, Van Oosterkamp PF (1997) The development of platinum-zirconia catalysts for the CO_2 reforming of methane. Stud Surf Sci Catal 107:537–546
33. Kikuchi E, Chen Y (1997) Low-temperature syngas formation by CO_2 reforming of methane in a hydrogen-permselective membrane reactor. Stud Surf Sci Catal 107:547–553
34. Ponelis AA, Van Zyl PGS (1997) CO_2 reforming of methane in a membrane reactor. Stud Surf Sci Catal 107:555–560

35. Hallische H, Bouarab R, Cherife O, Bettahar MM (1998) Effect of metal additives on deactivation of Ni/α-Al_2O_3 in the CO_2-reforming of methane. Stud Surf Sci Catal 119:705–710
36. Buarab R, Menad S, Hallische D, Cherifi O, Bettahar MM (1998) Reforming of methane with carbon dioxide over supported Ni catalysts. Stud Surf Sci Catal 119:717–722
37. Nichio NN, Casella ML, Ponzi EN, Ferretti OA (1998) Ni/Al_2O_3 catalysts for syngas obtention via reforming with O_2 and/or CO_2. Stud Surf Sci Catal 119:723–728
38. Gronchi P, Centola P, Kaddouri A, Del Rosso R (1998) Transient reactions in CO_2 reforming of methane. Stud Surf Sci Catal 119:735–740
39. Provendier H, Petit C, Estournes C, Keinnemann A (1998) Dry reforming of methane. Interest of La-Fe-Ni solid solutions compared to $LaNiO_3$ and $LaFeO_3$. Stud Surf Sci Catal 119:741–746
40. Kroll VCH, Tjatjopoulos GJ, Mirodatos C (1998) Kinetics of methane reforming over Ni/SiO_2 catalysts based on a step-wise mechanistic model. Stud Surf Sci Catal 119:753–758
41. Kim J-H, Suh DJ, Park T-J, Kim K-L (1998) Improved stability of nickel-alumina aerogel catalysts for carbon dioxide reforming of methane. Stud Surf Sci Catal 119:771–776
42. York APE, Suhartanto T, Green MLH (1998) Influence of molybdenum and tungsten dopants on nickel catalysts for dry reforming of methane with carbon dioxide to synthesis gas. Stud Surf Sci Catal 119:777–782
43. Suzuki S, Hayakawa T, Hamakawa S, Suzuki K, Shishido T, Takehira K (1998) Sustainable Ni catalysts prepared by SPC method for CO_2 reforming of CH_4. Stud Surf Sci Catal 119:783–788
44. Stagg SM, Resasco DE (1998) Effect of promoters on supported Pt catalysts for CO_2 reforming of CH_4. Stud Surf Sci Catal 119:813–818
45. O'Connor AM, Meunier FC, Ross JRH (1998) A kinetic and in-situ DRIFT spectroscopy study of carbon dioxide reforming over a Pt/ZrO_2 catalyst. Stud Surf Sci Catal 119:819–824
46. Quincoces CE, Perez de Vargas S, Diaz A, Montes M, González MG (1998) Morphological changes of Ca promoted Ni/SiO_2 catalysts and carbon deposition during CO_2 reforming of methane. Stud Surf Sci Catal 119:837–842
47. Nam JW, Chae H, Lee SH, Jung H, Lee K-Y (1998) Methane dry reforming over well-dispersed Ni catalyst prepared from perovskite-type mixed oxides. Stud Surf Sci Catal 119:843–848
48. Tomishige K, Chen Y, Yamazaki O, Himeno Y, Koganezawa Y, Fujimoto K (1998) Carbon-free CH_4-CO_2 and CH_4-H_2O reforming catalysts – structure and mechanism. Stud Surf Sci Catal 119:861–866
49. Fischer F, Tropsch H (1928) Brennstoff Chem 3:39
50. Bodrov IM, Apel'baum LO (1967) Kinet Katal 8:379
51. Bodrov IM, Apel'baum LO, Temkin MI. Kinet Katal 5:696
52. Takayasu O, Hirose E, Matsuda N, Matsurra I (1991) Chem Expr 6:447
53. Ashcroft AT, Cheetham AK, Green MLH, Vernon PDF (1991) Partial oxidation of methane to synthesis gas using carbon dioxide. Nature 352:225–226; see also Vernon PDF, Green MLH, Cheetham AK, Ashcroft AT (1992) Catal Today 13:417
54. Solymosi F, Kutsan GY, Erdohelyi A (1991) Catalytic reaction of CH_4 with CO_2 over alumina-supported Pt metals. Catal Lett 11:149
55. Masai M, Kado H, Miyake A, Nishiyama S, Tsuruya S (1988) Stud Surf Sci Catal 36:67
56. Levy M, Levitan R, Rosin H, Rubin R (1993) Solar-energy storage via a closed-loop chemical heat pipe. Solar Energy 50:179–189
57. Worner A, Tamme R (1998) CO_2 reforming of methane in a solar driven volumetric receiver-reactor. Catal Today 46:165–174
58. Wang SB, Lu GQM, Millar GJ (1996) Carbon dioxide reforming of methane to produce synthesis gas over metal-supported catalysts: state of the art. Energy Fuels 10:896–904
59. Hu YH, Ruckenstein E (2004) Catalytic conversion of methane to synthesis gas by partial oxidation and CO_2 reforming. Adv Catal 48:297–345

60. Ross JRH, Van Keulen ANJ, Hegarty MES, Seshan K (1996) The catalytic conversion of natural gas to useful products. Catal Today 30:193–199
61. Ross JRH (2005) Natural gas reforming and CO_2 mitigation. Catal Today 100:151–158
62. Bradford MCJ, Vannice MA (1999) CO_2 reforming of CH_4. Catal Rev Sci Eng 41:1–42
63. Verykios XE (2003) Catalytic reforming of natural gas for the production of chemicals and hydrogen. Int J Hydrogen Energy 28:1045–1063
64. Armor JN (1999) The multiple roles of catalysis in the production of H_2. Appl Catal A Gen 176:159–176
65. Ma J, Sun N, Zhang X (2009) A short review of catalysis for CO_2 conversion. Catal Today 148:221–231
66. Kodama T (2003) High-temperature solar chemistry for converting solar heat to chemical fuels. Progr Energy Combust Sci 29:567–597
67. Horiuchi T, Sakuma K, Fukui T, Kubo Y, Osaki T, Mori T (1996) Suppression of carbon deposition in the CO_2 reforming of CH_4 by adding basic metal oxides to a Ni/Al_2O_3 catalyst. Appl Catal A Gen 144:111–120
68. Wang SB, Lu GQ (1998) Role of CeO_2 in Ni/CeO_2-Al_2O_3 catalysts for carbon dioxide reforming of methane. Appl Catal B Environ 19:267–277
69. Wang SB, Lu GQM (1998) CO_2 reforming of methane on Ni catalysts: effects of the support phase and preparation technique. Appl Catal B Environ 16:269–277
70. Kim JH, Suh DJ, Park TJ, Kim KL (2000) Effect of metal particle size on coking during CO_2 reforming of CH_4 over Ni-alumina aerogel particles. Appl Catal A Gen 197:191–200
71. Martinez R, Romero E, Guimon C, Bilbao R (2004) CO_2 reforming of methane over coprecipitated Ni-Al catalysts modified with lanthanum. Appl Catal A Gen 274:139–149
72. Juan-Juan J, Roman-Martinez MC, Illan-Gomez MJ (2004) Catalytic activity and characterization of Ni/Al_2O_3 and NiK/Al_2O_3 catalysts for CO_2 methane reforming. Appl Catal A Gen 264:169–174
73. Laosiripojana N, Sutthisripok W, Assabumrungrat S (2005) Synthesis gas production from dry reforming of methane over CeO_2 doped Ni/Al_2O_3: influence of the doping of ceria on the resistance toward carbon formation. Chem Eng J 112:13–22
74. Goula MA, Lemonidou AA, Efstathiou AM (1996) Characterization of carbonaceous species formed during reforming of CH_4 with CO_2 over Ni/CaO-Al_2O_3 catalysts studied by various transient techniques. J Catal 161:626–640
75. Osaki T, Mori T (2001) Role of potassium in carbon-free CO_2 reforming of methane on K-promoted Ni/Al_2O_3 catalysts. J Catal 204:89–97
76. Rostrup Nielsen JR, Hansen JHB (1993) CO_2 reforming of methane over transition metals. J Catal 144:38–49
77. Tomishige K, Chen YG, Fujimoto K (1999) Studies on carbon deposition in CO_2 reforming of CH_4 over nickel-magnesia solid solution catalysts. J Catal 181:91–103. See also: Tomishige K, Yamazaki O, Chen YG, Yokoyama K, Li XH, Fujimoto K (1998) Development of ultra-stable Ni catalysts for CO_2 reforming of methane. Catal Today 45:35–39
78. Wei JM, Iglesia E (2004) Isotopic and kinetic assessment of the mechanism of reactions of CH_4 with CO_2 or H_2O to form synthesis gas and carbon on nickel catalysts. J Catal 224:370–383
79. Ruckenstein E, Hu YH (1995) Carbon dioxide reforming of methane over nickel alkaline earth metal oxide catalysts. Appl Catal A Gen 133:149–161
80. Ruckenstein E, Hu YH (1998) Combination of CO_2 reforming and partial oxidation of methane over NiO/MgO solid solution catalysts. Ind Eng Chem Res 37:1744–1747
81. Djaida A, Libs S, Keinnemann A, Barama A (2006) Characterization and activity in dry reforming of methane on NiMg/Al and Ni/MgO catalysts. Catal Today 113:194–200
82. Guczi L, Stefler G, Geszti O, Sajo I, Paszti Z, Tompos A, Schay Z (2010) Methane dry reforming with CO_2: a study on surface carbon species. Appl Catal A Gen 375:236–246
83. Wang H, Miller JT, Shakouri M, Xi C, Wu T, Zhao H, Cem Akatay M (2013) XANES and EXAFS studies on metal nanoparticle growth and bimetallic interaction of Ni-based catalysts

for CO_2 reforming of CH4. Catal Today 207:3–12. See also: Zhang J, Wang H, Dalai AK (2007) J Catal 249:298-; idem (2008) Appl Catal A Gen 339:321
84. Roh HS, Jun KW, Dong WS, Chang JS, Park SE, Joe YI (2002) Highly active and stable Ni/Ce-ZrO_2 catalyst for H_2 production from methane. J Mol Catal A Chem 181:137–142; see also: Li XS, Chang JS, Tian MY, Park SE (2001) CO_2 reforming of methane over modified Ni/ZrO_2 catalysts. Appl Organometal Chem 15:109–112; and Li X, Chang JS, Park SE (1999) Carbon as an intermediate during the carbon dioxide reforming of methane over zirconia-supported high nickel loading catalysts. Chem Lett 1099–1100
85. Montoya JA, Romero-Pascaul E, Gimon C, Del Angel P, Monzon A (2000) Methane reforming with CO_2 over Ni/ZrO_2-CeO_2 catalysts. Catal Today 63:71–85
86. Lercher JA, Bitter JH, Hally W, Niessen W, Seshan K (1996) Design of stable catalysts for methane-carbon dioxide reforming. Stud Surf Sci Catal 101:463–472; see also: Hally W, Bitter JH, Seshan K, Lercher JA, Ross JRH (1994) Problem of coke formation on Ni/ZrO_2 catalysts during the carbon dioxide reforming of methane. Stud Surf Sci Catal 88:167–173; and Ref. [28]
87. Nagaraja BM, Bulushev DA, Beloshapkin S, Ross JRH (2011) The effect of potassium on the activity and stability of Ni-MgO-ZrO_2 catalysts for the dry reforming of methane to give synthesis gas. Catal Today 178:132–136
88. Bradford MCJ, Vannice MA (1996) Catalytic reforming of methane with carbon dioxide over nickel catalysts. Part 1. Catalyst characterization and activity; and Part 2. Reaction. Appl Catal A Gen 142:73–96 and 97–122
89. Zhang ZL, Verykios XE, MacDonald SM, Affrossman S (1996) Comparative study of carbon dioxide reforming of methane to synthesis gas over Ni/La_2O_3 and conventional nickel-based catalysts. J Phys Chem 100:744–754; see also Zhang Z, Verykios XE (1977) Carbon dioxide reforming of methane to synthesis gas over Ni/La_2O_3 catalysts. Appl Catal A Gen 138:109–133; and Verykios XE (2003) Catalytic reforming of natural gas for the production of chemicals and hydrogen. Int J Hydrogen Energy 28:1045–1063
90. Swaan HM, Kroll VCH, Martin GA, Mirodatos C (1994) Deactivation of supported nickel catalysts during the reforming of methane by carbon dioxide. Catal Today 21:571–578; see also: Kroll VCH, Swaan HM, Mirodatos C (1996) Methane reforming reaction with carbon dioxide over Ni/SiO_2 catalyst. 1. Deactivation studies. J Catal 161:409–422
91. Valderrama G, Kiennemann A, Goldwasser MR (2010) La-Sr-Ni-Co-O based perovskite-type solid solutions as catalyst precursors in the CO_2 reforming of methane. J Power Sources 195:1765–1771
92. Ashcroft AT, Cheetham AK, Green MLH, Vernon PDF (1991) Partial oxidation of methane to synthesis gas using carbon dioxide. Nature 352:225–226; see also Vernon PDF, Green MLH, Cheetham AK, Ashcroft AT (1992) Partial oxidation of methane to synthesis gas, and carbon dioxide as an oxidizing agent for methane conversion. Catal Today 13:417–426
93. Stagg-Williams SM, Noronha FB, Fendley G, Resasco DE (2000) CO_2 reforming of CH_4 over Pt/ZrO_2 catalysts promoted with La and Ce oxides. J Catal 194:240–249
94. Damyanova S, Bueno JMC (2003) Effect of CeO_2 loading on the surface and catalytic behaviors of CeO_2-Al_2O_3-supported Pt catalysts. Appl Catal A Gen 253:135–150
95. O'Connor AM, Ross JRH (1998) The effect of O_2 addition on the carbon dioxide reforming of methane over Pt/ZrO_2 catalysts. Catal Today 46:203–210
96. Bitter JH, Seshan K, Lercher JA (1997) The state of zirconia supported Pt catalyst for CO_2/CH_4 reforming. J Catal 171:279–286
97. Nakamura J, Aikawa K, Sato K, Uchima T (1994) Role of support in reforming of CH_4 with CO_2 over Rh catalysts. Catal Lett 25:265–270
98. Richardson JT, Garrait M, Hung JK (2003) Carbon dioxide reforming with Rh and Pt-Re catalysts dispersed on ceramic foam supports. Appl Catal A Gen 255:69–82
99. Mark MF, Maier WF (1996) CO_2 reforming of methane on supported Rh and Ir catalysts. J Catal 164:122–130

100. Erdohelyi A, Cserenyi J, Solymosi F (1993) Activation of CH_4 and its reaction with CO_2 over supported Rh catalysts. J Catal 141:287–299
101. Qin D, Lapszewicz J (1994) Study of mixed steam and CO_2 reforming of CH_4 to syngas on MgO-supported metals. Catal Today 21:551–560
102. Maestri M, Vlachos DG, Beretta A, Groppi G, Tronconi E (2008) Steam and dry reforming of methane on Rh: microkinetic analysis and hierarchy of kinetic models. J Catal 259:211–222
103. Erdohelyi A, Cserenyi J, Papp E, Solymosi F (1994) Catalytic reaction of methane with carbon dioxide over supported palladium. Appl Catal A Gen 108:205–219
104. Donazzi A, Beretta A, Groppi G, Forzatti P (2008) Catalytic partial oxidation of methane over a 4 % Rh/alpha-alumina catalyst. Part II. Role of CO_2 reforming. J Catal 255:259–268
105. Claridge JB, York APE, Brungs AJ, Marquez-Alvarez C, Sloan J, Tsang SC, Green MLH (1998) New catalysts for the conversion of methane to synthesis gas: molybdenum and tungsten carbide. J Catal 180:85–100 (See also reference [25])
106. Treacy D, Ross JRH (2004) Carbon dioxide reforming of methane over supported molybdenum carbide catalysts. In: Bao X, Xu Y (eds) Natural gas conversion VII, vol 147, Studies in surface science and catalysis. Elsevier, Amsterdam, pp 193–198
107. Asencios YJO, Assaf EM (2013) Combination of dry reforming and partial oxidation of methane on NiO-MgO-ZrO_2 catalyst: effect of nickel content. Fuel Proc Technol 106:247–252
108. Zanganeh R, Rezaei M, Zamaniyan A (2013) Dry reforming of methane to synthesis gas on NiO-MgO nanocrystalline solid solution catalysts. Int J Hydrogen Energy 38:3012–3018
109. Zanganeh R, Rezaei M, Zamaniyan A, Bozorgzadeh HR (2013) Preparation of $Ni_{0.1}$ $Mg_{0.9}O$ nanocrystalline powder and its catalytic performance in methane reforming with carbon dioxide. J Ind Eng Chem 19:234–239
110. Chen W, Zhao G, Xue Q, Chen L, Lu Y (2013) High carbon-resistance Ni/$CeAlO_3$-Al_2O_3 catalyst for CH_4/CO_2 reforming. Appl Catal B Environ 136–137:260–268
111. Bhavani AG, Kim WY, Kim JY, Lee JS (2013) Improved activity and coke resistance by promoters of nanosized trimetallic catalysts for autothermal carbon dioxide reforming of methane. Appl Catal A Gen 450:63–72
112. Benrabaa R, Löfberg A, Rubbens A, Bordes-Richard E, Vannier RN, Barama A (2013) Structure, reactivity and catalytic properties of nanoparticles of nickel ferrite in the dry reforming of methane. Catal Today 203:188–195
113. Gardner TH, Spivey JJ, Kugler EL, Pakhare D (2013) CH_4–CO_2 reforming over Ni-substituted barium hexaaluminate catalysts. Appl Catal A Gen 455:129–136
114. Baeza BB, Pedrero CM, Soria MA, Ruiz AG, Rodemerck U, Ramos IR (2013) Transient studies of low-temperature dry reforming of methane over Ni-CaO/ZrO_2-La_2O_3. Appl Catal B Environ 129:450–459
115. Odedairo T, Chen J, Zhu Z (2013) Metal–support interface of a novel Ni–CeO_2 catalyst for dry reforming of methane. Catal Commun 31:25–31
116. Ozkara-Aydinoglu S, Aksoylu AE (2013) A comparative study on the kinetics of carbon dioxide reforming of methane over Pt–Ni/Al_2O_3 catalyst: effect of Pt/Ni Ratio. Chem Eng J 215–216:542–549
117. Tao K, Shi L, Ma Q, Wang D, Zeng C, Kong C, Wu M, Chen L, Zhou S, Hu Y, Tsubaki N (2013) Methane reforming with carbon dioxide over mesoporous nickel–alumina composite catalyst. Chem Eng J 221:25–31
118. Ma Q, Wang D, Wu M, Zhao T, Yoneyama Y, Tsubaki N (2013) Effect of catalytic site position: nickel nanocatalyst selectively loaded inside or outside carbon nanotubes for methane dry reforming. Fuel 108:430–438
119. Sun Y, Collins M, French D, McEvoy S, Hart G, Stein W (2013) Investigation into the mechanism of NiMg(Ca)bAlcOx catalytic activity for production of solarised syngas from carbon dioxide reforming of methane. Fuel 105:551–558

120. Zhu J, Peng X, Yao L, Deng X, Dong H, Tong D, Hu C (2013) Synthesis gas production from CO_2 reforming of methane over NieCe/SiO_2 catalyst: the effect of calcination ambience. Int J Hydrogen Energy 38:117–126
121. Albarazi A, Beaunier P, Costa PD (2013) Hydrogen and syngas production by methane dry reforming on SBA-15 supported nickel catalysts: on the effect of promotion by $Ce_{0.75}Zr_{0.25}O_2$ mixed oxide. J Hydrogen Energy 38:127–139
122. San Jose-Alonso D, Illan-Gomez MJ, Roman-Martɪnez MC (2013) Low metal content Co and Ni alumina supported catalysts for the CO_2 reforming of methane. J Hydrogen Energy 38:2230–2239
123. Nagaraja BM, Bulushev DA, Belshapkin S, Chansai S, Ross JRH (2013) Potassium-doped Ni–MgO–ZrO_2 catalysts for dry reforming of methane to synthesis gas. Topics Catal 56:1686–1694; see also Ref. [87]

Chapter 7
Carbon Dioxide as C-1 Block for the Synthesis of Polycarbonates

Peter T. Altenbuchner, Stefan Kissling, and Bernhard Rieger

Abbreviations

BDI	β-diiminate
BO	1-butene-oxide
CHC	cyclohexene carbonate
CHO	cyclohexene oxide
DFT	density functional theory
DMAP	Dimethylaminopyridine
DNP	2,4-dinitrophenolate
OAc	acetate
PC	propylene carbonate
PDI	Polydispersity index
PCHC	poly(cyclohexene carbonate)
PO	propylene oxide
PPC	poly(propylene carbonate)
PPNCl	*bis*(triphenylphosphine)iminium chloride
TBD	1,5,7-triabicyclo[4,4,0]dec-5-ene
T_g	glass transition temperature
T_m	melting point
TMS	Trimethylsilyl-
TOF	turn-over frequency
TON	turn-over number
VCHC	vinylcyclohexene oxide

P.T. Altenbuchner • S. Kissling • B. Rieger (✉)
Technische Universität München, WACKER-Lehrstuhl für Makromolekulare Chemie, Lichtenbergstrasse 4, Garching 85748, Germany
e-mail: rieger@tum.de

B.M. Bhanage and M. Arai (eds.), *Transformation and Utilization of Carbon Dioxide*, Green Chemistry and Sustainable Technology, DOI 10.1007/978-3-642-44988-8_7,

ZnAA zinc-adipate
ZnGA zinc-glutarate
ZnPA zinc-pimelate
ZnSA zinc-succinate

7.1 Introduction

Fossil energy sources became the dominant energy carriers at the beginning of the twentieth century. Since then, no alternatives to crude oil, gas, and coal have arisen to supplant them as a universal source of energy and raw materials for the chemical industry [1, 2]. The discovery of versatile possibilities for the use of crude oil as well as its low price and historical abundance made the steep rise in living standards in the last 100 years possible. As a result, the concentration of carbon dioxide in the atmosphere has risen significantly and reached 397 ppm in 2013 [3]. However, the finiteness of coal, gas, and especially oil reserves and the steadily increasing demand for them are likely to create a rising imbalance of supply and demand. Furthermore, the various negative implications of reliance on fossil energy carriers generate only limited incentives for industry and consumers to change their accustomed behavior. The reason for the disproportionate low price of CO_2 is that the resulting environmental damage is not or is only partially included in it. The rising generation of carbon dioxide however opens up a vast C-1 source for the synthesis of chemical raw materials. The attractive properties of CO_2 as a nontoxic, renewable, and low-cost C_1-building block are known, and it is currently used on an industrial scale in the production of urea (146×10^6 t/a), methanol (6×10^6 t/a), cyclic carbonate (0.040×10^6 t/a), and salicylic acid (0.060×10^6 t/a), among others [4]. However, the thermodynamic stability has thus far hampered its usage as widespread chemical reagent. Methods to overcome the high energy barriers are based upon reduction, oxidative coupling with unsaturated compounds on low valency metal complexes, and increasing electrophilicity of the carbonyl carbon [5].

The reaction of CO_2 with highly reactive substrates, such as epoxides, affords materials which can be produced on industrially relevant scale (Fig. 7.1). These polycarbonates from CO_2 have the potential to be the next industrial product with a high impact on the usage as commodity polymers. Consequently, the synthesis of highly active catalysts and understanding their mechanistic behavior is of upmost importance and the current developments will be discussed in this chapter.

7.2 Current Situation

Over 20 chemical reaction pathways for carbon dioxide have been developed over the course of the last two decades. Industrially viable reactions are scarce and only the production of urea, salicylic acid, and carbonates have reached

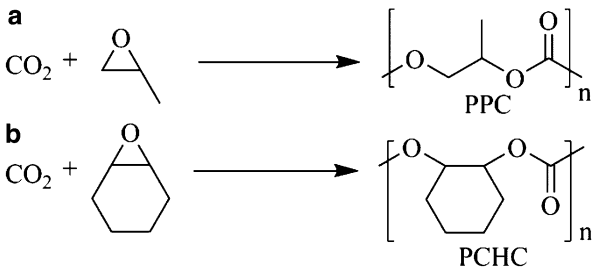

Fig. 7.1 Alternating copolymerization of propylene oxide (PO) (**a**) and cyclohexene oxide (CHO) (**b**) with CO_2

larger volumes [6, 7]. The amount of carbon dioxide consumed by these or any other chemical processes however cannot counteract anthropologically caused climate change. They rather have the potential to supplant oil-based starting materials in various synthetic pathways and thereby open up a more eco-friendly synthesis. The production of biodegradable polycarbonates from CO_2 and epoxides is currently receiving a lot of attention [5, 8, 9]. Aside from the polymeric product, cyclic carbonates also have potential applications such as in lithium ion batteries as electrolytes and as intermediates for the synthesis of linear dialkyl carbonates [4]. In this chapter cyclic carbonates will not be discussed in detail [9–11]. The focus will instead be on the catalysis behind the synthesis of polymeric materials with the recent developments at the center. Polycarbonates such as poly(propylene carbonate) (PPC) and poly(cyclohexene carbonate) (PCHC) have promising physical properties like lightness, durability, biodegradability, heat resistance, high transparency, and gas permeability which make them possible candidates for applications in the automotive, medical, and electronics industries.

7.2.1 Properties of Polycarbonates on the Example of Poly(propylene carbonate)

A large variety of epoxides are commercially available and subsequently have been tested for their behavior in copolymerization with carbon dioxide or even in terpolymerization with an additional epoxide. In industry though only ethylene oxide and propylene oxide are currently produced on large scale and have therefore a commercial advantage. Terpolymerizations promise a synthetic approach toward materials with better physical and material properties. Poly (propylene carbonate) and poly(cyclohexene carbonate) do not yet meet the demands of industry in respect of their glass transition temperatures, achieved molecular weights, elasticity, and their homogeneity. This justifies an academic approach toward better understanding of the polymerization behavior and properties of the produced materials.

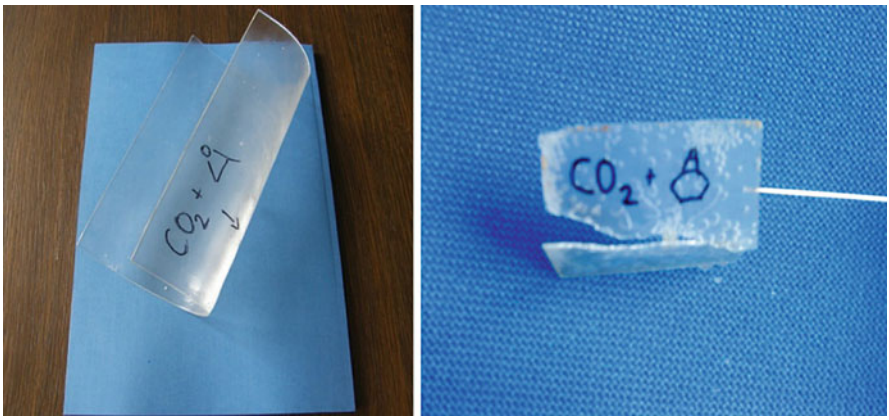

Fig. 7.2 Poly(propylene carbonate) (*left*), poly(cyclohexene carbonate) (*right*)

7.2.1.1 General Properties

Poly(propylene carbonate) is an aliphatic polycarbonate (Fig. 7.2). Due to irregular incorporation of carbon dioxide, polyether units can be presented in the polymer backbone. PPC is amorphous, hydrophobic, and soluble in organic solvents, e.g., dichloromethane, acetone, and cyclic propylene carbonate. The general properties strongly depend on the molecular weight, polydispersity, ratio of carbonate to ether linkages, microstructure, and possible catalyst contaminations in the polymer [12, 13]. Due to all the mentioned factors in literature, a temperature range from 25 to 46 °C for the glass transition temperature of PPC is given, and also other material characteristics like tensile strength and Young's modulus also show some variance [14, 15]. Cyclic carbonates act as plasticizers in the polymer and have the same effect as ether units in the polymer backbone: they decrease the glass transition temperature. Additionally, high amounts of ether linkages affect the material's thermal stability.

As the available analytical data is not always sufficient to correctly compare the investigated polymer samples, some properties only can be given as approximate ranges. For polymer samples with a T_g of about 40 °C, the range for the modulus was from 700 to 1,400 MPa, whereas for PPC with a T_g of 30 °C the modulus was reported to be 200 and 1,000 MPa [14, 15]. However, for strictly alternating PPC with less than 1 % cyclic carbonate content, an elongation at break of less than 50 % and a tensile strength of around 40 MPa (M_n = 180,000 g/mol) is reported in the literature [8]. One of the major disadvantages of PPC is its tendency to degrade at elevated temperatures. Earlier reports tested PPC with different molecular weights at temperatures between 150 and 180 °C. They observed severe degradation which of course has negative consequences for the material properties. Current publications suggest that the degradation is not solely induced by temperature, but that residual catalyst can enhance the degradation as well [16–20]. Already at 150 °C, a

PPC sample with a molecular mass over 200 kg/mol and a PDI of 1.2 show severe degradation to cyclic carbonate after 1 h if the catalyst residue is not completely removed from the polymer [12]. An increase in thermostability to 180 °C was made possible by a thorough catalyst removal from the sample. Further increases in temperature resulted in profound degradation even for the treated polymer sample. Blending of PPC with other engineering plastics is possible but difficult due to the fact that the optimum melt processing temperature for PPC is around 100–140 °C [21]. In general, polyesters and polyamides exhibit higher melting temperatures of above 200 °C [16]. The catalysts known in the literature so far show low productivity and produce at most 38 kg polymer per gram cobalt catalyst [22]. The catalysts cannot be left in the polymer due to their coloring- and degradation-enhancing properties. Furthermore, regulations concerning the amount of toxic metals like cobalt make a thorough clean up of the polycarbonates necessary.

7.2.1.2 Degradation Mechanism and Thermal Stability

In the previous subchapter, the thermal degradation of PPC was briefly addressed. Now the underlying mechanisms and possibilities for the formation of more stable PPC shall be discussed in more detail.

One form of thermal degradation is chain unzipping, whereby the nucleophile for the degradation can be located in the polymer chain or through an external nucleophile from another chain (Fig. 7.3a). Terminal hydroxyl groups can perform intramolecular backbiting reactions and thereby cause the formation of cyclic carbonates. The backbiting reaction can occur via a terminal alkoxide chain end which attacks at a carbonyl carbon. The backbiting route can also be via a terminal carbonate which attacks at an electrophilic carbon in the polymer chain. Intermolecular back biting leads to an attack at a random position in the polymer and forms shorter chains. The second degradation mechanism, which is assumed to take place increasingly at higher temperatures, is random chain scission (Fig. 7.3b) [23, 24]. At elevated temperatures, a decarboxylation reaction takes place and gives rise to carbon dioxide and an olefin moiety. As can be seen in Fig. 7.3c, catalyst impurities, water residues, acids, bases, and solvents promote degradation reactions and should therefore be thoroughly excluded or removed upon completion of the reaction [16].

The thermal stabilities reported in the literature are difficult to compare and to relate to one another due to a lack of information concerning both the polycarbonates and the testing conditions. Generally, the chain unzipping of poly (propylene carbonate) and other carbonates can be suppressed to a certain degree by end-capping, although the potential for depolymerization via chain scission is not affected by this alteration. In the end-capping process, the nucleophilic terminal hydroxyl groups of the poly(alkylene carbonates) are replaced with less reactive functionalities (e.g., isocyanates, carboxylic acid anhydrates, acetates, urethanes, sulfonates, phosphorous containing compounds) [23–27]. Analytical data concerning the remaining hydroxyl groups have not been published so far.

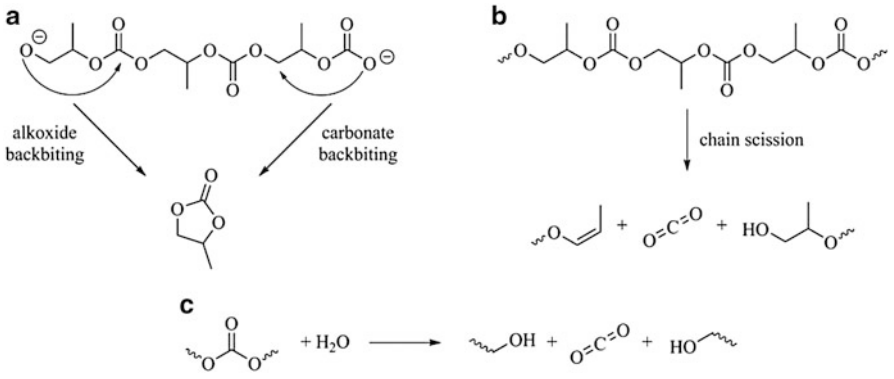

Fig. 7.3 Backbiting mechanisms for poly(propylene carbonate): (**a**) chain unzipping, (**b**) chain scission, and (**c**) residual water traces promoting the degradation

Hydrogen bonding has also been shown to improve the thermal stability of polycarbonates significantly. In a recent publication, octadecanoic acid was added to PPC by solution mixing. The resulting supramolecular complexes showed improved thermal stability, a thermotropic liquid crystalline character, and enhanced glass transition compared to an amorphous PPC copolymer [28]. Improvements in thermal stability were also obtained by adding wood flour [29] or nanoparticles [30–33] to polycarbonates by blending with other polymers [34–37].

The actual measured thermal stabilities are difficult to compare due to different testing conditions and the lack of information concerning the poly(propylene carbonates) themselves. It was reported that interactions between poly(propylene carbonate) and metal ions can in fact enhance the thermal stability [38–40]. Nevertheless, none of the modifications to poly(propylene carbonate) mentioned in the literature are able to inhibit degradation during processing at temperatures over 180 °C.

7.2.1.3 Terpolymerization

Terpolymerizations and block copolymerizations have the potential to overcome the poor properties of poly(propylene carbonate) and poly(cyclohexene oxide), respectively, and instead combine their strengths in one polymeric material. Other epoxides such as styrene oxide and epichlorohydrin offer additional opportunities as copolymers and also as substitutes for PO or CHO. Consequently, both the copolymerization and the terpolymerization of carbon dioxide and various epoxides have been investigated (Fig. 7.4) [41–54]. The incorporation of other monomers (lactones and anhydrides) in polycarbonate structures has also been studied [55–62].

Fundamental research on the reasons for the differing reactivities and on the inactivity of some catalysts toward some monomers is scarce. Rieger et al. published detailed kinetic studies supported by quantum chemical calculations in 2011 [63]. The homogeneous dinuclear zinc catalyst **26** of Williams et al. was chosen as a test system

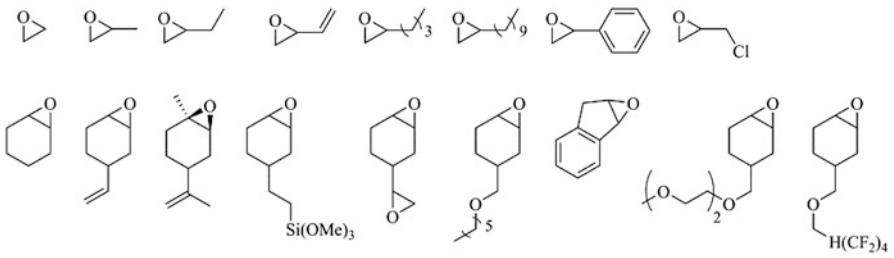

Fig. 7.4 Some epoxides used in the literature [41–54]

as it exhibits the highest activities for CHO/CO_2 copolymerization at one bar carbon dioxide pressure (TOF = 25 h^{-1}) [64]. The copolymerization of propylene oxide and carbon dioxide however is not possible with catalyst **26**: instead, only cyclic carbonate is formed. Many zinc-based catalyst systems share this inactivity for PO/CO_2 copolymerization or possess only low activities compared to other metals. Therefore, Rieger et al. systematically varied the reaction conditions to identify the underlying principles. They found that neither propylene oxide nor additionally added cyclic propylene carbonate does deactivate the catalyst for the formation of PCHC, although in the presence of cyclic propylene carbonate, the activity was decreased dramatically. Terpolymerizations with different ratios of CHO to PO resulted only in PCHC and no incorporation of PO was found, which can be attributed to a very fast backbiting reaction in the case of PO. DFT calculations showed that the ring strains of CHO and PO are comparable and that kinetic barriers to polymer formation in theory favor generation of PPC over PCHC. Consequently, the authors concluded that in the case of the studied zinc catalyst, the depolymerization rate of PPC is several magnitudes faster than that of PCHC. The limitations of zinc complexes gave cobalt catalysts an advantage in the field of CHO/PO and CO_2 terpolymerizations. In 2006 the first (salen)CoX catalysts with increased activities were discovered [46]. Catalyst **1**, in combination with [PPN]Cl, is able to terpolymerize at 25 °C and 15 bar CO_2 pressure equimolar quantities of PO and CHO with activities up to 129 h^{-1}. The resulting polymer had a narrow PDI of 1.24 and a high content of carbonate linkages and showed a single T_g. The authors varied the reaction conditions and were able to tune the CHO content from 30 to 60 % which gave polymers with T_g in the range of 50–100 °C. The highly alternating nature of the polymer was attributed to the inhibiting nature of CHO on PO which leaves both epoxides with matched reactivities in the copolymerization. The regioselective ring opening of PO was not disturbed by the competing binding of the epoxides to the metal center. Another cobalt-based catalyst (**7**) with covalently bound ionic groups was published in 2010 by Lee et al. They performed a multitude of experiments with various epoxides in different combinations [65]. Terpolymerizations of CO_2/PO/CHO, CO_2/PO/1-hexene oxide (HO), and CO_2/PO/1-butene oxide (BO) were carried out. Activities ranged between 4,400 and 14,000 h^{-1} and no cyclic carbonate formation was observed during the reactions. Furthermore, an increase in decomposition temperature was achieved by employing a third monomer and the results demonstrated that the T_g of PO/CO_2 can be

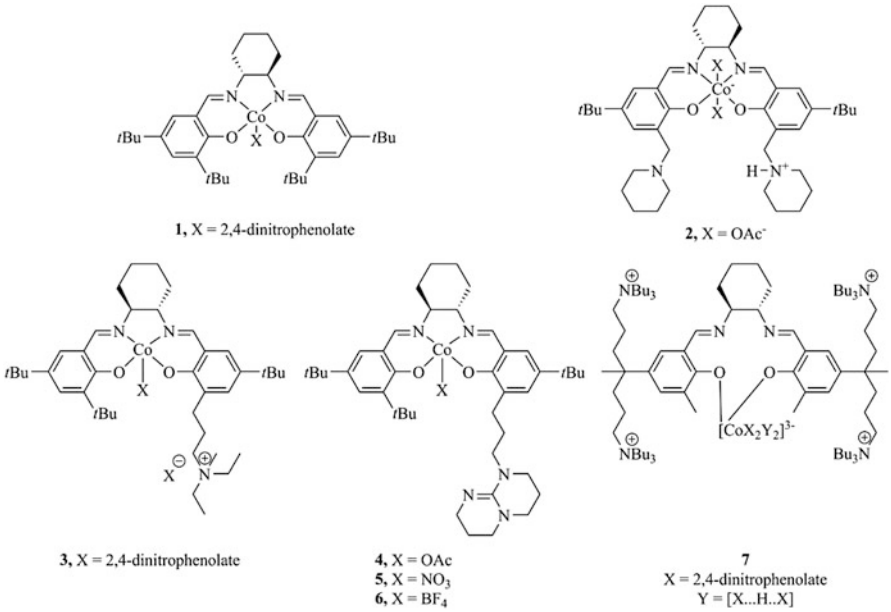

Fig. 7.5 Cobalt catalysts for the co- and terpolymerization of carbon dioxide and epoxides [22, 46, 65–67]

adjusted at will in a certain range (0–100 °C) by using a third monomer (CHO, HO, or BO). A linear dependency between the glass transition temperature in the terpolymer and the proportions of the third monomer was observed, which makes T_g adjustments possible. For the terpolymer CO_2/PO/HO, the temperature range was found to be from −15 to 32 °C and for CO_2/PO/BO from 9 to 33 °C. The authors also report that the incorporation of further epoxides (styrene oxide (SO), isobutylene oxide (IO), and glycidyl ether (GE)) in the PO/CO_2 copolymer failed under the tested reaction conditions due to remaining impurities in the monomers. Almost at the same time Lu et al. reported a bifunctional cobalt(III) catalyst (**3**) for the copolymerization of CHO/CO_2 and for terpolymerization with additional aliphatic epoxides such as PO, EO, BO, and HO (Fig. 7.5) [66].

The catalyst showed high activities (TOF) of 1,958–3,560 h^{-1} (90 °C, 25 bar, 1:1 = CHO: [PO,BO,HO,EO]) and molecular weights of the resulting terpolymers ranged between 40,000 and 60,000 g/mol (PDI ~ 1.1). The produced polymers had a content of 37–65 % of cyclohexene carbonate linkages and only one T_g was measured (32–79 °C).

Functionalized epoxides open up the possibility for post modification of the resulting carbonate structures. Already in 2007 Coates et al. used β-diiminate zinc(II) acetate catalysts ([(BDI)ZnOAc]$_2$) for the terpolymerization of CHO, vinylcyclohexene oxide (VCHO), and carbon dioxide to synthesize vinyl-functionalized polycarbonates [43]. The subsequent olefin metathesis using a Grubbs' catalyst [68] made the transformation of linear polycarbonates into nanoparticles of controlled size possible. The

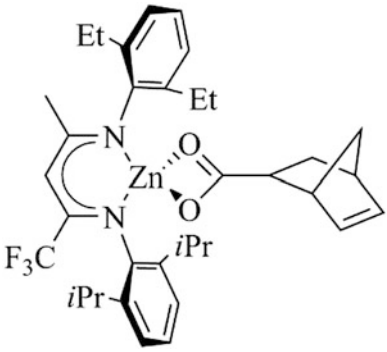

Fig. 7.6 BDI zinc catalyst with a norbornene carboxylate initiator [69]

employed epoxides had comparable reactivities, which enabled the generation of terpolymers with a VCHO content of 30 mol%. Medium molecular weights of 54,100 g/mol and low PDI ($M_w/M_n = 1.20$) were reached. It was observed that the cross-metathesis reaction progressed quickly in the beginning, but due to the formation of increasingly rigid polymer chains slowed down after 15 min. A remarkable increase in the T_g was observed from 114 to 194 °C at 76 % cross-linking. This increase was attributed to reduced chain mobility. A similar approach was used by Coates et al. in 2012 for the synthesis of multisegmented graft polycarbonates [69]. Norbornenyl-terminated multiblock poly(cyclohexene carbonate)s were again synthesized using a BDI zinc catalyst **8** with a norbornene carboxylate initiator (Fig. 7.6). The living nature of the copolymerization allowed the step-by-step addition of functionalized CHO. This generated variable block sequences which could subsequently be transformed to segmented graft copolymers by ring-opening metathesis polymerization.

Propylene oxide derivatives in terpolymers can also be found in the literature. Frey et al. terpolymerized 1,2-isopropylidene glyceryl glycidyl ether (IGG), glycidyl methyl ether (GME), and carbon dioxide [70]. After the acidic removal of the protecting acetal groups, a polycarbonate poly((glyceryl glycerol)-co-(glycidyl methyl ether) carbonate) (P((GG-co-GME)C)) is received. The analysis of the polymeric material showed monomodal molecular weight distributions and PDIs between 2.5 and 3.3, although the molecular mass was comparably low (12,000–25,000 g/mol). The T_g of the unprotected polymer was 3–5 °C higher than those of the corresponding protected copolymers. Interestingly, during investigations of the degradation behavior of the P((GG-co-GME)C) copolymers in THF solution, no backbone degradation was observed over 21 days. The authors ascribe this observation to the reduced stability of the resulting cyclic carbonate structures.

As can be seen in this chapter, the possibilities for further research are far from exhausted. Apart from the synthesis of ever more refined structures, the analytics must evolve simultaneously to access the microstructure. Therefore, current developments in the field of polymer NMR techniques will be discussed in detail in the next chapter.

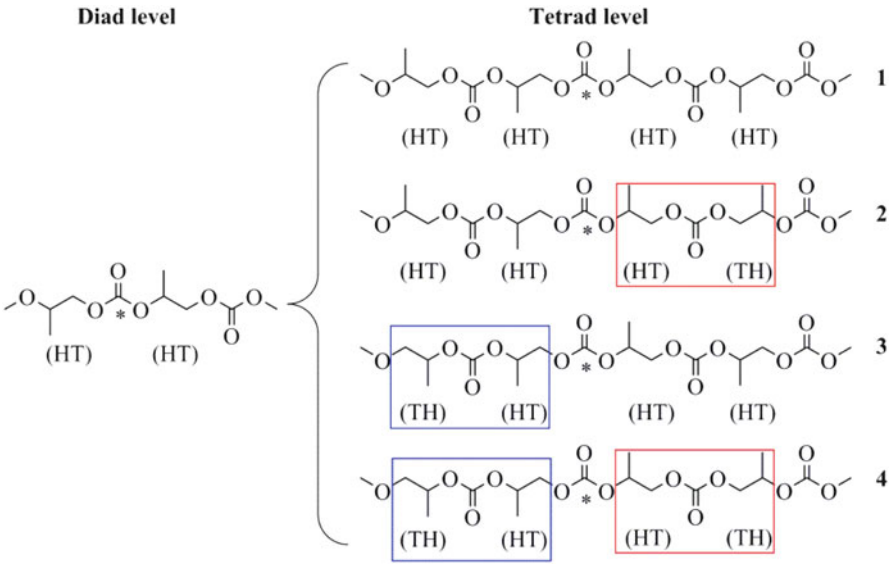

Fig. 7.7 *The four proposed* regiosequences with central HT junctions

7.2.1.4 Microstructure of Poly(propylene carbonate)

Since its first discovery, poly(propylene carbonate) has been characterized via a multiple analytical methods by various research groups [71–76]. NMR has been used extensively for microstructure analysis because PPC with higher stereoregularity has the potential to increase the glass transition temperature (T_g). In general, the ring opening of PO occurs via an S_N2 type mechanism at the methylene position resulting in a predominantly head-to-tail (HT) regiostructure of the CO_2/PO copolymer. By contrast, tail-to-tail (TT) or head-to-head (HH) connections arise if the ring opening of the epoxide takes place at the methine carbon. In 2002, Chisholm and colleagues assigned ^{13}C NMR spectra for different PPC copolymers using a statistical approach [17]. First, they studied the ^{13}C NMR spectrum of (*S*)-PPC obtained from the copolymerization of (*S*)-PO and CO_2 using a zinc glutarate catalyst. The carbonate carbon region showed more than one resonance, providing information about the possible regiosequences that occur at the tetrad level. Consequently, Chisholm et al. proposed four regiosequences with central head-to-tail (HT) junctions that are distinguishable by NMR for the carbonate carbons (Fig. 7.7).

The other carbonate carbon signals arising from TT and HH junctions at the diad level were assigned as *s*. Chisholm and colleagues applied the same statistical approach at the triad level for aliphatic carbon in PPC and later on they analyzed the structure of oligoether carbonates [17, 77]. Those compounds were potential models for the PPC microstructural assignments in NMR studies. It was possible to show with ^{13}C NMR investigations that the carbonate carbon signals have both

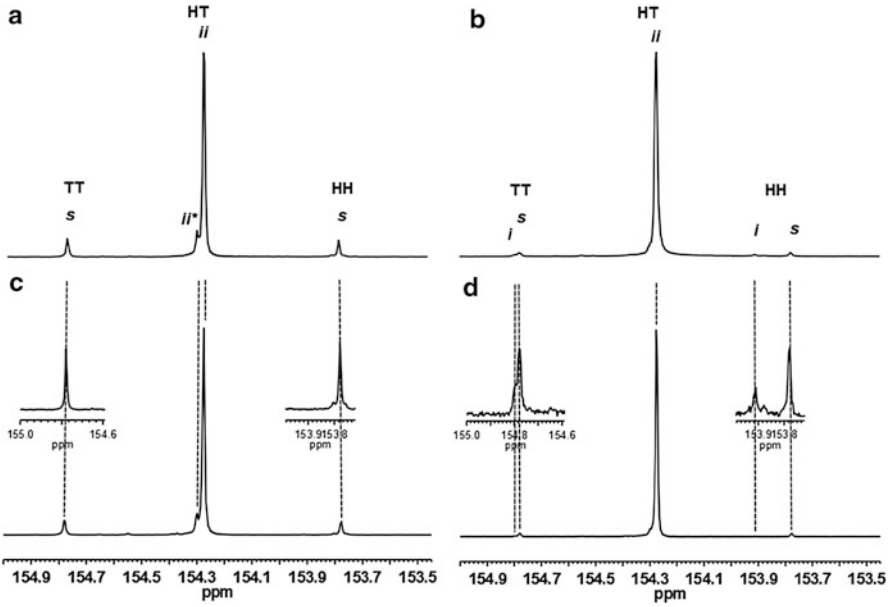

Fig. 7.8 ^{13}C (125 MHz, $CDCl_3$) NMR spectra (carbonate carbon region): (**a**) (*R*)-PPC copolymer, (**b**) (*R*)-PPC copolymer synthesized, (**c**) (*S*)-PPC copolymer, and (**d**) (*S*)-PPC copolymer, 1 equivalent [PPN]Cl, 1,000 eq. PO at 30 °C and 30 bar CO_2 for 20 h [(**a**) and (**d**) ((*R*,*R*)-(salen)CoCl) (**b**) and (**c**) (*S*,*S*)-(salen)CoCl] (Reprinted with permission from Ref. [78]. Copyright 2012, American Chemical Society)

regio- and stereosensitivity at the diad and tetrad levels to their adjacent ether units [77]. Density functional theory calculations were applied to the tested oligoether carbonates. These calculations indicated that the carbonate groups exist predominantly in *cis-cis* geometries with more than one stable conformation for each molecule. In addition, the ^{13}C chemical shifts predicted in the calculations were sensitive to the conformations of the molecules and the configurations of the stereocenters in PO ring-opened units. Recently, different poly(propylene carbonate) (PPC) microstructures have been synthesized by Rieger et al. from the alternating copolymerization of CO_2 with propylene oxide (PO) using chiral cobalt and (salen)Cr catalysts [78, 79].

The model which was presented in the study of Rieger et al. was based on triad structure obtained from ^{13}C NMR spectroscopy (HT carbonyl region). The ^{13}C NMR spectra of selected poly(propylene carbonate) samples were recorded using a 900 MHz (^1H) spectrometer, showing a previously unreported fine splitting of the carbonate resonances. Utilization of enantiopure and enantio-enriched PO allowed to apply the approach of isolated stereoerrors in the predominantly isotactic polymer to assign in detail the observed signals due to the stereo- and regioirregularities (Fig. 7.8). This assignment was performed under consideration of the direction of the polymer chain. Additional GC-analysis of the hydrolyzed polymers has shown a

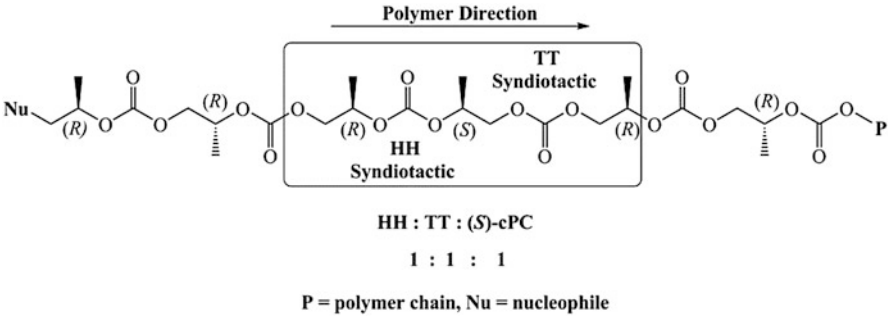

Fig. 7.9 Syndiotactic HH and TT in (*R*)-PPC synthesized using 1, resulting from "abnormal" epoxide ring opening at the methine position [78]

correlation between the extent of regioerror and the ring opening of PO with inversion of configuration at chiral atom, leading to *s*-HH diads. Signals of *i*-diads in the HH region were also observed in certain cases, which is referred to an "abnormal" PO-enchainment with retention of configuration of the stereocenters. The assignment of carbonate carbon signals at δ_C 153.8 and 154.8 ppm to HH and TT syndiotactic diads, respectively (Fig. 7.9), is consistent with the previous work of Chisholm and coworkers [80].

However, in the HT-region, a new low-intensity peak in the vicinity of the *ii*-signal at the lower field was observed, which could be assigned to an effect of an HH regioerror close to the isotactic triad. Accordingly, all observed low-intensity signals in the polymers with a lower isotacticity (δ_C 154.29, 154.30, 154.35, and 154.39 ppm) correlate well with the resonances in the HH region due to the regioerror (Fig. 7.10). Such correlation was also observed in case of the polymer with a predominantly syndiotactic structure, revealing a low-intensity peak at low field close to an *ss*-HT-signal.

Aside from the HT region, the splitting pattern of the signals in the HH region of the spectrum is informative with respect to the copolymer microstructure. The splitting of the signals in the TT region is not pronounced, therefore indicating a weak influence of the neighboring stereoconfiguration on the chemical shift of this junction. It is therefore expected that the HH junction has a stronger effect on chemical shifts in neighboring stereosequences than the TT sequence does.

In case of copolymers with a high extent of regioerrors, the described correlations are not so straightforward but still can be observed (Fig. 7.11). A greater number of peaks in the HT and HH regions are expected for such copolymers, where the model of isolated regioerrors is no longer valid.

Following the (S)-PO/(R)-PO ratios in the polymer chain during the rac-PO/CO_2 copolymerization reaction using GC and 500 MHz NMR spectroscopy provided insight into the understanding of the arising PPC microstructure. The suggested average microstructure of the copolymers shows a gradient change from *iso*-enriched to stereogradient microstructure with the polymerization time due to the catalyst enantioselectivity. Investigations by Nozaki et al. also led to the synthesis

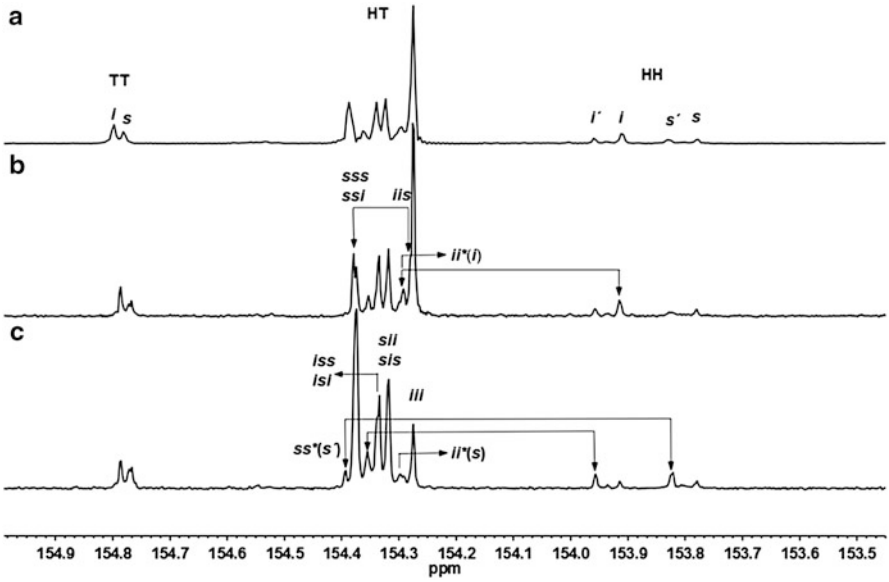

Fig. 7.10 ^{13}C NMR spectra of the carbonate carbon region of (**a**) *iso*-enriched PPC (125 MHz, $CDCl_3$), (**b**) *iso*-enriched PPC (225 MHz, $CDCl_3$), and (**c**) *syndio*-enriched PPC (225 MHz, $CDCl_3$) and the proposed assignment of signals on the tetrad level (Reprinted with permission from Ref. [78]. Copyright 2012, American Chemical Society)

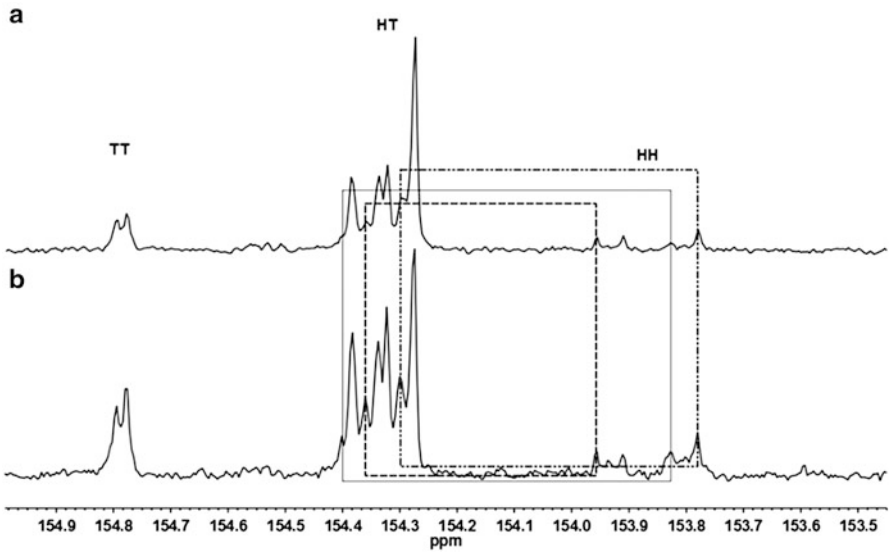

Fig. 7.11 ^{13}C (75 MHz, $CDCl_3$) NMR spectra for PPC copolymer synthesized using catalyst (salen)CrCl with 0.5 equivalent DMAP, (**a**) using 75 % (*S*)-PO and 25 % (*R*)-PO (**b**) using 25 % (*S*)-PO and 75 % (*R*)-PO at 50 °C and 50 bar CO_2 for 20 h (Reprinted with permission from Ref. [78]. Copyright 2012, American Chemical Society)

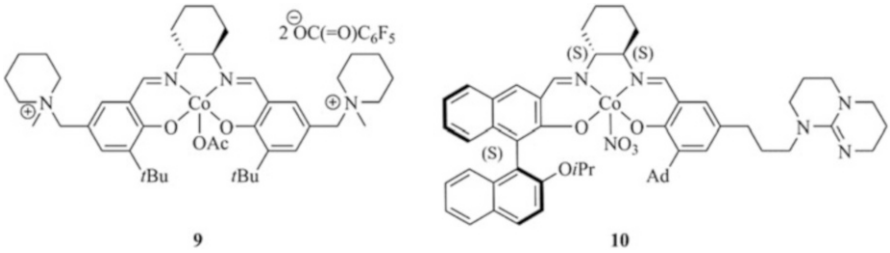

Fig. 7.12 (*left*) (salen)CoOAc **9** is capable of producing stereogradient PPC, (*right*) (salen)$CoNO_3$ **10** catalyst with pending TBD arm is capable of producing >99 % HT PPC [76, 81]

of stereogradient PPC which consisted of two enantiomeric structures on each end of the polymer chain [76]. The used catalyst was an optically active (salen)CoOAc with pendant ammonium arms. Thermal properties of the polymer were analyzed by differential scanning calorimetry (DSC) and thermogravimetry (TG).

Different regio- and stereoregularities did not show an influence on the glass transition temperatures ($T_g \sim 33$ °C) of the obtained polymers as was also confirmed by Rieger et al. [78]. But the stereogradient PPC and the stereoblock PPC exhibited higher thermal decomposition temperatures of up to 273 °C compared to PPCs with lower regio- and stereoregularities and iso-enriched PPC ($T_d = 240$ °C). The authors attributed their findings to a possible stereocomplex formation of a (S)-PPC block and (R)-PPC block in the same chain upon precipitation in methanol. Equimolar mixture of (S)-PPC and (R)-PPC did not show increased T_d values which might indicate a spatial dependence of the (S)-PPC and (R)-PPC for the stereoblock formation. Lu et al. achieved the synthesis of >99 % head-to-tail, >99 % carbonate linkage, and isotactic PPC with a multichiral (S,S,S)-(salen)$CoNO_3$ catalysts with a TBD group (1,5,7-triabicylco[4.4.0] dec-5-ene) anchored on the 5-position of one phenyl ring (Fig. 7.12) [81]. The isotactic PPC produced from (R)-PO exhibited elevated T_g values of up to 47 °C.

7.2.1.5 Microstructure of Poly(cyclohexene carbonate)

The copolymerization of *meso*-cyclohexene oxide and carbon dioxide produces poly(cyclohexene oxide) with different stereochemistry depending on the employed catalyst system. The ring opening of a meso-epoxide proceeds with inversion of the configuration at one of the two chiral centers (Fig. 7.13).

Nozaki et al. were the first to report asymmetric alternating copolymerization of *meso*-CHO with carbon dioxide. They used an equimolar mixture of Et_2Zn and (*S*)-diphenyl(pyrrolidin-2-yl)methanol as chiral catalyst [82]. Through alki-treatment, the PCHC was hydrolyzed into *trans*-1,2-diol and the degree of asymmetric induction was measured to be 70 % ee. These isotactic PCHCs were characterized via ^{13}C NMR spectroscopy using statistical methods and model compounds [83]. An

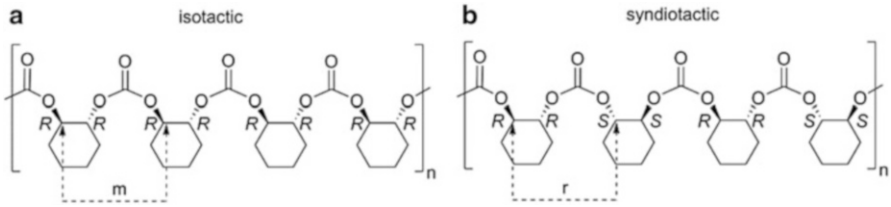

Fig. 7.13 Poly(cyclohexene oxide): isotactic (**a**) and syndiotactic (**b**)

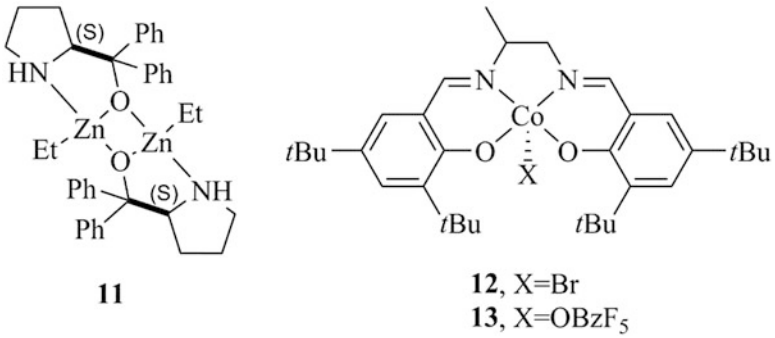

Fig. 7.14 Dinuclear zinc catalyst (**11**) (*left*), (salen)CoX catalyst (*right*) for the copolymerization of CHO and carbon dioxide [84, 85]

improved dimeric zinc system (**11**) was able to generate isotactic-enriched PCHC with 80 % ee [84]. End group analysis showed that the insertion of CO_2 happens at the zinc-ethoxy bond of the catalyst. Nevertheless, the obtained stereoregular copolymer (80 % ee) showed a T_g of 117 °C which is very close to that of non-stereoregular PCHC (115 °C) (Fig. 7.14).

The first syndiotactic-enriched PCHC was reported by Coates et al. who employed (salen)CoX catalysts for the copolymerization of CHO/CO_2 [85]. Catalyst (salen)CoBr (**12**) and (salen)CoOBzF_5 (**13**) were able to produce PCHC with up to 81 % r-centered tetrads. Through Bernoullian statistical methods, the PCHC triad and tetrad sequences were assigned in the ^{13}C NMR spectra in the carbonyl and methylene regions. The addition of cocatalyst ([PPN]Cl) resulted in the complete loss in syndiotacticity in the produced PCHC. The synthesis of enantiopure (salen)Co(III) catalysts (Fig. 7.15) by Lu et al. in 2012 made the synthesis of highly isotactic PCHC possible [86].

Chiral induction agents, such as (*S*)-2-methyltetrahydrofuran and (*S*)-propylene oxide, further improved the enantioselectivity regarding (*S*,*S*)-(salen)Co(III). PCHC with up to 98:2 *RR*:*SS* could be obtained with catalyst **1d**/[PPN]Cl in the presence of (*S*)-2-methyltetrahydrofuran. The highly isotactic PCHC was analyzed by DSC measurements and wide angle X-ray diffraction (WAXD). They found that PCHC samples with less than 90 % isotacticity did not show any crystallization.

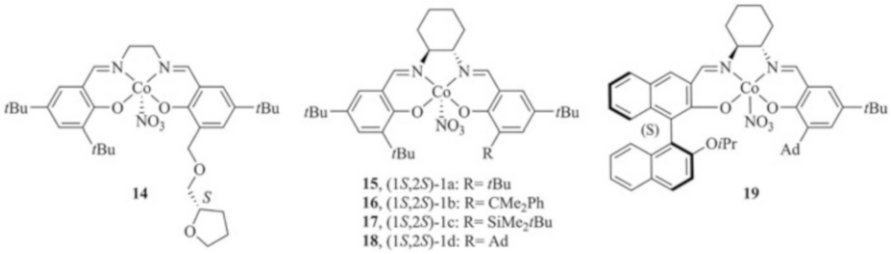

Fig. 7.15 Disymmetrical enantiopure (salen)Co(III) complexes[86]

(*R*)-PCHC with an *RR*:*SS* ratio of 92:8 ((*R*)-PCHC-92) gave a T_g of 122 °C and a small endothermic melting peak at 207 °C which stems from the low degree of crystallinity of the polymer. Contrary to amorphous PCHC, the (*R*)-PCHC-92 sample showed sharp diffraction peaks.

Aside from defined stereo- and regioregular synthesis of optical active PPC and PCHC, the catalytic side of the polymer formation has received much attention in recent years. The current development is refocusing on new possible ligand structures with less toxic metal centers which nevertheless can achieve high activities in the copolymerization. Those developments will be presented in the next section.

7.3 CO_2 Utilization in Polycarbonates

7.3.1 Development

Before diving into the broad field of polycarbonates and their synthesis and applications, a small review of historic developments is necessary to place the subsequent work in context. The earliest mention of the synthesis of poly(ethylene carbonate) was made in a patent in 1966 by Stevens [87]. However, it was not until 1969 that Inoue et al. presented their findings concerning the activity of a $ZnEt_2$/water mixture which was able to catalyze the formation of poly(propylene carbonate) from carbon dioxide and propylene oxide [73]. At pressures ranging from 20 to 50 bar and at 80 °C, the heterogeneous catalyst produced low molecular weight carbonates with turnover frequencies up to 0.12 h^{-1} and sparked a surge in developments over the next decades. In heterogeneous catalysis, Soga et al. synthesized the first well-defined catalyst system from a $Zn(OH)_2$/glutaric acid mixture, which is still the most active zinc-based system for copolymerization of CO_2 and propylene oxide [88]. By using different zinc carboxylates, Rieger et al. demonstrated the importance of the distance of the active zinc centers for catalytic activity. Problems arose in the evaluation of the active zinc centers, as well as the importance of crystallinity, surface, and particle size for this catalysis [10]. Furthermore, deeper understanding of the reaction mechanism was hampered by the drawbacks of heterogeneous catalysts in general. It is very

challenging to define the active sites in such systems and subsequently to ascribe structural alterations to activity increases or decreases. Furthermore, the multitude of active sites in the catalysts leads to broad polydispersity indices (PDI) which makes the characterization of physical properties of the polymer difficult. Consequently, it was not until 1978 that Inoue et al. published the first homogeneous catalyst system for the copolymerization reaction of CO_2 and epoxides [89]. The aluminum tetraphenylporphyrin complexes in combination with $EtPh_3PBr$ as cocatalyst were able to copolymerize not only cyclohexene oxide (CHO) but also propylene oxide (PO) with low PDIs. In 1995, *bis*(phenoxide)$Zn(THF)_2$ catalysts were synthesized and employed in the copolymerization of PO and also CHO and CO_2 [47, 90]. This catalyst system exhibited rather low activities and selectivities toward polycarbonate formation. The next important step toward well-defined and tunable catalysts was made by Coates et al. with the development of zinc β-diiminate complexes ((β-diiminate)ZnOR) [91]. This type of ligand allowed adjustment of the steric and electronic environment around the metal center and even small variations in the ligand framework already had drastic influences on activity and selectivity. Recently, Rieger et al. published a new dinuclear zinc catalyst system for the copolymerization of cyclohexene oxide and carbon dioxide. The catalyst **35** limits – in a certain broad pressure regime – the polymerization rate as a function of the applied CO_2 pressure. It is the first time that the rate determining step is shifted toward CO_2 insertion. This unique behavior is attributed to a flexible CH_2-tether that links both complex moieties. As a result, the highest known polymerization activities for CHO-based polycarbonates are reported.

Nowadays, development of these well-defined homogeneous catalysts and research on polycarbonates from carbon dioxide and epoxides are flourishing. Various review articles have been published in recent years in this field of research which demonstrates the growing interest in this material and the underlying mechanism [5, 9, 88, 92–97].

7.3.2 Mechanistic Aspects of the Epoxide and Carbon Dioxide Copolymerization

Homogeneous catalysts with the general structure L_nMX possess the great advantage of having only one defined active site. Tailoring the organic ligand L_n as well as the initiating group and the metal center provides a broad range of possibilities. Nevertheless, mechanistic investigations so far have not provided an unambiguous picture of the copolymerization of carbon dioxide and epoxides. Hence, three different possible reaction pathways shall be presented for a model salen complex.

The reaction pathway A requires interactions between two catalyst molecules and their active sites (Fig. 7.16). Thus, this mechanism is probable in the absence of a cocatalyst at low epoxide to catalyst loadings. It is rate dependent on the Lewis acidity of the corresponding metal center and on the nucleophilicity of the axial ligand X.

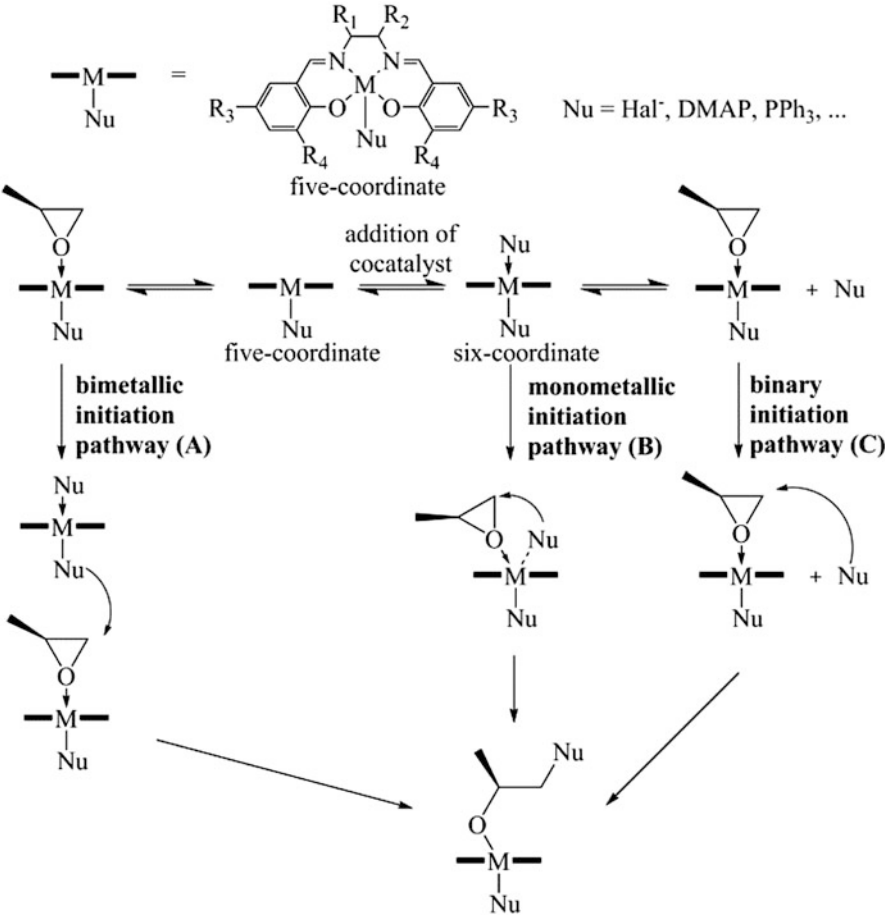

Fig. 7.16 Initiation mechanism for L_nMX for the copolymerization of carbon dioxide and PO: bimetallic pathway (**a**), monometallic pathway (**b**), and binary pathway (**c**) (Reprinted with permission from Ref. [88]. Copyright 2011, Elsevier)

Accordingly, the type of catalytic system used defines the mechanism. In the work of Jacobsen on the asymmetric nucleophilic ring opening of epoxides by chiral (salen)CrX complexes, this intermolecular, bimetallic pathway is a vital step in the absence of a cocatalyst [98]. The group of Rieger et al. also performed theoretical calculations concerning the chain-growth mechanism during the copolymerization of CO_2 and epoxides. The DFT calculations indicated that chain growth proceeds through the attack of a metal-bound alkyl carbonate on a precoordinated epoxide on a metal center [99]. However, other investigations indicated a bimetallic initiation step and subsequent monometallic chain propagation [71, 100–102]. Reaction pathway B is the monometallic mechanism and is comparable to an associative ligand exchange mechanism. In this scenario, the nucleophile and the epoxide are both bound to one metal center.

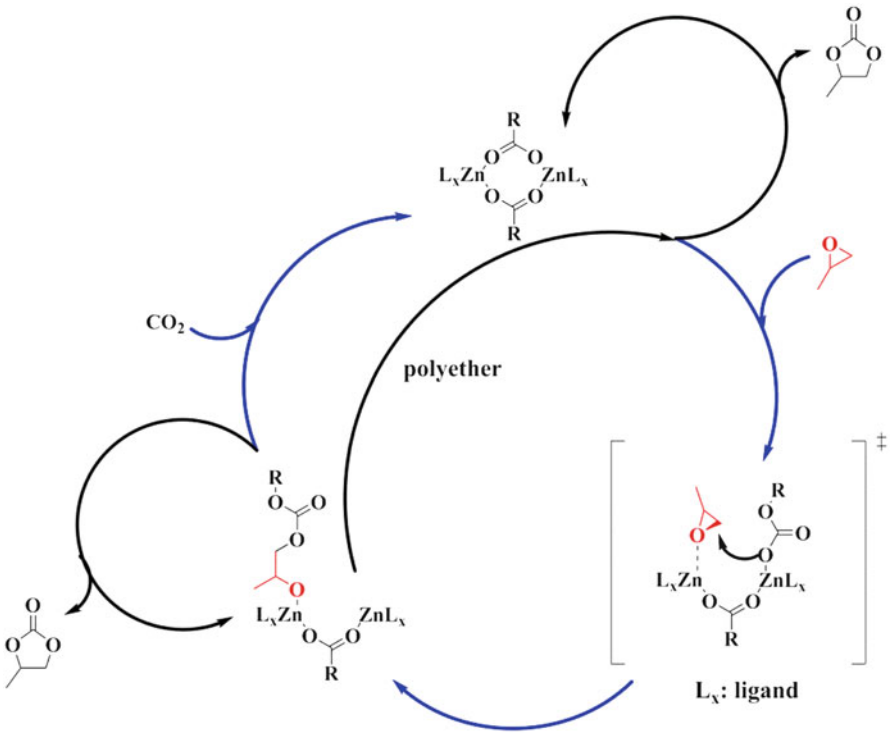

Fig. 7.17 Bimetallic propagation and the possible concomitant side reactions

In general, the epoxide is opened at the least hindered C-O bond but regioerrors may occur. Both the axial ligand and the nucleophile have the potential to open the epoxide and are therefore incorporated in the polymer chain as end groups. The thermally disfavored transition state makes this reaction mechanism unlikely for commonly used catalysts. Reaction pathway C takes place in the case of binary catalyst/cocatalyst systems where the added nucleophile attacks the precoordinated epoxide and opens the ring. Binary catalyst/cocatalyst systems have been under scrutiny from multiple research teams around the world in recent times [46, 85, 103–116].

The group of Coates et al. was able to show with (β-diiminate)ZnOR catalysts that a bimetallic mechanism is at play during their reactions [117]. Furthermore, they were able to find the rate determining step as the incorporation of the epoxide. The weak nucleophilic nature of the carbonate end group makes a preactivation of the epoxide necessary. Therefore, Lewis acids in the form of cocatalysts or a second metal center have to be used. After the ring opening of the epoxide, CO_2 is inserted into the metal alkoxy bond, for which an open coordination site at the metal is not obligatory. This mechanism explains the generally observed loss of activity of cocatalyst systems at higher dilutions (Fig. 7.17).

Undesired side reactions during the copolymerization are the formation of cyclic carbonates and the formation of polyether segments. The group of Darensbourg

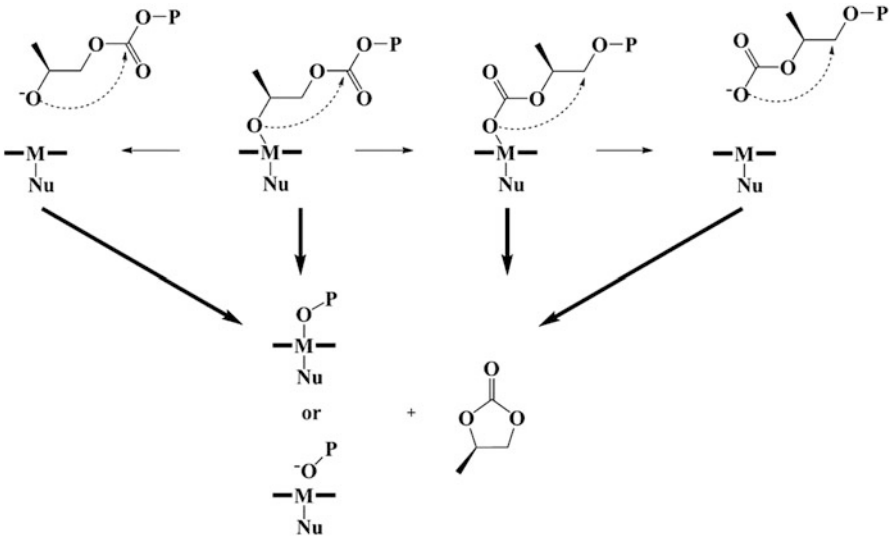

Fig. 7.18 Chain backbiting mechanism [88]

studied in detail the reasons for the product selectivity and the dependence on temperature, pressure, cocatalyst, and catalyst structure [101]. In general, both low temperatures and stronger coordination to the metal center decrease the amount of cyclic byproduct since these factors can suppress backbiting. During the backbiting reaction either the carbonato- or alkoxy-chain end of the polymer attacks at the growing chain (Fig. 7.18). This reaction is especially pronounced for aliphatic epoxides [63]. Alternatively, the growing chain end may dissociate from the metal center and more easily undergo backbiting in its unbound state [99]. The protonation of this unbound alkoxy- or carbonato-chain end is a possible strategy to reduce backbiting.

Chain transfer reactions during the copolymerization can be caused by traces of water, alcohols, or acids. Chain transfer can be exploited to tune the molecular weight by addition of, for example, adipic acid or telechelic polymers featuring alcohol end groups [118]. These chain transfer reactions lead to lower molecular weights than theoretically calculated. Furthermore, phosphoric acid and phenylphosphonic acids as additives have been tested to afford flame-retarding PPCs [42].

7.3.3 Catalysis

7.3.3.1 Bifunctional Catalysts

Owing to the desire to reach high selectivities and activities, catalyst design has shifted in recent years toward bifunctional catalysts. These complexes combine the

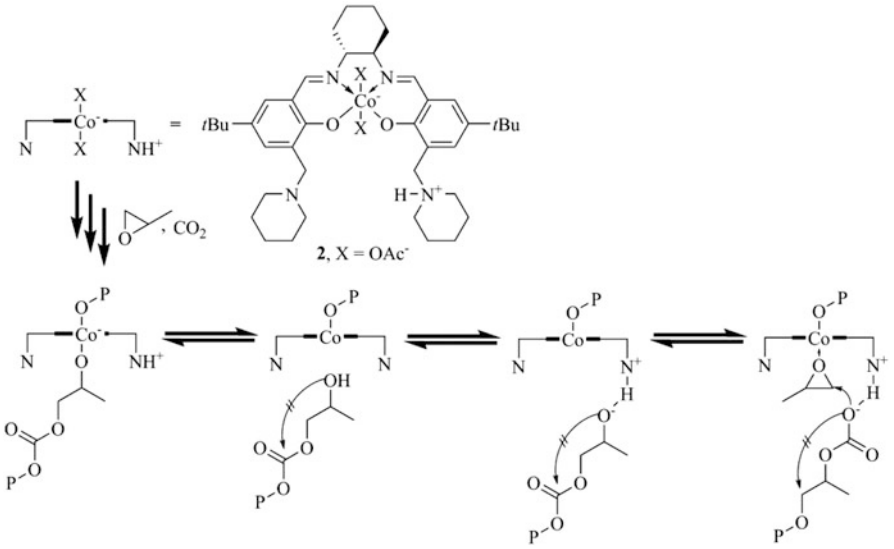

Fig. 7.19 Copolymerization mechanism for a bifunctional salenCo(III) complex with a piperidinium arm [67] (Reprinted with permission from Ref. [88]. Copyright 2011, Elsevier)

active metal site, coordinated by an organic ligand framework, with a covalently bound cocatalyst. With these considerations in mind Nozaki et al. incorporated a piperidinium arm into a (salen)CoOAc complex. It was proposed that cyclic carbonate formation is inhibited by the protonated piperidinium arm which can protonate the growing polymer chain upon dissociation from the metal center (Fig. 7.19). At a catalyst loading of PO/catalyst = 2,000, 14 bar and ambient temperatures, a selectivity of 99 % for poly(propylene carbonate) was achieved. Furthermore, it was shown that even at elevated temperatures of 60 °C, the cyclic carbonate formation could be suppressed to a certain degree [67].

The group of Lee et al. designed a series of ionic bifunctional catalyst structures in which the cocatalyst is covalently bound and is supposed to keep the growing polymer chain close to the reactive center [22, 119]. The anions also function as initiators for the copolymerization and have a pronounced effect on polymerization activity and product selectivity [120]. These catalysts were employed in copolymerization reactions with various epoxides, for example, cyclohexene oxide, hexene oxide, 1-butene oxide, and propylene oxide [48]. Polymerizations of PO and carbon dioxide at 80 °C and at dilutions as low as 0.67 mmol% were shown to be possible while retaining high activities and selectivities for the polycarbonate formation (TOF 12,400 h^{-1}, 96 %) [22]. The highest reported TOF is 26,000 h^{-1} (>99 %, M_n = 114 kg/mol, PDI = 1.29). It was possible to produce high molecular weight PPC at elevated temperatures with a M_n of up to 285 kg/mol and narrow molecular weight distributions of 1.18. Interestingly, the catalyst structure allowed the removal from the produced polymer after the copolymerization.

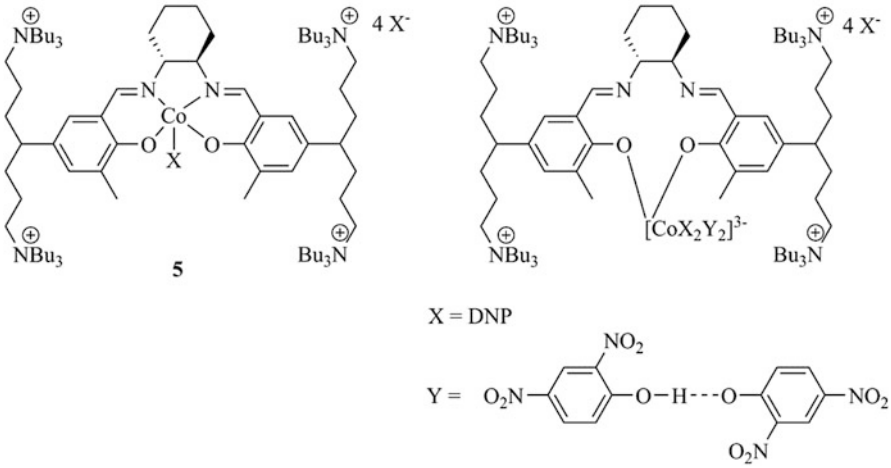

Fig. 7.20 Bifunctional ionic salenCo(III) catalyst **5** and its proposed bidentate coordination structure [121]

Filtration through a short pad of silica gel results in a catalyst which exhibits almost equivalent copolymerization activities even after several separation cycles. In their later work the group of Lee discovered an unusual coordination mode in their bifunctional catalysts. Though no crystal structure has yet been obtained from this proposed conformation, NMR studies and DFT calculations support the proposed structure. They postulated that the imine nitrogens of the salen ligand do not coordinate to the cobalt center (Fig. 7.20). Instead the DNPs coordinate to the cobalt, forming a negatively charged cobaltate complex. Structural variations of the ligand framework allowed the conclusion that sterically more demanding substituents in *ortho*-position reduce the activity. The authors attributed this to the fact that the formation of the aforementioned bidentate cobalt coordination is inhibited. High copolymerization activities were only observed on catalysts with the ability to form the cobaltate complex (Fig. 7.20 (right)) [121]. The employed 2,4-dinitrophenolate is explosive in its dry state as well as hazardous. Therefore, anion variations were performed using 2,4,5-trichlorophenolate, 4-nitrophenolate, 2,4-dichlorophenolate, and nitrate [118, 120]. It was found by chance that homoconjugated anion pairs of the phenols [X-H-Y] show increased activities and higher tolerance to water impurities leading to shorter induction periods [121]. Interestingly the rather long induction periods of the cobalt complexes during the copolymerization of epoxides and carbon dioxide are still unexplained. Further examples of bifunctional catalysts for the production of polycarbonates were published by Lu et al. These (salen)CoX complexes feature either an alkyl arm with pending quaternary ammonium salt at the 3-position of the phenyl ring or an alkyl arm bound to 1,5,7-triabicyclo[4,4,0] dec-5-ene (TBD). Catalyst **4** with the TBD group was able to polymerize with high selectivity for polycarbonate (97 %) at 100 °C and 20 bar. Activities up to 10,880 h^{-1} at a loading of 1 mmol% were

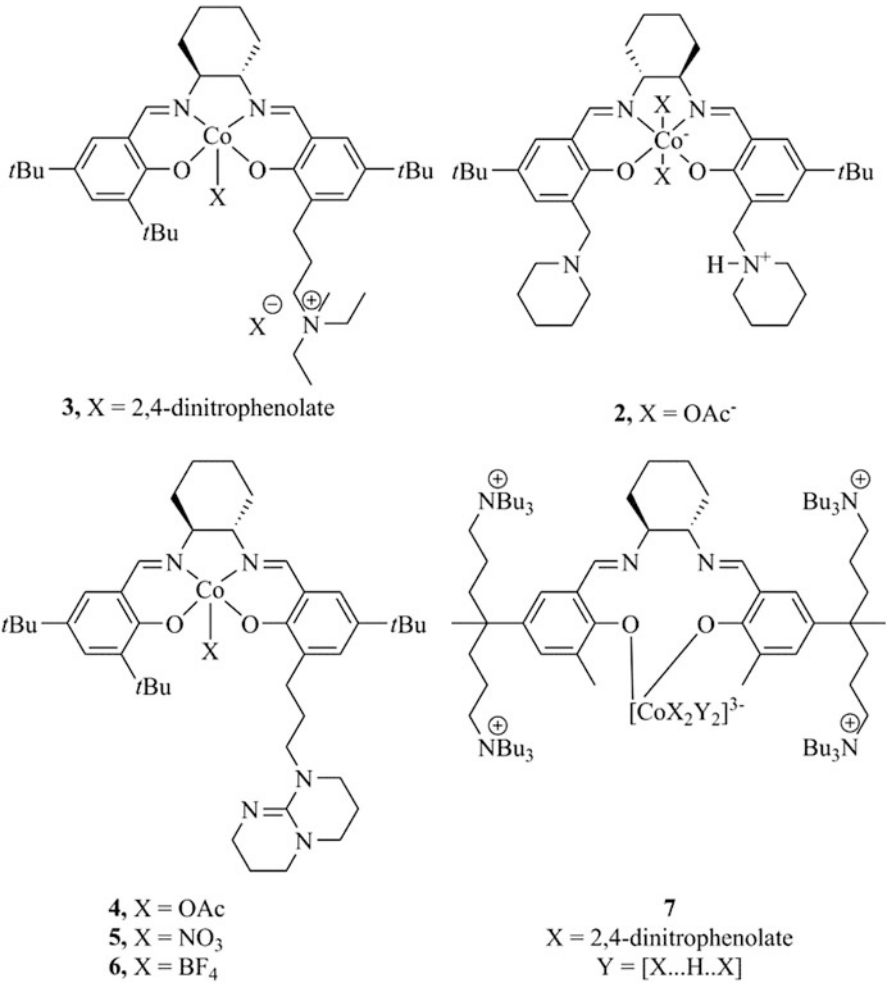

Fig. 7.21 Bifunctional salenCo(III) catalysts [22, 66, 67]

reached [122]. Through mass spectroscopy, it was possible to show that the pending TBD arm is activated after the insertion of one PO and carbon dioxide molecule. It stabilizes the Co(III) species against reduction to the inactive Co(II) by reversible intramolecular Co-O bond formation (Fig. 7.21).

The Co(III) catalyst (**3**) with an ammonium salt ($-NEt_2Me^+$) and 2,4-dinitrophenolate proved to be less active with TOF of 3,900 h^{-1} at 90 °C while nevertheless maintaining high selectivity for copolymer formation.

Bifunctional cobalt catalysts are currently the catalysts of choice for further scientific studies and improvements due to their excellent activities combined with high selectivities for the polymer formation. However, their main drawbacks cannot be solved by synthetic design as cobalt is toxic, prone to reduction, and has to be

removed from the polymer after copolymerization. This puts a considerable energetic burden on the produced polymer and hampers its chances to compete with already established polymers.

7.3.3.2 Zinc Catalysts

Due to their colorlessness, nontoxicity, and low price, it is not surprising that there is a considerable amount of literature on Zn(II)-based catalysts. For heterogeneous catalysis, the zinc glutarate (ZnGA) system is the most widely studied one. It is easy to prepare, nontoxic, economically viable, and easy to handle. But these heterogeneous catalysts are not only interesting for industrial applications as they offer the opportunity to better understand the reaction processes. The molecular structure of ZnGA was only recently reported and showed a unique structural constitution [123]. It consists of Zn centers coordinated by four carboxyl groups with the glutarate ligands either in a bent or an extended conformation. This structural type limits the activity for the copolymerization to the surface due to restricted monomer diffusion [124]. Consequently, methods for enlarging the surface were tested but with unsatisfactory results with respect to the achieved activity. Also the replacement of GA by derivatives (e.g., 2-ketoglutaric acid, 3,3-dimethylglutaric acid) with other functionalities in the hydrocarbon chain did not bring the expected success [125]. Experiments with different alkyl lengths (succinic acid (SA), adipic acid (AA), pimelic acid (PA)) in between the Zn centers showed that these are also active [126, 127]. It was not until 2011 that Rieger et al. published a detailed study of ZnSA, ZnGA, ZnAA, and ZnPA and their respective activities in the copolymerization of epoxides and CO_2 [128]. From the copolymerization experiments, the activity gap between ZnSA and the higher homologues was identified. The molecular structure was the crucial factor as the main difference between ZnSA and the tested homologues was the Zn-Zn distance. This indicated that the defined spatial structure which is influenced by the dicarboxylic acid has direct influence on the activity of heterogeneous zinc dicarboxylate systems. The Zn-Zn distance that is necessary for copolymerization is only found on one of the main *hkl*-indiced plains of the solid-state structure of ZnSA. However, in the solid-state structure of ZnGA, the corresponding distance of 4.6–4.8 Å is found on each main *hkl* plain (Fig. 7.22). These results show that two zinc centers have to be in close spatial proximity for high copolymerization activities to be possible. Theoretical calculations suggest that the optimal Zn-Zn distance for CO_2/epoxide copolymerization is between 4.3 and 5.0 Å [129].

This range gives an optimum between the activation energy and product selectivity toward polymer formation. The importance of the appropriate Zn-Zn distance for homogeneous catalysts was already described in literature. The study of Rieger et al. indicates that also in heterogeneous Zn catalysts a bimetallic mechanism is at play on the surface for which the spatial separation of the metal is crucial. To gain deeper insights into the copolymerization mechanism, homogeneous single-site

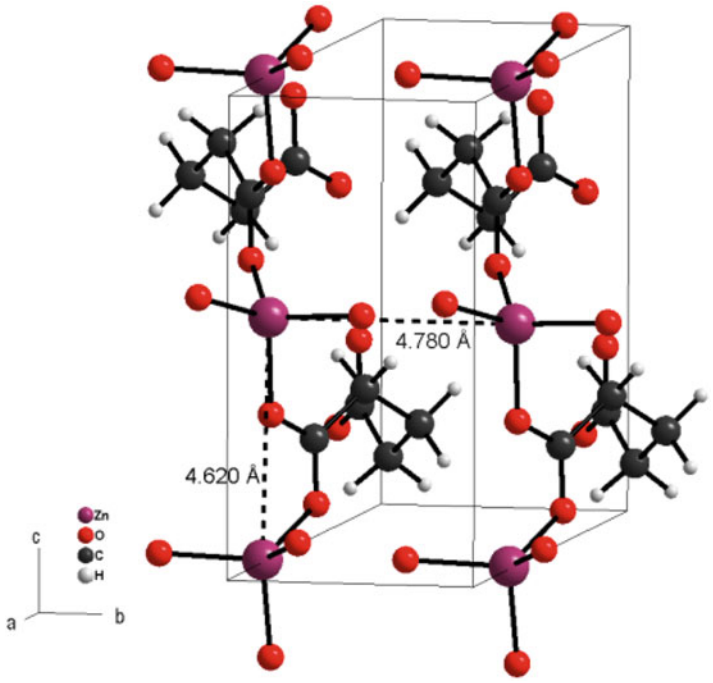

Fig. 7.22 Close-up view on unit cell and metal distances in zinc glutarate (Zn-Zn distance = 4.6-4.8 Å) (Reprinted with permission from Ref. [128]. Copyright 2011, American Chemical Society)

catalysts are required. Darensbourg et al. synthesized the first homogeneous zinc-based catalyst for the copolymerization of cyclohexene oxide and CO_2 [47]. These catalysts exhibited a strong tendency to form polyether even at elevated CO_2 pressures (55 bar). Major drawbacks of those early systems were the low activities and selectivities for polycarbonate formation. In the case of the phenoxide zinc complexes, another side reaction limited success as their phenoxide ligands were consumed as initiators during the polymerization [51, 130]. The unstable nature of the zinc phenoxide catalysts made mechanistic investigations and the defined synthesis of the ligand framework around the metal center difficult. The first breakthrough for copolymerization of epoxides and carbon dioxide was the discovery of β-diketiminato zinc catalysts (BDI) for the CHO/CO_2 copolymerization by Coates et al. which led to a more systematic catalyst design. Minor variations in the electronic and steric character of the BDI ligand framework resulted in dramatic changes in catalytic activity [47, 48]. These catalysts afforded polymers with narrow PDIs at low carbon dioxide pressures with high activities. In the copolymerization reaction of CHO/CO_2, minor changes in the backbone from R^1 = H, R^2, R^3 = Et to R^1 = CN, R^2 = Me and R^3 = *i*Pr led to an activity increase from 239 to 2,290 h^{-1} [91]. As shown in Fig. 7.23, these complexes are present in monomer/dimer equilibria which depend on sterics, electronics, and temperature.

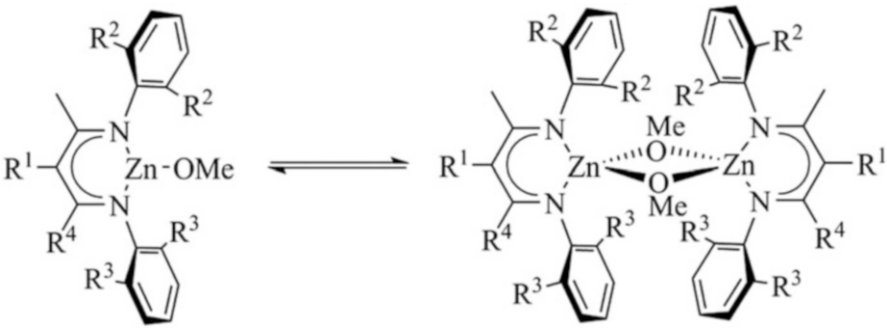

Fig. 7.23 Monomer/dimer equilibria for the zinc-based catalysts by Coates et al. [91]

Rate studies with in situ IR spectroscopy on the copolymerization resulted in a zero-order dependence in CO_2, a first-order dependence in CHO, and a varying dependency from 1.0 to 1.8 for zinc [117]. This variation can be constituted with the appearance of the mentioned equilibrium in Fig. 7.23. All results support the assumption that two zinc centers are interacting in the copolymerization and that the rate determining step is located at the ring opening of the epoxide. Additionally, it was found that sterical variation (R^1 = Et, R^2 = *i*Pr) at the aniline moiety and the introduction of electron withdrawing groups to the catalyst (**20**) backbone gave an active catalyst for the copolymerization of PO/CO_2 at 25 °C, 6.9 bar with a TOF of 235 h^{-1}. The resulting polymer featured a regioirregularity and a narrow molecular weight distribution [131] (Fig. 7.24).

Interestingly this complex structure also polymerized β-butyrolactone and β-valerolactone to afford atactic poly(3-hydroxybutyrate) (PHB) and poly (3-hydroxyvalerate) [132]. Research into the zinc BDI systems led to the discovery of ethylsulfinate as superior initiating group [133]. In 2005 Lee et al. presented an anilido-aldimine ligand for dinuclear zinc complexes (Fig. 7.25). Thereby, open (**22**) and closed (**21**–**24**) structures were synthesized with zinc-zinc distances of between 4.88 Å for the open structure and 4.69 Å for the closed structure. For the copolymerization of cyclohexene oxide and carbon dioxide, only the catalyst with the open structure was active. With this catalyst TOFs up to 200 h^{-1} were achieved. Increasing the Lewis acidity of the zinc centers led to an increase of activity up to 2,860 h^{-1} at high dilutions ([catalyst]:[CHO] = 1:50,000) [134, 135].

In 2011, Williams et al. published a rigid dinuclear zinc complex for low-pressure copolymerization of cyclohexene oxide and CO_2. Investigations of this catalyst system also revealed a zero-order dependence on CO_2 (between 1 and 40 bar CO_2 pressure) and a first-order dependence on CHO. These results confirmed the hypothesis that the incorporation of the epoxide is rate determining for their dinuclear rigid zinc catalysts [136]. This implies that at typical process conditions, an increase in CO_2 concentration does not automatically enhance polymerization activity. In subsequent work, Williams et al. replaced zinc with cobalt(II)/(III) [137] and iron [138] in the reduced Robson-type ligand structure (Fig. 7.26). The isolated complexes

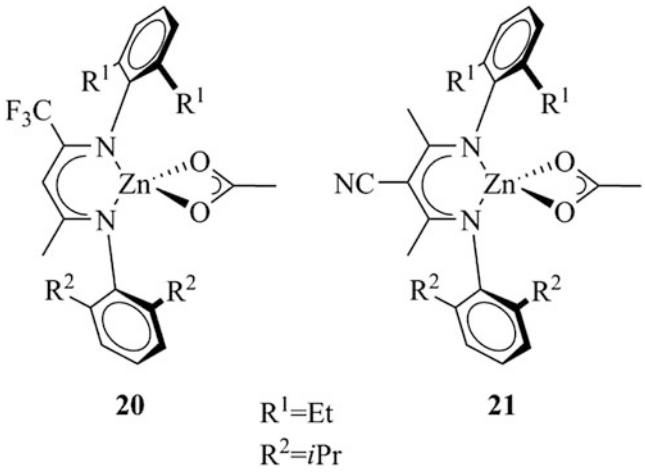

Fig. 7.24 Zinc catalyst for copolymerization of propylene oxide and carbon dioxide [131]

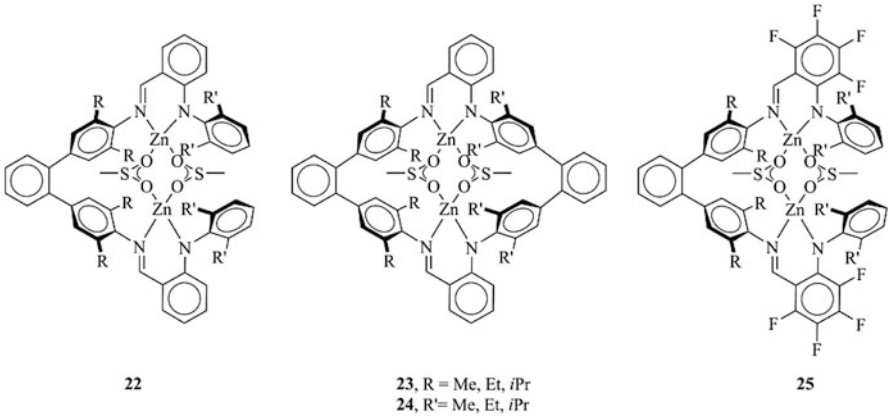

Fig. 7.25 Dinuclear anilido-aldimine zinc complexes [134, 135]

were all able to copolymerize CHO and carbon dioxide with good activities and high selectivities. The highest activities in the copolymerization of CHO and CO_2 were achieved with magnesium (**31**). Activities of up to 750 h^{-1} and very high selectivities of >99 % for the copolymer formation were observed with this structure (12 atm CO_2, [CHO]:[31] = 1:10,000, PDI = 1.03/1.10). The data gathered from these metal screenings show very nicely how the copolymerization activity can be tuned in dinuclear catalysts by the Lewis acidity of the metal itself.

In 2013, Rieger et al. presented a flexibly tethered dinuclear zinc complex **35**, in which two BDI zinc units are linked by a tether (Fig. 7.27). The linker allows to overcome the entropically disfavored aggregation of two individual complex molecules in solution. Catalyst **35** exhibits very high activities of up to 9,130 h^{-1} for the

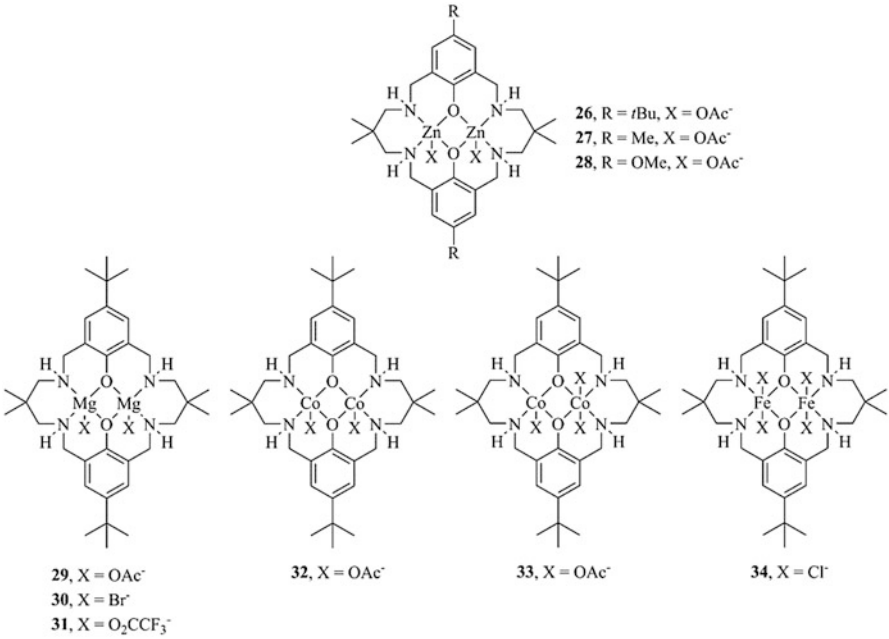

Fig. 7.26 Dinuclear reduced Robson-type complexes with Zn-, Mg-, Co-, and Fe-centers [64, 136–139]

Fig. 7.27 Flexibly tethered dinuclear zinc complex [140]

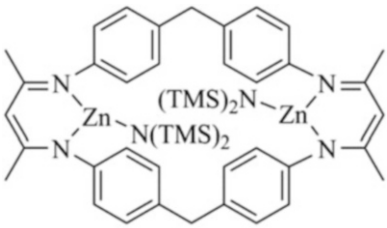

35

copolymerization of CHO and carbon dioxide (at 40 bar CO_2, 100 °C, [CHO]: [35] = 4,000:1) [140].

Kinetic measurements in an in situ IR reactor revealed a first-order dependence in catalyst. Interestingly, with constant catalyst and cyclohexene oxide concentration, the order in carbon dioxide was determined to be one in the range of 5–25 bar CO_2 pressure. For 25–45 bar, this order changes from one to zero. The assignment of the order in cyclohexene oxide was performed at two different pressure regimes: 10 and 30 bar, respectively. This resulted in a reaction order of zero for 10 bar and a reaction order of one at 30 bar. The subsequent rate laws are depicted below:

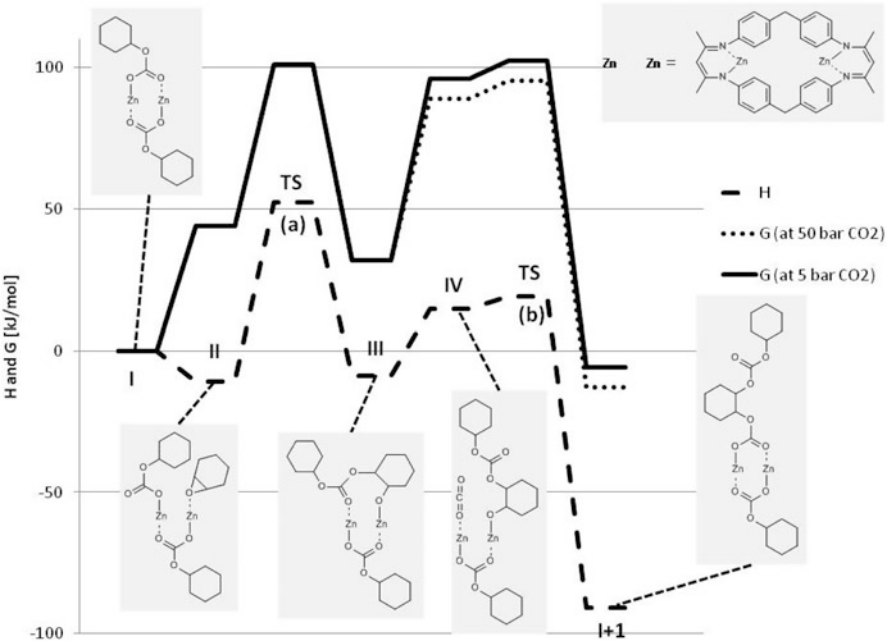

Fig. 7.28 Enthalpy and Gibbs free energy profile for the whole catalytic cycle of catalyst **35** (Reprinted with permission from Ref. [140]. Copyright 2013, Wiley-VCH Verlag GmbH & Co. KGaA)

Equation 7.1: Rate law of complex **35** for 5–25 bar CO_2 **(a)** and for 25–45 bar CO_2 **(b)** [140].

$$r = k \cdot [CHO]^0 \cdot [CO_2]^1 \cdot [Catalyst]^1 \quad 5-25 \text{ bar } CO_2 \quad (a)$$

$$r = k \cdot [CHO]^1 \cdot [CO_2]^0 \cdot [Catalyst]^1 \quad 25-45 \text{ bar } CO_2 \quad (b)$$

Catalyst **35** is the first dinuclear zinc catalyst which shows a shift in the rate determining step from ring opening of the epoxide to carbon dioxide insertion for the copolymerization of cyclohexene oxide and carbon dioxide in a certain pressure regime. This unique behavior is attributed to the flexible CH_2-tethers which links both complex moieties. Considering the first-order dependence with respect to CHO of all other catalysts, this suggests that the flexible tether between the two zinc centers facilitates the cooperative ring-opening step in an unprecedented manner. These results are supported by quantum chemical calculations. The computed results for the main steps, beginning from the dicarbonato complex as the starting point, followed by coordination of CHO, epoxide ring opening to form an alkoxide and subsequent insertion of CO_2 into the coordinated alkoxide bond, are summarized in Fig. 7.28.

As can be seen in Fig. 7.28, both elementary steps give similar computed G-values (~100 kJ/mol) which means that both transition states are equally difficult to overcome. It is notable that the enthalpy H is much bigger for the ring opening (TS (a) = 52.3 kJ/mol) compared to the H of the CO_2 insertion (TS(b) = 19.2 kJ/mol). At first glance, it appears surprising that elementary steps with such dissimilar activation energies can both be rate limiting. DFT calculations explain the similar activation energies as a consequence of Gibbs free energy which includes both activation enthalpy and entropy. The main point is that all alkoxide species are significantly higher in G if compared to the dicarbonato complex I, which is why all Gibbs free energies have to be considered in relation to complex I. As the resting state is in all cases the dicarbonato complex I, oxirane ring opening is a bimolecular reaction, i.e., the incorporation of one liquid species into the catalyst bound polymer chain. Otherwise, CO_2 insertion is effectively a trimolecular reaction, which consumes both one liquid epoxide and one gaseous CO_2. All the structural and electronic features of **35** lead to high copolymerization activities of over 9,130 h^{-1} and selectivities of >99 % toward polycarbonate formation.

In conclusion, zinc and other nontoxic, cheap, and abundant metals have tremendous advantages compared to other transition metals, namely, cobalt and chrome, which are currently predominantly employed for the copolymerization of carbon dioxide and epoxides. In recent publications, it was nicely shown how those economic and eco-friendly elements can achieve high activities and selectivities. An additional advantage of zinc and magnesium is their colorless ions. This opens up the possibility to leave the catalyst in the formed polymer and reduce work-up costs.

7.4 Conclusion

Carbon dioxide as feedstock for the generation of biodegradable polycarbonates has been known in the literature for almost 45 years. Since the discovery of the copolymerization reaction of carbon dioxide and epoxides, chemistry has made significant progress, and especially in the last 10 years, the search for better and more eco-friendly catalysts has gained momentum. As the stereoselective synthesis of poly(propylene carbonate) is still in its infancy and the analytical methods used have not yet been fully exploited, NMR techniques have the potential to help interpret the structures produced by catalyst systems and to pinpoint promising catalyst candidates for further development. Though heterogeneous catalysts still dominate industrial production processes, for mechanistic investigations, homogeneous systems do have the necessary advantages to tackle the underlying questions about the mechanism and within the catalysis. Cobalt(III) catalysts with a variety of accompanying ligand structures have become the center of attention since the discovery of bifunctional structures which allow the incorporation of the cocatalyst into the complex and thereby enable high activities and the production of polycarbonates with high molecular masses, low PDIs, and >99 % carbonate

content. However, cobalt as toxic and coloring metal has to be removed from the polymer after copolymerization. Any additional work-up increases the energetic burden on production and limits competitiveness of biodegradable polymers such as poly(propylene carbonate). Possible applications in food packaging also make the development of less toxic catalysts desirable. An applicable catalyst for large-scale industrial production in a continuous process has to exhibit a sufficient activity to make it economically viable. In recent years, research made great progress in the development of iron-, magnesium-, and zinc-based systems which show improved activities. It will be interesting and exciting to see the future development of catalyst systems which tolerate water contaminations and multiple epoxides and nevertheless show high activities in co- and terpolymerizations at ambient conditions.

References

1. Song C (2006) Global challenges and strategies for control, conversion and utilization of CO_2 for sustainable development involving energy, catalysis, adsorption and chemical processing. Catal Today 115:2–32
2. Energy, E.A.U.S.D.o. (2011) Annual Energy Review. http://www.eia.gov/totalenergy/data/annual/index.cfm. Accessed 02 May 2013
3. Tans P (2013) Trends in atmospheric carbon dioxide. www.esrl.noaa.gov/gmd/ccgg/trends/. Accessed 02 May 2013
4. Sakakura T, Kohno K (2009) The synthesis of organic carbonates from carbon dioxide. Chem Commun (Cambridge, UK) 11:1312–1330
5. Cokoja M, Bruckmeier C, Rieger B et al (2011) Transformation of carbon dioxide with homogeneous transition-metal catalysts: a molecular solution to a global challenge? Angew Chem Int Ed 50(37):8510–8537
6. Sakakura T, Choi JC, Yasuda H (2007) Transformation of carbon dioxide. Chem Rev 107:2365–2387
7. Peters M, Koehler B, Kuckshinrichs W et al (2011) Chemical technologies for exploiting and recycling carbon dioxide into the value chain. ChemSusChem 4:1216–1240
8. Darensbourg DJ, Wilson SJ (2012) What's new with CO_2? Recent advances in its copolymerization with oxiranes. Green Chem 14(10):2665–2671
9. Lu X-B, Darensbourg DJ (2012) Cobalt catalysts for the coupling of CO_2 and epoxides to provide polycarbonates and cyclic carbonates. Chem Soc Rev 41:1462–1484
10. Clements JH (2003) Reactive applications of cyclic alkylene carbonates. Ind Eng Chem Res 42:663–674
11. North M, Pasquale R, Young C (2010) Synthesis of cyclic carbonates from epoxides and CO_2. Green Chem 12(9):1514–1539
12. Varghese JK, Na SJ, Park JH et al (2010) Thermal and weathering degradation of poly (propylene carbonate). Polym Degrad Stab 95(6):1039–1044
13. Du LC, Meng YZ, Wang SJ et al (2004) Synthesis and degradation behavior of poly (propylene carbonate) derived from carbon dioxide and propylene oxide. J Appl Polym Sci 92:1840–1846
14. Luinstra GA (2008) Poly(propylene carbonate), old copolymers of propylene oxide and carbon dioxide with new interests: catalysis and material properties. Polym Rev (Philadelphia, PA, USA) 48(1):192–219
15. Qin Y, Wang X (2010) Carbon dioxide-based copolymers: environmental benefits of PPC, an industrially viable catalyst. Biotechnol J 5:1164–1180

16. Barreto C, Hansen E, Fredriksen S (2012) Novel solventless purification of poly(propylene carbonate): tailoring the composition and thermal properties of PPC. Polym Degrad Stab 97(6):893–904
17. Chisholm MH, Navarro-Llobet D, Zhou Z (2002) Poly(propylene carbonate). 1. More about poly(propylene carbonate) formed from the copolymerization of propylene oxide and carbon dioxide employing a zinc glutarate catalyst. Macromolecules 35:6494–6504
18. Kuran W, Gorecki P (1983) Degradation and depolymerization of poly(propylene carbonate) by diethylzinc. Makromol Chem 184:907–912
19. Gorecki P, Kuran W (1985) Diethylzinc-trihydric phenol catalysts for copolymerization of carbon dioxide and propylene oxide: activity in copolymerization and copolymer destruction processes. J Polym Sci Polym Lett Ed 23:299–304
20. Darensbourg DJ, Wei S-H, Wilson SJ (2013) Depolymerization of poly(indene carbonate). A unique degradation pathway. Macromolecules 46:3228–3233
21. Wang SJ, Du LC, Zhao XS et al (2002) Synthesis and characterization of alternating copolymer from carbon dioxide and propylene oxide. J Appl Polym Sci 85(11):2327–2334
22. Min SSJK, Seong JE, Na SJ et al (2008) A highly active and recyclable catalytic system for CO_2/propylene oxide copolymerization. Angew Chem Int Ed 47(38):7306–7309
23. Peng S, An Y, Chen C et al (2003) Thermal degradation kinetics of uncapped and end-capped poly(propylene carbonate). Polym Degrad Stab 80:141–147
24. Dixon DD, Ford ME, Mantell GJ (1980) Thermal stabilization of poly(alkylene carbonate)s. J Polym Sci Polym Lett Ed 18(2):131–134
25. Lai MF, Li J, Liu JJ (2005) Thermal and dynamic mechanical properties of poly(propylene carbonate). J Therm Anal Calorim 82:293–298
26. Yu T, Luo F-L, Zhao Y et al (2011) Improving the processability of biodegradable polymer by stearate additive. J Appl Polym Sci 120:692–700
27. Yao M, Mai F, Deng H et al (2011) Improved thermal stability and mechanical properties of poly(propylene carbonate) by reactive blending with maleic anhydride. J Appl Polym Sci 120:3565–3573
28. Yu T, Zhou Y, Zhao Y et al (2008) Hydrogen-bonded thermostable liquid crystalline complex formed by biodegradable polymer and amphiphilic molecules. Macromolecules 41(9):3175–3180
29. Ge XC, Zhu Q, Meng YZ (2006) Fabrication and characterization of biodegradable poly (propylene carbonate)/wood flour composites. J Appl Polym Sci 99:782–787
30. Bian J, Wei XW, Lin HL et al (2011) Preparation and characterization of modified graphite oxide/poly(propylene carbonate) composites by solution intercalation. Polym Degrad Stab 96:1833–1840
31. Shi X, Gan Z (2007) Preparation and characterization of poly(propylene carbonate)/montmorillonite nanocomposites by solution intercalation. Eur Polym J 43:4852–4858
32. Wang JT, Zhu Q, Lu XL et al (2005) ZnGA–MMT catalyzed the copolymerization of carbon dioxide with propylene oxide. Eur Polym J 41(5):1108–1114
33. Zhang Z, Lee J-H, Lee S-H et al (2008) Morphology, thermal stability and rheology of poly (propylene carbonate)/organoclay nanocomposites with different pillaring agents. Polymer 49:2947–2956
34. Chen L, Qin Y, Wang X et al (2011) Toughening of poly(propylene carbonate) by hyperbranched poly(ester-amide) via hydrogen bonding interaction. Polym Int 60:1697–1704
35. Ma X, Yu J, Wang N (2005) Compatibility characterization of poly(lactic acid)/poly(propylene carbonate) blends. J Polym Sci B 44:94–101
36. Wang N, Zhang X, Yu J et al (2008) Partially miscible poly(lactic acid)-blend-poly(propylene carbonate) filled with carbon black as conductive polymer composite. Polym Int 57:1027–1035
37. Peng S, Wang X, Dong L (2005) Special interaction between poly(propylene carbonate) and corn starch. Polym Compos 26:37–41

38. Spencer TJ, Chen Y-C, Saha R et al (2011) Stabilization of the thermal decomposition of poly (propylene carbonate) through copper ion incorporation and use in self-patterning. J Electr Mater 40:1350–1363
39. Yu T, Zhou Y, Liu K et al (2009) Improving thermal stability of biodegradable aliphatic polycarbonate by metal ion coordination. Polym Degrad Stab 94:253–258
40. Uzunlar E, Kohl PA (2012) Thermal and photocatalytic stability enhancement mechanism of poly(propylene carbonate) due to Cu(I) impurities. Polym Degrad Stab 97:1829–1837
41. Jeon JY, Lee JJ, Varghese JK et al (2012) CO_2/ethylene oxide copolymerization and ligand variation for a highly active salen-cobalt(iii) complex tethering 4 quaternary ammonium salts. Dalton Trans 42:9245–9254
42. Cyriac A, Lee SH, Varghese JK et al (2011) Preparation of flame-retarding poly(propylene carbonate). Green Chem 13(12):3469–3475
43. Cherian AE, Sun FC, Sheiko SS et al (2007) Formation of nanoparticles by intramolecular cross-linking: following the reaction progress of single polymer chains by atomic force microscopy. J Am Chem Soc 129:11350–11351
44. Cyriac A, Lee SH, Lee BY (2011) Connection of polymer chains using diepoxide in CO_2/propylene oxide copolymerizations. Polym Chem 2(4):950–956
45. Darensbourg DJ, Poland RR, Strickland AL (2012) (Salan)CrCl, an effective catalyst for the copolymerization and terpolymerization of epoxides and carbon dioxide. J Polym Sci Part A Polym Chem 50(1):127–133
46. Shi L, Lu X-B, Zhang R et al (2006) Asymmetric alternating copolymerization and terpolymerization of epoxides with carbon dioxide at mild conditions. Macromolecules 39:5679–5685
47. Darensbourg DJ, Holtcamp MW (1995) Catalytic activity of zinc(II) phenoxides which possess readily accessible coordination sites. Copolymerization and terpolymerization of epoxides and carbon dioxide. Macromolecules 28(22):7577–7579
48. Seong JE, Na SJ, Cyriac A et al (2009) Terpolymerizations of CO_2, propylene oxide, and various epoxides using a cobalt(III) complex of salen-type ligand tethered by four quaternary ammonium salts. Macromolecules 43(2):903–908
49. Harrold ND, Li Y, Chisholm MH (2013) Studies of ring-opening reactions of styrene oxide by chromium tetraphenylporphyrin initiators. Mechanistic and stereochemical considerations. Macromolecules 46(3):692–698
50. Kim JG, Cowman CD, LaPointe AM et al (2011) Tailored living block copolymerization: multiblock poly(cyclohexene carbonate)s with sequence control. Macromolecules 44(5):1110–1113
51. Darensbourg DJ, Wildeson JR, Yarbrough JC et al (2000) Bis 2,6-difluorophenoxide dimeric complexes of zinc and cadmium and their phosphine adducts: lessons learned relative to carbon dioxide/cyclohexene oxide alternating copolymerization processes catalyzed by zinc phenoxides. J Am Chem Soc 122(50):12487–12496
52. Wu G-P, Wei S-H, Lu X-B et al (2010) Highly selective synthesis of CO_2 copolymer from styrene oxide. Macromolecules 43(21):9202–9204
53. Wu G-P, Xu P-X, Lu X-B et al (2013) Crystalline CO_2 copolymer from epichlorohydrin via Co(III)-complex-mediated stereospecific polymerization. Macromolecules 46(6):2128–2133
54. Darensbourg DJ, Wilson SJ (2011) Synthesis of poly(indene carbonate) from indene oxide and carbon dioxide – a polycarbonate with a rigid backbone. J Am Chem Soc 133(46):18610–18613
55. Liu S, Xiao H, Huang K et al (2006) Terpolymerization of carbon dioxide with propylene oxide and ε-caprolactone: synthesis, characterization and biodegradability. Polym Bull 56:53–62
56. Liu Y, Huang K, Peng D et al (2006) Synthesis, characterization and hydrolysis of an aliphatic polycarbonate by terpolymerization of carbon dioxide, propylene oxide and maleic anhydride. Polymer 47(26):8453–8461

57. Hwang Y, Jung J, Ree M et al (2003) Terpolymerization of CO_2 with propylene oxide and ε-caprolactone using zinc glutarate catalyst. Macromolecules 36(22):8210–8212
58. Lu L, Huang K (2005) Synthesis and characteristics of a novel aliphatic polycarbonate, poly [(propylene oxide)-co-(carbon dioxide)-co-(γ-butyrolactone)]. Polym Int 54:870–874
59. Liu S, Wang J, Huang K et al (2011) Synthesis of poly(propylene-co-lactide carbonate) and hydrolysis of the terpolymer. Polym Bull 66:327–340
60. Wu G-P, Darensbourg DJ, Lu X-B (2012) Tandem metal-coordination copolymerization and organocatalytic ring-opening polymerization via water to synthesize diblock copolymers of styrene oxide/CO_2 and lactide. J Am Chem Soc 134:17739–17745
61. Zhang J-F, Ren W-M, Sun X-K et al (2011) Fully degradable and well-defined brush copolymers from combination of living CO_2/epoxide copolymerization, thiol-ene click reaction and ROP of ε-caprolactone. Macromolecules 44:9882–9886
62. Kröger M, Folli C, Walter O et al (2005) Alternating copolymerization of cyclohexene oxide and CO_2 catalyzed by zinc complexes with new 3-amino-2-cyanoimidoacrylate ligands. Adv Synth Catal 347(10):1325–1328
63. Lehenmeier MW, Bruckmeier C, Klaus S et al (2011) Differences in reactivity of epoxides in the copolymerisation with carbon dioxide by zinc-based catalysts: propylene oxide versus cyclohexene oxide. Chem Eur J 17(32):8858–8869
64. Kember MR, Knight PD, Reung PTR et al (2009) Highly active dizinc catalyst for the copolymerization of carbon dioxide and cyclohexene oxide at one atmosphere pressure. Angew Chem Int Ed 48:931–933
65. Seong JE, Na SJ, Cyriac A et al (2010) Terpolymerizations of CO_2, Propylene oxide, and various epoxides using a cobalt(III) complex of salen-type ligand tethered by four quaternary ammonium salts. Macromolecules 43(2):903–908
66. Ren W-M, Zhang X, Liu Y et al (2010) Highly active, bifunctional Co(III)-salen catalyst for alternating copolymerization of CO_2 with cyclohexene oxide and terpolymerization with aliphatic epoxides. Macromolecules 43:1396–1402
67. Nakano K, Kamada T, Nozaki K (2006) Selective formation of polycarbonate over cyclic carbonate: copolymerization of epoxides with carbon dioxide catalyzed by a cobalt(III) complex with a piperidinium end-capping arm. Angew Chem Int Ed 45(43):7274–7277
68. Scholl M, Ding S, Lee CW et al (1999) Synthesis and activity of a new generation of ruthenium-based olefin metathesis catalysts coordinated with 1,3-dimesityl-4,5-dihydroimidazol-2-ylidene ligands. Org Lett 1:953–956
69. Kim JG, Coates GW (2012) Synthesis and polymerization of norbornenyl-terminated multiblock poly(cyclohexene carbonate)s: a consecutive ring-opening polymerization route to multisegmented graft polycarbonates. Macromolecules 45(19):7878–7883
70. Geschwind J, Frey H (2013) Stable, hydroxyl functional polycarbonates with glycerol side chains synthesized from CO_2 and isopropylidene(glyceryl glycidyl ether). Macromol Rapid Commun 34(2):150–155
71. Cohen CT, Chu T, Coates GW (2005) Cobalt catalysts for the alternating copolymerization of propylene oxide and carbon dioxide: combining high activity and selectivity. J Am Chem Soc 127(31):10869–10878
72. Inoue S, Koinuma H, Tsuruta T (1969) Copolymerization of carbon dioxide and epoxide with organometallic compounds. Makromol Chem 130:210–220
73. Inoue S, Koinuma H, Tsuruta T (1969) Copolymerization of carbon dioxide and epoxide. J Polym Sci Part B Polym Lett 7(4):287–292
74. Aida T, Inoue S (1982) Synthesis of polyether-polycarbonate block copolymer from carbon dioxide and epoxide using a metalloporphyrin catalyst system. Macromolecules 15:682–684
75. Lednor PW, Rol NC (1985) Copolymerization of propylene oxide with carbon dioxide: a selective incorporation of propylene oxide into the polycarbonate chains, determined by 100 MHz carbon-13 NMR spectroscopy. Chem Commun (Cambridge, UK) 9:598–599
76. Nakano K, Hashimoto S, Nakamura M et al (2011) Stereocomplex of poly(propylene carbonate): synthesis of stereogradient poly(propylene carbonate) by regio- and

enantioselective copolymerization of propylene oxide with carbon dioxide. Angew Chem Int Ed 50(21):4868–4871
77. Byrnes MJ, Chisholm MH, Hadad CM et al (2004) Regioregular and regioirregular oligoether carbonates: a 13C{1H} NMR investigation. Macromolecules 37:4139–4145
78. Salmeia KA, Vagin S, Anderson CE et al (2012) Poly(propylene carbonate): insight into the microstructure and enantioselective ring-opening mechanism. Macromolecules 45:8604–8613
79. Salmeia KA (2012) Copolymerization of propylene oxide and CO_2 with salen-type catalysts; polymerization activities and polymer microstructure. Technische Universität München, Munich
80. Chisholm MH, Navarro-Llobet D, Zhou Z (2002) Poly(propylene carbonate). 1. More about poly(propylene carbonate) formed from the copolymerization of propylene oxide and carbon dioxide employing a zinc glutarate catalyst. Macromolecules 35(17):6494–6504. doi:10.1021/ma020348+
81. Ren W-M, Liu Y, Wu G-P et al (2011) Stereoregular polycarbonate synthesis: alternating copolymerization of CO_2 with aliphatic terminal epoxides catalyzed by multichiral cobalt (III) complexes. J Polym Sci Part A Polym Chem 49:4894–4901
82. Nozaki K, Nakano K, Hiyama T (1999) Optically active polycarbonates: asymmetric alternating copolymerization of cyclohexene oxide and carbon dioxide. J Am Chem Soc 121(47):11008–11009
83. Nakano K, Nozaki K, Hiyama T (2001) Spectral assignment of poly[cyclohexene oxide-alt-carbon dioxide]. Macromolecules 34(18):6325–6332
84. Nakano K, Nozaki K, Hiyama T (2003) Asymmetric alternating copolymerization of cyclohexene oxide and CO_2 with dimeric zinc complexes. J Am Chem Soc 125:5501–5510
85. Cohen CT, Thomas CM, Peretti KL et al (2006) Copolymerization of cyclohexene oxide and carbon dioxide using (salen)Co(III) complexes: synthesis and characterization of syndiotactic poly(cyclohexene carbonate). Dalton Trans 1:237–249
86. Wu G-P, Ren W-M, Luo Y et al (2012) Enhanced asymmetric induction for the copolymerization of CO_2 and cyclohexene oxide with unsymmetric enantiopure salenCo(III) complexes: synthesis of crystalline CO_2-based polycarbonate. J Am Chem Soc 134:5682–5688
87. Stevens HC (1966) High-molecular-weight polycarbonates. US 324,841
88. Klaus S, Lehenmeier MW, Anderson CE et al (2011) Recent advances in CO_2/epoxide copolymerization-new strategies and cooperative mechanisms. Coord Chem Rev 255(13–14):1460–1479
89. Takeda N, Inoue S (1978) Polymerization of 1,2-epoxypropane and copolymerization with carbon dioxide catalyzed by metalloporphyrins. Die Makromolekulare Chemie 179(5):1377–1381
90. Darensbourg DJ, Holtcamp MW, Struck GE et al (1999) Catalytic activity of a series of Zn (II) phenoxides for the copolymerization of epoxides and carbon dioxide. J Am Chem Soc 121(1):107–116
91. Moore DR, Cheng M, Lobkovsky EB et al (2002) Electronic and steric effects on catalysts for CO_2/epoxide polymerization: subtle modifications resulting in superior activities. Angew Chem Int Ed 41(14):2599–2602
92. Darensbourg DJ (2010) Chemistry of carbon dioxide relevant to its utilization: a personal perspective. Inorg Chem (Washington, DC, USA) 49(23):10765–10780
93. Darensbourg DJ (2007) Making plastics from carbon dioxide: salen metal complexes as catalysts for the production of polycarbonates from epoxides and CO_2. Chem Rev 107(6):2388–2410
94. Kember MR, Buchard A, Williams CK (2011) Catalysts for CO_2/epoxide copolymerization. Chem Commun (Cambridge, UK) 47(1):141–163
95. Ikpo N, Flogeras JC, Kerton FM (2013) Aluminium coordination complexes in copolymerization reactions of carbon dioxide and epoxides. Dalton Trans 42:8998–9006

96. Sugimoto H, Inoue S (2004) Copolymerization of carbon dioxide and epoxide. J Polymr Sci Part A Polym Chem 42(22):5561–5573
97. Coates GW, Moore DR (2004) Discrete metal-based catalysts for the copolymerization of CO_2 and epoxides: discovery, reactivity, optimization, and mechanism. Angew Chem Int Ed 43(48):6618–6639
98. Hansen KB, Leighton JL, Jacobsen EN (1996) On the mechanism of asymmetric nucleophilic ring-opening of epoxides catalyzed by (Salen)CrIII complexes. J Am Chem Soc 118:10924–10925
99. Luinstra GA, Haas GR, Molnar F et al (2005) On the formation of aliphatic polycarbonates from epoxides with chromium(III) and aluminum(III) metal-salen complexes. Chem Eur J 11:6298–6314
100. Darensbourg DJ, Yarbrough JC (2002) Mechanistic aspects of the copolymerization reaction of carbon dioxide and epoxides, using a chiral salen chromium chloride catalyst. J Am Chem Soc 124(22):6335–6342
101. Darensbourg DJ, Yarbrough JC, Ortiz C et al (2003) Comparative kinetic studies of the copolymerization of cyclohexene oxide and propylene oxide with carbon dioxide in the presence of chromium salen derivatives. In situ FTIR measurements of copolymer vs cyclic carbonate production. J Am Chem Soc 125(25):7586–7591
102. Darensbourg DJ, Rodgers JL, Mackiewicz RM et al (2004) Probing the mechanistic aspects of the chromium salen catalyzed carbon dioxide/epoxide copolymerization process using in situ ATR/FTIR. Catal Today 98(4):485–492
103. Rao D-Y, Li B, Zhang R et al (2009) Binding of 4-(N, N-dimethylamino)pyridine to Salen- and Salan-Cr(III) cations: a mechanistic understanding on the difference in their catalytic activity for CO2/epoxide copolymerization. Inorg Chem (Washington, DC, USA) 48:2830–2836
104. Lu X-B, Wang Y (2004) Highly active, binary catalyst systems for the alternating copolymerization of CO_2 and epoxides under mild conditions. Angew Chem Int Ed 43:3574–3577
105. Lu X-B, Shi L, Wang Y-M et al (2006) Design of highly active binary catalyst systems for CO_2/epoxide copolymerization: polymer selectivity, enantioselectivity, and stereochemistry control. J Am Chem Soc 128(5):1664–1674
106. Cohen CT, Coates GW (2006) Alternating copolymerization of propylene oxide and carbon dioxide with highly efficient and selective (salen)Co(III) catalysts: effect of ligand and cocatalyst variation. J Polym Sci Part A Polym Chem 44(17):5182–5191
107. Niu Y, Zhang W, Pang X et al (2007) Alternating copolymerization of carbon dioxide and propylene oxide catalyzed by (R, R)-SalenCoIII-(2,4-dinitrophenoxy) and Lewis-basic cocatalyst. J Polym Sci Part A Polym Chem 45(22):5050–5056
108. Qin Z, Thomas CM, Lee S et al (2003) Cobalt-based complexes for the copolymerization of propylene oxide and CO_2: active and for polycarbonate synthesis. Angew Chem Int Ed 42(44):5484–5487
109. Sugimoto H, Kuroda K (2008) The cobalt porphyrin-lewis base system: a highly selective catalyst for alternating copolymerization of CO_2 and epoxide under mild conditions. Macromolecules 41:312–317
110. Guo L, Wang C, Zhao W et al (2009) Copolymerization of CO_2 and cyclohexene oxide using a lysine-based (salen)CrIIICl catalyst. Dalton Trans 27:5406–5410
111. Darensbourg DJ, Bottarelli P, Andreatta JR (2007) Inquiry into the formation of cyclic carbonates during the (salen)CrX catalyzed CO_2/cyclohexene oxide copolymerization process in the presence of ionic initiators. Macromolecules 40(21):7727–7729
112. Darensbourg DJ, Phelps AL (2005) Effective, selective coupling of propylene oxide and carbon dioxide to poly(propylene carbonate) using (salen)CrN3 catalysts. Inorg Chem (Washington, DC, USA) 44(13):4622–4629
113. Darensbourg DJ, Mackiewicz RM (2005) Role of the cocatalyst in the copolymerization of CO_2 and cyclohexene oxide utilizing chromium salen complexes. J Am Chem Soc 127(40):14026–14038

114. Eberhardt R, Allmendinger M, Rieger B (2003) DMAP [4-(N, N-dimethylamino)pyridine]/Cr(III) catalyst ratio: the decisive factor for poly(propylene carbonate) formation in the coupling of CO_2 and propylene oxide. Macromol Rapid Commun 24(2):194–196
115. Darensbourg DJ, Mackiewicz RM, Rodgers JL et al (2004) Cyclohexene oxide/CO_2 copolymerization catalyzed by chromium(III) salen complexes and N-methylimidazole: effects of varying salen ligand substituents and relative cocatalyst loading. Inorg Chem (Washington, DC, USA) 43:6024–6034
116. Darensbourg DJ, Mackiewicz RM, Rodgers JL et al (2004) (Salen)CrIIIX catalysts for the copolymerization of carbon dioxide and epoxides: role of the initiator and cocatalyst. Inorg Chem (Washington, DC, USA) 43:1831–1833
117. Moore DR, Cheng M, Lobkovsky EB et al (2003) Mechanism of the alternating copolymerization of epoxides and CO_2 using β-diiminate zinc catalysts: evidence for a bimetallic epoxide enchainment. J Am Chem Soc 125(39):11911–11924
118. Cyriac A, Lee SH, Varghese JK et al (2010) Immortal CO_2/propylene oxide copolymerization: precise control of molecular weight and architecture of various block copolymers. Macromolecules 43(18):7398–7401
119. Noh EK, Na SJ, Sujith S et al (2007) Two components in a molecule: highly efficient and thermally robust catalytic system for CO_2/epoxide copolymerization. J Am Chem Soc 129 (26):8082–8083
120. Yoo J, Na SJ, Park HC et al (2010) Anion variation on a cobalt(III) complex of salen-type ligand tethered by four quaternary ammonium salts for CO_2/epoxide copolymerization. Dalton Trans 39(10):2622–2630
121. Na Sung J, Sujith S, Cyriac A et al (2009) Elucidation of the structure of a highly active catalytic system for CO_2/epoxide copolymerization: a salen-cobaltate complex of an unusual binding mode. Inorg Chem (Washington, DC, USA) 48(21):10455–10465
122. Ren W-M, Liu Z-W, Wen Y-Q et al (2009) Mechanistic aspects of the copolymerization of CO_2 with epoxides using a thermally stable single-site cobalt(III) catalyst. J Am Chem Soc 131(32):11509–11518
123. Zheng YQ, Lin JL, Zhang HL (2000) Crystal structure of zinc glutarate, Zn(C5H6O4). Zeitschrift fuer Kristallographie – New Crystal Struct 215(4):535–536
124. Ree M, Hwang Y, Kim J-S et al (2006) New findings in the catalytic activity of zinc glutarate and its application in the chemical fixation of CO_2 into polycarbonates and their derivatives. Catal Today 115:134–145
125. Eberhardt R, Allmendinger M, Zintl M et al (2004) New zinc dicarboxylate catalysts for the CO_2/propylene oxide copolymerization reaction: activity enhancement through zn(II)-ethylsulfinate initiating groups. Macromol Chem Phys 205(1):42–47
126. Zhu Q, Meng YZ, Tjong SC et al (2003) Catalytic synthesis and characterization of an alternating copolymer from carbon dioxide and propylene oxide using zinc pimelite. Polymer Int 52:799–804
127. Wang JT, Shu D, Xiao M et al (2006) Copolymerization of carbon dioxide and propylene oxide using zinc adipate as catalyst. J Appl Polym Sci 99:200–206
128. Klaus S, Lehenmeier MW, Herdtweck E et al (2011) Mechanistic insights into heterogeneous zinc dicarboxylates and theoretical considerations for CO_2-epoxide copolymerization. J Am Chem Soc 133:13151–13161
129. Lehenmeier M (2012) Synthese zweikerniger Zinkkatalysatoren zur Copolymerisation von Kohlenstoffdioxid und Epoxiden. Technische Universität München, Munich
130. Van Meerendonk WJ, Duchateau R, Koning CE et al (2005) Unexpected side reactions and chain transfer for zinc-catalyzed copolymerization of cyclohexene oxide and carbon dioxide. Macromolecules 38(17):7306–7313
131. Allen SD, Moore DR, Lobkovsky EB et al (2002) High-activity, single-site catalysts for the alternating copolymerization of CO_2 and propylene oxide. J Am Chem Soc 124(48):14284–14285

132. Rieth LR, Moore DR, Lobkovsky EB et al (2002) Single-site β-diiminate zinc catalysts for the ring-opening polymerization of β-butyrolactone and β-valerolactone to poly (3-hydroxyalkanoates). J Am Chem Soc 124:15239–15248
133. Eberhardt R, Allmendinger M, Luinstra GA et al (2003) The ethylsulfinate ligand: a highly efficient initiating group for the zinc β-diiminate catalyzed copolymerization reaction of CO_2 and epoxides. Organometallics 22:211–214
134. Lee BY, Kwon HY, Lee SY et al (2005) Bimetallic anilido-aldimine zinc complexes for epoxide/CO_2 copolymerization. J Am Chem Soc 127(9):3031–3037
135. Bok T, Yun H, Lee BY (2006) Bimetallic fluorine-substituted anilido-aldimine zinc complexes for CO_2/(cyclohexene oxide) copolymerization. Inorg Chem (Washington, DC, USA) 45(10):4228–4237
136. Jutz F, Buchard A, Kember MR et al (2011) Mechanistic investigation and reaction kinetics of the low-pressure copolymerization of cyclohexene oxide and carbon dioxide catalyzed by a dizinc complex. J Am Chem Soc 133(43):17395–17405
137. Kember MR, White AJP, Williams CK (2010) Highly active di- and trimetallic cobalt catalysts for the copolymerization of CHO and CO_2 at atmospheric pressure. Macromolecules 43:2291–2298
138. Buchard A, Kember MR, Sandeman KG et al (2011) A bimetallic iron(III) catalyst for CO_2/epoxide coupling. Chem Commun (Cambridge, UK) 47:212–214
139. Kember MR, Williams CK (2012) Efficient magnesium catalysts for the copolymerization of epoxides and CO_2; using water to synthesize polycarbonate polyols. J Am Chem Soc 134 (38):15676–15679
140. Lehenmeier MW, Kissling S, Altenbuchner PT et al (2013) Flexibly tethered dinuclear zinc complexes: a solution to the entropy problem in CO_2/epoxide copolymerization catalysis? Angew Chem Int Ed 52(37):9821–9826

Part II
Photocatalytic, Electrochemical and Inorganic Reactions

Chapter 8
Fixation of Carbon Dioxide Using Molecular Reactions on Flexible Substrates

Jacob Jensen and Frederik C. Krebs

8.1 Introduction

The largest chemical challenge in terms of scale is undoubtedly the control and management of carbon dioxide in the atmosphere. Due to annual man-made emissions of 24 gigaton CO_2, the atmospheric content of CO_2 has increased from 270 to 385 ppm. Totally this amounts to around 1 teraton excess carbon dioxide in the atmosphere stemming mainly from the combustion of fossil fuels [1]. This is a result of a very efficient and a highly distributed system for conversion of reduced forms of carbon into carbon dioxide (cars, households, etc.). The increased CO_2 generated by mankind is not balanced by an equal amount of fixation mainly due to deforestation. There is broad recognition worldwide that the emission of carbon dioxide must be brought down and preferably reverted such that a situation of a negative man-made carbon dioxide emission is reached. Currently the scale of that challenge exceeds our capacity for handling materials by several orders of magnitude, and developing solutions to this should be considered as a priority. Laboratory-scale catalysts are therefore not particularly useful unless they can be scaled to the required level without any carbon footprint. In addition to this problem, it is impossible to extract carbon dioxide directly from the atmosphere without generating more carbon dioxide in the process (i.e., the sequestration of 1 kg of carbon dioxide from the atmosphere will emit more than 1 kg of carbon dioxide). This fundamental problem has resulted in the passive view that man-made carbon dioxide emissions should be reduced but not reverted. This is done most efficiently by reducing carbon dioxide emissions directly at the source, e.g., flue gasses from coal fired power plants, iron smelters, and concrete factories. Extracting the carbon dioxide from the flue gasses is costly and the carbon sequestration and storage (CSS) costs can be as high as 50 % of the electricity costs.

J. Jensen • F.C. Krebs (✉)
Department of Energy Conversion and Storage, Technical University of Denmark, Frederiksborgvej 399, DK-4000 Roskilde, Denmark
e-mail: frkr@dtu.dk

B.M. Bhanage and M. Arai (eds.), *Transformation and Utilization of Carbon Dioxide*, Green Chemistry and Sustainable Technology, DOI 10.1007/978-3-642-44988-8_8,

In order to propose an efficient solution to the problem, one must use a renewable energy source to convert atmospheric carbon dioxide either for reuse of the stored energy or by fixation of it, thus reducing the amount of carbon dioxide in the atmosphere. The solar energy available at the surface of the Earth is around 1,000 $W \cdot m^{-2}$ (AM1.5G), and depending on the local climate, one can expect to receive between 1,000 and 2,000 kWh m^{-2} $year^{-1}$ from solar irradiation. Based on this, a rational approach seems to be one where sunlight is used to drive carbon dioxide converting reactions. In order to efficiently address the issue of scale, the development of chemical conversion systems must reflect this. A solution to this challenge is through the use of flexible substrates as carrier foils for the conversion agents. By employing flexible substrates, the large areas necessary for solar exposure conversion can be achieved through fast coating of low-cost photocatalysts or fixation agents using roll-to-roll processing at low temperatures. The following chapter will address the challenges encountered in utilizing this strategy.

8.2 Thermodynamical Considerations

The carbon dioxide molecule is linear and has two polar bonds between the electrophilic carbon and the nucleophilic oxygen atoms. CO_2 is a rather unreactive molecule, owing to the fact that it is in its most oxidized state. This is mirrored in the large standard enthalpy of formation at 298 K which is 393 $kJ \cdot mol^{-1}$ (reaction 8.1).

$$C + O_2 \rightarrow O{=}C{=}O \tag{8.1}$$

The stability of the CO_2 molecule requires that a large amount of energy is supplied in order for transformations to occur. Depending on the product, the energy requirements for reduction of CO_2 are as follows for carbon monoxide and methane:

$$CO_2 \rightarrow CO + \tfrac{1}{2}O_2 \quad \Delta H^\circ = 283\ kJ \cdot mol^{-1}; \quad \Delta G^\circ = 257\ kJ \cdot mol^{-1} \tag{8.2}$$

$$CO_2 + H_2O \rightarrow CH_4 + 2O_2 \quad \Delta H^\circ = 285\ kJ \cdot mol^{-1};$$

$$\Delta G^\circ = 237\ kJ \cdot mol^{-1} \tag{8.3}$$

For the Gibbs free energy to be zero, reaction (8.2) needs to be carried out at a minimum of 3,075 °C, if the process was to be accomplished thermochemically [2]. For this to be energetically viable, the energy should come from a renewable source, such as concentrated solar irradiation [3]. Such high temperatures are not compatible with the flexile substrate approach described in this chapter. For that approach to be useful, only low temperature (<100 °C) can be employed, and photocatalysis using transition metal oxide semiconductors is one way of achieving this.

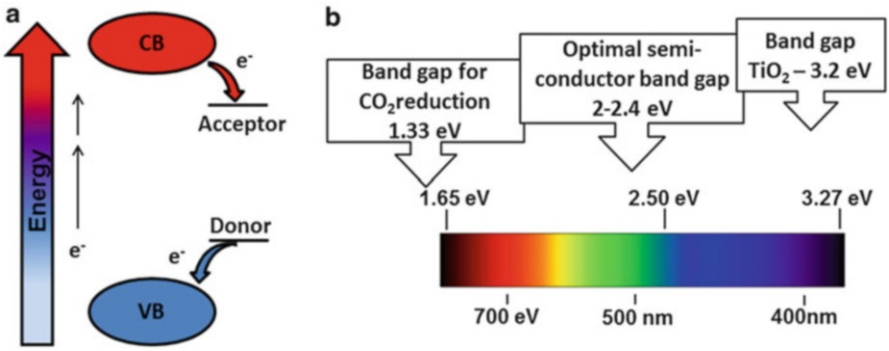

Fig. 8.1 The energy levels necessary for photocatalytic reduction. (**a**) Upon solar irradiation an electron is excited from the valence band (VB) to the conducting band (CB), from where it is accessible for reduction of an acceptor molecule (e.g., CO_2). The excitation creates an electron deficiency or hole in semiconductor. Simultaneously a donor molecule (e.g., water) donates an electron to the hole, completing the catalytic circle. (**b**) The visible part of the electromagnetic spectrum, showing the wavelength below and photon energies above. The *arrows* indicate the reduction potential of CO_2, the optimal band gap for practical purposes, and the band gap of TiO_2, respectively

8.2.1 Band Gap and Photocatalytic Properties

The basic process in photocatalysis is depicted in Fig. 8.1a. As semiconductors lack coherent energy levels, there is a void region between the valence band (VB) and the conducting band (CB), where energy transitions are not allowed, known as the band gap. If photons of energy equal to or higher than the band gap reaches the semiconductor surface, an electron is excited to the conducting band leaving behind a positively charged electron vacancy or hole (h^+). The energy levels at the bottom of the semiconductor conducting band is the reduction potential of the excited electron, while the top of the valence band is the oxidation potential of the holes generated [4]. The catalytic property of the semiconductor is the ability to simultaneously reduce one adsorbed species while oxidizing another. For reduction to occur, the reduction potential of the adsorbed species needs to be higher (more positive) than the conduction band of the photocatalyst, while oxidation requires the reduction potential (of the adsorbed species) be lower (more negative) than the energy of the valence band holes; this is shown in Fig. 8.1a. For carbon dioxide conversion, CO_2 is the acceptor molecule, while compounds such as hydrogen or water acts as donor molecules.

If reaction (8.2) is to occur by photocatalysis, the band gap of the photocatalyst should be at least 1.33 eV (per photon), which corresponds to wavelengths below 930 nm ($E(eV) = 1{,}240\ eV{\cdot}\lambda(nm)$). But as entropy changes and other losses associated with the splitting of CO_2 have to be taken into account, the optimal energy required per photon is in the region from 2 to 2.4 eV, see Fig. 8.1b [5]. Of the semiconductors commonly used, titanium dioxide is by far the most well studied. TiO_2 is found in several crystal forms, with anatase and rutile being the forms

usually employed for photocatalysis. Due to differences in lattice structures and electronic densities, anatase and rutile have different band gaps of 3.20 eV and 3.02 eV, respectively. This corresponds to absorption thresholds of 384 and 410 nm [4]. It is still unclear whether or not the band edges of TiO_2 is such that photocatalysis can occur without doping the catalyst, but it is our experience that photocatalytic reactions using unmodified TiO_2 are possible [4, 6–10].

8.3 Carbon Dioxide Conversion Reactors

In order to convert CO_2 into useful products, a suitable reactor needs to be developed. Ideally the source of CO_2 would come from the atmosphere, but since the amount of CO_2 in the atmosphere is approximately 0.04 %, the available CO_2 for conversion is low. Moreover, the conversion system risks being polluted by other atmospheric components such as volatile sulfur compounds. All in all purification of CO_2 must be accomplished before conversion. The carbon capture and sequestration technologies commonly used for CO_2 capture today are characterized by high energy consumption for desorption of CO_2, which makes using these technologies for purification of CO_2 in connection with photocatalytic reduction questionable. However, if efficient capture system like CO_2 diffusion selective membranes were employed, extraction from the atmosphere would be possible using a minimum amount of energy [11, 12]. Another solution is to use the Direct Air Capture (DAC) system, where air is cycled through solid alkali sorbents that binds the weakly acidic CO_2. The concentrated CO_2 becomes available by replacement by water at low temperatures (40–45 °C) [13]. By combining a membrane system with an appropriate photocatalyst or fixation reagent (roll-to-roll coated onto the polymer membrane), one can manufacture a large area foil that extracts CO_2 from the atmosphere and converts it to an energy-rich chemical form (e.g., a liquid fuel) when exposed to sunlight. A schematic for such a unit is shown in Fig. 8.2. In Fig. 8.2a, the conversion agent is coated onto a membrane that selectively allows CO_2 to permeate into the reaction chamber. The other side of the chamber consists of a window that allows sunlight to pass. The energy for conversion is supplied by solar irradiation, and products are recovered as liquid/gaseous energy carriers or as fixated precursors. A slightly different conversion unit is depicted in Fig. 8.2b, where CO_2 in a similar way is separated from the atmosphere by a membrane. The difference in this setup is that the conversion reagent is coated onto a flexible substrate that also functions as the reactor window.

The conversion unit suggested is a complex chemical system, and several issues must be solved in order for successful operation:

- Coating of conversion reagent
- Stability of window substrate
- Reactivity of conversion reagent
- Analysis of products

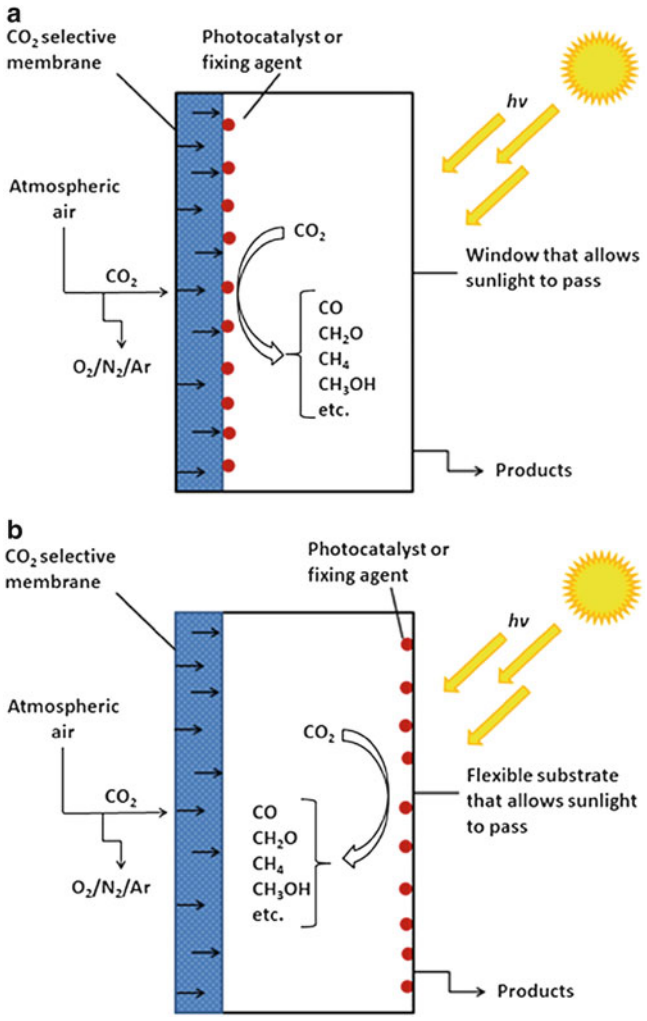

Fig. 8.2 Two examples of CO_2 conversion units that function by extraction of atmospheric CO_2 using a selective membrane. In (**a**) the conversion reagent is coated onto the membrane, whereas in (**b**) it is coated onto a flexible substrate that functions as the reactor window

To address these questions most efficiently, simple reactor designs that focus on one or two aspects are employed. An example of such a prototype is depicted in Fig. 8.3, which is comparable to similar reactors [10, 14, 15]. This reactor is made of a lathed aluminum chamber with an inner volume of 290 cm^3. In order to gain access to the chamber, changing of the front window, cleaning of the chamber, etc., the demountable top is removed by unscrewing, and it is tightly closed again by screwing the window against an o-ring gasket in the housing (see Fig. 8.3b, c).

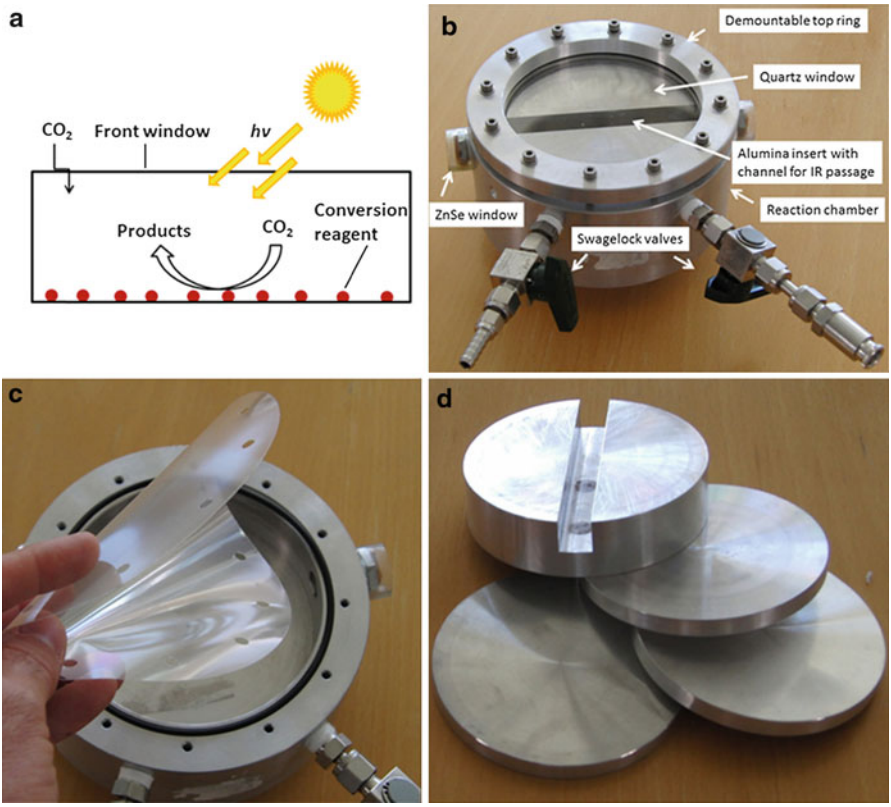

Fig. 8.3 (**a**) Schematic of simple prototype conversion unit. (**b**) An operational conversion reactor equipped with a quartz window. (**c**) PET foil to be used as reactor window. (**d**) Alumina inserts allowing variations in reactor volume

Introduction of gaseous components and flushing of the chamber are done through of Swagelock™ valves. Variation of the chamber volume is possible as blocks of aluminum were lathed to fit the chamber (see Fig. 8.3d). The chamber construction allows for several modes of usage as discussed previously (see schematics in Fig. 8.2). By placing the coated substrate inside the reactor facing out and using a window material that allows passage of solar irradiation, conditions like those in Fig. 8.2a are established. By choosing the appropriate material, the window can function as a solar filter, which is beneficial when optimizing operational parameters. A more unconventional operational mode, like that schematized in Fig. 8.2b, is to coat the conversion reagent onto the front window, which can be a flexible substrate like PET (Fig. 8.3c) or quarts (Fig. 8.3b).

8.3.1 Infrared Spectroscopy

The method of analysis is another thing that can successfully be integrated in the reactor design. In photocatalytic conversion reactors like the one in Fig. 8.3b, the products are generally gasses, which can be detected by either GC-MS or infrared spectroscopy [16–18]. The reactor in Fig. 8.3b is equipped with zinc-selenide (ZnSe) windows and makes use of in situ infrared spectroscopy for analysis. The setup is such that the reactor can be removed from the light source during operation. After IR analysis (<1 min), the reactor is placed back under the light source and irradiation is resumed. The use of in situ infrared spectroscopy was found particularly useful, being a nondestructive method that combines chemical fingerprinting with a reasonable sensitivity that enables detection of many different materials. As the products of photocatalytic CO_2 conversion are simple small molecules like CO, CH_4, and CH_3OH, the identification by IR is straightforward and can be a quantitative analytical tool by making standard calibration curves of components such as methane, formic acid, methanol, and carbon monoxide (the detection limit of CO using the reactor in Fig. 8.2b is around 0.01 %). Table 8.1 shows the major bands of some simple carbon volatiles [18–23].

Using isotopically labeled $^{13}CO_2$ is a particular useful way of distinguishing between reaction products formed from introduced carbon dioxide or carbon dioxide originating from sources such as the flexible substrate, surfactants, and catalyst precursor [25, 26]. The difference in the IR spectra of reduction products containing ^{13}C is determined using the harmonic equation [25].

In the case of carbon monoxide, the difference in IR spectra is shown in Fig. 8.4. Spectrum (A) displays the infrared spectrum of ^{12}CO, where the C–O stretching is centered at 2,143 cm^{-1}. This vibration has moved to 2,096 cm^{-1} in spectrum (B) that displays ^{13}CO. Spectrum C is a mixture of the two isotopes [10, 18, 20].

8.3.2 Adsorption of Carbon-Containing Volatiles

When designing reactor conversion reactors, one naturally has to think about the materials used. Using all quartz reactors is possible for small-scale reactors, but scaling these quickly becomes unsolvable, which is why most reactors consist of a chamber comprising a window. What might not be so obvious is that the gaseous components have the ability to adsorb onto the chamber surface and herby complicate the analysis of the products, when desorbing at a later stage. This was observed for the chamber in Fig. 8.3, where isotopically labeled $^{13}CO_2$ and ^{12}CO was detected in the reaction chamber devoid of any catalyst and after prolonged flushing with pure hydrogen gas and subsequent UV illumination. As a precaution, a flushing procedure aimed at desorbing CO_2 from the chamber surface prior to operation was installed. This consisted of heating the chamber to 65 °C for 60 min, flushing with hydrogen, and evaporation at reduced pressure; a procedure

Table 8.1 Major infrared bands for simple carbon volatiles. For additional spectral information, the reader is directed to the National Institute of Standards and Technology's Chemistry Webbook [24]

Compound	Major bands (cm^{-1})
CO_2	2,349
CO	2,143
CHO	2,850, 2,785, 1,750, 1,485, 1,250
CH_3OH	3,337, 2,934, 2,822, 1,029, 655
CH_4	3,020, 1,534, 1,305

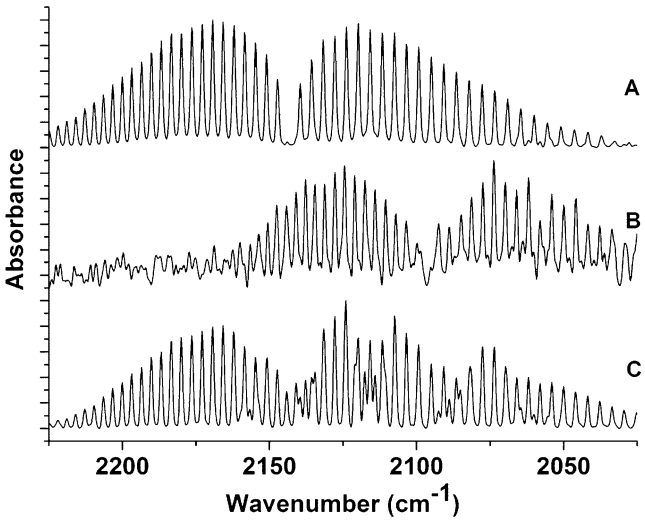

Fig. 8.4 Infrared absorbance spectra of gaseous carbon monoxide isotopes in argon (1 cm^{-1} resolution). (*a*) ^{12}CO. (*b*) ^{13}CO. (*c*) A mixture of ^{12}CO and ^{13}CO

that was repeated twice. $^{13}CO_2$ was believed to originate from earlier experiments performed in the reaction chamber as the aluminum surface was subjected to water vapor, oxygen, and light. Reaction conditions like these lead to the formation of alumina and aluminum hydroxide, which adsorbs volatiles such as CO_2 and CO [14, 27]; properties that has been exploited in carbon dioxide capture and sequestration processes. In addition, it has also been shown that a range of carbon-oxygen-containing species possibly resides on the alumina surface, including carbon monoxide that binds to Lewis acid sites on alumina, although to a lesser degree than carbon dioxide [28–30]. The complete desorption of carbon dioxide from alumina has been shown to take place at around 200 °C for mesoporous alumina and γ-alumina [31–33].

8.4 Coating

While numerous methods exist for depositing of material onto a substrate, energy considerations has to be acknowledged when developing devices that convert carbon dioxide. Employing energy-demanding deposition methods like sputtering, vacuum deposition, or thermal evaporation requires that the conversion agent is equally effective in order to compensate for the excessive energy used. Naturally all deposition methods require energy, but in order to avoid high CO_2 conversion requirements, the following section describes some of the deposition methods available that minimizes the impact on the energy balance. Common to these techniques are that a wet film of the dissolved material is formed upon deposition/coating, followed by evaporation of the solvent whereupon a thin film is formed. For laboratory scale, two established methods are spin- and spray coating, which are both facile with simple requirements to equipment. For spray coating, only a spray gun and a connection to pressurized gas are required (see Fig. 8.5). More advanced forms of this coating method are available, e.g., ultrasonic spray coating, thermal spray coating, and cold spray coating. In spray coating the dissolved photocatalyst is supplied to a nozzle where tiny aerosol droplets are formed when an inert gas (usually nitrogen or argon) is supplied. When vaporized the increased area of the droplets will cause partly evaporation of the solvent prior to impact. On impact the droplets are smashed and following the remaining solvent evaporate leaving behind a thin film of the desired material. Manually spray coating takes some practice as it is difficult to get an even film and it is preferable to use a solvent with a low vapor pressure, since this will increase the speed of evaporation. Solvents with high vapor pressures (e.g., chlorobenzene, dichlorobenzene) tend to produce uneven films due to streaks of runny solvents. Spray coating yields thin films with a rough surface, as it consists of clusters of materials (not necessarily in contact with other clusters). The surface roughness makes thickness determination troublesome, but the advantage of the roughness is an increased surface area that is beneficial in terms of photocatalytic activity.

Spray coating can be automatized and is in principle compatible with roll-to-roll coating. When spray coating it is preferable that the photocatalyst is dissolved prior

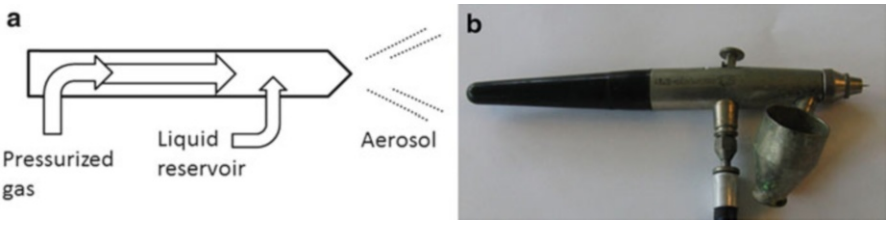

Fig. 8.5 (**a**) Schematic of a simple spray gun. The solution to be sprayed is supplied from a liquid reservoir and extruded through the nozzle as an aerosol by pressurized gas (typically N_2 or Ar). (**b**) Picture of a simple spray gun. This type has the reservoir directly attached to the gun

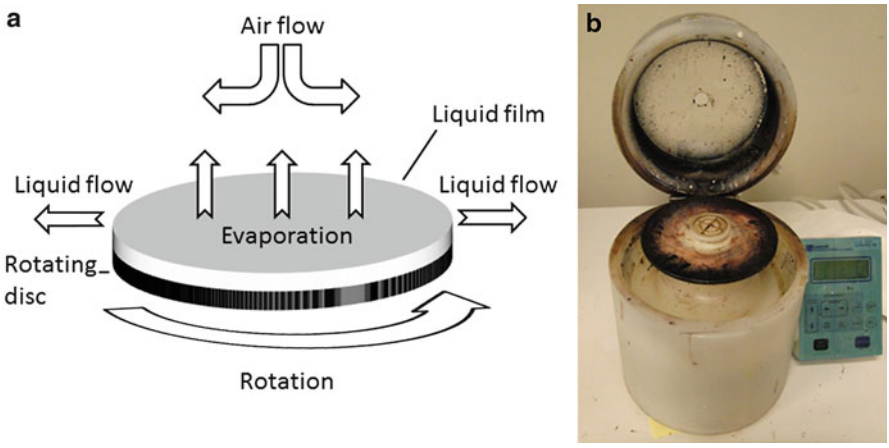

Fig. 8.6 (**a**) Schematic of the spin coating process. The ink to be spun cast is placed on the substrate prior to spinning and supplied while the substrate is in motion. By centrifugal forces, the ink is forced from the center of the disc to the edges. Evaporation of the solvent produces a thin solid film (Reproduced from Ref. [34] by permission of The Royal Society of Chemistry). (**b**) Picture of a spin coater. The substrate is put onto the rotating disc and held in place by vacuum while spinning. The panel on the left controls the rotational velocity and enables basic programming of the spin coater

to spraying, as the use of a slurry of precipitated photocatalyst will require a very low "concentration" equivalent of an increased amount of solvent.

Spin coating is another well-known technique that is fast, easy to use, and requires a minimum of equipment (see Fig. 8.6) [34]. An advantage of spin coating is that the results are highly reproducible, yielding films of identical thickness and morphology under identical conditions. These advantages make spin coating an excellent technique for small-scale laboratory experiments. The disadvantage is the large amount of material is wasted in the process, which makes this method very cost-inefficient and unsuitable for larger-scale production. In addition manually changing and cleaning substrates are time consuming.

While spin and spray coating are well suited for small-scale lab experiments, the disadvantages due to the large amount of manual work make them unsuited for larger-scale manufacturing tasks. Slot-die coating is ideally suited for this task as it is a fast and robust technique that is roll-to-roll compatible. In slot-die coating, the ink is dispersed onto a substrate through a coating head by a pump (see Fig. 8.7). The substrate is carried forward by a rotating drum. After solvent evaporation, a thin film is formed. The thickness of the film is controlled by ink concentration, rotational speed of the drum, and the speed of deposition. Laboratory-scale roll coaters enable limits on the amount of ink necessary for coating and are useful for optimizing procedures for larger-scale roll-to-roll equipment [35, 36].

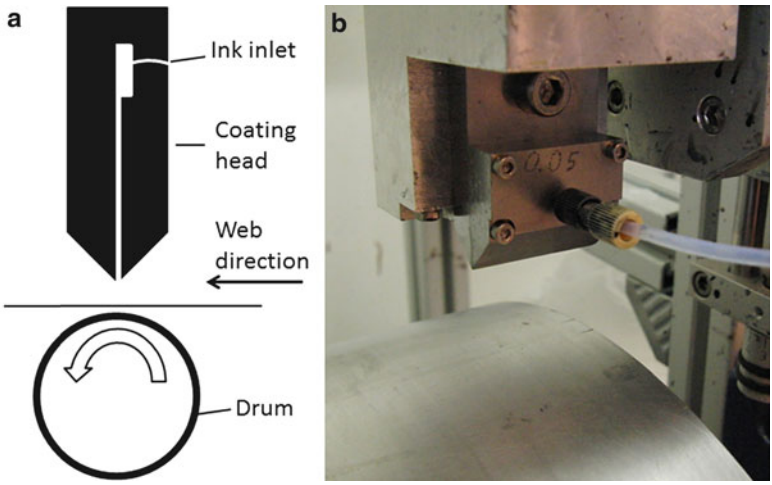

Fig. 8.7 (**a**) Schematic of the slot-die coating technique showing the coating head above the substrate. Following the inlet the ink is introduced into a small reservoir, where from it flows through void and is dispersed onto the substrate (Reprinted from Ref. [35], Copyright 2009, with permission from Elsevier). The substrate is carried forward by the rotating drum. (**b**) A picture of a slot-die coating head (*top*) with a tube attached to the ink inlet. Part of the rotating drum is seen at the *bottom* of the picture (no substrate attached)

8.4.1 Surfactants and Carbonaceous Residues

Inorganic photocatalysts usually require organic surfactants in order to meet the solubility requirement for the film-forming techniques described above. In addition to dissolution of the inorganic particles, the surfactants ensure the correct growth of the metal oxide nanoparticles and suppress aggregation, agglomeration, and precipitation [37–44]. The list of surfactants is extensive, and a few examples are given in Fig. 8.8.

Since the photocatalytic activity of a catalyst depend on the proper crystal phase of the catalyst, the surfactant group needs to be removed after coating. Of particular interest when working with flexible substrates is the removal of surfactants at low temperatures, as this allows for the exposure of the catalytic surface to reactants without thermal degradation of the polymer substrate. This can be done by exploiting the photooxidative abilities of TiO_2, whereby, e.g., oleic acid is decomposed to alkanes [45–49].

An example of photocatalytic removal of oleic acid on TiO_2 is given in Fig. 8.9. The graph shows the infrared spectra of TiO_2 nanoparticles in a KBr pellet during irradiation (1,200 $W \cdot m^{-1}$). The characteristic bands of oleic acid capped TiO_2 at 2,924, 2,852, 1,523, and 1,433 cm^{-1} are shown in spectrum A. Spectra B, C, and D shows the IR spectra after 60, 120, and 360 min of UV light, respectively. As seen from Fig. 8.5, the removal of oleic acid by UV light at low temperatures is a viable

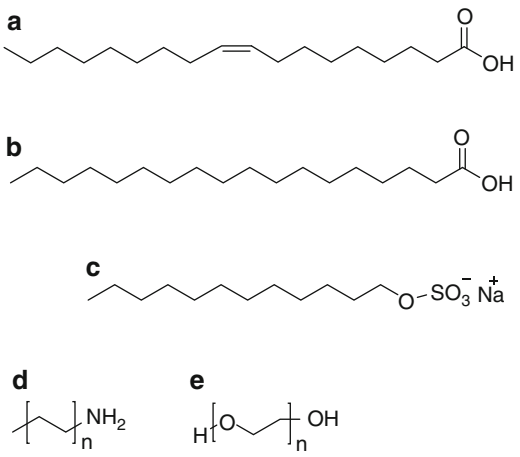

Fig. 8.8 Surfactants used for stabilization of photocatalyst nanoparticles. (**a**) Oleic acid, (**b**) stearic acid, (**c**) sodium dodecyl sulfate, (**d**) primary alkyl amines, (**e**) polyethylene glycol

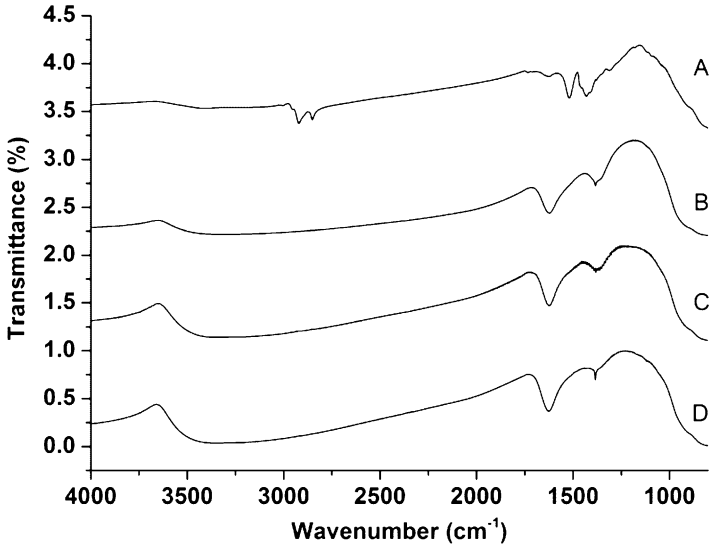

Fig. 8.9 Infrared analysis of the removal of oleic acid by UV-light. (*a*) Oleic acid capped TiO_2 particles prior to irradiation. (*b–d*) Sample following 60, 120, and 360 min of irradiation, respectively

process. The disappearance of the characteristic bands after a relatively short while (~60 min) leaves a broad band centered at 3,433 cm^{-1} and one at 1,626 cm^{-1}. The former is attributed to water adsorbed on titanium or hydroxyl groups; the latter is attributed to water adsorbed onto KBr. The presence of these bands is not disturbing, since water is introduced in the reaction chamber prior to the photochemical reaction [50, 51].

Fig. 8.10 Roll of flexible PET foil

Whether thermal or photocatalytic procedures are employed to decompose the surfactant group, it is important to realize the presence of carbonaceous residues on the catalyst surface following surfactant decomposition [52]. For oleic acid thermally decomposed in air, infrared analysis show absorption bands in the carbonyl region (2,200, 2,259 and 2,330 cm^{-1}), suggesting that the leftover residues are CO_x complexes [53]. In addition to the oxygen-containing species, amorphous carbon/graphite residues are formed when the decomposition takes place in an argon atmosphere, and alkane residues are believed to adsorb on the metal oxide surface beneath this graphite shell. The presence of carbon-containing species should be noted as they contribute to the complexity in analyzing the product mixture.

8.4.2 Flexible Substrates as Carrier Foils

By employing roll-to-roll coating of the photocatalyst onto flexible substrates, large area photocatalytic surfaces can be achieved at high production rates. The choice of substrate is wide as long as thin flexible foils are possible (see Fig. 8.10). Standard choices for roll-to-roll substrates are foils made of poly(ethylene terephthalate) (PET), poly(ethylene napthalate) (PEN), and poly(ethylene) (PE); the structures of these three polymer substrates are depicted in Fig. 8.11.

While employing flexible substrates is advantageous for large-scale manufacture and processing, there are questions that need to be addressed in order to use these as carrier foils for photochemical conversion of carbon dioxide. An obvious challenge is that polymeric films degrade when exposed to solar irradiation, oxygen, and moisture, i.e., conditions that are found outdoors where the photocatalytic system

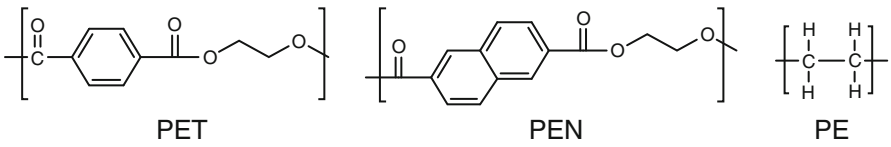

Fig. 8.11 Structure of poly(ethylene terephthalate) (*PET*), poly(ethylene napthalate) (*PEN*), and poly(ethylene) (*PE*). The figure shows the repeating unit of the polymeric structure

are to operate [54–59]. Moreover, as the oxidative degradation products include volatiles such as carbon dioxide and carbon monoxide, employing polymeric substrates for photoconversion of CO_2 could seem like Sisyphus' work [60–63]. In spite of this, polymeric substrates foils remain interesting as carrier foils since it is the total amount of carbon dioxide converted that matter, i.e., the amount of carbon dioxide photocatalytically converted or bound should be larger than the amount of oxidized carbon species released during substrate decomposition. Two other factors support this: (1) Coating of absorbing nanoparticle can in some instances protect the substrate material from solar irradiation. (2) By construction of a system that eliminates access to atmospheric oxygen. To assess the viability of polymeric substrates and aid in designing reactors for such, a short review of the fundamental degradation processes is appropriate.

It has been found that photodegradation of polymer substrates is a combination of two reactions: photolysis and photocatalytic oxidation [60, 63–70]. Photolysis is the "direct" cleavage, whereby photoinitiated radicals generated in the polymeric substrate lead to cleavage by, e.g., a Norrish type I reaction pathway as depicted in Scheme 8.2. Photooxidation is likewise initiated by radicals generated in the polymer but differs in that addition of oxygen generate hydroperoxide species that decompose as shown in Schemes 8.1 and 8.3 for PE and PET, respectively. Since photooxidation involves molecular oxygen, it should be possible to negate this reaction by employing an oxygen-free atmosphere. However, oxidation of the substrate has been found to occur even though oxygen-free conditions were employed [14]. This puzzling observation was attributed to the reduction of TiO_2 or residual substrate oxygen or carbon dioxide but do in any instance testify to the complexity of these chemical systems and the care that must be taken when evaluating results hereof.

Due to the difference in chemical composition of polyolefins (PE, PP, etc.) and polyesters (PET, PBT, etc.), the predominant degradation mechanism differs. Though multiple pathways might occur simultaneously, the predominant reaction for irradiated polyolefins in an oxygen-containing atmosphere is photocatalytic oxidation. This is due to the absence of chromophoric groups capable of absorbing energy from terrestrial sunlight (>290 nm), which result in insufficient energy for direct bond cleavage. However, light absorbing chromophores are found to develop in the films during processing and storage of polyolefins, which make generation of active intermediates on the surface possible. These react with oxygen and decompose as shown in Scheme 8.1 [66]. Since PET and related polyesters contain chromophoric groups as part of their molecular structure (aromatic and ester groups), they are

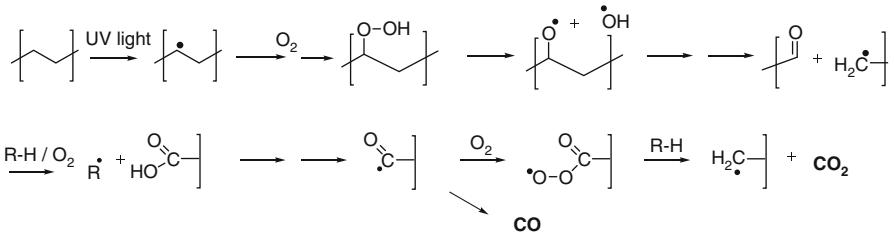

Scheme 8.1 Photooxidation of polyolefins. Reactive intermediates are generated on the surface of the substrate by UV irradiation. This is followed by addition of oxygen and proton abstraction to yield hydroperoxide species that decompose to carbonyl compounds and alkyl radicals. The alkyl radicals react further with oxygen to generate carbonyl radicals that decompose to CO or CO_2 via another sequence of oxygen addition and proton abstraction

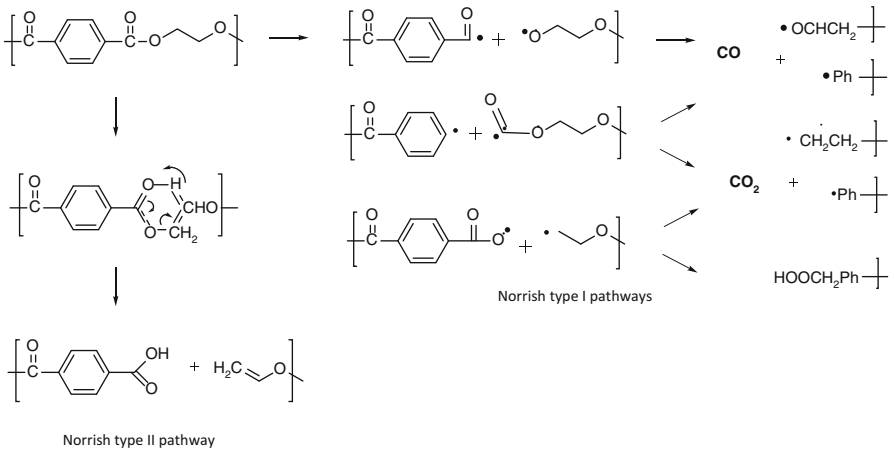

Scheme 8.2 Photolytic pathways for PET and related polyester substrates

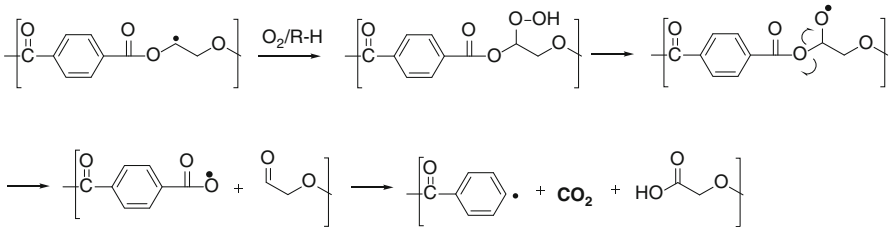

Scheme 8.3 Photocatalytic oxidation mechanism of PET and related polyesters

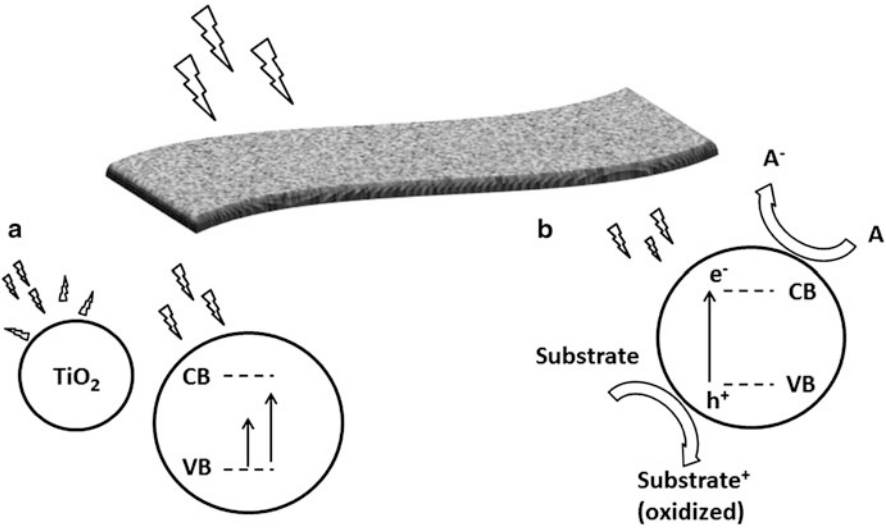

Fig. 8.12 Effect of TiO_2 nanoparticles on flexible substrates during irradiation. When flexible substrates are subjected to irradiation (*top*), the coated particles can affect the substrate in two ways. (**a**) Protect the substrate by scattering the irradiation or absorb irradiation without electron excitation. (**b**) Enhance photooxidation whereby the substrate donates electrons to the acceptor (designated A) via the photocatalyst

capable of absorbing high energy irradiation, which make them susceptible to direct photolytic cleavage that can proceed via Norrish type I or II pathways as illustrated in Scheme 8.2 [58, 60, 63–65].

While the photolytic cleavage is the predominant mechanism in PET and related polyesters, photooxidative decomposition is also observed analogous to that seen for polyolefins. Radical species, capable of reaction with oxygen, are produced in the surface by irradiation. This yields hydroperoxide species that decompose to various products including carbon dioxide (see Scheme 8.3) [14, 63, 71, 72].

8.4.3 Effect of TiO_2 Coatings

Chemical species on the substrate surface has been found to alter the photo and thermal stability, albeit the results of such coatings are ambiguous. On one hand, TiO_2 can attenuate decomposition and protect the substrate by scattering and absorbing UV irradiation. On the other hand, TiO_2 has been exploited in environmental management such as wastewater treatment and self-cleaning surfaces where it functions by photooxidizing organic molecules – a process that could enhance degradation in the substrate [45, 73–75]. The former situation is depicted in Fig. 8.12a, and the latter in Fig. 8.12b.

The effect of TiO_2 has been studied in some detail for paint (where TiO_2 is used as a filler/pigment) and films containing TiO_2. Results from these studies show that the effect depends on the crystal form of the oxide. Rutile TiO_2 contains stable OH groups on the surface and hence stabilize the substrate, whereas the anatase form of TiO_2 is reactive and consequently enhance photooxidation [14, 76–78]. Furthermore, commercially available foils contain various stabilizers, additives, and surfactants that could interact with TiO_2 and either enhance photooxidation or protection. In order to successfully convert small-scale laboratory experiments into large-scale photocatalytic systems, the atmosphere composition must be taken into account. Prior to operation, the amount of evolved CO_2 must be measured if flexible substrates are used as carrier foils. This is best done under CO_2-free conditions to be as reliable as possible, but at the same time the atmosphere should mimic the operational conditions as closely as possible. The operational conditions depend on the reactor and the concentration of CO_2 employed. But factors such as temperature and pressure are also of importance as described.

8.5 Conclusion and Perspectives

Photocatalytic reduction of CO_2 is a promising way of fighting the increasing content of atmospheric carbon dioxide, but as this technology is still being explored at laboratory scale, chances are that it takes several decades for efficient conversion systems to appear. For such a system to be effective, issues must be addressed that all relate to the enormous scale of the challenge.

The mechanism of photocatalytic reduction is not completely solved yet, even though qualified assumptions are plentiful. This leads to rough predictions on product composition, but most experiments seems to be on trial and error basis. As this chapter illustrates, monitoring CO_2 conversion is difficult. The adsorption-desorption of CO_2 from reactor surfaces, porous catalyst, foils, etc., combined with the fact that virtually any carbon-containing organic compound decomposes to CO_2 as an end product complicates the interpretation of experimental results and elucidation of the mechanism. By using isotopically labeled gases, true photocatalysis can be distinguished from reactions where the carbon source originates from adsorbed gasses or carbon-containing precursors.

The photocatalyst must be abundant, cheap, and chemically stable. These qualities are (among other transition metal oxides) found in TiO_2 possibly modified with dopants. But catalyst preparation is an issue that receives limited attention in connection with energy usage. Most catalysts require annealing at high temperatures for several hours to form an active crystal phase – an energy costly process that has to be repaid by catalytic action or carried out by using renewable energy, e.g., concentrated sunlight in solar ovens. The prize of manufacturing catalysts on a very large scale is also challenging, especially if doping with expensive metals such as platinum is required. To enhance the reactivity extension of the absorption (of the catalytic species) into the visible region of the electromagnetic spectrum

seems like a viable road forward if catalysts are to achieve conversion factors that outdo the manufacture of the catalytic species themselves.

Dispersion of photocatalytic species onto large areas is likewise an issue that needs addressing. We have, in this chapter, outlined the possibilities and difficulties in using flexible substrates as a solution. Flexible substrates can be coated with photocatalyst at a considerable rate and show promise to be compatible with membranes for carbon dioxide extraction. Roll-to-roll (R2R) coating is a low-tech method, which only requires moderate investments in equipment.

Construction of huge photocatalytic reactors is yet another challenge. Most reports are on laboratory size reactors, but this is very far from what is needed as the conditions under which tests are made. The challenge in going from the laboratory to the industrial scale seems to be huge, but it is definitely one that must be addressed.

References

1. Mikkelsen M, Jørgensen M, Krebs FC (2010) The teraton challenge. A review of fixation and transformation of carbon dioxide. Energy Environ Sci 3:43–81
2. Martin LR (1980) Use of solar energy to reduce carbon dioxide. Sol Energy 24:271–277
3. Traynor AJ, Jensen RJ (2002) Direct solar reduction of CO_2 to fuel: first prototype results. Ind Eng Chem Res 41:1935–1939
4. Carp O, Huisman CL, Reller A (2004) Photoinduced reactivity of titanium dioxide. Prog Solid State Chem 32:33–177
5. Varghese OK, Grimes CA (2008) Appropriate strategies for determining the photoconversion efficiency of water photoelectrolysis cells: a review with examples using titania nanotube array photoanodes. Sol Energy Mater Sol Cells 92:374–384
6. Lo C, Hung C, Yuan C, Wu J (2007) Photoreduction of carbon dioxide with H_2 and H_2O over TiO_2 and ZrO_2 in a circulated photocatalytic reactor. Sol Energy Mater Sol Cells 91:1765–1774
7. Roy SC, Varghese OK, Paulose M, Grimes CA (2010) Toward solar fuels: photocatalytic conversion of carbon dioxide to hydrocarbons. ACS Nano 4:1259–1278
8. Nguyen T, Wu JCS (2008) Photoreduction of CO_2 to fuels under sunlight using optical-fiber reactor. Sol Energy Mater Sol Cells 92:864–872
9. Linsebigler AL, Lu GQ, Yates JT (1995) Photocatalysis on TiO_2 surfaces – principles, mechanisms, and selected results. Chem Rev 95:735–758
10. Jensen J, Mikkelsen M, Krebs FC (2011) Flexible substrates as basis for photocatalytic reduction of carbon dioxide. Sol Energy Mater Sol Cells 95:2949–2958
11. Deng L, Hägg M (2010) Swelling behavior and gas permeation performance of PVAm/PVA blend FSC membrane. J Membr Sci 363:295–301
12. Nishimura A, Komatsu N, Mitsui G, Hirota M, Hu E (2009) CO_2 reforming into fuel using TiO_2 photocatalyst and gas separation membrane. Catal Today 148:341–349
13. Derichter RK, Ming T, Caillol S (2013) Fighting global warming by photocatalytic reduction of CO_2 using giant photocatalytic reactors. Renew Sustain Energy Rev 19:82–106
14. Jin C, Christensen PA, Egerton TA, Lawson EJ, White JR (2006) Rapid measurement of polymer photo-degradation by FTIR spectrometry of evolved carbon dioxide. Polym Degrad Stab 91:1086–1096
15. Robinson AJ, Searle JR, Worsley DA (2004) Novel flat panel reactor for monitoring photodegradation. Mater Sci Technol 20:1041–1048

16. Hong J, Zhang W, Ren J, Xu R (2013) Photocatalytic reduction of CO_2: a brief review on product analysis and systematic methods. Anal Methods 5:1086–1097
17. Su W, Fu X, Wei K, Zhang H, Lin H, Wang X, Li D (2001) Spectrum studies on titania photocatalysts. Guang Pu Xue Yu Guang Pu Fen Xi 21:34
18. Ulagappan N, Frei H (2000) Mechanistic study of CO_2 photoreduction in Ti silicalite molecular sieve by FT-IR spectroscopy. J Phys Chem A 104:7834–7839
19. Fredin L, Nelander B, Ribbegård G (1974) On the dimerization of carbon dioxide in nitrogen and argon matrices. J Mol Spectrosc 53:410–416
20. Mascetti J, Tranquille M (1988) Fourier transform infrared studies of atomic Ti, V, Cr, Fe, Co, Ni, and Cu reactions with carbon dioxide in low-temperature matrices. J Phys Chem 92:2177–2184
21. Burch DE, Williams D (1962) Total absorptance of carbon monoxide and methane in the infrared. Appl Optics 1:587–594
22. Falk M, Whalley E (1961) Infrared spectra of methanol and deuterated methanols in gas, liquid, and solid phases. J Chem Phys 34:1554–1568
23. Nelander B (1980) Infrared spectrum of the water formaldehyde complex in solid argon and solid nitrogen. J Chem Phys 72:77–84
24. Stein SE (2013) In: Linstrom J, Mallard WG (eds) NIST chemistry WebBook, NIST standard reference database 69. NIST, Gaithersburg, 20899
25. Yang C, Yu Y, Van Der Linden B, Wu JCS, Mul G (2010) Artificial photosynthesis over crystalline TiO_2-based catalysts: fact or fiction? J Am Chem Soc 132:8398–8406
26. Lin W, Han H, Frei H (2004) CO_2 splitting by H_2O to CO and O_2 under UV light in TiMCM-41 silicate sieve. J Phys Chem B 108:18269–18273
27. Kobayashi KLI, Shiraki Y, Katayama Y (1978) Study of adsorption phenomena on aluminium by interatomic Auger transition spectroscopy. I. Initial oxidation of Al. Surf Sci 77:449–457
28. Parkyns ND (1967) Surface properties of metal oxides. Part I. Infrared studies of the adsorption and oxidation of carbon monoxide on alumina. J Chem Soc A Inorg Phys Theor Chem:1910–1913. doi:10.1039/J19670001910
29. Mao C, Vannice MAS (1994) High surface area a-alumina. I. Adsorption properties and heats of adsorption of carbon monoxide, carbon dioxide, and ethylene. Appl Catal A Gen 111:151–173
30. Shiraki Y, Kobayashi KLI, Katayama Y (1978) Study of adsorption phenomena on aluminium by interatomic Auger transition spectroscopy. II. CO adsorption onto Al. Surf Sci 77:458–464
31. Chen C, Ahn W (2011) CO_2 capture using mesoporous alumina prepared by a sol-gel process. Chem Eng J 166:646–651
32. Morterra C, Magnacca G (1996) A case study: surface chemistry and surface structure of catalytic aluminas, as studied by vibrational spectroscopy of adsorbed species. Catal Today 27:497–532
33. Zhou Z, Zeng T, Cheng Z, Yuan W (2011) Preparation and characterization of titania-alumina mixed oxides with hierarchically macro-/mesoporous structures. Ind Eng Chem Res 50:883–890
34. Norrman K, Ghanbari-Siahkali A, Larsen NB (2005) Studies of spin-coated polymer films. Annu Rep Progr Chem Sect C 101:174–201
35. Krebs FC (2009) Fabrication and processing of polymer solar cells: a review of printing and coating techniques. Sol Energy Mater Sol Cells 93:394–412
36. Dam HF, Krebs FC (2012) Simple roll coater with variable coating and temperature control for printed polymer solar cells. Sol Energy Mater Sol Cells 97:191–196
37. Cozzoli PD, Kornowski A, Weller H (2003) Low-temperature synthesis of soluble and processable organic-capped anatase TiO_2 nanorods. J Am Chem Soc 125:14539–14548
38. Willis AL, Turro NJ, O'Brien S (2005) Spectroscopic characterization of the surface of iron oxide nanocrystals. Chem Mater 17:5970–5975

39. Satapathy S, Gupta PK, Srivastava H, Srivastava AK, Wadhawan VK, Varma KBR, Sathe VG (2007) Effect of capping ligands on the synthesis and on the physical properties of the nanoparticles of LiTaO3. J Cryst Growth 307:185–191
40. Liu GQ, Jin ZG, Liu XX, Wang T, Liu ZF (2007) Anatase TiO_2 porous thin films prepared by sol-gel method using CTAB surfactant. J Sol Gel Sci Technol 41:49–55
41. Kehres J, Andreasen JW, Krebs FC, Molenbroek AM, Chorkendorff I, Vegge T (2010) Combined in situ small- and wide-angle X-ray scattering studies of TiO_2 nanoparticle annealing to 1023K. J Appl Crystallogr 43:1400
42. Huo Q, Margolese DI, Ciesla U, Feng P, Gier TE, Sieger P, Leon R, Petroff PM, Schüth F, Stucky GD (1994) Generalized synthesis of periodic surfactant/inorganic composite materials. Nature 368:317–321
43. Li Z, Zhu Y (2003) Study on the surface-modification of TiO_2 nanoparticles. Appl Surf Sci 61:1484–1487
44. Shi X, Rosa R, Lazzeri A (2010) On the coating of precipitated calcium carbonate with stearic acid in aqueous medium. Langmuir 26:8474–8482
45. Parkin IP, Palgrave RG (2005) Self-cleaning coatings. J Mater Chem 15:1689–1695
46. Gohin M, Allain E, Chemin N, Maurin I, Gacoin T, Boilot J (2010) Sol-gel nanoparticulate mesoporous films with enhanced self-cleaning properties. J Photochem Photobiol A Chem 216:142–148
47. Kuai Q, Ye H, Gao Y (2010) Preparation of aluminum titanium pigments and its application in self-cleaning coating. Fenmo Yejin Cailiao Kexue yu Gongcheng 15:283–287
48. Rathouský J, Kalousek V, Kolář M, Jirkovský J, Barták P (2011) A study into the self-cleaning surface properties – the photocatalytic decomposition of oleic acid. Catal Today 161:202–208
49. Harwood HJ (1962) Reactions of the hydrocarbon chain of fatty acids. Chem Rev 62:99–154
50. Kang KS, Chen Y, Yoo KH, Jyoti N, Kim J (2009) Cause of slow phase transformation of TiO_2 nanorods. J Phys Chem C 113:19753–19755
51. Hao B, Li Y, Wang S (2010) Synthesis and structural characterization of surface-modified TiO_2. Adv Mater Res 129–131:154–158
52. Pradhan AR, Wu JF, Jong SJ, Tsai TC, Liu SB (1997) An ex situ methodology for characterization of coke by TGA and 13C CP-MAS NMR spectroscopy. Appl Catal A Gen 165:489–497
53. Roonasi P, Holmgren A (2009) A Fourier transform infrared (FTIR) and thermogravimetric analysis (TGA) study of oleate adsorbed on magnetite nano-particle surface. Appl Surf Sci 255:5891–5895
54. Gijsman P, Meijers G, Vitarelli G (1999) Comparison of the UV-degradation chemistry of polypropylene, polyethylene, polyamide 6 and polybutylene terephthalate. Polym Degrad Stab 65:433–441
55. Gulmine JV, Janissek PR, Heise HM, Akcelrud L (2003) Degradation profile of polyethylene after artificial accelerated weathering. Polym Degrad Stab 79:385–397
56. Hamid SH, Amin MB (1995) Lifetime prediction of polymers. J Appl Polym Sci 55:1385–1394
57. Day M, Wiles DM (1972) Photochemical degradation of poly(ethylene terephthalate). II. Effect of wavelength and environment on the decomposition process. J Appl Polym Sci 16:191–202
58. Day M, Wiles DM (1971) Photochemical decomposition mechanism of poly(ethylene terephthalate). J Pol Sci B 9:665–669
59. Kockott D (1989) Natural and artificial weathering of polymers. Polym Degrad Stab 25:181–208
60. Day M, Wiles DM (1972) Photochemical degradation of poly(ethylene terephthalate). III. Determination of decomposition products and reaction mechanism. J Appl Polym Sci 16:175–189
61. Philippart J, Posada F, Gardette J (1995) Mass spectroscopy analysis of volatile photoproducts in photooxidation of polypropylene. Polym Degrad Stab 49:285–290

62. Fernando SS, Christensen PA, Egerton TA, Eveson R, Martins-Franchetti SM, Voisin D, White JR (2009) Carbon dioxide formation during initial stages of photodegradation of poly (ethyleneterephthalate) (PET) films. Mater Sci Technol 25:549–555
63. Grossetete T, Rivaton A, Gardette JL, Hoyle CE, Ziemer M, Fagerburg DR, Clauberg H (2000) Photochemical degradation of poly(ethylene terephthalate)-modified copolymer. Polymer 41:3541–3554
64. Fechine GJM, Souto-Maior RM, Rabello MS (2007) Photodegradation of multilayer films based on PET copolymers. J Appl Polym Sci 104:51–57
65. Hurley CR, Leggett GJ (2009) Quantitative investigation of the photodegradation of polyethylene terephthalate film by friction force microscopy, contact-angle goniometry, and X-ray photoelectron spectroscopy. ACS Appl Mater Interfaces 1:1688–1697
66. Chew CH, Gan LM, Scott G (1977) Mechanism of the photo-oxidation of polyethylene. Eur Polym J 13:361–364
67. Gijsman P, Dozeman A (1996) Comparison of the UV-degradation chemistry of unstabilized and HALS-stabilized polyethylene and polypropylene. Polym Degrad Stab 53:45–50
68. Costa L, Luda MP, Trossarelli L (1997) Ultra high molecular weight polyethylene – II. Thermal- and photo-oxidation. Polym Degrad Stab 58:41–54
69. Lacoste J, Deslandes Y, Black P, Carlsson DJ (1995) Surface and bulk analyses of the oxidation of polyolefins. Polym Degrad Stab 49:21–28
70. Arnaud R, Moisan J, Lemaire J (1984) Primary hydroperoxidation in low-density polyethylene. Macromolecules 17:332–336
71. Rivaton A (1993) Photochemistry of poly(butyleneterephthalate): 2-Identification of the IR-absorbing photooxidation products. Polym Degrad Stab 41:297–310
72. Rivaton A (1993) Photochemistry of poly(butyleneterephthalate): 1-Identification of the IR-absorbing photolysis products. Polym Degrad Stab 41:283–296
73. Chong MN, Jin B, Chow CWK, Saint C (2010) Recent developments in photocatalytic water treatment technology: a review. Water Res 44:2997–3027
74. Fujishima A, Zhang X, Tryk DA (2008) TiO_2 photocatalysis and related surface phenomena. Surf Sci Rep 63:515–582
75. Hufschmidt D, Liu L, Selzer V, Bahnemann D (2004) Photocatalytic water treatment: fundamental knowledge required for its practical application. Water Sci Technol 49:135–140
76. Allen NS, Edge M, Corrales T, Catalina F (1998) Stabiliser interactions in the thermal and photooxidation of titanium dioxide pigmented polypropylene films. Polym Degrad Stab 61:139–149
77. Fechine GJM, Rabello MS, Souto-Maior RM (2002) The effect of ultraviolet stabilizers on the photodegradation of poly(ethylene terephthalate). Polym Degrad Stab 75:153–159
78. Allen NS, Khatami H, Thompson F (1992) Influence of titanium dioxide pigments on the thermal and photochemical oxidation of low density polyethylene film. Eur Polym J 28:817–822

Chapter 9
Reductive Conversion of Carbon Dioxide Using Various Photocatalyst Materials

Kojirou Fuku, Kohsuke Mori, and Hiromi Yamashita

9.1 Introduction

Although advances in science and technology have contributed to the development of society and have made people's lives increasingly comfortable, various environmental problems associated with technological advances have become global issues. In particular, global warming by greenhouse effect gas such as carbon dioxide (CO_2) and exhaustion of fossil fuels are already grave social problems of global dimensions. The catalytic conversion of CO_2 has widely been examined as one of the valuable approaches to solve these problems, but most of the processes require high temperature and pressures. However, various photocatalytic reactions have recently attracted considerable attention due to their milder reaction conditions (at room temperature and atmospheric pressure) and their ability to utilize solar light as inexhaustible energy source. Highly efficient and selective photocatalytic systems driven under sunlight and accompanied with a large positive change in the Gibbs free energy is of vital interest [1–8]. These reactions are considered to be an uphill reaction and are similar to the photosynthesis by green plants which produces glucose and oxygen from CO_2. The photocatalytic conversion of CO_2 emitted in large amounts into industrially beneficial compounds would be an alternative protocol from the viewpoints of *green and sustainable chemistry* by the solution of exhaustion of energy resources and global warming. Therefore, the development of efficient

K. Fuku
Division of Materials and Manufacturing Science, Graduate School of Engineering, Osaka University, 2-1 Yamada-oka, Suita, Osaka 565-0871, Japan

K. Mori • H. Yamashita (✉)
Division of Materials and Manufacturing Science, Graduate School of Engineering, Osaka University, 2-1 Yamada-oka, Suita, Osaka 565-0871, Japan

Elements Strategy Initiative for Catalysts Batteries ESICB, Kyoto University, Katsura, Kyoto 615-8520, Japan
e-mail: yamashita@mat.eng.osaka-u.ac.jp

B.M. Bhanage and M. Arai (eds.), *Transformation and Utilization of Carbon Dioxide*, Green Chemistry and Sustainable Technology, DOI 10.1007/978-3-642-44988-8_9,

photocatalytic systems enabling reduction and/or fixation of CO_2 is the most desirable and challenging goal [2, 3].

The utilization of solar energy for the conversion of CO_2 can be realized by considering the photocatalytic reduction and/or fixation of CO_2 into CO, HCOOH, CH_3OH, and CH_4, etc., by the active photocatalysts such as TiO_2, $SrTiO_3$, ZnO, or SiC semiconductors. Inoue and Fujishima et al. have first reported that HCOOH, HCHO, and CH_3OH are produced under irradiation of aqueous suspension systems involving a variety of semiconductor powders or single crystals [9]. Although the pioneering works on the photoreduction of CO_2 on semiconductors in aqueous suspension systems were summarized by Halmann, the efficiency was low when H_2O was used as the reductant [10]. Substantially improved yields of CH_3OH and CH_4 from CO_2 with H_2O have been reported by us, in which photocatalytic reactions successfully proceed in solid–gas systems at room temperature on isolated tetrahedral Ti centers of macro- or mesoporous silicate sieves instead of dense phase powdered TiO_2 materials [2, 3, 11–22]. We focus on the characteristic features of photocatalytic reduction and/or fixation of CO_2 with H_2O on various types of active titanium oxide catalysts under heterogeneous gas–solid conditions.

This review report about our approach on the efficient reduction and/or fixation of CO_2 using various titanium oxide photocatalysts. Additionally, other novel and unique systems enabling efficient conversion of CO_2 using various oxide semiconductors other than titanium oxide or localized surface plasmon resonance-enhanced photocatalysis are also introduced.

9.2 Various Titanium Oxide Photocatalysts

As shown in Fig. 9.1, the electronic properties as well as the photocatalytic activity of titanium oxide photocatalysts dramatically change depending on their local structure, from an extended semiconducting structure to nano-sized, extremely small nanoparticles and molecular-sized titanium oxide species. In the case of the bulk TiO_2 materials, photochemical excitation leads to charge separation in the particle, in which electrons (e^-) are promoted to the conduction band (cb) and holes (h^+) are left in the valence band (vb) upon light irradiation. The generated hole in the valence band and the conduction band electron can react with electron donors and electron acceptors adsorbed on the titanium oxide surface, respectively. On the contrary, the Ti-oxide moieties, which are spatially separated from each other, can be implanted and isolated in the silica matrixes of microporous zeolite and mesoporous silica materials at the atomic level, and have been named as “single-site photocatalysts.” The isolated Ti atoms can be substituted with Si atoms in the silica matrixes ($Si/Ti > 30$) and coordinated tetrahedrally with oxygen atoms. Such single-site catalysts can be simply synthesized by various anchoring techniques, such as hydrothermal synthesis, sol–gel method, and chemical vapor deposition, and are stable as far as the silica matrixes keep their porous structures. In the case of the isolated and tetrahedrally coordinated Ti-oxide moiety, excitation by UV irradiation brings about an electron transfer from the oxygen (O^{2-}) to Ti^{4+} ions, resulting in the

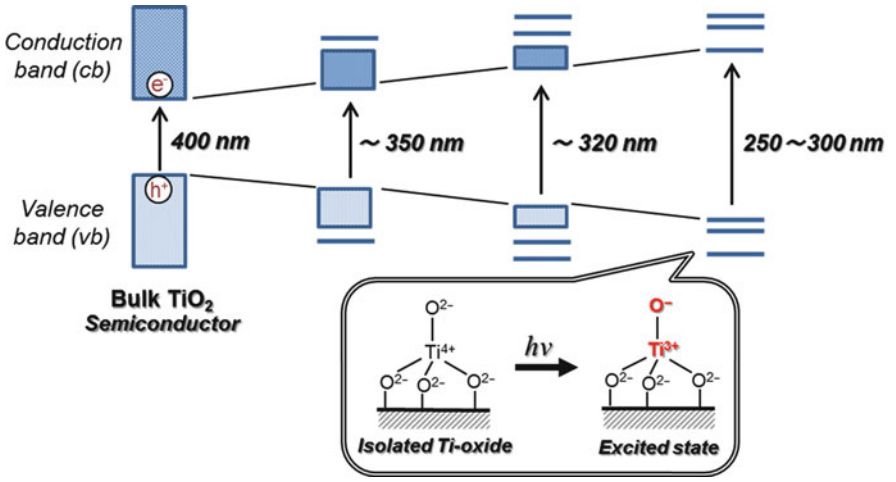

Fig. 9.1 The electronic state change in the titanium oxide photocatalysts from semiconducting bulk TiO_2 to the isolated Ti-oxide molecular species

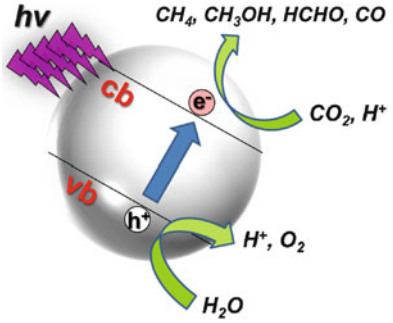

Fig. 9.2 Reaction scheme for the photocatalytic reduction of CO_2 with H_2O on bulk TiO_2

formation of pairs of trapped hole centers (O^-) and electron centers (Ti^{3+}). Such charge-transfer excited state, i.e., the excited electron–hole pair state which localizes quite near to each other as compared to the electron and hole produced in semiconducting materials, plays a significant role in various photocatalytic reactions.

The efficiency for the photocatalytic reduction and/or fixation of CO_2 with H_2O to produce CH_4 and CH_3OH strongly depends upon the type of the employed titanium oxide photocatalysts [11–22]. The primary processes on semiconducting TiO_2 photocatalysts are illustrated in Fig. 9.2. The band gap between the conduction band and the valence band becomes larger as the particle size of the semiconducting TiO_2 decreased, making it suitable and applicable to the reduction of CO_2 [2, 3]. For extremely fine TiO_2 particles less than 10 nm in diameter, the size quantum effect and/or the effects of the surface modification in its coordination geometry plays a significant role in the appearance of unique activity. Consequently, the electrons and holes which are produced by UV-light irradiation within the ultrafine particles of TiO_2 and the highly dispersed titanium oxide species exhibit more unique and high activities compared to those produced in large particle TiO_2 photocatalysts.

9.3 Small Particle TiO_2 Photocatalysts

UV irradiation of the powdered TiO_2 catalysts in the presence of a gaseous mixture of CO_2 and H_2O led to the evolution of CH_4 at 275 K, accompanied with the formation of trace amounts of C_2H_4 and C_2H_6 [13, 14]. The yields of these products increased with the UV-irradiation time, while no products were detected under dark conditions. The CH_4 yield was almost zero in the reaction of CO_2 without H_2O and increased with increasing the amount of H_2O. These results suggest that the photocatalytic reduction of CO_2 to produce CH_4 and C_2 compounds takes place photocatalytically in the solid–gas phase systems. The formation of CH_4 as the main product has also been observed by Saladin et al., and the partially reduced TiO_2 species formed under UV irradiation is proposed as an active species [23].

The yields of CH_4 formation in the photocatalytic reduction of CO_2 with H_2O on several TiO_2 photocatalysts with different physicochemical property are shown in Table 9.1. The photocatalytic activity, based on the CH_4 yields, was found to depend on the type of TiO_2 catalyst, in the order of JRC-TIO-4 > -5 > -2 > -3 [14]. This tendency corresponds with that in the photocatalytic hydrogenation of methyl acetylene with H_2O, proving that the reduction of CO_2 with H_2O undoubtedly occurs photocatalytically activated powdered TiO_2 catalyst [24, 25]. It is likely that the anatase-type TiO_2 possessing a large band gap as well as numerous surface –OH groups is preferable for efficient photocatalytic reactions. The band gap increase is accompanied by a shift in the conduction band edge to higher energy levels. This shift causes the reductive potential to shift to more negative values, which ultimately causes a great enhancement in the photocatalytic activity. The surface –OH groups and/or physisorbed H_2O also play a significant role in photocatalytic reactions via the formation of OH radicals and H radicals.

Preliminary studies by ESR measurement provide an insight into the reaction pathway. The ESR signals obtained under UV irradiation of the anatase-type TiO_2 catalyst in the presence of CO_2 and H_2O at 77 K can be ascribed to the characteristic photogenerated Ti^{3+} ions ($g_\perp = 1.9723$ and $g_\parallel = 1.9628$) and H radicals (with 490 G splitting), as well as CH_3 radicals having a hyperfine splitting ($H\alpha = 19.2$ G, $g = 2.002$) [14]. The signal intensity of CH_3 radicals decreased with increasing the amount of H_2O, indicating that CH_3 radicals are the intermediate species and react with H radicals that are formed by the reduction of protons (H^+) originated from H_2O adsorbed on the catalyst.

Table 9.1 Textural property and photocatalytic activity of TiO_2 catalysts

Catalyst	Crystal structure[a]	S_{BET} (m^2/g)	CO_2 ads. (μmol/g)	Relative –OH conc.	Band gap (eV)	Reduction of CO_2[b] (μmol/h·g)	Hydrogenation of methyl acetylene (μmol/h·g)
JRC-TIO-2	A	16	1	1	3.47	0.03	0.20
JRC-TIO-3	R	51	17	1.6	3.32	0.02	0.12
JRC-TIO-4	A	49	10	3.0	3.50	0.27	8.33
JRC-TIO-5	R	3	0.4	3.1	3.09	0.04	0.45

[a]A, anatase; R, rutile

[b]CH_4 yield in the reaction of CO_2 (0.12 mmol) and H_2O (0.37 mmol) for 6 h

9.4 Metal-Loaded TiO_2 Photocatalysts

The effect of metal loading on the photocatalytic reduction of CO_2 with H_2O on TiO_2 catalysts was investigated [14]. In the case of the Cu/TiO_2 photocatalyst (0.3–1.0 wt%), CH_4 yield was suppressed, but a new formation of CH_3OH could be observed. Characterization by XPS reveals that the main species of copper in the catalyst is 1+ oxidation state. It has been also reported that Cu^+ catalysts play a significant role in the photoelectrochemical production of CH_3OH from CO_2 and H_2O system [26]. Following the photocatalytic reduction, the Cu/TiO_2 catalysts exhibited a new peak at 299 eV in the C(1) XPS spectra, suggesting that carboxylate groups which accumulated on the catalyst may be the primary intermediate species for this reaction.

Further detailed study was performed by Gunlazuardi et al. by systematically varying the Cu loading on TiO_2 [27]. The CH_3OH yield increased with Cu loading, and the highest yield can be achieved by 3 % Cu/TiO_2, which was three times higher than the original TiO_2. Cu can serve as an electron trapper and prohibits the recombination of electron and hole, significantly increasing photoefficiency. However, catalysts with more than 3 wt% Cu loading do not further increase the CH_3OH yield due to its shading effects, consequently reducing the photo-exciting capacity of TiO_2. The activation energy for 3 % Cu/TiO_2 and the original TiO_2 was determined to be 12 and 26 kJ/mol, respectively. The apparent lower activation energy of 3 % Cu/TiO_2 catalyst indicates that the Cu also acts as active species to provide CH_3OH and enhances the photoefficiency of TiO_2 photocatalysts.

In the case of the Pt/TiO_2, the yield of CH_4 increased remarkably when the amount of Pt was increased (0.1–1.0 wt%), but the addition of excess Pt was undesirable for an efficient reaction [13]. Regarding the reaction intermediates, Solymosi et al. have observed the formation of CO_2^- species in bent form under UV irradiation of the Rh/TiO_2 in the presence of CO_2 using FT-IR [28]. The electron transfer from the irradiated catalyst to the adsorbed CO_2 takes place, resulting in the formation of a CO_2^- anion as the key step in the photochemical reduction of CO_2 using metal-loaded TiO_2 semiconductor.

9.5 TiO_2 Single Crystals

With a well-defined catalyst surface such as a single crystal, detailed information on the reaction mechanism can be obtained at the molecular level [2, 15]. Therefore, the photocatalytic reduction of CO_2 with H_2O on rutile-type TiO_2 (100) and TiO_2 (110) single crystal surfaces has been performed [15]. As shown in Table 9.2, the efficiency and selectivity of the photocatalytic reactions strongly depend on the type of TiO_2 single crystal surface. UV irradiation of the TiO_2 (100) single crystal catalyst in the presence of a mixture of CO_2 and H_2O led to the evolution of both CH_4 and CH_3OH at 275 K, whereas only CH_3OH was detected with the TiO_2 (110) single crystal catalyst.

Table 9.2 Yields of the formation of CH_4 and CH_3OH in the photocatalytic reduction of CO_2 (124 μmol g^{-1}) with H_2O (372 μmol g^{-1}) at 275 K

Single crystal of TiO_2	Yield of CH_3OH (μmol/h·g-cat)	Yield of CH_4 (μmol/h·g-cat)
(100)	2.4	3.5
(110)	0.8	0

It is likely that the photogenerated electrons localizing on the surface sites of the excited TiO_2 play a significant role in the photoreduction of CO_2 molecules into intermediate carbon species [2, 15]. The surface Ti atoms may act as a reductive site. According to the surface geometric models for TiO_2 (100) and TiO_2 (110), the atomic ratio (Ti/O) of the top-surface Ti and O atoms, which have geometric spaces large enough to have direct contact with CO_2 and H_2O molecules, is higher on TiO_2 (100) than on TiO_2 (110) surface. In the excited state, the surface with a higher Ti/O surface ratio, i.e., TiO_2 (100), exhibits a more reductive tendency than TiO_2 (110). Such a reductive surface allows a more facile reduction of CO_2 molecules especially for the formation of CH_4. In the HREELS spectrum of a clean TiO_2(100) single crystal surface after UV irradiation in the presence of CO_2 and H_2O, two peaks due to the C–H stretching vibration of the CH_x species and the O–H stretching of the surface hydroxyl groups at around 2,920 and 3,630 cm^{-1}, respectively. On the other hand, only a weak peak assigned to the O–H stretching vibration was observed without UV irradiation, suggesting that UV-light irradiation is indispensable for attaining CO_2 reduction and the formation of the active H and CH_x species.

9.6 Ti-Oxide Anchored on Zeolite (Ion Exchange)

The photocatalyst systems incorporated within the zeolite cavities and frameworks have been proven to be effective for various reactions [29–32]. The Ti-oxide anchored onto zeolite, Ti-oxide/Y-zeolite (1.1 wt% as TiO_2), was prepared by ion exchange with an aqueous titanium ammonium oxalate solution using Y-zeolite ($SiO_2/Al_2O_3 = 5.5$) (ex-Ti-oxide/Y-zeolite) [16–18].

Figure 9.3 shows the Ti K-edge XANES and the Fourier transformation of EXAFS (FT-EXAFS) spectra of the Ti-oxide/Y-zeolites. The XANES spectra of the bulk TiO_2 powder give rise to several well-defined pre-edge peaks attributable to the titanium in a symmetric octahedral environment [33]. The ex-Ti-oxide/Y-zeolite exhibits an intense single pre-edge peak at 4,967 eV, suggesting that the Ti-oxide species exist in a tetrahedral coordination [1–3]. On the other hand, the imp-Ti-oxide/Y-zeolite prepared by the impregnation exhibits three characteristic weak pre-edge peaks attributed to crystalline TiO_2. The FT-EXAFS spectra of the ex-Ti-oxide/Y-zeolite exhibit only peak at around 1.6 Å assigned to the neighboring oxygen atoms (Ti–O) indicating the presence of an isolated Ti-oxide species. These findings indicate that highly dispersed isolated tetrahedral Ti-oxide species are formed on the ex-Ti-oxide/Y-zeolite. On the other hand, the imp-Ti-oxide/Y-zeolite exhibits an intense peak

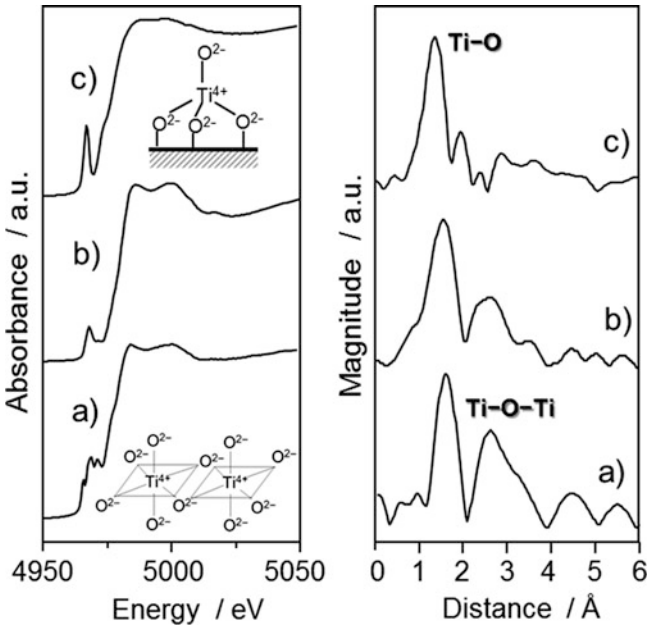

Fig. 9.3 Ti K-edge XANES and FT-EXAFS spectra of anatase TiO_2 powder (*a*), imp-Ti-oxide/Y-zeolite (10.0 wt% as TiO_2) (*b*), and the ex-Ti-oxide/Y-zeolite (*c*)

assigned to the neighboring titanium atoms (Ti–O–Ti) suggestive of the aggregation of the Ti-oxide species.

The photoluminescence spectra of the ex-Ti-oxide/Y-zeolite at 77 K are shown in Fig. 9.4. Excitation by light at around 250–280 nm brought about an electron transfer from the oxygen to titanium ion, resulting in the formation of pairs of the trapped hole center (O^-) and an electron center (Ti^{3+}) [1–3]. The observed photoluminescence is attributed to the radiative decay process from the charge-transfer excited state of the Ti-oxide moieties in a tetrahedral coordination geometry, $(Ti^{3+}—O^-)^*$, to their ground state [34, 35]. The addition of H_2O or CO_2 molecules onto the anchored Ti-oxide species leads to the efficient quenching of the photoluminescence. Such an efficient quenching suggests not only that tetrahedrally coordinated Ti-oxide species locate at positions accessible to the added CO_2 or H_2O but also that CO_2 or H_2O interacts and/or reacts with the Ti-oxide species in both its ground and excited states. Because the addition of CO_2 led to a less effective quenching than that with the addition of H_2O, the interaction of the emitting sites with CO_2 was weaker than that with H_2O.

UV irradiation of powdered TiO_2 and Ti-oxide/Y-zeolite catalysts in the presence of a mixture of CO_2 and H_2O led to the evolution of CH_4 and CH_3OH at 328 K, as well as trace amounts of CO, C_2H_4, and C_2H_6 [16–18]. The specific photocatalytic activities for the formation of CH_4 and CH_3OH are shown in Fig. 9.5. The ex-Ti-oxide/Y-zeolite exhibits a high activity and a high selectivity for the formation of CH_3OH, while the formation of CH_4 was predominated on bulk TiO_2 as well as on

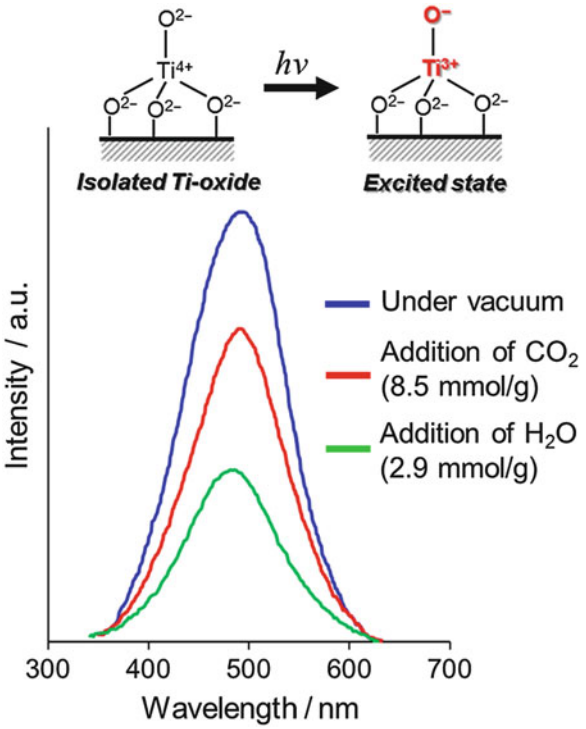

Fig. 9.4 Photoluminescence spectrum of the ex-Ti-oxide/Y-zeolite catalyst (a) and the effects of the addition of CO_2 and H_2O. Measured at 77 K, excitation at 290 nm, and emission monitored at 490 nm

the imp-Ti-oxide/Y-zeolite. The deposition of Pt improved the photocatalytic activity, but the CH_3OH selectivity significantly decreased. These findings clearly suggest that the tetrahedrally coordinated Ti-oxide species act as active photocatalysts for the reduction of CO_2 with H_2O exhibiting a high selectivity toward CH_3OH.

UV irradiation of the anchored Ti-oxide catalyst in the presence of CO_2 and H_2O at 77 K led to the appearance of ESR signals due to the Ti^{3+} ions, H atoms, and carbon radicals [2, 3]. After the disappearance of these ESR signals in this system at around 275 K, the formation of CH_4 and CH_3OH was observed. From these results, the reaction mechanism in the photocatalytic reduction of CO_2 with H_2O on the highly dispersed Ti-oxide catalyst can be proposed as shown in Scheme 9.1: CO_2 and H_2O molecules interact with the excited state of the photoinduced $(Ti^{3+}—O^{-})^*$ species and the reduction of CO_2 and the decomposition of H_2O proceed competitively. Furthermore, H atoms and OH• radicals are formed from H_2O and such radicals react with the carbon species formed from CO_2 to produce CH_4 and CH_3OH.

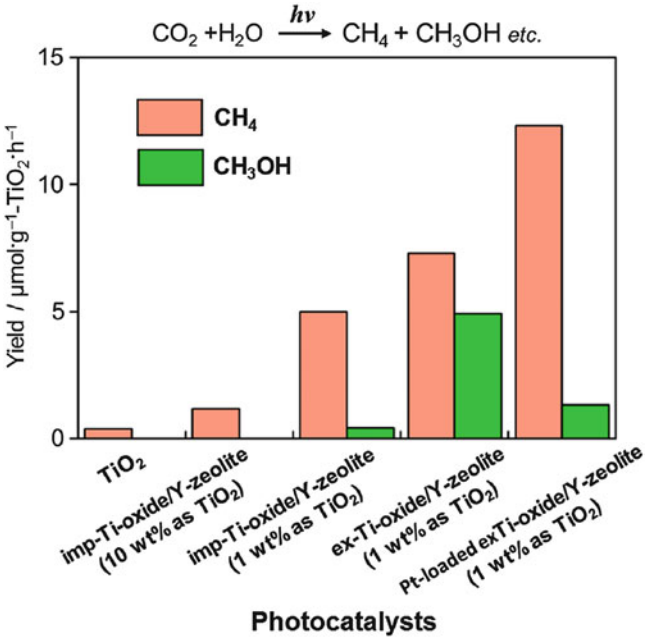

Fig. 9.5 The product distribution of the photocatalytic reduction of CO_2 with H_2O on anatase TiO_2 powder, the imp-Ti-oxide/Y-zeolite (10 wt% as TiO_2), the imp-Ti-oxide/Y-zeolite (1 wt% as TiO_2), the ex-Ti-oxide/Y-zeolite (1 wt% as TiO_2), and the Pt-loaded ex-Ti-oxide/Y-zeolite catalysts

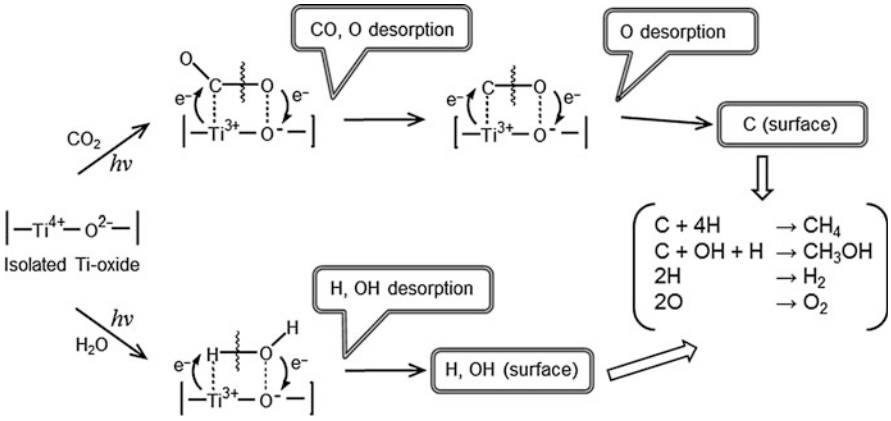

Scheme 9.1 Schematic illustration of the photocatalytic reduction of CO_2 with H_2O on the anchored titanium oxide species

9.7 Ti-Containing Zeolite and Mesoporous Molecular Sieves

The Ti-oxide species prepared within the ordered silica frameworks have revealed a unique local structure as well as a high selectivity in the oxidation of organic substances with hydrogen peroxide [34–36]. Hydrothermally synthesized Ti-containing zeolites (TS-1, Ti-Beta) and mesoporous molecular sieves (Ti-MCM, Ti-HMS, Ti-FSM) have been subjected to the photocatalytic reduction CO_2 with H_2O [18–22, 36–38].

In situ photoluminescence, ESR, UV–VIS and XAFS investigations indicated that the Ti-oxide species in the Ti-mesoporous molecular sieves (Ti-MCM-41 and Ti-MCM-48) and in the TS-1 zeolite are highly dispersed within the zeolite framework and exist in a tetrahedral coordination. Upon excitation with UV light at around 250–280 nm, these catalysts exhibit photoluminescence spectra at around 480 nm. The addition of CO_2 or H_2O onto these catalysts results in a significant quenching of the photoluminescence, suggesting the excellent accessibility of the CO_2 and H_2O to the Ti-oxide species [18–21].

UV irradiation of the Ti-mesoporous molecular sieves and the TS-1 zeolite in the presence of CO_2 and H_2O also led to the formation of CH_3OH and CH_4 as the main products [18–21]. The yields of CH_3OH and CH_4 per unit weight of the Ti-based catalysts are shown in Fig. 9.6. It can be seen that Ti-MCM-48 exhibits much higher activity than either TS-1 or Ti-MCM-41. The higher activity and selectivity for the formation of CH_3OH attained with the Ti-MCM-48 than that with the other catalysts may be due to the combined contribution of the high dispersion state of the Ti-oxide species and the large pore size with a three-dimensional channel structure: TS-1 has a smaller pore size (ca. 5.7 Å) and a three-dimensional channel structure; Ti-MCM-41 has a large pore size (>20 Å) but one-dimensional channel structure; and Ti-MCM-48 has both a large pore size (>20 Å) and three-dimensional channels. These results strongly suggest that mesoporous molecular sieves containing highly dispersed Ti-oxide species are promising candidates as effective photocatalysts.

The effect of Pt loading on the photocatalytic activity of Ti-containing mesoporous silica has also been investigated, and the changes in the yields of CH_4 and CH_3OH formation are shown in Fig. 9.6. The deposition of Pt onto the Ti-containing zeolites is effective for promoting the photocatalytic activity, but the formation of only CH_4 is promoted [18].

Ti-containing zeolite, Ti-Beta, has attracted much attention because of their large-pore structure compared to the Y-zeolite [36–38]. The other characteristic feature is that the H_2O affinity of Ti-Beta zeolites can be changed significantly depending on the preparation methods, and their hydrophobic–hydrophilic properties can modify the catalytic performances [36–38]. As shown in Fig. 9.7, the photocatalytic reduction of CO_2 with H_2O was found to proceed in the gas phase at 323 K with different activity and selectivity on hydrophilic Ti-Beta(OH) and hydrophobic Ti-Beta(F) zeolites prepared in the OH^- and F^- media, respectively.

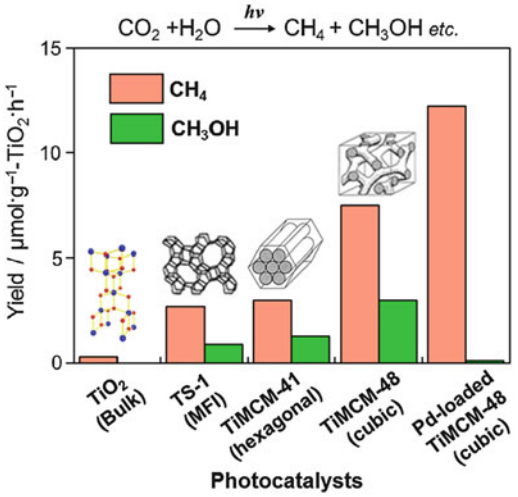

Fig. 9.6 The product distribution of the photocatalytic reduction of CO_2 with H_2O on TiO_2 powder, TS-1, Ti-MCM-41, Ti-MCM-48, and the Pt-loaded Ti-MCM-48 catalysts

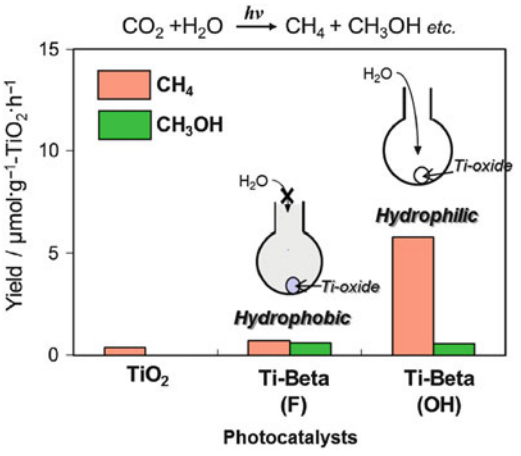

Fig. 9.7 The product distribution of the photocatalytic reduction of CO_2 with H_2O on Ti-Beta(F), Ti-Beta(OH), and TiO_2 powder (P-25) as the reference catalyst

The higher activity for the formation of CH_4 observed with Ti-Beta(OH) and the higher selectivity for the formation of CH_3OH observed with the Ti-Beta(F) may be attributed to the different abilities of zeolite pores on the H_2O affinity. These results suggest that the affinity of the H_2O molecules to adsorb on the zeolite is one of important factors for the selectivity in the photocatalytic reduction of CO_2 and H_2O.

For the reduction of CO_2 with H_2O on the Ti-containing zeolite and mesoporous molecular sieves, a similar reaction pathway with Ti-oxide anchored on zeolite is proposed by considering ESR spectroscopy at 77 K, in which CO_2 reduction and

H_2O splitting proceed competitively at the LMCT-excited Ti—O centers: CO_2 is reduced to CO and subsequently to C radicals, while H_2O photodecomposes to H and OH radicals. Reaction of H and OH radicals with carbon species is thought to yield CH_3OH and CH_4. Frei and co-workers carried out further mechanistic investigations by monitoring the visible light-induced reaction of $^{13}CO_2$ and H_2O gas mixtures in the framework Ti-MCM-41 molecular sieve with in situ FT-IR spectroscopy at room temperature [39]. ^{12}CO gas along with ^{13}CO were observed as the products by infrared, and the growth of ^{13}CO depended linearly on the photolysis laser power. This points out the presence of small amounts of carbonaceous residues on the high-surface area mesoporous silicates. H_2O was also confirmed as the stoichiometric electron donor. These results suggest that CO is a single-photon, 2-electron-transfer product of CO_2 at framework Ti centers with H_2O acting as a direct electron donor. By considering this, the mechanism is proposed as follows: Excitation of the framework Ti^{4+} centers leads to photoinduced $(Ti^{3+}—O^-)^*$ species. Electron transfer from transient Ti^{3+} to CO_2 splits the molecule into CO and O^-. The latter is spontaneously protonated by a Si–OH group or H^+ cogenerated upon H_2O oxidation to yield a surface OH radical. Another surface OH radical is formed as a result of the simultaneous H_2O oxidation by the framework oxygen hole. The OH radicals either combine to yield H_2O_2 or dismutate to give O_2 and H_2O.

9.8 Ti-Oxide Anchored on Porous Silica Glass (CVD)

The Ti-oxide anchored onto porous silica glass (PVG) plate was prepared using a facile reaction of $TiCl_4$ with the surface OH groups on the transparent porous Vycor glass (Corning Code 7930) in the gas phase at 453–473 K, followed by treatment with H_2O vapor to hydrolyze the anchored compound [11–13]. UV irradiation of the anchored Ti-oxide catalysts in the presence of a mixture of CO_2 and H_2O led to the evolution of CH_4, CH_3OH, and CO at 323 K. The total yield was larger under UV irradiation at 323 K than at 275 K. The efficiency of the photocatalytic reaction strongly depends on the ratio of H_2O/CO_2, and its activity increases with increasing the H_2O/CO_2 ratio; however, an excess amount of H_2O suppresses the reaction rates. Figure 9.8 shows the effect of the number of anchored Ti–O layers on the absorption edge in the UV–VIS spectra of the catalysts and the efficiency of the photocatalytic reactions as well as the relative yields of the photoluminescence. It was proven that only catalysts with highly dispersed monolayer Ti-oxide exhibit high photocatalytic activity and photoluminescence at around 480 nm. Only the tetrahedrally coordinated Ti-oxide species exhibit photoluminescence emission upon excitation at around 250–280 nm. These findings also clearly suggest that the tetrahedrally coordinated Ti-oxide species function as active photocatalysts for the reduction of CO_2 with H_2O.

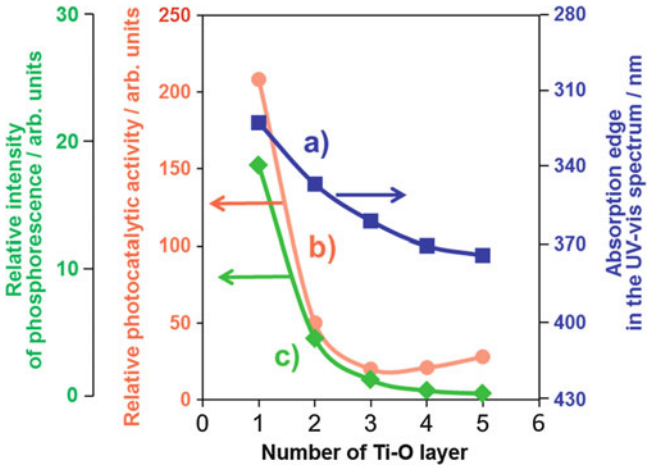

Fig. 9.8 The effects of the number of the Ti–O layers of the anchored titanium oxide catalysts on the absorption edge of the catalysts (*a*), the reaction yields (*b*), and the relative yields of the photoluminescence (*c*)

9.9 Ti-Containing Porous Silica Thin Film

In the syntheses of zeolites and mesoporous molecular sieves, the morphology of these materials was mainly in powdered form. However, powdered material systems are difficult to handle for practical use as photocatalysts. Therefore, the synthesis of transparent porous silica thin films is a subject of current interest. Such transparent porous silica thin films have a larger surface area, in contrast to metal oxide thin films on a quartz substrate, and can realize the efficient absorption of light, showing that they have potential for use as effective photocatalysts.

Self-standing Ti-containing porous silica (PS) thin films with different pore structures and Ti contents were synthesized by a solvent evaporation method. Ti-PS(h, 25) and Ti-PS(c, 50) mean hexagonal and cubic structure with a Si/Ti ratio of 25 and 50, respectively [40, 41]. The synthesized thin films are colorless and completely transparent. Mesoporous structure was confirmed by a characteristic diffraction peak at around 2–3° associated with the d_{100} spacing.

UV irradiation of these Ti-containing porous silica thin films in the presence of CO_2 and H_2O at 323 K led to the formation of CH_4 and CH_3OH as well as CO and O_2 as minor products. Ti-PS(h, 50) thin film was proven to be the most effective photocatalyst with a high quantum yield of 0.28 %, which was larger than the Ti-MCM-41 powder catalyst even with the same pore structure (Fig. 9.9). This quantum yields obtained with transparent Ti-PS (50) thin film photocatalyst has been improved in contrast to the value obtained with the titanium oxide anchored on transparent porous silica glass (0.02 %). In powdered form, the effect of the scattering of light on the particle surface would be large so that effective light

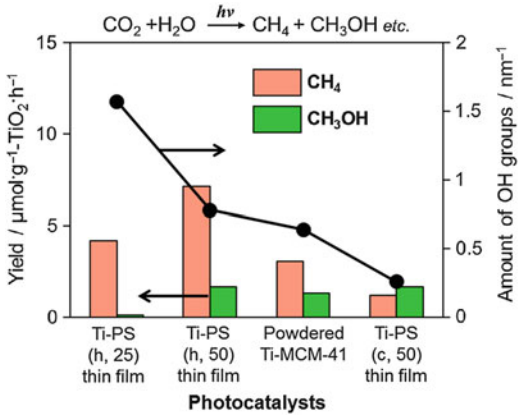

Fig. 9.9 The product distribution of the photocatalytic reduction of CO_2 with H_2O and amount of surface OH groups on Ti-PS(h, 25), Ti-PS(h, 50), powdered Ti-MCM-41, and Ti-PS(c, 50)

absorption and measurement may not be realized. Thus, the high photocatalytic activity of such thin films can be attributed to the efficient absorption of UV light due to its high transparency. From FT-IR investigations, it was found that these Ti-containing porous silica thin films had different concentrations of surface OH groups and showed different adsorption properties for the H_2O molecules toward the catalyst surface: photocatalysts having small amounts of surface OH groups showed high selectivity for the formation of CH_3OH.

9.10 Ti/Si Binary Oxide (Sol–Gel)

Ti/Si binary oxides involving different Ti contents were prepared by the sol–gel method using mixtures of tetraethylorthosilicate and titanium *iso*propoxide. Ti/Si binary oxides with only a small Ti contents exhibited the photoluminescence emission at around 480 nm upon excitation at around 280 nm [22, 42]. UV irradiation of the Ti/Si binary oxide catalysts in the presence of a gaseous mixture of CO_2 and H_2O led to the formation of CH_4 and CH_3OH as the main products. A parallel relationship between the specific photocatalytic activities of the titanium oxide species and the photoluminescence yields of the Ti/Si binary oxides was observed. This phenomenon clearly indicates that the appearance of high photocatalytic activity for the binary oxides is closely associated with the formation of the charge-transfer excited complex due to the highly dispersed tetrahedral Ti-oxide species.

The XAFS, ESR, and photoluminescence investigations of the Ti/Si binary oxide indicated that these catalysts prepared by the sol–gel method can keep tetrahedral coordination geometry of Ti-oxide species until the TiO_2 content approaches up to approximately 20 wt%. Consequently, the Ti/Si binary oxides having a high Ti content can be successfully utilized as active photocatalysts for the efficient reduction of CO_2 with H_2O in the gas–solid system.

9.11 Visible Light-Sensitive TiO_2-Based Catalysts

The development of visible light-sensitive photocatalysts was intensively pursued since the pure TiO_2 and Ti-oxide species only shows fascinating photocatalytic activities under UV-light irradiation, which limit the utilization of a small UV fraction of natural solar light. One of the most promising strategies to use higher wavelength of the solar spectrum is the dye sensitization of TiO_2. The organometallic dye, especially (2,2′-bipyridine) ruthenium (II) chloride hexahydrate, attached TiO_2 absorb sunlight and injects electrons into the conduction band of TiO_2, which ultimately promote the CO_2 reduction to produce CH_4 [43]. It was also reported that the perylene diimide derivatives have shown high light-harvesting capacity similar to the Ru complex dye.

Nguyen et al. found substantial improvements in the photoactivity of metal-doped TiO_2–SiO_2 mixed oxide-based photocatalysts toward CO_2 photoreduction in the presence of H_2O and concentrated sunlight in an optical fiber photoreactor (OFPR) [44]. Fe atoms are introduced into the TiO_2–SiO_2 lattice during sol–gel process, resulting in the full visible light absorption as well as the effect on product selectivity of the obtained catalyst. Cu–Fe/TiO_2 catalyst mainly produced ethylene with the quantum yield of 0.024 %, whereas Cu–Fe/TiO_2–SiO_2 catalyst exhibited favorable methane production with the quantum yield of 0.05 %. The overall energy efficiency is found to be higher on Cu–Fe/TiO_2–SiO_2 (0.018 %) than on its Cu–Fe/TiO_2 (0.016 %). The superior photoactivity of Cu–Fe/TiO_2–SiO_2 catalyst under natural sunlight could be ascribed to the efficient charge-transfer mechanism between TiO_2 and Cu as well as Fe as co-dopants and its full absorption of visible light.

9.12 Various Metal Oxide Photocatalysts

The reviews concerning the photocatalytic reduction of CO_2 using various metallic oxides other than TiO_2 have been previously summarized by Navalon et al. [45] In general, ZnO and NiO are widely known as versatile oxide semiconductors except for TiO_2. Because these ZnO and NiO semiconductors possess negatively high conduction band potential compared to the TiO_2 (TiO_2, −0.29 V; ZnO, −0.31 V; NiO, −0.50 V at pH 7) [46]. Yahaya et al. focused on these conduction band potential for efficient CO_2 reduction, and the photocatalytic reduction of CO_2 to CH_3OH was performed in an aqueous suspension of these oxide semiconductors under laser light irradiation at 355 nm [47]. The ZnO and NiO semiconductors exhibited more efficient CH_3OH production performance than the TiO_2. The amounts of produced CH_3OH decreased with irradiation time when TiO_2 and ZnO were used as photocatalysts, indicating that the produced CH_3OH was further oxidized to HCHO, HCOOH, or CO_2 by the high oxidation ability of these materials, while no decrease of produced CH_3OH was confirmed in the presence of the NiO semiconductor. In addition, they discovered that more efficient CH_3OH

production was achieved to convert CO_2 into H_2CO_3, because the pH of the system decreases by production of H_2CO_3 (dissolution of CO_2), resulting in the shift of conduction band edge to more positive value.

Novel oxide photocatalysts by composite compounds of various metal species were also reported for photoreduction of CO_2 [48]. Various cocatalyst nanoparticles such as NiO_x, Ru, Cu, Au, or Ag were loaded on $ALa_4Ti_4O_{15}$ (A = Ca, Sr, or Ba). Among those synthesized, 2 wt% Ag loaded on $BaLa_4Ti_4O_{15}$ ($Ag/BaLa_4Ti_4O_{15}$) exhibited the highest CO_2 reduction performance, resulting in the formation of CO as a main product. The Ag cocatalyst acted as a reduction site to produce CO from CO_2. Interestingly, the photocatalytic activity for CO_2 reduction strongly depends on the loading method of Ag nanoparticles. The small-size Ag nanoparticles (10 nm) were prepared on the edge of plate particle of the $BaLa_4Ti_4O_{15}$ by liquid-phase chemical reduction method, and the performance of photocatalytic CO_2 reduction was significantly improved compare to the $Ag/BaLa_4Ti_4O_{15}$ using conventional method such as impregnation or photodeposition. It is concluded that the separation of reaction sites (reduction and oxidation) and the loading of small-size Ag cocatalyst on the edge of plate play important roles to achieve efficient activation of CO_2 reduction using $Ag/BaLa_4Ti_4O_{15}$ photocatalyst.

As discussed in Sect. 9.11, the development of visible light-sensitive photocatalyst is also absolutely imperative for more efficient CO_2 reduction. The unique photocatalyst system for CO_2 reduction using composite oxide of $Pt/ZnAl_2O_4$ modified with mesoporous ZnGaNO was reported by Yan et al. [49]. The photocatalytic reduction of CO_2 to CH_4 was efficiently confirmed in the presence of H_2O under visible light irradiation ($\lambda > 420$ nm), because this novel and unique photocatalyst possesses high CO_2 adsorption property derived from mesoporous structure, basicity, and visible light absorption ability by narrow band gap structure to achieve efficient CO_2 reduction. This photocatalytic activity is about seven times higher than that of Pt-loaded N-doped TiO_2 known as versatile visible light-sensitive photocatalyst.

9.13 Localized Surface Plasmon Resonance-Enhanced Photocatalyst

Au nanoparticle can absorb visible and infrared light in particular regions due to localized surface plasmon resonance (LSPR) [50, 51]. In simple terms, LSPR is made up of collective oscillations of free electrons in metal NPs driven by the electromagnetic field of incident light [4]. This unique characteristic has given rise to a new approach to the fabrication of visible light-sensitive photocatalysts, known as plasmonic photocatalysts, through the deposition of Au nanoparticle onto suitable semiconductors [52]. It has been proposed that in the case of Au/TiO_2, at an excitation wavelength corresponding to the LSPR of Au, the Au nanoparticle absorb photons and inject photogenerated electrons into the TiO_2 conduction band [53].

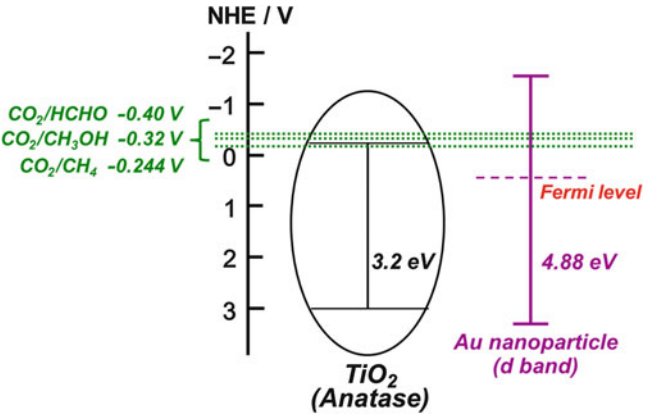

Fig. 9.10 The energy level of anatase-type TiO_2 and Au nanoparticle and reduction of CO_2 to HCHO, CH_3OH, or CH_4

The photocatalytic reduction of CO_2 to CH_4 using the unique LSPR property of Au/TiO_2 was recently performed by Hou et al. [54, 55]. In this system, the main product was CH_4, but the methanol and formaldehyde were also observed. When the light ($\lambda = 532$ nm) matched to the LSPR absorption of Au nanoparticle was utilized in this system, the reduction efficiency of CO_2 was about 24 times higher than that of bare TiO_2. They discussed that the excited electrons produced in the Au nanoparticles by the LSPR did not directly transfer to the conduction band of TiO_2. However, when the photon possessing high enough energy to excite the electrons in d-band of Au nanoparticles was irradiated, the charge was directly transferred between Au nanoparticle and TiO_2 (Fig. 9.10). Since the LSPR can absorb light of long-wavelength region, this unique photocatalytic system is one of promising approach for efficient CO_2 reduction by beneficial use of photo-energy.

9.14 Conclusions

In this chapter, we have focused on the progress in the very stimulating field of the photocatalytic reduction of CO_2 with H_2O on various types of Ti-oxide catalysts. Upon UV-light irradiation, the reactions on TiO_2 powders in the presence of gaseous CO_2 and H_2O at 275 K produced CH_4 as the major product, while on the highly dispersed titanium oxide anchored on porous glass or ordered porous silicas, the formations of CH_3OH as well as CH_4 were observed as the major products. In situ spectroscopic studies of the system indicated that the photocatalytic reduction of CO_2 with H_2O is linked to a much higher activity of the charge-transfer excited state, i.e., $(Ti^{3+}—O^{-})^*$ of the tetrahedral coordinated Ti-oxide species formed on the surface. Owing to the dramatically growing nature of this research field, we expect that the

design strategy described here can offer a helpful overview to the readers in this fascinating area. In recent report, the highly efficient reduction of CO_2 was achieved using various oxide semiconductors or the LSPR property of metallic nanoparticles. These photocatalytic systems are expected for solution of various global environment problems including CO_2 problem.

References

1. Anpo M, Yamashita H (1996) Photochemistry of surface species anchored on solid surface. In: Anpo M (ed) Surface photochemistry. Wiley, Chichester, pp 117–164
2. Schiavello M (ed) (1997) Heterogeneous photocatalysts. Wiley, Chichester
3. Anpo M (2000) Photofunctional zeolites. NOVA, New York
4. Anpo M, Yamashita H, Zhang SG (1996) Photoinduced surface chemistry. Curr Opin Solid State Mater Sci 1:630–635
5. Anpo M (1989) Photocatalysis on small particle TiO_2 catalysts. Reaction intermediates and reaction mechanisms. Res Chem Intermed 11:67–106
6. Anpo M, Ichihashi Y, Takeuchi M, Yamashita H (1998) Design of unique titanium oxide photocatalysts by an advanced metal ion-implantation method and photocatalytic reactions under visible light irradiation. Res Chem Intermed 24:143–149
7. Yamashita H, Ichihashi Y, Takeuchi M, Kishiguchi S, Anpo M (1999) Characterization of metal ion-implanted titanium oxide photocatalysts operating under visible light irradiation. J Synchrotron Radiat 6:451–452
8. Yamashita H, Honda M, Harada M, Ichihashi Y, Anpo M (1998) Preparation of titanium oxide photocatalysts anchored on porous silica glass by a metal ion-implantation method and their photocatalytic reactivities for the degradation of 2-propanol diluted in water. J Phys Chem B 102:10707–10711
9. Inoue T, Fujishima A, Konishi S, Honda K (1979) Photoelectrocatalytic reduction of carbon dioxide in aqueous suspensions of semiconductor powders. Nature 277:637–640
10. Halmann M (1983) Photochemical fixation of carbon dioxide. In: Grätzel M (ed) Energy resources through photochemistry and catalysis. Academic, New York, pp 507–565
11. Anpo M, Chiba K (1992) Photocatalytic reduction of carbon dioxide on anchored titanium oxide catalysts. J Mol Catal 74:207–302
12. Yamashita H, Shiga A, Kawasaki S, Ichihashi Y, Ehara S, Anpo M (1995) Photocatalytic synthesis of CH_4 and CH_3OH from CO_2 and H_2O on highly dispersed active titanium oxide catalysts. Energy Conv Manag 36:617–620
13. Anpo M, Yamashita H, Ichihashi Y, Ehara S (1995) Photocatalytic reduction of CO_2 with H_2O on various titanium oxide catalysts. J Electroanal Chem 396:21–26
14. Yamashita H, Nishiguchi H, Kamada N, Anpo M, Teraoka Y, Hatano H, Ehara S, Kikui K, Palmisano L, Sclafani A, Schiavello M, Fox MA (1994) Photocatalytic reduction of CO_2 with H_2O on TiO_2 and Cu/TiO_2 catalysts. Res Chem Intermed 20:815–823
15. Yamashita H, Kamada N, He H, Tanaka K, Ehara S, Anpo M (1994) Reduction of CO_2 with H_2O on $TiO_2(100)$ and $TiO_2(110)$ single crystals under UV-irradiation. Chem Lett 1994 (5):855–858
16. Anpo M, Yamashita H, Ichihashi Y, Fujii Y, Honda M (1997) Photocatalytic reduction of CO_2 with H_2O on titanium oxides anchored within micropores of zeolites: effects of the structure of the active sites and the addition of Pt. J Phys Chem B 101:2632–2636
17. Anpo M, Yamashita H, Fujii Y, Ichihashi Y, Zhang SG, Park DR, Ehara S, Park SE, Chang JS, Yoo JW (1998) Photocatalytic reduction of CO_2 with H_2O on titanium oxides anchored within zeolites. Stud Surf Sci Catal 114:177–182

18. Yamashita H, Fuji Y, Ichihashi Y, Zhang SG, Ikeue K, Park DR, Koyano K, Tatsumi T, Anpo M (1998) Selective formation of CH_3OH in the photocatalytic reduction of CO_2 with H_2O on titanium oxides highly dispersed within zeolites and mesoporous molecular sieves. Catal Today 45:221–227
19. Anpo M, Zhang SG, Fujii Y, Ichihashi Y, Yamashita H, Koyano K, Tatsumi T (1998) Photocatalytic reduction of CO_2 with H_2O on Ti-MCM-41 and Ti-MCM-48 mesoporous zeolite catalysts. Catal Today 44:327–332
20. Ikeue K, Yamashita H, Anpo M (1999) Photocatalytic reduction of CO_2 with H_2O on titanium oxides prepared within the FSM-16 mesoporous zeolite. Chem Lett 1999(11):1135–1136
21. Yamashita H, Ikeue K, Takewaki T, Anpo M (2002) In situ XAFS studies on the effects of the hydrophobic-hydrophilic properties of Ti-beta zeolites in the photocatalytic reduction of CO_2 with H_2O. Top Catal 18:95–100
22. Yamashita H, Kawasaki S, Fujii Y, Ichihashi Y, Ehara S, Park SE, Chang JS, Yoo JW, Anpo M (1998) Photocatalytic reduction of CO_2 with H_2O on Ti/Si binary oxide catalysts prepared by the sol-gel method. Stud Surf Sci Catal 114:561–564
23. Saladin F, Forss L, Kamber I (1995) Photosynthesis of CH_4 at a TiO_2 surface from gaseous H_2O and CO_2. J Chem Soc Chem Commun 5:533–534
24. Anpo M, Tomonari M, Fox MA (1989) In situ photoluminescence of titania as a probe of photocatalytic reactions. J Phys Chem 93:7300–7303
25. Yamashita H, Ichihashi Y, Harada M, Stewart G, Fox MA, Anpo M (1996) Photocatalytic degradation of 1-octanol on anchored titanium oxide and on TiO_2 powder catalysts. J Catal 158:97–101
26. Frese KW (1991) Electrochemical reduction of carbon dioxide at intentionally oxidized copper electrodes. J Electrochem Soc 138:3338–3343
27. Slamet HW, Nasution E, Purnama E, Kosela S, Gunlazuardi J (2005) Photocatalytic reduction of CO2 on copper-doped titania catalysts prepared by improved-impregnation method. Catal Commun 6:313–319
28. Raskö J, Solymosi F (1994) Infrared spectroscopic study of the photoinduced activation of CO_2 on TiO_2 and Rh/TiO_2 catalysts. J Phys Chem 98:7147–7152
29. Anpo M, Matsuoka M, Shioya Y, Yamashita H, Giamello E, Morterra C, Che M, Patterson HH, Webber S, Ouellette S, Fox MA (1994) Preparation and characterization of the Cu^+/ZSM-5 catalyst and its reaction with NO under UV irradiation at 275 K. In situ photoluminescence, EPR, and FT-IR investigations. J Phys Chem 98:5744–5750
30. Yamashita H, Matsuoka M, Tsuji K, Shioya Y, Anpo M, Che M (1996) In-situ XAFS, photoluminescence, and IR investigations of copper ions included within various kinds of zeolites. Structure of Cu(I) ions and their interaction with CO molecules. J Phys Chem 100:397–402
31. Yamashita H, Ichihashi Y, Anpo M, Hashimoto M, Louis C, Che M (1996) Cavities: the structure and role of the active sites. J Phys Chem 100:16041–16044
32. Yamashita H, Zhang SG, Ichihashi Y, Matsumura Y, Souma S, Tatsumi T, Anpo M (1997) Photocatalytic decomposition of NO at 275 K on titanium oxide catalysts anchored within zeolite cavities and framework. Appl Surf Sci 121:305–309
33. Farges F, Brown GE Jr, Rehr JJ (1996) Coordination chemistry of Ti(IV) in silicate glasses and melts: I. XAFS study of titanium coordination in oxide model compounds. Geochim Cosmochim Acta 60:3023–3060
34. Anpo M, Aikawa N, Kubokawa Y, Che M, Louis C, Giamello E (1985) Photoluminescence and photocatalytic activity of highly dispersed titanium oxide anchored onto porous Vycor glass. J Phys Chem 89:5017–5021
35. Anpo M, Aikawa N, Kubokawa Y, Che M, Louis C, Giamello E (1985) Photoformation and structure of oxygen anion radicals (O_2^-) and nitrogen-containing anion radicals adsorbed on highly dispersed titanium oxide anchored onto porous Vycor glass. J Phys Chem 89:5689–5694
36. Takewaki T, Hwang SJ, Yamashita H, Davis ME (1999) Synthesis of BEA-type molecular sieves using mesoporous materials as reagents. Micropor Mesopor Mater 32:265–273

37. Camblor MA, Corma A, Esteve P, Martines M, Valencia S (1997) Epoxidation of unsaturated fatty esters over large-pore Ti-containing molecular sieves as catalysts: important role of the hydrophobic-hydrophilic properties of the molecular sieve. Chem Commun 33:795–796
38. Tatsumi T, Jappar N (1998) Properties of Ti-beta zeolites synthesized by dry-gel conversion and hydrothermal methods. J Phys Chem B 102:7126–7131
39. Lin W, Han H, Frei H (2004) CO_2 splitting by H_2O to CO and O_2 under UV light in TiMCM-41 silicate sieve. J Phys Chem B 108:18269–18273
40. Ikeue K, Nozaki S, Ogawa M, Anpo M (2002) Photocatalytic reduction of CO_2 with H_2O on Ti-containing porous silica thin film photocatalysts. Catal Lett 80:111–114
41. Ikeue K, Nozaki S, Ogawa M, Anpo M (2002) Characterization of self-standing Ti-containing porous silica thin films and their reactivity for the photocatalytic reduction of CO_2 with H_2O. Catal Today 74:241–248
42. Yamashita H, Kawasaki S, Ichihashi Y, Harada M, Anpo M, Stewart G, Fox MA, Louis C, Che M (1998) Characterization of titanium-silicon binary oxide catalysts prepared by the sol-gel method and their photocatalytic reactivity for the liquid-phase oxidation of 1-octanol. J Phys Chem B 102:5870–5875
43. Ozcan O, Yukruk F, Akkaya EU, Uner D (2007) Dye sensitized CO2 reduction over pure and platinized TiO2. Top Catal 44:523–528
44. Nguyen TH, Wu JCS (2008) Photoreduction of CO2 to fuels under sunlight using optical-fiber reactor. Sol Energy Mater Sol Cells 92:864–872
45. Navalon S, Dhakshinamoorthy A, Alvaro M, Garcia H (2013) You have free access to this content photocatalytic CO_2 reduction using non-titanium metal oxides and sulfides. Chem Sus Chem 6:562–577
46. Xu Y, Schoonen MAA (2000) The absolute energy positions of conduction and valence bands of selected semiconducting minerals. Am Mineral 85:543–556
47. Yahaya AH, Gondal MA, Hameed A (2004) Selective laser enhanced photocatalytic conversion of CO2 into methanol. Chem Phys Lett 400:206–212
48. Iizuka K, Wato T, Miseki Y, Saito K, Kudo A (2011) Photocatalytic reduction of carbon dioxide over Ag cocatalyst-loaded $ALa_4Ti_4O1_5$ (A = Ca, Sr, and Ba) using water as a reducing reagent. J Am Chem Soc 133:20863–20868
49. Yan S, Yu H, Wang N, Li Z, Zou Z (2012) Efficient conversion of CO_2 and H_2O into hydrocarbon fuel over $ZnAl_2O_4$-modified mesoporous ZnGaNO under visible light irradiation. Chem Commun 48:1048–1050
50. Mori K, Kawashima M, Che M, Yamashita H (2010) Enhancement of the photoinduced oxidation activity of a ruthenium(II) complex anchored on silica-coated silver nanoparticles by localized surface plasmon resonance. Angew Chem Int Ed 49:8598–8601
51. Fuku K, Hayashi R, Takakura S, Kamegawa T, Mori K, Yamashita H (2013) The synthesis of size- and color-controlled silver nanoparticles by using microwave heating and their enhanced catalytic activity by localized surface plasmon resonance. Angew Chem Int Ed 52:7446–7450
52. Cushing SK, Li JT, Meng FK, Senty TR, Suri S, Zhi MJ, Li M, Bristow AD, Wu NQ (2012) Photocatalytic activity enhanced by plasmonic resonant energy transfer from metal to semiconductor. J Am Chem Soc 134:15033–15041
53. Tanaka A, Sakaguchi S, Hashimoto K, Kominami H (2012) Preparation of Au/TiO_2 exhibiting strong surface plasmon resonance effective for photoinduced hydrogen formation from organic and inorganic compounds under irradiation of visible light. Catal Sci Technol 2:907–909
54. Hou WB, Hung WH, Pavaskar P, Goeppert A, Aykol M, Cronin SB (2011) Photocatalytic conversion of CO_2 to hydrocarbon fuels via plasmon-enhanced absorption and metallic interband transitions. ACS Catal 1:929–936
55. Hou WB, Cronin SB (2013) A review of surface plasmon resonance-enhanced photocatalysis. Adv Funct Mater 23:1612–1619

Chapter 10
Electrochemical Fixation of Carbon Dioxide

Hisanori Senboku

10.1 Introduction

Electrochemical fixation of carbon dioxide means an incorporation of carbon dioxide in organic molecules as functional groups by the use of an electrochemical method. Fixation of carbon dioxide can be principally classified into two categories. One is fixation with C–C bond formation between carbon dioxide and organic molecules to yield carboxylic acid. The electrochemical fixation of carbon dioxide in most reports is in this category, and, consequently, electrochemical fixation of carbon dioxide yielding carboxylic acid is often called "electrochemical carboxylation" or "electrocarboxylation." The other one is fixation of carbon dioxide with C–heteroatom bond formation between a carbon atom of carbon dioxide and a heteroatom, such as an oxygen or nitrogen atom, in organic molecules. As heteroatom sources, alcohol and amine are used for this type of fixation to form carbonate and carbamate ions ($-X-CO_2^-$), respectively. Since the resulting carbonic acid and carbamic acid generally cannot be isolated due to their rapid decarboxylation, they are obtained and isolated as their esters, carbonate and carbamate, respectively, by the reaction of the forming carbonate or carbamate ions with appropriate electrophiles, such as alkyl halides, in situ after the fixation of carbon dioxide (Scheme 10.1).

Of the two types of electrochemical fixation of carbon dioxide in organic molecules, this chapter focuses on electrochemical fixation of carbon dioxide with C–C bond formation giving carboxylic acid.

C–C bond formation between carbon dioxide and organic molecules is thought to proceed generally via two different pathways. When the reduction potential of an organic substrate is more positive than that of carbon dioxide, electrochemical reduction of the organic substrate predominantly occurs to generate anionic species. Nucleophilic attack of the resulting anionic species on carbon dioxide yields

H. Senboku (✉)
Division of Chemical Process Engineering, Faculty of Engineering,
Hokkaido University, Sapporo, Hokkaido, Japan
e-mail: senboku@eng.hokudai.ac.jp

B.M. Bhanage and M. Arai (eds.), *Transformation and Utilization of Carbon Dioxide*,
Green Chemistry and Sustainable Technology, DOI 10.1007/978-3-642-44988-8_10,

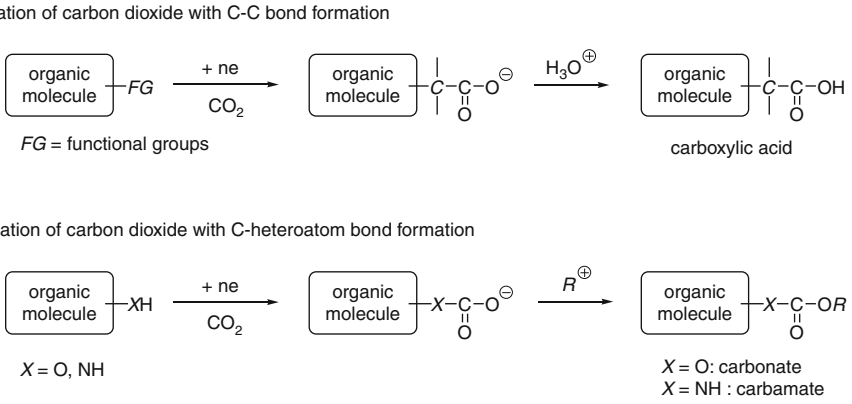

Scheme 10.1 Electrochemical fixation of carbon dioxide in organic molecules with C–C or C–heteroatom bond formation

carboxylic acid (*path* ***a*** in Scheme 10.2). On the other hand, when the reduction potential of the organic substrate is more negative than that of carbon dioxide, one-electron reduction of carbon dioxide predominantly occurs to generate the radical anion of carbon dioxide, which reacts with organic substrates, typically alkenes, to yield the corresponding mono- and/or dicarboxylic acids (*path* ***b*** in Scheme 10.2).

Fixation of carbon dioxide in organic molecules with C–C bond formation gives carboxylic acid. Carbon dioxide used as a source of a carboxyl group is not only abundant and economical but also nontoxic and attractive as an environmentally benign C1 chemical reagent for organic synthesis, same as the description in other chapters. By using an electrochemical method, efficient fixation of carbon dioxide in appropriate organic molecules can be achieved even under an atmospheric pressure of carbon dioxide under quite mild and almost neutral conditions. Electrochemical reduction of organic molecules in the presence of carbon dioxide using magnesium or aluminum as a sacrificial anode in a one-compartment electrochemical cell has been found to be the most convenient, useful, and effective method for efficient fixation of carbon dioxide to yield carboxylic acid in high yields [1–4]. Carbon dioxide is also used for synthesizing carboxylic acid in conventional methods. For example, reaction of a Grignard reagent or organolithium reagent with carbon dioxide in ether or tetrahydrofuran, flammable organic solvents, gives carboxylic acid. However, the reaction proceeds under highly basic conditions, and the use of these highly reactive reagents imposes limitation of usable functional groups in the reagents themselves and special caution in their handling is needed. As well as carbon dioxide, a cyanide ion, such as KCN and NaCN, and carbon monoxide (CO) are also effective C1 carbon sources in conventional methods for synthesis of a nitrile and ester, which are the precursors of carboxylic acid and are readily converted to carboxylic acid by hydrolysis. However, these C1 reagents are unfortunately toxic, and from the viewpoint of green and sustainable chemistry,

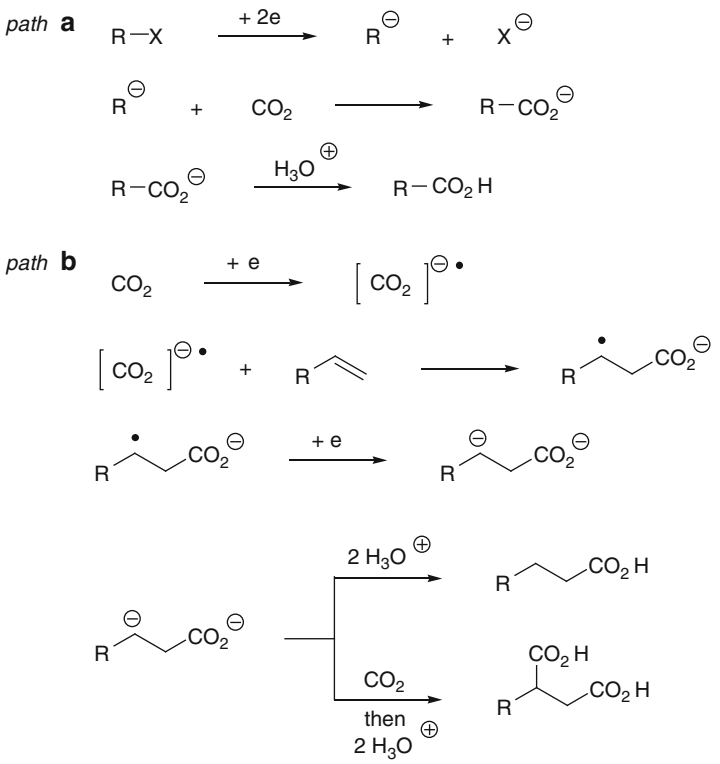

Scheme 10.2 Two general reaction pathways for electrochemical fixation of carbon dioxide with C–C bond formation

the use of these reagents is unfavorable. On the other hand, an electrochemical method is an environmentally benign method, and there is no need to use such toxic reagents and flammable solvents with special caution in electrochemical fixation of carbon dioxide to yield carboxylic acid in high yields. Although transition-metal catalyzed fixation of carbon dioxide in organic and organometallic compounds has recently been developed, an electrochemical method can achieve efficient fixation of carbon dioxide without such expensive and air-sensitive metal catalysts by using electrons as an essential reagent.

Platinum, grassy carbon, graphite, stainless steel, carbon fiber, silver, lead, mercury pool, and some other metals have been reported to be usable as cathode materials in electrochemical carboxylation. Among them, platinum, stainless steel, carbon fiber, and graphite are frequently used for efficient formation of carboxylic acid by electrochemical fixation of carbon dioxide with a sacrificial anode, such as magnesium and aluminum [1–4], as a couple in an undivided cell (one-compartment cell). DMF (*N*,*N*-dimethylformamide) and acetonitrile are mainly used for electrochemical carboxylation as solvents with low concentration of tetraalkylammonium salts and lithium perchlorate as supporting electrolytes. Acetone, DMSO (dimethyl sulfoxide), and THF (tetrahydrofuran) are also usable for fixation of carbon dioxide.

10.2 Synthetic Applications

Efficient fixation of carbon dioxide in various kinds of organic molecules has been successfully carried out by an electrochemical method with C–C bond formation; alkenes [5] and activated alkenes including styrenes [5–15], allenes [5, 16], alkynes [5, 17–19], enynes and diynes [5, 20–23], aromatic [1, 3, 24], allyl [3, 25, 26], propargyl [27], benzyl [1, 3, 28–50] and vinyl [3, 51–53] halides, aryl [54, 55] and vinyl triflates [56–60], aldehydes and ketones [61–64], imines [65], benzyl esters and carbonates [66, 67], and other organic substrates [68–70] are efficiently carboxylated by an electrochemical method to afford various kinds of useful carboxylic acids [4, 71]. For example, electrochemical carboxylation of halides **1** and **3** gave fluorine-containing carboxylic acids **2** and ester **4** in high yields, respectively [24, 34] (Scheme 10.3). Since synthesis of these carboxylic acids is difficult by conventional method using organometallic reagents, it is obvious that electrochemical method is of great use for synthesis of these carboxylic acids.

Electrochemical fixation of carbon dioxide into substituted allylic halide **5** was reported to occur at the α-position to give unsaturated carboxylic acid **6** regioselectively [25] while conventional reaction of the corresponding Grignard reagent **7** derived from halide **5** with carbon dioxide occurs at the γ-position via six-membered transition state to give regioisomer **8** as a sole product (Scheme 10.4).

Electrochemical debromination followed by carboxylation of 2-bromomethyl-1,4-dibromobut-2-ene (**9**) can take place efficiently by using manganine, alloy of 12–15 % Mn, 2–4 % Ni, and 80–85 % Cu as an anode metal to give 3-methylene-4-pentenoic acid (**10**). This result shows that tribromide **9** can work as a synthetic equivalent of isoprenyl carbanion **11**. Carboxylic acid **10** has an isoprene unit and can be used for aqueous Diels-Alder reaction as a water-soluble diene [26] (Scheme 10.5).

Electrochemical carboxylation is sometimes carried out in the presence of a transition-metal catalyst such as Pd [54–56, 72–74], Ni [5, 9, 16–23, 31, 32, 35, 38, 41, 52, 53, 60, 70, 75, 76], and cobalt [28, 36, 37, 44] complexes, the use of which

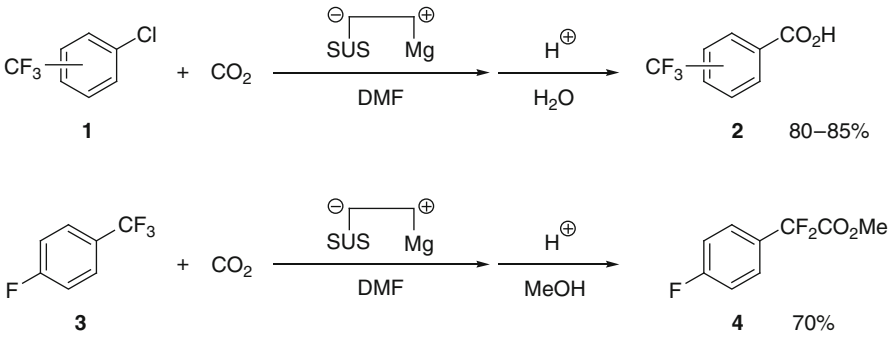

Scheme 10.3 Synthesis of fluorine-containing carboxylic acids and esters by electrochemical carboxylation of organic halides

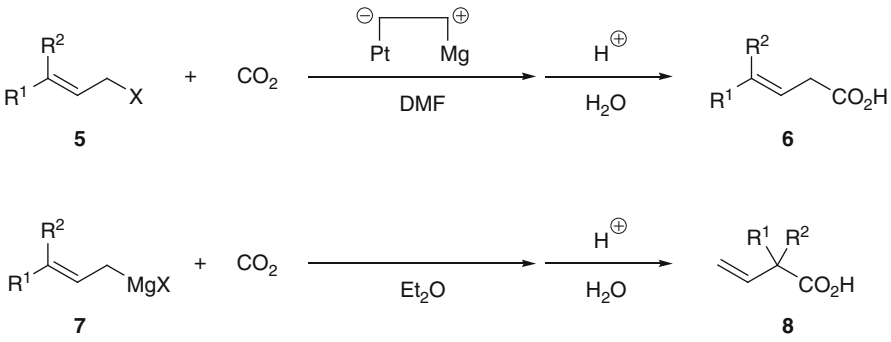

Scheme 10.4 Regioselective fixation of carbon dioxide in γ,γ-disubstituted allylic halides by electrochemical method and Grignard reagents

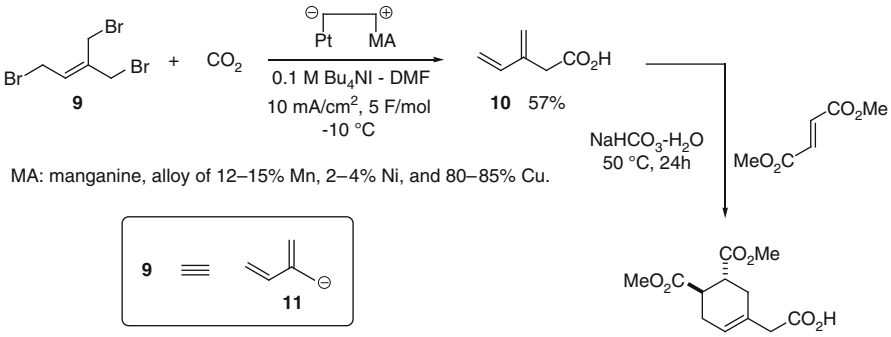

Scheme 10.5 Synthesis of 3-methylene-4-pentenoic acid by electrochemical carboxylation of 2-bromomethyl-1,4-dibromobut-2-ene and its application as a water-soluble diene in aqueous Diels-Alder reaction

often results in drastic enhancement and control of chemo- and regioselectivity and efficiency of carbon dioxide fixation. For instance, electrochemical carboxylation of lactone enol triflates **12**, readily prepared from the corresponding lactones, in the absence of any catalyst gives only a complex mixture in about 60 % conversion of **12**, while similar carboxylation in the presence of 20 mol% of $NiBr_2$•bpy results in efficient fixation of carbon dioxide to give the corresponding cyclic α-alkoxyl-α,β-unsaturated carboxylic acid **13** in high yields [60] (Scheme 10.6).

Electrochemical carboxylation of terminal alkynes **14** in the presence of Ni catalyst gave **15** as a major product along with isomer **16** [17, 18]. Carboxylic acids **17** and **18** are also synthesized by nickel-catalyzed electrochemical carboxylation of terminal alkyne **14** [19]. Consequently, selective synthesis of each carboxylic acid **15**, **16**, **17**, and **18** from terminal alkyne **14** and carbon dioxide can be accomplished even by selecting appropriate ligands on nickel(II) complexes in the electrochemical carboxylation (Scheme 10.7). As a similar manner, control

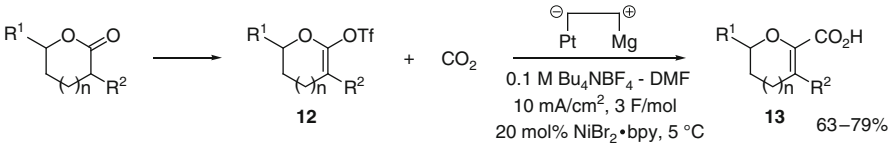

Scheme 10.6 Synthesis of cyclic α-alkoxyl-α,β-unsaturated carboxylic acids by nickel(0)-catalyzed electrochemical carboxylation of lactone enol triflates

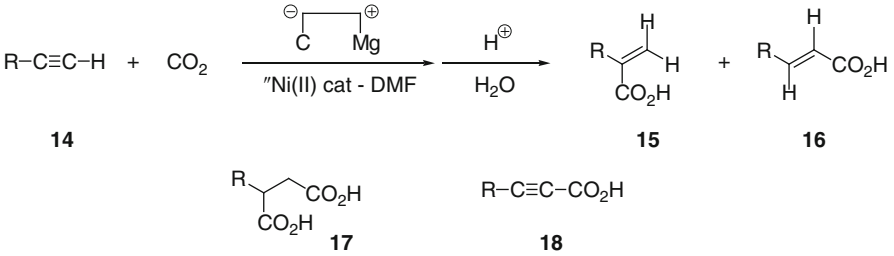

Scheme 10.7 Ligand-directed and nickel-catalyzed electrochemical carboxylation of terminal alkynes

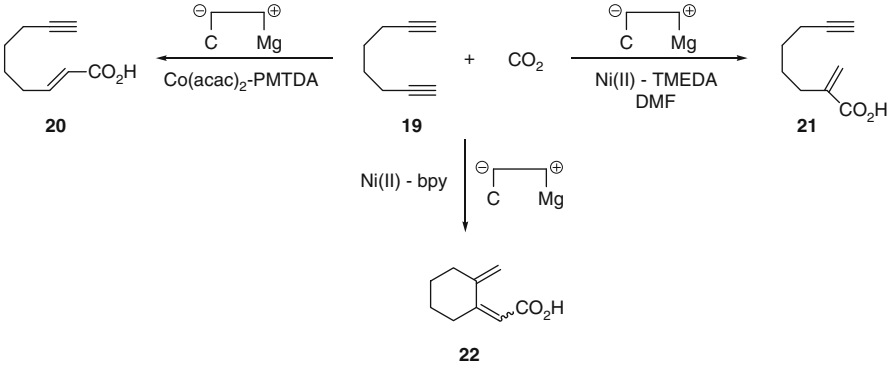

Scheme 10.8 Nickel-catalyzed electrochemical carboxylation of α,ω-diynes

of chemo- and regioselectivity by catalysts and ligands has also been achieved in electrochemical carboxylation of α,ω-diyne **19** to give each carboxylic acids **20**, **21**, and **22** selectively [22] (Scheme 10.8).

Carboxylation can take place with other electrochemically induced chemical reactions such as cyclization [75–77]. For example, electrochemical carboxylation of 2-allyloxybromobenzene (**23**) in the presence of nickel catalyst or electron transfer

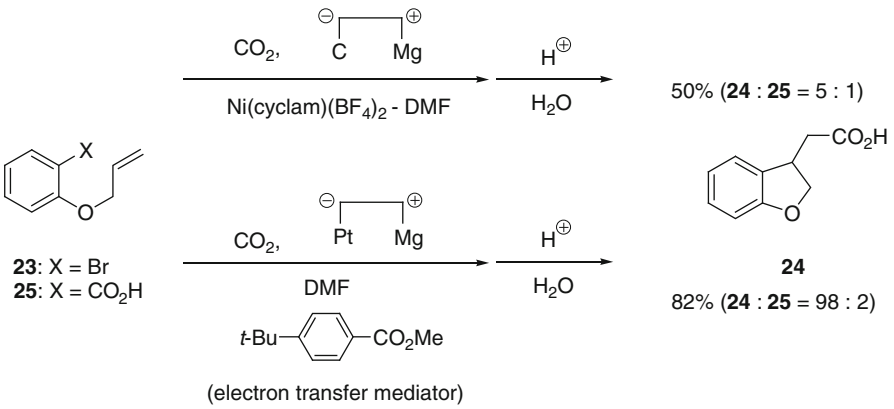

Scheme 10.9 Synthesis of dihydrobenzofuran-3-ylacetic acids by electrochemical sequential cyclization-carboxylation reaction

mediator results in cyclization followed by fixation of carbon dioxide to give carboxylic acid **24** in high selectivity toward direct-carboxylation product **25** (Scheme 10.9) [75, 77].

One notable synthetic application of electrochemical fixation of carbon dioxide is synthesis of 2-arylpropanoic acids, nonsteroidal anti-inflammatory drugs (NSAIDs), and their useful precursors (Scheme 10.10). Electrochemical carboxylations of benzyl halide **26** give 2-arylpropanoic acid **27**. Many successful syntheses of NSAIDs, such as ibuprofen and naproxen, have been reported by this type of reaction [1, 3, 30–33, 35–37, 40–44, 48–50, 71, 86, 87]. On the other hand, chiral 2-arylpropanoic acid **27** can be readily synthesized by electrochemical carboxylation of vinyl bromide **28** [51, 71] followed by enantioselective hydrogenation. For example, electrochemical carboxylation of vinyl bromide **28a** yields α, β-unsaturated carboxylic acid **29a** in 93 % yield [51], which can be readily transformed into (*S*)-ibuprofen **27a** by enantioselective hydrogenation [78, 79] (Scheme 10.10). The precursors of naproxen (**29b**), ketoprofen (**29c**), and flurbiprofen (**29c**) are also synthesized in high yields by similar electrochemical carboxylation. Consequently, synthesis of chiral NSAIDs can be readily achieved from vinyl bromide **28** and carbon dioxide only in two steps by electrochemical method (Scheme 10.11). α,β-Unsaturated carboxylic acid **29** can also be obtained from aryl methyl ketone **30** by electrochemical carboxylation followed by dehydration of the resulting α-hydroxycarboxylic acid **31**. Successful syntheses of **31** as the precursors of chiral NSAIDs have been reported by using this type of reaction [61, 63, 64, 71, 86, 87] (Scheme 10.10).

It is noteworthy that syntheses of fluorinated analogs of NSAIDs can also be achieved by electrochemical fixation of carbon dioxide [48–50]. For example, electrochemical reduction of α,α-difluoroethylarenes **32** in the presence of carbon dioxide by using a Pt cathode and a Mg anode resulted in the reductive cleavage of one C–F bond followed by a fixation of carbon dioxide at the benzylic

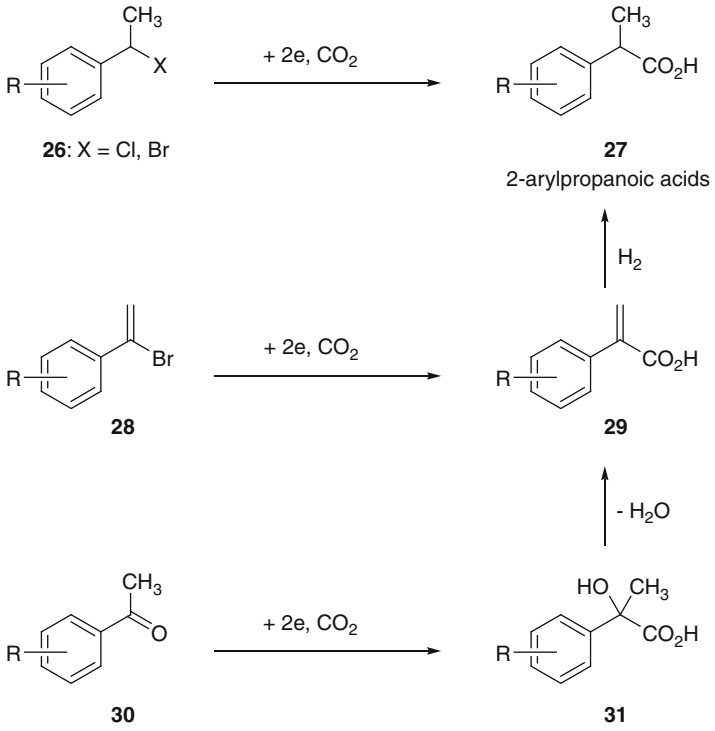

Scheme 10.10 Three synthetic routes for nonsteroidal anti-inflammatory drugs (NSAIDs) having 2-arylpropanoic acid skeleton through electrochemical fixation of carbon dioxide

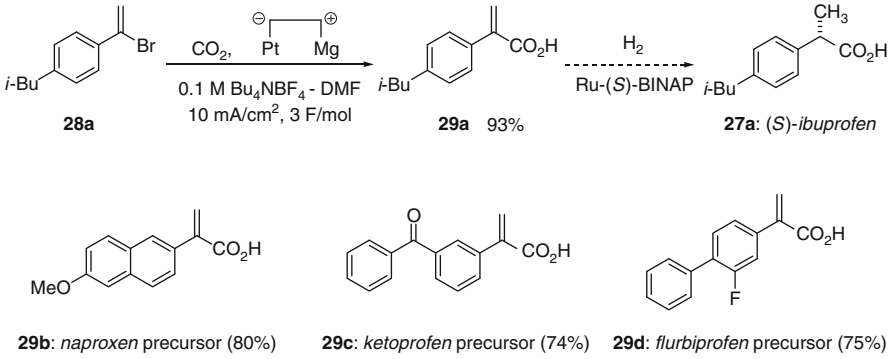

Scheme 10.11 Efficient synthesis of 2-arylpropenoic acids, the precursors of chiral NSAIDs, by electrochemical carboxylation of α-bromostyrene derivatives

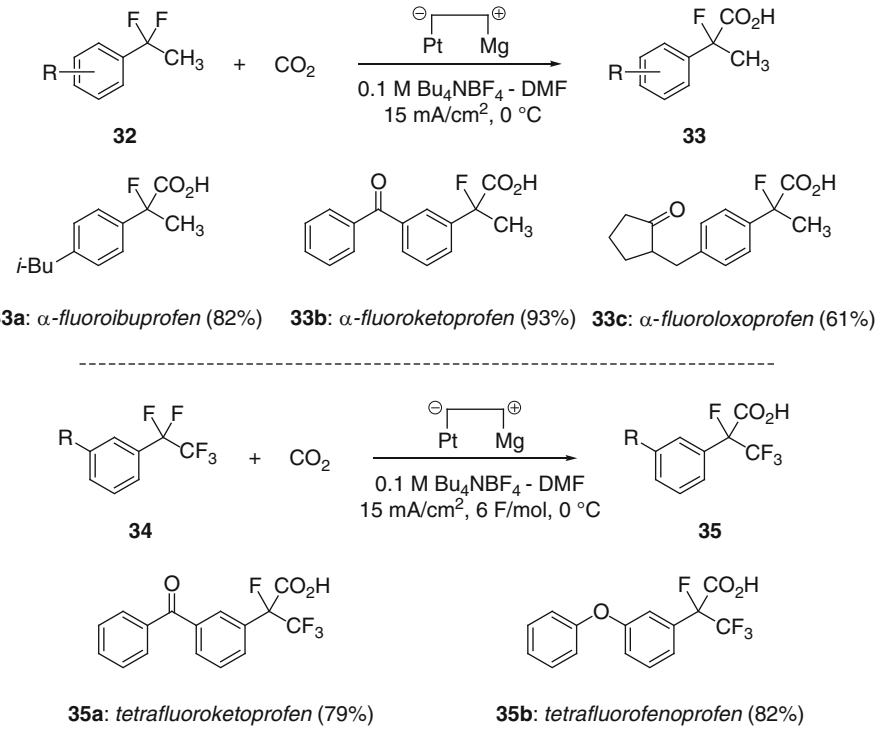

Scheme 10.12 Syntheses of mono- and tetrafluorinated NSAIDs by electrochemical carboxylation of benzylic fluorides

position to give 2-fluoro-2-arylpropanoic acids, α-fluorinated NSAIDs, **33** in good yields (Scheme 10.12). α-Fluoroibuprofen (**33a**), α-fluoroketoprofen (**33b**), α-fluoroloxoprofen (**33c**), and other α-fluorinated NSAIDs are successfully synthesized in high yields by similar electrochemical carboxylation [48]. Synthesis of tetrafluorinated ketoprofen (**35a**) and fenoprofen (**35b**) is also accomplished using pentafluoroethylarenes (**34**) as starting materials in similar electrochemical carboxylation [49] (Scheme 10.12).

Electrochemical fixation of carbon dioxide is also an effective and powerful tool for synthesis of β,β,β-trifluoro derivatives of ibuprofen, naproxen, and related NSAIDs [50]. Electrochemical reduction of benzyl bromide **36**, having trifluoromethyl group at the benzylic position, in the presence of carbon dioxide by using zinc, instead of magnesium, as an anode results in efficient fixation of carbon dioxide to give the corresponding carboxylated product **37** in good yields. Trifluoroibuprofen methyl ester (**37a**), trifluoronaproxen methyl ester (**37b**), and trifluorofenoprofen (**37c**) are successfully synthesized in moderate to good yields by the present electrochemical method (Scheme 10.13). Synthesis of **37** is quite difficult by conventional chemical fixation of carbon dioxide using organometallic reagents. Since β,β,β-trifluoroethyl anion such as **39** is mostly known to release a

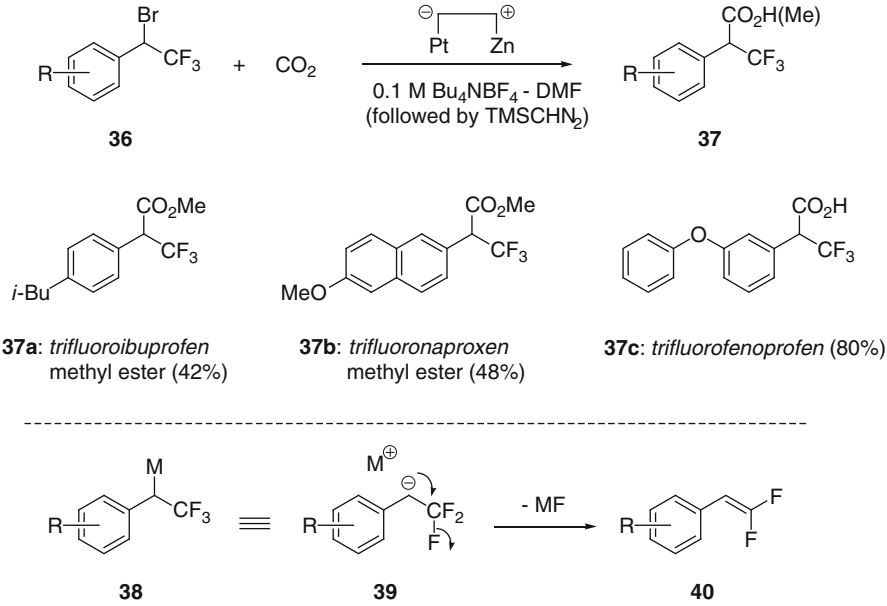

Scheme 10.13 Synthesis of 2-aryl-3,3,3-trifluoropropanoic acids, trifluorinated NSAIDs, by electrochemical carboxylation of (1-bromo-2,2,2-trifluoroethyl)arenes

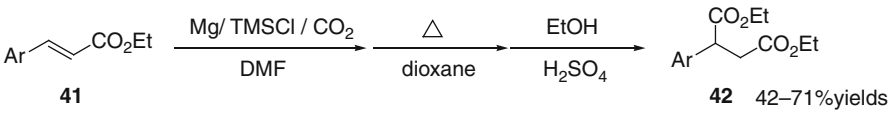

Scheme 10.14 Magnesium-promoted carboxylation of ethyl cinnamates

fluoride ion spontaneously to give difluoroalkenes such as **40** [50, 80], it is hard to prepare the corresponding organometallic reagents such as **38** by conventional chemical methods.

These successful syntheses of fluorinated NSAIDs **33**, **35**, and **37** strongly indicate the usefulness, significance, advantage, and convenience of an electrochemical fixation of carbon dioxide for synthesis of carboxylic acids.

Efficient fixation of carbon dioxide can also be achieved by using magnesium metal, instead of electrolysis, as an electron donor for the reduction of organic substrate. For example, magnesium-promoted carboxylation of ethyl cinnamate derivatives **41** for practical synthesis of arylsuccinate **42** has been successfully carried out [81] (Scheme 10.14).

It is well known that carbon dioxide can become supercritical fluid under relatively moderate conditions ($Tc = 31$ C, $Pc = 7.5$ MPa). Supercritical carbon dioxide ($scCO_2$) has significant potential as an environmentally benign solvent to replace the hazardous organic solvents, as carbon dioxide is abundant, economical,

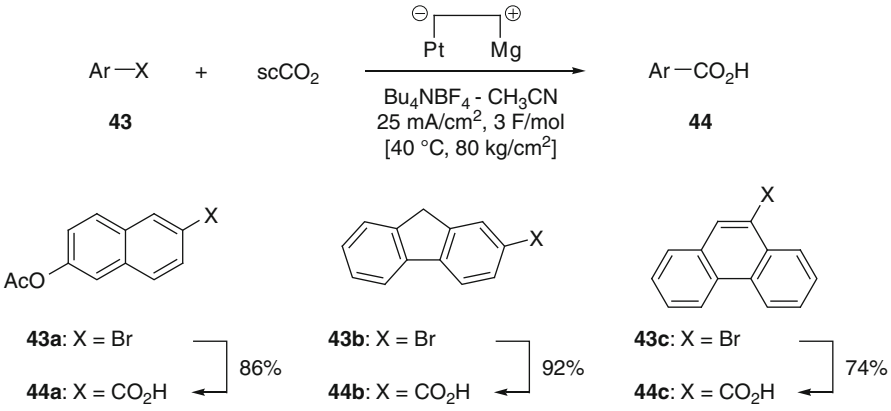

Scheme 10.15 Electrochemical carboxylation of aryl halides in supercritical carbon dioxide ($scCO_2$)

and nontoxic and can be recovered and reused after the reaction. The use of $scCO_2$ to electrochemical carboxylation has been studied, and a novel method for electrochemical carboxylation in $scCO_2$ by the use of small amount of acetonitrile (5–10 to 155 mL of $scCO_2$) as a cosolvent has been developed [82]. No current flows in pure supercritical carbon dioxide due to its poor conductivity.

Fixation of carbon dioxide to aromatic compounds successfully takes place in $scCO_2$. Electrochemical reduction of aromatic halides **43** in $scCO_2$ containing a small amount of acetonitrile with a platinum plate cathode and a magnesium anode results in efficient fixation of carbon dioxide to give aryl carboxylic acids such as **44a–c** in high yields [82, 83] (Scheme 10.15).

Electrochemical dicarboxylation of phenanthrene (**45**) and anthracene (**47**) also proceeds efficiently in $scCO_2$ to yield the corresponding dicarboxylic acids **46** and **48**, respectively, in high stereoselectivity and high yields [83, 84] (Scheme 10.16). Similar electrochemical dicarboxylation of **47** in acetonitrile solution in the presence of atmospheric pressure of carbon dioxide only gives 32 % yield of dicarboxylic acid **48**.

Electrochemical carboxylation in $scCO_2$ can also be applied to the synthesis of NSAIDs. For example, electrolysis of benzyl chloride **49** in $scCO_2$ yields *racemic* naproxen (**50**) in 74 % yield [83, 84] (Scheme 10.17).

Electrochemical carboxylation of aryl methyl ketone **51** in $scCO_2$ gives α-hydroxycarboxylic acid **52** in 78 % yield (Scheme 10.18), which can be transformed into chiral (*S*)-naproxen (**53**) by dehydration followed by enantioselective hydrogenation (Scheme 10.18; see also Scheme 10.10). Synthesis of loxoprofen precursor **55** is of considerable synthetic as well as electrochemical significance as the usual chemical reaction cannot control the reactivity of the two carbonyl groups in **54**. In the electrochemical reactions, however, aryl methyl ketone is more readily reduced than cyclopentanone, and the electrochemical carboxylation of **54** selectively takes place at the aryl ketone moiety to give expected α-hydroxypropanoic acid **55** in 91 %

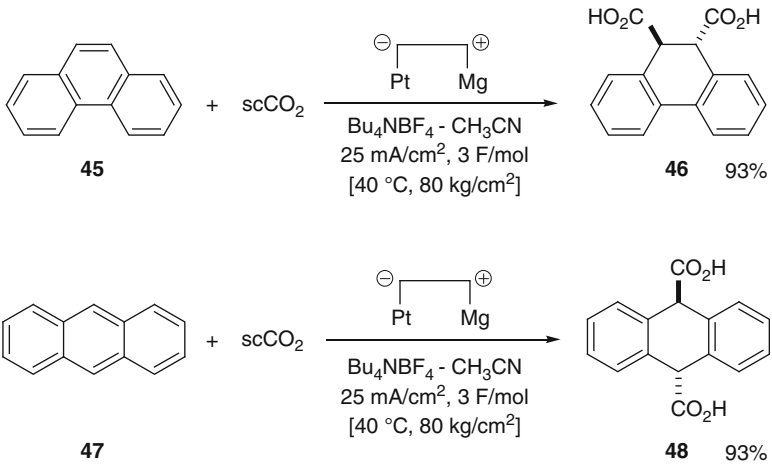

Scheme 10.16 Electrochemical carboxylation of phenanthrene and anthracene in $scCO_2$

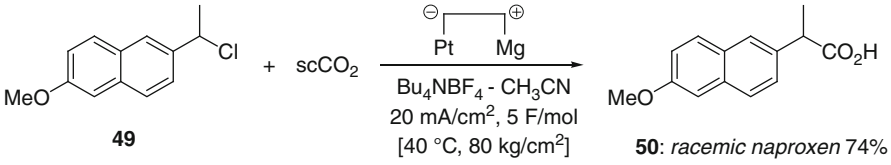

Scheme 10.17 Synthesis of naproxen by electrochemical carboxylation in $scCO_2$

yield [84], which can also be transformed into chiral loxoprofen (**56**) by dehydration followed by enantioselective hydrogenation (Scheme 10.18, see also Scheme 10.10).

Similar electrochemical carboxylation of vinyl bromides **28** in $scCO_2$ also gives the precursor of NSAIDs **29a**, **29b**, and **29d** in almost the same yields as those using atmospheric pressure of carbon dioxide [84] (see Scheme 10.11).

Although there are many reports on electrochemical carboxylation, only a few studies on diastereoselective [85, 86] and asymmetric [87, 88] fixation of carbon dioxide by electrochemical method have been reported. For example, diastereoselective electrochemical carboxylation using chiral *N*-(2-bromoacyl) oxazolidin-2-ones as substrates has been studied, and the best diastereomeric ratio (**58/59** = 2/98) with 80 % isolated yield is accomplished when amide **57** (R = Me) having Oppolzer's camphorsultam as chiral auxiliary is used as a substrate in electrochemical carboxylation [85] (Scheme 10.19).

Alkaloid-induced asymmetric electrochemical carboxylation of aryl alkyl ketone has been studied. Yields and enantiomeric excess of carboxylic acids are, however, still moderate, and further development of these areas including diastereoselective fixation of carbon dioxide with wide variety of examples and scopes are desirable.

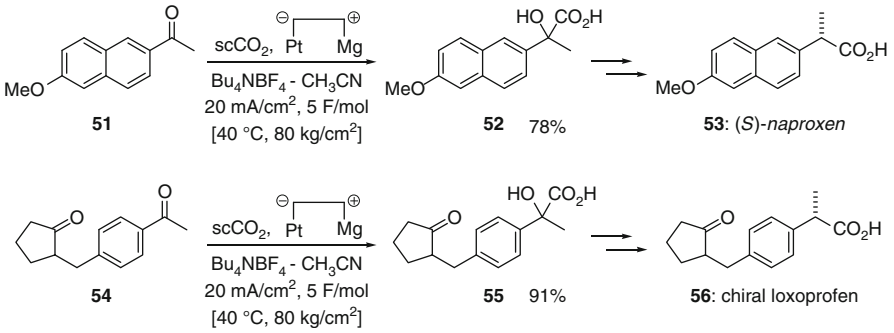

Scheme 10.18 Synthesis of the precursors of naproxen and loxoprofen by electrochemical carboxylation of aryl methyl ketones in $scCO_2$

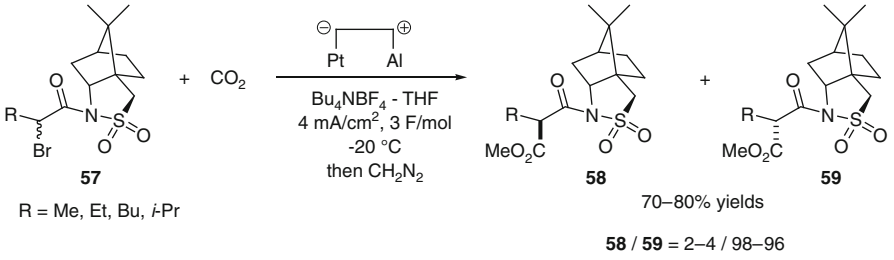

Scheme 10.19 Diastereoselective electrochemical carboxylation of chiral α-bromoamides

The use of an ionic liquid as a solvent and a supporting electrolyte for electrochemical fixation of carbon dioxide has been studied [89, 90]. Since ionic liquid can be readily recovered and reused after the reaction, it has significant possibility as a novel reaction medium not only for fixation of carbon dioxide but also for other electrochemical reactions. As well as diastereoselective and asymmetric electrochemical fixation of carbon dioxide, development of these research areas are now in progress and further studies are also expected.

10.3 Conclusion

The present electrochemical method for efficient fixation of atmospheric pressure of carbon dioxide to a variety of organic compounds yielding useful carboxylic acids has several advantages: use of simple one-compartment cell, simple electrolysis under constant current conditions, high yields of the produced carboxylic acid when a sacrificial anode such as magnesium and aluminum is used, and easy application to the synthesis of useful precursors of nonsteroidal anti-inflammatory

agents such as ibuprofen and naproxen and other high value-added substances. This electrochemical method might be used for industrial production of these compounds. The use of supercritical carbon dioxide for the electrochemical fixation of carbon dioxide would become a useful method for production of carboxylic acids in the future because the use of organic solvent will be highly limited and both environmentally benign procedures and recycle of carbon source should be important and necessary in organic synthesis from the viewpoint of green and sustainable chemistry.

References

1. Silvestri G, Gambino S, Filardo G, Gulotta A (1984) Sacrificial anodes in the electrocarboxylation of organic chlorides. Angew Chem Int Ed Engl 23:979–980
2. Silvestri G, Gambino S, Filardo G (1991) Use of sacrificial anodes in synthetic electrochemistry. Processes involving carbon dioxide. Acta Chem Scand 45:987–992
3. Sock O, Troupel M, Périchon J (1985) Electrosynthesis of carboxylic acids from organic halides and carbon dioxide. Tetrahedron Lett 26:1509–1512
4. Chaussard J, Folest JC, Nédélec JY, Périchon J, Sibille S, Troupel M (1990) Use of sacrificial anodes in electrochemical functionalization of organic halides. Synthesis 1990:369–381
5. Dérien S, Clinet J-C, Duñach E, Péricon J (1992) Electrochemical incorporation of carbon dioxide into alkenes by nickel complexes. Tetrahedron 48:5235–5248
6. Tyssee DA, Baiser MM (1974) Electrocarboxylation I. Mono- and dicarboxylation of activated olefins. J Org Chem 39:2819–2823
7. Harada J, Sakakibara Y, Kunai A, Sasaki K (1984) Electrochemical carboxylation of α, β-unsaturated ketones with carbon dioxide. Bull Chem Soc Jpn 57:611–612
8. Filardo G, Gambino S, Silvestri G, Gennaro A, Vianello E (1984) Electrocarboxylation of styrene through homogeneous redox catalysis. J Electroanal Chem 177:303–309
9. Chiozza E, Desigaud M, Greiner J, Duñach E (1998) First example of double bond migration in the electrochemical CO_2 incorporation into (perfluoroalkyl)alkenes. Tetrahedron Lett 39:4831–4834
10. Ballivet-Tkatchenko D, Folest JC, Tanji J (2000) Electrocatalytic reduction of CO_2 for the selective carboxylation of olefins. Appl Organometal Chem 14:847–849
11. Senboku H, Komatsu H, Fujimura Y, Tokuda M (2001) Efficient electrochemical dicarboxylation of phenyl-substituted alkenes: synthesis of 1-phenylalkane-1,2-dicarboxylic acids. Synlett 2001(3):418–420
12. Chowdhury MA, Senboku H, Tokuda M (2004) Electrochemical carboxylation of bicycle [n.1.0]alkylidene derivatives. Tetrahedron 60:475–481
13. Senboku H, Yamauchi Y, Kobayashi N, Fukui A, Hara S (2011) Electrochemical carboxylation of flavones: facile synthesis of flavanone-2-carboxylic acids. Electrochemistry 79:862–864
14. Senboku H, Yamauchi Y, Kobayashi N, Fukui A, Hara S (2012) Some mechanistic studies on electrochemical carboxylation of flavones to yield flavanone-2-carboxylic acids. Electrochim Acta 82:450–456
15. Gambino S, Filardo G, Silvestri G (1982) Electrochemical carboxylation of organic substrates. Synthesis of carboxylic derivatives of acenaphthylene. J Appl Electrochem 12:549–555
16. Dérien S, Clinet J-C, Duñach E, Péricon J (1990) Coupling of allenes and carbon dioxide catalyzed by electrogenerated nickel complexes. Synlett:361–364
17. Duñach E, Péricon J (1988) Electrochemical carboxylation of terminal alkynes catalyzed by nickel complexes: unusual regioselectivity. J Organometal Chem 352:239–246

18. Duñach E, Péricon J (1990) New catalytic system for the activation of carbon dioxide and alkynes based on electrogenerated nickel complexes. Synlett 1990(3):143–145
19. Labbé E, Duñach E, Péricon J (1988) Ligand-directed reaction products in the nickel-catalyzed electrochemical carboxylation of terminal alkynes. J Organometal Chem 353:C51–C56
20. Dérien S, Clinet JC, Duñach E, Péricon J (1992) New C-C bond formation through the nickel-catalysed electrochemical coupling of 1,3-enynes and carbon dioxide. J Organometal Chem 424:213–224
21. Dérien S, Clinet JC, Duñach E, Péricon J (1993) Activation of carbon dioxide: nickel-catalyzed electrochemical carboxylation of diynes. J Org Chem 58:2578–2588
22. Dérien S, Duñach E, Péricon J (1990) Electrogenerated nickel(0) catalyzed carbon dioxide incorporation into α, ω-diynes. J Organometal Chem 385:C43–C46
23. Dérien S, Clinet JC, Duñach E, Péricon J (1991) First example of direct carbon dioxide incorporation into 1,3-diynes: a highly regio- and stereo-selective nickel-catalyzed electrochemical reaction. J Chem Soc Chem Commun:549–550
24. Heintz M, Sock O, Saboureau C, Périchon J, Troupel M (1988) Electrosynthesis of arylcarboxylic acids from chlorobenzene derivatives and carbon dioxide. Tetrahedron 44:1631–1636
25. Tokuda M, Kabuki T, Kato Y, Suginome H (1995) Regioselective synthesis of β, γ-unsaturated carboxylic acids by the electrochemical carboxylation of allylic bromides using a reactive-metal anode. Tetrahedron Lett 36:3345–3348
26. Tokuda M, Yoshikawa A, Suginome H, Senboku H (1997) New and convenient synthesis of 3-methylenepent-4-enoic acid by electrochemical carboxylation. Synthesis 1997(10):1143–1145
27. Tokuda M, Kabuki T, Suginome H (1994) Electrochemical carboxylation of propargylic halides by the use of reactive-metal anode. Denki Kagaku (presently Electrochemistry) 62:1144–1147
28. Folest JC, Duprilot JM, Périchon J, Robin Y, Devynck J (1985) Electrocatalyzed carboxylation of organic halides by a cobalt-salen complex. Tetrahedron Lett 26:2633–2636
29. Silvestri G, Gambino S, Filardo G, Greco G, Gulotta A (1986) Electrochemical carboxylation of benzal chloride. Tetrahedron Lett 25:4307–4308
30. Fauvarque JF, Jutand A, Francois M (1986) Electrosynthesis of 2-arylpropionic acids from ArCHMeCl and carbon dioxide, catalyzed by nickel complexes. Synthesis of anti-inflammatory agents. Nouv J Chim 10:119–122
31. Fauvarque JF, Jutand A, Francois M (1988) Nickel catalysed electrosynthesis of anti-inflammatory agents. Part I – Synthesis of aryl-2 propionic acids, under galvanostatic conditions. J Appl Electrochem 18:109–115
32. Fauvarque JF, Jutand A, Francois M, Petit MA (1988) Nickel-catalyzed electrosynthesis of anti-inflammatory agents: Part II: Monitoring of the electrolyses by HPLC analysis: role of the catalyst. J Appl Electrochem 18:116–119
33. Chaussard J, Troupel M, Robin Y, Jacob G, Juhasz JP (1989) Scale-up of electrocarboxylation reactions with a consumable anode. J Appl Electrochem 19:345–348
34. Saboureau C, Troupel M, Sibille S, Périchon J (1989) Electroreductive coupling of trifluoromethyl arenes with electrophiles: synthetic applications. J Chem Soc Chem Commun:1138–1139
35. Fauvarque JF, De Zelicourt Y, Amatore C, Jutand A (1990) Nickel-catalyzed electrosynthesis of anti-inflammatory agents: Part III: A new electrolyzer for organic solvents: oxidation of metal power as an alternative sacrificial anodes. J Appl Electrochem 20:338–340
36. Isse AA, Gennaro A, Vianello E (1996) Electrochemical carboxylation of aryl methyl chlorides catalysed by [Co(salen)][H_2 salen = N,N′-bis(salicylidene)ethane-1,2-diamine]. J Chem Soc Dalton Trans:1613–1618
37. Chung WH, Guo P, Wong CP, Lau CP (2000) Electrocarboxylation of aryl methyl chlorides catalyzed by cobalt 6,6′-bis(2-hydroxyphenyl)-2,2′-bipyridine. J Electroanal Chem 486:32–39
38. Gennaro A, Isse AA, Maran F (2001) Nickel(I)(salen)-electrocatalyzed reduction of benzyl chloride in the presence of carbon dioxide. J Electroanal Chem 507:124–134
39. Isse AA, Gennaro A (2002) Electrocatalytic carboxylation of benzyl chlorides at silver cathodes in acetonitrile. Chem Commun:2798–2799

40. Stepanov AA, Volodin YY, Grachev MK, Kurochkina GI, Syrtsev AN, Grinberg VA (2002) Reactions of direct electrocarboxylation of 1-phenylethylbromide and 1-(4-isobutylphenyl) ethyl chloride in the presence of β-cyclodextrin. Russ J Electrochem 38:1346–1352
41. Isse AA, Ferlin MG, Gennaro A (2003) Homogeneous electron transfer catalysis in the electrochemical carboxylation of arylethyl chlorides. J Electroanal Chem 541:93–101
42. Isse AA, Ferlin MG, Gennaro A (2005) Electrocatalytic reduction of arylethyl chlorides at silver cathodes in the presence of carbon dioxide: synthesis of 2-arylpropanoic acids. J Electroanal Chem 581:38–45
43. Damodar J, Krishna Mohan S, Khaja Lateef S, Jayarama Reddy S (2005) Electrosynthesis of 2-arylpropionic acids from α-methylbenzyl chlorides and carbon dioxide by [Co(Salen)]. Synth Commun 35:1143–1150
44. Ramesh Raju R, Khaja Lateef S, Krishna Mohan S, Jayarama Reddy S (2006) Synthesis of aryl-2-propionic acids by electrocarboxylation of methyl aryl bromides. Arkivoc 2006(i):76–80
45. Isse AA, De Giusti A, Gennaro A, Falciola L, Mussini PR (2006) Electrochemical reduction of benzyl halides at a silver electrode. Electrochim Acta 51:4956–4964
46. Scialdone O, Galia A, Errante G, Isse AA, Gennaro A, Filardo G (2008) Electrocarboxylation of benzyl chlorides at silver cathode at the preparative scale level. Electrochim Acta 53:2514–2528
47. Niu DF, Xiao LP, Zhang AJ, Zhang GR, Tan QY, Lu JX (2008) Electrocatalytic carboxylation of aliphatic halides at silver cathode in acetonitrile. Tetrahedron 64:10517–10520
48. Yamauchi Y, Fukuhara T, Hara S, Senboku H (2008) Electrochemical carboxylation of α, α-difluorotoluene derivatives and its application to the synthesis of α-fluorinated nonsteroidal anti-inflammatory drugs. Synlett 2008:438–442
49. Yamauchi Y, Sakai K, Fukuhara T, Hara S, Senboku H (2009) Synthesis of 2-aryl-2,3,3,3-tetrafluoropropanoic Acids, tetrafluorinated fenoprofen and ketoprofen by electrochemical carboxylation of pentafluoroethylarenes. Synthesis:3375–3377
50. Yamauchi Y, Hara S, Senboku H (2010) Synthesis of 2-aryl-3,3,3-trifluoropropanoic acids using electrochemical carboxylation of (1-bromo-2,2,2-trifluoroethyl)arenes and its application to the synthesis of β, β, β-trifluorinated non-steroidal anti-inflammatory drugs. Tetrahedron 2009(66):473–479
51. Kamekawa H, Senboku H, Tokuda M (1997) Facile synthesis of aryl-substituted 2-alkenoic acids by electroreductive carboxylation of vinylic bromides using a magnesium anode. Electrochim Acta 42:2117–2123
52. Kamekawa H, Kudoh H, Senboku H, Tokuda M (1997) Synthesis of α, β-unsaturated carboxylic acids by nickel(II)-catalyzed electrochemical carboxylation of vinyl bromides. Chem Lett 26:917–918
53. Kuang C, Yang Q, Senboku H, Tokuda M (2005) Stereospecific electrochemical carboxylation of β-bromostyrene by use of nickel(II) catalyst. Chem Lett 34:528–529
54. Jutand A, Négri S, Mosleh A (1992) Palladium catalyzed electrosynthesis using aryl trifluoromethanesulfonates (triflates). Synthesis of biaryls and aromatic carboxylic acids. J Chem Soc Chem Commun:1729–1730
55. Jutand A, Négri S (1998) Activation of aryl and vinyl triflates by palladium and electron transfer–electrosynthesis of aromatic and α, β-unsaturated carboxylic acids from carbon dioxide. Eur J Org Chem 1998:1811–1812
56. Jutand A, Négri S (1997) Palladium-catalyzed carboxylation of vinyl triflates. Electrosynthesis of α, β-unsaturated carboxylic acids. Synlett 1997:719–721
57. Kamekawa H, Senboku H, Tokuda M (1998) New electrochemical carboxylation of vinyl triflates. Synthesis of β-keto carboxylic acid. Tetrahedron Lett 39:1591–1594
58. Senboku H, Fujimura Y, Kamekawa H, Tokuda M (2000) Divergent electrochemical carboxylation of vinyl triflates: new electrochemical synthesis of phenyl-substituted α, β-unsaturated carboxylic acids and aliphatic β-keto carboxylic acids. Electrochim Acta 45:2995–3003
59. Senboku H, Kanaya H, Fujimura Y, Tokuda M (2001) Stereochemical study on electrochemical carboxylation of vinyl triflates. J Electroanal Chem 507:82–88

60. Senboku H, Kanaya H, Tokuda M (2002) Convenient synthesis of cyclic α-alkoxyl-α, β-unsaturated carboxylic acids by nickel-catalyzed electrochemical carboxylation of lactone enol triflates. Synlett 2002:140–142
61. Silvestri G, Gambino S, Filardo G (1986) Electrochemical carboxylation of aldehydes and ketones with sacrificial aluminum anodes. Tetrahedron Lett 27:3429–3430
62. Mcharek S, Heintz M, Troupel M, Péricon J (1989) Electrocarboxylation de composés carbonyles aliphatiques, aromatiques et vinyliques: intérêt de l'utilisation d'une anode consumable en magnésium. Bull Chim Soc Fra:95–97
63. Chan ASC, Huang TT, Wagenknecht JH, Miller RE (1995) A novel synthesis of 2-arylacetic acids via electrocarboxylation of methyl aryl ketones. J Org Chem 60:742–744
64. Datt AK, Marron PA, King CJH, Wagenknecht JH (1998) Process development for electrocarboxylation of 2-acetyl-6-methoxynaphthalene. J Appl Electrochem 28:569–577
65. Silvestri G, Gambino S, Filardo G (1988) Synthesis of N-substituted α-amino acids by electrocarboxylation of imines with sacrificial metallic anodes. Gazz Chim Ital 118:643–648
66. Gal J, Folest JC, Troupel M, Moingeon MO, Chaussard J (1995) Synthesis of arylacetic and 2-arypropionic acids by electrocarboxylation of benzylic compounds bearing a leaving group other than a halogen. New J Chem 19:401–407
67. Ohkoshi M, Michinishi J, Hara S, Senboku H (2010) Electrochemical carboxylation of benzylic carbonates: alternative method for efficient synthesis of arylacetic acids. Tetrahedron 66:7732–7737
68. Pokhodenko VD, Koshechko VG, Titov VE, Lopushanskaja VA (1995) A convenient electrochemical synthesis of α-oxoacids. Tetrahedron Lett 36:3277–3278
69. Koshechko VG, Titov VE, Lopushanskaya VA (2002) Electrochemical carboxylation of benzoyl bromides as effective phenylglyoxylic acid synthesis route. Electrochem Commun 4:655–658
70. Medeiros MJ, Pintaric C, Olivero S, Duñach E (2011) Nickel-catalyzed electrochemical carboxylation of allylic acetates and carbonates. Electrochim Acta 56:4384–4389
71. Tokuda M (2006) Efficient fixation of carbon dioxide by electrolysis – facile synthesis of useful carboxylic acids. J Nat Gas Chem 15:275–281
72. Torii S, Tanaka H, Hamatani T, Morisaki K, Jutand A, Pfluger F, Fauvarque JF (1986) Pd(0)-catalyzed electroreductive carboxylation of aryl halides, β-bromostyrene, and allyl acetates with CO_2. Chem Lett 15:169–172
73. Amatore C, Jutand A, Khalil F, Nielsen MF (1992) Carbon dioxide as a C1 building block. Mechanism of palladium-catalyzed carboxylation of aromatic halides. J Am Chem Soc 114:7076–7085
74. Damodar J, Krishna Mohan S, Jayarama Reddy S (2001) Synthesis of 2-arylpropionic acids by electrocarboxylation of benzyl chlorides catalysed by $PdCl_2(PPh_3)_2$. Electrochem Commun 3:762–766
75. Olivero S, Dunach E (1999) Selectivity in the tandem cyclization – carboxylation reaction of unsaturated haloaryl ethers catalyzed by electrogenerated nickel complexes. Eur J Org Chem 1999:1885–1891
76. Tyssee DA, Baiser MM (1974) Electrocarboxylation II. Electrocarboxylative dimerization and cyclization. J Org Chem 39:2823–2828
77. Senboku H, Michinishi J, Hara S (2011) Facile synthesis of 2,3-dihydrobenzofuran-3-ylacetic acids by novel electrochemical sequential aryl radical cyclization-carboxylation of 2-allyloxybromobenzenes using methyl 4-tert-butylbenzoate as an electron-transfer mediator. Synlett 2011:1567–1572
78. Manimaran T, Wu TC, Klobucar WD, Kolich CH, Stahly GP, Fronczek FR, Watkins SE (1993) In situ generation of ruthenium-chiral phosphine complexes and their use in asymmetric hydrogenation. Organometallics 12:1467–1470
79. Zhang X, Uemura T, Matsumura K, Sayo N, Kumobayashi H, Takaya H (1994) Highly enantioselective hydrogenation of α, β-unsaturated carboxylic acids catalyzed by H8-BINAP-Ru(II) complexes. Synlett 1994:501–503

80. Uneyama K, Katagiri T, Amii H (2008) α-Trifluoromethylated carbanion synthons. Acc Chem Res 41:817–829
81. Maekawa H, Murakami T, Miyazaki T, Nishiguti I (2011) Practical synthesis of diethyl phenylsuccinate by Mg-promoted carboxylation of ethyl cinnamate. Chem Lett 40:368–369
82. Sasaki A, Kudoh H, Senboku H, Tokuda M (1998) Electrochemical carboxylation of several organic halides in supercritical carbon dioxide. In: Torii S (ed) Novel trends in electroorganic synthesis. Springer, Tokyo, pp 245–246
83. Tokuda M (1999) Electrolytic synthesis using supercritical carbon dioxide. Electrochemistry 67:993–996
84. Senboku H, Tokuda M (2002) Electrochemical organic synthesis in supercritical carbon dioxide. Fine Chemical 31:50–60
85. Feroci M, Orsini M, Palombi L, Sotgiu G, Colapietro M, Ineci A (2004) Diastereoselective electrochemical carboxylation of chiral α-bromocarboxylic acid derivatives: an easy access to unsymmetrical alkylmalonic ester derivatives. J Org Chem 69:487–494
86. Orsini M, Feroci M, Sotgiu G, Inesi A (2005) Stereoselective electrochemical carboxylation: 2-phenylsuccinates from chiral cinnamic acid derivatives. Org Biomol Chem 3:1203–1208
87. Zhang K, Wang H, Zhao S, Niu D, Lu J (2009) Asymmetric electrochemical carboxylation of prochiral acetophenone: an efficient route to optically active atrolactic acid via selective fixation of carbon dioxide. J Electroanal Chem 630:35–41
88. Zhao S, Zhu M, Zhang K, Wang H, Lu J (2011) Alkaloid induced asymmetric electrochemical carboxylation of 4-methylpropiophenone. Tetrahedron Lett 52:2702–2705
89. Wang H, Zhang G, Liu Y, Luo Y, Lu J (2007) Electrocarboxylation of activated olefins in ionic liquid $BMIMBF_4$. Electrochem Commun 9:2235–2239
90. Hiejima Y, Hayashi M, Uda A, Oya S, Kondo H, Senboku H, Takahashi K (2010) Electrochemical carboxylation of α-chloroethylbenzene in ionic liquids compressed with carbon dioxide. Phys Chem Chem Phys 12:1953–1957

Chapter 11
Accelerated Carbonation Processes for Carbon Dioxide Capture, Storage and Utilisation

Renato Baciocchi, Giulia Costa, and Daniela Zingaretti

11.1 Introduction

This chapter deals with the application of accelerated carbonation of alkaline minerals and industrial residues in the framework of the actions aimed at reducing carbon dioxide emissions to the atmosphere. Depending on the point of view and the type of application, carbonation can be seen as either a CO_2 capture, CO_2 storage or CO_2 utilisation process. The boundary between the three definitions is however not clear-cut and depends on the main environmental benefit brought by the implementation of the carbonation process. The definition of carbonation as a utilisation or storage option will eventually depend on the extent of storage capacity that we may be able to achieve with respect to the emissions of the process we are dealing with. For instance, if we consider the case of accelerated carbonation of alkaline industrial residues, we may consider this process either as a CO_2 storage or a CO_2 utilisation one; this will depend on the relevance we may give to the CO_2 uptake capacity of these materials or to the improvement of their environmental properties after carbonation. Although this chapter is part of a book on CO_2 utilisation, it is worth pointing out that, differently from the other utilisation options considered, carbonation allows for a net storage of CO_2 into a solid and thermodynamically stable form and thus may be considered as a truly effective measure for climate change mitigation.

This chapter will first address the fundamentals of carbonation, describing the thermodynamics and kinetics of the process with reference to suitable raw materials and minerals. This will lead to discuss naturally occurring carbonation, highlighting the main issues that hinder carbonation to take place extensively on the earth's crust and possibly constrain the operating conditions for the industrial application of this process. This will open the way to the discussion on the operating conditions

R. Baciocchi (✉) • G. Costa • D. Zingaretti
Laboratory of Environmental Engineering, Department of Civil Engineering and Computer Science Engineering, University of Rome "Tor Vergata", Via del Politecnico 1, 00133 Rome, Italy
e-mail: baciocchi@ing.uniroma2.it

B.M. Bhanage and M. Arai (eds.), *Transformation and Utilization of Carbon Dioxide*, Green Chemistry and Sustainable Technology, DOI 10.1007/978-3-642-44988-8_11,

needed to accelerate the process, making it suitable for industrial applications. The application of accelerated carbonation will then constitute the main core of this chapter. First, a few CO_2 capture processes based on the exploitation of the carbonation reaction will be discussed. In the following, the largest section will be devoted to the application of mineral carbonation as a CO_2 storage and/or utilisation process, providing details on the different materials that can be used (minerals or industrial residues) and the reaction routes applied so far. Finally, the performance of accelerated carbonation processes making use of specific routes and feedstocks will be compared in terms of material and energy requirements.

11.2 Fundamentals of Carbonation Processes

11.2.1 Basic Thermodynamics and Kinetics of Carbonation

Mineral carbonation is a naturally occurring process, by which carbon dioxide reacts with minerals typically found in mafic and ultramafic rocks (i.e. Mg_2SiO_4 olivine, $Mg_3Si_2O_5(OH)_4$ serpentine, $CaSiO_3$ wollastonite), forming geologically and thermodynamically stable mineral carbonates (i.e. $MgCO_3$ magnesite, $MgCa(CO_3)_2$ dolomite, $CaCO_3$ calcite, $FeCO_3$ siderite, $NaAl(CO_3)(OH)_2$ dawsonite) [1]. Carbonation is a thermodynamically favourable process at the moderate temperature and pressure conditions encountered on the earth's surface and in the more superficial earth crust. The free energy of calcium and magnesium minerals, such as wollastonite and forsterite, in fact, well exceeds that of the corresponding carbonates for temperatures up to about 500 K at 1 bar CO_2 partial pressure [2]. Besides, the carbonation reaction is also exothermic: for instance, the enthalpy of reaction of CaO to $CaCO_3$ is 90 kJ/mol, which compares well to the enthalpy of combustion of carbon to carbon dioxide, equal to 400 kJ/mol.

Nevertheless, the naturally occurring carbonation reaction is a slow process, taking place at geological time scales. According to an investigation by Haug et al. [3], the weathering rate of olivine is estimated to be $10^{-8.5}$ mol/(m^2s) considering the average ground temperature in Norway of 6 °C and a pH of 5.6, which corresponds to the acidity of rainwater.

11.2.2 Accelerated Carbonation

The acceleration of natural carbonation processes in order to make them suitable for industrial applications aimed to store anthropogenically derived carbon dioxide has been first proposed by Seifritz [4] and Lackner et al. [2] within the efforts to reduce the emissions of greenhouse gases. The accelerated carbonation process involves the reaction of carbon dioxide with oxides of alkali and alkaline earth metals:

$$MeO + CO_2 \leftrightarrow MeCO_3 \tag{11.1}$$

Usually alkali or alkaline earth metals are not found naturally in the form of free oxides, as the latter are generally produced by the energy intensive calcination of the corresponding naturally occurring carbonate minerals. This means that reaction (11.1) as such can be exploited only if the carbonate is regenerated back to its oxide form. This is typically the case of *CO_2 capture* processes based on carbonation and calcination cycles. In these applications, CaO or other free alkali or alkaline metal oxides are usually contacted with a diluted CO_2 source at a temperature high enough to rapidly convert the oxide to the corresponding carbonate form. Then, the carbonated material is conveyed to a calciner where it is heated in order to decompose the carbonate, allowing to regenerate the solid to the oxide form, while releasing carbon dioxide ready for storage [5]. This process will be discussed in more detail in Sect. 11.3.2, together with another capture process based on the use of hot potassium carbonate [6].

If carbonate regeneration cannot take place or if the goal of the process is *CO_2 storage* (see Sect. 11.4.1), another alkalinity source needs to be used. As discussed in the previous section, alkali and alkaline earth metals may represent such a source. These are abundant components of the earth's crust, where they are found in different minerals, such as serpentine, olivine and wollastonite. The carbonation of these mineral takes place through the following global reactions [7]:

Olivine	$Mg_2SiO_4 + 2CO_2 \leftrightarrow 2MgCO_3 + SiO_2$	(11.2a)
Serpentine	$Mg_3Si_2O_5(OH)_4 + 3CO_2 \leftrightarrow 3MgCO_3 + 2SiO_2 + H_2O$	(11.2b)
Wollastonite	$CaSiO_3 + CO_2 \leftrightarrow CaCO_3 + SiO_2$	(11.2c)

Although a worldwide comprehensive estimate of available alkaline minerals is missing, the studies that have been performed up to now suggest that these should be theoretically sufficient to store all the currently known fossil carbon reserves. Making reference to the US situation, serpentine reserves are estimated at about 9,700 Gt [8]. Assuming that 2.1 tons of mineral are needed per ton of CO_2 stored (100 % conversion of serpentine), the sequestration potential of this mass of material is estimated around 4,600 Gt of CO_2 or more than 500 years of the US current production of CO_2 [8]. Furthermore, the final products of mineral carbonation (carbonates and silica) are environmentally stable and can therefore be disposed of as mine filler materials or used for construction purposes [9]. Hence, unlike underground geological storage, there would be little or no need to monitor the disposal sites and the environmental risks would be very low [7]. In Fig. 11.1 the estimated capacities and storage timeframes associated to different sequestration techniques are represented; as can be noted, mineral carbonation in particular shows the largest potential both in terms of capacity (similar to underground injection in saline aquifers) and of storage timeframes.

Despite the large availability of these minerals, concerns have been raised on the costs and environmental impact of the large mining industry that should be developed to extract them from the earth's crust. The size of this industry would not be unfeasible but would probably be of the same scale of the coal mining industry [7].

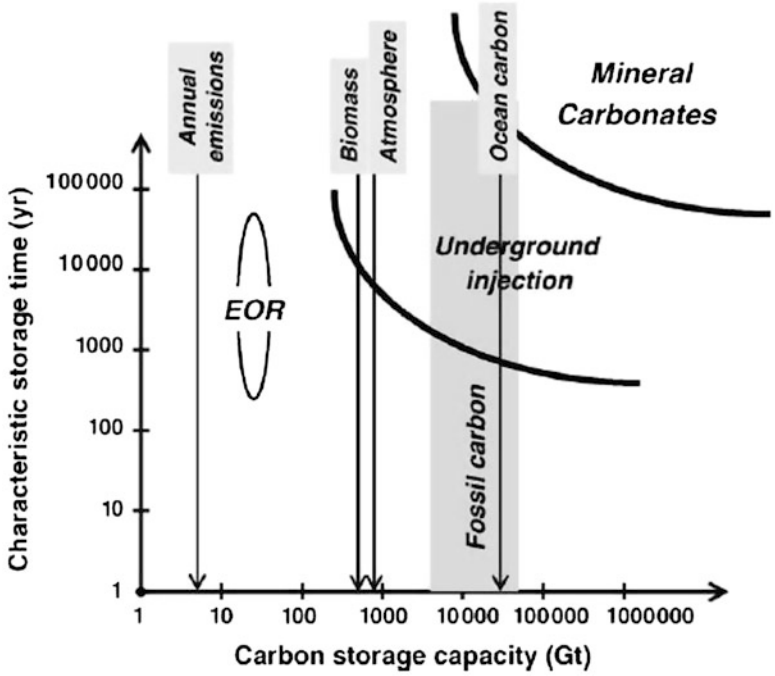

Fig. 11.1 Estimated storage capacities and relative timeframes for various sequestration methods (Reprinted from Ref. [10]. Copyright 2006, with permission from Elsevier)

An alternative alkalinity source is represented by some kinds of residues produced by different industrial activities. These include slags produced by iron and steelmaking plants (SS), fly and bottom ash (FA and BA, respectively) produced by power plants and solid waste incinerators and finally by cement kiln dust (CKD) or even waste cement [11]. Globally, a few hundred Mt of these materials is produced worldwide and part of it is already reused or recycled. Recently, Kirchofer et al. [12] provided an upper estimate of total Ca and Mg alkalinity available in the United States from CKD, FA and SS equal approximately to 7.65 Mt/year, with a carbonation capacity of approximately 6.98 Mt-CO_2/year, compared to about 6 Gt CO_2 emitted yearly in the United States. Figure 11.2 also indicates that the alkalinity and CO_2 emissions sources are well overlapped, suggesting that it is unlikely that carbonation reactants would need to be transported at great distances [12]. Clearly, these figures suggest that carbonation of industrial residues cannot be considered as a relevant global option for CO_2 storage. Nevertheless, it may help in reducing CO_2 emissions of some specific and small-scale emission sources.

Besides, carbonation of alkaline industrial residues may be considered as a CO_2 utilisation option aimed to improve the environmental properties of these materials and eventually to produce artificial aggregates that could replace natural ones in several civil engineering applications [13]. Based again on the US market data, the potential total synthetic aggregate production using FA, CKD and SS is estimated to be 20 Mt/year, approximately 1.7 % of total US mined aggregate

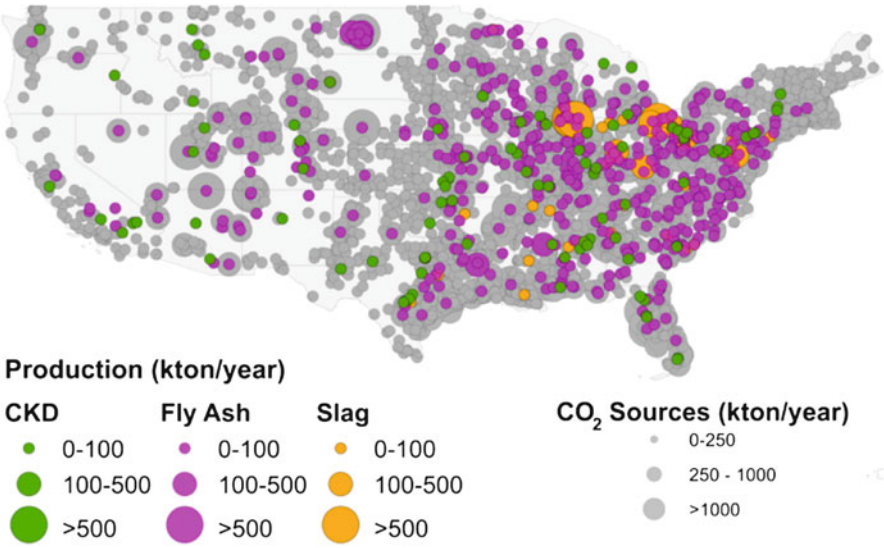

Fig. 11.2 Industrial alkalinity sources and stationary CO_2 sources in the conterminous United States (Reprinted with permission from Ref. [12]. Copyright 2013 American Chemical Society)

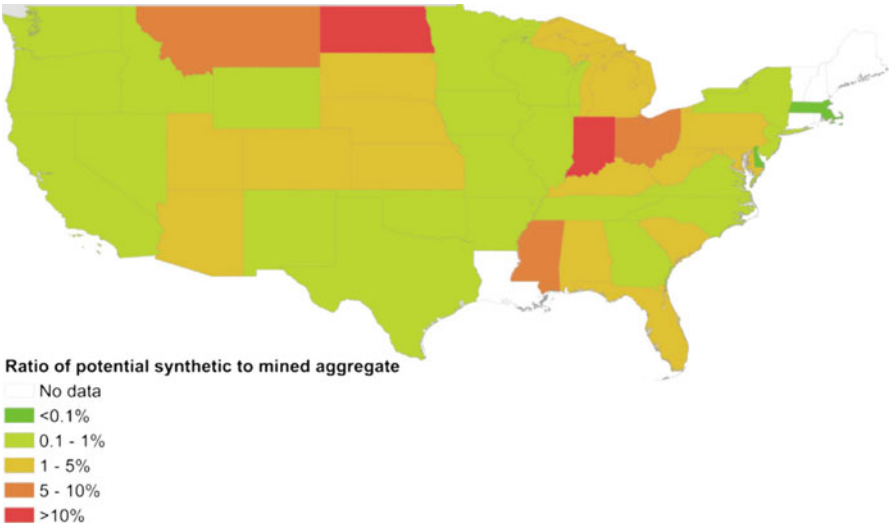

Fig. 11.3 Ratio between potential synthetic aggregate production from mineral carbonation to mined aggregate production (i.e. the potential market share of synthetic aggregate) in the conterminous United States (Reprinted with permission from Ref. [12]. Copyright 2013 American Chemical Society)

(i.e. 1.2 Gt/year) [12]. Figure 11.3 shows anyhow that this ratio is an average of a clearly dishomogeneous situation, characterised by US states where it may be expected that even more than 10 % of natural aggregates may be replaced by carbonated materials.

11.3 CO_2 Capture

11.3.1 Carbon Dioxide Sources and Capture Options

Carbon capture consists in the production of a concentrated CO_2 stream from a diluted source with the aim of conveying it to storage [7]. Diluted sources may include flue gases from combustion plants with CO_2 concentrations ranging between 3 and 10 % vol. depending on the fuel used and the excess air applied, flue gases from cement kilns with CO_2 concentrations up to 15 % vol. and syngas from integrated gasification combined cycle (IGCC) plants with CO_2 concentrations up to 40 %. The different CO_2 concentrations of the various emission sources pose different challenges in the development and choice of the most suitable separation process to use. Currently, capture processes based on chemical absorption using amine solutions represent the benchmark technology as they allow for the lowest energy penalty with respect to all other alternatives ready for use [7]. Nevertheless, the energy penalty of this process, mainly related to the heat requirements needed for amine regeneration, is approximately 25 % of the power plant thermal duty [7]. For this reason, currently, many efforts are being made to develop alternative capture processes characterised by lower energy penalties.

11.3.2 Capture Processes Based on Carbonation

This section will discuss three capture processes based on carbonation chemistry: calcium chemical looping, the Benfield process, based on the use of hot potassium carbonate, and absorption with alkali solutions. The former one is still under development; the second one is already applied at full scale, although its application seems limited to concentrated CO_2 sources; the latter one has been proposed for direct capture from air, although its feasibility is questionable, as will be discussed in this section.

11.3.2.1 Calcium Looping

Capture using calcium looping has been investigated for more than a decade. This process is based on two steps. First, carbon dioxide is captured in a carbonation reactor, where the following reaction takes place:

$$CaO + CO_2 \leftrightarrow CaCO_3 \tag{11.3}$$

Then, the carbonates are calcined at higher temperature, leading on the one hand to calcium oxide regeneration and on the other hand to produce a carbon dioxide stream suitable for disposal:

$$CaCO_3 \leftrightarrow CaO + CO_2 \tag{11.4}$$

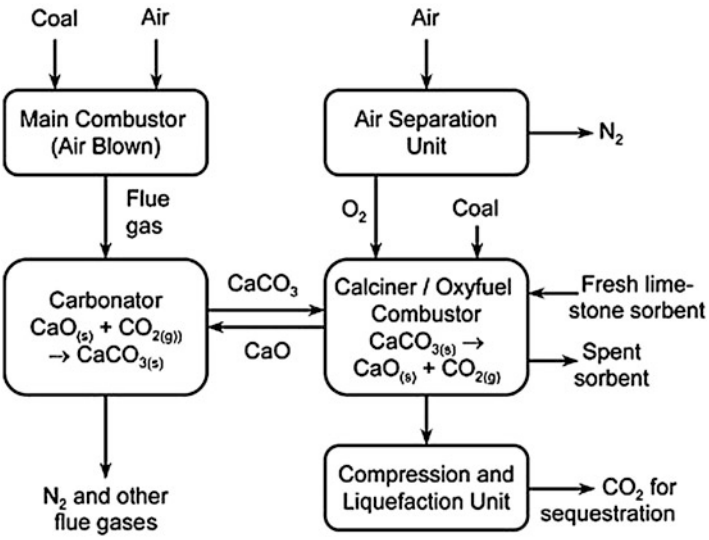

Fig. 11.4 Scheme of the calcium looping process applied to precombustion capture (Reprinted from Ref. [15]. Copyright 2010, with permission from Elsevier)

In the first applications that were not aimed at carbon capture and storage (CCS), the production of rather pure CO_2 was not an issue and the heat required for the calcination step was supplied by fuel combustion with air [5]. Shimizu et al. [14] first proposed to couple reactions (11.3) and (11.4) in the framework of CCS, following the process scheme outlined in Fig. 11.4. Carbon dioxide is captured in the carbonator at about 600 °C and the corresponding carbonates are calcined at 950 °C providing the heat required by oxy-fuel combustion, thus leading to a CaO stream that is recycled to the carbonator and a CO_2 stream of about 95 % purity, excluding the water that can be removed by condensation that can be disposed of.

The application of the calcium looping process requires that the sorbent is subjected to many cycles of carbonation and calcination [15]. Unfortunately, the CO_2 carrying capacity of the sorbent was shown to decline for increasing number of carbonation/calcination cycles (see Fig. 11.5). Increasing the regeneration temperature was also shown to negatively affect the performance of the sorbent after several cycles. This suggests that most of the observed loss of the CO_2 carrying capacity is due to sintering phenomena occurring during the calcination step. Sintering here refers to changes in pore shape, pore shrinkage and grain growth that particles of CaO undergo during heating. Sintering of CaO increases at higher temperatures and durations of calcination, as well as at higher partial pressures of steam and carbon dioxide [15].

Different options have been proposed to increase the lifetime of calcium-based sorbents. Among these, hydration of calcium oxide may represent one of the most promising options. Zeman [16] proposed to include a third hydration step in the calcium looping process, as reported in Fig. 11.6. Extrapolating the data collected in

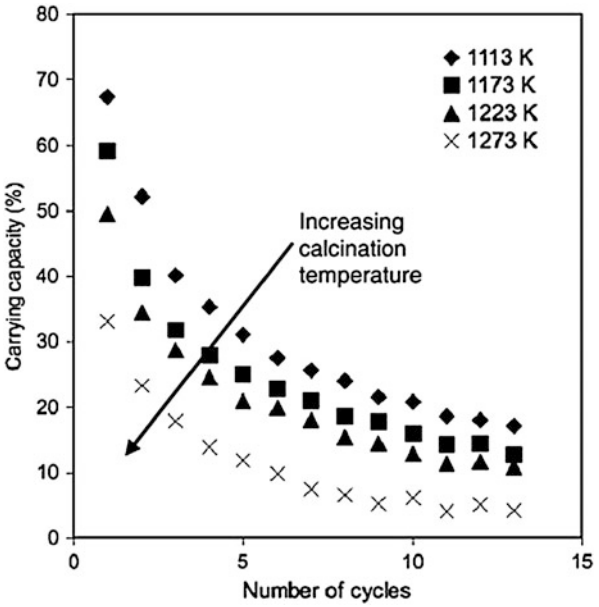

Fig. 11.5 CO_2 carrying capacity of the sorbent at increasing number of carbonation/calcination cycles (Reprinted from Ref. [15]. Copyright 2010, with permission from Elsevier)

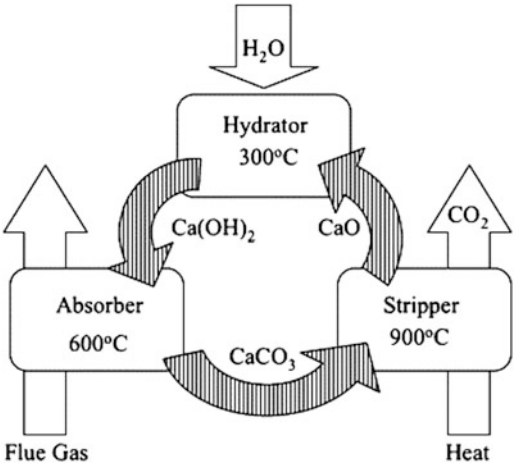

Fig. 11.6 Scheme of the hydrated calcium looping process (Reprinted from Ref. [16]. Copyright 2008, with permission from Elsevier)

ten TGA carbonation/calcination/hydration cycles, it was suggested that the long-term sorbent residual carrying capacity could increase up to 600 % with respect to dry carbonation/calcination cycles. According to Blamey et al. [15] this could in principle allow to reduce the sorbent makeup from the 1 mol of sorbent capturing 4.33 mol of CO_2 over ten cycles reported by Abanades et al. [17] up to 7.20 mol of CO_2 over ten cycles when the hydration step is included. Another interesting possibility to increase the lifetime of the sorbent is to develop synthetic products. One option relies on the use of pure calcium carbonate (PCC) that will also be discussed

later in the framework of CO_2 utilisation for the carbonation of industrial residues. High surface area PCC particles (5–20 nm) were synthetised through a wet precipitation process, allowing to achieve over 90 % carbonation over two calcium looping cycles [18]. The lifetime of the sorbent can also be improved by using mixed oxides with the formula $Ca_{0.9}\ M_{0.1}O_x$ where M = Cu, Cr, Co or Mn, CaO sorbents derived from organic salt precursors, CaO doped with Cs, sorbents derived from calcium lignosulphonate, sorbents based on Na_2CO_3 or NaCl, CaO-based sorbents using $CaTiO_3$ as binder and CaO-based sorbents using calcium aluminate ($Ca_{12}Al_{14}O_{33}$) as a stable matrix (see [19] and references therein).

11.3.2.2 Absorption with Hot Carbonate Solutions

The capture process is, in this case, based on the reaction of carbon dioxide with a potassium carbonate solution [6]:

$$CO_2 + K_2CO_3 + H_2O \leftrightarrow 2KHCO_3 \tag{11.5}$$

The CO_2 absorber is usually operated at high temperature and pressure. The higher the temperature is, the higher the concentration of potassium carbonate that can be used without precipitating the carbonate [20]. As the driving force of the process is given by the difference between the CO_2 partial pressure in the gas bulk and its equilibrium pressure at the gas–liquid interface, the process is usually operated at high pressure. Typical operating conditions of the absorber are 120–125 °C and 25 atm [20]. The bicarbonate solution is regenerated by steam stripping at approximately the same operating temperature and recycled to the absorption unit, whereas the CO_2 liberated may be disposed of. The energy requirement needed to regenerate thermally the bicarbonate back to carbonate is around 3–4 GJ/t CO_2 [21].

The chemistry of the hot carbonate absorption process is clearly in aqueous phase. At the typical pH (>8) encountered in the absorbing solution, the following reaction represents the rate-limiting step:

$$CO_2 + OH^- \leftrightarrow HCO_3^- \tag{11.6}$$

The CO_2 mass transfer rates may be improved through additives to the potassium carbonate solution [20]. These may include small amounts of diethanolamine (DEA), which significantly enhances the absorption rate, through the following reactions, leading to the formation of carbamate that then reacts with hydroxide ions forming back DEA and leading to the formation of bicarbonate ions:

$$CO_2 + R_2NH \leftrightarrow R_2N^+HCOO^- \tag{11.6a}$$

$$R_2N^+HCOO^- + OH^- \leftrightarrow R_2NH + HCO_3^- \tag{11.6b}$$

The Benfield industrial process, based on the chemistry discussed above, has been so far applied in 700 industrial plants for natural gas sweetening and in

ammonia plants. The relatively high partial pressure required for maximising the effectiveness of this process makes it more suitable for processing concentrated gas streams. For this reason, the Benfield process is used to treat the gas from the water-gas shift converter downstream a steam-reforming unit, where the CO_2 must be removed in order to obtain a pure nitrogen/hydrogen gas mixture for ammonia synthesis. In the framework of CCS technologies, it could be used as well to capture the CO_2 from syngas obtained from coal gasification units.

11.3.2.3 Absorption with Alkali Solutions

Carbon dioxide can be captured also using alkali solutions, such as NaOH or KOH ones. In this case, carbon dioxide is neutralised through the following general reaction:

$$CO_2 + NaOH \leftrightarrow Na_2CO_3 + H_2O \tag{11.7}$$

As already discussed for CaO, also NaOH is produced through an energy intensive process. Therefore, the regeneration of the carbonate to the hydroxide form is needed to make the process sustainable in terms of energy requirements and carbon capture. The traditional approach for the regeneration of potassium carbonate comes from the paper industry and is based on the so-called causticisation reaction, where potassium carbonate is reacted with lime:

$$Na_2CO_3 + Ca(OH)_2 \leftrightarrow NaOH + CaCO_3 \tag{11.8}$$

This reaction allows to regenerate NaOH, but once again requires lime as reagent, that is produced from hydration of quicklime (CaO). The latter, as already discussed, is produced by calcination of calcium carbonate (see Eq. 11.4).

The capture process given by Eqs. (11.7), (11.8) and (11.4) has been proposed to capture carbon dioxide from air and has been first assessed by Baciocchi et al. [22] and more recently has been the subject of a study of the American Physical Society [23]. The scheme of the process used as reference in both cited works is reported in Fig. 11.7.

In principle, the application of the alkali absorption process is well suited for CO_2 storage from very diluted sources, as air where CO_2 is present at about 380–390 ppm. This stems from the fact that hydroxyl ions accelerate the rate of CO_2 transfer from the gas to the liquid phase [24], which would be very slow if based on physical absorption or chemical absorption using weak bases, such as ethanolamines. Nevertheless, the main limitation of this capture process relies in the very high energy needed for regeneration. Baciocchi et al. [22] showed that this should amount to 12 GJ/t CO_2 against 9 and 20 GJ/t CO_2 generated by a power plant operating with coal or natural gas, respectively, and much higher than the 3–4 GJ/t CO_2 reported for flue gas capture using amines or hot potassium carbonate [21], thus making the process absolutely unfeasible in the first case and characterised by

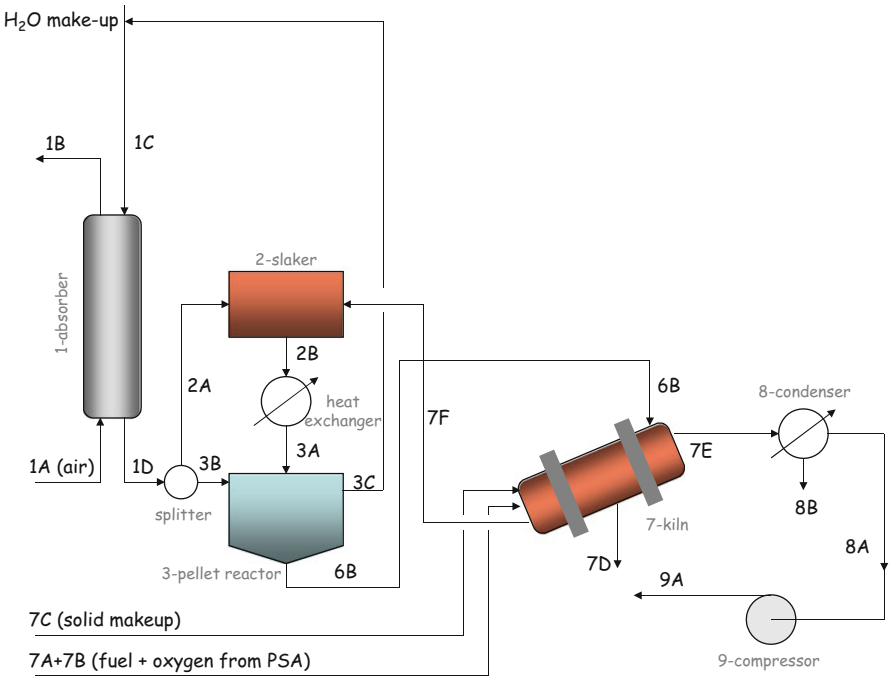

Fig. 11.7 Scheme of the air capture process based on alkali absorption and regeneration by causticisation and calcination reactions (Adapted and reprinted from Ref. [22]. Copyright 2006, with permission from Elsevier)

a too high energy penalty in the latter one. This conclusion was reinforced by APS [23] that gave a realistic estimate of air capture using alkali solutions of around 780 USD/t CO_2. In order to become a feasible capture option, the alkali absorption process would require a less energy intensive regeneration step. Nagasawa et al. [21] investigated how to increase its efficiency using a regeneration process based on the acidification of the carbonate solution obtained from the absorber, followed by liberation of gaseous carbon dioxide.

$$CO_2 + H^+ \rightarrow HCO_3^- \tag{11.9a}$$

$$HCO_3^- + H^+ \rightarrow H_2CO_3 \tag{11.9b}$$

$$H_2CO_3 \rightarrow H_2O + CO_2 \tag{11.9c}$$

As the reaction requires protons on the one hand and to remove alkaline metal ions from the solution on the other hand, this can be accomplished using electrodialysis for such an exchange. After an optimisation of the cell configuration, Nagasawa et al. [21] reduced the energy requirements to around 4 GJ/t CO_2. Nevertheless, the feasibility and applicability of this process need yet to be demonstrated.

11.4 CO_2 Storage

11.4.1 Processes and Reaction Routes

Accelerated carbonation for carbon storage has been investigated using different reaction routes (see Fig. 11.8). These can be broadly classified according to the reacting phases in gas-solid and aqueous phase routes. In the former one, gaseous carbon dioxide is assumed to react directly or indirectly with an alkaline mineral or residue. This route can be applied to materials characterised by a relatively high content of free calcium oxides or hydroxides. For the other alkaline materials, it is possible to apply the indirect route, where the reaction goes through the conversion of the alkaline material to the corresponding oxide or hydroxide, which is then carbonated in a subsequent step. As it will be discussed in more detail in the next sections, the gas-solid route does not seem promising for the scaleup of the process, in view of the slow kinetics of carbonation observed for both the indirect and direct options. As a consequence, most of the research on accelerated carbonation has

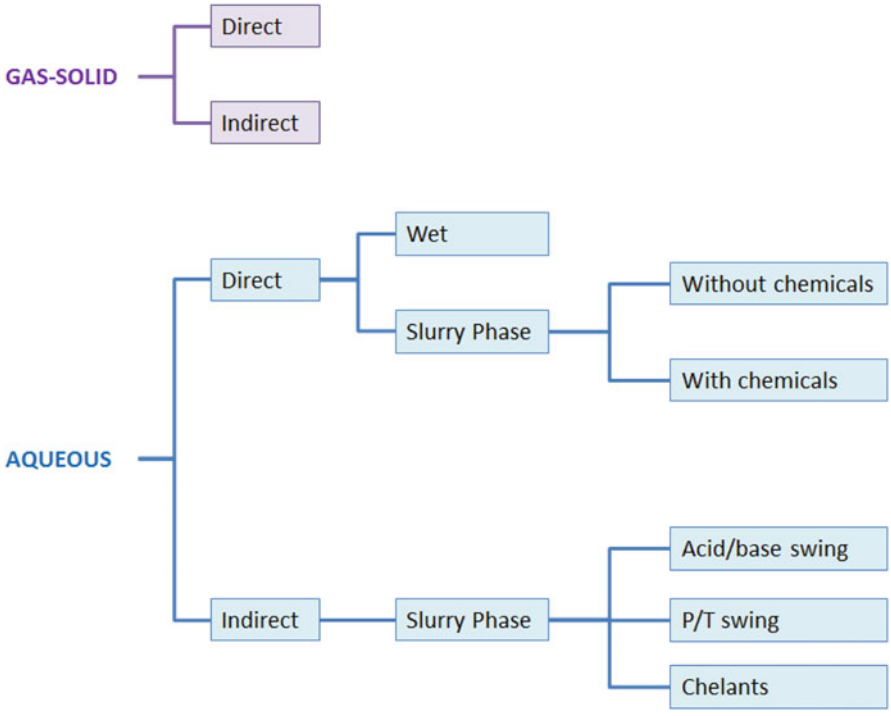

Fig. 11.8 Main routes of the accelerated carbonation processes tested for CO_2 storage

focused on the aqueous route, generally mixing the alkaline feedstock with water applying liquid to solid (L/S) ratios above 2 l/kg (slurry phase). Also in this case, both direct and indirect reaction routes have been proposed and tested. In the first case, mineral dissolution and carbonate precipitation take place in the same reactor. Eventually, chemicals, such as salts and bicarbonates, may be added in order to enhance the rate of the reaction by buffering the solution pH. As the optimal operating conditions for dissolution and precipitation are quite different, the indirect route may be preferred, as it allows running the dissolution and precipitation reactions in two different steps, switching the operating conditions as required. Finally, it is worth noting that the aqueous direct route may be run also using very low L/S ratios (typically below 1 l/kg), and in this case, it is often referred to as the "wet route". This route has been particularly investigated for the carbonation of industrial residues and will be discussed in Sect. 11.4.4.

11.4.2 Mineral Carbonation

11.4.2.1 Gas–Solid Carbonation

As discussed in Sect. 11.2.1, carbonation of minerals is thermodynamically favourable even at ambient conditions, with an exothermic overall chemistry that can be summarised as follows [25]:

$$x\mathrm{MgO}\ \ y\mathrm{SiO_2}\ \ z\mathrm{H_2O(s)} \leftrightarrow x\mathrm{MgO(s)} + y\mathrm{SiO_2(s)} + z\mathrm{H_2O} \tag{11.10a}$$

$$\mathrm{MgO(s)} + \mathrm{CO_2} \leftrightarrow \mathrm{MgCO_3(s)} \tag{11.10b}$$

Direct gas-solid carbonation of Mg silicate minerals would have been the preferred route for mineralisation of CO_2 due to its simplicity in design and better energy efficiency. More so, the overall carbonation reactions of olivine and serpentine are exothermic. However, these reactions suffer from very slow kinetics, low conversion and high energy requirements [26]. For this reason, Nduagu et al. [26] proposed an indirect gas-solid process based on the following steps: (1) production of $MgSO_4$ from the silicate, (2) conversion of $MgSO_4$ to $Mg(OH)_2$ and (3) gas-solid carbonation of $Mg(OH)_2$ to $MgCO_3$. One of the limitations of this process is given by the heat required to produce Mg hydroxide from the corresponding silicate, a process that requires temperatures of around 400–500 °C. Therefore, most of the feasibility of the process route comes from the possibility of using the heat released by the exothermic carbonation reaction. Besides, it is worth noting that the rate of $Mg(OH)_2$ carbonation is quite slow, with reasonable conversions achieved only after 6 h of reaction at about 35 bar and 500 °C (see Table 2 in [25]).

11.4.2.2 Aqueous Phase Carbonation

This process route takes place through the following chemical reactions, written making reference to forsterite, the main mineral constituent of olivine:

(a) Dissolution of carbon dioxide in water with release of protons:

$$CO_{2(g)} + 2H_2O_{(l)} \rightarrow H_2CO_{3(aq)} \rightarrow H^+{}_{(aq)} + HCO^-_{3(aq)}$$

(b) Dissolution of the mineral in water with release of alkaline cations:

$$Mg_2SiO_{4(s)} + 4H^+{}_{(aq)} \rightarrow 2Mg^{2+}{}_{(aq)} + SiO_{2(s)} + 2H_2O_{(l)}$$

(c) Precipitation of the carbonates:

$$Mg^{2+}{}_{(aq)} + HCO^-_{3(aq)} \rightarrow MgCO_{3(s)} + H^+{}_{(aq)}$$

In the direct aqueous phase route, the different reactions are assumed to take place in the same reactor at the same operating conditions. A comprehensive study of this route can be found in the works of the Albany Research Center [27] and of the Energy Research Centre of the Netherlands [28–30]. Gerdemann et al. [27] investigated the carbonation of different mineral feedstocks, including olivine, serpentine and wollastonite. They performed tests at different pressure, temperature and L/S ratio, which allowed them to select the best operating conditions in terms of conversion of the alkaline reactant (Mg or Ca depending on the feedstock). Namely, these were achieved at $T = 185$ °C and $pCO_2 = 150$ atm for olivine and $T = 155$ °C and $pCO_2 = 115$ atm for serpentine, using in both cases a 0.64 M $NaHCO_3$ and 1 M NaCl solution. For wollastonite the optimal operating conditions were slightly milder ($T = 100$ °C and $pCO_2 = 40$ atm) and distilled water was used. It is worth pointing out that the best operating conditions for serpentine were obtained assuming to use heat-activated serpentine (above 630 °C) and in all cases finely ground feedstocks (below 75 μm). Besides, for both olivine and serpentine, a pH buffer solution was needed to control the pH allowing both dissolution and carbonation to occur at a reasonable extent. The maximum extents of reaction achieved were around 50 % for olivine, 80 % for wollastonite and 73 % for serpentine. Huijgen et al. [28, 29] also investigated the carbonation of wollastonite in a direct route process. Wollastonite was observed to carbonate rapidly, with a maximum conversion in 15 min of 70 % at relatively mild conditions ($d < 38$ μm, $T = 200$ °C and $pCO_2 = 20$ bar).

The works performed on the direct route made clear that the limiting step of the whole process is represented by the dissolution of the mineral, especially for Mg-bearing ones. An increase of the dissolution rate can be achieved by performing a physical/chemical mineral surface pretreatment, increasing the specific area (grinding for size reduction), or by removing the silica-passivating layer (by abrasion/attrition). The first three options allow basically to modify the physicochemical

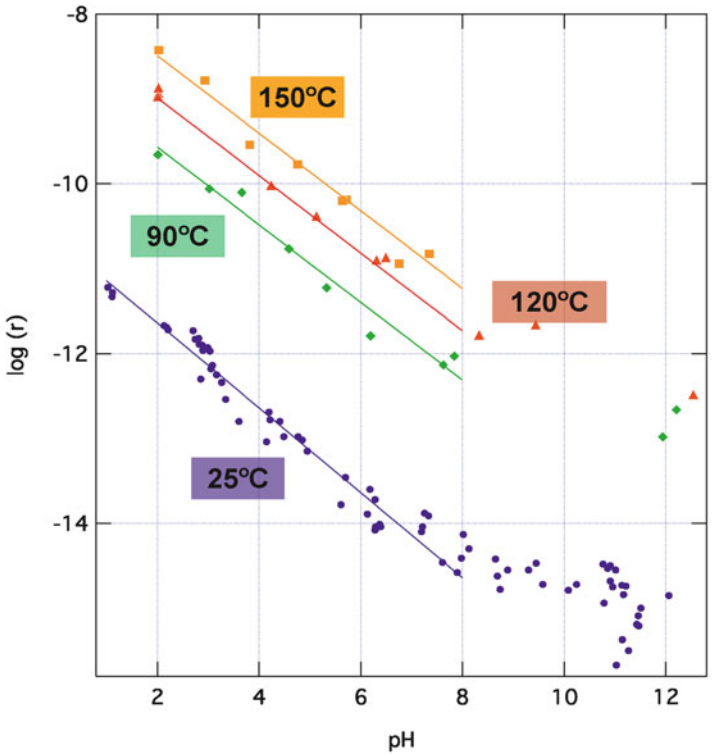

Fig. 11.9 Dissolution rate of olivine, r [mol cm^2 s^{-1}], vs. pH at different temperatures. Activation energy: −52.9 kj/mol (Adapted and reprinted from Ref. [31]. Copyright 2006, with permission from Elsevier)

properties of the material surface prior to dissolution. The latter one may allow to remove the residual silica layer on the mineral surface that prevents further dissolution of magnesium. For this reason, several works have been performed in order to better understand the dissolution mechanism and to increase the dissolution rate, especially of Mg-bearing minerals. Hänchen et al. [31] have specifically investigated the dissolution of olivine, showing the effect of the solution pH on the rate of dissolution at operating conditions suitable for mineral carbonation (see Fig. 11.9). Besides, the same group has more recently demonstrated that the addition of salts to the solution does not help in improving the dissolution rate of olivine [32], differently from what was expected based on the findings of Gerdemann et al. [27].

The findings on olivine dissolution are a clear example of the fact that the rate of silicate minerals dissolution is clearly enhanced at lower pH values, where precipitation of carbonates can hardly take place. This issue has prompted the development of a few indirect carbonation schemes, where minerals dissolution and carbonate precipitation are decoupled. Park et al. [33] developed a pH swing process, whose scheme is reported in Fig. 11.10. Dissolution of serpentine is

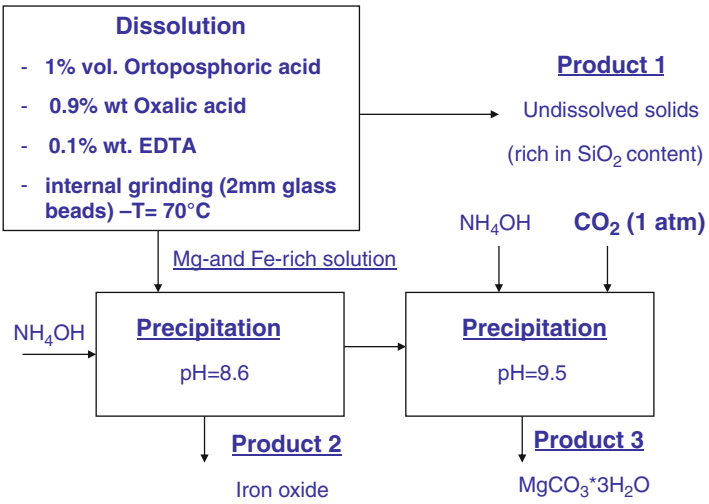

Fig. 11.10 Scheme of the pH swing process for serpentine carbonation developed by [33]

enhanced using a solution of weak acids and chelating agents coupled with internal grinding using glass beads. Then, two precipitation steps are foreseen: the first one, at pH = 8.6, aimed at iron oxide precipitation and the second one, at a higher pH, aimed at nesquehonite precipitation. Apart from the complexity of the different steps, the main open issue of this process remains how to recycle the different acid and basic amendments needed.

This is also the case for the other indirect process routes proposed in the last decade. Teir et al. [34] dissolved serpentine in HCl or HNO_3, and then hydromagnesite ($4MgCO_3$ $Mg(OH)_2$ $4H_2O$) was obtained by fixing the Mg-rich solution pH to 9 with addition of NaOH. Although a high carbonation conversion efficiency of Mg (80–90 %) was obtained, the chemicals involved, such as HCl and NaOH, could not be reused. More recently, Wang and Maroto-Valer [35] proposed a new pH swing mineral process by using recyclable ammonium salts. The process consists of the following main steps: (a) CO_2 is captured from flue gas using NH_3 and producing NH_4HCO_3; (b) a solution of NH_4HSO_4 is used to extract Mg from serpentine at mild operating conditions leading to a $MgSO_4$ solution; (c) the pH of the Mg-rich solution produced from mineral dissolution is switched to neutral pH by adding NH_4OH; (d) the $MgSO_4$ solution reacts with the NH_4HCO_3 solution allowing to precipitate carbonates at mild temperature, in fact since the formation of carbonate is determined by the operating temperature [36], nesquehonite ($MgCO_3{\cdot}3H_2O$) can be converted to hydromagnesite ($4MgCO_3{\cdot}Mg(OH)_2{\cdot}4H_2O$) above 70 °C; and (e) the $(NH_4)_2SO_4$ remaining in solution after the precipitation of hydromagnesite could be recovered by evaporation and subsequently heated up to regenerate NH_3 which is fed back to the capture step, whereas NH_4HSO_4 could be then reused for the mineral dissolution step.

11.4.3 Carbonation of Industrial Residues

As mentioned in Sect. 11.2.2, an alternative feedstock of alkaline phases suitable to be treated by accelerated carbonation for CO_2 storage is represented by waste by-products characterised by high calcium or magnesium (hydr)oxide or silicate contents; these include residues from thermal treatment plants or other activities such as mining, metallurgical processes, cement or paper manufacturing and construction and demolition [11, 37, 38]. Besides being often associated with CO_2 point source emissions, these materials tend to be chemically more unstable than geologically derived minerals [28]; therefore, typically they require a lower degree of pretreatment and less energy intensive operating conditions to enhance carbonation yields [28, 39]. Although as previously mentioned, the availability of these types of residues is too limited to exert a substantial effect in terms of the reduction of global CO_2 emissions, their use as feedstock for accelerated carbonation processes could be seen as a stepping stone towards the development of CCS processes based on natural minerals [37]. Furthermore, several studies have shown that accelerated carbonation is an effective treatment for reducing the release of specific metals from alkaline waste materials such as waste incineration bottom ash [40–43] and Air Pollution Control (APC) residues [44–46], steel slag [47–50] and oil shale ash [51], among others. The improvement in the leaching behaviour of these waste materials exerted by accelerated carbonation is important since it may broaden their management options, allowing e.g. to reuse them in selected civil engineering applications or to dispose of them in landfills for non hazardous or even inert waste. In addition, following specific reaction routes, accelerated carbonation can lead to the formation of products that can be employed for different applications, such as aggregates in construction or calcium carbonate to be used as filler or coating pigment in paper or plastics manufacturing.

11.4.3.1 Tested Materials

Accelerated carbonation has been tested on a variety of residues as a technique to achieve different objectives in different countries. In fact, issues of primary importance for this technology are the relative abundance of each waste stream, which determines the overall potential impact of the accelerated carbonation technique as a CO_2 mitigation strategy and the environmental behaviour of the residues. Both these issues may vary from country to country as a function of many factors including the main features of the industrial and energy sectors, available natural resources, implemented waste management strategies, adopted waste residue disposal and flue gas treatment technologies as well as environmental legislation. Thus, for example, in Estonia most of the energy demand is supplied by oil shale combustion, which emits significant amounts of CO_2 (emission factor of 29.1 tC/TJ) and generates large amounts of alkaline oil shale ash, thus making CO_2 sequestration via carbonation of oil shale ash a very attractive process [52];

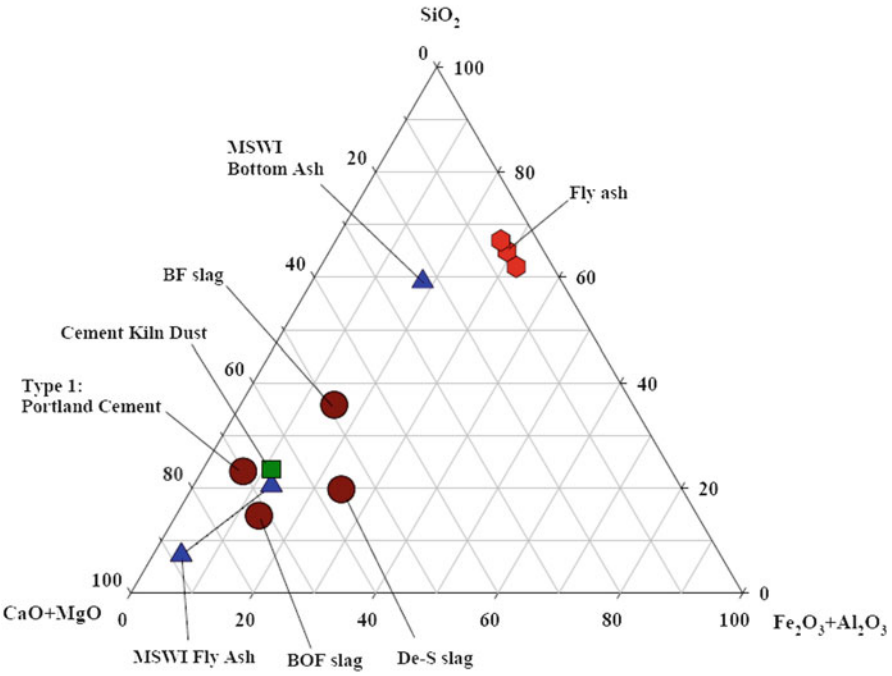

Fig. 11.11 Normalised CaO/MgO–SiO_2–Al_2O_3/Fe_2O_3 phase diagram of various types of alkaline waste (Reprinted with permission from Ref. [38]. Copyright 2012, Taiwan Association for Aerosol Research)

in Belgium instead, stringent legislative landfill acceptance criteria related to the leaching of specific heavy metals (such as Cu, Zn and Pb, in particular) do not allow waste incineration bottom ash to be directly landfilled even after natural weathering periods; hence, accelerated carbonation studies have been specifically undertaken to improve the chemical stability of these residues [40, 43, 53].

One of the fundamental aspects of accelerated carbonation investigations on alkaline industrial waste materials is the physical, chemical and mineralogical characterisation of the residues for the identification and quantification of the reactive phases. As shown in Fig. 11.11, the residues that exhibit the highest contents of CaO and MgO are municipal solid waste incineration (MSWI) fly ash or APC residues, basic oxygen furnace (BOF) steel slag and cement kiln dust (CKD) that present quite a similar content of major constituents to ordinary Portland Cement (PC). Other types of metallurgical residues such as desulphurisation (De-S) and blast furnace (BF) slags also present significant CaO and MgO contents, whereas MSWI bottom ash and coal combustion fly ash generally exhibit a predominance of Si phases and significant contents of Fe and Al oxides [38]. Some types of solid residues streams produced by coal-fired power stations, however, such as lignite combustion fly ash and oil shale ash typically exhibit higher CaO and MgO contents, i.e. 37 % CaO and 15 % MgO the

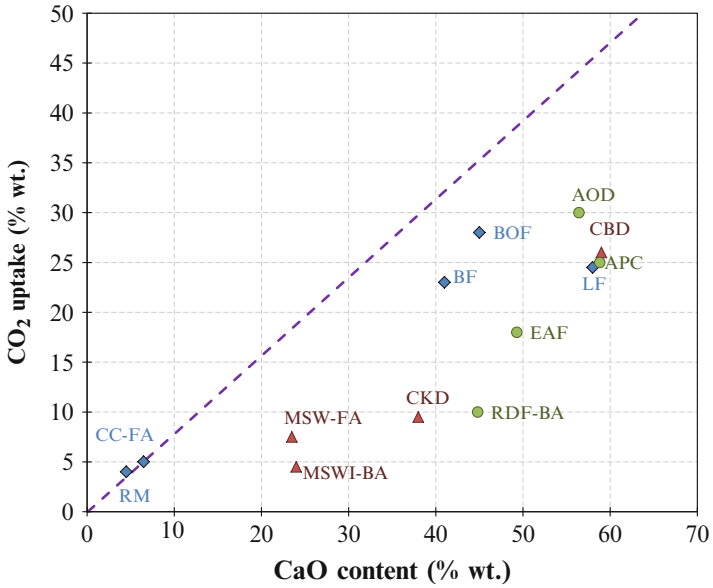

Fig. 11.12 Comparison of the average CO_2 uptakes obtained for different types of residues as a function of the CaO content of the materials, in which the *purple-dotted line* reports the maximum CO_2 uptake expected on the basis of the CaO content of the residues. Materials: *CKD* cement kiln dust [11], *CBD* cement bypass dust [11], *APC* air pollution control residues [45], *RDF-BA* refuse-derived fuel bottom ash [42], *MSWI-BA* municipal solid waste incineration bottom ash [11], *MSWI-FA* municipal solid waste incineration fly ash [11], *RM* red mud [38], *BOF* basic oxygen furnace slags [38], *EAF* electric arc furnace slag [48], *AOD* argon oxygen decarburisation slag [48], *BF* blast furnace slag [38], *LF* ladle furnace slags [38], *CC-FA* coal combustion fly ash [38]

former [54] and around 50 % CaO and 10–15 % MgO the latter type of material [52]. Accelerated carbonation has been applied also to alumina manufacturing residues, generally known as red mud, which typically contain around 8 % CaO and 1 % MgO [55].

The main composition of a residue can already provide a general indication on its reactivity with CO_2. As can be noted in Fig. 11.12 in fact, the average CO_2 uptakes resulting for each type of tested residue can be directly related in most cases to their CaO content, since Ca-based phases generally present a higher reactivity even under rather mild operating conditions, as opposed to Mg, Fe and Al ones. Hence, the residues that have shown to yield the highest CO_2 sequestration potential are those generated in steel-refining processes, such as AOD and LF slag, APC residues and by-products from cement manufacturing such as CBD (see Fig. 11.12). However, besides bulk chemical composition, important factors affecting the reactivity of industrial residues with CO_2 are also their mineralogy and particle size distribution. As previously mentioned, free oxide and hydroxide phases such as lime and portlandite, typically found in APC residues, CKD and paper mill waste, are very reactive with CO_2 even at mild operating conditions, while the reactivity of many of the different Ca- and Mg-containing silicates detected in

metallurgical slag, construction and demolition waste and MSWI bottom ash vary greatly depending on the types of crystal phases and of the presence of inclusions in the crystal lattice of various elements, such as Al, Cr and Fe. The reactivity of Ca silicates is indicated to increase for higher Ca/Si ratios [56]; in fact the most reactive silicate phases with CO_2 are generally reported to be tricalcium (alite, Ca_3SiO_5) and dicalcium (belite, Ca_2SiO_4) silicates, the latter in particular in the γ-polymorph phase that is formed during the cooling of steel-refining slag and results in the disintegration of the slag into a fine powder [48]. These types of silicate phases are generally retrieved in materials containing cementitious phases, such as concrete demolition waste [57] or steel manufacturing slag. Particle size, as indicated in Sect. 11.4.2, is one of the controlling factors for the dissolution kinetics of any kind of mineral or anthropogenically derived material. The by-products of flue gas treatment units, cement kiln dust and other ashes or particular products of industrial refining processes present average grain sizes (generally <100–150 μm) that are already in the optimum range for carbonation treatment, whereas slag residues from combustion or metallurgical processes or scraps from construction and demolition activities present a wider particle size distribution curve and a significant percentage of coarse particles.

11.4.3.2 Investigated Reaction Routes

Accelerated carbonation of alkaline solid waste has been up to now primarily investigated through the direct aqueous route (e.g. [40, 44, 45, 48, 52, 54, 58, 59]) or to a lower extent by means of the direct gas-solid reaction, applied only to materials with high lime and portlandite contents [60–62]. As mentioned in Sect. 11.4.1, direct aqueous accelerated carbonation studies have been performed in two different modes, either in slurry phase applying liquid to solid (L/S) ratios above 2 w/w (e.g. [54, 55, 58, 63, 64]), in particular for waste materials of low solubility in which CaO is generally bound as a silicate, or via the wet route, humidifying the material so as to set the L/S ratio below 1 w/w (e.g. [41, 42, 44, 45, 48, 49, 51, 59]). This latter type of treatment in which the CO_2 and Ca and Mg ions dissolution, as well as carbonation reactions, occur in the thin liquid film in direct contact with the solid residues has been originally applied for cement curing processes (see e.g. [65, 66]). It is specifically applied as a carbonation route also for industrial residues that present high contents of soluble elements such as salts and heavy metals so as to avoid the treatment and disposal of the processing liquid, as well as to favour dissolution kinetics at relatively mild operating conditions.

Carbonation of residues does not generally require the extraction of alkaline metals from the solid matrix, since the main reactive species are Ca-containing silicates, oxides and hydroxides. These minerals, as earlier mentioned, behave differently from those containing Mg, as hydration, solvation and carbonation of Ca-bearing phases can be carried out under the same operational conditions in a one stage operation [67]. However, for specific waste residues, characterised by high contents of silicate phases such as various types of steel slag or cement waste

residues, accelerated carbonation has also been tested applying the indirect aqueous route to slurry suspensions, separating the dissolution and precipitation steps so as to optimise each set of reactions by operating on the pH, dosing specific additives, similarly to the previously described pH swing process, (e.g. [68, 69]) or by varying some of the operating parameters, such as CO_2 pressure [57].

Depending chiefly on the main composition of the residues, the chosen process route and also the final aim of the study (CO_2 sequestration or improvement of the properties of the residue), a variety of operational conditions have been applied and quite different results in terms of CO_2 uptake have been achieved (see e.g. [37, 38, 67]).

Gas–Solid Carbonation

As previously mentioned, direct gas–solid carbonation was tested only on residues characterised by a high content of Ca (hydr)oxide phases and fine particle size. Jia and Anthony [60] carried out experiments with coal and petroleum coke fluidised bed combustion (FBC) fly ash in a pressurised thermogravimetric analyzer (PTGA) at 1 or 11 bar of 100 % CO_2; hydrated ash was found to react faster with CO_2 than unhydrated ash, presenting also a higher final CaO to $CaCO_3$ conversion ratio (60 % compared to 27.4 % respectively), owing to the effects of hydration on increasing the ash surface area [60]. Carbonation reactions showed to occur in the 300–600 °C temperature range for hydrated ash and in the 400–700 °C range for the unhydrated ash, while CO_2 pressure did not show to exert a significant effect on carbonation kinetics or the final calcium conversion yield [60]. More recently, Baciocchi et al. [61] and Prigiobbe et al. [62] performed gas-solid carbonation tests employing APC residues and confirmed that, under these conditions, carbonation is effective at temperatures equal to or above 350 °C. Maximum conversions between 60 and 80 % were obtained at temperatures between 350 and 500 °C and ambient pressure also applying diluted gas streams, i.e. characterised by a CO_2 concentration of 10–50 vol.% [62]. In addition, the kinetics of the reaction proved to be fast, achieving completion in less than 5 min and exhibiting a rapid chemically controlled reaction followed by a slower product layer diffusion-controlled process (see Fig. 11.13).

Slurry-Phase Carbonation

Slurry-phase accelerated carbonation has been performed mainly either under enhanced operating conditions (i.e. $T = 50–225$ °C and $pCO_2 = 5–30$ bar) (e.g. [43, 50, 58]) or alternatively at ambient temperature and atmospheric pressure using 10–100 % vol. CO_2 streams (e.g. [46, 52, 55]).

Slurry-phase carbonation experiments on ground BOF slag under enhanced conditions were performed in an autoclave reactor to assess the maximum CO_2 uptake of the material, as well as the corresponding Ca conversion yield and the

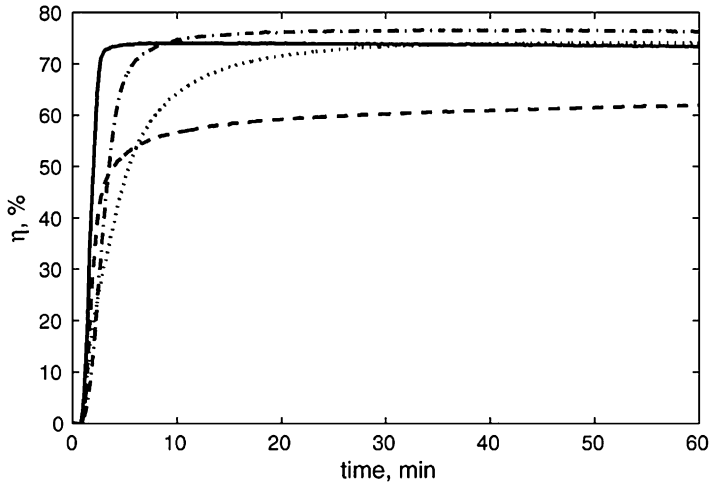

Fig. 11.13 Calcium conversion as a function of time for 10 % CO_2 flows at different temperature: 350 °C (- - -); 400 °C (—); 450 °C (···) and 500 °C (-·-·-) (Reprinted from Ref. [62]. Copyright 2009, with permission from Elsevier)

influence of operating conditions on process kinetics [58]. A maximum CO_2 uptake of about 180 g CO_2/kg BOF slag, corresponding to a carbonation conversion of 74 % of the Ca content of the slag, was achieved in 30 min at 19 bar CO_2 pressure and 100 °C for a slag particle size <38 μm. The reactive phases in the slag were found to be portlandite and Ca-(Fe) silicates and the only reaction product detected by XRD and SEM/EDX analysis was calcite [58]. As shown in Fig. 11.14, slag particle size was found to exert the most significant effects on the reaction, smaller grain sizes proving more reactive towards CO_2, while temperature, which enhanced silicate dissolution up to 200 °C, the L/S ratio and CO_2 partial pressure showed milder effects on Ca conversion yields. The diffusion of calcium through the solid matrix towards the surface of the slag particles appeared to be the rate-limiting reaction step, which was found to be hindered by the formation of a $CaCO_3$-coating and a Ca-depleted silicate layer on slag particles during the carbonation process [58]. A recent study confirmed that several Ca and/or Mg silicate phases (i.e. dicalcium silicate, bredigite, merwinite and cuspidine) as well as periclase, typically found in steelmaking slags such as AOD and continuous casting (CC) residues, present a significant reactivity to slurry-phase carbonation carried out under enhanced conditions ($T = 90$ °C, $pCO_2 = 6$ bar and L/S = 16 l/kg, $t < 2$ h) [50].

The CO_2 sequestration potential of metallurgical slags and of other types of residues such as fly ash from thermal treatment plants has also been investigated via the slurry-phase route at milder operating conditions. Carbonation of EAF and ladle slag carried out at 20 °C and ambient temperature with 15 % vol. CO_2 flows of 5 ml/min applying an L/S = 10 kg/kg resulted in a CO_2 uptake capacity of 17 g/kg EAF slag in 24 h and 247 g/kg ladle slag in 40 h, which was ascribed to the higher content

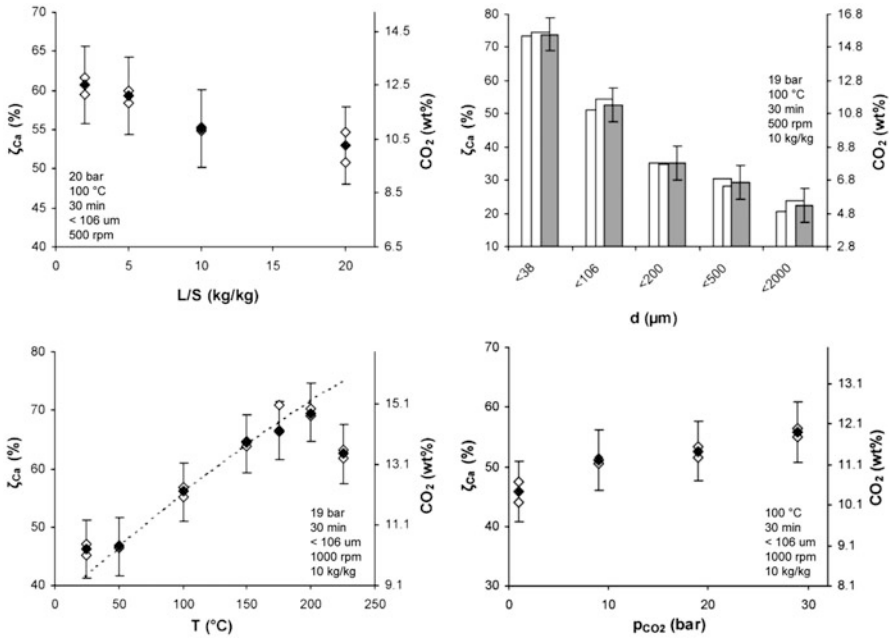

Fig. 11.14 Calcium conversion and CO_2 uptake as a function of the L/S ratio, particle size, reaction temperature (including Arrhenius-plot with $A = 6$ %Ca/min and $E_a = 3.6$ kJ/mol) and carbon dioxide pressure (Reprinted with permission from Ref. [58]. Copyright 2006 American Chemical Society)

of portlandite of the ladle slag suspension [63]. Studies on the CO_2 sequestration capacity of red mud reported a CO_2 uptake of 40 g CO_2/kg residues applying an L/S = 10 kg/kg at 20 °C and ambient pressure, bubbling a 15 % vol. CO_2 gas mixture with a flow rate of 5 ml/min for up to 24 h, which was attributed to the complete carbonation of the Ca and Na (hydr)oxides content of the residues [55]. Slurry-phase carbonation experiments carried out on fly ash from coal combustion power plants also showed a high reactivity of the lime content of the ash (over 80 %) with pure CO_2 at 30 °C and atmospheric pressure for 2 h; owing to the limited amount of CaO in the ash though, a CO_2 sequestration capacity of only 26 g CO_2/kg ash was reported [64]. For oil shale ash carbonation, 89–100 % and 48–73 % extents of carbonation were reported for experiments conducted on circulating FBC ash and pulverised FA, respectively, introducing a 10 % CO_2 gas mixture simulating flue gas in an aqueous slurry (L/S = 10 l/kg) at atmospheric pressure and room temperature for 20–40 min [52]. Lime was found to be the main CO_2 binding component, but also periclase and Ca silicates ($CaSiO_3$ and Ca_2SiO_4) were taken into account for calculating the maximal binding potential of oil shale ash [52]. The measured CO_2 uptakes varied between 100 and 160 g CO_2/kg residues, depending on the type of material tested. For lignite fly ash, a significantly higher CO_2 uptake (230 g CO_2/kg ash, with a Ca conversion yield of 75 %) was measured in a slurry system at 75 °C, using 10–30 % CO_2 at atmospheric pressure

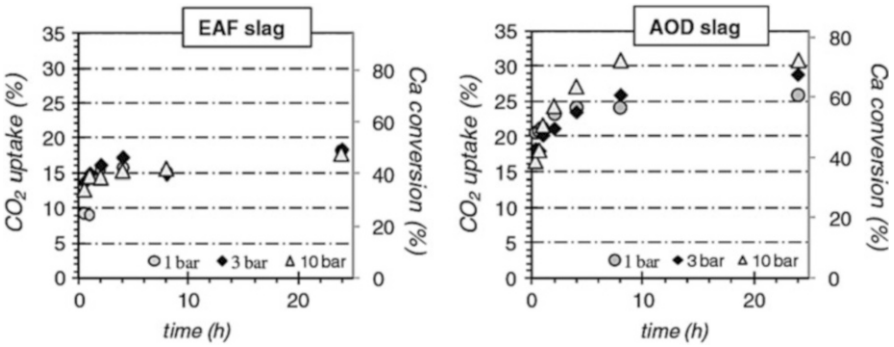

Fig. 11.15 Kinetics of CO_2 uptake and Ca conversion as a function of pressure ($T = 50$ °C, L/S = 0.4 l/kg) for EAF and AOD slag (Reprinted from Ref. [48], with kind permission from Springer)

for over 4 h [54]; the authors assessed that this result could account for a CO_2 sequestration capacity of 3.5 million tons of CO_2, corresponding to around 2 % of the CO_2 emissions from lignite power combustion in Germany [54].

Wet-Route Carbonation

Carbonation following the wet route (also called thin-film method [50]) has been tested on a wide range of residues, generally applying L/S ratios between 0.1 and 1 l/kg and mild operating conditions (30–50 °C and 1–10 bar), to investigate potential CO_2 uptakes as well as the effects on the leaching behaviour and on the mechanical properties of the materials. For stainless steel slag, Johnson et al. [70] found a maximum CO_2 uptake of 180 g/kg residue for milled (<125 μm) slag applying an L/S of 0.125 l/kg and 3 bar of 100 % CO_2 for 1 h, which led to a significant increase of the 28-day unconfined compressive strength of the material (around 10 MPa compared to below 0.6 MPa). The carbonation kinetics of different types of stainless steel slag was studied adopting a similar experimental approach by Baciocchi et al. [48]. An increase in the reaction temperature (to 50 °C) and L/S ratio (to 0.4 l/kg) showed to increase the reactivity of Ca silicate phases allowing to achieve higher CO_2 uptakes, whereas, as showed in Fig. 11.15, CO_2 pressure did not appear to exert significant effects, except for the AOD slag for reaction times above 1 h. The maximum Ca conversion yields achieved for the AOD slag appeared to be considerably higher than those resulting for milled EAF slag ($d < 0.150$ mm) and were related to the differences in the mineralogy of the two slags: the AOD residues mostly made up by γ-dicalcium silicate, while the others containing various Ca and Mg silicates [48]. Column carbonation experiments on two types of converter steel slag were also recently reported [49]. These experiments were carried out at atmospheric pressure, feeding 900 g of wetted steel slag with a water-saturated CO_2/Ar mixture at a flow rate of 400 ml/min for reaction times ranging

from 8 to 200 h and temperatures between 5 and 90 °C. The aim of this particular study was to assess the leaching behaviour of the slag more than its CO_2 storage potential; hence, relatively large (2–3.3 mm) steel slag grains were used and consequently lower carbonation degrees were achieved compared to other studies. CO_2 uptakes of 6 or 15 g/kg slag were reported for the two different types of converter steel slag in dependence of the free lime content of the material. Reaction kinetics showed to be enhanced by increasing temperature and humidity [49].

The CO_2 sequestration capacity of cement kiln dust (CKD) treated with humidified CO_2 was recently assessed in batch and column tests at ambient temperature and pressure applying gas compositions with CO_2 contents varying from 14 to 80 % [59]. The predominant reactive phase was found to be $Ca(OH)_2$ and, similarly to what was reported in other studies (e.g. [62]), reaction kinetics was found to follow the unreacted core model theory, exhibiting at early times a first-order trend indicating kinetics control by the chemical reaction and at longer times a zero-order trend induced by diffusion control due to coverage of the reacting particle surface by calcite [59]. A sequestration extent of over 60 % was observed within 8 h and the authors estimated that applying this process, a 6.5 % emission reduction in US cement-related emissions could be attained [59]. Compositions similar to those indicated in the previous study for cement kiln dust (around 50 % $Ca(OH)_2$) were indicated also for paper mill waste, which allowed to achieve a CO_2 net uptake of 218 g CO_2/kg paper waste, with pure CO_2 at 30 °C and atmospheric pressure for 2 h. A sequestration potential of round 15,000 tons of CO_2 for an average size cellulose pulp factory was estimated [71].

Wet-route carbonation of industrial residues has also been tested at pilot scale for specific applications. Mostbauer et al. [72] have investigated carbonation of the fine fraction of MSWI bottom ash as a landfill biogas-upgrading technique, i.e. to increase its methane content by removing CO_2. In addition, the treatment proved effective in reducing the H_2S content of the biogas and in improving the leaching behaviour of the slag [72]. Reddy et al. [73] tested carbonation in one of the largest coal-fired power plants of the United States by reacting flue gas with coal fly ash in a fluidised bed reactor for 1.5–2 h at 60 °C. Upon the treatment, the CO_2, SO_2 and Hg concentrations of the flue gas showed to decrease [73]. The feasibility of both types of applications mentioned, however, appears to be limited by the very low CO_2 uptakes that can be achieved by the tested materials (MSWI-BA and FA), which implies the requirement of very large amounts of residues in order to achieve significant uptakes.

Indirect Carbonation

Iizuka et al. [57] proposed to apply pressurised CO_2 for carbonating waste cement. The proposed process consists in a first step in which calcium is extracted from waste cement in an aqueous solution using pressurised 100 % CO_2 and a second step in which the pressure is reduced causing the extracted calcium to precipitate as

calcium carbonate. Experiments showed that up to 50 % of the calcium content of waste cement could be extracted with a CO_2 pressure of 9–30 bar [57].

Kodama et al. [68] developed a process for CO_2 sequestration from Ca silicate industrial residues using the pH swing of a weak base-strong acid solution. In particular, an ammonium chloride solution was chosen to extract Ca^{2+} ions from calcium silicate. As the reaction proceeds, due to NH_3 production, the solution becomes alkaline and, hence, when CO_2-containing gas is introduced in the extraction solution, $CaCO_3$ precipitates and NH_4Cl is regenerated. To avoid ammonia leakage with the flue gas, a NH_3 recovery tower was added after the CO_2 absorption unit [68]. Dissolution experiments of various size fractions of crushed converter steel slag were carried out with a 1 N NH_4Cl slurry solution for 1 h at atmospheric pressure and temperature between 60 and 90 °C. A Ca extraction yield of 60 % was achieved at 80 °C for the finest particle size fraction (<63 μm) with a very high Ca selectivity (>99 %), due to a final solution pH of 9.4, which allowed only Ca^{2+} to be dissolved differently from other extracting agents (i.e. HCl and CH_3COOH). Calcium carbonate precipitation conversion showed a maximum conversion of 80 % at 40 °C which decreased to 70 % at 80 °C, owing to lower CO_2 solubility. A $CaCO_3$ purity of 98 % was obtained, with the formation of calcite at lower temperature (plate-like morphology) and aragonite at higher temperature (needle-like morphology) [68].

Another research group investigated the feasibility of enhancing steelmaking slag dissolution with acetic acid solutions and other chemicals [69, 74–76]. Thermodynamic equilibrium calculations showed that at atmospheric pressure calcium extraction is exothermic and feasible at temperatures below 156 °C, whereas calcite carbonate precipitation may be obtained at temperatures above 45 °C [69]. A high Ca extraction yield was achieved with 33.3 % wt. solutions of acetic acid for different types of steelmaking slag (BF, AOD, EAF and converter slag) at 50 °C; however, due to the low pH values, other elements dissolved as well, including Mg, Al, Fe and Si; at 70 °C silicon was found to form a gel phase which could be separated by mechanical filtration and, hence, this temperature was chosen as the optimum reaction temperature for calcium extraction from steelmaking slag with acetic acid [69]. Carbonation experiments performed at 30–70 °C and 1–30 bar CO_2 on aqueous solutions of calcium extracted from blast furnace slag [74] and steel converter slag [75] with acetic acid showed that in order for significant calcite precipitation to occur, the addition of a strong base, such as NaOH, is needed to increase the pH of the solution. With NaOH addition, calcium carbonate phases (calcite, aragonite and calcite magnesium) were produced at 30 °C and atmospheric pressure from blast furnace slag [74]. The process scheme developed on the basis of these results as well as the amounts of reactants required to bind 1 kg CO_2 are reported in Fig. 11.16. Higher purity was achieved with carbonation tests carried out on aqueous solutions of calcium extracted from converter steel slags dissolved with weak acetic acid solutions [75]. In this case a maximum calcium conversion to carbonate of 86 %, with a precipitate purity of up to 99.8 %, was achieved at 30 °C with 10 % vol. CO_2. The main limits of this process are the high costs and requirements of additives such as NaOH and CH_3COOH; hence, other solvents

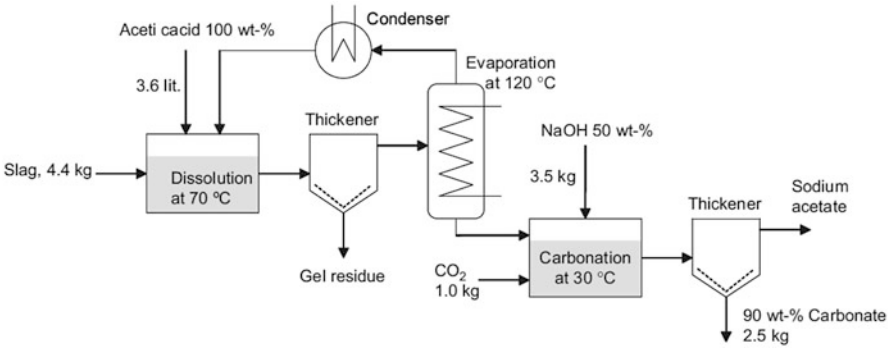

Fig. 11.16 Process scheme proposed for binding 1 kg of carbon dioxide by carbonating acetate produced from blast furnace slag (Reprinted from Ref. [74]. Copyright 2008, with permission from Elsevier)

have been tested for Ca^{2+} extraction from steelmaking slag [76]. Among these, ammonium salt solutions were found to be particularly selective in terms of Ca^{2+} dissolution and operational parameters showed similar effects to those described by [68].

11.4.3.3 Effects on the Leaching Behaviour of the Treated Residues

As previously mentioned, the effects of accelerated carbonation on the environmental behaviour of industrial residues and in particular on their potential release of inorganic contaminants such as metals, metalloids and salts has been the focus of many studies. As reviewed in [67], many works have concerned the effects of accelerated carbonation as opposed to natural weathering on the leaching behaviour of MSWI residues by performing different types of tests (e.g. compliance at native pH, pH dependence or column percolation tests). The multiple reaction mechanisms occurring during carbonation are accompanied by surface interactions between contaminants and neo-formation minerals and these will impact on the mobility of trace metals and metalloids in different ways. Hence, the effects exerted by carbonation on the leaching behaviour of industrial residues are quite complex and depend on many parameters, such as the specific properties of the individual trace metals, their solubility curves and behaviour as a function of pH and Eh and their affinity for minerals as calcite and Al and Fe (hydr)oxides [67]. In general terms, most studies have reported that carbonation determines a reduction in the pH of the leachates, which for most types of alkaline residues is above 12, and a consequent decrease in the mobility of amphoteric elements (such as Cu, Pb and Zn), whereas various effects on the release of other components such as oxyanion-forming elements (Cr, Mo and Sb in particular) depend on the characteristics of the material.

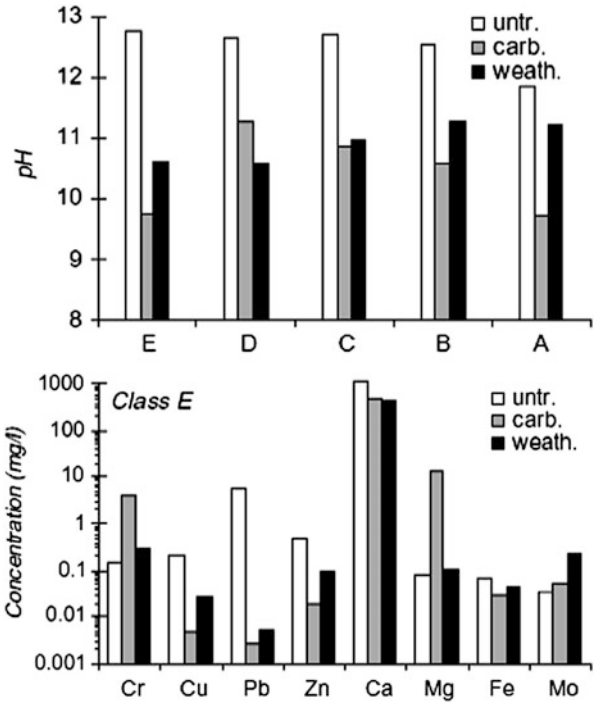

Fig. 11.17 Comparison of compliance leaching test results for untreated, carbonated ($T = 30$ °C, $P = 10$ bar, L/S = 0.3 l/kg, $t = 2$ h) and naturally weathered RDF-BA fractions: $A = 5.6$–12 mm; $B = 2$–5.6 mm; $C = 0.425$–2 mm; $D = 0.150$–0.425 mm; $E < 0.15$ mm (Reprinted from Ref. [42]. Copyright 2010, with permission from Elsevier)

As an example, Fig. 11.17 reports the effects exerted by accelerated carbonation on the leaching behaviour of specific size fractions of RDF incineration BA, resulting from the standardised compliance test (EN 12457-2) [42]. As can be noted, comparing the results obtained for the accelerated carbonation tests with those resulting for the same material after 1-year weathering, it may be observed that generally the accelerated treatment allowed to obtain lower pH values. For the macro-constituents of the slag, while for Ca leaching the two processes appeared to exert a very similar effect, Mg showed to be significantly mobilised only for the carbonated samples. This result may indicate hence that as a result of accelerated carbonation Mg may have partially formed more soluble phases than the original Mg silicate mineral constituents of the fresh slag. For amphoteric elements, accelerated carbonation appeared to generally exert a stronger effect on reducing the release of Pb in particular, but also of Cu and Zn. Cr and Mo leaching instead showed to be enhanced by both types of treatments. It is important to note finally that no significant variation between the $CaCO_3$ content of untreated and weathered slag was detected, whereas instead a CO_2 uptake of 140 g CO_2/kg residues was obtained for the finest particle size fraction; this suggests, as also indicated in previous studies (see [67] and references therein), that modifications of the leaching behaviour of BA do not depend directly on the amount of sequestered CO_2. Similar effects on the leaching behaviour of MSWI-BA were also reported by Rendek et al. [41], Santos et al. [43], Fernández-Bertos et al. [44], although

Rendek et al. [41] and Santos et al. [43] reported Cr leaching to decrease upon carbonation. In this latter study, slurry-phase carbonation was found to be more effective in reducing the mobility of elements such as Ba and Cu and to cause a lower mobilisation of V and Sb [43]. Also for APC residues, a significant reduction in the mobility of Pb, Cu, Zn and Cr was reported [44–46], along with an increase in Sb release [45, 46]; however, the critical compounds for the management of this type of residues are soluble salts, chlorides in particular, which do not appear to be significantly affected by the carbonation treatment.

As for steel slag, carbonation showed to exert a significant decrease in Ca leaching due to the formation of calcite, which is less soluble compared to (hydr) oxide and silicate phases, while to increase Mg and Si leaching, consistent with the pH decrease (for Mg leaching) and with the at least partial dissolution of the calcium silicate phases [47, 48]. Santos et al. [50] reported a reduction in the mobility of most trace contaminants (e.g. Mo, Pb, Zn, Ba, Ni, Sb) from AOD and CC slag, in particular upon slurry-phase carbonation under enhanced conditions. For V instead, a significant mobilisation effect was reported especially for carbonated BOF samples [47, 49], whereas a slight mobilisation effect for Cr was reported for EAF and AOD slag [48]. The effects of accelerated carbonation on the leaching behaviour of pulverised coal fly ash and oil shale ash were first analysed by Reddy et al. [51, 77]. Treating the humidified samples (20 % moisture) with 100 % CO_2 at around 3 bar for 120 h lowered the pH of the residues from 12.3–12.8 to 8.8–9.7 and showed to decrease the leaching of Mn, Cd, Pb and Zn for the fly ash and oil shale samples [51]. In an earlier study, the leaching of F and Mo was indicated to decrease as a result of accelerated carbonation treatment [77].

11.4.3.4 Effects on the Properties of Products to Use for Specific Applications

Wet-route carbonation has also been tested as a treatment to manufacture synthetic aggregates from thermal residues (i.e. MSWI residues, wood ash, paper ash, CBD and CKD) and waste quarry fines [13]. The process was tested at pilot scale in a unit designed to produce 100 kg of aggregates/h (see Fig. 11.18). The material is pelletised in a rotary carbonation reactor at ambient temperature and pressure and then discharged into a curing chamber circulated with dehumidified CO_2 for 7 days. The produced aggregates showed to present comparable properties to commercially available lightweight aggregates (e.g. bulk density below 1,000 kg/m^3 and a high water absorption capacity). Concrete blocks were manufactured with carbonated aggregates and their properties resulted adequate for specific applications, such as construction of internal partitioning walls [13]. As opposed to the commercially available fired or sintered aggregates, the proposed process relies on cold bonding with CO_2 and hence should allow to produce carbon-negative aggregates and construction materials [13].

One of the assets of applying indirect accelerated carbonation routes to minerals or residues such as steelmaking slag is that these treatments may be applied as a

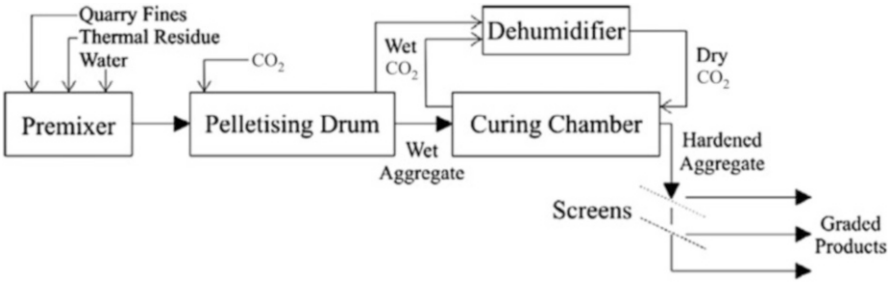

Fig. 11.18 Scheme of the pilot-scale process proposed for aggregates production based on carbonation of industrial residues (Reprinted from Ref. [13]. Copyright 2009, with permission from Elsevier)

technique for producing precipitated calcium carbonate (PCC) to use in industrial applications, e.g. as a filler and coating pigment in plastics, rubbers, paints and paper manufacturing [69, 74, 75]. PCC is currently produced by carbonating calcined natural limestone and during calcination more CO_2 than that which is sequestered during the carbonation process is emitted to the atmosphere [69]; hence, the use of calcium silicates for PCC production could contribute in reducing both CO_2 emissions and the consumption of natural resources such as limestone [75]. Solution temperature is an important parameter for this process since it affects calcium carbonate morphology [68, 75]; the precipitate formed at low temperature in fact displays a rhombohedral particle shape and small particle size, which are considered to be the appropriate characteristics for PCC commercialisation [75].

Recently carbonation of alkaline residues was also tested as a regeneration treatment for the spent solutions produced by CO_2 capture processes based on absorption with alkali solutions [78, 79]. As discussed in Sect. 11.3.2, the traditional approach for the regeneration of these solutions is to contact them with $Ca(OH)_2$ (see Eq. 11.8) that is produced by limestone calcination. Baciocchi et al. [78] investigated the use of a waste material as calcium hydroxide source so to reduce the consumption of alkali reagents and improve the economical and environmental performance of the alkali absorption process proposed as a biogas-upgrading technique with the additional benefit of permanently storing the separated CO_2 as calcite. On the basis of the results of preliminary lab-scale tests [78], a pilot-scale regeneration unit employing APC residues was designed, built and installed in a landfill site downstream of an absorption column treating landfill biogas with KOH/NaOH solutions [79]. Results of the combined absorption and regeneration pilot tests showed overall regeneration efficiencies of the alkali solutions of around 50–60 %. Furthermore, the performance of the absorption step appeared not to be affected by the use of regenerated solutions, while the solid product of the process, presenting a calcite content of over 80 %, presented an improved leaching behaviour compared to the raw APC residues [78, 79]. However, one of the critical aspects for the applicability of this process is related to the limited availability of $Ca(OH)_2$-rich residues such as APC residues.

11.4.4 Energy and Material Requirements of Accelerated Carbonation

Although the feasibility of accelerated carbonation of minerals and industrial residues was proven at lab scale, the significant requirement of materials and energy associated to the process has hindered so far its application at larger scale. Recently, several studies have focused on the evaluation of the energy penalties related to mineral carbonation adopting the slurry-phase route scheme [29, 80–82]. However, the energy penalties evaluated in these works differ considerably from one study to the other, even considering the different power plant types used as reference and also when the evaluation was based on the same experimental data, probably as a consequence of the differences in the assumptions made and in the selected process layout.

As discussed in Sect. 11.4.2, the Albany Research Center (ARC) presented a preliminary study aimed at developing an ex situ aqueous process to convert magnesium silicate-rich ultramafic rocks and minerals, such as olivine, wollastonite and serpentine, to magnesium carbonates by using gaseous CO_2 in an aqueous solution [80]. In this study seven kinds of ultramafic minerals were analysed considering various pretreatment options and operating conditions for the carbonation reaction and based on the results of lab-scale tests, the feasibility of the process was investigated. At the optimal operating conditions using olivine (L/S = 2.33 kg/kg, t = 120 min, T = 185 °C, pCO_2 = 150 bar and d < 37 μm), the authors determined an energy requirement of 352 MW for the storage of 100 % of the CO_2 emissions from a 1.3 GW coal-fired electric generation plant characterised by a heat release of around 10 GJ/tCO_2 emitted. The energy demand of this process using olivine, expressed in terms of CO_2 emissions, was estimated to be around 28 % of the total amount of carbon dioxide sequestered that corresponds to an energy requirement of 2.66 GJ/t CO_2 [80].

Huijgen et al. [29] evaluated the energetic performance of CO_2 sequestration by aqueous carbonation of Ca silicate ores and industrial residues. Specifically they considered data obtained from carbonation experiments carried out at lab scale using both a wollastonite and steel slag feedstock and on this basis they assumed a mineral carbonation process layout, thus determining the CO_2 sequestration efficiency at various operating conditions. The minimum energy penalties in terms of CO_2 emissions determined for wollastonite and steel slag were 16 % and 17 %, respectively (at L/S = 5 kg/kg, t = 15 min, T = 473 K, pCO_2 = 2 MPa, particle size lower than 38 μm), making reference to a power plant characterised by a heat release of 18 GJ/tCO_2 emitted. For an L/S = 2 kg/kg, higher energy penalties resulted for wollastonite and in particular for steel slag (i.e. 25 % and 31 %, respectively). The grinding of the feedstock and the compression of the carbon dioxide were identified as the main energy-consuming process steps. In addition, a sensitivity analysis has shown that further grinding (particularly for wollastonite) or reducing the CO_2 partial pressure (in the case of steel slag) can potentially improve the process efficiency [29].

Kelly et al. [81] performed a preliminary energy balance for three CO_2 mineralisation pathways at industrial scale, i.e. industrial caustics, naturally

occurring minerals and industrial wastes. The basis for this evaluation is a theoretical 1 GW coal-fired power plant emitting 8×10^6 t CO_2/y (i.e. a heat release of around 10 GJ/tCO_2 emitted), which is captured by one of the considered mineral carbonation pathways. The estimation of the energy penalties for the carbonation of olivine and wollastonite was performed on the basis of previous works [29, 80] taking also into account the requirements for mining and CO_2 separation. The resulting energy penalties ranged between 55 and 69 % for olivine and were over 100 % for wollastonite [81]. Regarding industrial residues, Kelly et al. [81] concluded that the energy penalty associated to CO_2 mineralisation of steel slag proposed by Huijgen et al. [29] is greater than 100 %, making this process unlikely to be feasible. On the other hand, the CO_2 mineralisation process with fly ash proposed by Reddy et al. [73] was considered feasible, as it presented a much lower energy penalty (9–22 %). It is worth pointing out that the energy penalties calculated by Kelly et al. [81] for steel slags were estimated assuming no energy recovery; however, as suggested also by Huijgen et al. [29], it is reasonable to assume that the heat of the water-mineral slurry can be recovered allowing to greatly reduce the energy penalties estimated by Kelly et al. [81].

Recently Kirchofer et al. [82] estimated the energy and material requirements of different aqueous carbonation processes using both natural silicate minerals (i.e. olivine and serpentine) and industrial by-products, such as cement kiln dust [59], coal fly ash [54] and steelmaking slag [29], in order to compare their environmental performance by life cycle assessment (LCA). The minimum energy penalty expressed in terms of percent CO_2 emitted per CO_2 sequestered, considering natural gas as energy source, was obtained for cement kiln dust at ambient temperature and pressure conditions, resulting equal to 14 %, while the results obtained for the other considered materials were 25 % for olivine, 75 % for serpentine, 34 % for steel slag and 45 % for fly ash. Furthermore, within the range of the considered operating conditions, heating provided the most relevant contribution, followed by mixing and grinding. It should be noted that in this study the energy requirements for CO_2 capture were not considered while those related to mining and transport of reactants and products were accounted for. Regarding the carbonation of minerals, in this study the energy penalties were estimated on the basis of the experimental results obtained in dissolution tests, assuming that all the dissolved cations react with CO_2 in the precipitation stage. This may explain the observed differences in the effects of the operating conditions and resulting energy requirements compared to the previously mentioned studies. As for the carbonation of residues, it is worth mentioning that the same process scheme was applied for all of the tested materials regardless of the applied L/S ratio.

11.5 Conclusions and Perspectives

Accelerated carbonation has been investigated for more than a decade as an option for carbon capture and storage. Apart from the well-established hot carbonate process, that has found an interesting market application in the ammonia synthesis

sector, the calcium looping technology seems to be the most promising and developed application of accelerated carbonation for carbon capture. Nevertheless, the process still suffers from the low stability of the calcium-based sorbents, whose CO_2 carrying capacity decreases sharply after a few carbonation/calcination cycles. Besides, the effective advantage of this process in terms of energy requirements with respect to commercial ethanolamine processes must still be demonstrated. Differently, the perspectives for the alkali absorption process are quite negative, in view of the very large energy inputs required to regenerate the solvent. The only solution to this issue may come from the use of alternative alkalinity sources, such as industrial residues rich in calcium hydroxide, that may be used for the solvent regeneration phase in place of raw calcium hydroxide; anyhow, the availability of these residues represents the main bottleneck for the deployment of this technology.

Accelerated carbonation as storage option has also been the subject of intense research efforts aimed at improving the efficiency of the process. So far, the direct aqueous route still represents the benchmark technology for mineral carbonation. Unfortunately, this route suffers from too high energy requirements, mostly related to the mechanical and thermal activation of the minerals and to the heat required to bring the mineral slurry to the optimal reaction temperature. The indirect route in principle could allow to reduce the energy requirements of the process; nevertheless, its feasibility is questionable due to the consumption of chemicals needed in these multistep processes and given the uncertainty on the effective possibility of recycling them. Thus summarising, the energy penalties associated to mineral carbonation would be of the same order of magnitude of the ones associated to carbon capture. Therefore, the only feasible perspective for the implementation of this technology seems to be represented by the application of mineral carbonation directly to the emission source, such as flue gas or syngas. Lumping capture and storage in a single step could probably reduce the overall energy penalty, allowing to fix CO_2 directly in a stable and definitive manner.

Differently from mineral carbonation, the many kinds of alkaline residues produced from thermal processes, steelmaking and cement industries allowed for the development of diverse strategies and reaction routes. Based on the overview made in this chapter, carbonation of industrial residues may represent a suitable option for storing at least part of the carbon dioxide emissions produced by these industrial sectors. These materials are typically more reactive than silicate minerals, allowing to achieve reasonable extents of carbonation at milder operating conditions. Besides, as these materials are already available at the CO_2 point source, all issues related to mining and transport would be avoided. Anyhow, also in this case the energy requirements associated to carbonation are not negligible. The wet route, at mild operating temperature and pressure, using a fairly concentrated CO_2 source, such as syngas or biogas, seems the most promising option for the application of the process.

Finally, the role of accelerated carbonation in CCUS must be briefly discussed. The term carbon utilisation suggests that some of the anthropogenically emitted CO_2 can be used for different purposes, but without any guarantee on the final destiny of the used carbon. On the other hand, the term storage means that the

anthropogenic CO_2 is isolated or fixed definitively. Given these definitions, as accelerated carbonation will always lead to the permanent fixation of some CO_2, we observe that it should be included among the storage options. The term utilisation could be eventually coupled to the term storage only when the storage capacity is negligible with respect to the emission source that we want to address and the main benefit of the process is given by the improvement of the environmental properties of the material or by the manufacturing of a product that can be employed for different applications.

References

1. Boschi C, Dini A, Dallai L et al (2010) Enhanced CO_2-mineral sequestration by cyclic hydraulic fracturing and Si-rich fluid infiltration into serpentinites at Malentrata (Tuscany, Italy). Chem Geol 265:209–226
2. Lackner KS, Wendt CH, Butt D et al (1995) Carbon dioxide disposal in carbonate minerals. Energy 20:1153–1170
3. Haug TA, Kleiv RA, Munz IA (2010) Investigating dissolution of mechanically activated olivine for carbonation purposes. Appl Geochem 25:1547–1563
4. Seifritz W (1990) CO_2 disposal by means of silicates. Nature 345:486
5. Abanades JC, Alvarez D (2003) Conversion limits in the reaction of CO_2 with lime. Energy Fuels 17:308–315
6. Yi F, Zou HK, Chu GW et al (2009) Modeling and experimental studies on absorption of CO_2 by Benfield solution in rotating packed bed. Chem Eng J 145:377–384
7. IPCC (2005) IPCC special report on carbon dioxide capture and storage. In: Metz B, Davidson O, de Coninck HC, Loos M, Meyer LA (eds) Prepared by Working Group III of the Intergovernmental Panel on Climate Change. Cambridge University Press, Cambridge/New York, 442 pp
8. Lackner K, Duby P, Yegulalp T et al (2008) AISI/DOE technology roadmap – TRP9957 Integrating steel production with mineral carbon sequestration. US DOE Technical Report, New York, doi: 10.2172/938528
9. Lackner KS (2002) Carbonate chemistry for sequestering fossil carbon. Annu Rev Energy Environ 27:193–232
10. Zevenhoven R, Teir S, Eloneva S (2006) Chemical fixation of CO_2 in carbonates: routes to valuable products and long-term storage. Catal Today 115:73–79
11. Gunning PJ, Hills CD, Carey PJ (2010) Accelerated carbonation treatment of industrial residues. Waste Manag 30:1081–1090
12. Kirchofer A, Becker A, Brandt A et al (2013) CO_2 mitigation potential of mineral carbonation with industrial alkalinity sources in the United States. Environ Sci Technol 47:7548–7554
13. Gunning PJ, Hills CD, Carey PJ (2009) Production of lightweight aggregate from industrial waste and carbon dioxide. Waste Manag 29:2722–2728
14. Shimizu T, Hirama T, Hosoda H et al (1999) A twin fluid-bed reactor for removal of CO_2 from combustion processes. Trans IChemE 77:62–68
15. Blamey J, Anthony EJ, Wang J et al (2010) The calcium looping cycle for large-scale CO_2 capture. Prog Energy Combust Sci 36:260–279
16. Zeman F (2008) Effect of steam hydration on performance of lime sorbent for CO_2 capture. Int J Greenh Gas Control 2:203–209
17. Abanades JC, Rubin ES, Anthony EJ (2004) Sorbent cost and performance in CO_2 capture systems. Ind Eng Chem Res 43:3462–3466

18. Gupta H, Fan LS (2002) Carbonation-calcination cycle using high reactivity calcium oxide for carbon dioxide separation from flue gas. Ind Eng Chem Res 41:4035–4042
19. Stendardo S, Andersen LK, Herce C (2013) Self-activation and effect of regeneration conditions in CO_2–carbonate looping with CaO–$Ca_{12}Al_{14}O_{33}$ sorbent. Chem Eng J 220:383–394
20. Sanyal D, Vasishtha N, Saraf DN (1988) Modeling of carbon dioxide absorber using hot carbonate process. Ind Eng Chem Res 27:2149–2156
21. Nagasawa H, Yamasaki H, Iizuka A et al (2009) A new recovery process of carbon dioxide from alkaline carbonate solution via electrodialysis. AIChE J 55:3286–3293
22. Baciocchi R, Storti G, Mazzotti M (2006) Process design and energy requirements for the capture of carbon dioxide from air. Chem Eng Process 34:1047–1058
23. APS (2011) Direct air capture of CO_2 with chemicals: a technology assessment for the APS panel on public affairs. American Physical Society Technical Report, Washington DC, April
24. Aroonwilas A, Tontiwachwuthikul P (2000) Mechanistic model for prediction of structured packing mass transfer performance in CO_2 absorption with chemical reactions. Chem Eng Sci 55:3651–3663
25. Zevenhoven R, Teir S, Eloneva S (2008) Heat optimisation of a staged gas–solid mineral carbonation process for long-term CO_2 storage. Energy 33:362–370
26. Nduagu E, Biörklöf T, Fagerlund J et al (2012) Production of magnesium hydroxide from magnesium silicate for the purpose of CO_2 mineralization – Part 2: Mg extraction modeling and application to different Mg silicate rocks. Miner Eng 30:87–94
27. Gerdemann SJ, O'Connor WK, Dahlin DC et al (2007) Ex situ aqueous mineral carbonation. Environ Sci Technol 41:2587–2593
28. Huijgen WWJ, Witkamp GJ, Comans RNJ (2006) Mechanisms of aqueous wollastonite carbonation as a possible CO_2 sequestration process. Chem Eng Sci 61:4242–4251
29. Huijgen WWJ, Ruijg GJ, Comans RNJ et al (2006) Energy consumption and net CO_2 sequestration of aqueous mineral carbonation. Ind Eng Chem Res 45:9184–9194
30. Huijgen WWJ, Comans RNJ, Witkamp G (2007) Cost evaluation of CO_2 sequestration by aqueous mineral carbonation. Energy Conv Manag 48:1923–1935
31. Hänchen M, Prigiobbe V, Storti G et al (2006) Dissolution kinetics of fosteritic olivine at 90–150 °C including effects of the presence of CO_2. Geochim Cosmochim Acta 70:4403–4416
32. Prigiobbe V, Costa G, Baciocchi R (2009) The effect of CO_2 and salinity on olivine dissolution kinetics at 120 °C. Chem Eng Sci 64:3510–3515
33. Park AAH, Fan LS (2004) CO_2 mineral sequestration: physically activated dissolution of serpentine and pH swing process. Chem Eng Sci 59:5241–5247
34. Teir S, Kuusik R, Fogelholm CJ et al (2007) Production of magnesium carbonates from serpentinite for long-term storage of CO_2. Int J Miner Process 85:1–15
35. Wang X, Maroto-Valer MM (2011) Dissolution of serpentine using recyclable ammonium salts for CO_2 mineral carbonation. Fuel 90:1229–1237
36. Hänchen M, Prigiobbe V, Baciocchi R et al (2008) Precipitation in the Mg-carbonate system—effects of temperature and CO_2 pressure. Chem Eng Sci 63:1012–1028
37. Bobicki ER, Liu Q, Xu Z et al (2012) Carbon capture and storage using alkaline industrial wastes. Prog Energy Combust 38:302–320
38. Pan SY, Chang EE, Chiang PC (2012) CO_2 capture by accelerated carbonation of alkaline wastes: a review on its principles and applications. Aerosol Air Qual Res 12:770–791
39. Huijgen WJJ, Comans RNJ (2003) Carbon dioxide sequestration by mineral carbonation: literature review. Technical Report ECN-C—03016, Petten, February
40. Van Gerven T, Van Keer E, Arickx S et al (2005) Carbonation of MSWI-bottom ash to decrease heavy metal leaching, in view of recycling. Waste Manag 25:291–300
41. Rendek E, Ducom G, Germain P (2006) Carbon dioxide sequestration in municipal solid waste incinerator (MSWI) bottom ash. J Hazard Mater B128:73–79
42. Baciocchi R, Costa G, Lategano E et al (2010) Accelerated carbonation of different size fractions of bottom ash from RDF incineration. Waste Manage 30:1310–1317

43. Santos RM, Mertens G, Salman M et al (2013) Comparative study of ageing, heat treatment and accelerated carbonation for stabilization of municipal solid waste incineration bottom ash in view of reducing regulated heavy metal/metalloid leaching. J Environ Manage 128:807–821
44. Fernández-Bertos M, Li X, Simons SJR et al (2004) Investigation of accelerated carbonation for the stabilization of MSW incinerator ashes and the sequestration of CO_2. Green Chem 6:428–436
45. Baciocchi R, Costa G, Di Bartolomeo E et al (2009) The effects of accelerated carbonation on CO_2 uptake and metal release from incineration APC residues. Waste Manage 29:2994–3003
46. Cappai G, Cara S, Muntoni A (2012) Application of accelerated carbonation on MSW combustion APC residues for metal immobilization and CO_2 sequestration. J Hazard Mater 207–208:159–164
47. Huijgen WJJ, Comans RNJ (2006) Carbonation of steel slag for CO_2 sequestration: leaching of products and reaction mechanisms. Environ Sci Technol 40:2790–2796
48. Baciocchi R, Costa G, Bartolomeo D et al (2010) Carbonation of stainless steel slag as a process for CO_2 storage and slag valorization. Waste Biomass Valor 1:467–477
49. van Zomeren A, van der Laan SR, Kobesen HBA et al (2011) Changes in mineralogical and leaching properties of converter steel slag resulting from accelerated carbonation at low CO_2 pressure. Waste Manage 31:2236–2244
50. Santos RM, Van Bouwel J, Vandevelde E et al (2013) Accelerated mineral carbonation of stainless steel slags for CO_2storage and waste valorization: effect of process parameters on geochemical properties. Int J Greenh Gas Control 17:32–45
51. Reddy KJ, Drever JI, Hausfurther VR (1991) Effects of a CO_2 pressure process on the solubilities of major and trace elements in oil shale solid wastes. Environ Sci Technol 25:1466–1469
52. Uibu M, Uus M, Kuusik R (2009) CO_2 mineral sequestration in oil-shale wastes from Estonian power production. J Environ Manage 90:1253–1260
53. Arickx S, Van Gerven T, Vandecasteele C (2006) Accelerated carbonation for treatment of MSWI bottom ash. J Hazard Mater B137:235–243
54. Back M, Kuehn M, Stanjek H et al (2008) Reactivity of alkaline lignite fly ashes towards CO_2 in water. Environ Sci Technol 42:4520–4526
55. Bonenfant D, Kharoune L, Sauvé S et al (2008) CO_2 sequestration by aqueous red mud carbonation at ambient pressure and temperature. Ind Eng Chem Res 47:7617–7622
56. Fernández-Bertos M, Simons SJR, Hills CD et al (2004) A review of accelerated carbonation technology in the treatment of cement-based materials and sequestration of CO_2. J Hazard Mater B112:193–205
57. Iizuka A, Fujii M, Yamasaki A et al (2004) Development of a new CO_2 sequestration process utilizing the carbonation of waste cement. Ind Eng Chem Res 43:7880–7887
58. Huijgen WJJ, Witkamp GJ, Comans RNJ (2005) Mineral CO_2 sequestration by steel slag carbonation. Environ Sci Technol 39:9676–2682
59. Huntzinger DN, Gierke JS, Kawatra SK et al (2009) Carbon dioxide sequestration in Cement Kiln Dust through mineral carbonation. Environ Sci Technol 43:1986–92
60. Jia L, Anthony EJ (2000) Pacification of FBC ash in a pressurized TGA. Fuel 79:1109–1114
61. Baciocchi R, Polettini A, Pomi R et al (2006) CO_2 sequestration by direct gas-solid carbonation of APC residues. Energy Fuels 20:1933–1940
62. Prigiobbe V, Polettini A, Baciocchi R (2009) Gas–solid carbonation kinetics of air pollution control residues for CO_2 storage. Chem Eng J 148:270–278
63. Bonenfant D, Kharoune L, Sauvé S et al (2008) CO_2 sequestration potential of steel slags at ambient pressure and temperature. Ind Eng Chem Res 47:7610–7616
64. Montes-Hernandez G, Pérez-López R, Renard F et al (2009) Mineral sequestration of CO_2 by aqueous carbonation of coal combustion fly-ash. J Hazard Mater 161:1346–1354
65. Young JF, Berger RL, Breese J (1974) Accelerated curing of compacted calcium silicate mortars on exposure to CO_2. J Am Ceram Soc 57:394–397
66. Papadakis VG, Vayenas CG, Fardis MN (1991) Experimental investigation and mathematical modelling of the concrete carbonation problem. Chem Eng Sci 46:1333–1338

67. Costa G, Baciocchi R, Polettini A et al (2007) Current status and perspectives of accelerated carbonation processes on municipal waste combustion residues. Environ Monit Assess 135:55–75
68. Kodama S, Nishimoto T, Yamamoto N et al (2008) Development of a new pH-swing CO_2 mineralization process with a recyclable reaction solution. Energy 33:776–784
69. Teir S, Eloneva S, Fogelholm CJ et al (2007) Dissolution of steelmaking slags in acetic acid for precipitated calcium carbonate production. Energy 32:528–539
70. Johnson DC, Macleod CL, Carey PJ et al (2003) Solidification of stainless steel slag by accelerated carbonation. Environ Technol 24:671–678
71. Pérez-López R, Montes-Hernandez G, Nieto JM et al (2008) Carbonation of alkaline paper mill waste to reduce CO_2 greenhouse gas emissions into the atmosphere. Appl Geochem 23:2292–2300
72. Mostbauer P, Lenz S, Lechner P (2008) MSWI bottom ash for upgrading of biogas and landfill gas. Environ Technol 29:757–764
73. Reddy KJ, Kohn S, Weber H et al (2011) Simultaneous capture and mineralization of coal combustion flue gas carbon dioxide (CO_2). Energy Proced 4:1574–83
74. Eloneva S, Teir S, Salminen J et al (2008) Fixation of CO_2 by carbonating calcium derived from blast furnace slag. Energy 33:1461–1467
75. Eloneva S, Teir S, Salminen J et al (2008) Steel converter slag as raw material for precipitation of pure calcium carbonate. Ind Eng Chem Res 47:7104–7111
76. Eloneva S, Mannisto P, Said A et al (2011) Ammonium salt-based steelmaking slag carbonation: precipitation of $CaCO_3$ and ammonia losses assessment. Greenh Gas Sci Technol 1:305–311
77. Reddy KJ, Gloss SP, Wang L (1994) Reaction of CO_2 with alkaline solid wastes to contaminant mobility. Water Res 28:1377–1382
78. Baciocchi R, Costa G, Gavasci R et al (2012) Regeneration of a spent alkaline solution from a biogas upgrading unit by carbonation of APC residues. Chem Eng J 179:63–71
79. Baciocchi R, Carnevale E, Corti A et al (2013) Innovative process for biogas upgrading with CO_2 storage: results from pilot plant operation. Biomass Bioenergy 53:128–137
80. O'Connor WK, Dahlin DC, Rush GE et al (2005) Aqueous mineral carbonation: mineral availability, pretreatment, reaction parametrics and process studies. Report DOE/ARC-TR-04-002. Albany Research Center, Albany
81. Kelly KE, Silcox GD, Sarofim AF et al (2011) An evaluation of ex situ, industrial-scale, aqueous CO_2 mineralization. Int J Greenh Gas Control 5:1587–1595
82. Kirchofer A, Brandt A, Krevor S et al (2012) Impact of alkalinity sources on the life-cycle energy efficiency of mineral carbonation technologies. Energy Environ Sci 5:8631–8641

Part III
Biological Reactions

Chapter 12
Carbon Dioxide Sequestration by Biological Processes

Kanhaiya Kumar and Debabrata Das

12.1 Introduction

Carbon dioxide is one among many greenhouse gases such as methane, ozone, NO_x, and water vapor. Greenhouse gases act as blanket, which retain the outgoing sun's heat (infrared rays) into the earth's atmosphere. In absence of greenhouse gases, earth would be colder. Contrary to this, increase in any one of the greenhouse gases will result in extra trapping of heat, causing global warming. CO_2 constitutes very small portion of the gases present in the earth's atmosphere. Natural range of CO_2 concentration over the last 650,000 years was in the range of 180–300 ppmv. However, presently CO_2 concentration has crossed the natural range and reached as high as 397.34 ppmv in March 2013. Moreover, the Keeling curve reveals progressively faster rise in CO_2 concentration after industrialization [1]. Rate of increase in atmospheric CO_2 was 1.94 ppm/year in 2011, which was more than twice the estimated value in 1959 [1]. Temperature contributes significantly to make planet habitable for the living beings. Therefore, trace amount of CO_2 in the earth's atmosphere is required for maintaining stable temperature. Increase or decrease of few degrees of global temperature can have a devastating effect on earth. Global atmosphere and ocean temperature have increased by 0.6 °C and 0.3 °C, respectively, in the last century despite the fact that solar output witnessed decline in the same period [2]. Rise in temperature is the reason for climate change and melting of glaciers, thus causing rise in the sea level. In addition, global warming will cause increase in soil microbe's respiration and further addition of greenhouse gas CO_2 [3]. In the last century, global sea level rose by 17 cm [2]. Nearly 2 billion tons of CO_2 is being absorbed in the upper layer of ocean per year. Increase in CO_2 absorption resulted in the increase of acidification that adversely affects the aquatic life [2]. The International Panel on Climate Change

K. Kumar • D. Das (✉)
Department of Biotechnology, Indian Institute of Technology Kharagpur,
I.I.T. Kharagpur, India
e-mail: ddas.iitkgp@gmail.com

B.M. Bhanage and M. Arai (eds.), *Transformation and Utilization of Carbon Dioxide*, Green Chemistry and Sustainable Technology, DOI 10.1007/978-3-642-44988-8_12,

(IPCC) forecast increase in CO_2 concentration up to 570 ppmv by the end of the twenty-first century. This will cause nearly a rise of 1.9 °C of mean global temperature, causing an increase in mean sea level by 38 cm [4]. It is disputable to link rise in temperature with increase in CO_2 concentration. Some reports suggest present temperature rise is the result of natural cycle of rise and fall in temperature over the earth's history. However, some researchers believe present rise in temperature is due to an increase in CO_2 concentration. It becomes more important as some reports reveal unprecedented rate of increase in temperature is contrary to natural cycle of earth temperature observed so far [2].

CO_2 is being injected into the atmosphere from natural as well as artificial sources. Natural sources of CO_2 are volcanic eruptions, decomposition of organic matters, and autotrophic and heterotrophic respiration [5]. However, there is a natural mechanism of CO_2 removal such as oceanic and terrestrial CO_2 removal from the atmosphere. Imbalance in natural CO_2 addition and removal from the atmosphere is due to anthropogenic emission of CO_2 by human activity despite the fact that natural processes remove 50 % of the anthropogenic CO_2 emissions. Therefore, increasing consumption of fossil fuels is the main matter of concern due to the anthropogenic CO_2 emissions. Total annual anthropogenic CO_2 emission due to fossil fuel consumption is 29 Gt per year [6]. Today, power plants, cement, steel manufacturing industries, transportation, and household usages are dependent on fossil fuels [7]. Coal-fired power plants consume nearly one third of the total fossil fuel consumption and the remaining from fossil fuel usages in other sectors such as transportation, industry, and homes [2, 8]. Increase in human population and modernization are the reasons for the booming of these sectors.

In this scenario, it is necessary to adopt some strategies to sequester CO_2 from the earth's atmosphere. CO_2 sequestration strategies can be divided into abiotic and biotic categories. Abiotic categories involve scrubbing, mineral carbonation, and geological and ocean injection. Several techniques are available to separate CO_2 from the flue gas. Further, they can be stored at various locations such as oceans, deep aquifers, and depleted oil and gas reservoirs [9]. However, these methods can pose potential threat for safety and environmental impact due to accidental leakage especially in long term [10]. Biotic categories include CO_2 sequestration in oceanic, terrestrial, and secondary carbonates. There are several natural phenomena occurring in the ocean, which ultimately remove atmospheric CO_2 [11]. Oceanic CO_2 at the surface is in equilibrium with atmospheric CO_2. CO_2 dissolved in water forms weak acid, which reacts with carbonate anions and water to form bicarbonate. Continuous supplies of cations are required to maintain the buffering capacity of bicarbonate system. CO_2 solubility gradient is another phenomenon by which large amount of CO_2 is being sent to the bottom of ocean. CO_2 is more soluble in cold and saline water. Therefore, cold dense water masses at higher latitude especially at the North Atlantic and Southern Ocean confluence sink into the interior of ocean carrying huge amount of CO_2 [11]. This eventually gets trapped by less dense water at the top for several hundred years. Further, oceanic phytoplanktons play a vital role by absorbing atmospheric CO_2 at the surface of the ocean during photosynthesis. Nearly 25 % of carbon fixed by these processes sinks to the bottom of the

ocean. It has been estimated that 11–16 Gt of carbon is removed from the atmosphere by this process [11]. Oceanic phytoplanktonic photosynthesis lowers the atmospheric CO_2 by 150–200 ppmv [11]. CO_2 is also absorbed naturally such as through sedimentation. CO_2 conversion into bicarbonate rocks is a natural process. Nearly 2 Gt of carbon is sequestered in the soil through burial of decomposed organic material from plants, animals, biomass, and agriculture by microbes [6]. However, most of those are released back into the atmosphere during soil erosion and oxidation. Biochar is another promising material helpful in CO_2 removal. Biochar is charcoal, which is produced when smoldering biomass is burnt in limited oxygen producing little heat. The advantage of biochar in CO_2 sequestration is that it gives stability to carbon present in the biomass against microbe's oxidation [6] and, thus, prevents the release of CO_2 into the atmosphere.

Land-based plants consume CO_2 in photosynthesis and release CO_2 during respiration. However, there is net CO_2 sequestration from the atmosphere. Plants are not capable of utilizing the concentrated CO_2 present in flue gas. It has been estimated that afforesting 22 % of earth's terrestrial surface, which is equal to present forested land, is required to sequester CO_2 emitted due to fossil fuel usages [12]. Other reports say only 345 million hectares is available for afforestation, which will result in 1.5 Gt C annually [6]. This can lead to little less than 20 % reduction in anthropogenic CO_2 emission. However, afforestation in total available area is not possible due to huge pressure on land for other purposes. Each year nearly 10 % of total atmospheric CO_2 is fixed into carbohydrates by the photosynthetic process [13]. Total global CO_2 removal by land-based plants and oceanic phytoplanktons are 403 Gt CO_2 (equivalent to 110 Gt carbon) and 385 Gt CO_2, respectively [8]. Microalgae, seaweeds, and higher aquatic plants are other alternatives for CO_2 sequestration because of their photosynthetic ability. However, the latter two are not promising because of low CO_2 and other nutrient mass transfer [14]. They require high amount of energy input for mixing. However, seaweeds are more promising compared to higher aquatic plants because it is difficult to achieve proper water exchange at the submerged plants and their dense stands [14]. Therefore, seaweeds are grown near the seashore and shallow ocean systems. Carbon is provided by seawater exchange system but requires high amount of energy for water pumping.

Use of microalgae, cyanobacteria, and other bacteria is another alternative available for CO_2 sequestration. A large number of microbes are known capable of utilizing CO_2. Except microalgae, all require some inorganic reducing agent such as H_2, H_2S, NH_3, etc. [14]. Photosynthetic efficiency of algae is 10 times higher than that of terrestrial plants. They are efficient in growing at relative higher concentration of CO_2 compared to plants. This makes them a suitable candidate for CO_2 sequestration from the flue gas. Cultivation of algae requires less water, and they can be grown in non-fertile land. Further, their biomass can be used for food and feed supplements, for the production of biofuels such as biohydrogen, bioethanol, biodiesel, and industrially important biomolecules and biofertilizers [7, 15, 16].

Use of carbonic anhydrase (CA) is another thrust area for CO_2 sequestration. Carbon content of earth's lithosphere is 42 % w/w in the form of $CaCO_3$ and other

carbonates which indicates transformation of gaseous CO_2 into solid carbonates is a geological stable process and has potential to exploit for CO_2 sequestration [17]. One of the reactions, hydration of CO_2 to carbonic acids, is the rate limiting step in CO_2 mineralization reaction [18]. CA is the catalyst of this reaction, and the use of this enzyme has been found to enhance the rate of reaction manifold [19]. Advantages of using CA for CO_2 sequestration are eco-friendliness, cost-effectiveness, simple process, and abundance of CA enzymes among microorganisms [20].

Thus, the present study aims to summarize various biological processes such as use of plants, microalgae, cyanobacteria, and other non-photosynthetic microbes for CO_2 sequestration. It also attempts to highlight different pathways occurring in biological systems along with the use of CA for this cause.

12.2 Biological Processes of CO_2 Sequestration

12.2.1 CO_2 Sequestration by Plants

The amount of CO_2 required for the terrestrial plants and crops is very less, nearly equal to atmospheric CO_2 concentration. Limited number of reports are available, demonstrating the long-term effect of CO_2 concentration on plants because of high amount of time and space required along with variation in experimental conditions. Therefore, it is not clear that the rise in CO_2 concentration will increase the CO_2 sequestration in existing forests [21]. Most suitable CO_2 concentration for plants obtained in greenhouses was nearly three times (0.1 %) the atmospheric CO_2. An experiment conducted by Norby et al. (2005) by analyzing four Free Air Carbon dioxide Enrichment (FACE) studies on forest reported that there will be 23 % increase in the plant productivity at the predicted level of CO_2 in 2050 compared to that of the present atmospheric CO_2 concentration [22]. However, they cautioned that increment in productivity may not increase the long-term CO_2 sequestration. Most of the trees in forest (~95 % of all higher plants) are C3 type having positive photosynthetic response to elevated CO_2 concentration [21, 23, 24]. Nearly one third of the global land is covered by forest. In another report, on average, 60 % and 27 % enhancement of photosynthesis and growth, respectively, for trees have been reported [25]. Elevated CO_2 concentration decreases the stomata aperture opening and reduces the water loss. Trees planted at CO_2 spring in Italy were found growing at similar rate compared to that of normal atmospheric CO_2 concentration [26]. Respiration rate has been found to decline in elevated CO_2 environment with little improvement in the photosynthetic ability of the plants. Thus, it is impractical to use terrestrial plants and crops for CO_2 sequestration from highly rich CO_2 stream of flue gas emitted from power plants [14]. The effect of temperature, one of the associated parameters with CO_2 concentration, has also been studied. Net CO_2 removal rate by plants was found to increase with temperature [27]. Further increase in temperature from optimum resulted in decreased CO_2 sequestration

rate. Therefore, CO_2 sequestration rate by green plants varies from day to day and season to season. It was observed that in CO_2-enriched atmosphere, plants shift the optimum temperature of CO_2 sequestration to higher level. Moreover, at this condition, process was found to be less sensitive to increase in temperature [27]. Despite the fact that plants have limited applicability in CO_2 sequestration at highly CO_2-rich environment, afforestation has a number of advantages. Firstly, nearly 30–40 % of captured carbon from atmosphere gets stored in depth of soil system through plant roots [28]. Secondly, cultivated agricultural crops contribute large amount of atmospheric CO_2 removal (in the order of 190 t ha^{-1} C) into the soil system acting as perpetual sink [28]. Thirdly, the lack of proper nitrogen fertilizer for land-based plants is one of the limiting factors. Therefore, CO_2 removal rate by plants can be enhanced significantly by the use of nitrogen fertilizer [8].

12.2.1.1 Mechanism of CO_2 Fixation

Each leaf cell contains nearly 50 chloroplasts [13]. Stomata are the entry sites of CO_2 into the leaf where it interacts with the RuBisCO present in chloroplasts and gaseous CO_2 reduced into carbohydrates. Stomata of leaves have been found unresponsive to higher CO_2 concentration. RuBisCO is the key enzyme of the Calvin cycle for all the three types of the plant C3, C4, and CAM. K_m of CO_2 for the C3 plants is 15–25 μM, and carboxylase activity of RuBisCO operates below the K_m of CO_2 and is not more than 25–30 % (equilibrium concentration of CO_2 in water and air is nearly 10 μM) of its maximum capacity (24, 29). However, C3 plants do not concentrate CO_2 using carbon concentrating mechanisms (CCMs) probably because of having large amount of RuBisCO and the presence of highly active β type of CA in the thylakoid stroma (Table 12.1). RuBisCO has both oxygenase and carboxylase activity. K_m for oxygenase activity is 700 times lower than that of carboxylase activity. Therefore, increase in atmospheric CO_2 concentration is associated with not only the increase in CO_2 assimilation but also the reduction in photorespiration consuming significant amount of oxygen [24]. However, at higher CO_2 concentration, rate of photosynthesis is limited by the regeneration of the ribulose-1,5-bisphosphate (RuBP). Triose phosphate produced during Calvin cycle releases inorganic phosphate P_i which is essential for ATP synthesis and RuBP regeneration from phosphorylated intermediates. Therefore, under these circumstances, photosynthesis is called P_i or triose phosphate limited use limited [24]. Fixed CO_2 can have three fates: (a) some of the CO_2 releases back into the atmosphere through respiration; (b) some of the CO_2 transfers to the soil through root exudates, root death, litter fall, and coarse woody debris which after decomposition releases back the CO_2 into the atmosphere; and (c) some of the CO_2 gets stored in the wood [21]. Contrary to C3 plants, C4 plants have the ability to grow efficiently in stress condition such as high temperature, low water availability, high irradiance, and saline soils. C4 plants on land have thick-ended walls of bundle-sheath cells, which help them in preventing the leakage of CO_2 outside [30]. CCM activates in plants by spatial separation of CO_2 fixation by

Table 12.1 Comparative study of CCMs occurring in plants (C3 and C4), microalgae, and cyanobacteria [29, 47]

Type of photosynthesis	CCM efficiency in DIC acquisition	K_m (CO_2) of RuBisCO	HCO_3^- accumulation over ambient concentration	DIC preference	Location of CA	Carbon concentrating mechanisms	RuBisCO location
Plants (C3)	Least efficient	15–25 μM	N.A	CO_2 as substrate	Highly active CA in stroma of chloroplast	One carboxylation reaction to form C3 compound	Chloroplast stroma of most of the leaf cells
Plants (C4)	Intermediately efficient	28–60 μM	N.A	PEP carboxylase (affinity with HCO_3^- only) more abundant than C3 plants	Abundance of CA in the cytosol of mesophyll cells Absent in bundle-sheath cells	Two carboxylation reactions to form C4 compound. Carboxylation and decarboxylation reactions are spatially separated	Bundle-sheath cells
Microalgae	Less efficient than cyanobacteria	20 μM	20 fold	CO_2 is preferred. Both CO_2 and HCO_3^- inside the cytosol	Periplasmic space; cytosol, thylakoid lumen; pyrenoid	HCO_3^-/Na^+ symporter; Na^+/H^+ antiporter; NADHdh-induced transport; ATP-fueled HCO_3^- transport; CO_2 transporter	Pyrenoid inside chloroplast
Cyanobacteria	Most efficient	≥200 μM	100 fold	Preference is less specific. Only HCO_3^- inside cytosol	Carboxysomes	Direct transfer of HCO_3^-; CA-mediated CO_2 diffusion	Carboxysomes

Calvin cycle. Normally PEP carboxylase catalyzes the CO_2 fixation in the mesophyll cells. C4 acids transported to bundle-sheath cells are decomposed to gaseous CO_2 by the action of NADP-malic enzyme and other decarboxylases. Both these processes are temporarily separated in CAM plants. Detailed discussions on Calvin cycle and CCMs in C4 and CAM plants are discussed in another section.

12.2.1.2 Oceanic Fertilization

Oceanic fertilization can be defined by adopting a practice of supplementing limiting nutrients to the phytoplanktons, causing increase in photosynthetic efficiency and CO_2 removal rate. For example, micronutrient Fe was added in 10 × 10 km patches of ocean, and 30 times increase in chlorophyll concentration with increase in 100,000 kg of carbon fixation was found [4]. However, its practice should be adopted cautiously as it can negatively interfere with the marine ecosystem. In addition, sinking organic matters on decomposition may produce other stronger greenhouse gases such as methane and NO_x [31].

12.2.1.3 Forest Fertilization

The study conducted by Oren et al. (2001) revealed that the enriched CO_2 concentration (550 ppmv) had only marginal positive effect on the biomass carbon increment. However, synergistic gain was observed when plants were grown in enriched CO_2 as well as nutrient condition. The gain was threefold and twofold larger at the poor site and at the moderate site, respectively. Fertilizing at higher CO_2 concentration is more prominent than the ambient CO_2 concentration [32]. Further, application of fertilizer in paddy soils has been found favoring the growth of autotrophic microorganisms, resulting in increased CO_2 sequestration [33].

12.2.2 CO_2 Sequestration by Microalgae and Cyanobacteria

12.2.2.1 Microalgae

Photosynthesis in microalgae takes place in chloroplast. Apart from other pigments such as β-carotene and xanthophylls, they have chlorophyll a and chlorophyll b as the major pigments, which give them bright green color. Light requirement of the typical algae is lower than the higher plants [34]. Light conversion efficiency and productivity are proportional to the increase in light intensity till it attains saturation light intensity [35]. Saturation light intensity of algae such as *Chlorella* and *Scenedesmus* sp. is of order 200 μ mol m^{-2} s^{-1} [36]. Photosynthesis is coupled with release of O_2 as by-product. High dissolved oxygen (DO) in the culture (>35 mg L^{-1}) has inhibitory effect on the photosynthesis [7, 37]. In the closed

photobioreactor, DO level has been found to increase as high as 400 %, thus severally affecting the photosynthetic process [38]. Further, cations dissolved in medium also negatively affect the photosynthetic process. Algae carry net negative charge in their surface and hence are a potential adsorber of polyvalent cations present in the surrounding medium. Adsorption of polyvalent cations on the surface of algae causes morphological changes in the cell morphology or can replace/block the prosthetic metal atoms in the active site of relevant enzymes leading to photosynthesis inhibition [34].

12.2.2.2 Cyanobacteria

Cyanobacteria is a gram-negative bacteria. Compared to other gram-negative bacteria, the cell wall of cyanobacteria has thicker peptidoglycan layer [39]. Cyanobacteria lack organelles in the cell. Respiratory chain is located in thylakoid membrane and plasma membrane. Photosynthesis takes place in thylakoid located in the cytoplasm, and photosynthetic electron transport takes place in its membranes. The photosynthetic apparatus of cyanobacteria is similar to the chloroplast of green algae and plants. However, major difference is in the antenna system. Cyanobacteria lack chlorophyll b and depend primarily on chlorophyll a and specialized protein complex known as phycobilisomes for harvesting light energy. Light harvesting complex can be lipophilic as well as hydrophilic in nature. Lipophilic pigments such as chlorophyll a and carotenoids are located within the thylakoid membranes whereas hydrophilic antenna pigments are housed in phycobilisomes attached outside of thylakoid membranes. Examples of hydrophilic pigments are allophycocyanin (APC), phycocyanin (PC), phycoerythrin (PE), or phycoerythrocyanin (PEC) [40]. Similar to green algae and plants, cyanobacteria carry out oxygenic photosynthesis, releasing O_2. However, in anaerobic condition, they can also carry out anoxygenic photosynthesis using PSI. Sources of electrons are smaller organic compounds such as succinate, hydrogen sulfide, and thiosulfate instead of water [41]. Anoxygenic photosynthesis results in generation of ATP by cyclic photophosphorylation around the PSI.

12.2.2.3 Photosynthesis: Key for CO_2 Sequestration

Photosynthesis, the key biological process occurring in plants and a wide number of microorganisms such as algae and cyanobacteria, helps in mitigating atmospheric CO_2. Photosynthesis occurs in the chloroplasts of plants and algae. Chloroplasts contain the thylakoid vesicles arranged in stacks, containing photosynthetic apparatus. Contrary to plants and algae, prokaryotic cyanobacteria do not have fixed organelles for keeping photosynthetic apparatus. They are located in cytoplasm as free and isolated photosynthetic lamellae [42]. Biological system uses photosynthesis for harnessing solar energy for the preparation of food with the help of CO_2 and water. Photosynthesis consists of two distinct processes: light-dependent process and light-independent

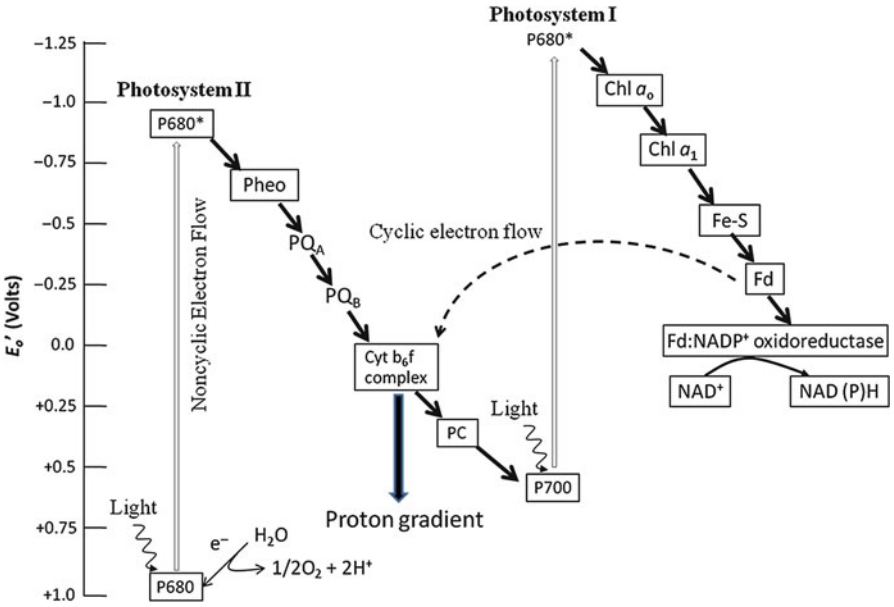

Fig. 12.1 Schematic diagram of Z scheme of photosynthetic process involving PSII and PSI. *Solid and dashed lines* show the noncyclic and cyclic flow of electrons. Abbreviation: PQ_A plastoquinone, PQ_B second quinine, *Chl* a_o chlorophyll a, *Chl* a_1 phylloquinone, *PC* plastocyanin [53]

process. In light-dependent process, they conserve light energy in the form of ATP and NADPH with the help of chlorophyll and light harvesting complex. Light-independent process utilizes ATP and NADPH for the fixation of CO_2 into triose phosphates, starch, sucrose, and other derived products. Photosynthetic apparatus of plants, algae, and cyanobacteria are similar in nature. Photosynthetic apparatus are found in the thylakoid membranes consisting of protein complex, electron carriers, and lipid molecules. The electron carriers are arranged in the shape of 90° tilted English alphabet Z. Two reaction centers, PSII and PSI, help in exciting the electrons by absorbing the light of 680 nm and 700 nm, respectively (Fig. 12.1). Two reaction centers are connected with series of electron carriers such as plastoquinone, cytochrome b_6f complex, and plastocyanine arranged in fixed increasing order of redox potential. Electron carriers between two centers help in transferring excited electrons at PSII to pass to PSI smoothly. Electrons at PSII come from breaking of water molecules into oxygen molecules, protons, and electrons. Two moles of water dissociates into four moles of protons and electrons and one mole of oxygen molecule (Eq. 12.1) [42].

$$2H_2O \rightarrow 4H^+ + 4e^- + O_2 \tag{12.1}$$

Protons accumulate into the lumen of thylakoid membranes, generating proton gradient across the membrane. Concentration gradient drives protons outside thylakoid membrane through ATP synthase producing ATP. Thus, ATP synthase

produces not only energy for the cell but also avails protons for the reduction of $NADP^+$ to produce NADPH. At PSII, light energy causes charge separation between P680 and pheophytin, creating P680+/Pheo−. Pheophytin transfers the electrons to a permanently bounded molecule (QA) to photosystem II. At QA site plastoquinone receives single electron instead of two. QB and QA sites differ from each other as the former requires two electrons to reduce instead of one, which is the case of the latter, causing two turnovers for the complete reduction of plastoquinone at QB. Due to close proximity of QB site, protons added to plastoquinone during its reduction come from the outside aqueous phase of the membrane [13]. At photosystem I, most of the antenna chlorophyll molecules are attached to the reaction center proteins [13]. Plastoquinone then transfers their electrons to next electron carrier cytochrome b_6f complex with simultaneous release of protons into the lumen. Cytochrome b_6f complex is attached with membrane-bound protein complex. Plastocyanin (PC) acts as a last protein carrier delivering electrons to PSI. PSI again excites the electrons received from electron carriers. Here, excited electrons are used to reduce ferredoxin (Fd), a protein loosely attached with thylakoid membranes from outside. Reduced Fd interacts with ferredoxin $NADP^+$ reductase (FNR) and the latter catalyzes the reduction of $NADP^+$ to NADPH as shown in (Eq. 12.2).

$$2Fd_{red} + 2H^+ + NADP^+ \rightarrow 2Fd_{ox} + NAD(P)H + H^+ \quad (12.2)$$

Each of the photosystem contributes one photon to the transfer of one electron. Therefore, two photons are required for the transfer of one electron along the electron carriers to the $NADP^+$. Two moles of water and eight photons are required to produce two moles of NAD(P)H as shown in (Eq. 12.3).

$$2H_2O + 2\ NADP^+ + 8\ photons \rightarrow O_2 + 2NAD(P)H + 2H^+ \quad (12.3)$$

Reduction of one molecule of CO_2 requires two moles of NAD(P)H. Energy content in photon is 480 KJ/mol, whereas energy gathered after reduction of one reduced CO_2 molecule is equivalent to 1,400 KJ. Therefore, theoretical maximum efficiency of the process is 36.4 %.

12.2.2.4 Carbon Concentrating Mechanisms (CCMs)

Cyanobacteria and algae behave like C3 plants but have much less affinity for CO_2 [29]. However, they develop CCMs similar to C4 and CAM plants, causing better photosynthetic efficiency compared to C3 plants [30]. Their RuBisCO have oxygenase as well as carboxylase activities, depending upon the concentration of local CO_2 in the compartment housing RuBisCO. Carboxylase activity of RuBisCO activates under high CO_2 pressure, whereas low concentration of CO_2 forces it to undergo oxygenase activity. Oxygenase reaction has many disadvantages. Firstly, glycolate 2-phosphate is the end product of oxygenase activity of RuBisCO

(Eq. 12.4). It has no use to algal cells; therefore, significant amount of cellular energy is wasted by consuming it. Secondly, it releases previously fixed CO_2, during the carboxylase activity of RuBisCO, which causes the loss of nearly 50 % of algal biomass [43]. Metabolism of glycolate 2-phosphate produces glycine, which on condensing with another glycine molecule produces serine, resulting in the loss of CO_2 [44]. Thirdly, loss of fixed carbon further negatively interferes with the regeneration of RuBP, required for the smooth functioning of the cycle.

$$\text{Ribulose 1,5 bisphosphate} + O_2 \rightarrow \text{glycerate 3-phosphate} + \text{glycolate 2-phosphate} \quad (12.4)$$

Affinity constant (Km) of microalgae and cyanobacteria for CO_2 is high compared to C3 plants, indicating low affinity of RuBisCO for CO_2 (Table 12.1). Under normal atmospheric air, RuBisCO is only half-saturated with CO_2 [7, 29]. The diffusion of CO_2 in aqueous solution is 10,000 times slower than the CO_2 diffusion in air [30]. Poor diffusion of atmospheric CO_2 in aqueous solution and low affinity of CO_2 by algae, cyanobacteria, and some chemoautotrophic bacteria pose a limitation to the carboxylase activity of RuBisCO [45]. Therefore, for maintaining this, it is necessary to saturate the compartment containing RuBisCO with CO_2. Fortunately, algae have carbon concentrating mechanisms (CCMs), which help them to increase the local CO_2 even when there is lower CO_2 concentration outside the algal cells [46]. Contrary to plants, algae and cyanobacteria have single-cell CO_2 concentrating mechanisms. However, they have internal compartments within the chloroplasts (pyrenoid in algae and carboxysome in cyanobacteria). Increase in concentration of CO_2 at close proximity of RuBisCO has many advantages. Firstly, it activates RuBisCO. Secondly, it increases carboxylase activity of RuBisCO, and, thirdly, dissolved inorganic carbon (DIC) influx may help in maintaining internal pH and dissipating excess light energy [47]. CCMs can be divided broadly into two categories: biochemical and biophysical CO_2 pumps. CCMs help in accumulation of large number of intracellular inorganic carbon inside the RuBisCO compartment. However, inorganic carbons are not available for fixation by RuBisCO. They must be converted back into gaseous CO_2 for the action of RuBisCO. CA is a vital enzyme, which overexpresses under low external CO_2 environment. CA acts as a catalyst in the interconversion of inorganic carbon back to gaseous CO_2.

Biochemical CO_2 Pump

C4 Mechanism – Biochemical pumps are mostly found in the terrestrial plants. However, some phytoplanktons and macroalgae also have evidence of biochemical pumps. C4 mechanisms have also been found in macroalgae such as *Udotea flabellum* and *Thalassiosira weissflogii* [43]. The role of C4 mechanism is to biochemically transport the DIC from the site excessive in it to the site where RuBisCO is active [43]. As the name indicates, CO_2 is stored in a four-carbon

compound, oxaloacetate. Phosphoenolpyruvate (PEP) is the carrier molecule, which combines with HCO_3^- using PEP carboxylase to form oxaloacetate. PEP carboxylase utilizes bicarbonates rather than CO_2; therefore, the gaseous CO_2 entering into the mesophyll cell must be rapidly converted to bicarbonate with the help of carbonic anhydrase [48]. At physiological CO_2 levels and pH, Km (HCO_3^-) of PEP carboxylase and HCO_3^- concentration in the cytoplasm of mesophyll cells were estimated to be about 8 μM and 50 μM, respectively. Therefore, unlike RuBisCO, PEP carboxylase is always saturated with HCO_3^- at ambient CO_2 concentration. Therefore, CA is mostly confined to mesophyll cell in the C4 plants compared to chloroplast in C3 plants [49]. Oxaloacetate further readily reduced to malate by the action of NADP-malate dehydrogenase. In plants, malate is transported to bundle-sheath cell where it is decarboxylated by the action of NADP-malic enzyme. At the site of RuBisCO, malate can be decarboxylated to pyruvate and releases gaseous CO_2 for the action of RuBisCO enzyme in Calvin cycle.

CAM Mechanism – CAM plants are usually found in desert area. In cool night, guard cells open to receive CO_2, while in daytime, it is closed to prevent water loss. This mechanism is also proposed in brown macroalgae for the assimilation of photosynthetic inorganic carbon [43]. PEP comes from the starch accumulated during daytime using Calvin cycle. Enzymes and compounds taking part in CAM mechanism are similar to C4 mechanism. However, end storage compound malate is temporarily separated over time rather than spatially as in C4 plants [43]. PEP carboxylase catalyzes the reaction of PEP and HCO_3^- to form oxaloacetate. NADP-malic dehydrogenase reduces oxaloacetate to malate, which is transported to vacuole having low pH at night. In daytime, whole pathways get reversed back and malic acid transported back to cytosol for the decarboxylation reaction, flooding cytosol with CO_2. Guard cell is closed during the daytime, preventing CO_2 diffusion outside the cell. It is to be noted that PEP carboxylase activity is also under control to prevent wasteful synthesis of C4 compounds during daytime.

Biophysical CO_2 Pump

CCMs in Cyanobacteria

Being simple in structure, algae and cyanobacteria cannot stop the diffusion of CO_2 [30]. Carboxysome is the key for the success of CCMs in cyanobacteria. It acts as a storehouse for CO_2 having limited permeability for CO_2 leakage. The ultimate target of CCMs is to transport DIC to the storehouse, carboxysome. Along with cyanobacteria, carboxysomes are also found in some chemoautotrophic bacteria growing in CO_2 concentration lower than the K_m of RuBisCO [45]. Carboxysomes have mainly icosahedral structures with the diameter of 100–200 nm. The number of carboxysomes present in per cell of cyanobacteria varies from 5 to 20 depending upon the growth conditions and species to species [45].

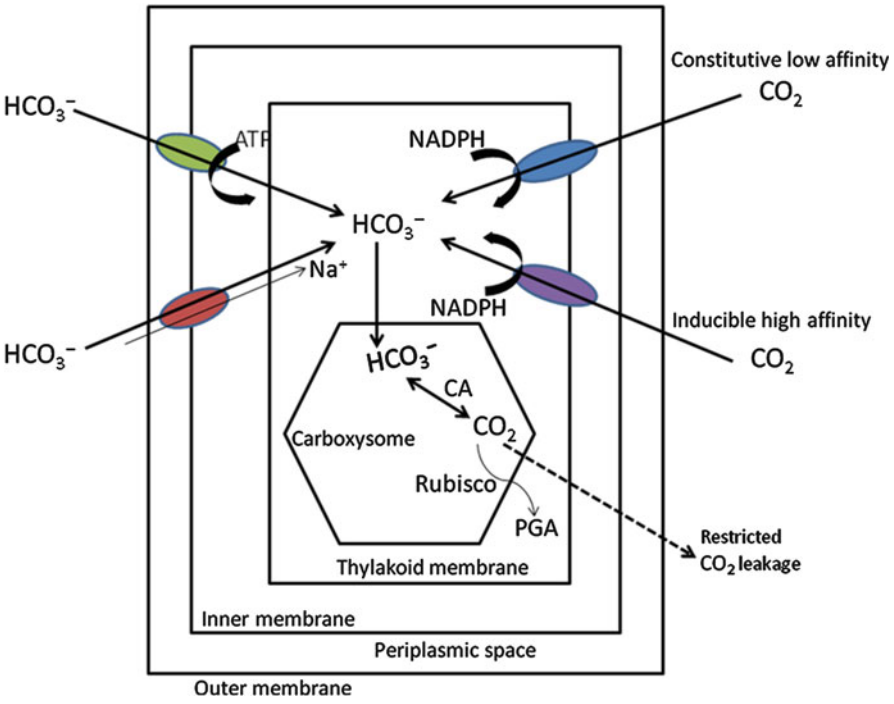

Fig. 12.2 Schematic diagram of CCMs occurring in cyanobacteria [29, 43, 49]

Most of algae and cyanobacteria examined so far have been found to have transporter for both CO_2 and HCO_3^-. However, few algae can also assimilate either CO_2 or HCO_3^-. CCMs are extensively studied in cyanobacteria compared to microalgae. Active transport occurs across the membrane having low permeability to DIC. In cyanobacteria, transport of CO_2 or HCO_3^- occurs via plasmalemma or thylakoid membranes. All the DIC removed from the outside by various DIC transporters are delivered only in the form of HCO_3^- into the cytosol of cell [45]. Bicarbonate concentrating ability of cyanobacteria is nearly five times greater than the microalgae, causing higher photosynthetic and CO_2 consumption efficiency of the former [30]. Outside, DIC including CO_2 penetrate the plasma membrane and reach the closest membrane of the chloroplast with the help of various transporter proteins. At least three mechanisms of active transport have been proposed in cyanobacteria (Fig. 12.2) [29, 49, 50]: (1) HCO_3^- can be transported to cytosol with the help of ABC-type transporter utilizing energy in the form of ATP, which is a high-affinity, low-CO_2-induced, and sodium-independent mode of HCO_3^- assimilation; (2) HCO_3^- transport into cytosol may also be the result of HCO_3^-/Na^+ symporter or the regulation of pH through Na^+/H^+ antiporter; and (3) for the active transport of CO_2, NADH dehydrogenase may have constitutively low or inducible high affinity for CO_2. In either case, CO_2 is first converted to HCO_3^- by NADHdh at plasmalemma of cyanobacteria and then

transported into the cytosol. Intracellular pH of cyanobacteria is near to 8, causing HCO_3^- as predominant species inside the cytoplasm (equilibrium ratio of HCO_3^- and CO_2 is near to 100). HCO_3^- is the charged ion and therefore cannot escape the lipid bilayer of the cyanobacteria [45]. HCO_3^- then diffuses into carboxysome where it is acted upon by CA enzyme to flood the compartment with gaseous CO_2 for the action of RuBisCO of Calvin cycle [43]. Remaining amount of CO_2 in carboxysome is diffused outward [47]. In addition, it has also been proposed to have direct access of HCO_3^- to cytoplasm of cyanobacteria. Rate of direct transport of HCO_3^- across plasma membrane is less significant compared to its active transport [51]. In yet another mechanism, compartment containing high concentration of HCO_3^- is acidified using proton pump and flooding with CO_2 (Eq. 12.5). In acidic compartment, HCO_3^- decomposes into CO_2 by the action of CA or proton-driven catalysis of HCO_3^- to CO_2. The high level of CO_2 then diffuses into the more alkaline compartment housing RuBisCO for the action of RuBisCO [43].

$$\text{Alkaline } (HCO_3^-) \rightarrow \text{ Acidic } (HCO_3^- \rightarrow CO_2) \rightarrow \text{ Alkaline } (CO_2) \quad (12.5)$$

CCMs in Algae

Compared to cyanobacteria, CCMs in microalgae are less understood because of more compartments inside the cell and very diverse group of microorganisms [29]. Microalgae composed of one or few cells do not have impermeable cell walls like plants to prevent leakage of CO_2. The challenging task is to prevent the leakage of concentrated CO_2 while allowing other nutrients to come in. The efficiency of acquisition of DIC depends on environmental conditions. For example, acquisition of DIC in low atmospheric CO_2 was found higher compared to high atmospheric CO_2 condition. However, the amount of RuBisCO did not change during adaptation from low to high CO_2 condition. This indicated the existence of transport system for the uptake of DIC into the cells. Cyanobacteria and microalgae can accumulate nearly 100- and 20-fold increase in HCO_3^- within the cells, respectively, over ambient CO_2 level [29]. DIC accumulation in algae is generally lower than cyanobacteria probably due to higher affinity of RuBisCO present in the former for CO_2. CCMs in microalgae have been hypothesized similar in nature as cyanobacteria by most of the researchers. Similar to carboxysome of cyanobacteria, microalgae also have a compartment (pyrenoid) in chloroplast densely packed with RuBisCO. Accumulation of charged HCO_3^- ions lessens the chance of leakage. Freshwater and marine green algae are capable of utilizing HCO_3^-. However, in most of the microalgae, CO_2 is main form of carbon entering into the cell and HCO_3^- in chloroplast. In *Chlamydomonas reinhardtii*, active transport of CO_2 has been found to have preference over HCO_3^- [51]. CO_2 uptake in whole cell is due to diffusion, while through the chloroplast, it is mediated by transfer [47]. A range of CAs participate in each of the compartment to maintain the equilibrium between CO_2 and HCO_3^- (Fig. 12.3). Eventually DIC entering into the pyrenoid is in the form of HCO_3^-, which needs to be converted back to CO_2 to enrich RuBisCO compartment for the carboxylase reaction. Cell membrane of pyrenoid does not

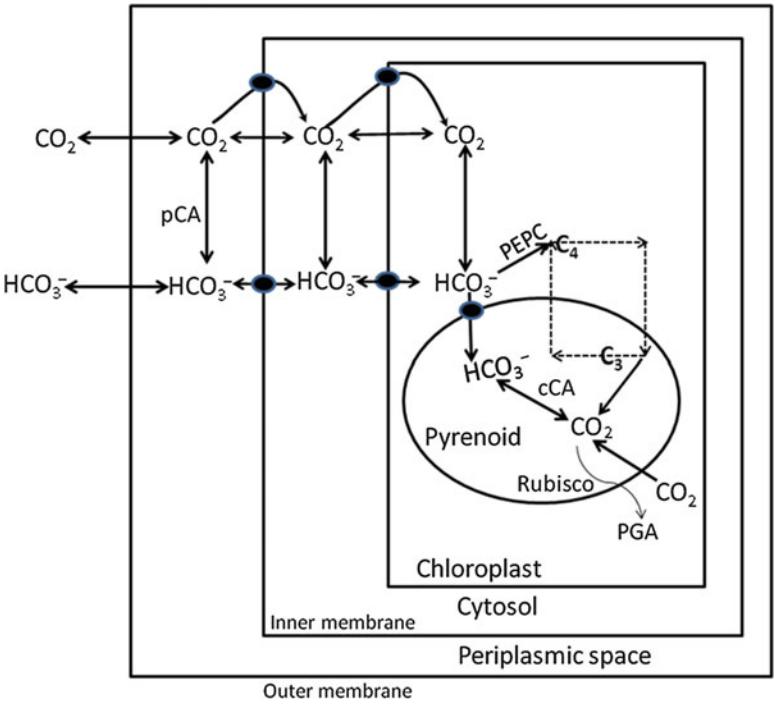

Fig. 12.3 Schematic diagram of CCMs occurring in green algae [29, 43, 49]

allow CO_2 to leak out, allowing sufficient time for RuBisCO to use CO_2 in the Calvin cycle. CA is an important enzyme for the successful operation of CCM. CA in microalgae is of different type and located in different places inside the cell. It has been found in periplasmic space, cytosol, as well as inside the pyrenoid. Direct uptake of HCO_3^- and CO_2 diffusion facilitated by periplasmic CA across the plasma membrane have been proposed [29]. Periplasmic CA probably helps in the diffusion of CO_2 and supply of HCO_3^- into the cytosol across the plasma membrane. However, in every case examined so far, electrochemical potential gradient for HCO_3^- was outward. By examining the HCO_3^- transport in *Ulva*, HCO_3^- uptake in microalgae has been proposed to occur through the HCO_3^-/OH^- antiport [47].

12.2.3 Bacteria

The non-photosynthetic bacteria play an important role in global carbon cycle. Advantages of these microorganisms are their ability to adapt to and survive extreme conditions of the environment. However, consumption of large amount of H_2 as electron donor limits their practical application [52]. Enzymes involved in

the CO_2 fixation pathway are sensitive to oxygen; therefore, they grow best in anaerobic environment [52]. Their ability to sequester CO_2 under anaerobic environment can be helpful for their application in O_2-deficient but CO_2-rich environment such as under the soil and flue gas [52].

Photosystem of some of the bacteria looks like either PSI or PSII. Lack of PSII deprives bacteria to use electrons of water and evolve oxygen as by-product of photosynthesis. Some simple inorganic or organic molecules substitute the water for the electrons needed to reduce CO_2 into useful simple sugar. They have bacteriochlorophyll, a family of molecules similar to chlorophyll, but absorb light in the range of 700–1,100 nm. Similar to oxygenic photosynthesis, electron transfer results in the generation of proton gradient across the thylakoid membrane. Outward protein gradient drives the proton out through ATP synthase, causing synthesis of ATP. Energy for CO_2 reduction comes from ATP and NADH. Electron carriers are quinone such as ubiquinone, menaquinone, and the cytochrome bc complex, which work similarly to cytochrome b_6f complex present in the oxygenic photosynthetic system [13].

Green gliding bacteria such as *Chloroflexus aurantiacus* harvest light using chlorosomes similar to green sulfur bacteria. CO_2 fixation in these microorganisms does not involve Calvin or Krebs cycle. They usually do photosynthesis under anaerobic condition. Green and purple bacterial membranes are in the form of lamellae, vesicles, or specialized structures (chlorosomes) where light reaction takes place. Sulfur purple bacteria such as *Chromatium vinosum* fix CO_2 for their survival using Calvin cycle.

12.2.3.1 Purple Bacteria

Photosynthetic machinery of purple bacteria such as *Rhodospirillum rubrum, Rhodopseudomonas viridis*, and *Rhodobacter sphaeroides* is of pheophytin-quinone type. Pheophytin is similar to chlorophyll but lacks central Mg^{2+} ions. Purple bacteria have single reaction center called P870. Electrons at the reaction center get excited, absorbing light of 870 nm. Excited electrons pass to cytochrome bc1 complex through pheophytin and quinine sequentially [53, 54]. Cytochrome bc1 complex is the hub that pumps the protons to generate proton gradient and electrons back to reaction center via cytochrome c_2 (Fig. 12.4a). Light-driven cyclic flow of electrons enables to produce ATP using ATP synthase. Purple bacteria are of two types: non-sulfur purple, such as *Rhodopseudomonas viridis* and *Rhodobacter sphaeroides*, and sulfur purple bacteria, such as *Chromatium vinosum*. Electron source for non-sulfur bacteria is organic compounds such as malate and succinate, whereas sulfur purple bacteria extract electrons from inorganic sulfur compounds such as hydrogen sulfide. CO_2 is fixed in purple bacteria using Calvin cycle.

12.2.3.2 Green Sulfur Bacteria

Reaction center of green sulfur bacteria such as *Chlorobium vibrioforme* and *Chlorobium thiosulfatophilum* is similar to PSI of oxygenic photosynthesis.

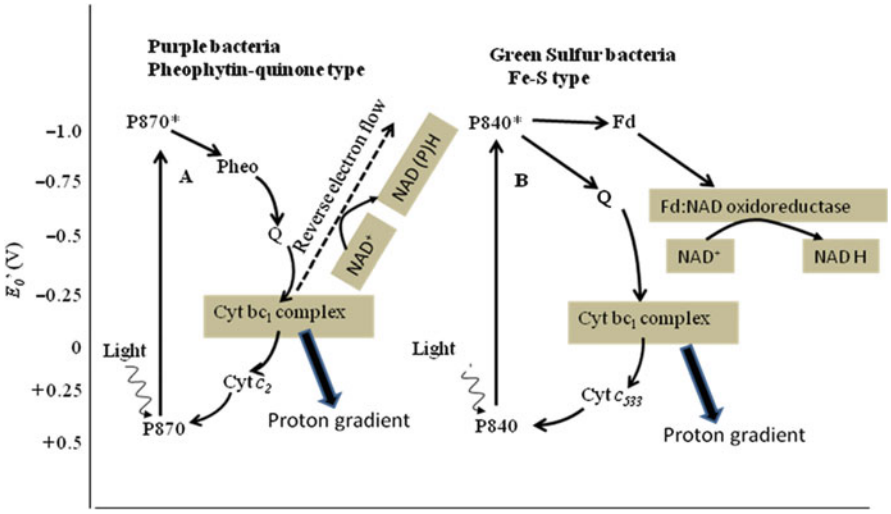

Fig. 12.4 Schematic diagram of photosynthetic process involving only PSI in (**a**) purple bacteria and (**b**) green sulfur bacteria. *Solid and dashed lines* show the noncyclic and cyclic flow of electrons. Abbreviation: *Q* quinine [53]

Similar to phycobilisomes of cyanobacteria, the antenna system of the green sulfur bacteria such as bacteriochlorophyll and carotenoids is contained in complexes known as chlorosomes attached to the surface of the photosynthetic membrane through baseplate containing antenna bacteriochlorophyll a [13]. Reaction center involved in green sulfur bacteria is called Fe–S type. Therefore, green sulfur bacteria are not dependent on the reverse electron flow for the carbon reduction as the reduced ferredoxin uses its electrons to reduce $NAD^+/NADP^+$ using ferredoxin–NAD(P)+ oxidoreductase enzyme. At reaction center, electrons get excited by absorbing light intensity of 840 nm. Excited electrons can follow two pathways: one cyclic flow of electrons back to the reaction center via Q, Cyt bc_1 complex, and Cyt c_{553}, and another noncyclic flow of electrons through iron–sulfur protein ferredoxin (Fd) to reduce NAD^+ to NADPH using ferredoxin/NAD reductase (Fig. 12.4b) [53, 54]. Similar to purple bacteria, protons are pumped by the cytochrome bc1 complex to generate ATP. Electrons at reaction center are replaced by the oxidation of H_2S to elemental S^o and then to SO_4^{2-}. Electron carriers in green sulfur bacteria are much better placed according to their electronegativity than the purple bacteria which ensure reduction of NAD without the need of reverse electron flow. Green sulfur bacteria reduce free CO_2 by reversing original tricarboxylic acid cycle (Krebs cycle) with the input of energy. Thus, green sulfur bacteria can fix CO_2 even in the absence of RuBisCO. Green sulfur bacteria extract both electrons and hydrogen from sulfur compounds [13].

12.3 CO_2 Sequestration Pathways

12.3.1 Calvin Cycle

CO_2 is fixed into carbohydrate in light-independent stage using Calvin–Benson cycle. Proteins participating in CO_2 fixation have been found outside the thylakoid membrane in aqueous phase [13]. CO_2 fixation reaction is catalyzed by the carboxylase activity of ribulose-1,5-bisphosphate carboxylase/oxygenase (RuBisCO) [55]. Calvin cycle can be divided into carboxylation, reduction, and regeneration reaction (Fig. 12.5). In carboxylation reaction, three molecules of CO_2 combine with three molecules of ribulose-1,5-bisphosphate (5 C) using carboxylase activity of RuBisCO enzyme to form six molecules of glycerate 3-phosphate (Eq. 12.6). Glycerate 3-phosphate further reduces to glyceraldehyde 3-phosphate in the reduction step. Reduction reaction is followed by regeneration reaction where ribulose-1,5-bisphosphate, the starting material of Calvin cycle, is regenerated using five molecules of glyceraldehyde 3-phosphate, while the remaining one molecule of glyceraldehyde 3-phosphate is used for the synthesizing biosynthetic material [56].

$$\text{Ribulose 1,5 bisphosphate} + CO_2 + H_2O \rightarrow 2\,\text{glyceraldehyde 3-phosphate} \quad (12.6)$$

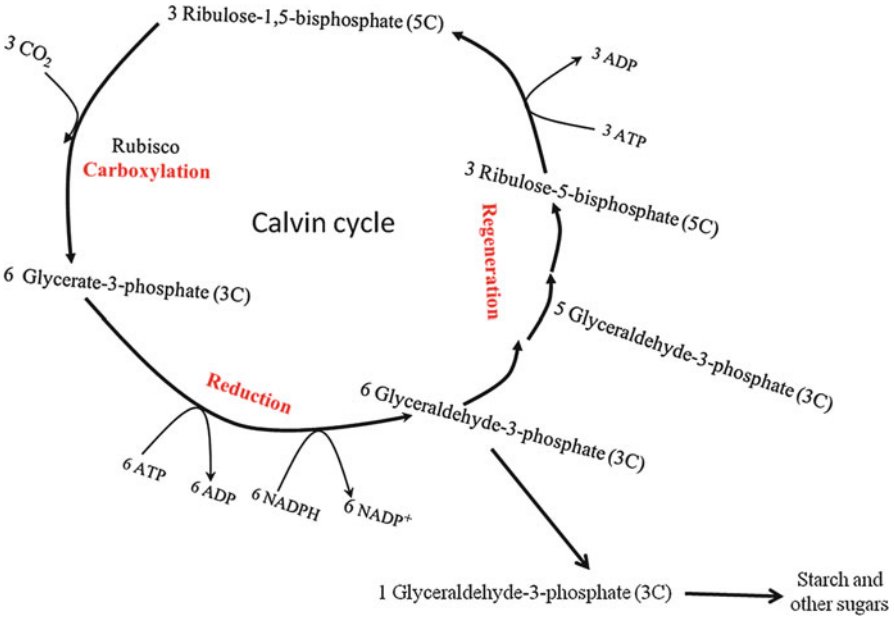

Fig. 12.5 Schematic diagram of Calvin cycle

Standard free energy for the synthesis of one mole of glucose is equal to 2,870 KJ [13]. Photosynthetic process is further generalized by Van Niel (Eq. 12.7).

$$CO_2 + 2H_2A + \text{light} \rightarrow (CH_2O)_n + 2A + H_2O \tag{12.7}$$

where A is O and S for oxygenic photosynthesis and anoxygenic photosynthesis (taking H_2S as electron donor), respectively. Later, it was demonstrated by Van Niel that molecular oxygen comes from dissociation of water rather than CO_2. The end product of Calvin cycle, glyceraldehyde 3-phosphate, is used in synthesizing cellular biosynthetic material for immediate energy source and sucrose that is transported to cytosol for storage as starch in chloroplast of green algae and glycogen in cyanobacteria [57]. Considering acetyl-CoA as the end product, seven molecules of ATP and four molecules of NAD(P)H are required to reduce two molecules of CO_2. Thus, Calvin cycle is the most energy intensive pathway for CO_2 sequestration [58].

$$2\,CO_2 + 7\,ATP + 4\,NAD(P)H + HS\text{-}CoA \rightarrow \text{Acetyl-CoA} + 7\,ADP + 4\,NAD\,(P)^+ \tag{12.8}$$

12.3.2 Wood–Ljungdahl (WL) or Reductive Acetyl-CoA Pathway

Wood–Ljungdahl (WL) or reductive acetyl-CoA pathway is a bidirectional pathway, which is predominant primarily in strict anaerobic bacteria and archaea of phyla Firmicutes and Euryarchaeota, respectively [58]. This pathway is used for chemoautotrophic carbon fixation in acetogens such as *Clostridium thermoaceticum* and *Acetobacterium woodii* and methanogens such as *Methanobacterium thermoautotrophicum* and most autotrophic sulfate reducers such as *Desulfobacterium autotrophicum*. Wood–Ljungdahl (WL) pathway was found to be the most efficient non-photosynthetic pathway based on the most expensive substrate (i.e., H_2 or electrons), for the production of acetate and ethanol [58]. Reductive acetyl-CoA pathway uses only four moles of H_2 to form one mole of acetate. Two molecules of CO_2 directly combine to form one molecule of acetate. This pathway is different from other six known CO_2 fixation pathways as it does not undergo in cyclic manner. In addition to the use of Fd for reduction reaction, carbon monoxide dehydrogenase and acetyl-CoA synthase are the main enzymes involved in this pathway. These enzymes are very sensitive to oxygen. It has both carbonyl as well as methyl components (Fig. 12.6). Out of two molecules of CO_2, one is reduced to carbonyl group (C=O) catalyzed by CO dehydrogenase, and the other CO_2 is captured on special tetrahydrofolate cofactor and reduced to a methyl group. Carbonyl group bonded with enzyme is combined with the methyl group to form acetyl-CoA by enzyme acetyl-CoA synthase complex. The reducing equivalents for the pathway are obtained by oxidation of molecular hydrogen during autotrophic growth or NADH and reduced ferredoxin during heterotrophic growth [59]. For the formation of one molecule of acetyl-CoA using two molecules

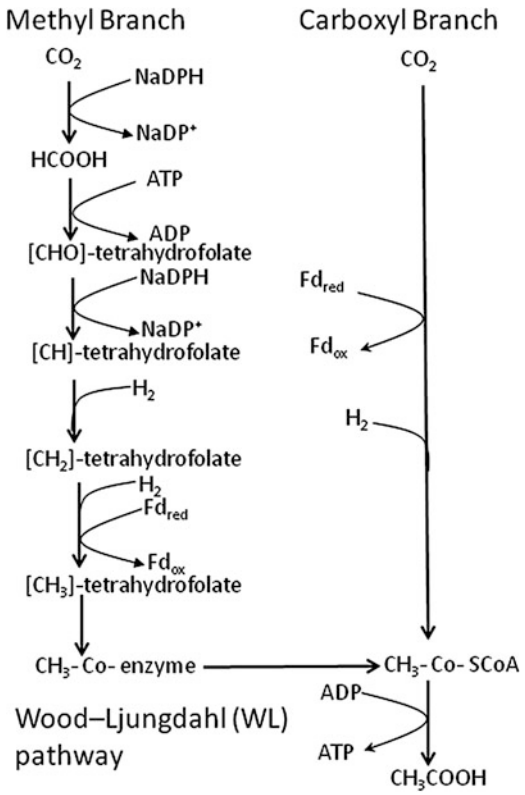

Fig. 12.6 Schematic diagram of Wood–Ljungdahl (WL) or reductive acetyl-CoA pathway. (Reprinted from Ref. [60]. Copyright 2011, with permission from Elsevier)

of CO_2, WL pathways need one molecule of ATP and four molecules of NAD(P)H (Eq. 12.9) [58]. Among the four pathways discussed above, WL pathway is most efficient based on CO_2 sequestration per ATP consumed. Moreover, ATP consumed in WL pathway is even less than one, as some of the energy is conserved in the membrane gradient in the form of ATP. rTCA cycle comes next to WL pathway in terms of energy efficiency. Both the pathways are found in highly reduced environments in which carbon reduction is more favorable [58].

$$2\,CO_2 + 1\,ATP + 4\,NAD(P)H + HS\text{-}CoA \rightarrow \text{Acetyl-CoA} + 1\,ADP + 4\,NAD(P)^+ \quad (12.9)$$

12.3.3 Reductive Tricarboxylic Acid Cycle (rTCA) or Reverse Citric Acid Cycle

Reductive tricarboxylic acid cycle (rTCA) has been found in bacteria under anaerobic or microaerobic conditions. Bacteria dwelling under these conditions are green sulfur bacteria such as *Chlorobium* sp. (*Chlorobium limicola, Chlorobium*

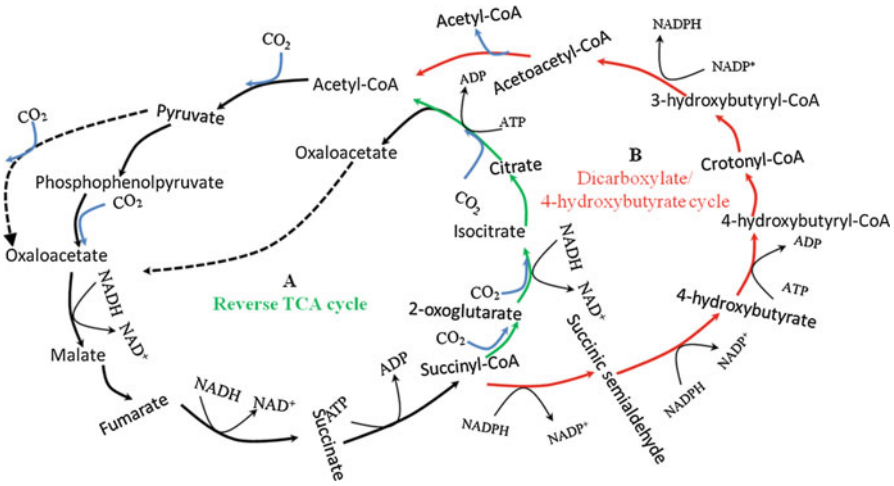

Fig. 12.7 Schematic diagram of (**a**) reductive tricarboxylic acid cycle (rTCA) or reverse citric acid cycle shown in *green arrow* and (**b**) dicarboxylate/4-hydroxybutyrate cycle shown in *red arrow*. *Black arrows* showing reaction pathways are common to both of them (Reprinted from Ref. [60]. Copyright 2011, with permission from Elsevier)

thiosulfatophilum, etc.), sulfur-reducing bacteria (*Desulfobacter*), knallgas bacteria or hydrogen-oxidizing bacteria (*Hydrogenobacter, Aquifex*), and archaea (*Thermoproteus*). They utilize this cycle to fix atmospheric CO_2 through anoxygenic photosynthesis [59]. Reductive citric acid cycle is oxidative citric acid cycle running in reverse direction [61]. In TCA cycle, one molecule of acetyl-CoA breaks down to form two molecules of CO_2 and energy. However, in reverse TCA cycle, two molecules of CO_2 are used to synthesize one molecule of acetyl-CoA using 2 ATP and H^+ from NADH and NADPH (Fig. 12.7a). Two carbon fixing enzymes, pyruvate synthase (pyruvate:ferredoxin oxidoreductase) and 2-oxoglutarate synthase (2-oxoglutarate:ferredoxin oxidoreductase), are the key enzymes of rTCA cycle and were found to be dependent on Fd [61, 62]. Two reactions involving ferredoxin (Fd) significantly help in reversal of some of the reactions, which are otherwise nonreversible in nature. Another enzyme citrate lyase was discovered which is dependent on ATP [63]. ATP-citrate lyase cleaves citrate, a six-carbon compound, into oxaloacetate, a four-carbon compound, and acetyl-CoA. These three enzymes work together to make energetically unfavorable reverse reactions possible. One molecule of succinyl-CoA combines with one molecule of CO_2 to form one molecule of 2-oxoglutarate using 2-oxoglutarate synthase. 2-Oxoglutarate further takes one molecule of CO_2 to form isocitrate using isocitrate dehydrogenase (IDH). Aconitase converts isocitrate to citrate, which is acted upon by citrate lyase to form oxaloacetate and acetyl-CoA. Acetyl-CoA combines with another molecule of CO_2 to form pyruvate using pyruvate synthase. It is followed by synthesis of PEP which combines with another molecule of CO_2 to regenerate oxaloacetate or other intermediates of the cycle in an

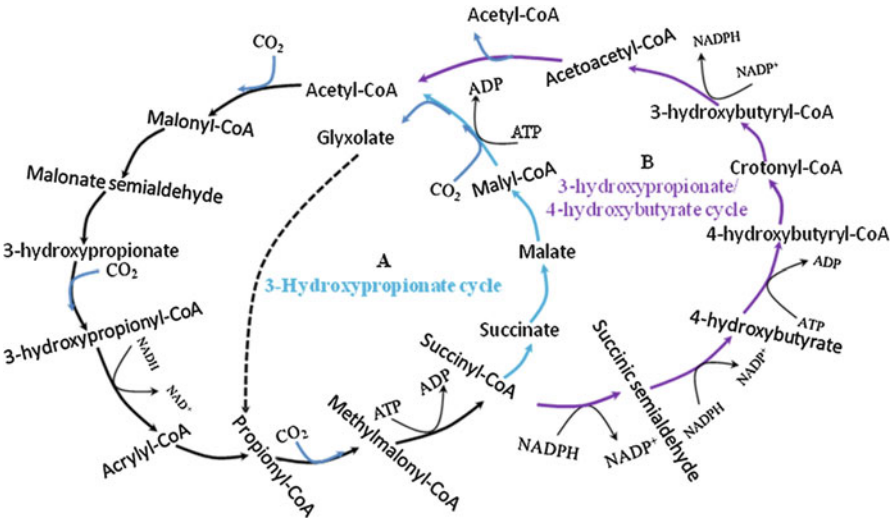

Fig. 12.8 Schematic diagram of (**a**) 3-hydroxypropionate cycle shown in *light blue arrow*, (**b**) 3-hydroxypropionate/4-hydroxybutyrate cycle shown in *purple arrow*. *Black arrows* showing reaction pathways are common to both of them (Reprinted from Ref. [60]. Copyright 2011, with permission from Elsevier)

anaplerotic manner [61]. Shiba et al. (1985) reported direct conversion of pyruvate into oxaloacetate in *H. thermophilus* by an enzyme pyruvate carboxylase [64]. In one complete cycle, four molecules of CO_2 are fixed to generate one molecule of oxaloacetate, which itself is an intermediate of the cycle. It requires two molecules of CO_2, 2 ATP, and 4 NAD(P)H for the formation of one molecule of acetyl-CoA as the end product as shown in Eq. (12.10) [58].

$$2\,CO_2 + 2\,ATP + 4\,NAD(P)H + HS\text{-}CoA \rightarrow Acetyl\text{-}CoA + 2\,ADP + 4\,NAD(P)^+ \quad (12.10)$$

12.3.4 3-Hydroxypropionate Cycle

CO_2 fixation in phototrophic green non-sulfur bacteria takes place using 3-hydroxypropionate pathway unique to eubacterium *Chloroflexus aurantiacus* and some chemotrophic archaebacteria such as *Sulfolobus metallicus, Ignicoccus hospitalis, Acidianus brierleyi*, and *Acidianus infernus* [60, 65, 66]. Enzymes participating in this pathway are not sensitive to oxygen [60, 67]. Acetyl-CoA is the starting precursor of 3-hydroxypropionate cycle. It combines with HCO_3^- to form malonyl-CoA with the help of ATP-dependent acetyl-CoA carboxylase (Fig. 12.8a). Acetyl-CoA carboxylase is also an essential enzyme for the synthesis of fatty acid. It is followed by the conversion of malonyl-CoA to

3-hydroxypropionate by malonyl-CoA reductase in an NADPH-dependent reaction. Malonyl-CoA reductase is a bifunctional enzyme, which reduces malonyl-CoA to 3-hydroxypropionate via malonate-semialdehyde as an intermediate using its aldehyde dehydrogenase and alcohol dehydrogenase domain. Reductive conversion of 3-hydroxypropionate to propionyl-CoA is catalyzed by propionyl-CoA synthase. Propionyl-CoA synthase is a trifunctional enzyme and formally requires three enzymatic reactions. In the first step, activation to 3-hydroxypropionyl-CoA is catalyzed by CoA ligase, which is followed by dehydration of 3-hydroxypropionyl-CoA to acrylyl-CoA by an enoyl-CoA hydratase. Finally, acrylyl-CoA is reduced to propionyl-CoA by an enoyl-CoA reductase using NADPH [65, 68, 69]. Propionyl-CoA undergoes carboxylation, catalyzed by ATP-dependent propionyl-CoA carboxylase to form methylmalonyl-CoA. Isomerization of methylmalonyl-CoA takes place in two sequential steps, catalyzed by methylmalonyl-CoA epimerase and methylmalonyl-CoA mutase to form succinyl-CoA. Succinyl-CoA transfers CoA for malate activation and forms succinate and malyl-CoA [65, 68, 69]. Malyl-CoA, a four-carbon compound, breaks down by malyl-CoA lyase to regenerate starting acetyl-CoA and glyxolate. Carboxylations of acetyl-CoA and propionyl-CoA are the main CO_2 fixation reactions. It is to be noted that actual substrate for both the carboxylation reactions is HCO_3^- rather than CO_2. Each turn of cycle results in net fixation of two molecules of bicarbonate to produce one molecule of glyxolate. Glyoxylate is considered as the initial CO_2 fixation product. Glyxolate is further utilized in the synthesis of the cellular material. Intermediate 3-hydroxypropionate is the characteristic of the cycle, which on reductive conversion produces propionyl-CoA [65, 68, 69]. In 3-hydroxypropionate cycle, six molecules of ATP and four molecules of NAD(P)H are required to reduce two molecules of CO_2 to form one molecule of acetyl-CoA as shown in Eq. (12.11) [58].

$$2\,CO_2 + 6\,ATP + 4\,NAD(P)H + HS\text{-}CoA \rightarrow Acetyl\text{-}CoA + 6\,ADP + 4\,NAD(P)^+ \quad (12.11)$$

12.3.5 Other Pathways

12.3.5.1 Dicarboxylate/4-Hydroxybutyrate Cycle

Dicarboxylate/4-hydroxybutyrate cycle is the newly discovered autotrophic pathway for carbon dioxide fixation in *Ignicoccus hospitalis* (*Desulfurococcales), Thermoproteus neutrophilus*, and an anaerobic member of *Thermoproteales* [70–72]. Evidence of dicarboxylate/4-hydroxybutyrate cycle has been reported by Ramos-vera et al. (2009) in *T. neutrophilus* [72]. This pathway can also be divided into two parts: the first part involves formation of succinyl-CoA from acetyl-CoA using two inorganic carbons and the second part deals with regeneration of acetyl-CoA from succinyl-CoA. Thus, this pathway has similarity with both

reductive tricarboxylic acid cycle (rTCA) and 3-hydroxypropionate/4-hydroxybutyrate cycles (Fig. 12.7b). The first part of the cycle involves the intermediates of reductive tricarboxylic acid cycle (rTCA) and the second part involves the intermediates of 3-hydroxypropionate/4-hydroxybutyrate cycle via the route similar to 4-hydroxybutyrate pathway to succinyl-CoA using pyruvate synthase and pyruvate carboxylase, as carboxylating enzyme. So, the only difference between this and the 3-hydroxypropionate/4-hydroxybutyrate cycle is the way succinyl-CoA is created.

12.3.5.2 3-Hydroxypropionate/4-Hydroxybutyrate Cycle

Another pathway has been reported in some bacteria called 3-hydroxypropionate/4-hydroxybutyrate cycle. This pathway was found in aerobic autotrophic members of Sulfolobales. 3-Hydroxypropionate/4-hydroxybutyrate pathway was discovered in *Metallosphaera sedula* which was earlier believed to fix CO_2 using 3-hydroxypropionate cycle. Malyl-CoA lyase, an enzyme used in the regeneration of acetyl-CoA, was absent in the cell extract of *M. sedula*, resulting in the proposed alternative pathway for the regeneration of starting material of cycle. Therefore, 3-hydroxypropionate and 3-hydroxypropionate/4-hydroxybutyrate cycle share the same steps from acetyl-CoA to succinyl-CoA (Fig. 12.8b). However, the enzymes involved in the reaction steps from acetyl-CoA to succinyl-CoA are not same in both cases. Detailed structure of acetyl-CoA carboxylase participating in 3-hydroxypropionate cycle reveals that the enzyme is composed of four subunits. Contrary to this, acetyl-CoA carboxylase taking part in 3-hydroxypropionate/4-hydroxybutyrate cycle has only three subunits. Similarly, malonyl-CoA reductase of both the cycles is not the same. They differ in the different intermediates through which regeneration of acetyl-CoA takes place from succinyl-CoA. The intermediates between acetyl-CoA and succinyl-CoA in 3-hydroxypropionate/4-hydroxybutyrate cycle are succinic semialdehyde, 4-hydroxybutyrate, 4-hydroxybutyryl-CoA, crotonyl-CoA, 3-hydroxybutyryl-CoA, and acetoacetyl-CoA, formations of which are catalyzed by succinyl-CoA reductase, succinate semialdehyde reductase, 4-hydroxybutyryl-CoA synthetase, 4-hydroxybutyryl-CoA dehydratase, crotonyl-CoA hydratase, 3-hydroxybutyryl-CoA dehydrogenase, and acetoacetyl-CoA β-ketothiolase, respectively [60].

12.4 Enzymes for CO_2 Sequestration

Carbonic anhydrase (CA) is zinc metalloenzyme which catalyzes conversion of free CO_2 into bicarbonates and protons. It is one of the fastest known enzymes catalyzing 10^4–10^6 reactions per second [73]. It has been found in a wide number of living beings such as plants, animals, and microorganisms as they have been found growing well in CO_2-rich conditions, and CA was found essential for this purpose

[74, 75]. In human body, CA is present in the erythrocyte and converts poorly soluble CO_2 in aqueous solution, such as blood plasma to water-soluble bicarbonate (HCO_3^-) anion [76]. Human isozyme HCA II having molecular mass of 30,000 is the fastest CA known so far, having a hydration rate of 1.4×10^6 molecules of CO_2 per second per molecule of CA [19]. Some of the microalgae which have been found containing CA are *Chlamydomonas reinhardtii, Scenedesmus obliquus, Dunaliella tertiolecta, Chlorella saccharophila, Chlorella vulgaris, Chlorella pyrenoidosa,* and *Chlorococcum littorale* [77]. BCA (bovine carbonic anhydrase) has been found stable in wide range of pH (5–10) and temperature (up to 70 °C) [9]. Sulfate and zinc have been found to enhance CA activity.

There are contradictory reports on the effect of CO_2 concentration on the activity of CA in photosynthetic microorganisms such as plants, green algae, and cyanobacteria. In most of the reports, activity of CA isolated from algae is inversely proportional to the CO_2 concentration. It was explained with the fact that RuBisCO can catalyze both oxygenase and carboxylase activities depending upon the nearby CO_2 concentration [29]. CA helps in increasing the concentration of CO_2 near the RuBisCO site. CA can enhance the internal CO_2 concentration up to 1,000 times higher than the external fluid. Therefore, at lower CO_2 concentration, expression of CA increases to maintain carboxylase activity of RuBisCO which in turn reduces atmospheric CO_2 into cellular constituents such as starch, lipid, and protein. However, in few reports, activity of CA initially increases with increase in CO_2 concentration and later starts decreasing with further increase in CO_2 concentration, thus making bell-shaped curve [20]. The reason behind the decreasing trend of CA at higher CO_2 was postulated due to feedback inhibition by bicarbonate and/or decrease in pH at this concentration.

Extracellular and intercellular crude extract of enzyme CA II isolated from *Chlorella vulgaris* were 72 and 160 mg $CaCO_3$ per milligram of protein, comparable to 225 mg $CaCO_3$ per milligram of protein with the purified enzyme from *Citrobacter freundii* [78].

12.4.1 Mechanism of CO_2 Captured by CA

Hydration of CO_2 into solid carbonate such as calcium carbonate is a natural process. There are five reactions required for the transformation of CO_2 into minerals [9, 19, 76].

1. Dissolution of gaseous CO_2 in liquid (Eq. 12.12)
2. Hydration of aqueous CO_2 into carbonic acids (H_2CO_3) (Eq. 12.13)
3. Dissociation of carbonic acid into bicarbonate ions (HCO_3^{2-}) and protons (Eq. 12.16)
4. Dissociation of bicarbonate ions into carbonate ions (CO_3^-) (Eq. 12.17)
5. Reaction of carbonate ions and calcium to form solid calcium carbonate (Eq. 12.18)

12.4.1.1 CO_2 Dissolution

$$CO_{2(g)} \leftrightarrow CO_{2(aq)} \tag{12.12}$$

12.4.1.2 Carbonic Acid Formation

$$CO_{2(aq)} + H_2O \leftrightarrow H_2CO_3 \tag{12.13}$$

$$K_2 = \frac{k_2}{k_{-2}} = \frac{6.2 \times 10^{-2} s^{-1}}{23.7\, s^{-1}} = 2.6 \times 10^{-3}$$

Where k_2, k_{-2} and K_2 are forward rate, reverse rate and equilibrium constants respectively. As shown in Eq. (12.13), hydration of CO_2 to carbonic acids is the rate limiting step having very less forward reaction constant 6.2 $\times$ 10^{-2} s at 25 °C [18]. However, catalysis by CA increases the rate of reaction manifold showing the high substrate specificity of this enzyme [19]. Enzyme catalyzes the CO_2 hydration reaction in the following two half reactions (Eqs. 12.14 and 12.15) [79]:

$$E - Zn - H_2O \leftrightarrow E - Zn + OH^- + H^+ \tag{12.14}$$

$$E - Zn - OH + CO_2 \leftrightarrow E - Zn - CO_3{}^- + H^+ \rightarrow E - Zn - H_2O + CO_3{}^- \tag{12.15}$$

The above reaction was found dominating when the pH is higher than 10 while it was found negligible at pH less than 8 [80].

12.4.1.3 Bicarbonate Formation

$$H_2CO_3 \leftrightarrow H^+ + HCO_3{}^- \tag{12.16}$$

$$K_3 = \frac{k_3}{k_{-3}} = \frac{8 \times 10^6\, s^{-1}}{4.7 \times 10^{10}\, s^{-1}} = 1.7 \times 10^{-4}$$

Where k_3, k_{-3} and K_3 are forward rate, reverse rate and equilibrium constants respectively. Bicarbonate formation reaction is diffusion controlled and very fast in nature.

12.4.1.4 Carbonate Formation

$$HCO_3{}^- \leftrightarrow H^+ + CO_3{}^{2-} \tag{12.17}$$

$$K_4 = \frac{k_4}{k_{-4}} = \frac{8 \times 10^6\, s^{-1}}{4.7 \times 10^{10}\, s^{-1}} = 4.69 \times 10^{-11}$$

Where k_4, k_{-4} and K_4 are forward rate, reverse rate and equilibrium constants respectively.

12.4.1.5 Calcium Carbonate Reaction

$$Ca^{2+} + CaCO_3{}^{2-} \leftrightarrow CaCO_3 \downarrow \tag{12.18}$$

Calcium carbonate precipitates quickly at the saturation concentration of calcium and carbonate ions. Therefore, continuous supply of carbonate ions by hydration of CO_2 and water is requisite [19]. CA was also found to enhance the calcium carbonate precipitation reaction [9]. However, contrary to enhanced hydration reaction, higher concentration of CA did not increase $CaCO_3$ precipitation reaction [9].

Some of the approaches which have been applied for improving the performance of CA are (1) isolating CAs from thermophilic microorganisms, (2) use of protein engineering to create thermotolerant enzymes, and (3) immobilizing the enzyme for stabilization and confinement to cooler regions and process modification that minimize the stresses such as cooling of the flue gas [81].

12.4.2 Immobilization of CA

Use of CA in aqueous solution has many disadvantages such as reusability and recovery. Immobilization of the CA in the nanoparticles significantly improves the catalytic property, storage, and thermal stability of the enzyme. Immobilized BCA and HCA enzymes were found retaining nearly 90 % of enzymatic activity for more than 20 cycles. Carbonic anhydrase (CA) can be immobilized on functionalized and metal nanoparticles confined mesoporous silica for CO_2 hydration and its sequestration to $CaCO_3$ [76, 82]. Surface-modified magnetic nanoparticle is one of such attractive templates for enzyme immobilization. Enzyme can be easily recovered from a reaction medium by applying a static magnetic field near the immobilized CA in the reactor [76, 82]. Inert materials such as chitosan and sodium alginate are widely used for immobilization of enzymes and microorganism. Whole cells of *Pseudomonas fragi, Micrococcus lylae*, and *Micrococcus luteus* 2 were immobilized on different biopolymer matrices [83]. Bovine carbonic anhydrase (BCA) was covalently immobilized by Vinoba et al. (2012) onto OAPS (octa(aminophenyl)silsesquioxane)-functionalized Fe_3O_4/SiO_2 nanoparticles by using glutaraldehyde as a spacer [76]. Immobilization of CA can be done in many ways such as adsorption on surfaces, entrapment within matrices, and cross-linking within polymeric scaffold [80]. Polyurethane foam is a highly porous hydrophilic polymeric material where enzyme immobilization was easy and fast. CA had 100 % activity over time, and thus reusability was not a concern [80].

12.4.3 Application of CA

Bovine CA has been proposed to inject into wellbore of geological formations to prevent CO_2 leakage through it [84]. CO_2 sequestration by mineral carbonation can use CA to make the process feasible at large scale. Alkaline silicates are abundant and high enough to sequester all the CO_2 emitted from total fossil fuels. Alkaline silicates can dissolve to provide cations in acidic conditions. However, high alkalinity is required for the increase of the rate of gaseous CO_2 dissolving into the carbonate ions CO_3^{2-}. Therefore, enhancing the release of divalent cations from the alkaline silicates and enhancing alkalinity are some of the challenges of the process. Increase in alkalinity increases the rate of dissolution of CO_2 into the carbonate ions CO_3^{2-}, and acidic conditions release the divalent cations required for the formation of carbonates [17]. Denitrification, methane production, and sulfate reduction are some of the alkalinity-producing metabolic processes. Therefore, these processes enhance the carbonation process. Integrating acid-producing process for silicate dissolution and alkaline-producing process for carbonate precipitation together can be used for CO_2 mitigation using biological mineral carbonation. Dupraz et al. (2009) has experimentally shown the use of *Bacillus pasteurii* as a model carbonate precipitating bacteria on the geological sequestration of CO_2 and its transformation into solid carbonate phases [85].

12.4.4 Challenges in Use of CA for CO_2 Sequestration

Enzyme works better at optimum temperature, pH, and enzyme concentration [83]. At lower pH, carbonates prefer to be in dissolved state than the precipitated form, while at higher pH, carbonate ions form but concerns about economical and environmental aspect arise [19]. Lifetime and activity of enzyme greatly depend upon pH, temperature, other ions such as CN^-, and higher concentration of SO_x and NO_x [19]. Higher cost of enzyme and its large-scale production are other bottlenecks to overcome to make the process successful in reality.

12.5 Conclusions

Imbalance between CO_2 emission and sink is the reason for steep rise in the earth's atmospheric CO_2 concentration. This may be the reason for the rise in global mean temperature, causing melting of glaciers, rise in sea level, ocean acidification, unpredicted climate changes, etc. Several biological processes are available for CO_2 mitigation. Carbonic anhydrase (CA) enzyme, algae, cyanobacteria, bacteria, and terrestrial plants are some of the biological methods used for CO_2 sequestration. However, these processes are slow and limited in application. Identifying limiting

parameters and application of technology can accelerate the natural processes manifold. For example, CO_2 hydration, the limiting step in the transformation of gaseous CO_2 to solid bicarbonates, can be accelerated by catalyzing the reaction using CA. Forest and oceanic fertilization can be applied to enhance the photosynthetic efficiency of terrestrial plants and oceanic phytoplanktons, respectively. Similarly, algae and cyanobacteria can be exploited for CO_2 sequestration as they can be grown efficiently at higher CO_2 concentration with higher photosynthetic efficiency.

Acknowledgments The authors gratefully acknowledge the Council of Scientific and Industrial Research (CSIR), Govt. of India, for senior research fellowship and Department of Biotechnology (DBT) and Ministry of New and Renewable Energy (MNRE), Govt. of India, for the financial support. The authors also acknowledge Ms. Pallavi Sinha for reviewing the manuscript.

References

1. Tans P (2010) Trends in atmospheric carbon dioxide. In: Earth System Research Laboratory Global Monitoring Division. http://www.esrl.noaa.gov/gmd/ccgg/trends. Accessed 15 May 2013
2. http://climate.nasa.gov/evidence/
3. Bardgett RD, Freeman C, Ostle NJ (2008) Microbial contributions to climate change through carbon cycle feedbacks. ISME J 2:805–814
4. Stewart C, Hessami M (2005) A study of methods of carbon dioxide capture and sequestration–the sustainability of a photosynthetic bioreactor approach. Energy Convers Manage 46:403–420
5. Sharma A, Bhattacharya A, Shrivastava A (2011) Biomimetic CO_2 sequestration using purified carbonic anhydrase from indigenous bacterial strains immobilized on biopolymeric materials. Enzyme Microb Technol 48:416–426
6. Oelkers EH, Cole DR (2008) Carbon dioxide sequestration: a solution to a global problem. Elements 4:305–310
7. Kumar K, Dasgupta CN, Nayak B et al (2011) Development of suitable photobioreactors for CO_2 sequestration addressing global warming using green algae and cyanobacteria. Bioresour Technol 102:4945–4953
8. Lee JW, Li R (2001) A novel strategy for CO_2 sequestration and clean air protection. In: Proceedings of fire national conference on carbon sequestration, Washington, DC, 14–17 May 2001
9. Mirjafari P, Asghari K, Mahinpey N (2007) Investigating the application of enzyme carbonic anhydrase for CO_2 sequestration purposes. Ind Eng Chem Res 46:921–926
10. Bachu S (2000) Sequestration of CO_2 in geological media: criteria and approach for site selection in response to climate change. Energy Convers Manage 41:953–970
11. Falkowski P, Scholes RJ, Boyle E et al (2000) The global carbon cycle: a test of our knowledge of earth as a system. Science 290:291–296
12. Hall DO, Woods J, House J (1992) Biological systems for uptake of carbon dioxide. Energy Convers Manage 33(5–8):721–728
13. Whitmarsh J, Govindjee (1999) The photosynthetic process. In: Singhal GS, Renger G, Sopory SK, Irrgang K-D, Govindjee (eds) Concepts in photobiology: photosynthesis and photomorphogenesis. Narosa Publishers/Kluwer, New Delhi/Dordrecht, pp 11–51
14. Benemann JR (1993) Utilization of carbon dioxide from fossil fuel-burning power plants with biological systems. Energy Convers Manage 34(9–11):999–1004
15. Skjånes K, Lindblad P, Muller J (2007) BioCO$_2$ – a multidisciplinary, biological approach using solar energy to capture CO_2 while producing H_2 and high value products. Biomol Eng 24:405–413

16. Loubiere K, Olivo E, Bougaran G et al (2009) A new photobioreactor for continuous microalgal production in hatcheries based on external-loop airlift and swirling flow. Biotechnol Bioeng 102(1):132–147
17. Salek SS, Kleerebezem R, Jonkers HM et al (2013) Mineral CO_2 sequestration by environmental biotechnological processes. Trends Biotechnol 31(3):139–146
18. Druckenmiller ML, Maroto-Valer MM (2005) Carbon sequestration using brines of adjusted pH to form mineral carbonates. Fuel Process Technol 86:1599–1614
19. Bond GM, Stringer J, Brandvold DK et al (2001) Development of integrated system for biomimetic CO_2 sequestration using the enzyme carbonic anhydrase. Energy Fuels 15:309–316
20. Ramanan R, Kannan K, Sivanesan SD et al (2009) Bio-sequestration of carbon dioxide using carbonic anhydrase enzyme purified from *Citrobacter freundii*. World J Microbiol Biotechnol 25:981–987
21. Beedlow PA, Tingey DT, Phillips DL et al (2004) Rising atmospheric CO_2 and carbon sequestration in forests. Front Ecol Environ 2(6):315–322
22. Norby RJ, DeLucia EH, Gielen B et al (2005) Forest response to elevated CO_2 is conserved across a broad range of productivity. Proc Natl Acad Sci U S A 102:18052–18056
23. Norby RJ, Wullschleger SD, Gunderson CA (1999) Tree responses to rising CO_2 in field experiments: implications for the future forest. Plant Cell Environ 22:683–714
24. Griffin KL, Seemann JR (1996) Plants, CO_2 and photosynthesis in the 21st century. Chem Biol 3(4):245–254
25. Karnosky DF (2003) Impacts of elevated atmospheric CO_2 on forest trees and forest ecosystems: knowledge gaps. Environ Int 29:161–169
26. Tognetti R, Cherubini P, Innes JL (2000) Comparative stem growth rates of Mediterranean trees under background and naturally enhanced ambient CO_2 concentrations. New Phytol 146:59–74
27. Idso SB, Idso KE, Garcia RL et al (1995) Effects of atmospheric CO_2 enrichment and foliar methanol application on net photosynthesis of sour orange tree (*Citrus aurantium*; Rutaceae) leaves. Am J Bot 82:26–30
28. Manning DAC, Renforth P (2013) Passive sequestration of atmospheric CO_2 through coupled plant-mineral reactions in urban soils. Environ Sci Technol 47:135–141
29. Moroney JV, Somanchi A (1999) How do algae concentrate CO_2 to increase the efficiency of photosynthetic carbon fixation. Plant Physiol 119:9–16
30. Tsai DDW, Ramaraj R, Chen PH (2012) Growth condition study of algae functions in ecosystem for CO_2 bio-fixation. J Photochem Photobiol B Biol 107:27–34
31. Yang H, Xu Z, Fan M et al (2008) Progress in carbon dioxide separation and capture: a review. J Environ Sci 20:14–27
32. Oren R, Ellsworth DS, Johnsen KH et al (2001) Soil fertility limits carbon sequestration by forest ecosystems in a CO_2-enriched atmosphere. Nature 411:469–471
33. Yuan H, Ge T, Wu X et al (2012) Long-term field fertilization alters the diversity of autotrophic bacteria based on the ribulose-1,5-biphosphate carboxylase/oxygenase (RuBisCO) large-subunit genes in paddy soil. Appl Microbiol Biotechnol 95:1061–1071
34. Munoz R, Guieysse B (2006) Algal-bacterial processes for the treatment of hazardous contaminants: a review. Water Res 40:2799–2815
35. Kumar K, Sirasale A, Das D (2013) Use of image analysis tool for the development of light distribution pattern inside the photobioreactor for the algal cultivation. Bioresour Technol 143:88–95
36. Hanagata N, Takeuchi T, Fukuju Y et al (1992) Tolerance of microalgae to high CO_2 and high temperature. Phytochemistry 31:3345–3348
37. Carvalho AP, Meireles LA, Malcata FX (2006) Microalgal reactors: a review of enclosed systems design and performances. Biotechnol Prog 22:1490–1506
38. Lee JS, Lee JP (2003) Review of advances in biological CO_2 mitigation technology. Biotechnol Bioprocess Eng 8:354–359

39. Castenholz RW, Waterbury JB (1989) Group I. Cyanobacteria. In: Staley JT, Bryant MP, Pfennig N, Holt JG (eds) Bergey's manual of systematic bacteriology, vol 3. Williams & Wilkins, Baltimore, pp 1710–1727
40. Garofalo R (2009) Algae and aquatic biomass for a sustainable production of 2nd generation biofuels. AquaFUELs Taxon Biol Biotechnol, pp 1–258
41. Garlick S, Oren A, Padan E (1977) Occurrence of facultative anoxygenic photosynthess among unicellular and filamentous cyanobacteria. J Bacteriol 129:623–629
42. Srirangan K, Pyne ME, Chou CP (2011) Biochemical and genetic engineering strategies to enhance hydrogen production in photosynthetic algae and cyanobacteria. Bioresour Technol 102:8589–8604
43. Giordano M, Beardall J, Raven JA (2005) Mechanisms in algae: mechanisms, environmental modulation, and evolution. Annu Rev Plant Biol 56:99–131
44. Zeng X, Danquah MK, Chen XD et al (2011) Microalgae bioengineering: from CO_2 fixation to biofuel production. Renew Sust Energy Rev 15:3252–3260
45. Cannon GC, Heinhorst S, Kerfeld CA (2010) Carboxysomal carbonic anhydrases: structure and role in microbial CO_2 fixation. Biochim Biophys Acta 1804:382–392
46. Coleman JR (1991) The molecular and biochemical analysis of CO_2 concentrating mechanisms in cyanobacteria and microalgae. Plant Cell Environ 14:861–867
47. Kaplan A, Reinhold L (1999) CO_2 concentrating mechanisms in photosynthetic microorganisms. Annu Rev Plant Physiol Plant Mol Biol 50:539–570
48. Leegood RC (2002) C4 photosynthesis: principles of CO_2 concentration and prospects for its introduction into C3 plants. J Exp Bot 53(369):581–590
49. Badger MR, Price GD (2003) CO_2 concentrating mechanisms in cyanobacteria: molecular components, their diversity and evolution. J Exp Bot 54(383):609–622
50. Price GD, Maeda S, Omata T et al (2002) Modes of active inorganic carbon uptake in the cyanobacterium *Synechococcus* sp. PCC7942. Funct Plant Biol 29:131–149
51. Spalding MH (2008) Microalgal carbon dioxide concentrating mechanisms: *Chlamydomonas* inorganic carbon transporters. J Exp Biol 59(7):1463–1473
52. Hu JJ, Wang L, Zhang SP et al (2011) Enhanced CO_2 fixation by a non-photosynthetic microbial community under anaerobic conditions: optimization of electron donors. Bioresour Technol 102:3220–3226
53. Nelson DL, Cox MM (2005) Lehninger principles of biochemistry, 4th edn. W.H. Freeman & Co, New Jersey
54. Madigan MT, Martinko JM, Parker J (2003) Brock: biology of microorganisms. Prentice Hall, Upper Saddle River
55. Calvin M, Benson AA (1948) The path of carbon in photosynthesis. Science 107:476–480
56. Kumar K, Das D (2012) Growth characteristics of *Chlorella sorokiniana* in airlift and bubble column photobioreactors. Bioresour Technol 116:307–313
57. Kumar K, Roy S, Das D (2013) Continuous mode of carbon dioxide sequestration by *C. sorokiniana* and subsequent use of its biomass for hydrogen production by *E. cloacae* IIT-BT 08. Bioresour Technol 145:116–122
58. Fast AG, Papoutsakis ET (2012) Stoichiometric and energetic analyses of non-photosynthetic CO_2-fixation pathways to support synthetic biology strategies for production of fuels and chemicals. Curr Opin Chem Eng 1:1–16
59. Müller V (2003) Bacteria energy conservation in acetogenic bacteria. Appl Environ Microbiol 69(11):6345–6353
60. Saini R, Kapoor R, Kumar R et al (2011) CO_2 utilizing microbes – a comprehensive review. Biotechnol Adv 29:949–960
61. Atomi H (2002) Microbial enzymes involved in carbon dioxide fixation. J Biosci Bioeng 94(6):497–505
62. Evans MC, Buchanan BB, Arnon DI (1966) A new ferredoxin-dependent carbon reduction cycle in a photosynthetic bacterium. Proc Natl Acad Sci U S A 55:928–934
63. Sintsov NV, Ivanovskii RN, Kondrateva EN (1980) ATP-dependent citrate lyase in the green phototrophic bacterium, *Chlorobium limicola*. Mikrobiologiia 49:514–516

64. Shiba H, Kawasumi T, Igarashi Y et al (1985) The CO_2 assimilation via the reductive tricarboxylic acid cycle in an obligately autotrophic, aerobic hydrogen-oxidizing bacterium, *Hydrogenobacter thermophilus*. Arch Microbiol 141:198–203
65. Alber BE, Fuchs G (2002) Propionyl-coenzyme A synthase from *Chloroflexus aurantiacus*, a key enzyme of the 3-hydroxypropionate cycle for autotrophic CO_2 fixation. J Biol Chem 277:12137–12143
66. Burton NP, Williams TD, Norris PR (1999) Carboxylase genes of *Sulfolobus metallicus*. Arch Microbiol 172:349–353
67. Strauss G, Fuchs G (1993) Enzymes of a novel autotrophic CO_2 fixation pathway in the phototrophic bacterium *Chloroflexus aurantiacus*, the 3-hydroxypropionate cycle. Eur J Biochem 215:633–643
68. Herter S, Fuchs G, Bacher A et al (2002) A bicyclic autotrophic CO_2 fixation pathway in *Chloroflexus aurantiacus*. J Biol Chem 277:20277–20283
69. Hügler M, Menendez C, Schagger H et al (2002) Malonyl-coenzyme A reductase from *Chloroflexus aurantiacus*, a key enzyme of the 3-hydroxypropionate cycle for autotrophic CO_2 fixation. J Bacteriol 184:2404–2410
70. Berg IA, Ramos-Vera WH, Petri A et al (2010) Study of the distribution of autotrophic CO_2 fixation cycles in Crenarchaeota. Microbiology 156:256–259
71. Huber H, Gallenberger M, Jahn U et al (2008) A dicarboxylate/4-hydroxybutyrate autotrophic carbon assimilation cycle in the hyperthermophilic archaeum *Ignicoccus hospitalis*. Proc Natl Acad Sci U S A 105:7851–7856
72. Ramos-Vera WH, Berg IA, Fuchs G (2009) Autotrophic carbon dioxide assimilation in *Thermoproteales* revisited. J Bacteriol 191:4286–4297
73. Heck RW, Tanhauser SM, Manda R et al (1994) Catalytic properties of mouse carbonic anhydrase V. J Biol Chem 269:24742–24746
74. Karlsson J, Clarke AK, Chen ZY et al (1998) A novel a-type carbonic anhydrase associated with the thylakoid membrane in *Chlamydomonas reinhardtii* is required for growth at ambient CO_2. EMBO J 17(5):1208–1216
75. Kusian B, Sultemeyer D, Bowien B (2002) Carbonic anhydrase is essential for growth of *Ralstonia eutropha* at ambient CO_2 concentrations. J Bacteriol 184(18):5018–5026
76. Vinoba M, Bhagiyalakshmi M, Jeong SW et al (2012) Carbonic anhydrase immobilized on encapsulated magnetic nanoparticles for CO_2 sequestration. Chem Eur J 18:12028–12034
77. Miyachi S, Iwasaki I, Shiraiwa Y (2003) Historical perspective on microalgal and cyanobacterial acclimation to low and extremely high CO conditions. Photosynth Res 77:139–153
78. Li L, Fu M, Zhao Y et al (2012) Characterization of carbonic anhydrase II from *Chlorella vulgaris* in bio-CO_2 capture. Environ Sci Pollut Res 19:4227–4232
79. Brauer M, Perez-Lustres JL, Weston J (2002) Quantitative reactivity model for the hydration of carbon dioxide by biomimetic zinc complexes. Inorg Chem 41:1454–1463
80. Ozdemir E (2009) Biomimetic CO_2 sequestration: 1. Immobilization of carbonic anhydrase within polyurethane foam. Energy Fuels 23:5725–5730
81. Savile CK, Lalonde JJ (2011) Biotechnology for the acceleration of carbon dioxide capture and sequestration. Curr Opin Biotechnol 22:818–823
82. Vinoba M, Yoon Y, Nam SC et al (2012) CO_2 conversion to $CaCO_3$ by immobilized carbonic anhydrase. KIC News 15(2):32–40
83. Sharma N, Nayak RK, Dadhwal VK et al (2011) Diurnal and seasonal variation of measured atmospheric CO_2 at Dehradun during 2009. In: International archives of the photogrammetry, remote sensing and spatial information sciences, volume XXXVIII-8/W20, 2011 ISPRS Bhopal 2011 workshop, Bhopal, 8 Nov 2011
84. Mahinpeya N, Asghari K, Mirjafari P (2011) Biological sequestration of carbon dioxide in geological formations. Chem Eng Res Des 89:1873–1878
85. Dupraz S, Ménez B, Gouze P et al (2009) Experimental approach of CO_2 biomineralization in deep saline aquifers. Chem Geol 265:54–62

Part IV
Reactions in/Under Dense Phase Carbon Dioxide

Chapter 13
Homogeneous Catalysis Promoted by Carbon Dioxide

Ran Ma, Zhen-Feng Diao, Zhen-Zhen Yang, and Liang-Nian He

13.1 Introduction

The global increase in environmental awareness has led to an ever-increasing control over the use and disposal of hazardous materials by the chemical industry and searching for "cleaner" alternatives for organic synthetic processes. One obvious target area is the replacement of conventional organic solvents by suitable candidates, such as supercritical fluids (particularly CO_2), ionic liquids [1], water [2], or even solvent-free systems [3]. Supercritical CO_2 ($scCO_2$), which is recognized as CO_2 heated and pressurized beyond its critical point ($T_c = 31.06\ ^\circ C$, $P_c = 7.38$ MPa), is considered to offer numerous advantages as reaction medium offering safe environment owing to its unique physical properties, such as abundantly available and cheap; nontoxic and environmentally benign even under oxidative conditions; high gaseous miscibility with hydrogen, oxygen, carbon monoxide, and methane; effective mass transfer; easily tunable properties with variation of pressure or temperature; and weakening of the solvent interactions around the reacting species [4–7]. In addition, surface tension effects can be eliminated since $scCO_2$ has negligible surface tension like a gas [8, 9]. Most importantly, separation of products and solvent ($scCO_2$) can easily be performed by depressurization, and the separated CO_2 can be reused by pressurization. On the other hand, in the case of aerobic oxidation reactions, the miscibility of organic substrates and catalysts with O_2 is crucial to achieve high oxidation rate, but the metal component of catalysts tends to undergo overoxidation, thus leading to the catalyst deactivation [10]. Hence, dense-phase (liquid or supercritical) CO_2 has been recently recognized as an innovative and environmentally friendly reaction medium for chemical syntheses and especially for the metal-catalyzed processes, mainly as an alternative to conventional organic solvents [11, 12]. This chapter

R. Ma • Z.-F. Diao • Z.-Z. Yang • L.-N. He (✉)
State Key Laboratory of Elemento-Organic Chemistry, Nankai University, Tianjin 300071, People's Republic of China
e-mail: heln@nankai.edu.cn

B.M. Bhanage and M. Arai (eds.), *Transformation and Utilization of Carbon Dioxide*, Green Chemistry and Sustainable Technology, DOI 10.1007/978-3-642-44988-8_13,

summarizes the utilization of $scCO_2$ as a solvent and promoter in organic reactions including hydrogenation, carbonylation, C–C forming reaction, oxidation reaction, and polymerization.

13.2 Hydrogenation

13.2.1 Asymmetric Hydrogenation

The monodentate phosphites containing *ortho*- and *meta-closo*-dodecarboranyl groups have widely been used as chiral ligands in the Rh-catalyzed asymmetric hydrogenation of dimethyl itaconate with high enantioselectivities (up to 93 % ee in $scCO_2$) [13, 14]. In order to achieve the comparable enantioselective with bidentate phosphines (97–99 % ee), the easily accessible monodentate phosphite-type ligands, for instance, PipPhos (**L1**) and MorfPhos (**L2**), are successfully applied to the hydrogenation of dimethyl itaconate **1** and methyl 2-acetamidoacrylate **3** in $scCO_2$ with high enantioselectivity (up to 99 % ee) and complete conversion within 35–50 min as depicted in Scheme 13.1 [15]. The high reaction rates could

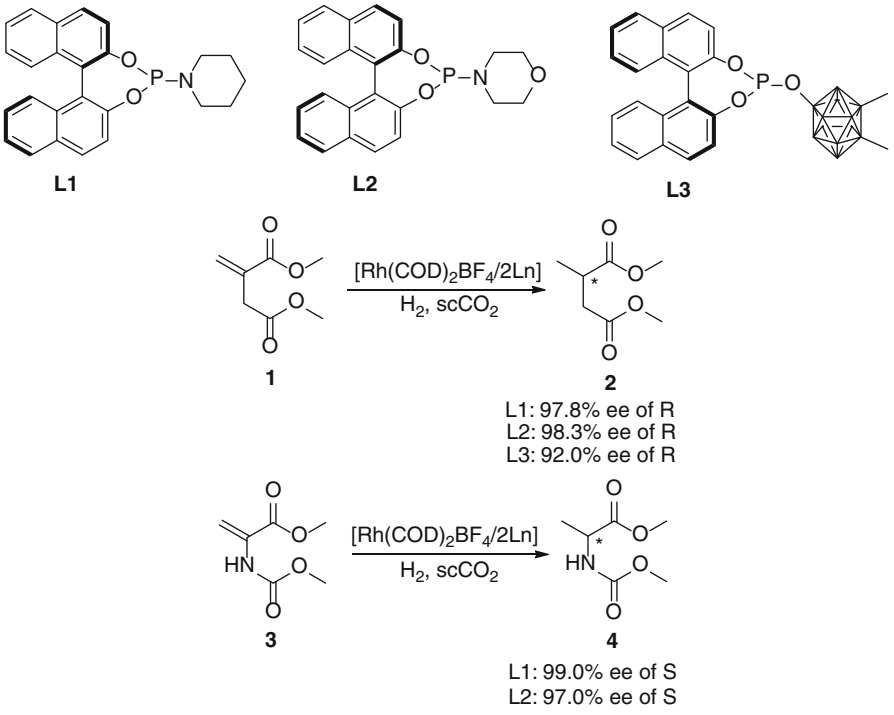

Scheme 13.1 Rhodium-catalyzed hydrogenation of prochiral olefins in $scCO_2$ [15]

presumably be attributed to the higher miscibility and diffusivity of gaseous hydrogen in the supercritical medium, thereby eliminating mass transfer resistance compared to that in CH_2Cl_2 [15, 16].

A successive application of monodentate phosphoramidite ligands has been covered successfully in the Rh-catalyzed hydrogenation of α-dehydroamino acid derivatives in $scCO_2$ with high enantioselectivity (up to 97 % ee) and excellent reaction rates [16]. Recently, sterically congested carborane-containing monodentate ligands (**L3**, Scheme 13.1) have been designed and synthesized as chiral ligands in Rh-catalyzed hydrogenation of prochiral olefins in $scCO_2$ [17]. High enantioselectivity (up to 92 % ee) and reactivities (100 % conversion in 45–60 min) are obtained when hydrogen pressure and total pressure are adjusted within H_2 8 MPa and total pressure 20 MPa [17].

The Ru complex is also found to be an efficient catalyst for the hydrogenation reactions in the environmentally friendly solvents [18–20]. While the solubility issues for most aromatic substrates, reagents, ligands, and catalysts in $scCO_2$ represented a critical factor for this type of asymmetric hydrogenation reaction, in this context, cosolvent, such as alcohol, is necessary for some substrates in order to increase the solubility in $scCO_2$ [21]. For example, the fluorinated alcohols such as $CF_3(CF_2)_6CH_2OH$ can increase both enantioselectivity (up to 89 % ee) and reactivity (over 99 % yield) for the hydrogenation of tiglic acid in $scCO_2$ to afford 2-methylbutanoic acid catalyzed by (*S*)-H_8-BINAP-Ru(II) [22]. On the other hand, perfluoroalkylBINAP is successfully used as a soluble chiral ligand for the asymmetric hydrogenation in $scCO_2$ with trifluorotoluene as cosolvent (Scheme 13.2) [23].

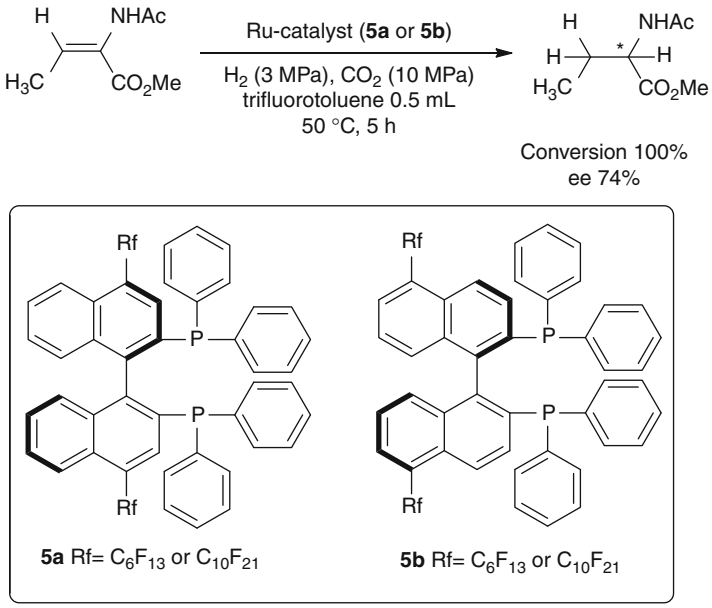

Scheme 13.2 The perfluoroalkylBINAP ligands for the asymmetric hydrogenation [23]

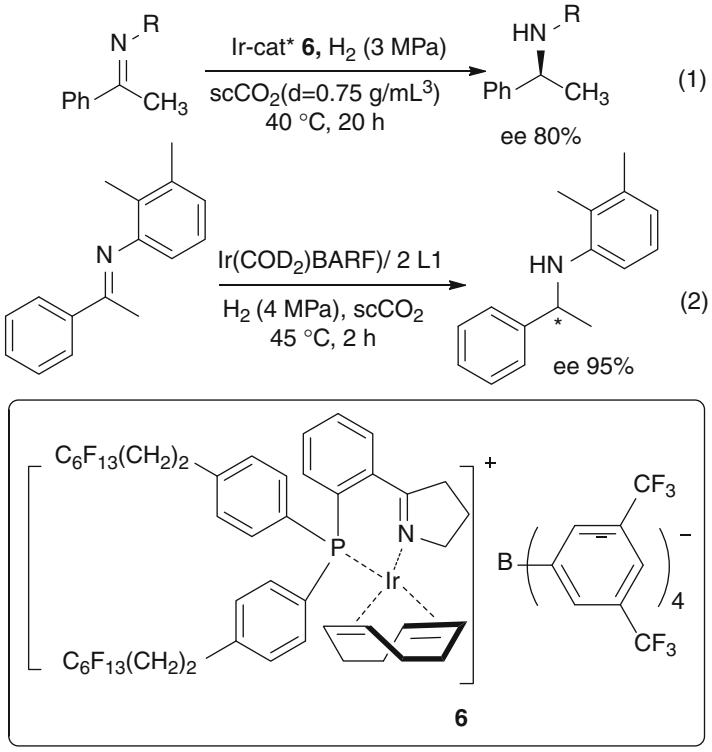

Scheme 13.3 Ir-catalyzed hydrogenation of acyclic arylimines in $scCO_2$ [25, 26]

The enantioselective hydrogenation of imines provides an attractive route to the preparation of optical-active amines and has attracted much attention in both academic and industrial research [24]. Leitner has showed that the cationic iridium complex **6** with chiral phosphinodihydrooxazoles, modified with perfluoroalkyl groups for enhancing the solubility in $scCO_2$, has been tested in the hydrogenation of N-(1-phenylethylidene)aniline in $scCO_2$, resulting in ee of up to 80 % (Scheme 13.3 (1)) [25]. Recently, the monodentate phosphite-type ligands have also been successfully used in the Ir-catalyzed asymmetric hydrogenations of acyclic arylimines in $scCO_2$ (Scheme 13.3 (2)) [26]. High yields (100 % conversion in 50–120 min) and enantioselectivities (up to 95 %) can be obtained under the optimal conditions (4 MPa H_2, 25 MPa total pressure, 45 °C) when **L1** (Scheme 13.1) is used as chiral ligands. It is worth noting that electron-donating or electron-withdrawing groups at the para-position of the N-aryl ring almost have no effect on the enantioselectivity [26].

$ScCO_2$ has also been demonstrated as a benign solvent for the asymmetric homogeneous hydrogenation of carbon–oxygen double bond [27]. A ruthenium complex, i.e., $[RuCl_2(C_6H_6)]_2$-(R)-BINAP derived in situ from the ruthenium source $[RuCl_2(C_6H_6)]_2$ and (R)-BINAP, is successfully found to be active for the

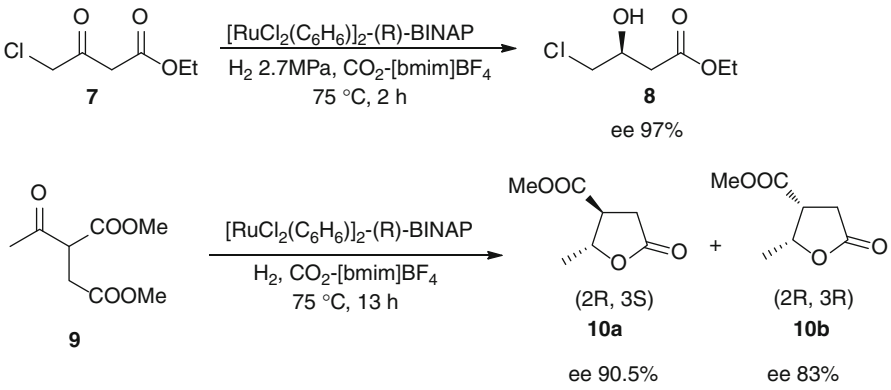

Scheme 13.4 Asymmetric hydrogenation of keto esters by Ru–BINAP catalyst [28]

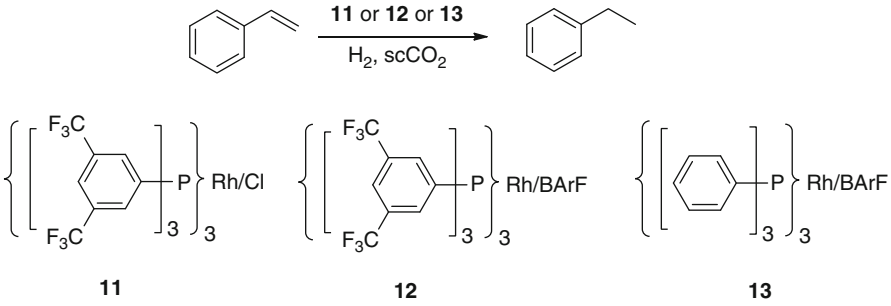

Scheme 13.5 Hydrogenation of styrene catalyzed by fluorinated rhodium–phosphine complexes [32]

asymmetric hydrogenation of ethyl 4-chloro-3-oxobutyrate **7** and dimethyl acetylsuccinate **9** with high enantioselectivity [28]. Interestingly, when the ionic liquid [bmim]BF_4 is added as a polar cosolvent, the hydrogenation enantioselectivity increases accordingly to give the target hydroxy ester **8** and lactones **10** (Scheme 13.4).

13.2.2 Hydrogenation of Styrene

Fluorine groups attached to ligands and fluorinated solvents such as $scCH_2F_2$ can increase the solubility of the catalyst containing fluorinated substituents in $scCO_2$ [29]. $BArF^-$ counterion and CF_3 groups are commonly used in asymmetric hydrogenation reactions with an increasing effect on solubility in the $scCO_2$ [25, 30, 31]. Three different fluorinated rhodium–phosphine complexes, $[P(Ph(CF_3)_2)_3]_3RhCl$ **11**, $[P(Ph(CF_3)_2)_3]_3RhBArF$ **12**, and $[P(Ph)_3]_3RhBArF$ **13**, which are observed to be soluble in $scCO_2$, thus are developed as efficient homogeneous catalysts for the hydrogenation of styrene (Scheme 13.5) [32]. The synthesized Rh-catalyst **12**

Scheme 13.6 Ru-catalyzed hydroboration of styrene derivatives to boronate esters in $scCO_2$ [35]

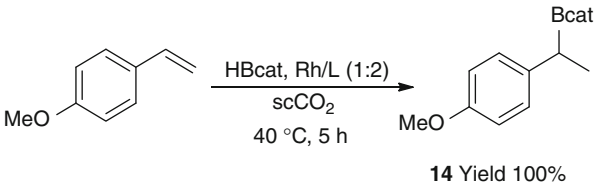

is the most effective catalyst with a conversion of 77.4 %, owing to the electron-withdrawing effect of fluoroalkyl moieties which presumably could have an important impact on the catalytical efficiency.

13.2.3 Hydroboration of Styrene

Boronate esters are one of the most extensively used intermediates in organic synthesis and pharmaceutical chemistry [33, 34]. Tumas and co-workers have demonstrated the first production of boronate esters from hydroboration of styrene derivatives in $scCO_2$ with a rhodium precursor and phosphorus ligands [35]. Incorporation of fluorinated functional groups into phosphine-based ligands can not only boost the solubility of the corresponding metal complexes but also control the stereoelectronic environment of catalysts [36]. Alkylboronate ester **14** is found as the unique product when the cyclohexyl-substituted phosphine $PR_2(OR_F)$ (L/Rh ratio = 2:1) is employed as a ligand, while a mixture of alkylboronate ester isomers are obtained when tetrahydrofuran (THF) is used as solvent instead of $scCO_2$ under the identical conditions (Scheme 13.6).

13.3 Carbonylation

13.3.1 Hydroformylation

Hydroformylation, which is adding one CO and H_2 to a carbon–carbon double bond to produce linear and branched aldehydes containing one more carbon number than the starting olefin, is an important transformation process of significant interest for academia as well as industry. Using $scCO_2$ as a reaction medium for homogeneous hydroformylation and as a means to tune selectivity or activity has received much attention with the potential benefits as applicable to this system as they have been shown to be with hydrogenation.

Rathke et al. have reported the first example of homogeneous hydroformylation in $scCO_2$ with a cobalt carbonyl catalyst (soluble in CO_2 without the need of any modification) by virtue of high-pressure NMR spectroscopy (Scheme 13.7) [37]. Improved yield of linear to branched butyraldehyde products up to 88 % is

Scheme 13.7 Hydroformylation of propylene in $scCO_2$ with $Co_2(CO)_8$ [37]

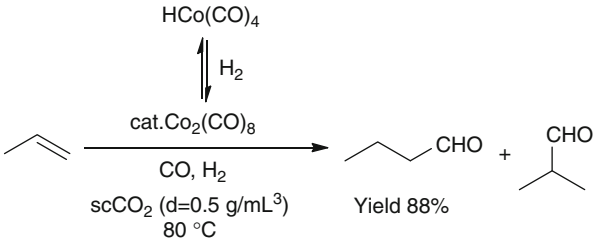

Scheme 13.8 $MnH(CO)_5$-catalyzed hydroformylation of cyclopropene [39]

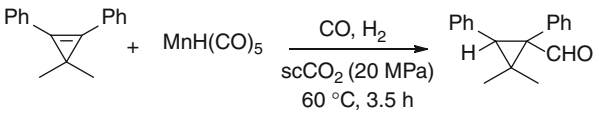

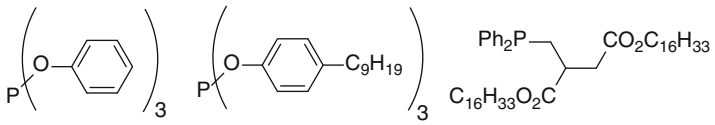

Scheme 13.9 Phosphite ligand for hydroformylation of long chain alkenes [41]

obtained when the hydroformylation proceeds in CO_2 at 80 °C without stirring. The rates of formation of both cobalt intermediate, i.e., $HCo(CO)_4$, and aldehydes are found to be comparable to reactions being performed in conventional nonpolar solvents. Activation energy (23.3 ± 1.4 kcal/mol) in $scCO_2$ is comparable to those measured in conventional organic solvents (27–35 kcal/mol) [38].

Subsequently, hydroformylation of 3,3-dimethyl-1,2-diphenylcyclopropene catalyzed by $MnH(CO)_5$ in $scCO_2$ at 60 °C has been developed by Jessop's group, to produce 66 % of alkane and 34 % of aldehydes, with the same chemoselectivity in hexane and pentane (Scheme 13.8). The aldehydes are primarily formed through nonradical pathways [39].

Simple trialkylphosphines, e.g., PEt_3, which are readily available, give high catalytic activity for the hydroformylation of hex-1-ene in $scCO_2$ [40]. A slight higher normal-to-branched ratio of aldehydes can be obtained taking $[Rh_2(OAc)_4]$ and PEt_3 as catalyst precursors, while a similar rate is obtained in toluene. Furthermore, Sellin and Cole–Hamilton have developed an alternative approach to the hydroformylation of long chain alkenes using insoluble phosphite-modified rhodium catalysts in $scCO_2$ (Scheme 13.9) [41]. Rhodium catalyst prepared in situ from $Rh_2(OAc)_4$ and $P(OPh)_3$ gave reasonable activity and high regioselectivity. The catalyst can be reused several times because the reaction products can be easily removed from the reaction by flushing the reactor with $scCO_2$.

Leitner et al. [29] as well as Erkey et al. [42] have independently investigated hydroformylation of an olefin in $scCO_2$ using fluorinated catalysts in order to enhance the CO_2 philicity and catalytic activity in $scCO_2$. A CO_2-soluble Rh complex **15** with a polyfluoroalkyl-substituted triarylphosphine ligand is developed

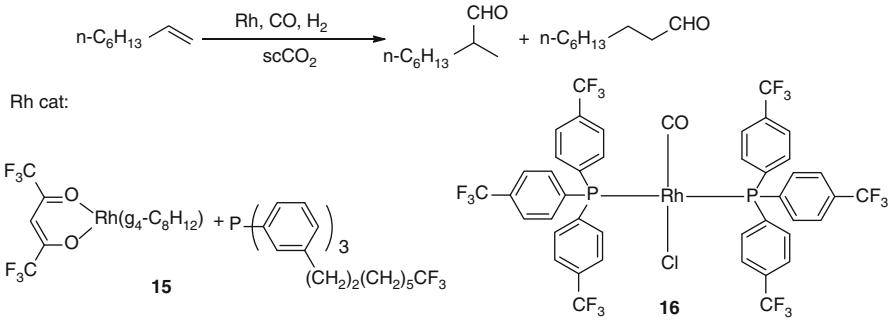

Scheme 13.10 Fluorinated catalysts for hydroformylation [29, 42]

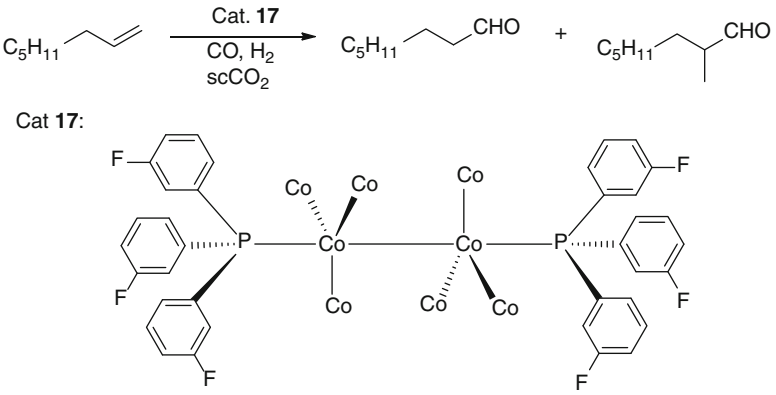

Scheme 13.11 Hydroformylation of 1-octene in $scCO_2$ by complex **17** [43]

for this purpose [29]. Hydroformylation of 1-octene gives a linear aldehyde in a good yield with 82 % selectivity (Scheme 13.10). Side reactions such as hydrogenation or isomerization of the olefin can be effectively suppressed in $scCO_2$. The trans-$RhCl(CO)(P(p\text{-}CF_3C_6H_4)_3)_2$ **16** (Scheme 13.10) with moderate solubility in $scCO_2$ also shows high activity for the hydroformylation of 1-octene. In addition, hydrogenation and isomerization products are insignificant, and the normal-to-branched ratio of 2.4 is acceptable with the complete conversion of 1-octene.

A bi-cobalt complex, i.e., $Co_2(CO)_6[P(3\text{-}FC_6H_4)_3]_2$ **17**, is designed and prepared for the hydroformylation of 1-octene in $scCO_2$ as shown in Scheme 13.11 [43]. Substantial improvement of the selectivity toward aldehyde is reached by using **17** in comparison with $Co_2(CO)_8$. An additional excess of phosphine is unnecessary for the conversion. Complex **17** can be efficiently separated from the reaction mixture because it is insoluble in the cold reaction mixture while completely soluble in the supercritical reaction medium.

Phosphite ligands to form rhodium catalysts give higher reactivity than phosphines [44]. Masdeu-Bultó and co-workers show soluble rhodium–phosphite catalytic systems for hydroformylation of 1-octene in $scCO_2$ [45]. A series of aryl phosphite ligands (**18–21**) are prepared with different donor and steric properties,

Scheme 13.12 Structures of phosphite ligands containing CF_3 group [45]

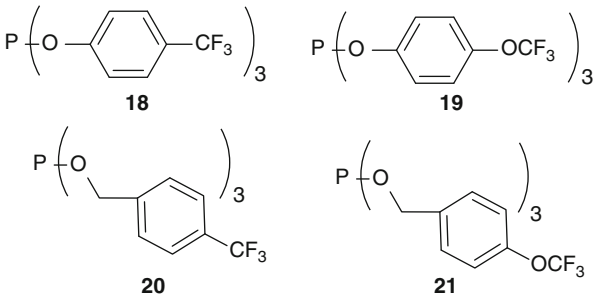

Scheme 13.13 Structures of phosphorus ligands without perfluoroalkyl substituents [46]

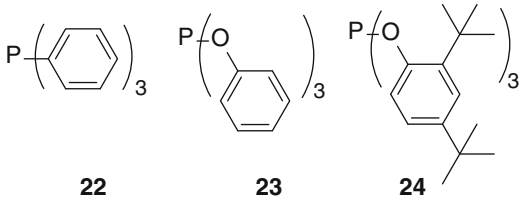

and the introduction of a CF_3 group could increase the π-acceptor ability of the phosphite (Scheme 13.12). High-pressure IR and NMR spectroscopies are used to investigate reactivity of rhodium precursors with these ligands in the presence of CO and H_2, showing that [RhH(CO)(**18**–**21**)$_3$] is formed as the main species in solution. High conversion (up to 93–99 %) for [Rh(acac)$(CO)_2$]/**18**,**19**,**21** is obtained with selectivities up to 94 % for [Rh(acac)$(CO)_2$]/**20** system.

A series of rhodium catalysts modified with phosphorus ligands (**23–24**) without perfluoroalkyl substituents have also been evaluated for the hydroformylation of 1-octene using CO_2 as the solvent (Scheme 13.13) [46]. It is demonstrated that the catalyst derived from **24** is very effective at different CO_2 densities, and an initial turnover frequency (TOF) of 3×10^4 $mol_{aldehyde}mol_{Rh}h^{-1}$ can be obtained.

$ScCO_2$ can also be applied as a reaction medium for asymmetric hydroformylation [47–49]. High enantioselectivity and regioselectivity are achieved in rhodium-catalyzed asymmetric hydroformylation with the perfluoroalkyl-substituted ligand (R,S)-3-H^2F^6-BINAPHOS in compressed CO_2 (Scheme 13.14) [47]. The isomer (R)-**25** is preferentially formed with up to 94 % ee.

Xiao et al. have also examined homogeneous hydroformylation in CO_2 [50, 51]. Fast and regioselective hydroformylation of alkyl acrylates can readily be accomplished in $scCO_2$ via specific solvent–solute interactions [50]. TOF of up to 1,827 h^{-1} is obtained for the formation of aldehyde by using Rh-P(p-$C_6H_4C_6F_{13}$)$_3$ as catalyst in $scCO_2$ while less than 200 h^{-1} in toluene. A fluorous polymeric phosphine could enhance the solubility of aryl phosphine in $scCO_2$ and thus promotes reaction (Scheme 13.15) [51]. Unique chemoselectivities are obtained in the hydroformylation of usually unreactive alkyl acrylates. When equimolar mixture of dec-1-ene and ethyl acrylate is used as substrate, only a TOF of 872 h^{-1} is measured for ethyl acrylate converting into the branched aldehyde, while no product arising from dec-1-ene could be detected.

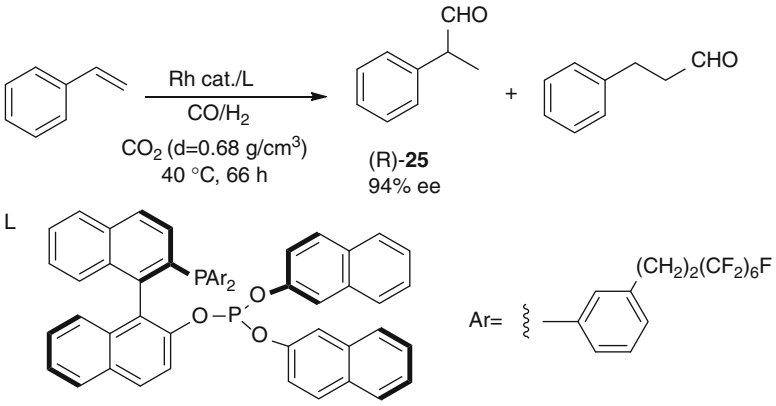

Scheme 13.14 Asymmetric hydroformylation in compressed CO_2 catalyzed by rhodium catalyst [47]

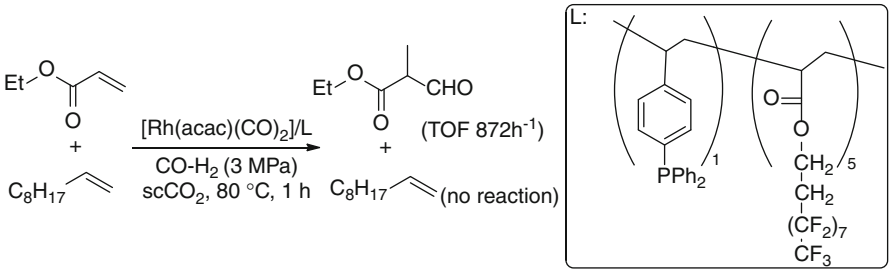

Scheme 13.15 Chemoselective hydroformylation of C═C bonds in $scCO_2$ [51]

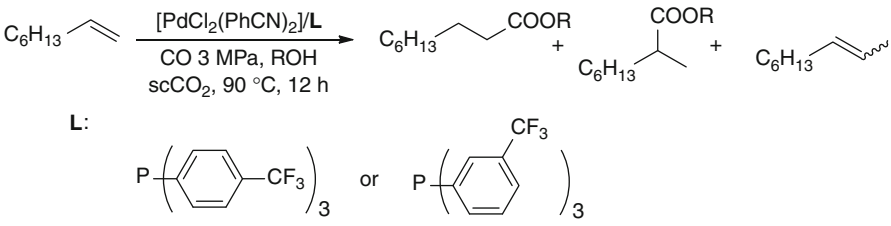

Scheme 13.16 Hydroesterification of oct-1-ene in $scCO_2$ [52]

13.3.2 Hydroesterification

Masdeu-Bultó has presented the first hydroesterification of linear alkenes in $scCO_2$ using palladium catalysts with phosphines containing $–CF_3$ groups (Scheme 13.16) [52]. Conversions up to 67 % with selectivities toward the ester up to 64 % can be obtained by using the catalytic precursor formed from $[PdCl_2(PhCN)_2]$ and phosphine ligands.

13.4 Carbon–Carbon Bond Formation

13.4.1 Diels–Alder Cycloaddition

A mass of literatures exist in relation to Diels–Alder chemistry in supercritical fluids, especially $scCO_2$. In 1987, Paulaitis and Alexander investigated the earliest Diels–Alder reaction of maleic anhydride and isoprene in $scCO_2$ (Scheme 13.17) [53]. Reaction rates are measured over a range of pressures (8–43 MPa) and at three temperatures (35, 45, and 60 °C). At 35 °C, the rate constants obtained in $scCO_2$ (above approximately 20 MPa) are similar to those obtained in liquid ethyl acetate. Ikushima has also studied the Diels–Alder reaction between maleic anhydride and isoprene catalyzed by aluminum chloride in $scCO_2$ [54]. High-pressure FT–IR spectroscopy is used to explore this reaction. A modification to the generally accepted concerted mechanism is proposed that the product is formed in a two-step sequence of sigma bond formation, followed by cyclization as depicted in Scheme 13.18.

Regiochemical course of Diels–Alder reactions in $scCO_2$ and conventional media is also investigated [55]. On analysis of the total reaction mixture, no deviation from the normal selectivity is observed when performing the reaction under single-phase conditions (50 °C, 9.5 MPa), and similar selectivity is observed in $scCO_2$ and toluene (Scheme 13.19).

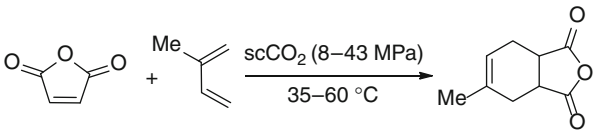

Scheme 13.17 Diels–Alder reaction of maleic anhydride and isoprene in $scCO_2$ [53]

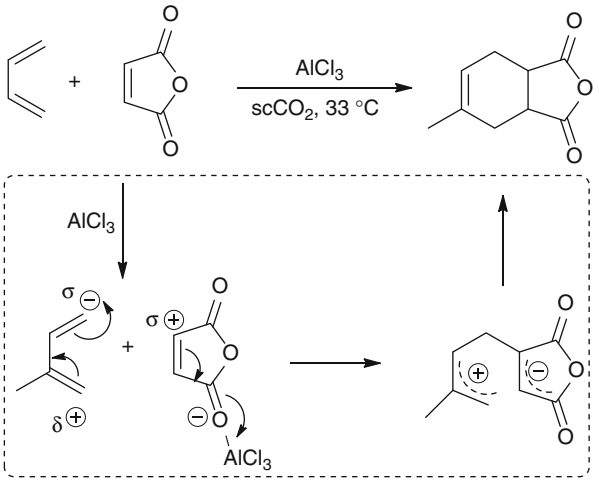

Scheme 13.18 A two-step mechanism for the Diels–Alder reaction in $scCO_2$ [54]

Scheme 13.19 Regioselectivity of Diels–Alder reactions in $scCO_2$ [55]

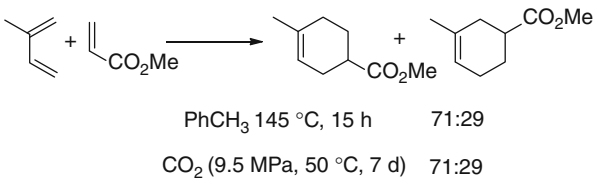

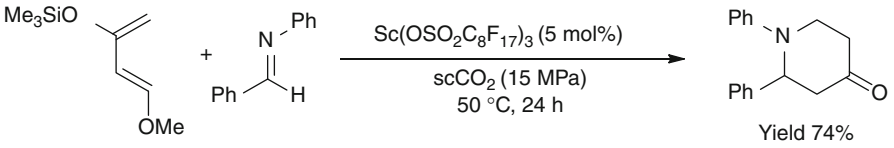

Scheme 13.20 Lewis acid-catalyzed aza-Diels–Alder reactions in $scCO_2$ [57]

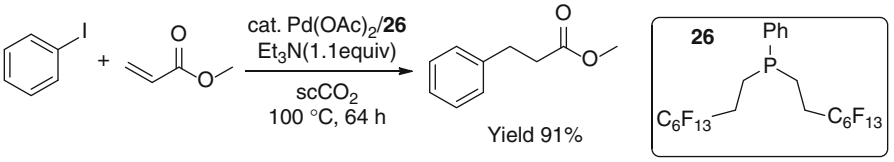

Scheme 13.21 Palladium-catalyzed carbon–carbon bond formation in $scCO_2$ [58]

The deficient rates and selectivities of the uncatalyzed Diels–Alder reaction limit its synthetic value. In this context, Rayner and co-workers have developed the Lewis acid-catalyzed Diels–Alder system by $Sc(OTf)_3$ [56]. Quantitative conversion can be achieved with a catalyst loading of 6.5 mol% at 50 °C, within 15 h, whereas the uncatalyzed reaction gives only 10 % complete after 24 h under similar conditions. $Sc(OSO_2C_8F_{17})_3$ can also be used as Lewis acid catalyst for Diels–Alder reaction and aza-Diels–Alder reaction in $scCO_2$ [57]. 99 % Yield of the aza-Diels–Alder reaction of Danishefsky's diene and imine is obtained with catalyst loading of 5 mol% employed (Scheme 13.20).

13.4.2 Coupling Reaction

Palladium-catalyzed coupling reactions in $scCO_2$ have received much attention. In 1988, Holmes et al. as well as Tumas et al. have independently developed the palladium-catalyzed carbon–carbon coupling reactions in $scCO_2$ [58, 59]. The solubility of the palladium complexes can be dramatically enhanced by introducing fluorinated phosphine ligand **26**. In this regard, the Heck reaction between iodobenzene and electron-deficient alkenes catalyzed by soluble palladium complexes in $scCO_2$ gives a superior yield (up to 92 %) than that reported in conventional solvents (Scheme 13.21). The workup procedures are significantly easier than

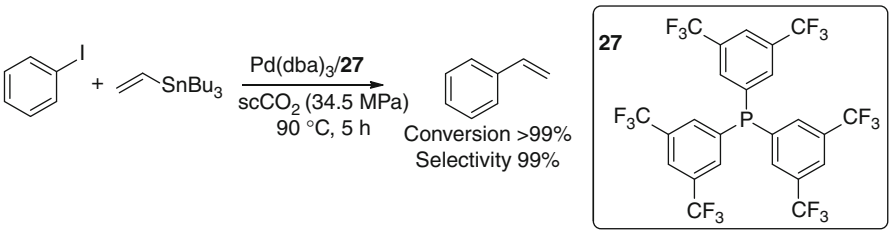

Scheme 13.22 Stille cross-coupling reaction in $scCO_2$ [59]

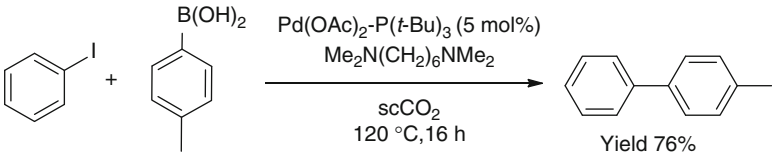

Scheme 13.23 Non-fluorous system for coupling reaction in $scCO_2$ [61]

those associated with standard reaction conditions because the extraction of the product with an organic solvent is no longer needed. Tumas has found that fluorinated phosphines, particularly tris[3,5-bis(trifluoromethyl)phenyl]phosphine **27**, show good activity (86 % conversion) and a quantitative conversion (>99 %) for Stille cross-coupling reaction between iodobenzene and vinyl(tributyl)tin in $scCO_2$ (Scheme 13.22).

The nature of the initial palladium source is also crucial. In this context, fluorinated palladium sources such as $Pd(OCOCF_3)_2$ and $Pd(F_6\text{-acac})_2$ are superior catalyst in comparison with the non-fluorinated sources such as $Pd(OCOCH_3)_2$ and $Pd_2(dba)_3$ for carrying out a variety of the palladium-catalyzed coupling reactions in $scCO_2$ with lower catalyst loadings and in shorter reaction times [60]. Although some phosphine ligands are usually considered to be inferior ligands for coupling reactions, they also give pleased conversions under this catalytic system. While the completely non-fluorous $Pd(OAc)_2$–$P(t\text{-}Bu)_3$ catalyst system is also highly active to promote Heck and Suzuki reactions in $scCO_2$ (Scheme 13.23) [61].

Recently, a convenient procedure for the Suzuki–Miyaura cross-coupling has been developed in $scCO_2$ [62]. The catalyst system is composed of $Pd(OCOCF_3)_2$, Buchwald phosphine ligand, cheap inorganic base such as potassium carbonate, and a crown ether, giving high yields of the corresponding cross-coupling products. Markedly, three or even four chlorine atoms in 1,2,4,5-tetrachlorobenzene are replaced by phenyl groups through treatment with phenylboronic acid (5 equiv.) in $scCO_2$ in the presence of the developed catalytic system (Scheme 13.24).

Taking a different process, Pd(II) complexes **28** containing various fused bicyclic oxadiazoline and tricyclic ketoimine ligands are described as highly efficient system in the Suzuki–Miyaura reaction in $scCO_2$ [63]. Quantitative cross-coupling yields are obtained of the aryl halides with phenylboronic acid in short reaction times (1 h) and very low catalyst loadings (2.5×10^{-5} mmol) as shown in Scheme 13.25.

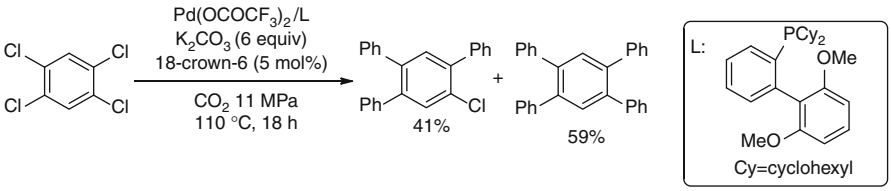

Scheme 13.24 Suzuki–Miyaura cross-coupling of tetrachloroarenes in $scCO_2$ [62]

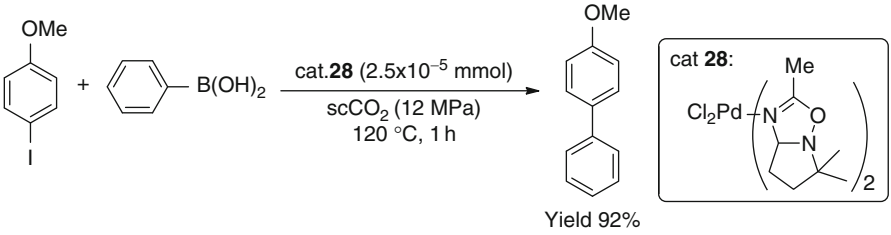

Scheme 13.25 A Pd(II) complex with bicyclic oxadiazoline for Suzuki–Miyaura reaction [63]

13.4.3 Olefin Metathesis

Supercritical fluids are also useful reaction media for the olefin metathesis which refers to the mutual alkylidene exchange reaction of alkenes [64, 65]. Transition metal-catalyzed olefin metathesis reactions in compressed CO_2 media have been developed by Leitner and co-workers [66]. Ring-opening metathesis polymerization (ROMP) of norbornene and cyclooctene gives the corresponding polymer in excellent yields by using the conventional metathesis catalysts **29** and **30** (Scheme 13.26), both in liquid CO_2 and $scCO_2$. This methodology for ring-closing metathesis (RCM) is also remarkable by using the same carbene complexes. A remarkable influence of the density of the supercritical medium on the product of RCM of **31** is observed with the 16-membered ring **32** being formed in excellent yield at CO_2 density of 0.65 $g \cdot ml^{-1}$, oligomers are obtained by acyclic diene metathesis (ADMET) at lower CO_2 density ($d < 0.65\ g \cdot ml^{-1}$) as depicted in Scheme 13.26.

Another remarkable feature is increasing the scope of this versatile transformation and applying $scCO_2$ as a protective medium. The epilachnene **34** has been synthesized by RCM of diene **33** without the need for N-protection (Scheme 13.27) [67].

13.4.4 Aldol Reaction

Ikariya has disclosed the first catalytic asymmetric Mukaiyama aldol reaction by a chiral binaphthol–titanium(IV) catalyst in $scCO_2$, although, giving a very low yield

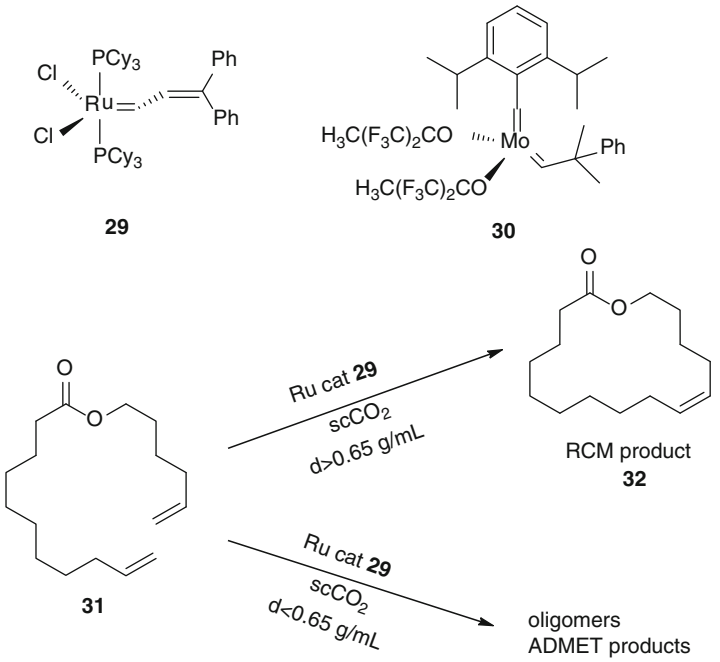

Scheme 13.26 Ring-closing metathesis catalyzed by carbene complexes in $scCO_2$ [66]

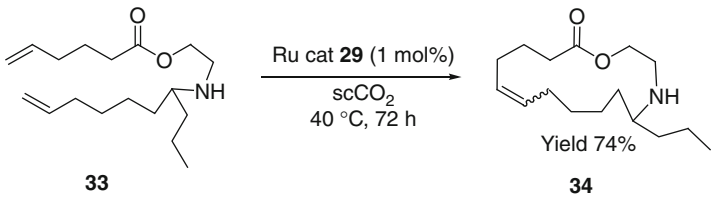

Scheme 13.27 Synthesized epilachnene **34** by RCM of diene **33** in $scCO_2$ [67]

of the aldol product [68]. Poly(ethylene glycol) (PEG) derivatives have remarkable effect on Mannich and aldol reactions in $scCO_2$ [69, 70]. It is envisaged that utilization of PEG as surfactants media can accelerate the reactions by forming emulsions in a single $scCO_2$ phase. Indeed, PEG_{400} is found to be effective in the $Yb(OTf)_3$-catalyzed Mannich reactions of imine with silyl enolate, giving rise to 72 % yield of product, while only 10 % yield of the product is obtained without PEG (Scheme 13.28). In the case of the $Sc(OTf)_3$-catalyzed aldol reactions of silyl enolates with aldehydes, the poly(ethylene glycol) dimethyl ether ($PEG(OMe)_2$, average Mw = 500) is more efficient than PEG itself (Scheme 13.29).

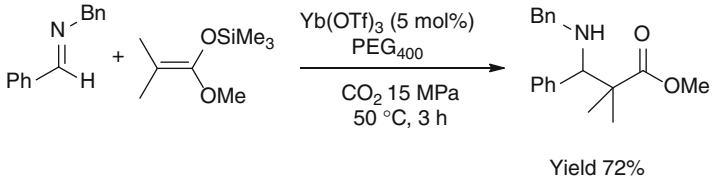

Scheme 13.28 Mannich reaction catalyzed by $Yb(OTf)_3$ in $scCO_2$ [69]

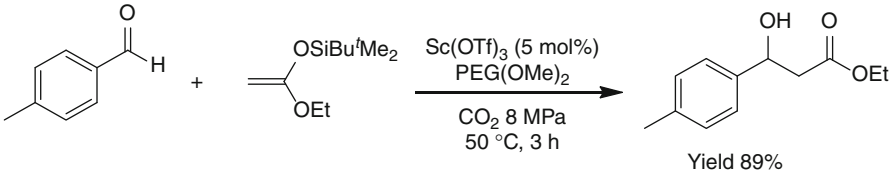

Scheme 13.29 Aldol reaction in CO_2–$PEG(OMe)_2$ system [69]

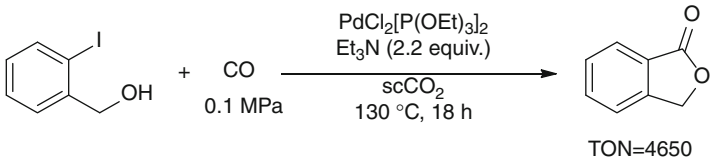

Scheme 13.30 Pd complex-catalyzed intramolecular carbonylation in $scCO_2$ [71]

13.4.5 Miscellaneous Reactions

Pd complexes with non-fluorous ligands have been developed as catalyst for the intramolecular carbonylation reactions of aryl halides in $scCO_2$ [71]. Turnover number (TON) of 1,880 is obtained when $PdCl_2(MeCN)_2$ is used as a catalyst in $scCO_2$ for the intramolecular carbonylation of 2-iodobenzyl alcohol. No marked effect of CO pressure on the TON values is observed in $scCO_2$, because of the higher diffusivity of $scCO_2$ as well as the high solubility of CO in this medium. Near completion (TON = 4,650) of the carbonylation can be reached even proceeding at low CO pressure (0.1 MPa) with the more soluble triethylphosphite as a ligand (Scheme 13.30). The rate of the intramolecular carbonylation reaction is found to be higher than that in toluene.

The Pauson–Khand reaction, the catalytic co-cyclization of an alkyne with an alkene and CO, leading to cyclopentanone, has been recognized as one of the most optimal routes to the synthesis of cyclopentenones [72, 73]. Jeong et al. have reported several examples of the intramolecular Pauson–Khand reaction catalyzed by $Co_2(CO)_8$ in $scCO_2$ [74]. Reaction of the intramolecular enynes and CO is optimized to give 85 % yield of cyclopentanones with 2.5 mmol% catalyst loading under a total pressure of 18 MPa (Scheme 13.31). The reaction also proceeds pretty

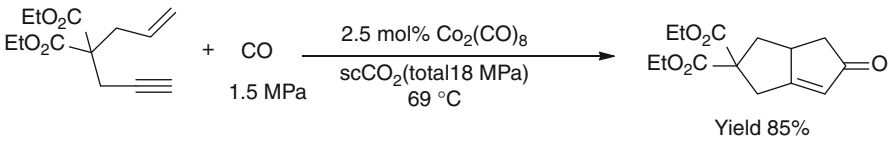

Scheme 13.31 Intramolecular Pauson–Khand reaction in $scCO_2$ [74]

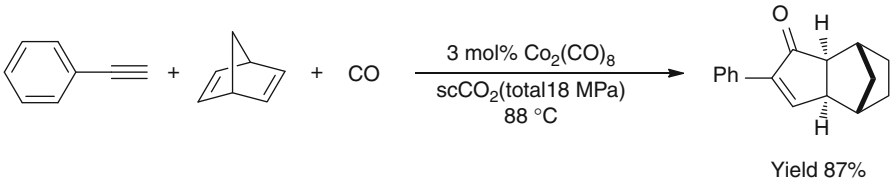

Scheme 13.32 Intermolecular Pauson–Khand reaction in $scCO_2$ [74]

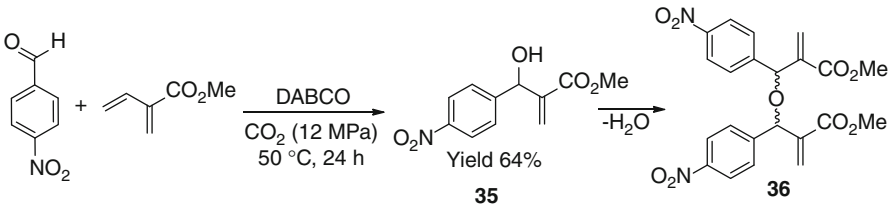

Scheme 13.33 DABCO catalyzed the Baylis–Hillman reaction in $scCO_2$ [77]

for a number of substituted enynes. Intermolecular coupling reaction between phenyl acetylene and norbornadiene also runs well, giving the bicyclic compound in 87 % yield (Scheme 13.32).

The Baylis–Hillman reaction is considered to be the useful carbon–carbon bond forming reaction between activated alkenes and aldehydes, introducing a hydroxyalkyl moiety at the α-position of Michael acceptors [75, 76]. The reaction between acrylate and a variety of aromatic aldehydes can be efficiently carried out in $scCO_2$ by using DABCO (1,4-diazabicyclo[2.2.2]octane) as a catalyst [77]. Enhanced reaction rates comparable to the solution-phase reactions are observed under this catalyst system. It is noted that an unprecedented dimerization **36** is observed as dimers of the original Baylis–Hillman adducts **35** at low pressure (Scheme 13.33).

Palladium-catalyzed cyclotrimerization of different substituted alkynes occurs smoothly in good yield and regioselectivity in $scCO_2$ (Scheme 13.34) [78]. $CuCl_2$, as a co-catalyst, could play an important role in enhancing the reaction rate and regenerating the active $PdCl_2$. Addition of methanol can increase the solubility of $PdCl_2$ and $CuCl_2$ in $scCO_2$. Also, environmentally friendly $scCO_2$ may be a substitute for toxic organic solvents and show potential utility in industry. $CpCo(CO)_2$ also has been reported as a catalyst for the cyclotrimerization of monosubstituted and disubstituted alkynes in $scCO_2$ [79].

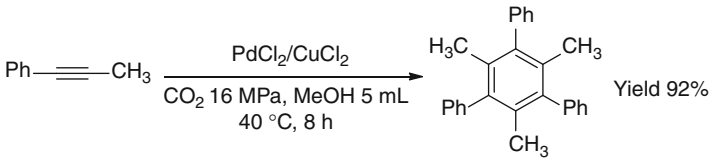

Scheme 13.34 Palladium-catalyzed cyclotrimerization in $scCO_2$ [78]

13.5 Oxidation Reaction

Since CO_2 is the highest oxidation state of carbon, its further oxidation will not proceed. Therefore, by-products originating from CO_2 can be depressed by using compressed CO_2 as reaction media. On the other hand, compressed CO_2 provides a safe reaction environment for reactions due to its excellent mass and heat transfer properties. Dense CO_2 appears to be a unique solvent for oxidation reactions [80, 81]. Moreover, the high miscibility of the oxidants, especially gaseous O_2, in $scCO_2$ also can eliminate interphase transport limitations [5, 82].

13.5.1 Oxidation Reaction of Alcohols

Selective aerobic oxidation of alcohols to aldehydes or ketones has been widely studied not only in conventional liquid solvents but also in $scCO_2$. The key to achieve high selectivity of aldehydes is to suppress the formation of carboxylic acid, which can further react with reactant alcohols to yield esters, leading to a further decline of the aldehyde selectivity [10].

The copper-based catalyst with a small amount of cosolvent (toluene or fluorobenzene) is successfully developed for the oxidation of cyclohexanol to cyclohexanone in compressed CO_2 [83]. The results indicate that the selectivity of the reaction in compressed CO_2 with or without cosolvent is much higher than that in the liquid solvents or without solvent (Table 13.1). Cosolvent could enhance the reaction rate by the means of tuning the properties of $scCO_2$ and the kinetic and thermodynamic properties of reactions.

The copper acetate complex **38**, i.e., the polydimethylsiloxane-functionalized pyridine **37**, is developed for the aerobic oxidation of alcohols to the corresponding aldehydes in $scCO_2$ as depicted in Scheme 13.35 [84]. In combination with 2,2,6,6-tetramethylpiperidin-1-yloxy (TEMPO) as co-catalyst, complete conversion of 4-nitrobenzyl alcohol could be achieved at 15 MPa CO_2, 1 MPa O_2, and 60 °C within 4 h (Scheme 13.36). However, the analogous copper derivatives containing simpler pyridine substituents, $[Cu(AcO)_2(py)]_2$ and $[Cu(AcO)_2(4VP)]_2$ (4VP = 4-vinylpyridine), show similar activities in spite of the negligible solubility in $scCO_2$. In addition, the solubility of the metal complex is unnecessary for the oxidation of alcohols.

Table 13.1 Solvent effect on the aerobic oxidation of cyclohexanol

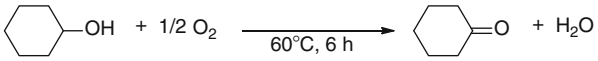

Solvent	Conversion of alcohol (%)	Selectivity of product (%)
No solvent	19.8	70.6
Toluene	33.4	77.9
Fluorobenzene	26.5	75.2
CO_2[a]	7.51	98.9
CO_2[a,b]	30.0	89.4
CO_2+toluene[a,c]	18.6	97.3

[a]Apparent density, 0.77 g/mL
[b]Reaction time, 36 h
[c]The amount of cosolvent in CO_2 is 0.5 mol%

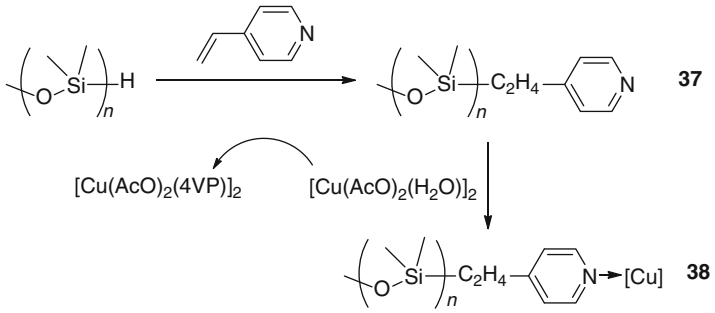

Scheme 13.35 Synthesis of compounds **37** and **38** [84]

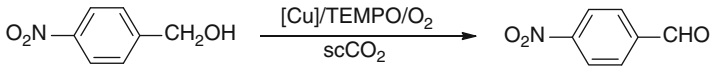

Scheme 13.36 Alcohol oxidation catalyzed by Cu-TEMPO [84]

13.5.2 CO_2 as a Soft Oxidant for the Oxidation of Aldehydes

The utilization of CO_2 as a soft oxidant is a promising concept for industrial applications, such as the oxidative coupling of CH_4 and the oxidative dehydrogenation of alkanes and alkyl aromatics [85]. On the other hand, aromatic aldehydes can also be oxidized to the corresponding carboxylic acids under mild conditions using CO_2 as a soft oxidant.

The catalytic oxidation of aromatic aldehydes under mild conditions is developed by using CO_2 as oxidant and N-heterocyclic carbenes (NHCs) as organocatalysts (Scheme 13.37) [86]. Under the optimized conditions, various aldehydes are oxidized to corresponding acids with 10 mol% 1,3-dimesitylimidazol-2-ylidene (IMes) as organocatalyst at room temperature.

Scheme 13.37 Aldehyde oxidation reaction with CO_2 catalyzed by NHC [86]

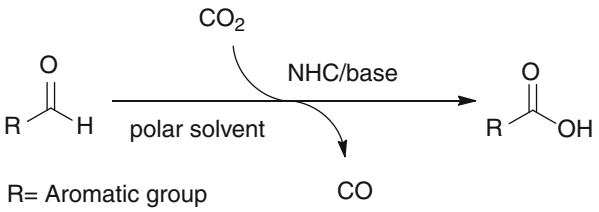

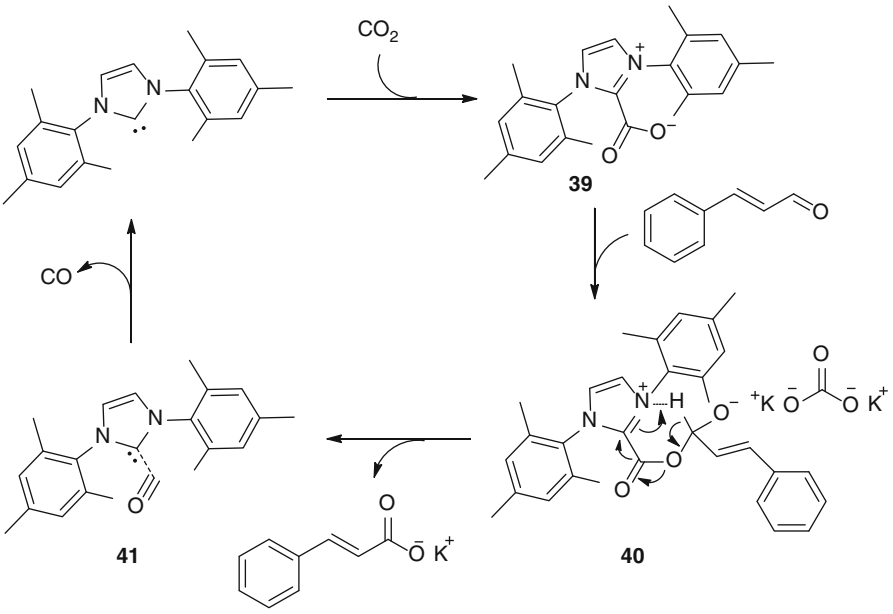

Scheme 13.38 Catalytic cycle in oxidation of cinnamaldehyde by NHC [86]

The mechanism of direct activation of CO_2 by the NHC is proposed as depicted in Scheme 13.38. Firstly, NHC reacts with CO_2 resulting in imidazolium carboxylate **39**, which attacks the 2-position of cinnamaldehyde, generating the possible intermediate **40**. And then, the hydrogen from the 2-position carbon on cinnamaldehyde is trapped by the nitrogen on imidazolium carboxylate, forming a stable six-membered ring intermediate. Finally, CO is released from NHC–CO complex **41**, and NHC is reused for the next cycle.

NHC-mediated oxidation of aldehydes could also proceed via the addition of CO_2 to the readily formed Breslow intermediate as illuminated in Scheme 13.39 [87]. The reaction implements via the addition of CO_2 to the readily formed Breslow intermediate **42** to form the hydroxycarboxylate **43** and the tautomer **44**, which could lose CO and hydroxide to afford the benzoic acid as depicted in Scheme 13.40.

Support for this hypothesis is obtained by the detection of CO in the reaction mixture. Indirect evidence for the mechanistic postulate outlined above is accrued by the formation of benzoic acid when phenylglyoxylic acid is exposed to NHC

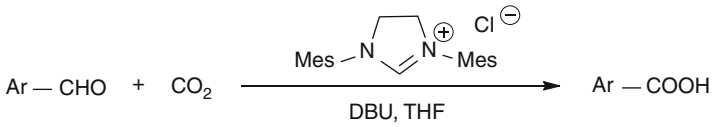

Scheme 13.39 Oxidation of aromatic aldehydes to carboxylic acids with CO_2 [87]

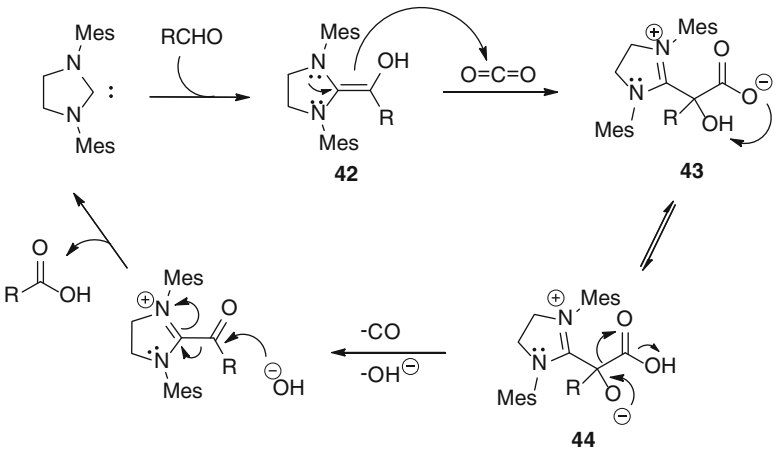

Scheme 13.40 Proposed mechanistic pathway for the oxidation of aldehydes through Breslow intermediate [87]

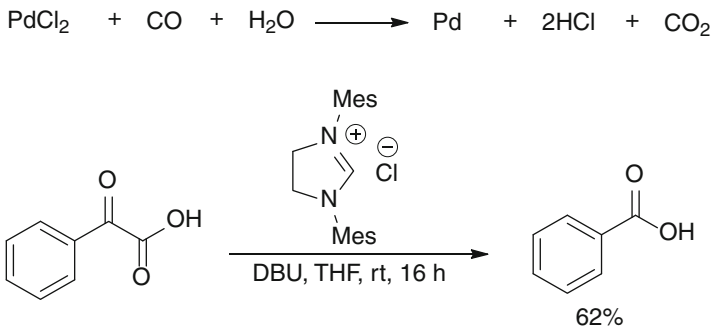

Scheme 13.41 Evidence for NHC-mediated oxidation of aldehydes [87]

under the same experimental conditions in which benzaldehyde is transformed to benzoic acid as illustrated in Scheme 13.41.

However, there is debate about the oxidation ability of CO_2 for the transformation of cinnamic aldehydes to acids catalyzed by NHCs. A study on NHC-catalyzed oxidation of aldehydes by using CO_2 as the stoichiometric oxidant is conducted,

Scheme 13.42 Oxidation of cyclohexane catalyzed by [Fe(TPP)Cl] in $scCO_2$ [90]

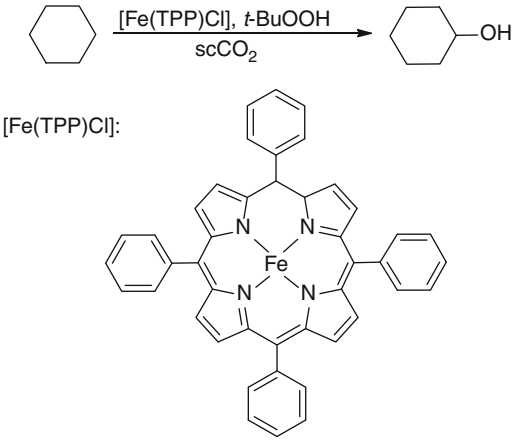

concluding that the apparent NHC-catalyzed oxidation of aldehydes with CO_2 actually involves air as the stoichiometric oxidant [88]. Series of computational and experimental investigation on the role of CO_2 in NHC-catalyzed oxidation of aldehydes is also carried out, indicating that this reaction could not be performed at room temperature and without the assistance of H_2O [89].

13.5.3 Oxidation Reaction of Hydrocarbons

Oxidation of cyclohexane could be achieved in $scCO_2$ catalyzed by iron tetraphenylporphyrin ([Fe(TPP)Cl]) with *tert*-butyl-hydroperoxide (*t*-BuOOH) as terminal oxidants (Scheme 13.42) [90]. CO_2 density is an important variable for the selectivity in the oxidation process. The selectivity is higher in $scCO_2$ than that in organic solvents with up to 15 % yield of cyclohexanol.

The aerobic oxidation of cyclohexene could be achieved by Fe(III)(5,10,15,20-tetrakis(pentafluorophenyl)porphyrin)Cl catalyzed at 50 °C, 16.5 MPa of the total pressure with 2 MPa O_2 partial pressure [91]. The reaction is retarded in the presence of the radical inhibitor 2,6-di-*tert*-butyl-4-methylphenol, suggesting that the product is formed through free radical allylic oxidation mechanism.

13.5.4 Oxidation Reaction of Olefins

An alternative product of oxidation of olefins in CO_2 medium is epoxide. Cyclohexene is epoxidized to 1,2-cyclohexene oxide and 1,2-cyclohexanediol by using $scCO_2$ as both solvent and reactant in combination with aqueous H_2O_2, which is made possible through the in situ formation of peroxycarbonic acid [92]. By adding $NaHCO_3$ and the hydrophilic cosolvent N, N-dimethylformamide (DMF), cyclohexene conversion is increased from 0.4 to 12.6 mol%.

Scheme 13.43 The proposed mechanism for the Wacker reaction in ROH/$scCO_2$ [93]

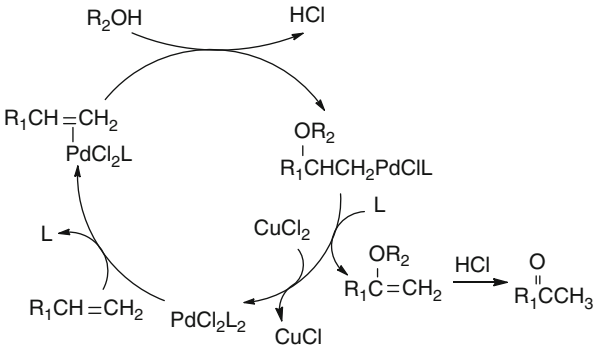

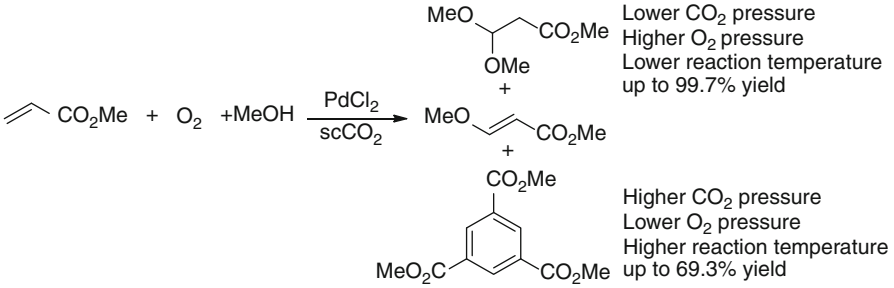

Scheme 13.44 $PdCl_2$-catalyzed aerobic oxidation of terminal alkenes with methanol in $scCO_2$ [94]

Wacker reaction is one of the most important reactions for the functionalization of alkene feedstock. The Wacker reaction could be carried out smoothly in $scCO_2$ or ROH/$scCO_2$ [93]. In order to increase the solubility of catalysts and accelerate the reaction rate, a suitable amount of MeOH/EtOH is added to modify the solvent polarity of $scCO_2$. The reaction in $scCO_2$ or MeOH/$scCO_2$ is homogeneous since organopalladium complexes are formed during the oxidative process as illuminated in Scheme 13.43.

Acetalization of terminal alkenes with alcohols, which undergo a Wacker-type process, is another important reaction for the functionalization of alkene feedstock. The $PdCl_2$-catalyzed aerobic oxidation of terminal alkenes with electron-withdrawing groups is performed in $scCO_2$ (Scheme 13.44). The $PdCl_2$-catalyzed aerobic oxidation of terminal alkenes with electron-withdrawing groups runs in $scCO_2$ through optimizing reaction conditions, to yield acetals and benzene derivatives (Scheme 13.44) [94]. Higher CO_2 pressure, lower O_2 pressure, and higher reaction temperature could favor the formation of the trisubstituted benzene, whereas the opposite tendency is observed for the generation of the dimethoxy adduct.

13.5.5 Baeyer–Villiger Reaction

The Baeyer–Villiger oxidation of ketones into esters or lactones is one of the most widely applied transformations in organic synthesis [95]. The aerobic Baeyer–Villiger oxidation can be performed very efficiently in compressed CO_2 at room temperature using oxygen as primary oxidant and an aldehyde as co-reductant [96]. No additional catalyst is required, and good to excellent yields are achieved for a wide range of cyclic and acyclic ketones.

13.6 Polymerization

13.6.1 Free Radical Polymerization in $ScCO_2$

Supercritical fluids can also provide insight into the general roles that solvents play in polymerization reactions. In 1992, the successful synthesis of high molar mass fluoropolymers was covered by using homogeneous free radical polymerization methods in $scCO_2$ [97]. Azobisisobutyronitrile (AIBN) is found to be a more efficient radical generator in $scCO_2$ than in benzene while with a slower decomposition rate, due to the absence of a cage effect in the low viscosity of CO_2. The perfluoropolymer **46** made in $scCO_2$ (59.4 °C, 207 bar) through the homopolymerization of 1,1-dihydroperfluorooctyl acrylate (FOA) **45** has a molar weight of 270,000 g · mol^{-1} with 65 % yield (Scheme 13.45).

13.6.2 Cationic Polymerization in $ScCO_2$

The choice of solvent plays an important role in controlling the course of cationic polymerizations. The utilization of liquid and supercritical CO_2 can perform as a solvent-dispersing medium for the cationic polymerization of vinyl ethers and oxetanes [98]. Interestingly, polymerization of the hydrocarbon vinyl ether **47** catalyzed by $EtAlCl_2$ and initiated by isobutyl vinyl ether adduct **50** is initially homogenous in $scCO_2$ and then becomes heterogeneous as the polymer **49**

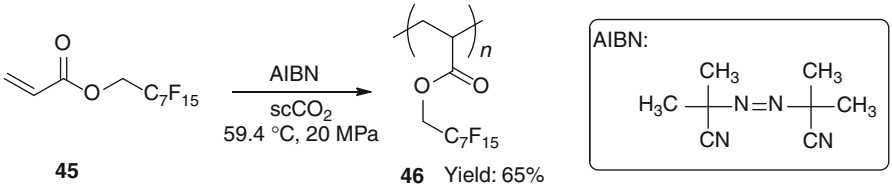

45 46 Yield: 65%

Scheme 13.45 Homopolymerization of 1,1-dihydroperfluorooctyl acrylate in $scCO_2$ [97]

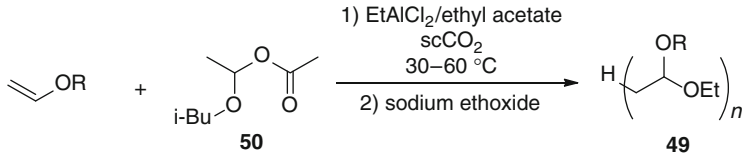

Scheme 13.46 Polymerization of vinyl ethers $EtAlCl_2$ in $scCO_2$ [98]

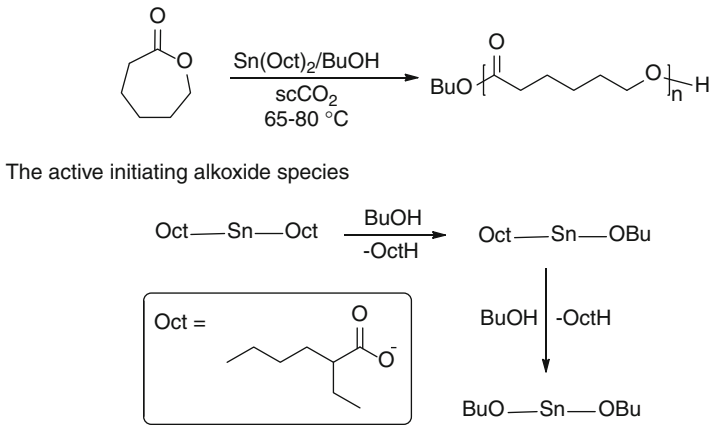

Scheme 13.47 $Sn(Oct)_2$-catalyzed ring-opening polymerization of ε-CL in $scCO_2$ [100]

forms and precipitates (Scheme 13.46). Polymers with high molar mass and broad molecular weight distributions are obtained in the absence of initiator **50**. Fluorocarbon-based alkyl vinyl ether **48** in the absence of initiator **50** is also polymerized in CO_2, and the polymerization remains homogeneous throughout the course of the reaction with a narrow molecular weight distribution.

13.6.3 Metal-Catalyzed Polymerization in $ScCO_2$

Ring-opening polymerization (ROP) is one of the most facile routes to obtain a number of linear aliphatic polyesters [99]. The ROP of ε-caprolactone (ε-CL) catalyzed by the industrially important catalyst $Sn(Oct)_2$ has been developed in $scCO_2$ [100]. The active initiating alkoxide species in the polymerization is a tin alkoxide species formed by $Sn(Oct)_2$ and an alcohol as illustrated in Scheme 13.47. The molecular weight of the product is controlled by the ratio of monomer to initiator, i.e., the [CL]/[BuOH] ratio, and increasing the ratio leads to an increase in molecular weight. Increasing the temperature results in an increase in the rate of

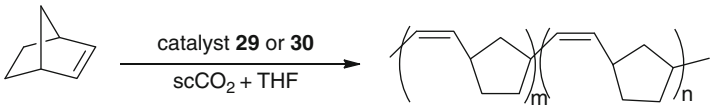

Scheme 13.48 ROMP of norbornene by metal carbene catalysts in $scCO_2$ [102]

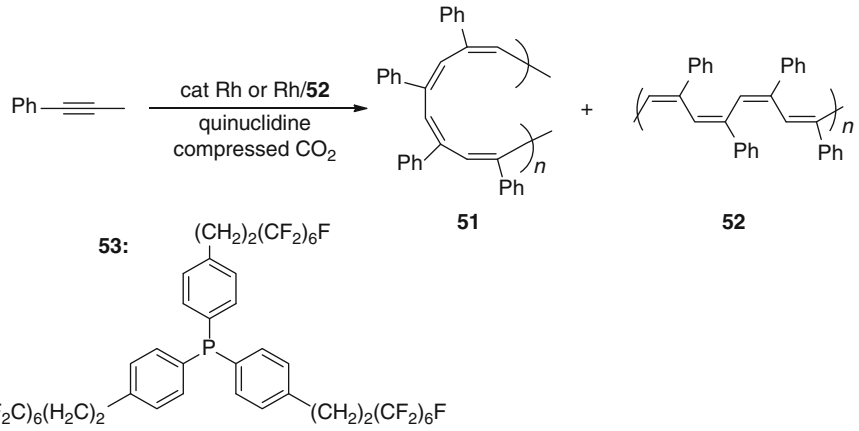

Scheme 13.49 Rh-catalyzed phenylacetylene polymerization in compressed CO_2 [103]

polymerization, while increasing the initial pressure of the reaction medium has the opposite effect and leads to a decrease in rate. The rate of ROP is generally slower in $scCO_2$ compared to bulk or solution polymerization conducted in toluene.

$Ru(H_2O)_6(Tos)_2$ has been reported as a catalyst for the ring-opened metathesis polymers (ROMP) of norbornene in liquid CO_2, leading to formation of high *cis*, syndiotactic poly(norbornene) [101]. Notably, the former polymers of bulk monomer in pure CO_2 are more *cis* stereospecific than those in methanol or CO_2/methanol and have a blocky distribution of *cis* and *trans* double bonds. Subsequently, the metal carbene catalysts (**29** and **30**, Scheme 13.26) have been developed for the ROMP of norbornene in $scCO_2$ (Scheme 13.48) [102]. Polynorbornenes prepared in $scCO_2$ are similar to that made in the THF in molecular weight, molecular weight distribution, and thermal stability. Neither the reaction temperature nor pressure makes significant differences in the trans/cis ratio of the polynorbornenes obtained in $scCO_2$, while higher temperature gives higher molecular weights.

The polymerization of phenylacetylene catalyzed by rhodium complex also has been performed in compressed CO_2 [103]. The unmodified catalyst, (norborna-2,5-diene)rhodium acetylacetanoate [Rh(nbd)(acac)], is insoluble in compressed CO_2. However, the polymerization in CO_2 proceeds more efficiently than that in conventional solvents such as THF or hexane, resulting in the *cis-cisoidal* product **51** in a 65 % yield. Using the fluorinated phosphine $[4\text{-}F(CF_2)_6(CH_2)_2C_6H_4]_3P$ **53**, modified rhodium catalyst gives rise to an increase in selectivity toward the *cis-transoidal* polymer **52** as shown in Scheme 13.49.

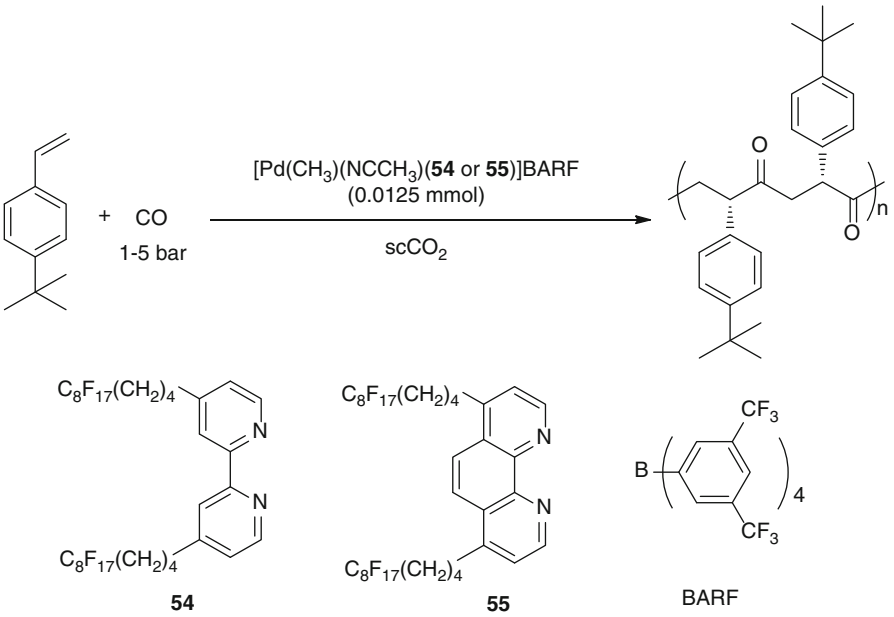

Scheme 13.50 CO/*tert*-butylstyrene copolymerization by palladium cationic complexes in $scCO_2$ [104]

Polyketone has been formed from the copolymerization of CO and *tert*-butylstyrene in $scCO_2$ as a reaction medium, avoiding the use of classical organic or fluorinated solvents as illustrated in Scheme 13.50 [104]. Palladium cationic complexes of general formula $[Pd(CH_3)(NCCH_3)(L)]BARF$ containing mono-chelated bipyridine **54** or phenanthroline ligands **55** with perfluorinated chains are used as catalysts in $scCO_2$ for this kind of copolymerization and give rise to the polyketone of highly syndiotactic and controllable molecular weights.

References

1. Welton T (1999) Room-temperature ionic liquids. Solvents for synthesis and catalysis. Chem Rev 99(8):2071–2084
2. Lindström UM (2002) Stereoselective organic reactions in water. Chem Rev 102 (8):2751–2772
3. Singh MS, Chowdhury S (2012) Recent developments in solvent-free multicomponent reactions: a perfect synergy for eco-compatible organic synthesis. RSC Adv 2 (11):4547–4592
4. Jessop PG, Ikariya T, Noyori R (1995) Homogeneous catalysis in supercritical fluids. Science 269(5227):1065–1069
5. Jessop PG, Ikariya T, Noyori R (1999) Homogeneous catalysis in supercritical fluids. Chem Rev 99(2):475–494

6. Beckman EJ (2004) Supercritical and near-critical CO_2 in green chemical synthesis and processing. J Supercrit Fluids 28(2–3):121–191
7. Jessop PG (2006) Homogeneous catalysis using supercritical fluids: recent trends and systems studied. J Supercrit Fluids 38(2):211–231
8. Page SH, Goates SR, Lee ML (1991) Methanol/CO_2 phase behavior in supercritical fluid chromatography and extraction. J Supercrit Fluids 4(2):109–117
9. Woods HM, Silva MMCG, Nouvel C et al (2004) Materials processing in supercritical carbon dioxide: surfactants, polymers and biomaterials. J Mater Chem 14(11):1663–1678
10. Seki T, Baiker A (2009) Catalytic oxidations in dense carbon dioxide. Chem Rev 109(6):2409–2454
11. Darr JA, Poliakoff M (1999) New directions in inorganic and metal-organic coordination chemistry in supercritical fluids. Chem Rev 99(2):495–542
12. Beckman EJ (2003) Green chemical processing using CO_2. Ind Eng Chem Res 42(8):1598–1602
13. Lyubimov SE, Tyutyunov AA, Kalinin VN et al (2007) Carboranylphosphites—new effective ligands for rhodium-catalyzed asymmetric hydrogenation of dimethyl itaconate. Tetrahedron Lett 48(46):8217–8219
14. Lyubimov SE, Said-Galiev EE, Khokhlov AR et al (2008) The use of monodentate phosphites and phosphoramidites as effective ligands for Rh-catalyzed asymmetric hydrogenation in supercritical carbon dioxide. J Supercrit Fluids 45(1):70–73
15. Lyubimov SE, Davankov VA, Said-Galiev EE et al (2008) Chiral phosphoramidites as inexpensive and efficient ligands for Rh-catalyzed asymmetric olefin-hydrogenation in supercritical carbon dioxide. Catal Commun 9(9):1851–1852
16. Lyubimov SE, Kuchurov IV, Davankov VA et al (2009) Synthesis of chiral amino acid derivatives in supercritical carbon dioxide using Rh-PipPhos catalyst. J Supercrit Fluids 50(2):118–120
17. Lyubimov SE, Kuchurov IV, Tyutyunov AA et al (2010) The use of new carboranylphosphite ligands in the asymmetric Rh-catalyzed hydrogenation. Catal Commun 11(5):419–421
18. Jessop PG, Hsiao Y, Ikariya T et al (1994) Catalytic production of dimethylformamide from supercritical carbon dioxide. J Am Chem Soc 116(19):8851–8852
19. Munshi P, Heldebrant DJ, McKoon EP et al (2003) Formanilide and carbanilide from aniline and carbon dioxide. Tetrahedron Lett 44(13):2725–2727
20. Krocher O, Koppel RA, Baiker A (1997) Highly active ruthenium complexes with bidentate phosphine ligands for the solvent-free catalytic synthesis of N,N-dimethylformamide and methyl formate. Chem Commun 1997, (5):453–454
21. Ting SST, Tomasko DL, Foster NR et al (1993) Solubility of naproxen in supercritical carbon dioxide with and without cosolvents. Ind Eng Chem Res 32(7):1471–1481
22. Xiao J, Nefkens SCA, Jessop PG et al (1996) Asymmetric hydrogenation of α, β-unsaturated carboxylic acids in supercritical carbon dioxide. Tetrahedron Lett 37(16):2813–2816
23. Berthod M, Mignani G, Lemaire M (2004) New perfluoroalkylated BINAP usable as a ligand in homogeneous and supercritical carbon dioxide asymmetric hydrogenation. Tetrahedron Asymmetry 15(7):1121–1126
24. Johansson A (1995) Methods for the asymmetric preparation of amines. Contemp Org Synth 2(6):393–407
25. Kainz S, Brinkmann A, Leitner W et al (1999) Iridium-catalyzed enantioselective hydrogenation of imines in supercritical carbon dioxide. J Am Chem Soc 121(27):6421–6429
26. Lyubimov SE, Rastorguev EA, Petrovskii PV et al (2011) Iridium-catalyzed asymmetric hydrogenation of imines in supercritical carbon dioxide using phosphite-type ligands. Tetrahedron Lett 52(12):1395–1397
27. Wang S, Kienzle F (2000) The syntheses of pharmaceutical intermediates in supercritical fluids. Ind Eng Chem Res 39(12):4487–4490

28. Turova OV, Kuchurov IV, Starodubtseva EV et al (2012) Ru–BINAP-catalyzed asymmetric hydrogenation of keto esters in high pressure carbon dioxide. Mendeleev Commun 22(4):184–186
29. Kainz S, Koch D, Leitner W et al (1997) Perfluoroalkyl-substituted arylphosphanes as ligands for homogenous catalysis in supercritical carbon dioxide. Angew Chem Int Ed 36(15):1628–1630
30. Guzel B, Omary MA, Fackler JP Jr et al (2001) Synthesis and characterization of {[(COD)Rh (bis-(2R,3R)-2,5-diethylphospholanobenzene)]+BARF−} for use in homogeneous catalysis in supercritical carbon dioxide. Inorg Chim Acta 325(1–2):45–50
31. Horishi Nishida NT, Yoshimura M, Sonoda T, Kobyrashi H (1984) Tetrakis[3,5-bis (trifluoromethyl)phenyl]borate. Highly lipophilic stable anionic agent for solvent-extraction of cations. Bull Chem Soc Jpn 57(9):2600–2604
32. Altinel H, Avsar G, Guzel B (2009) Fluorinated rhodium-phosphine complexes as efficient homogeneous catalysts for the hydrogenation of styrene in supercritical carbon dioxide. Transit Metal Chem 34(3):331–335
33. Burkhardt ER, Matos K (2006) Boron reagents in process chemistry: excellent tools for selective reductions. Chem Rev 106(7):2617–2650
34. Zhu Y, Jang SHA, Tham YH et al (2011) An efficient and recyclable catalytic system comprising nano-Iridium(0) and a pyridinium salt of nido-carboranyldiphosphine for the synthesis of one-dimensional boronate esters via hydroboration reaction. Organometallics 31(7):2589–2596
35. Carter CAG, Baker RT, Tumas W et al (2000) Enhanced regioselectivity of rhodium-catalysed alkene hydroboration in supercritical carbon dioxide. Chem Commun 2000, (5):347–348
36. Bhattacharyya P, Gudmunsen D, Hope EG et al (1997) Phosphorus(III) ligands with fluorous ponytails. J Chem Soc Perkin Trans 1(24):3609–3612
37. Rathke JW, Klingler RJ, Krause TR (1991) Propylene hydroformylation in supercritical carbon dioxide. Organometallics 10(5):1350–1355
38. Guo Y, Akgerman A (1997) Hydroformylation of propylene in supercritical carbon dioxide. Ind Eng Chem Res 36(11):4581–4585
39. Jessop PG, Ikariya T, Noyori R (1995) Selectivity for hydrogenation or hydroformylation of olefins by hydridopentacarbonylmanganese(I) in supercritical carbon dioxide. Organometallics 14(3):1510–1513
40. Bach I (1998) Hydroformylation of hex-1-ene in supercritical carbon dioxide catalysed by rhodium trialkylphosphine complexes. Chem Commun 1998, (14):1463–1464
41. Sellin MF, Cole-Hamilton DJ (2000) Hydroformylation reactions in supercritical carbon dioxide using insoluble metal complexes. J Chem Soc Dalton Trans (11):1681–1683
42. Palo DR, Erkey C (1998) Homogeneous catalytic hydroformylation of 1-octene in supercritical carbon dioxide using a novel Rhodium catalyst with fluorinated arylphosphine ligands. Ind Eng Chem Res 37(10):4203–4206
43. Patcas F, Maniut C, Ionescu C et al (2007) Supercritical carbon dioxide as an alternative reaction medium for hydroformylation with integrated catalyst recycling. Appl Catal B Environ 70(1–4):630–636
44. Van Rooy A, de Bruijn JNH, Roobeek KF et al (1996) Rhodium-catalysed hydroformylation of branched 1-alkenes; bulky phosphite vs. triphenylphosphine as modifying ligand. J Organomet Chem 507(1–2):69–73
45. Estorach CT, Orejón A, Masdeu-Bultó AM (2008) New rhodium catalytic systems with trifluoromethyl phosphite derivatives for the hydroformylation of 1-octene in supercritical carbon dioxide. Green Chem 10(5):545
46. Koeken ACJ, Benes NE, van den Broeke LJP et al (2009) Efficient hydroformylation in dense carbon dioxide using phosphorus ligands without perfluoroalkyl substituents. Adv Synth Catal 351(9):1442–1450
47. Francio G, Leitner W (1999) Highly regio- and enantio-selective rhodium-catalysed asymmetric hydroformylation without organic solvents. Chem Commun 1999, (17):1663–1664

48. Franciò G, Wittmann K, Leitner W (2001) Highly efficient enantioselective catalysis in supercritical carbon dioxide using the perfluoroalkyl-substituted ligand (R, S)-3–H2F6-BINAPHOS. J Organomet Chem 621(1–2):130–142
49. Kainz S, Leitner W (1998) Catalytic asymmetric hydroformylation in the presence of compressed carbon dioxide. Catal Lett 55(3–4):223–225
50. Hu Y, Chen W, Osuna AMB et al (2001) Rapid hydroformylation of alkyl acrylates in supercritical CO. Chem Commun 2001, (8):725–726
51. Hu Y, Chen W, Osuna AMB et al (2002) Fast and unprecedented chemoselective hydroformylation of acrylates with a fluoropolymer ligand in supercritical CO_2. Chem Commun 2(7):788–789
52. Estorach CT, Masdeu-Bultó AM (2007) Hydroesterification of 1-alkenes in Supercritical Carbon dioxide. Catal Lett 122(1–2):76–79
53. Paulaitis ME, Alexander GC (1987) A case study of the thermodynamic solvent effects on a Diels-Alder reaction in supercritical carbon dioxide. Reactions in supercritical fluids. Pure Appl Chem 59:61–68
54. Ikushima Y, Saito N, Arai M (1991) High-pressure Fourier transform infrared spectroscopy study of the Diels-Alder reaction of isoprene and maleic anhydride in supercritical carbon dioxide. Bull Chem Soc Jpn 64(1):282–284
55. Renslo AR, Weinstein RD, Tester JW et al (1997) Concerning the regiochemical course of the Diels–Alder reaction in supercritical carbon dioxide. J Org Chem 62(13):4530–4533
56. Scott Oakes R, J. Heppenstall T, Shezad N et al (1999) Use of scandium tris(trifluoromethanesulfonate) as a Lewis acid catalyst in supercritical carbon dioxide: efficient Diels-Alder reactions and pressure dependent enhancement of endo:exo stereoselectivity. Chem Commun 1999, (16):1459–1460
57. Matsuo J-I, Tsuchiya T, Odashima K et al (2000) Lewis acid catalysis in supercritical carbon dioxide. Use of Scandium tris(heptadecafluorooctanesulfonate) as a Lewis acid catalyst in Diels-Alder and aza Diels-Alder reactions. Chem Lett 29(2):178–179
58. Carroll MA, Holmes AB (1998) Palladium-catalysed carbon–carbon bond formation in supercritical carbon dioxide. Chem Commun 1998, (13):1395–1396
59. Morita DK, David SA, Tumas W et al (1998) Palladium-catalyzed cross-coupling reactions in supercritical carbon dioxide. Chem Commun 1998, (13):1397–1398
60. Shezad N, Oakes RS, Clifford AA et al (1999) Use of fluorinated palladium sources for efficient Pd-catalysed coupling reactions in supercritical carbon dioxide. Tetrahedron Lett 40(11):2221–2224
61. Early TR, Gordon RS, Carroll MA et al (2001) Palladium-catalysed cross-coupling reactions in supercritical carbon dioxide. Chem Commun 1(19):1966–1967
62. Kuchurov IV, Vasil'ev AA, Zlotin SG (2010) The Suzuki–Miyaura cross-coupling of bromo- and chloroarenes with arylboronic acids in supercritical carbon dioxide. Mendeleev Commun 20(3):140–142
63. Fernandes RR, Lasri J, da Silva MFCG et al (2011) Oxadiazoline and ketoimine Palladium (II) complexes as highly efficient catalysts for Suzuki–Miyaura cross-coupling reactions in supercritical carbon dioxide. Adv Synth Catal 353(7):1153–1160
64. Grubbs RH, Miller SJ, Fu GC (1995) Ring-closing metathesis and related processes in organic synthesis. Acc Chem Res 28(11):446–452
65. Schrock RR, Murdzek JS, Bazan GC et al (1990) Synthesis of molybdenum imido alkylidene complexes and some reactions involving acyclic olefins. J Am Chem Soc 112(10):3875–3886
66. Fürstner A, Koch D, Langemann K et al (1997) Olefin metathesis in compressed carbon dioxide. Angew Chem Int Ed 36(22):2466–2469
67. Theruvathu JA, Aravindakumar CT, Flyunt R et al (2001) Fenton chemistry of 1,3-dimethyluracil. J Am Chem Soc 123(37):9007–9014
68. Mikami K, Matsukawa S, Kayaki Y et al (2000) Asymmetric Mukaiyama aldol reaction of a ketene silyl acetal of thioester catalyzed by a binaphthol–titanium complex in supercritical fluoroform. Tetrahedron Lett 41(12):1931–1934
69. Komoto I, Kobayashi S (2001) Lewis acid catalysis in a supercritical carbon dioxide ($scCO_2$)-poly(ethylene glycol) derivatives (PEGs) system: remarkable effect of PEGS as additives on

reactivity of Ln(OTf)-catalyzed Mannich and Aldol reactions in $scCO_2$. Chem Commun 2001, (18):1842–1843
70. Komoto I, Kobayashi S (2004) Lewis acid catalysis in supercritical carbon dioxide. Use of poly(ethylene glycol) derivatives and perfluoroalkylbenzenes as surfactant molecules which enable efficient catalysis in $scCO_2$. J Org Chem 69(3):680–688
71. Kayaki Y, Noguchi Y, Iwasa S et al (1999) An efficient carbonylation of aryl halides catalysed by palladium complexes with phosphite ligands in supercritical carbon dioxide. Chem Commun 1999, (13):1235–1236
72. Pauson PL (1985) The khand reaction: a convenient and general route to a wide range of cyclopentenone derivatives. Tetrahedron 41(24):5855–5860
73. Schore NE (1988) Transition metal-mediated cycloaddition reactions of alkynes in organic synthesis. Chem Rev 88(7):1081–1119
74. Jeong N, Hwang SH, Lee YW et al (1997) Catalytic Pauson–Khand reaction in super critical fluids. J Am Chem Soc 119(43):10549–10550
75. Li G, Gao J, Wei H-X et al (2000) New CC bond formation via nonstoichiometric Titanium (IV) halide mediated vicinal difunctionalization of α, β-unsaturated acyclic ketones. Org Lett 2(5):617–620
76. Shi M, Xu Y-M (2003) An unexpected highly stereoselective double aza-Baylis–Hillman reaction of sulfonated imines with phenyl vinyl ketone. J Org Chem 68(12):4784–4790
77. Rose PM, Clifford AA, Rayner CM (2002) The Baylis-Hillman reaction in supercritical carbon dioxide: enhanced reaction rates, unprecedented ether formation, and a novel phase-dependent 3-component coupling. Chem Commun 2002, (9):968–969
78. Cheng J-S, Jiang H-F (2004) Palladium-catalyzed regioselective cyclotrimerization of acetylenes in supercritical carbon dioxide. Eur J Org Chem 2004(3):643–646
79. Montilla F, Avilés T, Casimiro T et al (2001) $CpCo(CO)_2$-catalysed cyclotrimerisation of alkynes in supercritical carbon dioxide. J Organomet Chem 632(1–2):113–118
80. Musie G, Wei M, Subramaniam B et al (2001) Catalytic oxidations in carbon dioxide-based reaction media, including novel CO_2-expanded phases. Coord Chem Rev 219–221:789–820
81. Maayan G, Ganchegui B, Leitner W et al (2006) Selective aerobic oxidation in supercritical carbon dioxide catalyzed by the $H_5PV_2Mo_{10}O_{40}$ polyoxometalate. Chem Commun 2006 (21):2230–2232
82. Leitner W (1999) Reactions in supercritical carbon dioxide. Top Curr Chem 206:107–132
83. Chang Y, Jiang T, Han B et al (2003) Aerobic oxidation of cyclohexanol to cyclohexanone in compressed CO_2 and liquid solvents. Ind Eng Chem Res 42(25):6384–6388
84. Herbert M, Montilla F, Galindo A (2010) Supercritical carbon dioxide, a new medium for aerobic alcohol oxidations catalysed by copper-TEMPO. Dalton Trans 39(3):900–907
85. Ansari MB, Park S-E (2012) Carbon dioxide utilization as a soft oxidant and promoter in catalysis. Energy Environ Sci 5(11):9419–9437
86. Gu L, Zhang Y (2010) Unexpected CO_2 splitting reactions to form CO with N-heterocyclic carbenes as organocatalysts and aromatic aldehydes as oxygen acceptors. J Am Chem Soc 132(3):914–915
87. Nair V, Varghese V, Paul RR et al (2010) NHC catalyzed transformation of aromatic aldehydes to acids by carbon dioxide: an unexpected reaction. Org Lett 12(11):2653–2655
88. Chiang P-C, Bode JW (2011) On the role of CO_2 in NHC-catalyzed oxidation of aldehydes. Org Lett 13(9):2422–2425
89. Ren X, Yuan Y, Ju Y et al (2012) Oxidation ability of CO_2 for the transformation of cinnamic aldehydes to acids catalyzed by N-heterocyclic carbene: combining computational and experimental studies. ChemCatChem 4(12):1943–1951
90. Olsen MHN, Salomão GC, Drago V et al (2005) Oxidation of cyclohexane in supercritical carbon dioxide catalyzed by iron tetraphenylporphyrin. J Supercrit Fluids 34(2):119–124
91. Kokubo Y, Wu X-W, Oshima Y et al (2004) Aerobic oxidation of cyclohexene catalyzed by Fe(III)(5,10,15,20-tetrakis(pentafluorophenyl)porphyrin)Cl in supercritical CO_2. J Supercrit Fluids 30(2):225–235

92. Nolen SA, Lu J, Brown JS et al (2002) Olefin epoxidations using supercritical carbon dioxide and hydrogen peroxide without added metallic catalysts or peroxy acids. Ind Eng Chem Res 41(3):316–323
93. Jiang H, Jia L, Li J (2000) Wacker reaction in supercritical carbon dioxide. Green Chem 2(4):161–164
94. Jiang H-F, Shen Y-X, Wang Z-Y (2008) Palladium-catalyzed aerobic oxidation of terminal olefins with electron-withdrawing groups in $scCO_2$. Tetrahedron 64(3):508–514
95. ten Brink GJ, Arends IWCE, Sheldon RA (2004) The Baeyer–Villiger reaction: new developments toward greener procedures. Chem Rev 104(9):4105–4124
96. Bolm C, Palazzi C, Francio G et al (2002) Baeyer–Villiger oxidation in compressed CO_2. Chem Commun 2002, (15):1588–1589
97. DeSimone JM, Guan Z, Elsbernd CS (1992) Synthesis of fluoropolymers in supercritical carbon dioxide. Science 257:945–947
98. Clark MR, DeSimone JM (1995) Cationic polymerization of vinyl and cyclic ethers in supercritical and liquid carbon dioxide. Macromolecules 28(8):3002–3004
99. Albertsson A-C, Varma IK (2003) Recent developments in ring opening polymerization of lactones for biomedical applications. Biomacromolecules 4(6):1466–1486
100. Bratton D, Brown M, Howdle SM (2005) Tin(II) ethyl hexanoate catalyzed precipitation polymerization of ε-caprolactone in supercritical carbon dioxide. Macromolecules 38(4):1190–1195
101. Hamilton JG, Rooney JJ, DeSimone JM et al (1998) Stereochemistry of ring-opened metathesis polymers prepared in liquid CO_2 at high pressure using $Ru(H_2O)_6(Tos)_2$ as catalyst. Macromolecules 31(13):4387–4389
102. Hu X, Blanda MT, Venumbaka SR et al (2005) Ring-opening metathesis polymerization (ROMP) of norbornene in supercritical carbon dioxide using well-defined metal carbene catalysts. Polym Advan Technol 16(2–3):146–149
103. Hori H, Six C, Leitner W (1999) Rhodium-catalyzed phenylacetylene polymerization in compressed carbon dioxide. Macromolecules 32(10):3178–3182
104. Gimenez-Pedros M, Tortosa-Estorach C, Bastero A et al (2006) Alternating CO/tert-butylstyrene copolymerisation using soluble cationic palladium complexes in supercritical carbon dioxide. Green Chem 8(10):875–877

Chapter 14
Multiphase Catalytic Reactions in/Under Dense-Phase Carbon Dioxide: Utilization of Carbon Dioxide as a Reaction Promoter

Hiroshi Yoshida, Shin-ichiro Fujita, Masahiko Arai, and Bhalchandra M. Bhanage

14.1 Introduction

Carbon dioxide serves as a building block for organic compounds, and various interesting examples are shown in the other chapters of this book. Carbon dioxide may be transformed into value-added organic compounds through chemical, photochemical, electrochemical, and biochemical reactions. In addition to the role of CO_2 as a useful reactant, CO_2 acts as a promoter/modifier in organic reactions in liquid phases although it is not involved as a reactant. In order for CO_2 to show such actions, pressurization is necessary to dissolve CO_2 in a certain quantity in an organic phase. When an organic liquid (substrate, solvent) is pressurized by CO_2, its volume may increase to some extent depending on the nature of the liquid. In some cases, a considerable amount of CO_2 is dissolved, and this expands the volume of the organic liquid phase significantly. This phase is often called as CO_2-dissolved expanded liquid phase (CXL) [1–3]. The dissolution of CO_2 changes the solvent properties of a liquid phase from pure organic liquid state to high-density CO_2 state, depending on its pressure applied. The liquid-phase dissolving CO_2 is beneficial to dissolution of gaseous reactants such as oxygen, hydrogen, and carbon monoxide. Thus, the pressurization with CO_2 would accelerate the liquid-phase chemical reactions involving gaseous reactants, including oxidation, hydroformylation, and hydrogenation. That is, CO_2 can act as an accelerator in organic synthetic reactions on simple pressurization of the reaction mixtures with CO_2

H. Yoshida • S.-i. Fujita • M. Arai (✉)
Division of Chemical Process Engineering, Faculty of Engineering, Hokkaido University, Sapporo 060-8628, Japan
e-mail: marai@eng.hokudai.ac.jp

B.M. Bhanage
Department of Chemistry, Institute of Chemical Technology, Mumbai 400019, India

B.M. Bhanage and M. Arai (eds.), *Transformation and Utilization of Carbon Dioxide*, Green Chemistry and Sustainable Technology, DOI 10.1007/978-3-642-44988-8_14,

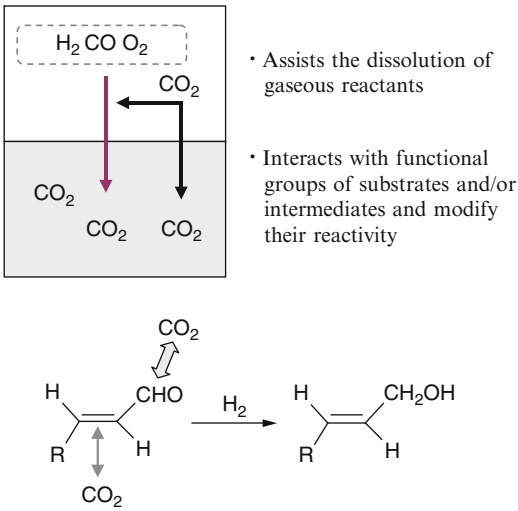

Fig. 14.1 Multiphase catalytic reactions in the presence of pressurized CO_2. The liquid phase includes substrate, solvent, and catalyst (homogeneous or heterogeneous). The dissolution of CO_2 may improve the dissolution of gaseous reactants and modify the reactivity of certain functional groups of organic substrates. An example given is the selective hydrogenation of carbonyl group, than carbon-carbon double bond, of α,β-unsaturated aldehyde to unsaturated alcohol

(Fig. 14.1). Under certain conditions, however, the dissolved CO_2 molecules act only as a diluent and have a negative effect of retarding the reactions. Whether the promotional effect of CO_2 pressurization will appear or not depends on a relative balance between those positive and negative factors.

In addition to the above-mentioned *macro (physical)* functions, CO_2 has interesting and significant *micro (chemical)* functions in organic synthetic reactions through direct interactions with reacting species in the liquid phases. The dissolved CO_2 molecules interact with functional groups of substrates and/or reaction intermediates, as proved by in situ high-pressure Fourier transform infrared spectroscopy [4]. The direct interaction with CO_2 changes the reactivity of certain functional groups of substrates and/or reaction intermediates, and, as a result, this may improve the selectivity to the production of desired products. That is, CO_2 acts as a reaction modifier, which is expected for liquid-phase synthetic reactions including no gaseous reactants (e.g., Heck coupling) as well as those including gaseous reactants. This chapter reviews several interesting examples of *micro (chemical)* effects of CO_2 in organic synthetic reactions and possible explanations for these effects observed. The reactions dealt with this chapter include oxidation, hydroformylation, hydrogenation, acid-catalyzed reactions, Heck reactions, and Diels–Alder reactions.

14.2 Multiphase Catalytic Reactions in the Presence of Dense-Phase CO_2

14.2.1 Oxidation

Oxidation is one of the widely investigated reactions in both academia and industry, and O_2 and H_2O_2 are generally used as oxidants. The use of dense-phase CO_2 prevents oxidation reactions from combustion and explosion, and mass transfer limitation can be improved in multiphase catalytic oxidations using gaseous oxidants. Therefore, several researchers investigated the utilization of CO_2 in oxidation reactions.

Yoo et al. reported the chemical functions of CO_2 as an active component for the liquid-phase O_2 oxidation of *o*-, *m*-, and *p*-xylenes at 468 K with Co/Mn/HBr catalyst, which is called "MC-type O_2 oxidation" [5]. They showed that the amount of O_2 consumed in O_2 oxidation of *m*-xylene was enhanced by the copresence of CO_2, and the purity of isophthalic acid (IPA) in the recovered solid product was also increased. Moreover, the promoting effects of CO_2 increased with increasing concentration of CO_2, indicating that both catalytic activity and selectivity to IPA were influenced by the presence of CO_2 in the reaction media. The O_2 oxidation of *p*-toluic acid, which was produced as an intermediate from *p*-xylene, was also examined, and they concluded that there were three mechanistic interpretations of the effects of CO_2. Firstly, copresence of CO_2 enhanced the solubility of the substrates as well as the intermediates; secondly, decarboxylation of the intermediates can be suppressed by the presence of CO_2. Thirdly, a synergistic interaction of CO_2 and O_2 molecules may create a cyclic peroxocarbonate species on the metal center of the MC-type catalyst, and these species play a key role in initiating the free radical propagation via the hydrogen abstraction process and accelerating the oxidation. The possible pathways of formation of peroxocarbonate species are shown in Scheme 14.1.

The metal-O_2 complex is initially formed on either Co or Mn center, and the CO_2 molecule is then inserted into the O-O bond to produce an active species (Type I).

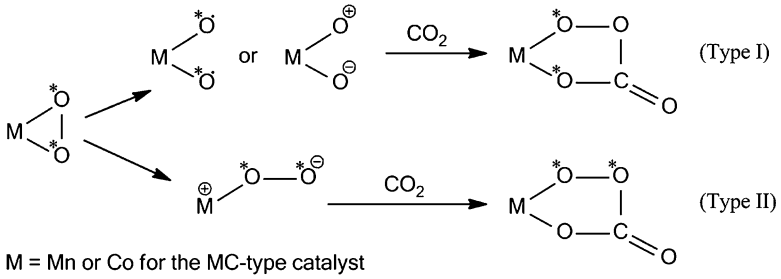

Scheme 14.1 Possible pathways of formation of peroxocarbonate species from O_2 and CO_2 with metal center of MC-type catalyst

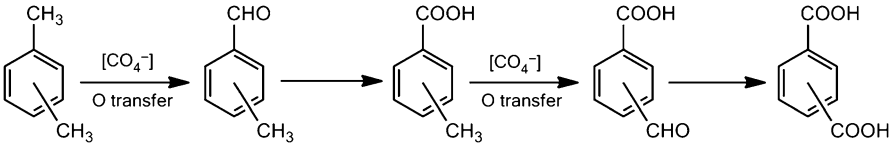

Scheme 14.2 Reaction pathways of O_2 oxidation of xylenes over Co/Mn/HBr catalyst in the presence of CO_2

Scheme 14.3 The formation of peroxycarbonic acid from CO_2 and H_2O_2

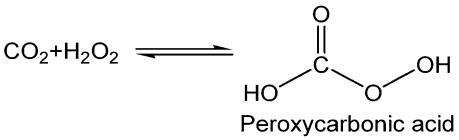

Another type of peroxocarbonate species can also be formed by a different mode of interaction (Type II). Aresta et al. reported that the oxygen atom directly bonded to the metal center in these species can transfer to the oxophile substrates [6], indicating that the peroxocarbonate species formed from O_2 and CO_2 accelerated the oxidation of methyl group in aromatic compounds to corresponding aldehydes as shown in Scheme 14.2.

Eckert et al. have investigated the olefin epoxidations using H_2O_2 as oxidant in the presence of dense-phase CO_2 with no metallic catalyst [7] and mentioned the formation of peroxycarbonic acid from CO_2 and H_2O_2, which facilitates the olefin epoxidation (Scheme 14.3). The mass transfer limitation is one of the crucial problems in this reaction because the epoxidation occurs in aqueous phase. Dense-phase CO_2 contributes to improve the mass transfer. Subramaniam et al. indicated that the peroxycarbonate is the most likely reactive intermediate in the olefin epoxidation [8]. In addition, they note that hydrogen bonding and polarity of CXLs are key factors in the epoxidation, which can be controlled by CO_2 pressurization and the kind of organic solvent used.

14.2.2 Hydroformylation

Hydroformylation of olefin with H_2 and CO is an industrially important reaction, and homogeneous Rh or Co complex catalysts are generally used. The cost of Rh complex catalyst is relatively expensive than Co complex catalyst, but the reaction can occur with high activity and selectivity under milder conditions. The utilization of dense-phase CO_2 in hydroformylation has been investigated by several researchers [9–11]. It is indicated that the increase of the solubility of syngas into liquid phase by using CXLs as reaction media gives the most significant effect in the hydroformylation reactions.

Tominaga et al. have first shown that the hydroformylation can indeed proceed with a mixture of H_2 and CO_2 instead of CO [12, 13]. CO can be formed from H_2

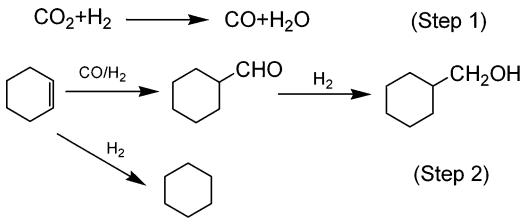

Scheme 14.4 One-pot hydroformylation of cyclohexene using H_2 and CO_2

and CO_2 through the reverse water gas shift reaction, and it can be directly used for hydroformylation with H_2, indicating that one-pot hydroformylation from H_2 and CO_2 can be achieved. Fujita et al. investigated the effect of H_2 and CO_2 pressures on the hydroformylation of cyclohexene with a catalyst system of $Ru_3(CO)_{12}$ and LiCl in *N*-methyl-2-pyrrolidone [14]. The hydroformylation with CO_2 and H_2 has a two-step process, as shown in Scheme 14.4, and the aldehyde produced is further reduced to the corresponding alcohol. In their work, gaseous CO was detected during the reaction, and its amount was comparable to those of aldehyde and alcohol formed. The step 1 proceeds faster compared with the step 2, which means that the hydroformylation reaction is the rate-determining step. The formation of CO was accelerated with increasing total pressure of H_2 and CO_2, and the yield of cyclohexanecarboxaldehyde was also increased. However, both the hydrogenation of cyclohexanecarboxaldehyde to cyclohexane-methanol and that of cyclohexene to cyclohexane were suppressed with increasing CO_2 pressure. The chemical functions of CO_2 as a promoter as well as a reactant were examined by in situ high-pressure FTIR measurements, and molecular interactions of CO_2 with cyclohexene and intermediates were not observed. They also examined the structure of Ru complexes at different pressures of H_2 and CO_2, and the results indicated the presence of $[H_3Ru_4(CO)_{12}]^{-1}$ and $[HRu_3(CO)_{11}]^{-1}$ under the reaction conditions used. These species may be active for the reduction of CO_2 to CO and the following hydroformylation reaction, respectively.

14.2.3 Hydrogenation

Liquid-phase hydrogenation is one of industrially important reactions, and different homogeneous and heterogeneous catalysts are used [15, 16]. Heterogeneous catalysts are more desirable than homogeneous ones when we consider the post-reaction treatments of catalyst separation and recycling. The reaction mixtures of our interest here are a multiphase system containing a liquid phase (substrate, solvent) and/or a gas phase (H_2, CO_2) with a solid phase (heterogeneous catalyst). The pressurization of organic liquid phases with CO_2 may have an interesting impact on the reaction rate and/or the product selectivity for the hydrogenation reactions in these phases.

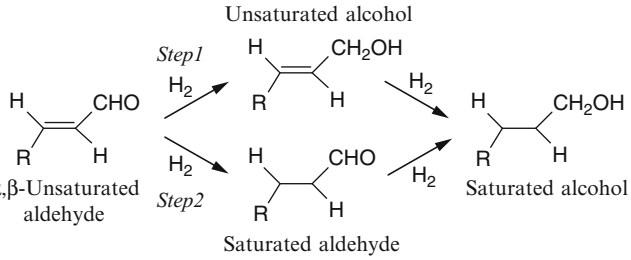

Scheme 14.5 Reaction pathways in hydrogenation of α,β-unsaturated aldehyde

The acceleration of hydrogenation reactions in the presence of dense-phase CO_2 was reported in the literature [17–20]. For example, Chouchi et al. compared the rates of hydrogenation of α-pinene with a Pd/C catalyst under different conditions at 323 K. They showed that the rate of hydrogenation in a gas–liquid system under CXL conditions was even faster compared to that in a homogeneous $scCO_2$ system [20].

In selective hydrogenation of α,β-unsaturated aldehydes with supported Pt catalysts, the C═C group is more easily hydrogenated rather than the C═O group, and so it is difficult to produce the corresponding unsaturated alcohols in high selectivity [21] (Scheme 14.5). The high selectivity to unsaturated alcohols may be achieved by modifying the properties of supported Pt particles with Sn and other additives. Bhanage et al. revealed that the presence of dense-phase CO_2 was effective for improving the hydrogenation of the carbonyl bond of cinnamaldehyde, α-methyl-trans-cinnamaldehyde, and crotonaldehyde with a Pt/Al_2O_3 catalyst at 323 K [22]. For crotonaldehyde, for example, the selectivity to crotyl alcohol was 46 % in neat ethanol at a H_2 pressure of 4 MPa, while it was improved to >70 % in the presence of 14 MPa CO_2. For cinnamaldehyde, the selectivity to cinnamyl alcohol was enhanced from 78 % in ethanol to 93 % at a CO_2 pressure of 14 MPa; in addition, the rate of hydrogenation was also improved with increasing CO_2 pressure. Zhao et al. measured in situ FTIR spectra of cinnamaldehyde and benzaldehyde dissolved in pressurized CO_2 gas phase at 323 K [23, 24]. They observed a significant red shift of the frequency of the stretching vibration of the C═O bond with increasing CO_2 pressure for cinnamaldehyde but a marginal red shift for benzaldehyde. The frequency of the vibration of the C═C bond was found to change little with the pressure. Therefore, they assumed that CO_2 molecules were able to interact with the carbonyl group, decrease the bond strength, and then increase its reactivity to hydrogenation. Those molecular interactions between CO_2 species and the carbonyl group were studied and confirmed by theoretical model calculations by Zhao et al. [25]. The function of CO_2 as an accelerator/modifier was also observed for the same hydrogenation reactions of α,β-unsaturated aldehydes using homogeneous metal complex catalysts [26–28].

The dense-phase CO_2 also has an impact on liquid-phase hydrogenation of aromatic nitro compounds, which is important in industry for the manufacture of aniline compounds [29], and several metals are used as active catalysts [30–34].

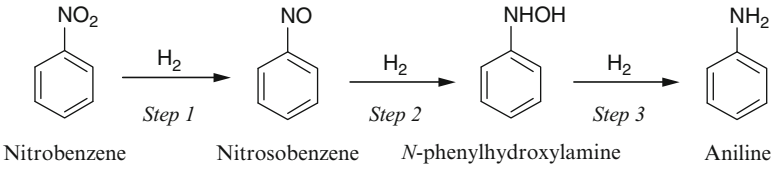

Scheme 14.6 Hydrogenation of nitrobenzene toward aniline

In this hydrogenation (Scheme 14.6), the production of such intermediates as nitrosobenzene and *N*-phenylhydroxylamine and such coupling by-products as azoxybenzene, azobenzene, and hydrazobenzene should be avoided, and a high selectivity to aniline should be achieved at a high conversion.

Meng et al. studied the selective hydrogenation of nitrobenzene to aniline with Al_2O_3-supported Ni catalysts at 323 K and at a H_2 pressure of 4 MPa [35]. The reaction runs were conducted in the presence of CO_2 at different pressures and no additional organic solvent. Under the conditions used, the rate of hydrogenation was observed to increase with increasing CO_2 pressure up to about 12 MPa, below which the reaction mixture was a gas–liquid–solid three-phase system and the reaction occurred mainly in the liquid phase. The dissolution of a gaseous reactant of H_2 should be improved by CO_2 pressurization, and this effect may be superior to the dilution of the reacting species in the liquid phase. The reaction mixture changed to a gas-solid two-phase system at higher CO_2 pressure, and the dilution became more significant, resulting in a decrease in the rate of reaction. It is noteworthy that the selectivity to the desired product of aniline is almost 100 % at any conversion level, and this complete selective hydrogenation can be achieved at CO_2 pressures of 6–18 MPa, that is, irrespective of the phase behavior of the reaction mixture. Meng et al. measured in situ FTIR spectra of nitrobenzene, nitrosobenzene, and *N*-phenylhydroxylamine dissolved in dense-phase CO_2 at different pressures. They observed that the frequency of stretching vibration of N–O bond of the nitro group was blue-shifted on CO_2 pressurization and believed that the reactivity of the nitro group was reduced in the presence of dense-phase CO_2. They assumed that for nitrosobenzene and *N*-phenylhydroxylamine, in contrast, their reactivity was promoted by the action of CO_2 species in the liquid phase. Thus, CO_2 is believed to slow down the rate of step 1 but accelerate the rates of steps 2 and 3. As a result, aniline can be produced in 100 % selectivity with no undesired intermediates and coupling products. The dilution of intermediates of nitrosobenzene and *N*-phenylhydroxylamine by the dissolution of CO_2 and H_2 would contribute to the suppression of their coupling reactions.

Meng et al. made a similar study with chloronitrobenzene substrates [36]. They demonstrated that the pressurization with CO_2 is also effective for the 100 % selective hydrogenation to the desired chloroaniline products at any conversion level. No dechlorination was observed to occur in this multiphase reaction system. Zhao et al. investigated the effects of metal particle size in hydrogenation of nitrobenzene with several supported noble metal catalysts in the presence of

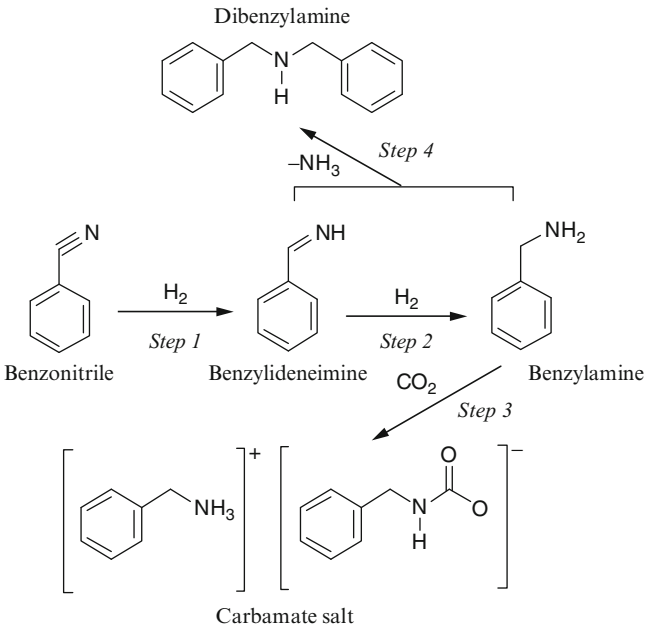

Scheme 14.7 Reaction pathways in hydrogenation of benzonitrile

dense-phase CO_2 [37, 38]. They showed that the turnover frequency decreased with the degree of metal dispersion in similar fashions for the reactions in ethanol and in compressed CO_2.

An interesting result was further reported by Meng et al. that the positive effect of CO_2 pressurization on the selective hydrogenation of nitrobenzene to aniline appeared at a low CO_2 pressure of about 1 MPa when an additional phase of water was also added to the reaction system [39]. Lin et al. reported the effectiveness of compressed CO_2/water system for ring hydrogenation of aromatic alcohols and aldehydes [40]. The function of water added is not clear at present. The multiphase organic reaction systems including dense-phase CO_2 and water are interesting and worth investigating in detail. A recent review article demonstrates the significance of on-water organic reactions, in which organic-water interface is important [41]. The combination of dense-phase CO_2 and water could give additive or synergistic effects on the reaction rate and/or the product selectivity in organic synthetic reactions.

Yoshida et al. reported different CO_2 actions for hydrogenation of benzonitrile with a Pd/Al_2O_3 catalyst in multiphase media including dense-phase CO_2 and water at 323 K [42]. The selective hydrogenation of benzonitrile to the primary amine may be achieved in a selectivity >95 % in a medium including both CO_2 and water. In this system, the primary amine formed may easily transform with CO_2 to a water-soluble carbamate salt (Scheme 14.7), and this hinders its further hydrogenation to the secondary amine in the organic phase, resulting in the high selectivity to benzylamine. The carbamate salt is not stable, and so the benzylamine can be

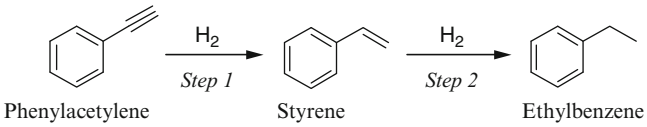

Scheme 14.8 Hydrogenation of phenylacetylene to styrene and ethylbenzene

Scheme 14.9
Hydrogenation of the nitro and vinyl groups of nitrostyrene

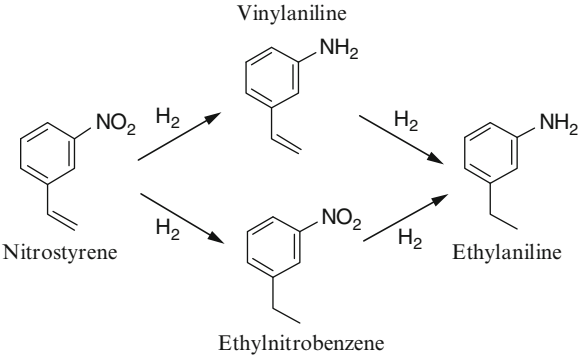

regenerated by heating [43]. When water is absent, the carbamate salt deposits on the surface of catalyst and causes its deactivation. The primary amine is soluble somewhat in water, but the production of the secondary amine cannot be avoided in the absence of CO_2.

The action of CO_2 as a protecting agent was earlier reported for hydrogenation [44] and other synthetic reactions [45, 46] using homogeneous catalysts. Eckert et al. studied the selective hydrogenation of benzonitrile with $NiCl_2/NaBH_4$ in ethanol at 303 K [44]. The yield of the primary amine was markedly promoted by simple pressurization of the organic phase with CO_2. This is ascribable to the formation of carbamate salt that prevents the side reaction of the primary amine with imine intermediate giving the secondary amine.

Recently Wei et al. investigated the partial hydrogenation of phenylacetylene with several monometallic and bimetallic Pd-based catalysts in hexane at 313 K [47] (Scheme 14.8). The pressurization with CO_2 was shown to improve the selectivity to styrene; at a total pressure of 3.4 MPa including 20 % CO_2, styrene was produced in a selectivity of 92 % at 100 % conversion in 0.5 h with a Pd-Ag bimetallic catalyst. Further increase of CO_2 partial pressure to 40 % increased the selectivity to 98 % but decreased the conversion to 74 % under the conditions used. Namely, the further hydrogenation of an alkene of styrene to an alkane of ethylbenzene can be suppressed although the function of CO_2 molecules is still unclear.

The extent of impact of CO_2 pressurization should be different from one organic liquid to another depending on their solvent properties; above-mentioned positive effects would be expected for some organic liquids but not for others. The dissolution of a certain amount of CO_2 into a liquid is required for CO_2 to have positive (or negative) effects in the liquid phase. Yoshida et al. studied the effects of CO_2 for a test reaction of nitrostyrene hydrogenation (Scheme 14.9) with a Pt/TiO_2 catalyst

using two organic solvents of toluene and ethanol at 323 K [48]. The two solvents indicated similar degrees of volume expansion at the same CO_2 pressure, as confirmed by phase behavior observations at the reaction temperature. In neat toluene, neat ethanol, and ethanol pressurized by CO_2, the nitro group of nitrostyrene was hydrogenated to vinylaniline in a high selectivity. In contrast, the vinyl group was selectively hydrogenated to ethylnitrobenzene in toluene pressurized by CO_2. These results may be explained by relative interactions among the two functional groups, the solvent molecules, and the CO_2 species in the liquid phase. The interactions of the vinyl group with CO_2 are weak, but those of the nitro group with CO_2 are significant, which decrease its reactivity to hydrogenation. The interactions of the nitro group with the dissolved CO_2 can appear in the case of toluene, in which the nitro group is likely to be surrounded by CO_2 species rather than toluene molecules because of no interaction between the nitro group and toluene molecules. So, the impact of CO_2 pressurization appears even at low pressures, decreasing the reactivity of the nitro group and then relatively increasing the hydrogenation of the vinyl group. In the case of ethanol, however, the interactions of the nitro group with the solvent molecules are strong as compared to those with CO_2, and, hence, the impact of CO_2 pressurization does not appear even at a high pressure of 10 MPa. These explanations are supported by molecular dynamics simulations, which determine the local composition around the nitro group of nitrostyrene in either toluene or ethanol pressurized by CO_2. It is thus important to select a suitable solvent when we expect positive effects of CO_2 pressurization on liquid-phase hydrogenation and other organic reactions. Solvent properties of substrates, solvents, and CO_2 are important to consider [49].

Those results demonstrate the importance of interactions of CO_2 molecules with substrates and intermediates. Akiyama et al. studied these molecular interactions of CO_2 with various organic compounds of ketones, esters, and amides by using in situ high-pressure FTIR [4]. The results would be helpful in discussing the impact of CO_2 on reactions with those substrates. In the hydrogenation reactions in the presence of dense-phase CO_2 over supported metal catalysts, CO is formed from CO_2 and H_2 and adsorbed on the surface of supported metal particles, and this would cause the deactivation of catalysts [50–54]. The occurrence of catalyst deactivation may depend on competitive adsorption of CO, substrates, and/or intermediates. Dong et al. studied the hydrogenation of the aromatic rings of polystyrene in a CXL of decahydronaphthalene pressurized by CO_2 using 5 % Pd/SiO_2 and 5 % Pd/Al_2O_3 catalysts at 423 K [55]. They observed the catalyst deactivation in a relatively early stage of reaction due to the formation and adsorption of CO formed from CO_2 and H_2. They detected CO at the end of hydrogenation reaction. It is interesting to note that the catalyst deactivation can be avoided by physically mixing an additional methanation catalyst (5 % Ru/Al_2O_3, 65 % Ni/SiO_2-Al_2O_3) and a hydrogenation catalyst into a single particle. The methanation catalyst could convert CO into CH_4 and regenerate the surface of the hydrogenation catalysts. The use of the methanation catalysts does not influence the desired reaction of the aromatic ring hydrogenation of polystyrene. Using in situ high-pressure FTIR, Yoshida et al. studied the formation and adsorption of CO

Scheme 14.10 In situ formation of alkylcarbonic acid from CO_2 and alcohol

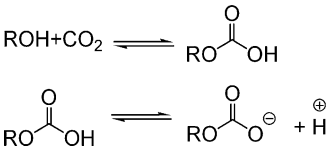

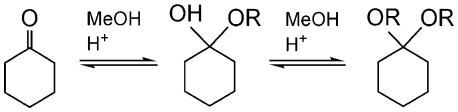

Scheme 14.11 Formation of dimethyl acetal of cyclohexanone catalyzed by in situ generated acid in CO_2-expanded methanol

from H_2 and CO_2 over Al_2O_3-supported Pt, Pd, Rh, and Ru catalysts at 323 K [56]. They collected FTIR spectra of adsorbed CO at different CO_2 pressures and in the presence and absence of water (H_2O, D_2O) for heat-treated and untreated noble metal catalysts. They discussed the types of CO species adsorbed on the metal particles depending on their surface structure and the influence of water vapor on the CO adsorption behavior. Water molecules may be adsorbed more preferentially on atomically rough surfaces rather than CO species. Our attention is herein given to interactions of CO_2 with organic substrates and intermediates. The CO_2 may affect the properties of supported metal particles through the formation and adsorption of CO in hydrogenation reactions, as mentioned above. Note, further, that CO_2 molecules could have a direct impact on supported metal particles, which was speculated from the optical absorption measurements of supported Au particles in the compressed CO_2 gas phase at different pressures [57]. Liu et al. recently reported that the properties and activity of a TiO_2 catalyst were modified by the accumulation of CO_2 species on its surface assisted by the action of a surfactant [58]. The photocatalytic activity of TiO_2 for the production of H_2 through water splitting was improved by about one order of magnitude.

14.2.4 Acid-Catalyzed Reactions

Acid-catalyzed reactions in CXLs using in situ generated catalysts from the reaction of CO_2 with alcohol or water were pioneered by the joint group of Eckert and Liotta [59–63]. Alkylcarbonic acids can be formed in alcohols with compressed CO_2 and used as acid catalysts (Scheme 14.10). This reaction system is desirable because the decomposition of the acid can automatically occur by simple depressurization after the reactions without any post-reaction neutralization and salt disposal.

They found that the formation of dimethyl acetal of cyclohexanone in methanol (Scheme 14.11) was up to 130 times faster by CO_2 pressurization. The greatest

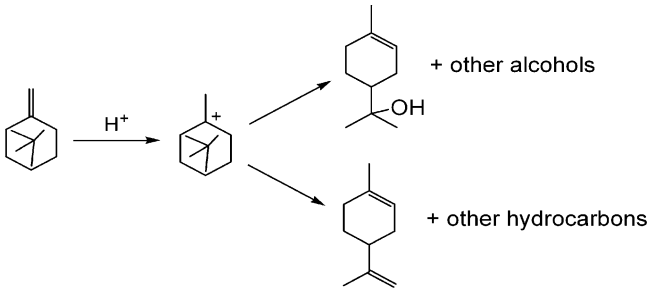

Scheme 14.12 Hydrolysis of β-pinene in the CO_2-expanded MeOH/H_2O mixture

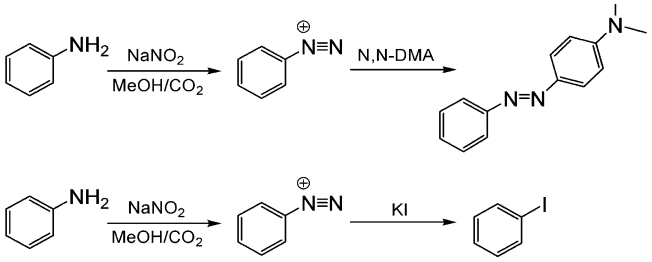

Scheme 14.13 In situ acid catalysis for single-pot synthesis of methyl yellow and iodobenzene in CO_2-expanded methanol

enhancement was found at a pressure of 22 bar; presumably higher pressures are undesirable due to decreasing polarity of the expanded solvent inhibiting the dissociation of the acid.

The application of in situ generated alkylcarbonic acid as a catalyst for the hydrolysis of β-pinene to terpineol and other alcohols was also investigated [61]. Good selectivity for alcohols rather than hydrocarbons was obtained in CXLs and hot water (Scheme 14.12). Eckert et al. used several kinds of CXLs with different compositions of methanol, water, and CO_2 for the reactions. A selectivity of 84.0 % for the hydrolysis product at the highest conversion (70.9 %) was achieved in the CO_2-expanded 1:1 methanol/water mixture (348 K, 3 mol% CO_2). The reaction did not proceed when the CO_2 was absent.

Eckert et al. demonstrated the catalytic performance of in situ acid catalysis for the diazotization of aniline, which is either coupled with *N*,*N*-dimethyl aniline to form methyl yellow or reacted with iodide to form iodobenzene (Scheme 14.13) [63]. A 97 % conversion of aniline with a 72 % yield of methyl yellow was obtained at 278 K in 72 h with an excess nitrile salt and a high CO_2 loading. This reaction did not occur in the absence of CO_2. They also used THF as a solvent instead of methanol, but the yield was only 0.3 %, which may come from the lack of alkylcarbonic acid and the formation of carbamates from aniline and CO_2. These results strongly suggest that a suitable acid source like alcohol must be present for utilization of dense-phase CO_2 in the acid-catalyzed reactions.

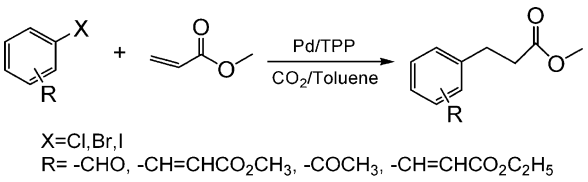

Scheme 14.14 Heck reactions of halogenated benzene derivatives with methyl acrylate in CO_2-expanded toluene with Pd/TPP catalyst

14.2.5 Heck and Diels–Alder Reactions

There are many advantages of using dense-phase CO_2 in multiphase catalytic reactions as mentioned above. Recently, some positive effects in liquid organic reactions without any gaseous reactants were also found.

$ScCO_2$ has been investigated as a reaction media of Heck coupling reactions using homogeneous complex catalysts; there are some advantages such as the extraction of the product, resulting in the controlling of the product distribution. The modification of metal complex catalysts with fluorinated functional groups is effective for increasing their solubility into $scCO_2$ phase [64, 65]. Such a catalyst modification may not always be necessary for multiphase reactions, in which the solubility of the catalysts in the organic phase is not so a serious problem. Multiphase Heck reactions in the presence of dense-phase CO_2 were investigated [66]. Fujita et al. reported the effects of CO_2 pressurization on liquid-phase Heck reactions of methyl acrylate with various aryl bromides over homogeneous Pd/TPP catalyst in toluene in the presence of compressed CO_2 (Scheme 14.14) [67]. For the Heck reaction of iodobenzene and non-activated bromobenzene with methyl acrylate, the conversion simply decreased with CO_2 pressure due to the dilution effect of CO_2 molecules in the liquid organic phase. However, the conversion increased with CO_2 pressure in the range up to 3 MPa for the reaction of 2-bromoacetophenone with methyl acrylate. This promoting effect was not observed in the case of using 3- and 4-bromoacetophenone. From the results of high-pressure FTIR measurements of 2-, 3-, 4-bromoacetophenones in the presence of CO_2, they conclude that the dissolved CO_2 molecules interact with the aryl bromide substrates in different manners depending on their structures. It is suggested that the C-Br bonds of the three substrates are modified by the presence of CO_2, indirectly through interactions of CO_2 with the other moieties or directly with the C-Br moiety. The rate of the liquid-phase Heck reaction can be enhanced by pressurizing the reaction mixture with CO_2 at a low pressure of 2–4 MPa, although the enhancement effect is limited to a few bromoarenes of a certain structure.

Fujita et al. studied the impact of CO_2 pressurization for the Diels–Alder reactions of isoprene with methyl acrylate, methyl vinyl ketone, and acrolein in the CO_2-expanded toluene and ethanol at 393 K with a heterogeneous $SiO_2 \cdot Al_2O_3$ catalyst [67] (Scheme 14.15). The conversion simply decreased with CO_2 pressure in the reactions with three dienophile substrates, which may be caused by the dilution effect of CO_2 molecules in the liquid phases. However, the product selectivity remarkably changed with CO_2 pressure; the ratio of [3] adduct to [2]

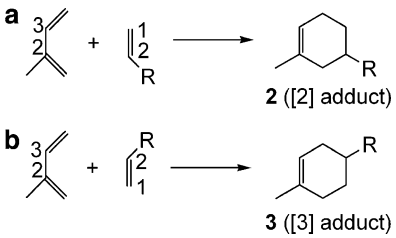

Scheme 14.15 Two approaches (**a**) and (**b**), yielding [2] adduct and [3] adduct

adduct could be altered, which changed most extensively for acrolein from 47:53 to 73:27 at pressure up to 16 MPa. The change was less significant for the other dienophiles, but the ratio did also change from 70:30 to 75:25 and from 63:37 to 73:27 for methyl acrylate and methyl vinyl ketone, respectively. At a high pressure of 16 MPa, very similar **3** to **2** ratios were seen for the three dienophiles, which are similar to those with Diels–Alder reactions of cyclopentadiene with methyl vinyl ketone and methyl acrylate in dense-phase CO_2 reported by Tester et al. [68]. They concluded that the product selectivity was not affected by CO_2 pressure, while Ikushima et al. mentioned about the effect of CO_2 pressurization in the reaction of isoprene and methyl acrylate in dense-phase CO_2 [69]. The pressurization and dissolution of CO_2 in the toluene phase will scarcely change its features as a continuum of solvent for the reactions. CO_2 molecules dissolved surround the substrate molecules inducing interactions between the substrate and CO_2 molecules in the liquid phase. As the pressure is raised, the state of such a clump of substrate-CO_2 molecules in toluene may become similar to that in a dense-phase CO_2 medium, resulting in the similar **3** to **2** ratios as obtained.

The molecular interaction of CO_2 with three dienophiles in the presence of dense-phase CO_2 was discussed using in situ high-pressure FTIR measurements, and the results indicated that the interactions of dense-phase CO_2 with the carbonyl group may be stronger for acrolein compared with the other two carbonyl compounds, as estimated from the peak shift of ν(C═O) absorption band with increasing CO_2 pressure. Fujita et al. speculated that CO_2 molecules interact with the carbonyl group of a dienophile, and this makes its C-1 carbon more positive compared to the C-2 carbon. As a result, the approach b of Scheme 14.15 may be more favorable to occur than that between the dienophile and isoprene in which C-3 may be more positive than C-2 owing to the electron-withdrawing nature of the methyl group attached to C-2. These interactions may cause steric effects on the product selectivity, resulting in the increase of the **3** to **2** ratio with CO_2 pressure. Eckert et al. also investigated the interactions between CO_2 and the substrates for the Diels–Alder reaction between 4-phenyl-1,2,4-triazoline-3,5-dione (PTAD) and anthracene in CO_2-expanded acetonitrile [70] (Scheme 14.16). From the reaction results, they speculate that CO_2 dissolved in the liquid organic phase acts as a Lewis acid, and the interaction between Lewis acid and carbonyl oxygen of the PTAD would destabilize the azo bond, increasing the reactivity of the dienophile toward the diene (Scheme 14.17).

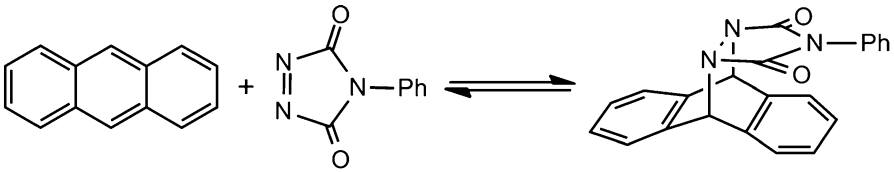

Scheme 14.16 Diels–Alder reaction of anthracene and PTAD

Scheme 14.17 Lewis acid–base interaction between CO_2 and PTAD molecules

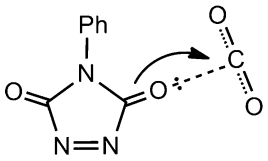

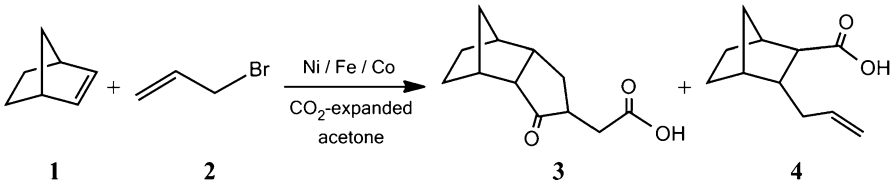

1 **2** **3** **4**

Scheme 14.18 The catalytic carbonylative cycloaddition between norbornene **1** and allyl bromide **2** in CO_2-expanded acetone

14.2.6 Other Reactions

Recently, many researchers are making efforts to extend the application of dense-phase CO_2 for new chemical reactions including multiphase reactions and liquid-phase organic reactions.

Moral et al. reported excellent chemoselectivity in the Ni-catalyzed cyclocarbonylation reaction with both alkynes and strained alkenes by tuning the operational parameters, using CO_2-expanded acetone as a reaction medium instead of liquid acetone [71]. The carbonylative cycloaddition between norbornene **1** and allyl bromide **2** with CO over Ni/Fe catalyst at 298 K in liquid or CO_2-expanded acetone was investigated (Scheme 14.18). The norbornene and allyl bromide tested were highly soluble in both pure CO_2 and CO_2-expanded acetone, but the catalyst was only soluble in CO_2-expanded acetone under certain conditions. Thus, the reaction was feasible under homogeneous conditions in the latter medium. Cyclopentanone **3** was obtained as a main product in a selectivity of 77 % in the absence of CO_2, and the selectivity to **3** can slightly be improved to 80 % by CO_2 pressurization. Interestingly, they added a certain amount of H_2O into the reaction system, and the selectivity to **3** was enhanced to 98 % with no retardation of the reaction. They speculated the acidification of reaction media with CO_2 and H_2O, which decreased the OH^- concentration, resulting in preventing hydroxyl attack at the acyl metal intermediate and interrupting the cyclization.

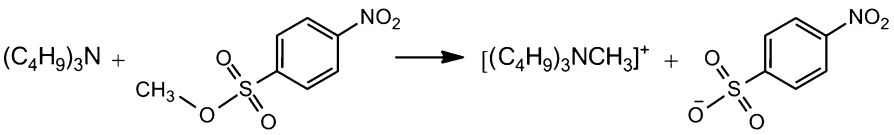

Scheme 14.19 Menschutkin reaction of TBA and MNBS

Ford et al. focused on the controlling of local polarity in CXLs by changing CO_2 pressure. They examined several probes as indicators of either local or bulk polarity in CO_2-expanded acetonitrile [72]. The Menschutkin reaction is a nucleophilic substitution reaction proceeding by an S_N2 mechanism between a nitrogen base, typically a tertiary amine, and an organic electrophile such as an alkyl halide or sulfonate to form a quaternary ammonium salt. The transition state of this reaction is much more polar than the reactants, thus making the reaction kinetics strongly depend on the polarity of the surrounding medium. The Menschutkin reaction of tributylamine (TBA) with methyl *p*-nitrobenzenesulfonate (MNBS) in CO_2-expanded acetonitrile at 313 K was studied (Scheme 14.19), and it is found that at a mole fraction of $CO_2 > 0.60$, the value of the rate constant is significantly higher than that at a mole fraction of $CO_2 < 0.60$. At high CO_2 loading, the charge-separated transition state of the reactant may be stabilized by acetonitrile with decreasing polarity of the liquid phase. Another factor is that the polar solutes would be clustered and/or aggregated as CXL increasingly becomes nonpolar.

14.3 Conclusions

Several examples described in this chapter demonstrate that CO_2 can act as a promoter/modifier in organic synthetic reactions. CO_2 has different macro (physical) and micro (chemical) functions depending on the reactions and conditions used. The reaction rate and/or the product selectivity in a liquid-phase reaction may be improved by the actions of CO_2 dissolved in the liquid phase. CO_2 interacts with organic substrates, intermediates, and/or products and changes their reactivity. Some pressure is needed for CO_2 to dissolve in a certain amount, and the pressurization with CO_2 is a simple procedure. When water is also present with dense-phase CO_2, the reaction mixture is more complicated, but interesting reaction outcome would be obtained through additive and/or synergistic effects of CO_2 and water. The multiphase reactions in the presence of dense-phase CO_2 and/or water are an interesting topic to be investigated in more detail, and the effects of CO_2 and water should be explained at molecular level. For practical application, the multiphase reactions should be analyzed from the viewpoint of chemical engineering (mixing, phase behavior, mass transfer, and reaction kinetics), and the costs of CO_2 pressurization and depressurization, post-purification of water, and so on should be considered.

References

1. Jessop PG, Subramaniam B (2007) Gas-expanded liquids. Chem Rev 107:2666–2694
2. Akien GR, Poliakoff M (2009) A critical look at reactions in class I and II gas-expanded liquids using CO_2 and other gases. Green Chem 11:1083–1100
3. Arai M, Fujita S, Shirai M (2009) Multiphase catalytic reactions in/under dense phase CO_2. J Supercrit Fluids 47:351–356
4. Akiyama Y, Fujita S, Senboku H, Rayner CM, Brough SA, Arai M (2008) An in situ high pressure FTIR study on molecular interactions of ketones, esters, and amides with dense phase carbon dioxide. J Supercrit Fluids 46:197–205
5. Yoo JS, Jhung SH, Lee KH, Park YS (2002) An advanced MC-type oxidation process – the role of carbon dioxide. Appl Catal A Gen 223:239–251
6. Aresta M, Tommasi I, Quaranta E, Fragale C, Mascetti J, Tranquille M, Galan F, Fouassier M (1996) Mechanism of formation of peroxocarbonates $RhOOC(O)O(Cl)(P)_3$ and their reactivity as oxygen transfer agents mimicking monooxygenases. The first evidence of CO_2 insertion into the O-O Bond of $Rh(\eta^2\text{-}O_2)$ complexes. Inorg Chem 35:4254–4260
7. Nolen SA, Lu J, Brown JS, Pollet P, Eason BC, Griffith KN, Gläser R, Bush D, Lamb DR, Liotta CL, Eckert CA (2002) Olefin epoxidations using supercritical carbon dioxide and hydrogen peroxide without added metallic catalysts or peroxy acids. Ind Eng Chem Res 41:316–323
8. Rajagopalan B, Wei M, Musie GT, Subramaniam B, Busch DH (2003) Homogeneous catalytic epoxidation of organic substrates in CO_2-expanded solvents in the presence of water-soluble oxidants and catalysts. Ind Eng Chem Res 42:6505–6510
9. Rathke JW, Klingler RJ, Krause TR (1991) Propylene hydroformylation in supercritical carbon dioxide. Organometallics 10:1350–1355
10. Hemminger O, Marteel A, Mason MR, Davies JA, Tadd AR, Abraham MA (2002) Hydroformylation of 1-hexene in supercritical carbon dioxide using a heterogeneous rhodium catalyst. 3. Evaluation of solvent effects. Green Chem 4:507–512
11. Jin H, Subramaniam B (2004) Homogeneous catalytic hydroformylation of 1-octene in CO_2-expanded solvent media. Chem Eng Sci 59:4887–4893
12. Tominaga K, Sasaki Y (2004) Ruthenium-catalyzed one-pot hydroformylation of alkenes using carbon dioxide as a reactant. J Mol Catal A Chem 220:159–165
13. Tominaga K (2006) An environmentally friendly hydroformylation using carbon dioxide as a reactant catalyzed by immobilized Ru-complex in ionic liquids. Catal Today 115:70–72
14. Fujita S, Okamura S, Akiyama Y, Arai M (2007) Hydroformylation of cyclohexene with carbon dioxide and hydrogen using ruthenium carbonyl catalyst: influence of pressures of gaseous components. Int J Mol Sci 8:749–759
15. Weissermal K, Arpe HJ (1997) Industrial organic chemistry, 3rd edn. Wiley-VCH, Weinheim
16. Smith GV, Notheisz F (1995) Heterogeneous catalysis in organic chemistry. Academic, London
17. Seki T, Grunwaldt JD, Baiker A (2008) Heterogeneous catalytic hydrogenation in supercritical fluids: potential and limitations. Ind Eng Chem Res 47:4561–4585
18. Solinas M, Pfaltz A, Cozzi PG, Leitner W (2004) Enantioselective hydrogenation of imines in ionic liquid/carbon dioxide media. J Am Chem Soc 126:16142–16147
19. Devetta L, Giovanzana A, Canu P, Bertucco A, Minder BJ (1999) Kinetic experiments and modeling of a three-phase catalytic hydrogenation reaction in supercritical CO_2. Catal Today 48:337–345
20. Chouchi D, Gourgouillon D, Courel M, Vital J, da Ponte MN (2001) The influence of phase behavior on reactions at supercritical conditions: the hydrogenation of α-pinene. Ind Eng Chem Res 40:2551–2554
21. Gallezot P, Richard D (1998) Selective hydrogenation of α, β-unsaturated aldehydes. Catal Rev Sci Eng 40:81–126

22. Bhanage BM, Ikushima Y, Shirai M, Arai M (1999) The selective formation of unsaturated alcohols by hydrogenation of α, β-unsaturated aldehydes in supercritical carbon dioxide using unpromoted Pt/Al_2O_3 catalyst. Catal Lett 62:175–177
23. Zhao F, Fujita S, Akihara S, Arai M (2005) Hydrogenation of benzaldehyde and cinnamaldehyde in compressed CO_2 medium with a Pt/C catalyst: a study on molecular interactions and pressure effects. J Phys Chem A 109:4419–4424
24. Zhao F, Fujita S, Sun J, Ikushima Y, Arai M (2004) Carbon dioxide-expanded liquid substrate phase: an effective medium for selective hydrogenation of cinnamaldehyde to cinnamyl alcohol. Chem Commun 40:2–4
25. Wang J, Wang M, Hao J, Fujita S, Arai M, Wu Z, Zhao F (2010) Theoretical study on interaction between CO_2 and carbonyl compounds: influence of CO_2 on infrared spectroscopy and activity of CO. J Supercrit Fluids 54:9–15
26. Fujita S, Akihara S, Zhao F, Liu R, Hasegawa M, Arai M (2005) Selective hydrogenation of cinnamaldehyde using ruthenium-phosphine complex catalysts with multiphase reaction systems in and under pressurized carbon dioxide: significance of pressurization and interfaces for the control of selectivity. J Catal 236:101–111
27. Liu R, Zhao F, Fujita S, Arai M (2007) Selective hydrogenation of citral with transition metal complexes in supercritical carbon dioxide. Appl Catal A Gen 316:127–133
28. Bhanage BM, Ikushima Y, Shirai M, Arai M (1999) Multiphase catalysis using water-soluble metal complexes in supercritical carbon dioxide. Chem Commun 35:1277–1278
29. Rappoprt Z (ed) (2007) The chemistry of anilines. Wiley, Chichester
30. Diao S, Qjan W, Luo G, Wei F, Wang Y (2005) Gaseous catalytic hydrogenation of nitrobenzene to aniline in a two-stage fluidized bed reactor. Appl Catal A Gen 286:30–35
31. Nishimura S (2001) Handbook of heterogeneous catalytic hydrogenation for organic synthesis. Wiley, New York
32. Li H, Zhao Q, Wan Y, Dai W, Qiao M (2006) Self-assembly of mesoporous Ni-B amorphous alloy catalysts. J Catal 244:251–254
33. Xu R, Xie T, Zhao Y, Li Y (2007) Quasi-homogeneous catalytic hydrogenation over monodisperse nickel and cobalt nanoparticles. Nanotechnology 18:055602–055606
34. Höller V, Wegricht D, Yuranov I, Kiwi-Minsker L, Renken A (2000) Three-phase nitrobenzene hydrogenation over supported glass fiber catalysts: reaction kinetic study. Chem Eng Technol 23:251–255
35. Meng X, Cheng H, Akiyama Y, Hao Y, Qiao W, Yu Y, Zhao F, Fujita S, Arai M (2009) Selective hydrogenation of nitrobenzene to aniline in dense phase carbon dioxide over $Ni/\gamma\text{-}Al_2O_3$: significance of molecular interactions. J Catal 264:1–10
36. Meng X, Cheng H, Fujita S, Hao Y, Shang Y, Yu Y, Cai S, Zhao F, Arai M (2010) Selective hydrogenation of chloronitrobenzene to chloroaniline in supercritical carbon dioxide over Ni/TiO_2: significance of molecular interactions. J Catal 269:131–139
37. Zhao F, Ikushima Y, Arai M (2004) Hydrogenation of nitrobenzene with supported platinum catalysts in supercritical carbon dioxide: effects of pressure, solvent, and metal particle size. J Catal 224:479–483
38. Zhao F, Zhang R, Chatterjee M, Ikushima Y, Arai M (2004) Hydrogenation of nitrobenzene with supported transition metal catalysts in supercritical carbon dioxide. Adv Synth Catal 346:661–668
39. Meng X, Cheng H, Fujita S, Yu Y, Zhao F, Arai M (2011) An effective medium of H_2O and low-pressure CO_2 for the selective hydrogenation of aromatic nitro compounds to anilines. Green Chem 13:570–572
40. Lin HW, Yen CH, Tan CS (2012) Aromatic hydrogenation of benzyl alcohol and its derivatives using compressed CO_2/water as the solvent. Green Chem 14:682–687
41. Chanda A, Fokin VV (2009) Organic synthesis on water. Chem Rev 109:725–748
42. Yoshida H, Wang Y, Narisawa S, Fujita S, Arai M (2013) A multiphase reaction medium including pressurized carbon dioxide and water for selective hydrogenation of benzonitrile with a Pd/Al_2O_3 catalysts. Appl Catal A Gen 456:215–222

43. George M, Weiss RG (2002) Chemically reversible organogels via latent gelators. Aliphatic amines with carbon dioxide and their ammonium carbamates. Langmuir 18:7124–7135
44. Xie X, Liotta CL, Eckert CA (2004) CO_2-protected amine formation from nitrile and imine hydrogenation in gas-expanded liquids. Ind Eng Chem Res 43:7907–7911
45. Fürstner A, Koch D, Langemann K, Leitner W, Six C (1997) Olefin metathesis in compressed carbon dioxide. Angew Chem Int Ed 36:2466–2469
46. Wittmann K, Wisniewski W, Mynott R, Leitner W, Kranemann CL, Rische T, Eilbracht P, Kluwer S, Ernsting JM, Elsevier CJ (2001) Supercritical carbon dioxide as solvent and temporary protecting group for rhodium-catalyzed hydroaminomethylation. Chem Eur J 7:4584–4589
47. Wei HH, Yen CH, Lin HW, Tang CS (2013) Synthesis of bimetallic Pd-Ag colloids in CO_2-expanded hexane and their application in partial hydrogenation of phenylacetylene. J Supercrit Fluids 81:1–6
48. Yoshida H, Kato K, Wang J, Meng X, Narisawa S, Fujita S, Wu Z, Zhao F, Arai M (2011) Hydrogenation of nitrostyrene with a Pt/TiO_2 catalyst in CO_2-dissolved expanded polar and nonpolar organic liquids: their macroscopic and microscopic features. J Phys Chem C 115:2257–2267
49. Reichardt C (2003) Solvents and solvent effects in organic chemistry, 3rd edn. Wiley-VCH, Weinheim
50. Minder B, Mallat T, Pickel KH, Steiner K, Baiker A (1995) Enantioselective hydrogenation of ethyl pyruvate in supercritical fluids. Catal Lett 34:1–9
51. Ferri D, Bürgi T, Baiker A (2002) Probing boundary sites on a Pt/Al_2O_3 model catalyst by CO_2 hydrogenation and in situ ATR-IR spectroscopy of catalytic solid–liquid interfaces. Phys Chem Chem Phys 4:2667–2672
52. Burgener M, Ferri D, Grunwaldt JD, Mallat T, Baiker A (2005) Supercritical carbon dioxide: an inert solvent for catalytic hydrogenation? J Phys Chem B 109:16794–16800
53. Arunajatesana V, Subramaniama B, Hutchensonc KW, Herkes FE (2007) In situ FTIR investigations of reverse water gas shift reaction activity at supercritical conditions. Chem Eng Sci 62:5062–5069
54. Zeinalipour-Yazdi CD, Cooksy AL, Efstathiou AM (2007) A diffuse reflectance infrared Fourier-transform spectra and density functional theory study of CO adsorption on $Rh/\gamma\text{-}Al_2O_3$. J Phys Chem C 111:13872–13878
55. Dong LB, McVicker GB, Kiserow DJ, Roberts GW (2010) Hydrogenation of polystyrene in CO_2-expanded liquids: the effect of catalyst composition on deactivation. Appl Catal A Gen 384:45–50
56. Yoshida H, Narisawa S, Fujita S, Liu R, Arai M (2012) In situ FTIR study on the formation and adsorption of CO on alumina-supported noble metal catalysts from H_2 and CO_2 in the presence of water vapor at high pressures. Phys Chem Chem Phys 14:4724–4733
57. Arai M, Nishiyama Y, Ikushima Y (1998) Optical absorption of fine gold particles in supercritical carbon dioxide for the characterization of solvent properties. J Supercrit Fluids 13:149–153
58. Liu R, Yoshida H, Narisawa S, Fujita S, Arai M (2012) The dispersion of TiO_2 modified by the accumulation of CO_2 molecules in water: an effective medium for photocatalytic H_2 production. RSC Adv 2:8002–8006
59. West KN, Wheeler C, McCarney JP, Griffith KN, Bush D, Liotta CL, Eckert CA (2001) In situ formation of alkylcarbonic acids with CO_2. J Phys Chem A 105:3947–3948
60. Xie X, Liotta CL, Eckert CA (2004) CO_2-catalyzed acetal formation in CO_2-expanded methanol and ethylene glycol. Ind Eng Chem Res 43:2605–2609
61. Chamblee TS, Weikel RR, Nolen SA, Liotta CL, Eckert CA (2004) Reversible in situ acid formation for β-pinene hydrolysis using CO_2 expanded liquid and hot water. Green Chem 6:382–386
62. Weikel RR, Hallett JP, Liotta CL, Eckert CA (2006) Self-neutralizing in situ acid catalysts from CO_2. Top Catal 37:75–80

63. Weikel RR, Hallett JP, Liotta CL, Eckert CA (2007) Self-neutralizing in situ acid catalysis for single-pot synthesis of iodobenzene and methyl yellow in CO_2-expanded methanol. Ind Eng Chem Res 46:5252–5257
64. Morita DK, Pesiri DR, David SA, Glaze WH, Tumas W (1998) Palladium-catalyzed carbon-carbon bond formation in supercritical carbon dioxide. Chem Commun 1397–1398
65. Fujita S, Yuzawa K, Bhanage BM, Ikushima Y, Arai M (2002) Palladium-catalyzed Heck coupling reactions using different fluorinated phosphine ligands in compressed carbon dioxide and conventional organic solvents. J Mol Cat A Chem 180:35–42
66. Bhanage BM, Fujita S, Arai M (2003) Heck reactions with various types of palladium complex catalyst: application of multiphase catalysis and supercritical carbon dioxide. J Organomet Chem 687:211–218
67. Fujita S, Tanaka T, Akiyama Y, Asai K, Hao J, Zhao F, Arai M (2008) Impact of carbon dioxide pressurization on liquid phase organic reactions: a case study on Heck and Diels-Alder reactions. Adv Synth Catal 350:1615–1625
68. Weinstein RD, Renslo AR, Danheiser RL, Tester JW (1999) Silica-promoted Diels-Alder reactions in carbon dioxide from gaseous to supercritical conditions. J Phys Chem B 103:2878–2887
69. Ikushima Y, Saito N, Arai M (1992) Supercritical carbon dioxide as reaction medium: examination of its solvent effects in the near-critical region. J Phys Chem 96:2293–2297
70. Ford JW, Lu J, Liotta CL, Eckert CA (2008) Solvent effects on the kinetics of a Diels-Alder reaction in gas-expanded liquids. Ind Eng Chem Res 47:632–637
71. Moral D, Osuna AMB, Córdoba A, Moretó JM, Veciana J, Ricart S, Ventosa N (2009) Versatile chemoselectivity in Ni-catalyzed multiple bond carbonylations and cyclocarbonylations in CO_2-expanded liquids. Chem Commun 31:4723–4725
72. Ford JW, Janakat ME, Lu J, Liotta CL, Eckert CA (2008) Local polarity in CO_2-expanded acetonitrile: a nucleophilic substitution reaction and solvatochromic probes. J Org Chem 73:3364–3368